



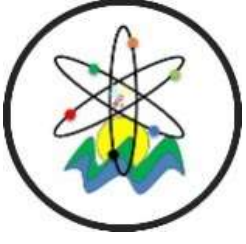
Black Sea Journal of Engineering and Science

Volume 7 | Issue 3



ISSN: 2619 - 8991


BS Journals



BLACK SEA JOURNAL OF ENGINEERING AND SCIENCE
(BSJ ENGIN SCI)


BS Journals

Black Sea Journal of Engineering and Science (BSJ Eng Sci) is a double-blind peer-reviewed, open-access international journal published electronically 6 times (January, March, May, July, September, and November) in a year by since January 2018. It publishes, in English and Turkish, full-length original research articles, innovative papers, conference papers, reviews, mini-reviews, rapid communications or technical note on advances in a wide range of scientific disciplines from all fields of engineering and science and from any source.

ISSN 2619 - 8991

Phone: +90 362 408 25 15

Fax: +90 362 408 25 15

Email: bsjsci@blackseapublishers.com

Web site: <http://dergipark.gov.tr/bsengineering>

Sort of publication: Periodically 6 times (January, March, May, July, September, and November) in a year

Publication date and place: May 15, 2024 - Samsun, TÜRKİYE

Publishing kind: Electronically

OWNER

Assoc. Prof. Dr. Uğur ŞEN

DIRECTOR IN CHARGE

Prof. Dr. Hasan ÖNDER

EDITOR BOARDS

EDITOR IN CHIEF

Prof. Dr. Hasan ÖNDER, Ondokuz Mayıs University, TÜRKİYE

Assoc. Prof. Dr. Uğur ŞEN, Ondokuz, Mayıs University, TÜRKİYE

SECTION EDITORS*

Prof. Dr. Ahmet UYANIK, Section Editor of Chemistry, Ondokuz Mayıs University, TÜRKİYE

Prof. Dr. Amila Sandaruwan RATNAYAKE, Section Editor of Geological Engineering, Uva Wellassa University, SRI LANKA

Prof. Dr. Berna KILIÇ, Section Editor of Fisheries Engineering, Ege University, TÜRKİYE

Prof. Dr. Çiğdem TAKMA, Section Editor of Statistics, Ege University, TÜRKİYE

Prof. Dr. Ertan BUYRUK, Section Editor of Mechanical Engineering, Sivas Cumhuriyet University, TÜRKİYE

Prof. Dr. Fahrul Zaman HUYOP, Section Editor of Biology, Universiti Teknologi Malaysia, MALAYSIA

Prof. Dr. Fauziatul FAJAROH, Section Editor of Chemical Engineering, Universitas Negeri Malang, INDONESIA

Prof. Dr. Fuad ALHAJOMAR, Section Editor of Electrical and Electronics Engineering, University of South Wales, UNITED KINGDOM

Prof. Dr. Gökhan CİVELEKOĞLU, Section Editor of Environmental Engineering, Akdeniz University, TÜRKİYE

Prof. Dr. Hasan TANAK, Section Editor of Physics, Amasya University, TÜRKİYE

Prof. Dr. Hasan TEMİZ, Section Editor of Food Engineering, Ondokuz Mayıs University, TÜRKİYE

Prof. Dr. Hojjat SADEGHİ-ALIABADI, Section Editor of Chemistry, Isfahan University, IRAN

Prof. Dr. İbrahim Özgür DENEME, Section Editor of Civil Engineering, Aksaray University, TÜRKİYE

Prof. Dr. İbrahim UĞUR, Section Editor of Mining Engineering, Süleyman Demirel University, TÜRKİYE

Prof. Dr. Jamrun EBBAH, Section Editor of Fisheries Engineering, Mindanao State University, PHILIPPINES

Prof. Dr. Messaoud SAIDANI, Section Editor of Civil Engineering, Coventry University, UNITED KINGDOM

Prof. Dr. Perarasu THANGAVELU, Section Editor of Aerospace Engineering, Anna University, INDIA

Prof. Dr. Sema PALAMUTCU, Section Editor of Textile Engineering, Pamukkale University, TÜRKİYE

Prof. Dr. Ümit Cafer YILDIZ, Section Editor of Forest Engineering, Karadeniz Technical University, TÜRKİYE

Assoc. Prof. Dr. Belgin KARABACAKOĞLU, Section Editor of Chemical Engineering, Eskişehir Osmangazi University, TÜRKİYE

Assoc. Prof. Dr. Bülent BOSTANCI, Section Editor of Geomatics Engineering, Erciyes University, TÜRKİYE

Assoc. Prof. Dr. Edit MİKÓ, Section Editor of Agricultural Engineering, University of Szeged, HUNGARY

Assoc. Prof. Dr. Ergün EKİCİ, Section Editor of Industrial Engineering, Çanakkale Onsekiz Mart University, TÜRKİYE

Assoc. Prof. Dr. Helal Uddin MOLLA, Section Editor of Physics, Rajshahi University of Engineering and Technology, BANGLADESH

Assoc. Prof. Dr. Kadyrbay CHEKİROV, Section Editor of Biology, Kyrgyz Turkish Manas University, KYRGYZSTAN

Assoc. Prof. Dr. Mehmet EBEOĞLUGİL, Section Editor of Metallurgical and Materials Engineering, Dokuz Eylül University, TÜRKİYE

Assoc. Prof. Dr. Nilüfer YURTAY, Section Editor of Computer Engineering, Sakarya University, TÜRKİYE

Assoc. Prof. Dr. Özgür Hakan AYDOĞMUŞ, Section Editor of Mathematics, Social Sciences University of Ankara, TÜRKİYE

Assoc. Prof. Dr. Rita ISMAİLOVA, Section Editor of Computer Engineering, Kyrgyz - Turkish Manas University, KYRGYZSTAN

Assoc. Prof. Dr. Samia Chehbi GAMOURA, Section Editor of Statistics, Strasbourg University, FRANCE

Assoc. Prof. Dr. Silvio DE OLIVEIRA JUNIOR, Section Editor of Mechanical Engineering, University of São Paulo, BRAZIL

Assoc. Prof. Dr. Sinan AKISKA, Section Editor of Geological Engineering, Ankara University, TÜRKİYE

Asst. Prof. Dr. Abdul JABBAR, Section Editor of Textile Engineering, National Textile University, PAKISTAN

Asst. Prof. Dr. Arsheed Ahmad RATHER, Section Editor of Forest Engineering, Annamalai University, INDIA

Asst. Prof. Dr. Ezenwanyi OCHULOR, Section Editor of Metallurgical and Materials Engineering, University Of Lagos, NIGERIA

Asst. Prof. Dr. Francis INEGBEDION, Section Editor of Industrial Engineering, University of Benin, NIGERIA

Asst. Prof. Dr. Haniyeh RASOULI PIROUZIAN, Section Editor of Food Engineering, Tabriz University, IRAN

Asst. Prof. Dr. Jun-wei LIM, Section Editor of Environmental Engineering, Universiti Teknologi Petronas, MALAYSIA

Asst. Prof. Dr. Mehmet GÜÇYETMEZ, Section Editor of Electrical and Electronics Engineering, Kırşehir Ahi Evran University, TÜRKİYE

Asst. Prof. Dr. Melahat CİHAN, Section Editor of Aerospace Engineering, Samsun University, TÜRKİYE

Asst. Prof. Dr. Muhammad GULİSTAN, Section Editor of Mathematics, Hazara University, PAKISTAN

Asst. Prof. Dr. Sedat KARADAVUT, Section Editor of Agricultural Engineering, Trakya University, TÜRKİYE

Asst. Prof. Dr. Seyedeh Narges SADATI, Section Editor of Mining Engineering, University of Mohaghegh Ardabili, IRAN

Asst. Prof. Dr. Xinyi WANG, Section Editor of Geomatics Engineering, Henan Polytechnic University, CHINA

* The ranking is arranged alphabetically within the academic title

EDITORIAL - ADVISORY BOARD*

Prof. Dr. Aglaia (Litsa) LIOPA-TSAKALIDI, Institute of Western Greece, GREECE

Prof. Dr. Ercan EFE, Kahramanmaraş Sutcu Imam University, TÜRKİYE

Prof. Dr. Mohammad Masood TARIQ, University of Balochistan, PAKISTAN

Prof. Dr. Mustafa Çağatay TUFAN, Ondokuz Mayıs University, TÜRKİYE

Prof. Dr. Özkan GÖRGÜLÜ, Ahi Evran University, TÜRKİYE

Assoc. Prof. Dr. Taner TUNÇ, Ondokuz Mayıs University, TÜRKİYE

Asst. Prof. Dr. Emil OMURZAK, Kyrgyz-Turkish Manas University, KYRGYZSTAN

Asst. Prof. Dr. Yılmaz KAYA, Ondokuz Mayıs University, TÜRKİYE

* The ranking is arranged alphabetically within the academic title

STATISTIC EDITOR

Prof. Dr. Mehmet TOPAL, Kastamonu University, TÜRKİYE

ENGLISH EDITOR

Asst. Prof. Dr. Betül ÖZCAN DOST, Ondokuz Mayıs University, TÜRKİYE

TURKISH EDITOR

Prof. Dr. Serkan ŞEN, Ondokuz Mayıs University, TÜRKİYE

REVIEWERS OF THE ISSUE*

Prof. Dr. Adem ASAN, Ondokuz Mayıs University, Department of Chemistry, Analytical Chemistry, TÜRKİYE

Prof. Dr. Arda ÖZTÜRKCAN, İstanbul Gelişim University, Department of Nutrition and Dietetics, Organic Chemistry, TÜRKİYE

Prof. Dr. Cahit GÜRER, Afyon Kocatepe University, Department of Civil Engineering, Transportation and Traffic, TÜRKİYE

Prof. Dr. Cemil GÜRÜNLÜ, Karadeniz Technical University, Department of Electrical and Electronics Engineering, Energy, TÜRKİYE

Prof. Dr. Cemil ÖZ, Sakarya University, Department of Computer Engineering, Neural Networks, TÜRKİYE

Prof. Dr. Derya BIRANT, Dokuz Eylül University, Department of Computer Science, Machine Learning, TÜRKİYE

Prof. Dr. Erkan YASLIOĞLU, Bursa Uludağ University, Department of Biosystem Engineering, Agricultural Structures, TÜRKİYE

Prof. Dr. Muhammet KARATON, Fırat University, Department of Civil Engineering, Earthquake Engineering, TÜRKİYE

Prof. Dr. Recep ÖZEN, Mersin University, Department of Chemistry, Organic Chemistry, TÜRKİYE

Assoc. Prof. Dr. Ahmet ATALAY, Atatürk University, Department of Civil Engineering, Transportation and Traffic, TÜRKİYE

Assoc. Prof. Dr. Aysel VEYİSOĞLU, Sinop University, Department of Medical Services and Techniques, Bacteriology, TÜRKİYE

Assoc. Prof. Dr. Demet TATAR, Hitit University, Department of Medical Services and Techniques, Bacteriology, TÜRKİYE

Assoc. Prof. Dr. Emre ŞİRİN, Kırşehir Ahi Evran University, Department of Agricultural Biotechnology, Animal Reproduction and Breeding, TÜRKİYE

Assoc. Prof. Dr. Fadime ÖZDEMİR, Bilecik Şeyh Edebali University, Department of Molecular Biology and Genetics, Bacteriology, TÜRKİYE

Assoc. Prof. Dr. Hacı Mehmet ALAKAŞ, Kırıkkale University, Department of Industrial Engineering, Optimization in Manufacturing, TÜRKİYE

Assoc. Prof. Dr. Hare KILIÇASLAN, Karadeniz Technical University, Department of Architecture, Built Environment and Design, TÜRKİYE

Assoc. Prof. Dr. Hilal AYCI, Gazi University, Department of Architecture, Built Environment and Design, TÜRKİYE

Assoc. Prof. Dr. Hüseyin ŞANLI, Tekirdağ Namık Kemal University, Department of Automotive Technology, Automotive Combustion and Fuel Engineering, TÜRKİYE

Assoc. Prof. Dr. Kadir GÜÇLÜER, Adıyaman University, Department of Civil Engineering, Construction Materials, TÜRKİYE

Assoc. Prof. Dr. Kenan ALTUN, Sivas Cumhuriyet University, Department of Electronics and Automation, Electronics, TÜRKİYE

Assoc. Prof. Dr. Mürsel Ozan İNCETAŞ, Alanya Alaaddin Keykubat University, Department of Computer Technologies, Artificial Intelligence, TÜRKİYE

Assoc. Prof. Dr. Rukiye UZUN ARSLAN, Zonguldak Bülent Ecevit University, Department of Electrical and Electronics Engineering, Data Mining and Knowledge Discovery, TÜRKİYE

Assoc. Prof. Dr. Şaban ÖZTÜRK, Ankara Hacı Bayram Veli University, Department of Management Information Systems, Artificial Intelligence, TÜRKİYE

Assoc. Prof. Dr. Şahika ÖZDEMİR, İstanbul Sabahattin Zaim University, Department of Interior Architecture and Environmental Design, Architectural Design, TÜRKİYE

Assoc. Prof. Dr. Sedat BEHREM, Aksaray University, Department of Animal Science and Animal Nutrition, Sheep and Goat Breeding and Treatment, TÜRKİYE

Assoc. Prof. Dr. Seyit Ahmet SİS, Balıkesir University, Department of Electrical and Electronics Engineering, Electrical Engineering, TÜRKİYE

Assoc. Prof. Dr. Sinan KUL, Bayburt University, Department of Emergency Aid and Disaster Management, Environmental Sciences and Engineering, TÜRKİYE

Assoc. Prof. Dr. Tunahan ERDEM, Çukurova University, Department of Agricultural Machinery, Agricultural Tools and Machines, TÜRKİYE

Assoc. Prof. Dr. Tuncay ERCAN, Yaşar University, Department of Management Information Systems, Information and Computing Sciences, TÜRKİYE

Assoc. Prof. Dr. Yavuz ÖZDEMİR, İstanbul Health and Technology University, Department of Industrial Engineering, Industrial Engineering, TÜRKİYE

Assoc. Prof. Dr. Yunus DEMİR, Bursa Technical University, Department of Industrial Engineering, Artificial Intelligence, TÜRKİYE

Assist. Prof. Dr. Behcet DÜNDAR, Osmaniye Korkut Ata University, Department of Civil Engineering, Construction Materials, TÜRKİYE

Assist. Prof. Dr. Bilgehan ERKAL, Karabük University, Department of Electrical and Electronics Engineering, Electrical Engineering, TÜRKİYE

Assist. Prof. Dr. Dilan ALP, Şırnak University, Department of Energy Systems Engineering, Energy Systems Engineering, TÜRKİYE

Assist. Prof. Dr. Elif ACAR, Yozgat Bozok University, Department of Business Administration, Multiple Criteria Decision Making, TÜRKİYE

Assist. Prof. Dr. Emre ALARSLAN, Bandırma Onyedi Eylül University, Department of Animal Science, Sheep and Goat Breeding and Treatment, TÜRKİYE

Assist. Prof. Dr. Evrim GÜLER, Bartın University, Department of Computer Engineering, Artificial Intelligence, TÜRKİYE

Assist. Prof. Dr. Gökhan GÖKSU, Yıldız Technical University, Department of Mathematics Engineering, Control Engineering, TÜRKİYE

Assist. Prof. Dr. Görkem SERBES, Yıldız Technical University, Department of Biomedical Engineering, Biosignal Processing, TÜRKİYE

Assist. Prof. Dr. Hasan Ali İRİK, Erciyes University, Department of Biosystem Engineering, Agricultural Structures, TÜRKİYE

Assist. Prof. Dr. İlker KARADAĞ, Sivas Cumhuriyet University, Department of Industrial Engineering, Multiple Criteria Decision Making, TÜRKİYE

Assist. Prof. Dr. Mahmut DURMAZ, Siirt University, Department of Civil Engineering, Construction Materials, TÜRKİYE

Assist. Prof. Dr. Mustafa NİL, Manisa Celal Bayar University, Department of Electrical and Electronics Engineering, Power Electronics, TÜRKİYE

Assist. Prof. Dr. Onur SÖZÜDOĞRU, Atatürk University, Department of Emergency Aid and Disaster Management, Environmental Sciences and Engineering, TÜRKİYE

Assist. Prof. Dr. Osman GÖKALP, İzmir Yüksek Teknoloji Institute, Department of Computer Engineering, Evolutionary Computation, TÜRKİYE

Assist. Prof. Dr. Özlem KARABİBER CURA, İzmir Katip Çelebi University, Department of Clinical Engineering, Machine Learning, TÜRKİYE

Assist. Prof. Dr. Serdar KARGIN, İstanbul Arel University, Department of Biomedical Engineering, Communications Engineering, TÜRKİYE

Assist. Prof. Dr. Sevtap TIRINK, Iğdır University, Environmental Health Program, Environmental Sciences and Engineering, TÜRKİYE

Assist. Prof. Dr. Talha Enes GÜMÜŞ, Sakarya University, Department of Electrical and Electronics Engineering, Power Plants, TÜRKİYE

Assist. Prof. Dr. Tuğçe GÖVER, Selçuk University, Department of Pharmacy, Analytical Chemistry, TÜRKİYE

Assist. Prof. Dr. Veli BAYSAL, Bartın University, Department of Computer Engineering, Computational Physiology, TÜRKİYE

Assist. Prof. Dr. Yaşar Barış DOLUKAN, OSTİM Technical University, Biomedical Device Technology Program, Biomedical Sciences and Technology, TÜRKİYE

Assist. Prof. Dr. Yeliz KARACA, University of Massachusetts Chan Medical School, Machine Learning, USA

Dr. Abdulhamit SEVGİ, OSTİM Technical University, Department of Mechatronics, Control Theory and Applications, TÜRKİYE

Dr. Ebru ERGÜNEŞ BERKİN, Hassa District Directorate of Agriculture, Biometry, TÜRKİYE

Dr. Ehsan SHEYDAEE, University of Tehran, Department of Biosystem Engineering, Agricultural Structures, IRAN

Dr. Kenan ERİN, Tarsus University, Department of Machine Engineering, Industrial Automation, TÜRKİYE

Dr. Mehmet Emin VURAL, GAP International Agricultural Research and Training Center Directorate, Sheep and Goat Breeding and Treatment, TÜRKİYE

Dr. Muhammet KAPTAN, Zonguldak Bülent Ecevit University, Department of Food Processing, Sheep and Goat Breeding and Treatment, TÜRKİYE

Dr. Mutlu BULUT, Incirlik Air Base Meteorology Directorate, Agricultural Land Management, TÜRKİYE

Dr. Nurdoğan CEYLAN, Adıyaman University, Department of Machine Engineering, Industrial Automation, TÜRKİYE

Dr. Okan GÜNGÖR, Bayburt University, Department of Electronics and Automation, Electrical-Electronics and Communication Engineering, TÜRKİYE

* The ranking is arranged alphabetically within the academic title

Table of Contents

Research Articles

1. **RESPIRATORY ANALYSIS WITH ELECTROCARDIOGRAM DATA: EVALUATION OF PANTOMPKINS ALGORITHM AND CUBIC CURVE INTERPOLATION METHOD**
Mert Süleyman DEMİRSOY, Ayşe Nur AY GÜL..... 374-383
2. **EFFECT OF SOLAR COLLECTOR GEOMETRY ON DRYING TIME AND NUTRITIONAL PROPERTIES OF LEVANT QUALITY HAZELNUTS**
Mithat AKGÜN, Cemalettin AYGÜN, Mehmet AKGÜN, Emre TURAN.....384-391
3. **TÜRKİYE ÖLÇEĞİNDE KARAYOLU YOL- BAKIM MALİYETLERİ VE GELECEK TAHMİNİ**
Fatma Pınar GÖKSAL.....392-400
4. **UTILIZATION OF SLIP CASTING PROCESS FOR RECYCLING CAD/CAM DENTAL ZIRCONIA WASTES**
Cemile Betül EMRULLAHOĞLU ABİ, Hatice Şule ÇOBAN TETİK, Erdiñç ABİ.....401-408
5. **INVESTIGATION OF LINEAR AND NONLINEAR BEHAVIOUR OF REINFORCED CONCRETE COLUMN EXPOSED TO CORROSION EFFECT FOR DIFFERENT DAMAGE LIMIT LEVELS**
Halit Erdem ÇOLAKOĞLU, Muhammed ÖZTEMEL.....409-422
6. **İÇ LOJİSTİK FAALİYETLERİNDE YALIN TEKNİKLERİN KULLANILMASI VE BİR UYGULAMA**
Ayşe UÇAR, Betül TURANOĞLU ŞİRİN.....423-435
7. **ROBOTIC ARM TRAJECTORY TRACKING USING IMAGE PROCESSING AND KINEMATIC EQUATIONS**
Yusuf Hamida EL NASER, Durmuş KARAYEL, Mert Süleyman DEMİRSOY, Muhammed Salih SARIKAYA, Nur Yasin PEKER.....436-444
8. **USAGE OF WEKA SOFTWARE BASED ON MACHINE LEARNING ALGORITHMS FOR PREDICTION OF LIVER FIBROSIS/CIRRHOSIS**
Rukiye UZUN ARSLAN, Ziyet PAMUK, Ceren KAYA.....445-456
9. **A GAME-THEORETICAL INTEGRATED APPROACH FOR SUSTAINABLE PORTFOLIO SELECTION: AN APPLICATION ON BIST PARTICIPATION SUSTAINABILITY INDEX STOCKS**
Furkan GÖKTAŞ.....457-464
10. **MODELING CLIMATE CHANGE SCENARIOS FOR SPRING BARLEY IN SOUTHEAST OF ALMATY IN KAZAKHSTAN USING THE LINTUL APPROACH**
Aidana SABITOVA, Gulnur SULEIMANOVA, Tefide KIZILDENİZ, Ali Kaan YETİK.....465-472
11. **İVESİ KUZULARINDA BÜYÜME ÖZELLİKLERİ İÇİN PRATİK BİR DAMIZLIK SEÇME YÖNTEMİ: KOLAY İNDEKS UYARLAMASI**
Yusuf KAPLAN, İrfan GÜNGÖR, Kürşat ALKOYAK, Mustafa TEKERLİ.....473-477
12. **SUSTAINABLE AIRPORT MANAGEMENT AND AIRLINE MARKETING**
Sevgi AYDIN.....478-487
13. **THE IMPACT OF DEVICE TYPE NUMBER ON IOT DEVICE CLASSIFICATION**
Ahmet Emre ERGÜN, Özgü CAN.....488-494

14. BIODIVERSITY OF Actinobacteria FROM KULA GEOPARK IN TÜRKİYE	
<i>Betül BAYRAKTAR, Kamil ISIK.....</i>	<i>495-508</i>
15. GEBELİKTE ANNE SAĞLIĞI RİSK GRUPLARININ TAHMİNİNE YÖNELİK MAKİNE ÖĞRENMESİ TABANLI BİR KARAR DESTEK SİSTEM TASARIMI	
<i>İrem ŞENYER YAPICI, Rukiye UZUN ARSLAN.....</i>	<i>509-520</i>
16. ADSORPTION OF THE ANTIBIOTIC ROXITHROMYCIN ON LOW-COST FOOD WASTE MATERIALS: BATCH AND COLUMN STUDIES	
<i>İlknur TOSUN SATIR, Bediha AKMEŞE.....</i>	<i>521-528</i>
17. HANÖNÜ (KASTAMONU) GÜNEŞ ENERJİSİ SANTRALİNİN FARKLI SİMÜLASYON PROGRAMLARI İLE TASARIMI VE ELEKTRİK ENERJİSİ ÜRETİM SONUÇLARININ DEĞERLENDİRİLMESİ	
<i>Sefa KIRNAPCI, Nihat PAMUK.....</i>	<i>529-538</i>
18. ELECTROCHEMICAL HYDROGEN PEROXIDE GENERATION AND REMOVAL OF MOXIFLOXACIN BY ELECTRO-FENTON PROCESS	
<i>Gökçe Didar DEĞERMENCİ, Nejdet DEĞERMENCİ.....</i>	<i>539-546</i>
19. NATURE INSPIRED PRACTICES IN SUPER TALL BUILDING DESIGNS: SIMILARITIES OF FORM	
<i>Aslı YILDIZ, Güneş Mutlu AVINÇ.....</i>	<i>547-559</i>
20. FLUOKSETİN VE NORFLUOKSETİNİN SENTEZİ ÜZERİNE ÇALIŞMALAR VE ANTİOKSİDANT ÖZELLİĞİNİN ARAŞTIRILMASI	
<i>Nesimi ULUDAĞ.....</i>	<i>560-565</i>
21. EVALUATION OF AGING EFFECTS OF ZINC OXIDE ON THE OPTICAL PROPERTIES OF POROUS SILICON-ZINC OXIDE HETEROJUNCTION PHOTODETECTOR DEVICE	
<i>Safiye KARAÇAM, Meltem GÖR BÖLEN.....</i>	<i>566-574</i>
22. PROTEİN KAYNAKLARININ İN VİTRO OLGUNLAŞTIRILMIŞ SIĞIR OOSİTLERİNİN GLUTATYON PEROKSİDAZ ENZİM AKTİVİTESİ ÜZERİNE ETKİSİ	
<i>Nisa Nur YILMAZ.....</i>	<i>575-579</i>
23. FORECASTING ROAD FREIGHT AND PASSENGER TRANSPORT DEMANDS IN TURKEY USING THE EXPONENTIAL SMOOTHING	
<i>Hümeyra BOLAKAR TOSUN.....</i>	<i>580-586</i>
24. A COMPACT GAN POWER AMPLIFIER MODULE FOR NEW GENERATION CELLULAR BASESTATIONS	
<i>Burak Berk TÜRK, Furkan HÜRÇAN, Hüseyin Şerif SAVCI, Hakan DOĞAN.....</i>	<i>587-593</i>
25. MEETING THE ENERGY NEEDS OF POULTRY HOUSES WITH WIND TURBINE SYSTEM UNDER TEKİRDAĞ CONDITIONS AND ITS ENVIRONMENTAL EFFECTS	
<i>Elif TÜRKBOYLARI, Ahmet Nedim YÜKSEL.....</i>	<i>594-600</i>
26. ELEKTRİKLİ ARAÇ DEVRESİNDE KULLANILAN BOOST DÖNÜŞTÜRÜCÜNÜN ANALİZİNE FARKLI YAKLAŞIMLAR	
<i>Ayşe Tuğba YAPICI, Nurettin ABUT, Ali Bekir YILDIZ.....</i>	<i>601-609</i>



RESPIRATORY ANALYSIS WITH ELECTROCARDIOGRAM DATA: EVALUATION OF PAN-TOMPKINS ALGORITHM AND CUBIC CURVE INTERPOLATION METHOD

Mert Süleyman DEMİRSOY^{1*}, Ayşe Nur AY GÜL²

¹Sakarya University of Applied Sciences, Faculty of Technology, Department of Mechatronics Engineering, 54050, Sakarya, Türkiye


²Sakarya University of Applied Sciences, Biomedical Technologies Application and Research Center, 54050, Sakarya, Türkiye


Abstract: Advancements in bioinstrumentation have facilitated the easier monitoring of biometric signals such as electrocardiogram (ECG) and respiration. This development is particularly crucial for the diagnosis and management of various conditions like stress and sleep disorders. Two commonly used features in heart rate variability (HRV) analysis derived from ECG data are standard deviation and serial correlation coefficients of R-R intervals (the time durations between heartbeats). The former utilizes the fundamental components of QRS complexes, while the latter is designed to extract relationships between respiration and heart rate. In the proposed methodology, R-R wave detection is performed on processed ECG data using the Pan-Tompkins algorithm, and the respiration duration for each R-R interval from respiration data is selected. Additionally, missing respiration data for selected R-R intervals is interpolated based on the interpolation method. The results of this study are compared with the standard interpolation and cubic spline interpolation models to assess the effectiveness of the proposed method and its ability to capture temporal fluctuations. Since standard interpolation fails to accurately detect respiration data from R-R intervals and cannot precisely handle missing R-R intervals in short samples, cubic spline interpolation is recommended as a replacement and its results are presented. The obtained results provide insights into the effectiveness and application of the Pan-Tompkins algorithm, FFT (Fast fourier transform) implementation, and cubic spline interpolation in the selection of respiration and R-wave features. According to the findings of the study, in the analysis conducted on 2-second samples with a 1000 Hz sampling frequency created from each participant's respiratory data set, missing respiratory data were successfully reconstructed from the R-R intervals of the ECG data using standard and cubic curve interpolation methods. Upon examination of RMSE (Root mean square error) values, it was observed that for 30% of the participants, as RMSE values increased, completion counts for standard interpolation increased, while completion counts for cubic curve interpolation decreased. Conversely, when RMSE values decreased, 60% of the participants showed a decrease in completion counts for standard interpolation and an increase in completion counts for cubic curve interpolation. A 10% participant group was identified where there was no apparent relationship between RMSE values and interpolation method. This indicates that in 90% of the participants, there is a linear relationship between the study's interpolation method, RMSE values, and completion counts for missing R-R intervals.

Keywords: Electrocardiogram, Respiration, Pan-Tompkins algorithm, Curve interpolation

*Corresponding author: Sakarya University of Applied Sciences, Faculty of Technology, Department of Mechatronics Engineering, 54050, Sakarya, Türkiye

E mail: mertdemirsoy@subu.edu.tr (M. S. DEMİRSOY)

Mert Süleyman DEMİRSOY  <https://orcid.org/0000-0002-7905-2254>

Ayşe Nur AY GÜL  <https://orcid.org/0000-0002-4448-4858>

Received: January 12, 2024

Accepted: February 26, 2024

Published: May 15, 2024

Cite as: Demirsoy MS, Ay Gül AN. 2024. Respiratory analysis with electrocardiogram data: evaluation of Pan-Tompkins algorithm and cubic curve interpolation method. BSJ Eng Sci, 7(3): 374-383.

1. Introduction

Electrocardiogram (ECG) is a graphical representation of electrical waves generated during a process, providing crucial information about the cardiac cycle (Kohler et al., 2002; Luz et al., 2016). Cardiologists utilize ECG to diagnose and monitor heart diseases, including conditions such as arrhythmia detection (Ye et al., 2010; Apandi et al., 2018; Marinho et al., 2019). A normal rhythmic ECG signal includes P-waves, QRS complexes, and T-waves. QRS complexes and R-peaks play a significant role in automated ECG analyses, forming the basis for many algorithms (Harikumar and Shivappriya, 2011; Benosman et al., 2017). By identifying QRS complexes and R-peaks, other waves and features in the ECG can be detected (Kohler et al., 2002). The

measurement of biological information such as electrocardiogram (ECG) and respiration has become possible in recent times using devices like wearable sensors and cameras (Rahman et al., 2016; Dias and Paulo Silva Cunha, 2018). Advanced technologies in bioinstrumentation enable the monitoring of physical and psychological conditions in daily life. For instance, it is employed to monitor the elderly based on heart rate (Shin et al., 2012), assess parasympathetic activity using high-frequency components of R-R intervals (the durations between heartbeats) (Hayano and Yuda, 2019), and measure sleep stages using heart rate and respiration (Suzuki et al., 2009). The reliability of vital data obtained from devices is crucial for accurate monitoring. When a portion of vital data is lost due to



external factors such as noise, the reliability of indices calculated from vital data will be low.

For example, R-R intervals are commonly used in the calculation of various indices like heart rate. However, movements of the body causing electrode displacement or potential fluctuations caused by artifacts can lead to incorrect measurements of the R-wave. Since missing vital data results in missing R-R intervals, the reliability of indices based on R-R intervals will be low. To fill in missing data or predict values in a specific range of the dataset, linear interpolation and curve interpolation (Choi and Shin, 2018) methods are used. Standard and cubic spline interpolation are two commonly used methods for this purpose. These two methods are employed to predict missing or specific interval data. Cubic spline interpolation generally provides smoother and more accurate results due to the use of a higher-degree polynomial. However, depending on the nature of the data and the characteristics of the dataset, standard interpolation can be sufficient in some cases. However, the longer the missing segment, the greater the deviation between the calculated R-R intervals and the actual R-R intervals. For example, frequencies calculated from interpolated R-R intervals will also be incorrect. Therefore, to interpolate missing R-R intervals accurately, it is necessary to consider heart rate variability (HRV) during the missing period to complete missing R-R intervals. In this study, a dataset was used where 20 healthy and drug-free participants (age ranging from 18 to 28; 9 males and 11 females) were subjected to tasks requiring arithmetic or attention.

This article proposes a method for completing missing RR intervals based on the respiratory duration using the Pan-Tompkins algorithm applied to ECG data in states of mental activity and calmness. Along with this method, cubic spline interpolation also helps complete missing R-R intervals and prevents temporal fluctuations occurring in R-R intervals. As R-R intervals are biometric data, they are influenced by the individual and measurement conditions. Therefore, the proposed method selects respiratory features according to the measured data.

1.1. Studies Related to the Data Set

The dataset known as 'PsPM-CogSF,' created by Bach and Staib (2015), comprises measurements of respiration and electrocardiogram (ECG) during mental arithmetic tasks and resting periods. These measurements are used to investigate physiological responses associated with cognitive processes and relaxation states. The matching pursuit algorithm has provided a fast and effective method for extracting tonic sympathetic arousal from spontaneous skin conductance fluctuations. This algorithm has offered a significant alternative for assessing autonomous responses during cognitive tasks and resting periods. Similarly, dynamic causal modeling (DCM) has been employed to predict tonic sympathetic arousal arising from spontaneous skin conductance fluctuations. This methodology, utilizing data obtained from skin conductance fluctuations, has shed light on the

physiological relationships between sympathetic arousal and emotional states, contributing to the understanding of cognitive-emotional processes (Bach and Staib, 2015). The 'PsPM-CogSF' dataset has played a crucial role in developing psychophysiological models for evaluating fear learning and sympathetic activity. These models have provided valuable insights into the relationship between autonomic arousal and cognitive-emotional phenomena, deepening the understanding of fear memory and sympathetic responses. This dataset, utilized by Jelsma and others as well as Cheadle and others to investigate the relationship between sympathetic arousal and experiences of racial discrimination and psychological characteristics, has explored the dynamics of the sympathetic nervous system arousal by examining responses to real-life experiences and psychological features based on physiological measurements in the dataset (Cheadle et al., 2020; Jelsma et al., 2021). Finally, a study titled "Marked Point Process Filtering Approach for Tracking Sympathetic Arousal from Skin Conductance" by Wickramasuriya and Faghih (2020) has been presented. In summary, the 'PsPM-CogSF' dataset has contributed significantly to research on sympathetic arousal, fear learning, and psychophysiological models. The use of matching pursuit algorithms, dynamic causal modeling, and psychophysiological models has enhanced the understanding of autonomic responses during cognitive tasks, emotional experiences, and real-life stress factors.

2. Materials and Methods

2.1. Completing Missing RRs

The goal was to fill in the missing R-R intervals in the dataset using standard and cubic spline interpolation methods, aiming to complete the missing data and address the gaps. Figure 1 illustrates how R-R intervals can be obtained from the ECG. Initially, a high-amplitude R-wave is extracted from the ECG.

Subsequently, each RR is calculated from the interval between one R wave and the next R wave. However, when there are artifacts in the ECG and R waves are not accurately detected, the R-R intervals will be abnormal. Consequently, data in that region will be lost. The literature suggests various approaches to overcome this problem: improving the accuracy of R-wave detection, identifying abnormal values in R-R intervals, and completing missing R-R intervals. Several methods have been proposed to enhance the accuracy of R-wave detection, such as noise reduction techniques that decrease the impact of noise and enhance the accuracy of R-wave detection (Akshay et al., 2010; Sahoo et al., 2015). Additionally, there is a method using neural networks for R-wave detection (Vijaya et al., 1998). The main method for removing outliers is to decide whether R-R intervals are within the normal range. For example, reliability is determined based on whether R-R intervals are between 250 ms and 1500 ms (Izumi et al., 2015). Linear or second-degree/cubic function-based curve

interpolation has been utilized to predict missing R-R intervals (Choi and Shin, 2018). As curve interpolation requires minimal computation, it can be easily applied even in wearable devices. However, as mentioned above, the deviation between real and calculated R-R intervals grows as the duration of data loss increases. To address this issue, methods to complete heart rate using blood pressure and blood flow have been suggested (Li and Clifford, 2008; Borges and Brusamarello, 2016). Respiration has been identified as one of the key factors in increasing heart rate variability (HRV) (Berntson et al., 1993). Moreover, respiration is known to cause changes in heart rate through respiratory sinus arrhythmia (Berntson et al., 1993). Similarly, heart rate can fluctuate with changes in both deep breathing and respiratory rate (Sroufe, 1971; Chang et al., 2013). For instance, when both respiration and R-R intervals are measured simultaneously, both can be recorded as missing. However, while R-R intervals fluctuate between 250 ms and 1500 ms per beat (Izumi et al., 2015), respiratory

changes can range from 3000 ms to 5000 ms per breath (Berntson et al., 1993). Thus, respiration is expected to be useful in completing missing R-R intervals, and changes can be more easily observed than in ECG signals. It is known that heart rate variability (HRV) varies depending on the depth of respiration (Sroufe, 1971). HRV deepens during deep breathing (Sroufe, 1971). Therefore, in this study, respiration depth is utilized. Additionally, changes in respiratory rate will also create variability in heart rate (Chang et al., 2013). Moreover, HRV is high during slow breathing and low during fast breathing. Therefore, in our approach, respiration duration is used. Figure 2 illustrates the representation of respiration durations in the data set at a sampling frequency of 1000 Hz, showing the data numbers in the periods of mental activity and resting states (data between 0-1400 representing the resting state, and data between 1400-2800 representing the mental activity state).

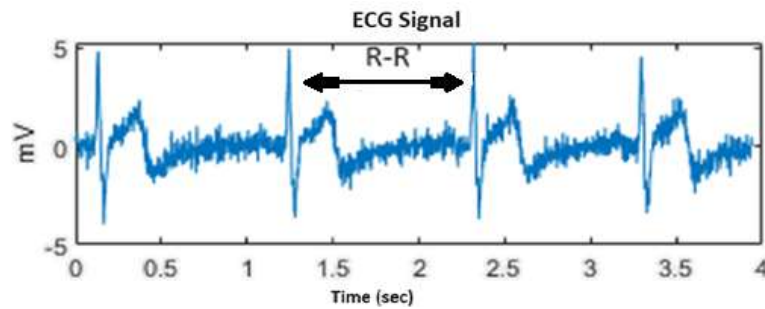


Figure 1. R-R intervals.

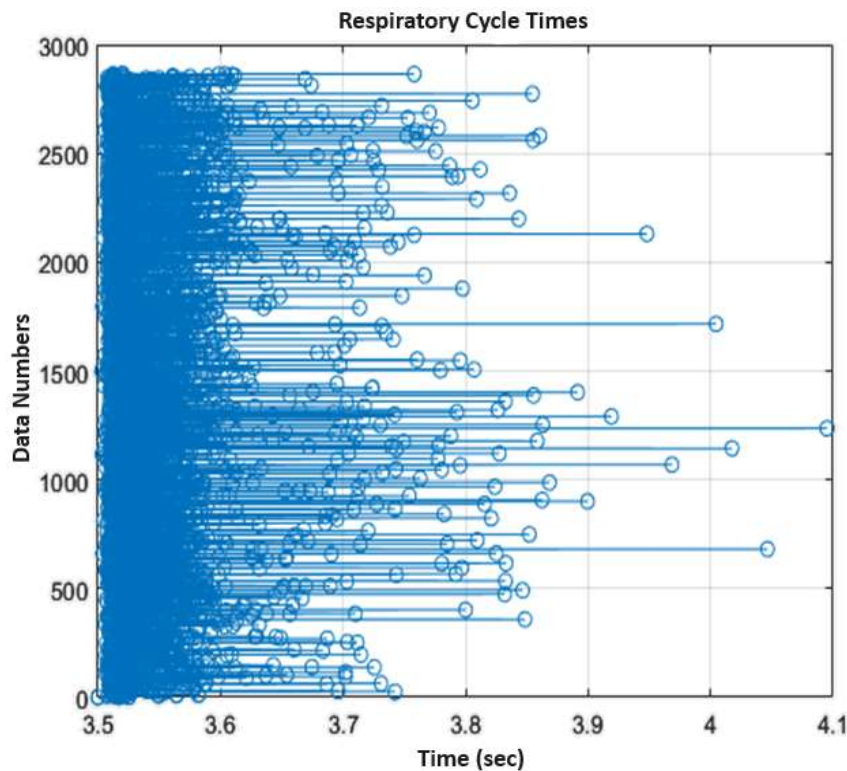


Figure 2. Respiratory time graph during mental activity and rest (x-axis represents time, y-axis represents the number of data).

As shown in Figure 2, signal processing on the FFT model reveals that the average respiration duration during rest is 3.87 seconds at 50 Hz, whereas during mental activity, the average respiration duration is 3.69 seconds. From this, it can be inferred that the heart rate variability (HRV) during rest, indicating the change in heart rate, will be more profound. This implies that RR waves can be more easily detected during rest.

2.2. Preprocessing

Vital signs such as heart rate are known to be significantly influenced by individual characteristics such as gender (Ryan et al., 1994; Chester and Rudolph, 2011). If missing R-R intervals are completed using the same method for everyone, the accuracy of the completed R-R intervals will be debated. This difference also affects the nerves. R-R intervals vary on sympathetic and parasympathetic nerves. When the sympathetic nerves are active, the heart rate variability (HRV) is low. On the other hand, when the parasympathetic nerves are active, the HRV is high. Therefore, reflecting the tendency of the autonomic nervous system during periods of missing R-R intervals is important. The proposed method processes time series data using fast fourier transformation (FFT). Figure 3 illustrates the workflow of the proposed method.

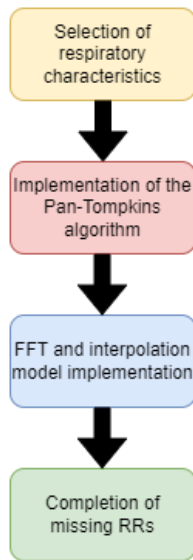


Figure 3. Method flow chart.

Initially, the raw ECG data were processed using a low-pass filter with a cutoff frequency of 100 Hz and a filter order of 3. Subsequently, a high-pass filter with a cutoff frequency of 10 Hz and a filter order of 3 was applied to remove unwanted low-frequency components. Additionally, 50 Hz power line noise was eliminated using a notch filter (Ay et al., 2017). Following these steps, the Pan-Tompkins algorithm was implemented to detect R waves. This algorithm was utilized by testing threshold values separately for each subject's data. Subsequently, the interval wave between Rs and the next R wave was calculated, and RR tachograms were generated. Finally, the graph illustrating the variation of R-R intervals over time was resampled at 30 Hz. To

address potential high-frequency electrical noise in the raw respiratory data, a median filter (window size of 0.15 seconds) was applied for smoothing (Ay et al., 2017). Furthermore, the relationship between respiratory features and HRVs was observed by applying FFT after the median filter to calculate respiratory durations. Figure 4 illustrates the preprocessing steps for the ECG data.

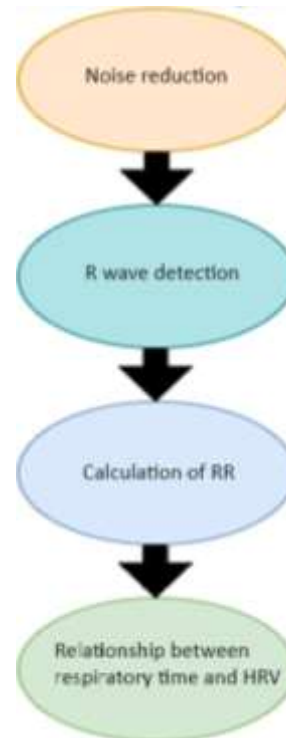


Figure 4. Signal preprocessing steps.

Heart Rate Variability (HRV) analysis is a non-invasive measurement that reflects the autonomic nervous system's regulation of heart rate, extensively utilized in the medical field for evaluating stress, sleep quality, and various cardiovascular conditions. This analysis involves a sequence of signal processing steps for the accurate detection and analysis of R-R intervals, which are the time intervals between consecutive R-waves in an electrocardiogram (ECG) signal. These steps encompass noise reduction, R-wave detection, calculation of R-R intervals, and elucidation of the relationship between respiratory time and HRV. Noise Reduction is the initial step in processing ECG signals for HRV analysis, addressing the contamination of signals with various types of noise (Ay and Yildiz, 2021; Ay and Yildiz, 2023). This phase is crucial for accurate R-wave detection. Techniques such as band-pass filtering and more advanced methods like wavelet transform are employed for effective noise suppression without distorting the ECG signal. R-Wave Detection follows noise reduction and is pivotal for calculating R-R intervals. The Pan-Tompkins algorithm is a popular method in this context, involving filtering, differentiation, squaring, and integration of the ECG signal to emphasize the R-wave feature. Calculation of R-R Intervals is conducted upon

accurate R-wave detection. This process measures the time between successive R-wave peaks, typically in milliseconds, and analyzes the variability within these intervals to assess HRV. The relationship between respiratory time and HRV is the final step in the signal processing for HRV analysis. Respiration affects heart rate through respiratory sinus arrhythmia (RSA), significantly impacting HRV measurements. To analyze this relationship, the respiratory signal can be extracted from the ECG signal itself or through other sensors measuring thoracic expansion, with techniques like spectral analysis or time-frequency analysis used to quantify the influence of respiration on HRV. In summary, the signal processing steps involved in HRV analysis, from noise reduction and R-wave detection to the calculation of R-R intervals and understanding the respiratory influence on HRV, are complex but crucial for an accurate and reliable assessment of heart rate variability. These processes enable clinicians and researchers to better comprehend the autonomic regulation of heart rate and its implications for health and disease.

2.3. Development Methods

The accuracy of completing incomplete R-Rs was evaluated using the following methods.

2.3.1. Correlation coefficients

HRV (Heart Rate Variability), is a measure of the variability in heart rate and is typically calculated based on the R-R intervals (time intervals between heartbeats). The changes in the time series of R-R intervals are used to assess HRV. The relationship between HRV and respiration is often examined through the correlation coefficient between respiration and HRV. The correlation coefficient is a statistical measure used to quantify the relationship between two variables. The Pearson Correlation Coefficient is commonly employed to calculate the correlation coefficient on R-R intervals and respiratory data in ECG recordings, and its formula is presented in Equation 1.

$$r = \frac{\sum_{i=1}^n (x_i - \bar{x})(y_i - \bar{y})}{\sqrt{\sum_{i=1}^n (x_i - \bar{x})^2 \sum_{i=1}^n (y_i - \bar{y})^2}} \quad (1)$$

Equation 1 represents the number of samples, n. Here, x_i and y_i denote each sample in the R-R intervals and respiratory data, respectively. Additionally, \bar{x} , \bar{y} represent the means of R-R intervals and respiratory data. The correlation coefficient takes values between -1 and +1. A positive (+1) correlation indicates a direct linear relationship between the two variables, while a negative (-1) correlation signifies an inverse relationship. A value of 0 indicates no apparent relationship.

The obtained correlation coefficient in this manner represents the connection between R-R intervals and respiratory data. A positive correlation suggests a linear relationship between respiration and HRV, while a negative correlation indicates an inverse relationship. A value close to 0 indicates a lack of a significant relationship between the two datasets. In the utilized

dataset (comprising a total of 20 subjects), positive correlations were observed for all but 3 subjects. Subjects 1 and 2 exhibited a negative correlation, while subject 3 showed a correlation coefficient of 0, indicating no discernible relationship between the two variables.

2.3.2. Root Mean Square Error (RMSE)

Root Mean Square Error (RMSE) is a measure of the difference between actual and predicted values, commonly employed to assess the performance of a predictive model. It allows evaluating prediction errors on HRV and R-R intervals in ECG and respiratory data. Denoting the predicted values for HRV and R-R intervals as \hat{y} and the actual values as y_i , the RMSE formula is expressed in Equation 2.

$$RMSE = \sqrt{\frac{\sum_{i=1}^n (y_i - \hat{y}_i)^2}{n}} \quad (2)$$

For instance, using this formula for the actual and predicted values of R-R intervals, we can assess the predictive capability of your model. The lower the RMSE value, the higher the predictive power of your model. This evaluation is commonly preferred as a method to measure the prediction performance on R-R intervals or HRV. A lower RMSE value indicates that the model makes predictions closer to the actual data. In our dataset, the RMSE values were measured at a level considered low for 14 subjects and at a level considered high for 6 subjects. This suggests that obtaining more accurate results in completing missing R-R intervals can be achieved by using the data of the 14 subjects, resulting in a lower RMSE.

2.3.3 Pan-Tompkins Algorithm

The Pan-Tompkins algorithm is an algorithm used for QRS detection and is commonly employed to identify R-peaks in ECG signals. This algorithm is designed to define R-peaks in QRS complexes by utilizing the width, slope, and amplitude of an integrated window. The algorithm typically consists of two stages: preprocessing and decision stages. In the preprocessing stage, the raw ECG signal is prepared before entering the QRS detection process. This stage involves reducing noise, organizing the signal, and enhancing the visibility of QRS complexes. It is performed to diminish unwanted noise in the signal and make QRS complexes more easily detectable. In the decision stage, only significant peak points in the signal are considered using a specific threshold, while noise peak points are ignored. This step is taken to identify crucial points in the signal to clearly determine R-peaks.

The Pan-Tompkins algorithm, employing these stages, identifies R-peaks in QRS complexes and is widely used for real-time ECG analysis. Thus, it enables the rapid and reliable detection of prominent points of heartbeats in the ECG signal. In this article, the missing data in respiratory signals will be completed using the curve interpolation method based on the R-peaks detected with the Pan-Tompkins algorithm. As the R-R intervals are identified in the ECG data with the Pan-Tompkins algorithm, the respiratory signals containing missing R-R

intervals will be identified through cubic interpolation. Figure 5 illustrates the block diagram of the Pan-Tompkins algorithm.

The detection graph of the R peaks of the filtered ECG signal, where the Pan-Tompkins algorithm was applied and whose threshold value was selected as 60% of the maximum signal amplitude (Hamida El Naser and Naser, 2023), is shown in Figure 6.

2.3.4. Interpolation method

Curve interpolation is a method used to fit a smooth curve or polynomial to a dataset. In the analysis of HRV and R-R intervals in ECG and respiratory data, curve interpolation is employed to complete missing data or

represent the dataset more smoothly. Curve interpolation utilizes polynomials to create a smooth curve between data points. This process allows the data to be combined with a smooth curve and aids in the completion of missing or corrupted data. Cubic curves (third-degree polynomials) are commonly used for curve interpolation (Hao et al., 2021). For both data signals (ECG and respiration), cubic curves using these polynomials are applied at each data point to create a smooth curve. The output of the original and cubic curve interpolation applied signals for ECG and respiration data is illustrated in Figure 7.

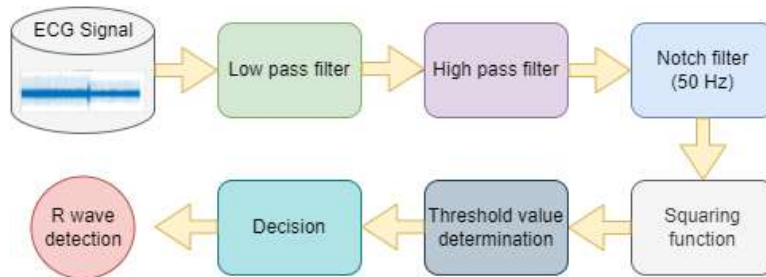


Figure 5. Pan-Tompkins algorithm block diagram.

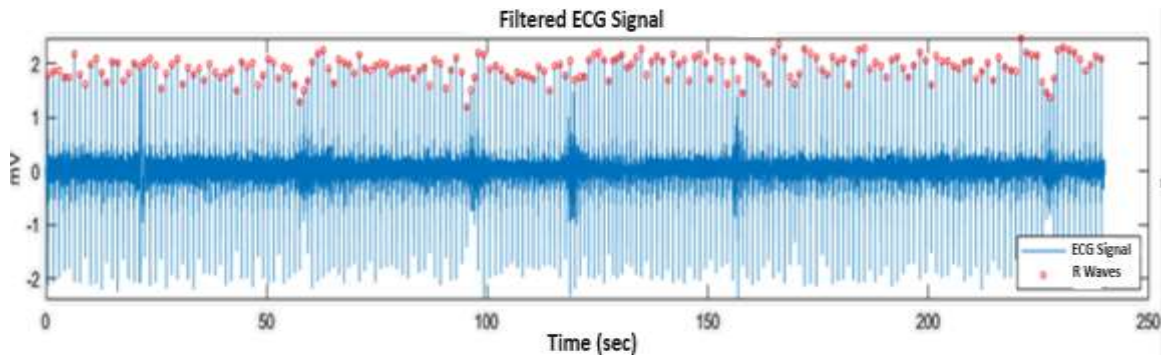


Figure 6. R-peaks with Pan-Tompkins algorithm applied.

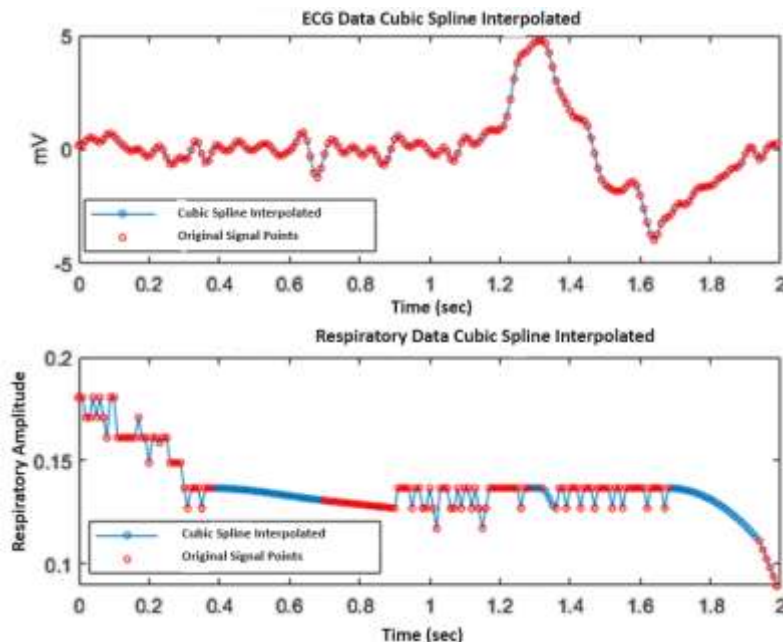


Figure 7. Cubic curve interpolation application in ECG and respiratory data.

In Figure 7, it can be observed that there is no loss in the original ECG data, and when cubic curve interpolation is applied, the values are identical to the original signal. However, in the respiratory data, deviations are present in the original signal, and these discrepancies are detected and mitigated by applying cubic curve interpolation using R-R intervals from the ECG data.

Standard interpolation (first-degree polynomials) applied to both data signals (ECG and Respiration) is illustrated in Figure 8, showing the output of the applied signals.

As depicted in Figure 8, it accurately predicts the ECG data similar to cubic curve interpolation, identifying the

real data as it is. However, it is observed that it falls short in detecting the lost respiratory data for the test from the respiratory dataset by relying on R-R intervals in the ECG data. It failed to identify and apply 10 missing respiratory data points between 0.4 and 0.8 seconds in the original data.

3. Results and Discussion

After applying the proposed methods to the ECG and respiratory data in the dataset, the R-peak counts and associated average respiratory durations of the subjects were calculated, and they are presented in Table 1.

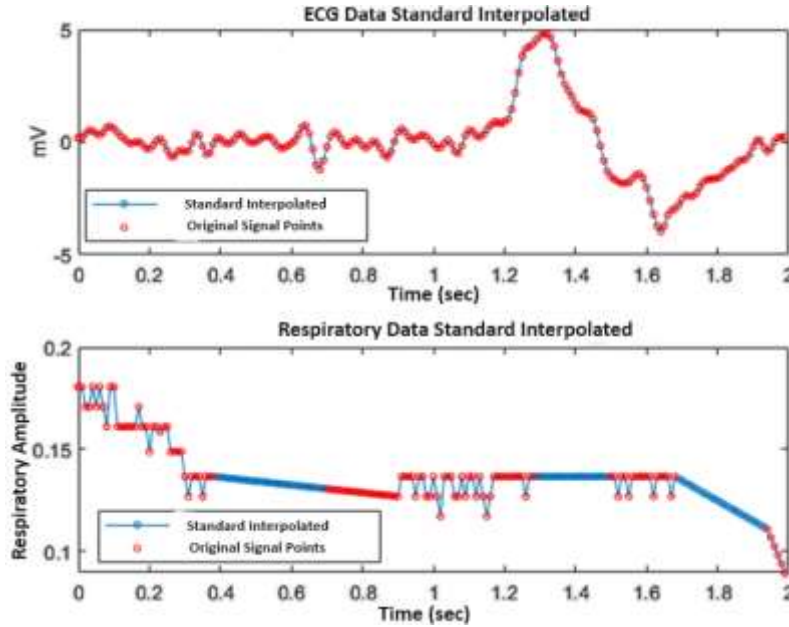


Figure 8. Application of standard interpolation in ECG and respiratory data.

Table 1. R peak numbers and corresponding average breathing times in mental activity and calm states of the subjects in the data set

Subject Order	Number of R peaks between 0-2 min	Number of R peaks between 2-4 min	Average Respiratory Time (sec)
1	135	130	3.32
2	161	165	3.11
3	141	140	3.20
4	231	178	2.05
5	246	201	1.84
6	168	125	2.83
7	251	177	1.92
8	250	145	2.01
9	176	140	2.66
10	235	171	2.03
11	191	165	2.41
12	221	184	1.98
13	165	141	2.71
14	201	179	2.34
15	198	181	2.22
16	155	139	3.04
17	199	146	2.69
18	235	203	1.89
19	181	168	2.45
20	228	184	2.11

In Table 1, it can be observed that the counts of R-peaks during the mental activity state (0-2 minutes) vary compared to the counts during the rest state (2-4 minutes). Generally, R-peak counts tend to be higher during mental activity, while decreasing during the rest state. Most subjects exhibit higher R-peak counts during mental activity, suggesting an increased occurrence of heartbeats. Notably, subjects 4, 5, and 7 demonstrate significantly higher R-peak counts. Overall, a trend of decreased respiratory durations during mental activity compared to the rest state is observed. The increased heart rate is often associated with faster respiratory durations. Additionally, a positive correlation is observed except for subject 3 (subjects 1, 2, and 3). Negative correlation is observed for subjects 1 and 2, while the correlation coefficient for subject 3 is 0, indicating no relationship between respiration and heartbeats for this subject.

In summary, Table 1 highlights the relationship between R-peak counts and respiratory durations during mental activity and rest states. Higher heart rates and shorter respiratory durations are observed during mental activity, whereas lower heart rates and longer respiratory durations are observed during the rest state.

In Table 2, 2-second samples were created from the respiratory data sets for each subject with a sampling frequency of 1000 Hz. An equal number of data points (200 data points for each subject's data set) were randomly removed from the respiratory data sets. Using standard and cubic curve interpolation methods, missing respiratory data were reconstructed from the R-R

intervals of the ECG data. The detected data points and RMSE values for the subjects' ECG data, based on the applied methods, are presented in Table 2.

In Table 2, the data completion counts for standard interpolation are lower compared to cubic curve interpolation. This indicates that standard interpolation completes fewer missing data points and fills in fewer data values. Upon examining the RMSE values, it is observed that standard interpolation sometimes has lower and sometimes higher values compared to cubic curve interpolation. This suggests that both methods can exhibit different performances based on the structure of the data set and the distribution of missing data, emphasizing the need to consider these factors to determine which method yields better results. Additionally, when RMSE values approach the mean value of the ECG signal, it is observed that standard interpolation completes more data. However, in this scenario, cubic curve interpolation has completed fewer data points compared to other RMSE values that can be considered low.

If we look at subjects 15, 1, 6, 9, 11, and 10 in order, as RMSE values increase, the completion counts for standard interpolation also increase, while the completion counts for cubic curve interpolation decrease. Conversely, as RMSE values decrease, the completion counts for standard interpolation decrease, and the completion counts for cubic curve interpolation increase. It can be inferred from Table 2 that there is a linear relationship with RMSE values.

Table 2. Relationship between data completion numbers of standard and cubic spline interpolation methods and RMSE values

Subject Order	Standard interpolation number of data completions	Cubic spline interpolation number of data completions	RMSE values (mV)
1	18	161	1.67
2	37	152	2.11
3	25	112	1.94
4	39	95	2.21
5	30	135	1.63
6	26	154	1.74
7	20	196	1.51
8	32	185	1.96
9	27	126	1.84
10	63	76	2.47
11	41	85	2.39
12	18	169	1.71
13	19	152	1.79
14	55	89	2.51
15	15	133	1.46
16	37	185	2.02
17	29	146	1.91
18	18	105	1.79
19	28	151	2.09
20	16	118	1.61

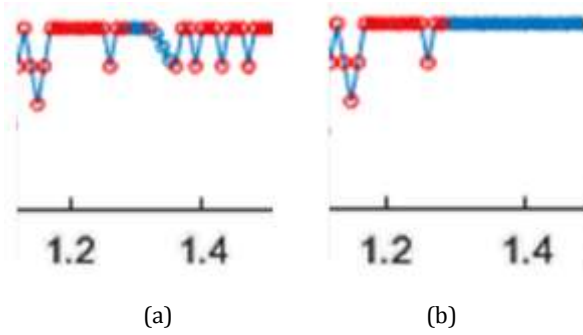


Figure 9. Cubic curve interpolation method (a) Standard interpolation method (b) (Blue line interpolated signal, red circles original respiratory signal points).

For both methods used to complete missing respiration data from R-R intervals, the respiration data has been reduced to the same number and order for both methods. In Figure 9(a), the cubic curve interpolation method shows that between 1.2 and 1.4 seconds, the original signal is actually in a downward triangular shape. However, in Figure 9(b), standard interpolation draws the period between 1.2 and 1.4 seconds as a straight line. Upon closer examination, cubic curve interpolation appears to provide more accurate and precise results in completing missing data.

The method utilizing 3rd-degree cubic curve interpolation, which leverages respiration features, has yielded significantly more accurate results compared to standard (1st-degree) interpolation when compared with the proposed method. These results indicate an increase in the variability of R-R intervals even in the presence of missing R-R intervals during resting conditions. However, in other situations (e.g., mental activity or arithmetic operations), the autonomic nervous system can fluctuate, potentially leading to decreased accuracy. On the other hand, short-term repeated results have shown very little difference between the proposed method and 1st-degree standard interpolation for missing R-R intervals (e.g., Figure 8). One possible explanation for this is the short duration of the periods in Figure 8 and Figure 7. However, it is evident that 1st-degree standard interpolation is not suitable for completing missing data. 1st-degree standard interpolation linearly replaces changing R-R intervals over time, ultimately producing R-R intervals with temporal fluctuations. These results suggest that using 3rd-degree cubic curve interpolation without temporal fluctuations will provide more accurate and precise results in completing missing R-R intervals. In the future, it is planned to assess what kind of temporal fluctuations may occur in missing R-R intervals when the proposed methods are used under different conditions.

4. Conclusion

This study aimed to investigate the relationship between heart rate variability (HRV) and respiration and explore appropriate methods for accurately completing missing

R-R intervals. The results obtained using Pearson correlation coefficient revealed both positive and negative correlations between respiration and HRV under specific conditions. Consequently, the cubic curve interpolation method facilitated the accurate integration of missing R-R intervals in respiration signals. Analyses conducted indicated that 3rd-degree cubic curve interpolation provided more accurate results compared to standard (1st-degree) interpolation and was more effective in completing missing R-R intervals. This allowed for the more precise completion of changing R-R intervals over time. According to the findings of the study, 85% of the participants exhibited higher R-peak counts during mental activity, particularly noticeable in subjects 4, 5, 7, 8, and 10. This indicates an increase in heartbeats. The tendency of decreased respiratory durations during mental activity compared to the rest state was observed, reflecting the common association of increased heart rate with shorter respiratory durations. These findings suggest that respiration features can be utilized to enhance the accuracy of completing R-R intervals and warrant further evaluation under different conditions in future research.

Author Contributions

The percentage of the author(s) contributions is presented below. All authors reviewed and approved the final version of the manuscript.

	M.S.D.	A.N.A.G.
C	70	30
D	80	20
S	50	50
DCP	90	10
DAI	80	20
L	40	60
W	80	20
CR	50	50
SR	50	50

C=Concept, D= design, S= supervision, DCP= data collection and/or processing, DAI= data analysis and/or interpretation, L= literature search, W= writing, CR= critical review, SR= submission and revision.

Conflict of Interest

The author declared that there is no conflict of interest.

Ethical Consideration

Ethics committee approval was not required for this study because of there was no study on animals or humans.

References

Akshay N, Jonnabhotla NAV, Sadam N, Yeddanapudi ND. 2010. ECG noise removal and QRS complex detection using UWT. International Conference on Electronics and Information Engineering, 2: 438.
 Apandi ZFM, Ikeura R, Hayakawa S. 2018. Arrhythmia detection using MIT-BIH dataset: A review. International Conference on

- Computational Approach in Smart Systems Design and Applications ICASSDA, August 15-17, Serawak, Malaysia, pp: 1-5. IEEE.
- Ay AN, Yildiz MZ, Boru B. 2017. Real-time feature extraction of ECG signals using NI LabVIEW. *Sakarya Univ J Sci*, 21(4): 576-583.
- Ay AN, Yildiz MZ. 2021. The effect of attentional focusing strategies on EMG-based classification. *Biomed Eng*, 66(2): 153-158.
- Ay AN, Yildiz MZ. 2023. The performance of an electromyography-based deep neural network classifier for external and internal focus instructions. *Concurr Comput: Pract Exper*, 35(2): e7470.
- Bach DR, Staib M. 2015. A matching pursuit algorithm for inferring tonic sympathetic arousal from spontaneous skin conductance fluctuations. *Psychophysiology*, 52(8): 1106-1112.
- Benosman MM, Bereksi-Reguig F, Salerud, EG. 2017. Strong real-time QRS complex detection. *J Mech Medic Biol*, 17(08): 1750111.
- Berntson GG, Cacioppo JT, Quigley KS. 1993. Respiratory sinus arrhythmia: Autonomic origins, physiological mechanisms, and psychophysiological implications. *Psychophysiology*, 30(2): 183-196.
- Borges G, Brusamarello V. 2016. Sensor fusion methods for reducing false alarms in heart rate monitoring. *J Clin Monit Comput*, 30: 859-867.
- Chang Q, Liu R, Shen Z. 2013. Effects of slow breathing rate on blood pressure and heart rate variabilities. *Int J Cardiol*, 169(1): e6-e8.
- Cheadle JE, Goosby BJ, Jochman JC, Tomaso CC, Kozikowski Yancey CB, Nelson TD. 2020. Race and ethnic variation in college students' allostatic regulation of racism-related stress. *Proc National Acad Sci*, 117(49): 31053-31062.
- Chester JG, Rudolph JL. 2011. Vital signs in older patients: age-related changes. *J American Medic Direct Assoc*, 12(5): 337-343.
- Choi A, Shin H. 2018. Quantitative analysis of the effect of an ectopic beat on the heart rate variability in the resting condition. *Front Physiol*, 9: 922.
- Dias D, Paulo Silva Cunha J. 2018. Wearable health devices-vital sign monitoring, systems and technologies. *Sensors*, 18(8): 2414.
- Hamida El Naser Y, Karayel D. 2023. Modeling the effects of external oscillations on mucus clearance in obstructed airways. *Biomechan Model Mechanobiol*, 2023: 1-14.
- Hao W, Rui D, Song L, Ruixiang Y, Jinhai Z, Juan C. 2021. Data processing method of noise logging based on cubic spline interpolation. *Appl Math Nonlinear Sci*, 6(1): 93-102.
- Harikumar R, Shivappriya SN. 2011. Analysis of QRS detection algorithm for cardiac abnormalities-A review. *Int J Soft Comput Eng*, 1(5): 80-88.
- Hayano J, Yuda E. 2019. Pitfalls of assessment of autonomic function by heart rate variability. *J Physiol Anthropol*, 38(1): 1-8.
- Izumi S, Nakano M, Yamashita K, Nakai Y, Kawaguchi H, Yoshimoto M. 2015. Noise tolerant heart rate extraction algorithm using short-term autocorrelation for wearable healthcare systems. *IEICE Transact Info Syst*, 98(5): 1095-1103.
- Jelsma EB, Goosby BJ, Cheadle JE. 2021. Do trait psychological characteristics moderate sympathetic arousal to racial discrimination exposure in a natural setting?. *Psychophysiology*, 58(4): e13763.
- Kohler BU, Hennig C, Orglmeister R. 2002. The principles of software QRS detection. *IEEE Eng Medic Biol Magazine*, 21(1): 42-57.
- Li Q, Clifford GD. 2008. Suppress false Arrhythmia alarms of ICU monitors using heart rate estimation based on combined arterial blood pressure and ECG analysis. 2nd International Conference on Bioinformatics and Biomedical Engineering, May 16-18, London, UK, pp: 2185-2187.
- Luz EJDS, Schwartz WR, Cámara-Chávez G, Menotti D. 2016. ECG-based heartbeat classification for arrhythmia detection: A survey. *Comput Methods Prog Biomed*, 127: 144-164.
- Marinho LB, de MM Nascimento N, Souza JWM, Gurgel MV, Rebouças Filho PP, de Albuquerque VHC. 2019. A novel electrocardiogram feature extraction approach for cardiac arrhythmia classification. *Future Gener Comput Syst*, 97: 564-577.
- Rahman H, Ahmed MU, Begum, S, Funk P. 2016. Real time heart rate monitoring from facial RGB color video using webcam. 29th Annual Workshop of the Swedish Artificial Intelligence Society (SAIS), June 2-3, Malmö, Sweden, No: 129.
- Ryan SM, Goldberger AL, Pincus SM, Mietus J, Lipsitz LA. 1994. Gender-and age-related differences in heart rate dynamics: are women more complex than men?. *J American College Cardiol*, 24(7): 1700-1707.
- Sahoo SK, Subudhi AK, Kanungo B, Sabut SK. 2015. Feature extraction of ECG signal based on wavelet transform for arrhythmia detection. International Conference on Electrical, Electronics, Signals, Communication and Optimization, January 24-25, Andhrapradesh, India, pp: 24-25.
- Shin DI, Song JH, Joo S.K, Huh SJ. 2012. Hybrid vital sensor of health monitoring system for the elderly. Wireless Mobile Communication and Healthcare: Second International 4-4-ICST Conference, MobiHealth 2011, October 5-7, Kos Island, Greece, pp: 329-334.
- Sroufe LA. 1971. Effects of depth and rate of breathing on heart rate and heart rate variability. *Psychophysiology*, 8(5): 648-655.
- Suzuki T, Ouchi K, Kameyama KI, Takahashi M. 2009. Development of a sleep monitoring system with wearable vital sensor for home use. International Conference on Biomedical Electronics and Devices, January 14-17, Porto, Portugal, pp: 326-331.
- Vijaya G, Kumar V, Verma HK. 1998. ANN-based QRS-complex analysis of ECG. *J Medic Eng Technol*, 22(4): 160-167.
- Wickramasuriya DS, Faghieh RT. 2020. A marked point process filtering approach for tracking sympathetic arousal from skin conductance. *IEEE Access*, 8: 68499-68513.
- Ye C, Coimbra MT, Kumar BV. 2010. Arrhythmia detection and classification using morphological and dynamic features of ECG signals. Annual International Conference of the IEEE Engineering in Medicine and Biology, August 30 - September 4 Buenos Aires, Brazil, pp: 1918-1921.



EFFECT OF SOLAR COLLECTOR GEOMETRY ON DRYING TIME AND NUTRITIONAL PROPERTIES OF LEVANT QUALITY HAZELNUTS

Mithat AKGÜN^{1*}, Cemalettin AYGÜN², Mehmet AKGÜN³, Emre TURAN⁴

¹Ordu University, Institute of Science and Technology, Department of Renewable Energy, 52200, Ordu, Türkiye

²Karadeniz Technical University, Faculty of Marine Sciences, Department of Marine Engineering Operations, 61080, Trabzon, Türkiye

³Giresun University, Hazelnut Specialization Coordinatorship, 28100, Giresun, Türkiye


⁴Ordu University, Institute of Science and Technology, Department of Food Engineering, 52200, Ordu, Türkiye


Abstract: This study examines the impact of drying Levant quality hazelnut samples, including husk and shell, using hot air heated by solar panels at a constant speed of 6 m/s. The study also investigates the impact of collector irradiation absorption surface geometries on hazelnut drying time. A solar collector with four types of air duct geometry was used to dry hazelnuts. The radiation-absorbing surface of the air duct was manufactured flat, and three different trapezoidal geometries (30, 45 and 60 angles) were used. The mass losses of hazelnuts were measured and determined at regular intervals. In addition, the total phenolic content, the DPPH radical scavenging activity, the FRAP, the free fatty acid content, the peroxide value and the moisture content were measured. For the purpose of comparison, some of the products have been dried by means of unheated air at ambient temperature. The pre-drying process (withering process) to separate the hazelnuts from husk, only took 1.5 days (14 h excluding night). In these systems, the shelled fresh hazelnuts, separated from the husk, fell below the equilibrium moisture content of 6% in 2 days (except for 18 h at night). It was found that the most suitable collector geometry for all the parameters studied in the drying of hazelnuts with solar collectors was 45 degrees, and that other geometries could be used in terms of food properties.


Keywords: Drying, Solar collector, Hazelnut traits, Husk


*Corresponding author: Ordu University, Institute of Science and Technology, Department of Renewable Energy, 52200, Ordu, Türkiye

E mail: makgun@odu.edu.tr (M. AKGÜN)

Mithat AKGÜN  <https://orcid.org/0000-0002-5514-1236>

Cemalettin AYGÜN  <https://orcid.org/0000-0002-6033-3558>

Mehmet AKGÜN  <https://orcid.org/0000-0001-5148-5544>

Emre TURAN  <https://orcid.org/0000-0002-4289-0107>

Received: February 06, 2024

Accepted: March 15, 2024

Published: May 15, 2024

Cite as: Akgün M, Aygün C, Akgün M, Turan E. 2024. Effect of solar collector geometry on drying time and nutritional properties of Levant quality hazelnuts. *BSJ Eng Sci*, 7(3): 384-391.

1. Introduction

Hazelnut (*Corylus avellana* L.) is classified as hard-shelled fruits and is cultivated in countries with temperate climates. Türkiye is considered as the homeland of hazelnut because it has been cultivated for many years and is home to the highest quality varieties (Özçağırın et al., 2014). Approximately 68% of the world's hazelnut production is carried out on the Black Sea coast of Türkiye, which is the most suitable area in terms of ecological conditions (TUIK, 2021). In the Black Sea region, hazelnuts are grown up to 60 km inland from the coast and up to 750 m altitude (Köksal, 2002). Of these areas, those between 0-250 m altitudes are called the coastal part, those between 251-500 m altitudes are called the middle part, those at altitudes higher than 500 m are called the high part, and the hazelnut variety grown according to altitude varies (Turan and Islam, 2018). Generally, Tombul, Palaz, Kara, Sivri, Uzunmusa, Çakıldak, and Foşa hazelnut varieties are grown in the region and many varieties are produced together in the same garden, especially in the gardens located in the

coastal area. These varieties differ in terms of physical and chemical fruit characteristics and are named according to their quality. Considering the quality parameters, hazelnuts in Türkiye are classified as Giresun and Levant quality hazelnuts. While Giresun quality refers to Tombul hazelnut, Levant quality refers to the dominant varieties and the mixture of these varieties in the city where cultivation is carried out. In Ordu, where hazelnut production is the highest, Kalınkara, Sivri, Palaz, Uzunmusa, and Çakıldak hazelnuts are called Levant quality (Uzundumlu et al., 2019). Threshing is the process of drying harvested hazelnuts using various methods. Threshing machines are used to sort hazelnuts with high moisture content after withering for 3-5 days. The sorted nuts are typically laid on soil, concrete, or grass and sun-dried for 5-15 days. Harvest in central and upland areas tends to coincide with late summer and mid-autumn, exposing these areas to high rainfall and mist. Rain can make the hazelnuts difficult to harvest and thresh and can also affect the quality of the nuts. During the drying process, hazelnuts can be damaged in terms of quality parameters, depending on



the duration of the process and climatic factors. If hazelnuts are dried in the sun, there is a risk of contamination with pathogens, microbial spoilage, formation of aflatoxins, deterioration of antioxidants and fatty acids, as well as loss of quality and yield (Kontaş, 2022). Hazelnuts contain secondary metabolites with antioxidant properties, such as phenolic acids, flavonoids, water and fat-soluble vitamins and tannins, in addition to the main components of fat, carbohydrates and protein. The harvesting and drying conditions determine the presence of these properties.

A number of techniques have been developed to prevent the hazelnuts from being damaged by the threshing conditions and to dry them quickly and efficiently with a minimum of energy input. Traditional dryers are commonly used for this, with the flow rate, temperature, and humidity of the mass transfer fluid being adjusted to achieve optimum results. Recent advancements in drying systems have led to the increasing popularity of new technologies such as infrared, microwave, heat pump, LED dryers, and hybrid dryers, which combine two or more drying systems (Akgün et al., 2018; Aksüt et al., 2023; Kian-Pour, 2020; Huang et al., 2021; Fenandes et al., 2024).

Drying and storage are required for nuts such as hazelnuts, walnuts, almonds, and peanuts. Sun drying is more challenging for hazelnuts than for other fruits as they are typically grown in rainy and humid regions. As a result, there has been a need for eco-friendly drying systems that preserve fruit quality, minimize energy costs, and are affordable for growers (Danso-Boateng, 2013; Topdemir, 2019). Recently, there has been an increasing focus on drying methods that use energy from solar panels and the design of such systems (Mohana et al., 2020; Memur, 2022).

The aim of using solar energy as a renewable energy source in the drying sector is to increase energy efficiency and minimize damage to the environment. These systems use the sun as the dryer source, resulting in low operating costs (Yıldız and Gökayaz, 2019). Numerous studies have employed solar collectors for drying purposes to enhance energy efficiency and speed. These studies have explored various food types and emphasized the importance of improving collector efficiency (Reddy, 1987; Shariah et al., 2002; Aktaş, 2003; Ceylan et al., 2006; Saleh and Gatea, 2010; Behera et al., 2022; EL-Mesery et al., 2022; Harini et al., 2022).

The drying of Levant hazelnuts harvested in their shells before and after patching is the subject of this experimental study. The effects of air heated by solar collectors at different drying temperatures on the drying times and the characteristics of the nuts are being studied.

2. Materials and Methods

This study focuses on Levant of *Corylus avellana* L, which is extensively cultivated in the Perşembe district of Ordu province, located in the coastal region of the Black Sea in

Türkiye. The initial moisture content of the hazelnuts is between 27.3% and 32.2%, while the initial moisture content of the hazelnut shells is between 72.2% and 77.6%.

The shelled hazelnuts of the Levant have a size of 14-22 mm. The hazelnuts used in this study have not been sized. Hazelnuts were harvested by hand from the branches of plants of Levant quality cultivars. The hazelnut harvest in the coastal area takes place between 5-20 August, during which time the Black Sea coast experiences humidity and rainfall. Hazelnuts have unique characteristics that require them to be sun-dried by laying them on the ground to separate them from their husks. Depending on the climate, the drying time for hazelnuts varies from 3 to 7 days. Hazelnuts are dried in the sun until they reach 6% humidity. This process can take 3-12 days, and unfavorable drying conditions can lead to the formation of aflatoxins.

2.1. Drying Equipment

In the drying process, 5 air type solar collectors designed and manufactured by us were used as heat source (Figure 1). The radiation absorption surface of solar collector 1 given in Figure 1 is flat, the radiation absorption surface of the collector 2 is closed for drying at ambient temperature, the radiation absorption surface of the collector 3 is 30 degrees trapezoidal, the radiation absorption surface of the collector 4 is 45 degrees trapezoidal and the radiation absorption surface of the collector 5 is 60 degrees trapezoidal. The channel heights are taken equal in order to ensure equal air flow rates through the collectors.

The radiating surface of the collectors measures 1 m². Adjustable fans for air flow rate were placed at each collector inlet. The air velocity was measured at the inlet of the hazelnut drying box using a thermo-anemometer. The air temperature was measured in a time-dependent manner at the inlet and the outlet of the collector. The heated and accelerated air passes through the collector and is discharged into the environment through the spiral pipe, which is located above the nuts that are laid on the net in the box.

2.2. Method

Hazelnuts harvested from the orchard were weighed without separation and placed in Polyfoam boxes, with 4 kg per treatment. To prevent the collector outlet temperatures from getting too high and affecting the quality of the hazelnuts, the air speed through the collectors has been increased. The air velocity passing over the hazelnuts was 6 m/s constant.

Moisture losses were measured by weighing the samples at regular intervals during the drying process. Once the moisture losses of the samples with husks reached a constant level, they were manually sorted and separated from the husks. The moisture content of each sample was then measured. The fresh hazelnut samples were sorted, weighed, and placed in polyfoam boxes with a weight of 1.5 kg per treatment.



Figure 1. Five solar collectors used in the drying system.

Table 1. Measurement tools

Measureme	Measurement	Tool	Range	Precision
Temperature	K-type thermocouple	Vert	-220 – 1370 °C	0.1 °C
Temperature	Infrared thermometer	Fluke-62 Max	-30 – 500 °C	0.1 °C
Air speed	Hot wire anemometer	Cem Dt-8880	0.1 – 25 m/s	0.01 m/s
Weight loss	Digital scale	Necklife Agt S2	0 – 6 kg	0.1 g
Moisture	Moisture analyzer	Precisa-XM60	0.02 – 124 g	0.001 g

During the drying process, the mass loss of hazelnuts was measured at regular intervals (every hour) with an electronic balance. The purpose of this weighing is to determine whether the hazelnut has reached 6% equilibrium moisture. When the hazelnut reached the equilibrium moisture, the drying experiment was terminated. Air temperature was measured at the inlet and outlet of each panel. In sun drying, the surface temperature of the hazelnut was measured with an infrared thermometer. Air velocity was measured by telescopic hot wire anemometer in both panel drying and sun drying. Hazelnut wet and dry moisture values were determined by infrared moisture measuring device. The instruments used and the sensitivity values for the measurements performed in the experiments are shown in Table 1.

2.2.1. Hazelnut oil extraction

Hexane was used as a solvent for cold-extracting oil from homogenised hazelnut samples. The extraction process was carried out by stirring the samples on a MR-12 Rocker-Shaker (Biosan, Latvia) at 50 rpm for 2 hours at room temperature. The resulting supernatant was obtained by centrifugation (Nüve 800R, Türkiye) at 4500 rpm for 10 minutes and then decanted. The hexane-oil mixture was then subjected to rotary evaporation (Heidolph Laborota 4000, Germany) at 45°C to remove the hexane. The free fatty acidity and peroxide value of the obtained oil were analyzed (Akgün and Akgün, 2023).

2.2.2. Free fatty acids (FFA)

Hazelnut oils (2 g) were weighed to an accuracy of 0.01 g and treated with 12 mL of a neutral mixture of diethyl ether:ethanol (1:1, v:v). The titration was then carried out using a 0,01 N solution of potassium hydroxide in

ethanol with 1 % of phenolphthalein as an indicator. The results for free fatty acids (FFA) are presented as a percentage of oleic acid (AOAC, 1990).

2.2.3. Peroxide value (PV)

The oil sample was weighed in a glass jar using a precision balance. Then, 10 mL of chloroform and 15 mL of acetic acid were added and mixed. Next, 1 mL of saturated potassium iodide solution was added to the mixture and kept in the dark for 5 minutes. Titration was carried out with 0.002 N sodium thiosulphate solution followed by the addition of 75 mL distilled water and 1 mL 1% starch solution. The PV was calculated as meq O₂/kg (according to AOAC, 1990).

2.2.4. Extraction procedure of bioactive components

To extract the hazelnut samples, a mixture of 80% methanol and 20% distilled water was added to one gram of defatted hazelnut. The mixture was then subjected to extraction on an MR-12 Rocker-Shaker (Biosan, Latvia) at 50 rpm for 6 hours at room temperature. After extracting, the mixture was centrifuged for 10 min at 5000 rpm and the supernatant was decanted. The procedure was repeated for the residue and the combined extracts were analyzed for the total phenolic content and antioxidant activity (according to DPPH, ABTS and FRAP assays).

2.2.5. Total phenolic content

An aliquot of the sample extract was mixed with FC reagent and a 20% w/v solution of sodium carbonate in a test tube and the total volume was adjusted to 5 ml with distilled water according to the Folin-Ciocalteu test (Singleton et al., 1999). After 30 minutes at room temperature, the absorbance of the prepared mixtures was recorded at 760 nm using a UV mini-1240

spectrophotometer (Shimadzu, Japan). Using a gallic acid standard curve, the results are expressed as milligrams of gallic acid equivalent (GAE) per 100 g dry weight.

2.2.6. Antioxidant activity assays

The hazelnut samples' antioxidant activity was determined by calculating $\mu\text{mol trolox-equivalent (TE)}/\text{g}$ dry weight using three different in vitro antioxidant assays: DPPH, ABTS, and FRAP.

To determine DPPH, 100 μl of the sample extract was mixed with 0.1 mM DPPH solution (2.9 ml) in a test tube. After incubating the mixtures at 30 °C for 30 min, the absorbance was measured at 517 nm (Brand-Williams et al., 1995).

The determination of ABTS was carried out according to the protocol developed by Re et al. (1999). In order to allow the formation of radical cations, a 7 mM ABTS stock solution containing 2.45 mM potassium persulfate was kept in the dark for 12 h. The resulting radical mixture was then diluted with ethanol until the absorbance at 734 nm was 0.700 ± 0.02 , yielding the ABTS test solution. Next, 100 μl of the sample extract was added to the test tube and reacted with the diluted ABTS test solution (2900 μl) for 6 minutes. The absorbance was read at 734 nm and recorded.

For FRAP analysis, the FRAP reagent was prepared by mixing TPTZ (10 mmol/L), $\text{FeCl}_3 \cdot 6\text{H}_2\text{O}$ (20 mmol/L) and acetate buffer (0.3 mol/L, pH 3.6) solutions in appropriate volumetric ratios (1:1:10 v/v). Absorbance values of the mixture prepared with the sample extract and FRAP reagent were measured at 593 nm in a spectrophotometer after incubation at 37 °C for 4 minutes (Benzie and Strain, 1996).

The statistical analysis of all values obtained from the study was conducted using the One-Way ANOVA method in the SPSS 25 software package (Genç and Soysal, 2018).

3. Results and Discussion

This section presents the results of the study in two parts: the hazelnut drying process and the resulting

changes in kernel quality characteristics.

3.1. Hazelnut Drying

Figure 2 shows the ambient temperature change of Levant during pre-drying (withering process) to remove hazelnuts from the husk. It took 1.5 days to complete the pre-drying process. The moisture contents of the shelled hazelnuts were as follows: Sample 1 (21.3%), Sample 2 (25.6%), Sample 3 (20.8%), Sample 4 (20.0%), and Sample 5 (21.2%). These measurements were taken after 14 hours of operation, excluding nighttime.

The temperature at night, when the system was not operated, was not measured, and is represented as intermittent on the graph. Sample 4 experienced a higher moisture loss due to the higher ambient temperature (46.3 °C) compared to the other samples, despite having the same flow rates. In system no. 2, the humidity value was high as expected since the air flow was at ambient temperature (max. 30.1 °C). At the end of the pre-drying process, the humidity of the solar collectors at the end of the drying process was close to each other and lost about 30% more moisture than the drying directly at ambient temperature. This finding is consistent with earlier research (Demirtaş, 1996).

The objective of the drying process following pre-drying is to reduce the moisture content of the shelled hazelnuts to below 6% equilibrium moisture. This drying process lasted 18 hours.

Figure 3 shows the time-dependent ambient temperature of shelled hazelnuts that were separated from the husk and dried again. It is clearly seen that sample 1 and the air velocity without heated drying will dry more slowly than the others. The temperature curve of sample 2 shows that the hazelnuts can be dried in a shorter time by increasing the temperature of the air. This is clearly seen when compared with the temperature curve of sample 1. To prevent hazelnuts from spoiling in rainy regions, it is recommended to heat them slightly above atmospheric air and pass them under cover, this will also shorten the drying time.

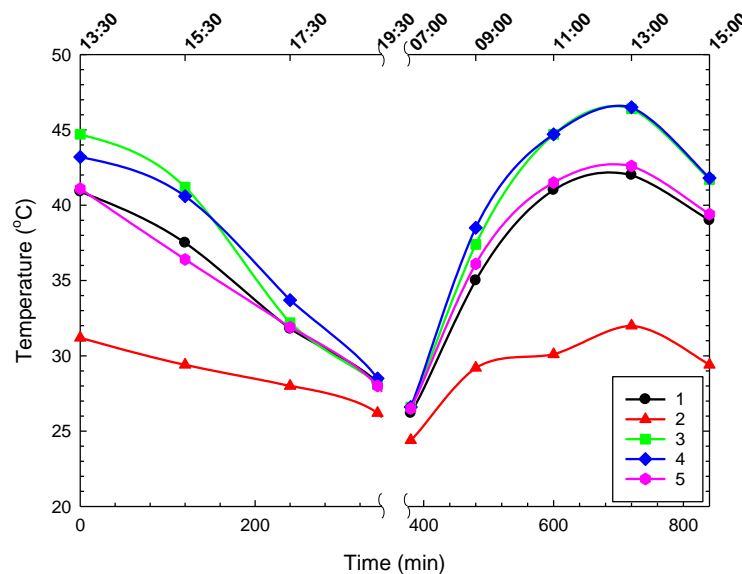


Figure 2. The variation of in-husk hazelnut drying ambient temperature over time.

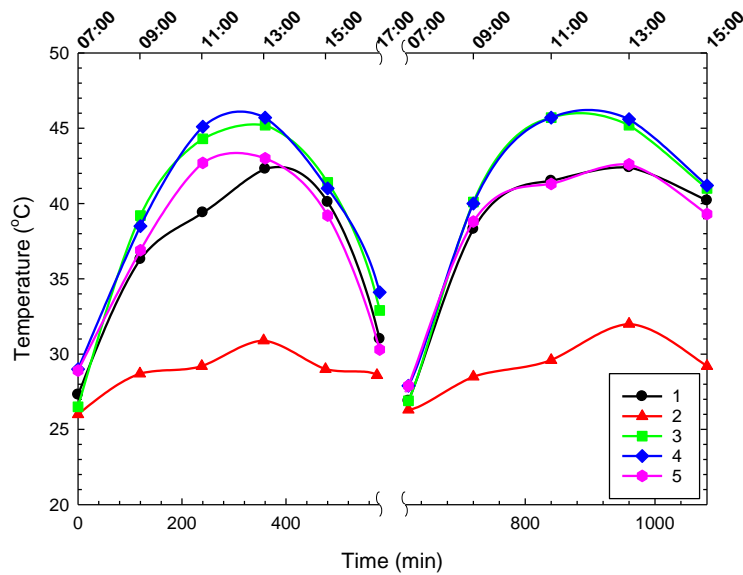


Figure 3. The variation of hazelnut without husk drying ambient temperature over time.

The drying process was completed in 18 hours. However, despite the humidity dropping below 6% in the solar collectors (Sample 2), the process continued for an additional 8 hours at ambient temperature.

After the hazelnuts were dried, their moisture content was measured and recorded as follows: Sample 1 (5.3%), Sample 2 (7.4%), Sample 3 (5.1%), Sample 4 (5.4%), and Sample 5 (5.2%). Although sample 4 has the highest average temperature (Figure 3), it also has a higher humidity level compared to samples 3 and 5. Hazelnut size is mainly responsible for the variation in moisture content during the same process. Drying slows down as the size increases, and moisture diffuses more slowly from the interior to the hazelnut shell. Sample 2 was not completely dry by the end of the experiment. It was therefore dried separately until it reached an equilibrium moisture content of 6%.

3.2. Hazelnut traits

The study investigated the effect of different drying rates on oxidation parameters. Both free fatty acid and peroxide levels were found to be significant ($P < 0.05$) by statistical analysis.

Table 2 presents the TPC, and antioxidant capacity of hazelnut samples dried using various methods. The utilization of different drying methods significantly affected the TPC and antioxidant capacity of the hazelnut samples ($P < 0.01$). The TPC of the hazelnut samples ranged from 312.79-449.19 mg GAE/100 g. The highest TPC was observed in hazelnuts dried using 45° and Flat solar collectors (SCs), while hazelnuts dried with 30° SC had the lowest TPC ($P < 0.05$). In this study, the continuous system had the lowest drying temperature (26-32°C), but the longer drying time compared to other methods had a negative effect on the bioactive properties. A similar trend to TPC results was also observed for antioxidant activity assays. The highest values ($P < 0.05$) for all three antioxidant activity assays were presented by 45° and Flat SCs, while the antioxidant

capacity of the hazelnuts dried by the SC system with 30° tilt angle was the lowest ($P < 0.05$). Previous studies have shown a positive correlation between TPC and antioxidant capacity in hazelnut samples, which is in agreement with our findings Yılmaz et al. (2019). The TPC and antioxidant activity findings were consistent with previous studies on hazelnuts (Yılmaz et al., 2019; Balık et al., 2021; Çelik et al., 2023; Yaman et al., 2023). However, some researchers reported lower values (Ghirardello et al., 2013; Karaosmanoğlu, 2022; Akgün and Akgün, 2023). Yılmaz et al. (2019) determined the DPPH and FRAP values of hazelnuts of different sizes to be 31.60-44.18 mmol/kg and 33.48-58.83 mmol/kg, respectively. Balık (2021) reported TPC, DPPH and FRAP values for different Turkish hazelnuts in the range of 280.35-1130.06 mg GAE/100 g, 1.22-2.54 mmol TE/kg, and 2.9-26.99 mmol TE/kg, respectively. The hazelnut's bioactive component content and antioxidant capacity vary depending on agricultural factors, variety, size, processing method, extraction procedure, and storage conditions (Ghirardello et al., 2013; Simsek et al., 2017; Yılmaz et al., 2019; Karaosmanoğlu, 2022). Additionally, the bioactive properties of hazelnuts are significantly affected by the drying method used. In their study, Özcan and Uslu (2023) found that drying hazelnuts using different methods (room temperature, conventional oven, and microwave) increased the total phenolic content (TPC) and the antioxidant activity (measured by DPPH). They recommended the use of conventional oven drying over the other methods.

Table 3 presents the FFA (%oleic acid) and PV (meq O₂/kg) values of hazelnuts dried using different methods. The hazelnut oils were found to have FFA and PV values in the range of 0.21-0.23% and 0.26-0.37%, respectively. The FFA and PV values of hazelnut samples dried using different methods were similar ($P > 0.05$). Therefore, the drying methods used in this study did not have a significant ($P > 0.05$) effect on the oxidation parameters of

hazelnuts. Similarly, Kashaninejad et al. (2003) found no significant difference between the FFA values of pistachios dried by different methods. However, in the present study, all samples had FFA values below the threshold value ($\geq 1\%$) accepted as an indicator of quality deterioration (Turan, 2018b). Our results were lower than the values found in previous studies (Celik et al., 2023; Akgun and Akgun, 2023), but similar to those reported by Turan (2018a, 2018b). Previous studies (Ghirardello et al., 2013; Turan, 2018a, Turan, 2018b; Mokhtarian and Tavakolipour, 2019) have shown that the FFA and PV of nuts can vary depending on environmental factors, drying, processing, storage, and

packaging conditions. In order to prevent oxidation, Turan (2018b) emphasized that hazelnuts should be dried at a maximum temperature of 45 °C for a short time. Mokhtarian and Tavakolipour (2019) found that pistachios dried using conventional solar drying systems with air recycling had a lower peroxide value than those dried without air recycling, due to the longer drying time associated with the latter method. A study conducted by Akgün and Akgün (2023) found that hazelnuts preserved their oxidative quality better when dried using a solar collector with an air flow rate of 3.00 m/s, compared to sun drying.

Table 2. Changes in total phenolics and antioxidant capacity of hazelnuts dried by various drying methods

Drying Method	TPC (mg GAE/100 g)	DPPH ($\mu\text{mol TE/g}$)	ABTS ($\mu\text{mol TE/g}$)	FRAP ($\mu\text{mol TE/g}$)
Flat-SC	431.84±2.82 ^a	49.81±1.21 ^a	15.63±0.52 ^{ab}	25.83±1.70 ^a
Continuous	360.10±12.39 ^c	42.89±1.52 ^b	14.11±0.44 ^{bc}	22.18±0.73 ^b
30° SC	312.79±8.22 ^d	35.33±2.73 ^c	10.78±0.65 ^d	17.38±0.30 ^c
45° SC	449.19±7.05 ^a	50.01±1.22 ^a	16.93±0.70 ^a	26.70±1.99 ^a
60° SC	389.94±16.55 ^b	43.65±1.18 ^b	13.91±0.34 ^c	21.35±0.51 ^b

SC= solar collector, TPC= total phenolic content, DPPH= DPPH antiradical activity, ABTS= ABTS antiradical activity, FRAP= ferric ion reducing antioxidant power, ^(a-d) Significant differences (Türkiye test; P<0.05) between means in the same column are indicated by different lowercase letters.

Table 3. Changes in FFA and PV values of hazelnuts dried by various drying methods

Drying Method	FFA (%)	PV (meq O ₂ /kg)
Flat-SC	0.22±0.02	0.33±0.08
Continuous	0.21±0.01	0.26±0.04
30° SC	0.21±0.01	0.28±0.14
45° SC	0.23±0.02	0.35±0.07
60° SC	0.23±0.01	0.37±0.08

SC= solar collector, FFA= free fatty acids, PV= peroxide value.

4. Conclusion

The study examined the effects of solar-heated air at different types solar collectors on the drying of Levant quality hazelnuts and drew the following conclusions:

1. In wet climates, it may be preferable to heat the hazelnuts slightly above the air temperature and dry them under cover to prevent spoilage and shorten the drying time.
2. Drying with air without heating took a long time. However, it allowed the hazelnuts to dry without spoiling.
3. At the end of the pre-drying process, the humidity of the solar collectors at the end of the drying process was close to each other (Sample 1, 3, 4, and 5) and lost about 30% more moisture than the drying directly at ambient temperature (Sample 2).
4. In the pre-drying stage, as expected, the shortest drying time was achieved with a Sample 4 (45 trapezoidal angle).

5. The drying time decreases as the heat of the air increases when a solar collector is used for the drying process.
6. It is seen that the most suitable collector geometry for TPC, DPPH, ABTS and FRAP values of hazelnut in hazelnut drying with solar collectors is 45 degrees.
7. The results indicate that the geometry of the collector does not have a statistically significant effect on the FFA and PV values of hazelnuts during solar drying.

Solar collectors are recommended for drying hazelnuts due to their environmentally friendly nature, lack of energy costs, and ability to preserve food properties.

Author Contributions

The percentage of the author(s) contributions is presented below. All authors reviewed and approved the final version of the manuscript.

	M.A.	C.A.	M.A.	E.T.
C	25	25	25	25
D	25	25	25	25
S	25	25	25	25
DCP	25	25	25	25
DAI	25	25	25	25
L	25	25	25	25
W	25	25	25	25
CR	25	25	25	25
SR	25	25	25	25
PM	25	25	25	25
FA	25	25	25	25

C=Concept, D= design, S= supervision, DCP= data collection and/or processing, DAI= data analysis and/or interpretation, L= literature search, W= writing, CR= critical review, SR= submission and revision, PM= project management, FA= funding acquisition.

Conflict of Interest

The authors declared that there is no conflict of interest.

Ethical Consideration

Ethics committee approval was not required for this study because of there was no study on animals or humans.

References

Akgün M, Akgün M. 2023. Effect of solar collector drying on the nutritional properties of Çakıldak hazelnut. *Turkish J Food Agri Sci*, 5(2): 130-140.

Akgün M, Kandemir L, Öztürk B. 2018. Effect of led drying on drying behavior of *Prunus domestica* L. fruit. *Indian J Pharmac Edu Res*, 52(4): 115-118.

Aksüt B, Dinçer E, Saraçoğlu O, Polatçı H. 2023. Kurutma yöntemi ve sıcaklık değerlerinin mor reyhanın kuruma kinetiği ve renk kalitesi üzerine etkisi. *Anad Tarım Bilim Derg*, 38 (1): 187-198.

Aktaş M. 2003. Optimization of fins in indirect hot water preparation systems with solar energy natural circulation. MSc thesis, Gazi University Institute of Science and Technology, Ankara, Türkiye, pp: 53-99.

AOAC. 1990. Oils and fats official methods of analysis of the association of official analytical chemists. Washington DC, US, pp: 485-518.

Balık HI, Balık SK, Duyar Ö. 2021. Hazelnut genetic resources project. 2nd International Cukurova Agriculture and Veterinary Congress, January 4-5, Adana, Türkiye, p: 75-76.

Balık HI. 2021. Bioactive compounds and fatty acid composition of new Turkish hazelnut cultivars. *Int J Fruit Sci*, 21(1): 106-114.

Behera DD, Mohanty AM, Mohanty RC. 2022. Recent advances in solar drying technologies: A Comprehensive review. *JES*, 6(4): 503-519.

Benzie IF, Strain JJ. 1996. The ferric reducing ability of plasma (FRAP) as a measure of "antioxidant power": the FRAP assay. *Analytical Biochem*, 239(1): 70-76.

Brand-Williams W, Cuvelier ME, Berset CLWT. 1995. Use of a

free radical method to evaluate antioxidant activity. *LWT- Food Sci Technol*, 28(1): 25-30.

Çelik ÖF, Aktaş N, Tugay Mİ, Tuncil YE. 2023. Hazelnut (*Corylus avellana* L.) skin, a by-product of hazelnut industry, possesses oil with high oxidative and thermal stabilities. *Int J Food Sci Technol*, 58(10): 5471-5477.

Ceylan İ, Aktaş M, Doğan H. 2006. Apple drying in a solar drying oven. *Polytechnic J*, 9(4): 289-294.

Danso-Boateng E. 2013. Effect of drying methods on nutrient quality of Basil (*Ocimum viride*) leaves cultivated in Ghana. *Inter Food Res J*, 20(4): 1569-1573.

Demirtaş C. 1996. Fındık kurutma şartlarının belirlenmesi. PhD Thesis, Institute of Science and Technology, Karadeniz Technical University, Trabzon, Türkiye, pp: 151.

EL-Mesery HS, EL-Seesy AI, Hu Z, Li Y. 2022. Recent developments in solar drying technology of food and agricultural products: A review. *Renew Sustain Energy Rev*, 157: 112070.

Fernandes L, Tavares PB. 2024. A review on solar drying devices: Heat transfer, air movement and type of chambers. *Solar*, 4(1): 15-42.

Genç S, Soysal Mİ. 2018. Parametric and nonparametric post hoc tests. *BSJ Eng Sci*, 1(1): 18-27.

Ghirardello D, Contessa C, Valentini N, Zeppa G, Rolle L, Gerbi V, Botta R. 2013. Effect of storage conditions on chemical and physical characteristics of hazelnut (*Corylus avellana* L.). *Postharvest Biol Technol*, 81: 37-43.

Harini, S, Kavva, VS, Ramana, AS. 2022. Recent developments in design and operations of solar dryer. *IOP Conference Series: Earth and Environmental Science*, 1100: 012007.

Huang D, Yang P, Tang X, Luo L, Sunden B. 2021. Application of infrared radiation in the drying of food products. *Trends Food Sci Technol*, 110: 765-777.

Karaosmanoğlu H. 2022. Lipid characteristics, bioactive properties, and mineral content in hazelnut grown under different cultivation systems. *J Food Proces Preserv*, 46(7): e16717.

Kashaninejad M, Tabil LG, Mortazavi A, Safe Kordi A. 2003. Effect of drying methods on quality of pistachio nuts. *Drying Technol*, 21(5): 821-838.

Kian-Pour N. 2020. Fundamental drying techniques applied in food science and technology. *Int J Food Eng Res*, 6(1): 35-63.

Köksal AI. 2002. Turkish hazelnut cultivars. Hazelnut Promotion Group, Ankara, Türkiye, pp: 136.

Kontaş E. 2022. Periyodik kurutma şartlarının fındığın kurutma davranışına etkisi. MSc Thesis, Institute of Science and Technology, Ordu University, Ordu, Türkiye, pp: 71.

Memur E. 2022. Drying performance evaluations with solar food dryer design. *Yekarum*, 7(2): 48-57.

Mohana Y, Mohanapriya R, Anukiruthika T, Yoha KS, Moses JA, Anandharamakrishnan C. 2020. Solar dryers for food applications: Concepts, designs, and recent advances. *Solar Energy*, 208: 321-344.

Mokhtarian M, Tavakolipour H. 2019. The effects of solar drying systems and packaging types on the quality indicators of dried pistachio nuts. *Pistachio Health J*, 2(1): 71-82.

Özçağırın R, Ünal A, Özeker E, İsfendiyoğlu M. 2014. Temperate climate fruit species. Ege University Press House, No: 566, İzmir, Türkiye, pp: 262.

Özcan MM, Uslu N. 2023. Investigation of changes in total phenol, flavonoid, antioxidant activity, fatty acids, polyphenol and mineral profiles of hazelnut kernels dried in air, oven and microwave. *JSFA Rep*, 3(2): 72-81.

Re R, Pellegrini N, Proteggente A, Pannala A, Yang M, Rice-Evans C. 1999. Antioxidant activity applying an improved

- ABTS radical cation decolorization assay. *Free Radical Biol Medic*, 26(9-10): 1231-1237.
- Reddy TA. 1987. The design and sizing of active solar thermal systems. Oxford University Press, New York, US, pp: 4-10.
- Saleh SM, Gatea AA. 2010. Design, construction, and performance evaluation of solar maize dryer. *Iraqi J Mechan Mater Eng*, 10(3): 365-376.
- Shariah A, Al-Akhras M-Ali, Al-Omari IA. 2002. Optimizing the tilt angle of solar collectors. *Renew Energy*, 26: 587-598.
- Simsek A, Artik N, Konar N. 2017. Phenolic profile of meals obtained from defatted hazelnut (*Corylus avellana* L.) varieties. *Int J Life Sci Biotechnol Pharma Res*, 6(1): 7-12.
- Singleton VL, Orthofer R, Lamuela-Raventós RM. 1999. Analysis of total phenols and other oxidation substrates and antioxidants by means of Folin-ciocalteu reagent. *Methods Enzymol*, 299: 152-178.
- Topdemir A. 2019. Mikroçoğaltımla üretilmiş fesleğenin (*Ocimum basilicum* L.) tepsili kurutucuda kuruma karakteristiğinin belirlenmesi. *Fırat Üniv Müh Bilim Dergi*, 31(2): 545-550.
- TÜİK 2021. <https://data.tuik.gov.tr/Kategori/GetKategori?p=tarim-111&dil=1> (accessed date: January 21, 2023).
- Turan A, İslam A. 2018. Effect of drying methods on some chemical characteristics of hazelnuts (*Corylus avellana* L.) during storage. *J Inst Sci Technol*, 8(3): 11-19.
- Turan A. 2018a. Effect of drying methods on fatty acid profile and oil oxidation of hazelnut oil during storage. *European Food Res Technol*, 244(12): 2181-2190.
- Turan A. 2018b. Effect of drying methods on nut quality of hazelnuts (*Corylus avellana* L.). *J Food Sci Technol*, 55(11): 4554-4565.
- Uzundumlu AS, Bilgiç A, Ertek N. (2019). Forecasting hazelnut production of Turkey's leading hazelnut producing provinces between 2019 and 2025 with ARIMA model. *Acad J Agri*, 8(Special Issue): 115-126.
- Yaman M, Balta MF, Karakaya O, Kaya T, Necas T, Yildiz E, Dirim E. 2023. Assessment of fatty acid composition, bioactive compounds, and mineral composition in hazelnut genetic resources: Implications for nutritional value and breeding programs. *Horticulturae*, 9(9): 1008.
- Yıldız Z, Gökayaz L. 2019. Drying of apple slices with different solar drying methods. *J Food Feed Sci Technol*, 22: 29-36.
- Yılmaz M, Karakaya O, Balta MF, Balta F, Yaman İ. 2019. Change of biochemical characteristics depending on kernel size in Çakıldak hazelnut cultivar. *Acad J Agri*, 8(Special Issue): 61-70.



TÜRKİYE ÖLÇEĞİNDE KARAYOLU YOL- BAKIM MALİYETLERİ VE GELECEK TAHMİNİ

Fatma Pınar GÖKSAL^{1*}

¹Aksaray University, Faculty of Engineering, Department of Industrial Engineering, 68100, Aksaray, Türkiye

Özet: Karayolu ulaşımında dikkat edilmesi gereken en önemli unsur ekonomi olgusudur. Ülkemizde de halihazırda yapımı hızla artmakta olan artan esnek üst yol kaplamaları, taşıt sayısı artışları vb. gerekçelerdeki artışlar sebebi ile ekonomik verilerin önemini göz önüne sermektedir. Bugüne kadar karayolu üstyapısı bozulma örnekleri üzerine detaylı incelemeler yapılmıştır. Bu çalışmada farklı olarak amaç, maliyet araştırmalarında gelecek tahmin modelleri oluşturmaktır. Çalışmada bölgesel düzeyde yol bakım onarım için harcanan rakamlar yıllara göre incelenmiştir. Verilerin analizinde SPSS programından yararlanılmıştır. Karayolları genel müdürlüğünden alınan yol bakım onarım verilerinin 2023-2025 tahminlerinde Winters yöntemi kullanılmıştır. Çalışma sonuçlarına göre 2025 yılı için artan trafik hacminden dolayı yol bakım maliyetinin ciddi oranda artacağı gözlemlenmiş ve bunu azaltabilmek için yapılabilecek önlemler ve politikalar sunulmuştur.

Anahtar kelimeler: Esnek yol kaplama, Ulaştırma, Yol bozulması, Ekonomi, Winters yöntemi

Highway Maintenance Costs and Future Forecast in Türkiye

Abstract: The most important factor to consider in road transportation is the phenomenon of economy. Increasing flexible pavements, the increase in the number of vehicles, etc., which are currently being constructed rapidly in our country. It reveals the importance of economic data due to the increases in the reasons. To date, detailed studies have been carried out on examples of highway pavement deterioration. Differently, the aim of this study is to create future prediction models in cost research. In the study, the figures spent on road maintenance and repair at the regional level were examined by year. SPSS program was used to analyze the data. Winters methods were used in the 2023-2025 estimates of road maintenance and repair data received from the General Directorate of Highways. According to the study results, it has been observed that the cost of road maintenance will increase significantly due to the increasing traffic volume for 2025, and measures and policies that can be taken to reduce this are presented.

Keywords: Flexible road pavement, Transportation, Road degradation, Economy, Winters method

*Sorumlu yazar (Corresponding author): Aksaray University, Faculty of Engineering, Department of Industrial Engineering, 68100, Aksaray, Türkiye

E mail: fatmapinargoksal@aksaray.edu.tr (F. P. GÖKSAL)

Fatma Pınar GÖKSAL



<https://orcid.org/0000-0002-6007-9297>

Gönderi: 03 Ocak 2024

Kabul: 15 Mart 2024

Yayınlanma: 15 Mayıs 2024

Received: January 03, 2023

Accepted: March 15, 2024

Published: May 15, 2024

Cite as: Göksal FP. 2024. Highway maintenance costs and future forecast in Türkiye. BSJ Eng Sci, 7(3): 392-400.

1. Giriş

Günümüz dünyasında gelişmekte ve değişmekte olan teknoloji ışığında kar edebilme kabiliyeti kişiler ya da bütün kuruluşlar için oldukça önemlidir. Bu bağlamda alınan kararların ve önlemlerin özellikle ekonomik olması, modernleşmeyi zorunlu hale getirmiştir. Türkiye de yolcu taşımacılığının %97'si, yük taşımacılığının ise %89'u karayolu ulaşımı ile gerçekleştirilmektedir (Çetin ve ark., 2011). Karayolu asfalt kaplama endüstrisinin hızla gelişmesiyle, asfalt üstyapı karışım sistemleri hakkında birçok detaylı çalışma başlamış ve kullanımı hızla yaygınlaşmıştır (Öztürk, 2004). Ülkemiz için en önemli maliyetlerden biri asfalt yol yapımı uygulamasıdır. Ülkemizde yolların, Mayıs 2016 itibari ile 20000 km'ye yakını asfalt betonu, 40000 km'den fazlası ise sathi kaplama yoldur. Asfalt kaplama yolların, maliyeti yüksek birçok malzeme gibi belirli aralıklarla önleyici bakım ve onarımlara ihtiyacı olduğu bilinmektedir. Bu bakım ve onarımların gelecek yıllar için daha yüklü bir mali yük getirebileceği düşünülmektedir. Böyle bir ekonomik

yükümlülük ışığında alınabilecek kararların detaylı incelenerek yeni teknoloji destekli analizlerle alınması oldukça önemlidir. Asfalt yolların ekonomik ömürlerinin ortalama 20 ile 40 yıl arasında değiştiği ve bu yolların bakım onarımları düzenli olarak yapılırsa sürenin dahada artacağı bilinmektedir (Karahacıoğlu ve Corum, 2020). Tsunokawa ve ark. (2002) yapmış olduğu çalışmada üstyapı tasarım farklılık gösterdiği ve tasarım standartlarına göre yolun ilk yapım maliyeti ile bakım maliyetleri arasındaki ve kuruluş maliyetleri ile kullanıcı maliyetleri arasındaki farklılıklar nedeniyle işin ekonomik boyutunu ortaya koymuşlardır. Carnahan ve ark. (1986) yapmış olduğu çalışmada yol üstyapısındaki bozulmalar için en uygun bakım aralıklarını elde edebilmek için yöntemler geliştirmişlerdir. Nihayetinde bakım-onarım maliyetlerini en aza indireyecek ve yol performansını maksimum şekilde yerine getirebilecek yöntemler üretmişlerdir. Esnek üstyapılarda oluşabilecek bozulmalarda trafik yükü ve yol yapım aşamasında kullanılan bitüm miktarı arasında lineer bir ilişki olduğu



bilinmektedir (Kuloğlu ve ark., 2004). Lamptey ve ark. (2005) yapmış olduğu çalışmada esnek yol üstyapılarında optimum düzeyde bakım maliyetleri elde etmek amaçlı INDOT tasarım standartlarını temel alarak bir analiz geliştirmişlerdir. Geleneksel olarak bir otoyol kurumunun uzun vadeli planlama kararı yalnızca rehabilitasyon ve yeniden inşa faaliyetlerini dikkate alıyordu. Ancak son yıllarda yapılan birçok çalışma, önleyici bakım faaliyetlerinin yani yol kaplamasının bozulmasının yavaşlatılması yada servis ömrünün uzatılması gibi birçok faaliyetinin önemini vurgulamıştır (Chong, 1989; Ponniah ve Kennepohl, 1996; Labi ve Sinha, 2003; Mamlouk ve Dosa, 2014). Varlıkların kuruluşlar tarafından uzun vadeli kârlılığının sürdürülebilmesi için temel bir işlev olan bakım onarım maliyeti, varlığın orijinal durumuna veya gerekli işlevi yerine getirebileceği duruma getirilmesi veya korunması amacıyla yapılan tüm eylemlerin birleşimi olarak tanımlanır ve bakım performansı ölçümü son yıllarda uygulayıcılar ve araştırmacılardan büyük ilgi görmektedir (Tee ve Ekpiwhre, 2020). Canver ve ark. (2020) yapmış olduğu çalışmada yol geometrik standartlarındaki iyileştirmenin, karayolu bakım maliyetlerini ciddi oranda azalttığını gözlemlemiştir. Ayrıca, mevcut ulaşım altyapısının bakımının düzenli ve zamanında yapılması da gelecek toplam maliyeti önemli ölçüde azaltmaktadır. Buna benzer şekilde literatürde yapılan birçok çalışmada yol bakım onarım maliyetinin birçok etmene bağlı olduğunu ifade edilmektedir (Qiao ve ark., 2019). Geçmişten günümüze çalışılan birçok konu, yol bakım maliyetlerinin azaltılarak üretilen yol kapasitesinden optimum düzeyde faydalanmak üzerine geliştirilmiştir.

Karayolu ulaştırmasında dikkate alınması gereken en önemli unsurlardan biri ekonomidir. Türkiye’de yapımı hala artmakta olan yol kaplamaları, taşıt sayısındaki ve çeşitliliğindeki artışlar sebebiyle fazla deformasyona uğramaktadır. Bu çalışmada bağlamında, karayolu bakım onarım maliyetleri incelenmiş ve gelecek için tahminlerde bulunulmuştur. Bu çalışma, özgün yaklaşımı nedeniyle yol bakım endüstrisine ve literatüre bir katkı niteliğindedir. Bu nedenle araştırmanın sonuçları, yol bakım maliyetlerini azaltmak için alınabilecek önlemlerin yaygınlaştırılmasını teşvik edebilir durumdadır. Ayrıca, çalışma ana hatları verilen yol bakım maliyetlerini azaltmada gelecekteki çalışmalara yol gösterici niteliktedir.

2. Materyal ve Yöntem

Verilerin analizinde SPSS programından yararlanılmıştır. Karayolları genel müdürlüğünden alınan yol bakım onarım verilerinin 2023-2025 tahminlerinde winters yöntemleri kullanılmıştır. Literatüre bakıldığında bahsedilen model üzerinden yapılmış olan çalışmalar incelenince bu çalışmada yöntem olarak winters yöntemi belirlenmiştir ve mevsim gibi bazı etkiler düşünüldüğünde bu yöntemi daha etkili olacağı düşünülmüştür. Winters Yöntemi, elde edilen verilere ait

son tespit edilen değişimleri dikkate almaktadır. Bu değişimler, sıçramalar, açıklanamayan bazı etkiler ya da önce algılanamayan bazı gözden kaçırılmış gelişmelerden oluşmaktadır (Çuhadar, 2014). Winters Yöntemi, içerisinde mevsimsel etkiler bulunduran zaman serilerinde uygulamak amaçlı geliştirilmiştir. Bu yöntem uygulanan zaman serisinin trendine, ortalama düzeyine ve mevsimsel bileşenlerine uygulanabilir (Irmak ve ark., 2012). Sabit katsayılar kullanan regresyon modellerinden gelen tahminlerin aksine, Winters yöntemlerinden gelen tahminler geçmiş tahmin hatalarına göre ayarlanır (Bowerman ve Connell, 1979). Kullanılan yöntem, doğrusal bir eğilime sahip olması ve mevsimsel bileşen içermemesi açısından çift yumuşatma yöntemine benzer. Çift yumuşatma yöntemi, yalnızca bir parametre kullandığı için daha ayırıştırıcıdır, bu yöntem ise iki parametrelidir. Düzleştirilmiş \hat{y}_t serisi aşağıdaki formülden elde edilir (eşitlik 1):

$$\hat{y}_{t+k} = \alpha + bk \quad (1)$$

burada a ve b, denklemde gösterildiği şekilde kalıcı bileşen ve eğilimdir. Bu katsayılar şu şekilde ifade edilebilir (eşitlik 2 ve 3):

$$a(t) = \alpha y_t + (1 - \alpha)(a(t) - 1) + b(t) - 1) \quad (2)$$

$$b(t) = \beta(a(t) - a(t - 1)) + 1 - \beta b(t) - 1) \quad (3)$$

burada $0 < \alpha, \beta, \gamma < 1$ sönümlenme faktörleri olarak tanımlanır. Bu yöntemde tahminler şu şekilde ifade edilir (eşitlik 4):

$$\hat{y}_{T+k} = a(T) + b(T)k \quad (4)$$

Bu yöntemde ifade edilen tahminler, eğim ile kesişen doğrusal bir eğilim üzerindedir.

3. Bulgular ve Tartışma

3.1. Asfalt Yol Bakım Giderlerine İlişkin Bulgular

3.1.1. Bölge şubelerine göre 2012-2022 asfalt yama giderlerine ilişkin bulgular

Tablo 1’de bölge şubelerine göre 2012-2022 asfalt yama giderlerine yer verilmiştir. Tablo 1’deki asfalt yama giderleri incelendiğinde en yüksek asfalt yama giderinin 2022 yılında gerçekleştiği, 2012-2022 yılları arasında yalnızca 1. Bölge ve 15. Bölgeye ait giderlerin her yıl olduğu, diğer bölgelerde asfalt-yama giderlerinin 2012-2022 yılları arasında bulunmadığı görülmektedir. 2012 yılında en yüksek asfalt yama giderinin 15. Bölgede olduğu, 2022 yılında ise en yüksek asfalt yama giderinin 1. Bölgede olduğu görülmektedir. Şekil 1’de 2012-2022 yılları arasında asfalt yama giderlerinin yıllara göre seyrine ait görünüme yer verilmiştir.

Tablo 2’de bölge şubelerine göre 2012-2022 asfalt yama

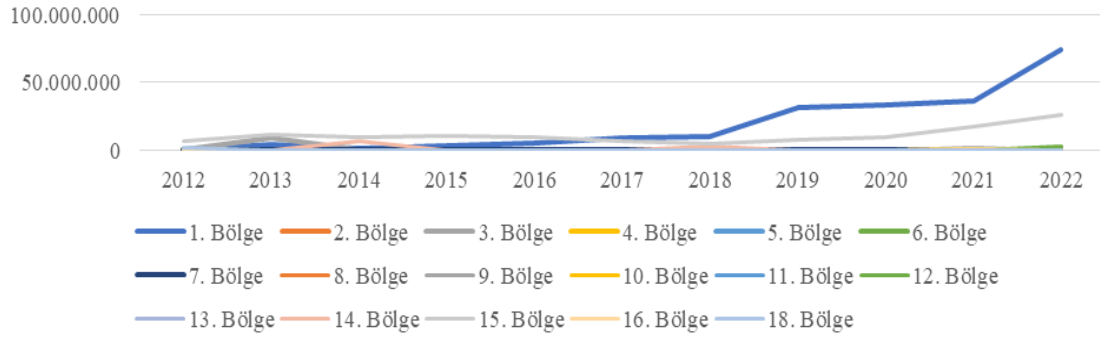
giderlerinin bir önceki yıla göre değişimine yer verilmiştir. Tablo 2'ye göre bir önceki yıla göre oransal olarak en fazla artış %202 ile 2013 yılında gerçekleşmiştir. 2012 yılı baz alındığında 2022 yılında

meydana gelen toplam asfalt yama gideri %1208 artış düzeyindedir. Bölge düzeyinde bir önceki yıla göre oransal olarak en fazla artış %208 ile 2015 yılında 1. Bölgede gerçekleşmiştir.

Tablo 1. Bölge şubelerine göre 2012-2022 asfalt yama giderleri

Bölge	2012	2013	2014	2015	2016	2017	2018	2019	2020	2021	2022
1	0	4.163.746	918.200	2.829.100	4.866.619	8.929.260	10.119.846	31.588.074	33.013.185	35.661.480	74.326.916
2	67.819	0	0	0	0	0	0	0	0	0	0
3	0	8.564.410	0	0	0	0	0	0	0	0	0
4	0	0	0	0	0	0	0	0	0	0	0
5	0	0	0	0	0	0	0	0	0	0	0
6	0	0	0	0	0	0	0	0	0	0	0
7	0	0	0	0	0	0	0	0	0	0	0
8	0	0	0	0	0	0	0	0	0	0	0
9	0	0	0	0	0	0	0	0	0	1.428.474	0
10	0	0	0	0	0	0	0	0	0	616.485	0
11	0	0	0	0	0	0	0	0	0	0	0
12	0	0	0	0	0	0	0	0	0	0	2.358.175
13	0	0	0	0	0	0	0	0	0	0	0
14	0	0	6.331.076	0	0	0	2.693.188	0	0	0	0
15	6.628.881	11.069.779	9.203.089	10.021.208	8.931.037	6.508.481	4.778.163	7.584.622	9.539.058	17.234.663	26.370.549
16	0	0	0	0	0	0	0	0	0	875.000	0
18	1.176.474	0	0	0	0	0	0	0	0	0	0
Toplam	7.873.174	23.797.935	16.452.365	12.850.309	13.797.656	15.437.741	17.591.197	39.172.696	42.552.243	55.816.102	103.055.639

BÖLGELERE GÖRE ASFALT YAMA GİDERLERİ (2012-2022)

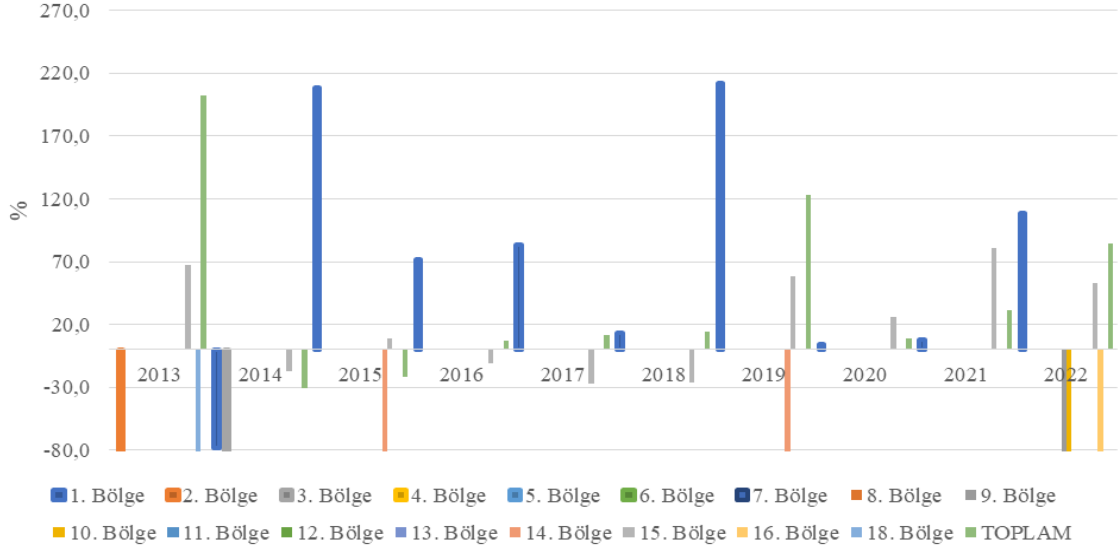


Şekil 1. Bölge düzeyinde 2012-2022 asfalt yama giderlerinin seyri.

Tablo 2. Bölge şubelerine göre 2012-2022 asfalt yama giderlerinin bir önceki yıla göre değişimi (%)

Bölge	2013	2014	2015	2016	2017	2018	2019	2020	2021	2022	13-22
1	-	-77,9	208,1	72,0	83,5	13,3	212,1	4,5	8,0	108,4	-
2	-	-	-	-	-	-	-	-	-	-	-
3	-	-	-	-	-	-	-	-	-	-	-
4	-	-	-	-	-	-	-	-	-	-	-
5	-	-	-	-	-	-	-	-	-	-	-
6	-	-	-	-	-	-	-	-	-	-	-
7	-	-	-	-	-	-	-	-	-	-	-
8	-	-	-	-	-	-	-	-	-	-	-
9	-	-	-	-	-	-	-	-	-	-	-
10	-	-	-	-	-	-	-	-	-	-	-
11	-	-	-	-	-	-	-	-	-	-	-
12	-	-	-	-	-	-	-	-	-	-	-
13	-	-	-	-	-	-	-	-	-	-	-
14	-	-	-	-	-	-	-	-	-	-	-
15	67,0	-16,9	8,9	-10,9	-27,1	-26,6	58,7	25,8	80,7	53,0	297,8
16	-	-	-	-	-	-	-	-	-	-	-
18	-	-	-	-	-	-	-	-	-	-	-
Toplam	202,3	-30,9	-21,9	7,4	11,9	13,9	122,7	8,6	31,2	84,6	1208,9

BİR ÖNCEKİ YILA GÖRE ASFALT YAMA GİDERLERİ ORANSAL DEĞİŞİM (2012-2022)



Şekil 2. Bölge şubelerine göre 2012-2022 asfalt yama giderlerinin bir önceki yıla göre değişimi (%).

Tablo 3'te bölge şubelerine göre asfalt yama giderleri 2023-2025 tahmin sonuçlarına yer verilmiştir. Tahmin yöntemi olarak mevsimsel olmayan Winters yönteminden yararlanılmıştır. Tablo 3'teki Winters mevsimsel olmayan çift parametrelili yönteme göre tahmin sonuçları incelendiğinde asfalt yama giderlerinin 2025 yılında 182.842.408 TL değerine ulaşması, bölge düzeyinde incelendiğinde 2025 yılında en yüksek asfalt yama giderinin 1. Bölgede olması beklenmektedir.

Tablo 3. Bölge şubelerine göre asfalt yama giderleri 2023-2025 tahmin sonuçları

Bölge	2023	2024	2025
1	77.877.801	96.769.201	115.660.601
15	35.305.439	44.806.123	54.306.807
Toplam	119.546.671	151.194.540	182.842.408

3.1.2. Bölge şubelerine göre 2012-2022 üstyapı yenilenmesi ve yol iyileştirme giderlerine ilişkin bulgular

Tablo 4'te bölge şubelerine göre 2012-2022 üstyapı yenilenmesi ve yol iyileştirme giderlerine yer verilmiştir. Tablo 4'deki üstyapı yenilenmesi ve yol iyileştirme giderleri incelendiğinde en yüksek üstyapı yenilenmesi ve yol iyileştirme giderinin 2022 yılında gerçekleştiği, 2012 yılında en yüksek üstyapı yenilenmesi ve yol iyileştirme giderinin 7 ve 4. bölgelerde olduğu, 2022 yılında ise yalnızca 1, 3 ve 12. bölgelerde karşılaştırılabilir olduğu ve en yüksek üstyapı yenilenmesi ve yol iyileştirme giderinin 12. Bölgede olduğu görülmektedir. Şekil 3'te 2012-2022 yılları arasında üstyapı yenilenmesi ve yol iyileştirme giderlerinin yıllara göre seyrine ait görünüme yer verilmiştir.

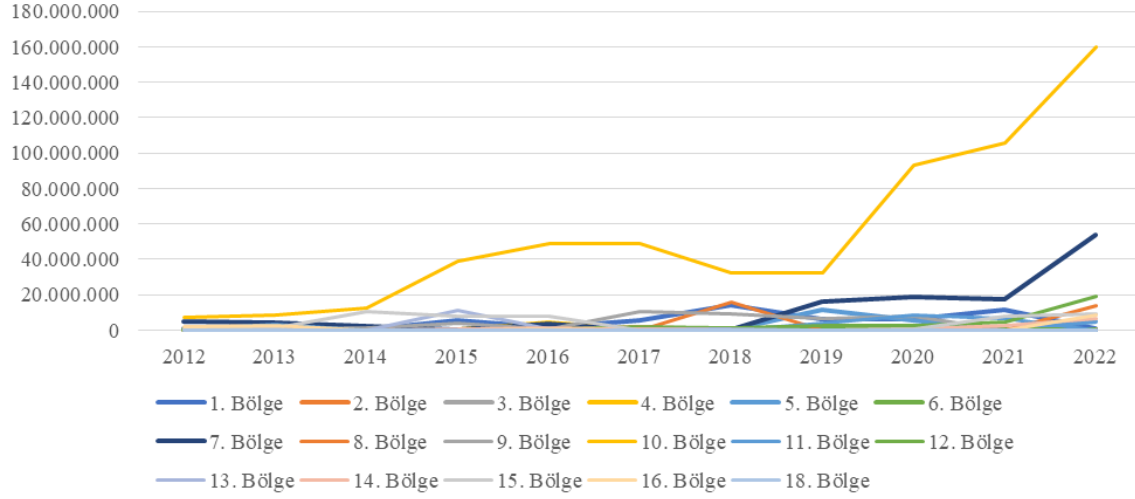
Tablo 4. Bölge şubelerine göre 2012-2022 üstyapı yenilenmesi ve yol iyileştirme giderleri

Bölge	2012	2013	2014	2015	2016	2017	2018	2019	2020	2021	2022
1	1.384.086	740.863	3.846.953	2.519.928	1.349.859	1.921.822	1.186.327	401.106	1.376.195	6.150.807	6.341.952
2	2.105.301	0	0	514.411	380.233	504.616	7.183.622	3.038.965	0	0	0
3	2.593.198	1.814.425	0	1.393.618	1.747.194	3.074.790	3.113.997	3.606.974	5.175.120	4.270.331	17.403.155
4	4.626.665	0	418.379	0	5.136.727	447.137	0	0	0	0	0
5	1.329.500	1.675.306	0	2.538.257	4.430.515	0	0	0	0	4.274.539	0
6	976.173	2.873.343	0	1.768.348	2.267.702	1.869.738	7.041.785	15.163.238	5.253.724	6.813.397	0
7	4.932.640	3.282.800	0	0	0	0	0	1.585.298	0	0	0
8	890.412	138.296	754.375	2.036.145	3.465.420	0	0	0	0	0	0
9	56.934	0	0	1.907.069	1.064.537	5.309.664	1.775.977	2.524.750	10.029.450	6.856.026	0
10	2.819.622	0	0	0	0	0	0	0	0	0	4.196.281
11	4.041.982	0	0	0	3.064.607	3.877.221	6.285.448	5.310.435	2.325.771	869.461	7.037
12	3.732.976	453.120	0	0	124.254	4.808.790	1.979.263	2.354.240	1.866.157	2.812.331	22.150.278
13	2.124.778	0	0	0	0	330.326	3.401.232	0	0	0	0
14	0	0	0	1.910.836	1.327.438	2.205.392	2.503.793	0	0	0	0
15	0	6.622.504	4.349.650	3.903.634	5.369.508	4.207.079	0	317.902	894.502	2.337.948	0
16	664.312	0	0	0	0	0	0	0	0	0	0
18	0	190.806	34.250	501.766	669.495	0	0	0	0	0	0
Toplam	32.278.579	17.791.462	9.403.607	18.994.011	30.397.487	28.556.574	34.471.443	34.302.910	26.920.919	34.384.841	50.098.702

Tablo 4'deki üstyapı yenilenmesi ve yol iyileştirme giderleri incelendiğinde en yüksek üstyapı yenilenmesi ve yol iyileştirme giderinin 2022 yılında gerçekleştiği, 2012 yılında en yüksek üstyapı yenilenmesi ve yol iyileştirme giderinin 7 ve 4. bölgelerde olduğu, 2022 yılında ise yalnızca 1, 3 ve 12. bölgelerde

karşılaştırılabilir olduğu ve en yüksek üstyapı yenilenmesi ve yol iyileştirme giderinin 12. Bölgede olduğu görülmektedir. Şekil 3'te 2012-2022 yılları arasında üstyapı yenilenmesi ve yol iyileştirme giderlerinin yıllara göre seyrine ait görünüme yer verilmiştir.

BÖLGELERE GÖRE ÜSTYAPI YENİLENMESİ VE YOL İYİLEŞTİRME GİDERLERİ (2012-2022)



Şekil 3. Bölge düzeyinde 2012-2022 üstyapı yenilenmesi ve yol iyileştirme giderlerinin seyri.

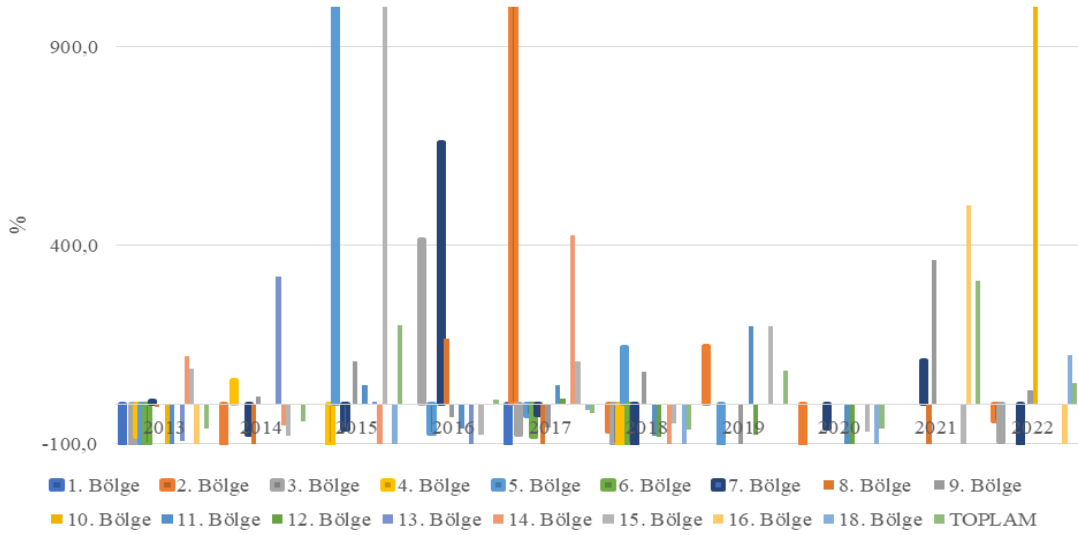
Tablo 5'te bölge şubelerine göre 2012-2022 üstyapı yenilenmesi ve yol iyileştirme giderlerinin bir önceki yıla göre değişimine yer verilmiştir. Tablo 5'e göre bir önceki yıla göre oransal olarak en fazla artış %311 ile 2021 yılında gerçekleşmiştir. 2012 yılı baz alındığında 2022 yılında meydana gelen toplam üstyapı yenilenmesi ve yol

iyileştirme gideri %1,8 azalış düzeyindedir. Bölge düzeyinde bir önceki yıla göre oransal olarak en fazla artış %4088 ile 2017 yılında 2. bölgede gerçekleşmiştir. Şekil 4'te 2012-2022 yılları arasında üstyapı yenilenmesi ve yol iyileştirme giderlerindeki oransal artışın bölge düzeyindeki seyrine ait görünüme yer verilmiştir.

Tablo 5. Bölge şubelerine göre 2012-2022 üstyapı yenilenmesi ve yol iyileştirme giderlerinin bir önceki yıla göre değişimi (%)

Bölge	2013	2014	2015	2016	2017	2018	2019	2020	2021	2022	13-22
1	-	-	-	-	-	-	-	-	-	-	-
2	-	-	-	-	4088,4	-70,2	146,2	-	-	-43,6	-
3	-	-	-	415,9	-77,1	-	-	-	-	-95,6	-91,3
4	-82,3	59,9	-	-	-	-	-	-	-	-	-
5	-	-	4194,5	-74,4	-30,9	143,9	-	-	-	-	-
6	-	-	-	-	-81,6	-	-	-	-	-	-70,2
7	8,9	-76,9	-64,7	659,7	-28,0	-	-	-60,2	111,3	-	-
8	-7,3	-	-	165,4	-	-	-	-	-	-	-
9	-	20,5	106,7	-32,8	-59,8	80,8	-	-	362,0	34,8	-
10	-	-	-	-	-	-	-	-	-	1686,2	-45,6
11	-	-	46,9	-62,0	48,6	-80,5	197,4	-	-	-	-
12	-	-	-	-	15,3	-82,4	-77,9	-	-	-	-
13	-91,8	321,3	6,8	-	-	-	-	-	-	-	182,4
14	120,1	-52,4	-	-	424,6	-	-	-	-	-	354,6
15	89,6	-79,2	1054,9	-77,8	108,6	-48,2	196,9	-69,1	-	-	-
16	-	-	-	-	-	-	-	-	500,8	-99,1	-98,5
18	-	-	-	-	-14,4	-	-	-	-	123,7	-
Toplam	-60,6	-42,7	200,2	12,8	-20,9	-64,6	83,4	-60,0	311,9	52,2	-1,8

BİR ÖNCEKİ YILA ÜSTYAPI YENİLENMESİ VE YOL İYİLEŞTİRME GİDERLERİ ORANSAL DEĞİŞİM (2012-2022)



Şekil 4. Bölge şubelerine göre 2012-2022 üstyapı yenilenmesi ve yol iyileştirme giderlerinin bir önceki yıla göre değişimi (%)

Tablo 6’de bölge şubelerine göre üstyapı yenilenmesi ve yol iyileştirme giderleri 2023-2025 tahmin sonuçlarına yer verilmiştir. Tahmin yöntemi olarak mevsimsel olmayan Winters yönteminden yararlanılmıştır. Tablo 6’deki Winters mevsimsel olmayan çift parametrelili yönteme göre tahmin sonuçları incelendiğinde üstyapı yenilenmesi ve yol iyileştirme giderlerinin yalnızca 1. Bölge ve toplam olarak hesaplanabildiği, 2025 yılında 34.245.643 TL değerine ulaşması beklenmektedir.

Tablo 6. Bölge şubelerine göre üstyapı yenilenmesi ve yol iyileştirme giderleri 2023-2025 tahmin sonuçları

Bölge	2023	2024	2025
9	20.875.243	25.283.165	29.691.087
Toplam	41.522.724	37.884.184	34.245.643

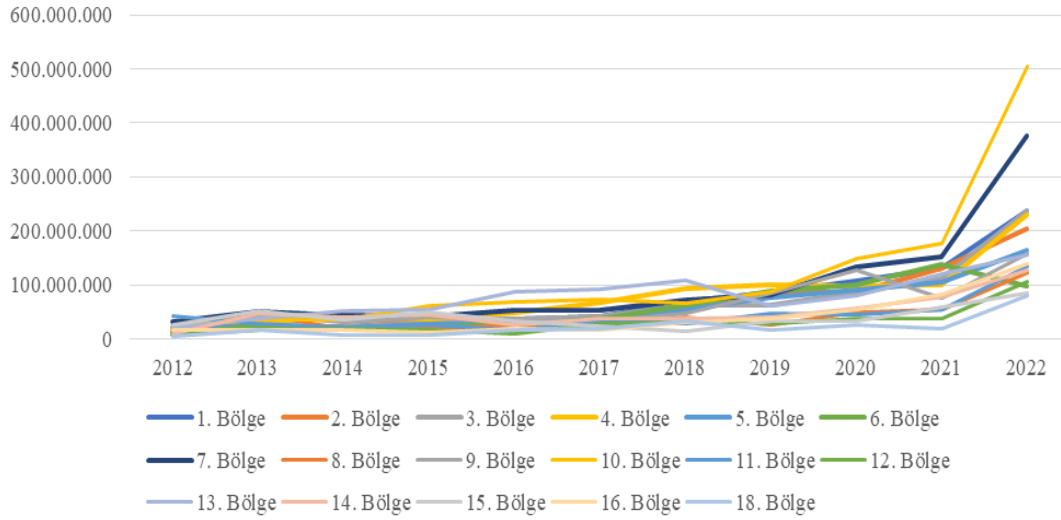
3.2. Bölge Şubelerine Göre 2012-2022 Asfalt Yol Bakım Toplam Giderlerine İlişkin Bulgular

Tablo 7’de bölge şubelerine göre 2012-2022 asfalt yol bakım toplam giderlerine yer verilmiştir. Tablo 7’deki asfalt yol bakım toplam giderleri incelendiğinde en yüksek asfalt yol bakım toplam giderinin 2022 yılında gerçekleştiği, bölge düzeyinde incelendiğinde 2022 yılında 10. Bölgede en yüksek asfalt yol bakım giderinin olduğu görülmektedir. 2012 yılında en yüksek asfalt yol bakım toplam giderinin 11. Bölgede olduğu, 2022 yılında ise en yüksek asfalt yol bakım toplam giderinin 10. Bölgede olduğu görülmektedir. Şekil 5’te 2012-2022 yılları arasında asfalt yol bakım toplam giderlerinin yıllara göre seyrine ait görünümü yer verilmiştir.

Tablo 7. Bölge şubelerine göre 2012-2022 asfalt yol bakım toplam giderleri

Bölge	2012	2013	2014	2015	2016	2017	2018	2019	2020	2021	2022
1	9.809.777	25.222.020	23.554.739	32.075.933	37.715.190	42.336.008	69.816.414	86.492.251	107.469.838	129.947.556	236.568.920
2	16.352.577	35.670.512	39.720.455	28.701.713	28.724.829	41.178.314	51.968.990	85.655.108	85.401.115	130.714.578	202.953.537
3	10.327.216	21.733.788	21.604.069	28.905.883	35.742.559	42.379.037	61.505.020	63.695.973	86.706.965	112.886.595	236.433.618
4	18.685.730	29.650.559	42.839.894	36.894.022	49.239.185	67.830.843	92.912.628	100.086.881	97.348.783	100.363.772	229.123.708
5	22.270.852	22.066.463	19.016.433	26.457.023	29.012.996	34.377.928	55.431.264	77.773.386	90.290.929	105.089.678	163.641.530
6	8.553.097	24.839.865	20.443.362	23.450.584	27.813.359	35.618.614	61.654.244	88.769.178	99.737.245	137.308.169	97.241.416
7	30.748.196	50.759.709	43.216.319	40.337.853	52.534.155	52.754.644	72.929.416	81.940.648	133.545.626	152.027.011	377.250.887
8	18.214.608	44.849.118	19.799.215	19.709.750	26.236.558	25.643.722	40.396.034	26.726.426	50.666.032	54.184.877	123.731.051
9	17.411.421	45.241.000	30.386.291	40.636.511	35.834.773	32.890.681	47.224.900	85.939.080	126.952.938	75.653.629	157.921.672
10	23.001.639	36.571.797	35.580.437	60.509.096	67.591.364	73.165.461	66.012.351	87.555.775	149.633.793	176.964.857	204.684.552
11	43.095.177	28.882.705	21.451.268	25.539.532	16.902.135	32.442.829	28.665.288	46.374.696	45.168.185	55.150.808	134.989.856
12	7.621.555	16.009.476	18.527.308	17.658.452	8.911.739	29.279.268	30.589.961	28.077.316	37.100.993	37.907.886	106.640.365
13	20.234.203	38.051.455	52.364.636	54.308.682	86.306.602	92.670.055	107.449.405	62.016.254	80.962.692	120.088.121	155.597.902
14	10.640.175	48.298.539	39.526.129	43.726.557	25.023.124	38.498.750	36.717.142	39.563.098	56.530.713	77.195.035	127.670.516
15	24.972.649	52.431.619	34.641.105	50.475.857	33.311.991	24.462.788	15.171.068	32.876.203	32.131.075	59.437.348	85.147.719
16	17.164.608	16.604.085	16.873.278	10.953.257	18.890.235	17.652.196	29.655.778	38.485.952	53.819.247	81.530.300	139.770.151
18	4.260.750	17.509.702	7.638.574	6.992.909	16.281.430	17.935.691	32.360.880	16.096.977	25.517.154	19.489.472	80.365.837
Toplam	303.364.230	554.392.412	487.183.512	547.333.614	596.072.224	701.116.829	900.460.783	1.048.125.202	1.358.983.323	1.625.939.692	3.159.733.237

BÖLGELERE GÖRE ASFALT YOL BAKIM TOPLAM GİDERLERİ
(2012-2022)



Şekil 5. Bölge düzeyinde 2012-2022 asfalt yol bakım toplam giderlerinin seyri

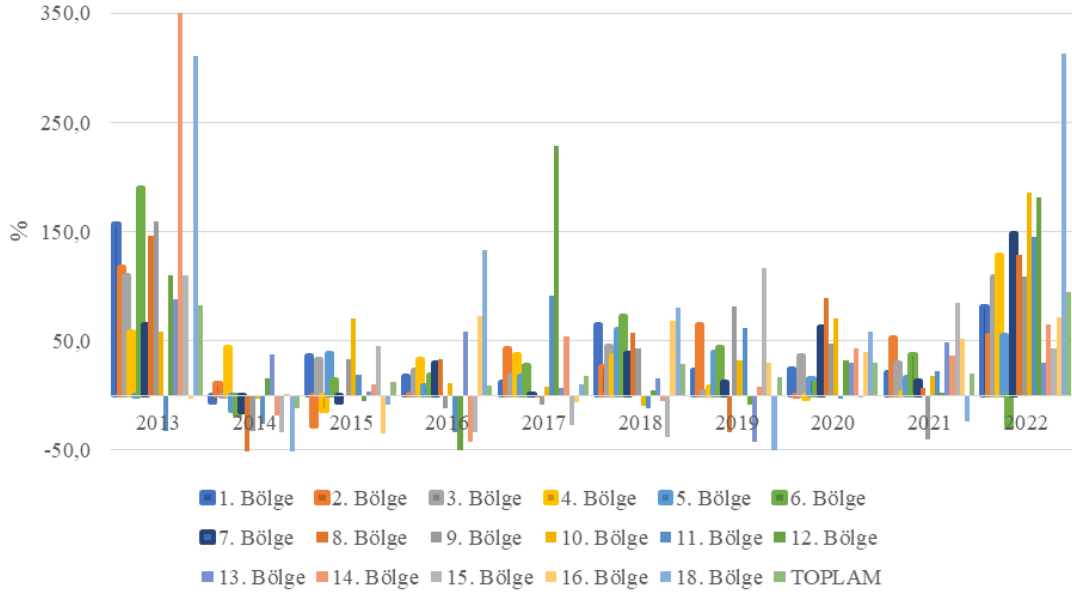
Tablo 8'de bölge şubelerine göre 2012-2022 asfalt yol bakım toplam giderlerinin bir önceki yıla göre değişimine yer verilmiştir. Tablo 8'e göre asfalt yol bakım toplam giderlerinde bir önceki yıla göre oransal olarak en fazla artış %82 ile 2013 yılında gerçekleşmiştir. 2012 yılı baz alındığında 2022 yılında meydana gelen toplam asfalt yol bakım gideri %941 artış düzeyindedir. Bölge düzeyinde bir önceki yıla göre oransal olarak en fazla artış %353 ile

2013 yılında 14. Bölgede gerçekleşmiştir. Bölge düzeyinde 2012 yılı baz alındığında 2022 yılında asfalt yol bakım giderlerinde en fazla artışın %2311 ile 1. Bölgede gerçekleştiği görülmektedir. Şekil 6'da 2012-2022 yılları arasında asfalt yol bakım toplam giderlerindeki oransal artışın bölge düzeyindeki seyrine ait görünüme yer verilmiştir.

Tablo 8. Bölge şubelerine göre 2012-2022 asfalt yol bakım toplam giderlerinin bir önceki yıla göre değişimi (%)

Bölge	2013	2014	2015	2016	2017	2018	2019	2020	2021	2022	13-22
1	157,1	-6,6	36,2	17,6	12,3	64,9	23,9	24,3	20,9	82,0	2311,6
2	118,1	11,4	-27,7	0,1	43,4	26,2	64,8	-0,3	53,1	55,3	1141,1
3	110,5	-0,6	33,8	23,7	18,6	45,1	3,6	36,1	30,2	109,4	2189,4
4	58,7	44,5	-13,9	33,5	37,8	37,0	7,7	-2,7	3,1	128,3	1126,2
5	-0,9	-13,8	39,1	9,7	18,5	61,2	40,3	16,1	16,4	55,7	634,8
6	190,4	-17,7	14,7	18,6	28,1	73,1	44,0	12,4	37,7	-29,2	1036,9
7	65,1	-14,9	-6,7	30,2	0,4	38,2	12,4	63,0	13,8	148,1	1126,9
8	146,2	-55,9	-0,5	33,1	-2,3	57,5	-33,8	89,6	6,9	128,3	579,3
9	159,8	-32,8	33,7	-11,8	-8,2	43,6	82,0	47,7	-40,4	108,7	807,0
10	59,0	-2,7	70,1	11,7	8,2	-9,8	32,6	70,9	18,3	185,2	2094,1
11	-33,0	-25,7	19,1	-33,8	91,9	-11,6	61,8	-2,6	22,1	144,8	213,2
12	110,1	15,7	-4,7	-49,5	228,5	4,5	-8,2	32,1	2,2	181,3	1299,2
13	88,1	37,6	3,7	58,9	7,4	15,9	-42,3	30,6	48,3	29,6	669,0
14	353,9	-18,2	10,6	-42,8	53,9	-4,6	7,8	42,9	36,6	65,4	1099,9
15	110,0	-33,9	45,7	-34,0	-26,6	-38,0	116,7	-2,3	85,0	43,3	241,0
16	-3,3	1,6	-35,1	72,5	-6,6	68,0	29,8	39,8	51,5	71,4	714,3
18	311,0	-56,4	-8,5	132,8	10,2	80,4	-50,3	58,5	-23,6	312,4	1786,2
Toplam	82,7	-12,1	12,3	8,9	17,6	28,4	16,4	29,7	19,6	94,3	941,6

BİR ÖNCEKİ YILA GÖRE ASFALT YOL BAKIM TOPLAM GİDERLERİ ORANSAL DEĞİŞİM (2012-2022)



Şekil 6. Bölge şubelerine göre 2012-2022 asfalt yol bakım toplam giderlerinin bir önceki yıla göre değişimi (%)

Tablo 9'da bölge şubelerine asfalt yol bakım toplam giderleri 2023-2025 tahmin sonuçlarına yer verilmiştir. Tahmin yöntemi olarak mevsimsel olmayan Winters yönteminden yararlanılmıştır. Tablo 9'daki Winters mevsimsel olmayan çift parametrelili yönteme göre

tahmin sonuçları incelendiğinde asfalt yol bakım toplam giderlerinin 2025 yılında 6.435.183.692 TL değerine ulaşması, bölge düzeyinde incelendiğinde 2025 yılında en yüksek yol bakım - onarım ve temizliği giderinin 1. Bölgede olması beklenmektedir.

Tablo 9. Bölge şubelerine göre asfalt yol bakım toplam giderleri 2023-2025 tahmin sonuçları

Bölge	2023	2024	2025
1	264.276.303	331.491.581	398.706.859
2	261.280.514	319.607.490	377.934.467
3	343.162.526	458.640.955	574.119.384
4	173.995.948	204.282.086	234.568.224
5	180.143.058	215.678.809	251.214.560
6	110.684.205	116.097.308	121.510.412
7	453.540.877	603.372.600	753.204.323
8	126.074.462	163.010.352	199.946.242
9	145.926.659	169.743.486	193.560.312
10	663.012.282	905.122.151	147.232.020
11	128.270.547	163.906.954	199.543.360
12	55.268.524	59.600.066	63.931.609
13	169.872.325	184.359.495	198.846.666
14	161.199.176	203.376.591	245.554.005
15	109.905.705	138.485.333	167.064.961
16	195.506.567	252.820.622	310.134.677
18	36.781.168	40.337.082	43.892.997
Toplam	4.027.182.221	5.231.182.956	6.435.183.692

4. Sonuç

Trafik hacmi ve buna bağlı olarak, kaplama gerilmelerindeki artış, üstyapı problemlerinin daha sık yaşanmasına ve yolların servis ömürlerinde azalmalara,

yol bakım maliyetlerinde artmalara sebep olmaktadır. Bu durum ise ekonomik yönden büyük kayıpları beraberinde getirmektedir. Çalışma sonuçları incelendiğinde, yıllara göre belirlenen bölgelerde asfalt

yol bakım giderlerinin giderek arttığı 2025 yılı için yapılan tahmine göre de, artmaya devam edeceği tespit edilmiştir. Bölgesel olarak artışların en çok 1. Bölge olarak Karayolu Genel Müdürlüğü tarafından İstanbul iline ait olacağı belirlenmiştir. Başta endüstriyel anlamda hızla gelişen ve gelişmekte olan 1. Bölgenin ve ardından diğer bölgelerin, rakamsal olarak gelecek tahmini yol bakım maliyetinin azaltılması ülke ekonomisine büyük ölçüde katkı sağlayacaktır. Bu maliyetlerin azaltılabilmesi için alınabilecek önlemler şu şekilde sıralanabilir:

- Maliyet analizi yapılmalı, yıllık olarak öngörülen harcamalar için mali bütçe hazırlanmalı ve burada bir kısma olmaksızın uygulanabilmelidir.
- Bilimsel birtakım çalışmaya yol gösterebilmesi için ülkemizde yapılan yol bakım verilerinin sağlıklı bir şekilde kayıt altına alınması oldukça önemlidir.
- Yola ait, gerekli düzeyde yeterli bakım yaparak yol üst yapısının dayanımını yükseltilmelidir.
- Bölgesel bazda iklim koşullarının göz önünde bulundurularak uygulamalar yapılmalıdır.

Katkı Oranı Beyanı

Yazarın katkı yüzdesi aşağıda verilmiştir. Yazar makaleyi incelemiş ve onaylamıştır.

	F.Ö.K.
K	100
T	100
Y	100
VTI	100
VAY	100
KT	100
YZ	100
KI	100
GR	100
PY	100
FA	100

K= kavram, T= tasarım, Y= yönetim, VTI= veri toplama ve/veya işleme, VAY= veri analizi ve/veya yorumlama, KT= kaynak tarama, YZ= Yazım, KI= kritik inceleme, GR= gönderim ve revizyon, PY= proje yönetimi, FA= fon alımı.

Çatışma Beyanı

Yazar bu çalışmada hiçbir çıkar ilişkisi olmadığını beyan etmektedirler.

Etik Onay Beyanı

Bu çalışmada hayvanlar ve insanlar üzerinde herhangi bir çalışma yapılmadığı için etik kurul onayı alınmamıştır.

Kaynaklar

- Bowerman BL, Connell RTO. 1979. Time series and forecasting: an applied approach. Duxbury Press, New York, USA, pp: 145.
- Canver S, Halit Ö, Saraçoğlu A, Maltaş A. 2020. Yol geometrik standartlarının karayolu işletme maliyetleri üzerindeki etkisinin incelenmesi. Mehmet Akif Ersoy Üniv Uygulamalı Bilim Derg, 4(1): 209-226.
- Carnahan JV, Davis WJ, Shahin MY, Keane PL, Wu MI. 1986. Optimal maintenance decisions for pavement management. J Transport Engin, 113(5): 554-572.
- Çetin B, Barış S, Saroğlu S. 2011. Türkiye’de karayollarının gelişimine tarihsel bir bakış. Çankırı Karatekin Üniv İktisadi İdari Bilim Fak Derg, 1(1): 123-150.
- Chong GJ. 1989. Rout and seal cracks in flexible pavement – a cost-effective preventive maintenance procedure. Ontario Ministry of Transport Rec, 1268: 8- 16.
- Çuhadar M. 2014. Muğla iline yönelik dış turizm talebinin modellenmesi ve 2012-2013 yılları için tahminlenmesi. Inter J Econ Administ Stud, 6(12): 1307-9832.
- Irmak S, Köksal CD, Asilkan Ö. 2012. Hastanelerin gelecekteki hasta yoğunluklarının veri madenciliği yöntemleri ile tahmin edilmesi. Uluslararası Alanya İşletme Fak Derg, 4(1): 101-114.
- Karahacıoğlu İA, Corum A. 2020. Asfalt yolların yaşam döngüsü maliyet analizi: İstanbul O3 otoyolunda uygulanması. Inter J Engin Res Develop, 12(1): 32-39.
- Kuloğlu N, Kök BV, Öndaş M. 2004. Sathi kaplamalarda kusma olayına etki eden faktörler. 4. Ulusal Asfalt Sempozyumu, 25-26 Aralık, Ankara, Türkiye, pp: 141-148.
- Labi S, Sinha KC. 2003. The effectiveness of maintenance and its impact on capital expenditures. Joint Transportation Research Program, Indiana Department of Transportation and Purdue University, West Lafayette, Indiana, pp: 64.
- Lamprey G, Ahmad MZ, Labi S, Sinha KC. 2005. Life cycle cost analysis for INDOT pavement design procedures. Joint Transportation Research Program, Indiana Department of Transportation and Purdue University, West Lafayette, Indiana, pp: 128.
- Mamlouk MS, Dosa M. 2014. Verification of effectiveness of chip seal as a pavement preventive maintenance treatment using LTPP data. Int J Pavement, 15(10): 879-888.
- Öztürk E. A. 2004. Karayolu esnek üst yapı tasarımında yeni bir yöntem: yüksek performanslı asfalt kaplama. Gazi Üniv Müh Mimar Fak Derg, 19(2): 175-184.
- Ponniah JE, Kennepohl GJ. 1996. Crack sealing in flexible pavements: a life-cycle cost analysis. Transp Res Rec, 1529: 86-94.
- Qiao Y, Fricker J. D, Labi S. 2019. Influence of project bundling on maintenance of traffic costs across highway project types. J Construct Engin Manage, 145(8): 05019010.
- Tee KF, Ekpiwhre E. 2020. Strategic cost modelling and optimisation for highway asset maintenance. J Qual Mainten Engin, 26(2): 198-212.
- Tsunokawa K, Islam R, Changyu G. 2002. Optimal strategies for highway pavement management in developing countries. Comput Aided Civil Infrast Engin, 17: 194-202.



UTILIZATION OF SLIP CASTING PROCESS FOR RECYCLING CAD/CAM DENTAL ZIRCONIA WASTES

Cemile Betül EMRULLAHOĞLU ABİ^{1*}, Hatice Şule ÇOBAN TETİK^{2,3}, Erdinç ABİ⁴

¹Afyon Kocatepe University, Department of Materials Science and Engineering, 03200, Afyonkarahisar, Türkiye

²Ağrı İbrahim Çeçen University, Central Research and Application Laboratory, 04100, Ağrı, Türkiye

³Ağrı İbrahim Çeçen University, Department of Computer Engineering, 04100, Ağrı, Türkiye

⁴Afyon Kocatepe University, Afyon Vocational School, 03200, Afyonkarahisar, Türkiye

Abstract: This study aimed to find the ideal parameters for shaping waste zirconia powders from dental laboratories using the slip-casting process. Additionally, the qualities of ceramic products created in this manner were evaluated using microstructural characterization and physical-mechanical tests. Various dental laboratories provided the waste CAD/CAM zirconia powder used in the investigation. Wastes in powder form were first calcined. Afterward, an attritor mill was used to grind the grain size until it was usable, following the completion of the grain size distribution analysis. Waste and commercial zirconia powders were combined using various dispersants to create slip-casting slurries. The rheological characteristics of these slurries were then ascertained. By evaluating the rheological properties of slip-casting slurries prepared in this way, the most suitable casting parameters were determined, and ceramic products were formed by slip-casting technique from the slurries to be prepared in accordance with these parameters. The shaped samples were dried and sintered at two different temperatures, 1400-1450°C, and samples were designed for physical, mechanical, and microstructural characterization. The pore percentages, bulk densities, and water absorption of the sintered samples, according to Archimedes' principle, as well as their strengths, were determined by the three-point bending strength test. Phase analysis was performed with XRD (X-ray diffractometer) microstructure studies with SEM (Scanning Electron Microscopy). It has been concluded that waste zirconia can be used in dental applications.

Keywords: Dental zirconia, Waste zirconia, CAD/CAM, Slip casting, Recycling

*Corresponding author: Afyon Kocatepe University, Department of Materials Science and Engineering, 03200, Afyonkarahisar, Türkiye

E mail: cbetul@aku.edu.tr (C. B. EMRULLAHOĞLU ABİ)

Cemile Betül EMRULLAHOĞLU ABİ  <https://orcid.org/0000-0003-0326-6122>

Hatice Şule ÇOBAN TETİK  <https://orcid.org/0000-0002-4775-9706>

Erdinç ABİ  <https://orcid.org/0000-0002-7041-364X>

Received: February 12, 2024

Accepted: March 15, 2024

Published: May 15, 2024

Cite as: Emrullahoğlu Abi CB, Çoban Tetik HŞ, Abi E. 2024. Utilization of slip casting process for recycling CAD/CAM dental zirconia wastes. BSJ Eng Sci, 7(3): 401-408.

1. Introduction

Zirconia (ZrO₂) is one of the most attractive dental materials, with the most research today. Yttria-stabilized tetragonal zirconia (Y-TSZ) was first used in biomedical applications in orthopedics in hip joints thanks to its excellent mechanical properties and biocompatibility (Christel et al., 1989; Denry and Kelly, 2008; Kelly and Benetti, 2011; Zhang and Lawn, 2018).

In dentistry, zirconia is preferred in orthodontic applications, post and support systems, and implants. Among these, its use of ceramic supports in crown and bridge prostheses constitutes the most considerable portion. High mechanical strength (900-1200 MPa) and fracture toughness (9-10 MPa.m^{1/2}) make using zirconia in crown and bridge applications on front and back teeth is possible. Zirconia support is obtained by processing semi-sintered and fully sintered blocks in automatic or manual devices with computer-aided design/computer-aided manufacturing (CAD/CAM) systems. While some blocks used after shaping become products, most become waste. Waste zirconia in powder and block form can be reused for different purposes by going through various

processes. Considering the economic and environmental factors, it is crucial to evaluate these material wastes, which are widely used today (Shenoy and Shenoy, 2010; Madfa et al., 2014; Mundhe et al., 2015; Duraccio et al., 2015; Gautam et al., 2016; Zhang et al., 2016).

However, the use of different production methods in evaluating dental zirconia waste has been examined in a limited way in the literature, and a basic understanding has not been provided yet. Another production method that is alternative to this production method is the slip casting method. Slip casting is one of the methods used for many years in shaping ceramics. This method is carried out by pouring slurry onto the refractory mold. Thanks to the porous structure of the refractory mold, water is removed from the mud by the capillary effect. This piece is then thickened by firing at high temperatures. Ceramics shaped by slip casting have less porosity and higher density than traditional porcelains (Pröbster and Diehl, 1992; Denry, 1996; Denry and Holloway, 2010; Shen, 2013).

Gouveia et al. (2017) in their study, various physical and mechanical properties of the samples obtained by



sintering the powder consisting of 100% CAD/CAM zirconia waste and the mixtures they prepared by adding 5-10-15% waste by volume to commercial zirconia powder and sintering at 1500 °C. According to their results, they concluded that the residue powders are highly suitable for prosthodontic zirconia sandblasting, as well as raw materials in refractory and pigment industries. In another study, Guazzato et al. (2004), in their research on zirconia-based ceramics, showed that the flexural strength (630±58 MPa) they obtained for In-Ceram Zirconia (IZ) processed by slip casting was higher than that of machine-processed ones (476±50 MPa). On the other hand, new applications are being tried in slip-casting studies. Roulet et al. (2021), in a survey conducted by Y-TZP, ceramics produced using a patent-pending slip casting method (Slurry, Decema GmbH) were compared with the hot isostatic pressing (HIP) method. As a result, the biaxial bending strength and characteristic strength of ceramics produced using the Slurry method were significantly higher than those of ceramics produced using HIP. In addition, dispersants are used for good shaping in ceramics. Dispersant selection is significant in obtaining a well-dispersed powder and a homogeneous ceramic suspension. The interaction of dispersant and ceramic powder is one of the most critical parameters. Therefore, it should be well characterized when choosing a dispersant. To determine dispersion properties, sedimentation and viscosity behaviors of suspensions are generally examined at the macroscopic scale (Schultz and Burckhardt, 1993; Singh et al., 2004). Studies show that evaluating both waste zirconia and considering alternative methods is essential. Since dental zirconia is expensive and imported into our country, the country's economy needs to be recycled. Therefore, in this study, optimum parameters were determined for shaping CAD/CAM tetragonal zirconia waste powders from dental laboratories using the slip casting method, and the usability of these materials in the production of high-density ceramic materials such as dental ceramics was evaluated with various physical and mechanical tests and microstructure characterization.

2. Materials and Methods

2.1. Starting Materials

Commercial yttria-stabilized zirconia powder from Saint-Gobain Ceramics (SGZ) with high purity and waste zirconia (ZrO₂) powders (WZ) gathered from several dental prosthesis laboratories of the machining CAD/CAM were employed in this investigation. Table 1 presents the suppliers' information, including the chemical composition, grain size distribution, and specific surface area. On the other hand, Darvan 821-A and Darvan C-N (Vanderbilt Minerals, LLC) dispersants, which are used in shaping ceramics by slip casting, were used in the experiments. The first of the dispersants used in this study is Darvan 821 A, an ammonium polyacrylate with a molecular weight of 3500g/mol and pH between 7 and 8 at room temperature. The second one is Darvan C-

N ammonium polymethacrylate with a molecular weight of 15000g/mol and pH between 7.5 and 9 at room temperature. In addition, polyethylene glycol was used as a binder.

Table 1. Chemical yttria-stabilized zirconia powder from saint-gobain ceramics

Chemical composition	wt%	ppm
LOI	0.61	
Y ₂ O ₃	5.56	
Na ₂ O		<10
Fe ₂ O ₃		10
SiO ₂		135
TiO ₂		<10
CaO		<15
MgO		25
Al ₂ O ₃		<20
SiO ₄ ⁻²		<100
Cl ⁻		<50
Physical properties	µm	m ² /g
Grain size distribution		
D10	0.15	
D50	0.57	
D90	1.44	
Specific surface area		6.4

2.2. Preparing Recycled Powder, Slip-Casting Slurry and Testing Samples

Materials such as wax processed on the same device can also be mixed into the waste powders generated from zirconia blocks processed with CAD/CAM in dental laboratories. For this reason, the waste powders were calcined at 850 °C for 2 hours to remove wax before use. The powder residues from the machining process presented a more extensive particle size distribution than the commercial powders. The commercial powders gave D50;0.57; the residues ranged from 0.1 to 1000 µm. The waste powder was ground with an attritor milling for 2 hours in isopropyl alcohol to match the commercial powder's mean size. Then, the slip-casting slurry was prepared to be 65% solid and 35% water. 6% by weight of selected dispersant and 2% by weight of binder were added and mixed in a magnetic stirrer for 2 hours. The prepared mixture was shaped by the slip-casting method. After the shaped samples were removed from the mold, they were kept covered with nylon for 4–5 days in order to dry slowly and in a humid environment, and then they were dried in an oven at a speed of 5 °C/hour to 100 °C and dried at this temperature for 1 night. The dried samples were pre-sintered at 1000 °C, and then their surfaces were smoothed and their dimensions adjusted using grinding and polishing machines. The oven was allowed to cool naturally after the sintering process, which was conducted at temperatures of 1400 and 1450 °C with a heating rate of 5 °C/min for two hours.

2.3. Characterization

In the first phase of this study, Zeta potential and

sedimentation tests were carried out to determine the optimum parameters for shaping two groups of samples consisting of zirconia and waste zirconia powders. Zeta potential measurements were made between pH 1-10 to determine both zirconia powders' isoelectrostatic points (IEP). Measurements were made on the Malvern Nano-Z Zeta potential measuring device. Sedimentation tests were conducted on zirconia powders in the pH range of 1 to 10. Subsequently, two distinct dispersants were added at pH 7 with different additive ratios for both zirconia powders. Tests were performed using 4 wt% zirconia powder in 25 mL tubes. First, the pH of the required amount of deionized water for each pH was fixed using HCl or NaOH. Then, the same amount of powder was weighed for each tube, added into the pH-adjusted water, and mixed in a magnetic stirrer for 4 hours. At the end of 4 hours, pH measurement was made, the suspension was transferred into the tube, its mouth was closed, and the height of the suspension was measured (h0). After being kept vertically for 24 hours, the height of the precipitate formed was measured and recorded (h). Finally, h/h0 values were calculated for the tubes prepared according to each pH value. These processes were repeated for both zirconia and dispersants for increasing amounts of dispersant (0-0.2-0.4-0.6-0.8-1 wt%) at pH 7. The total porosity, mass density, and water absorption percentages of the sintered samples were calculated based on Archimedes' method. The equation 1 calculated the relative density:

$$D = \rho / \rho_0 \times 100 \quad (1)$$

where ρ_0 is the theoretical density of yttrium-stabilized tetragonal zirconia polycrystals (6.10 g/cm^3 (Jiang et al., 2011)). A cold modulus of rupture (3-point bending strength) test was applied to the samples to measure the strength of the materials. The tests were conducted on a Shimadzu AG-IS model 100kN capacity mechanical testing device. Three-point bending strength tests followed ISO 6872 'Dental Ceramic' Standard. Furthermore, SEM microstructure investigations and XRD phase analysis were performed on the samples.

3. Results and Discussion

3.1. Waste Zirconia Characterization

First, it was necessary first to analyze the crystal phases and particle sizes to comprehend the existing state of waste zirconia. Figure 1a presents the particle size distribution, and Figure 1b X-ray diffraction pattern of sample WZ. The waste powders are currently undergoing examination for their potential application in dental ceramics. Their particle size distribution is quite complex, ranging from 0.1-1000 μm , and featuring multimodal modes. Upon conducting X-ray diffraction analysis, it was discovered that the powders contain monoclinic and tetragonal zirconia crystalline phases, which are highly desirable for dental ceramics. No other phases indicating contamination or impurities were detected during the analysis. Based on these findings, it can be confidently concluded that the waste powders are suitable for dental ceramics.

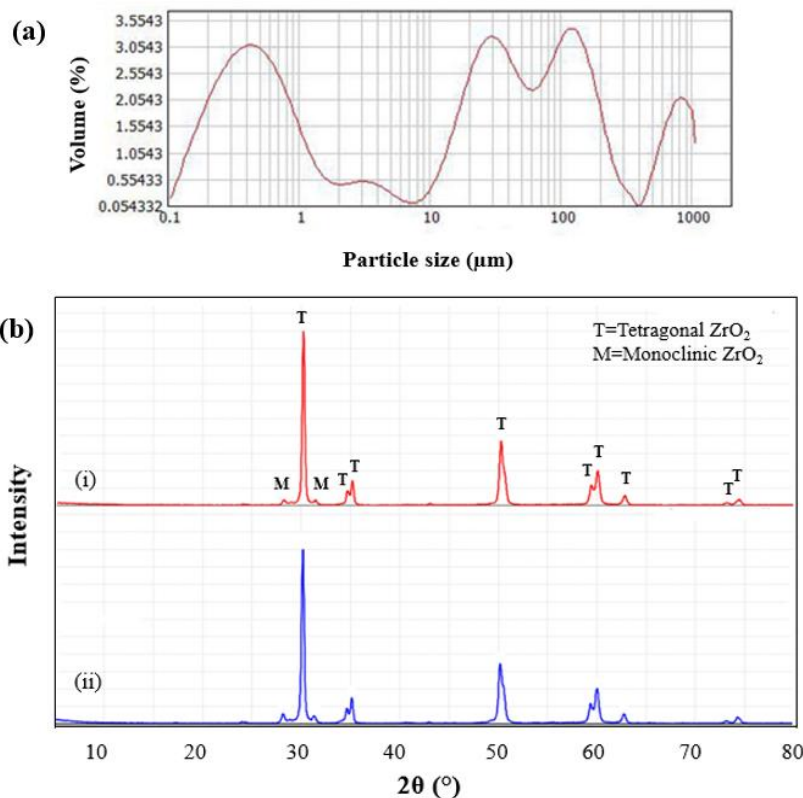


Figure 1. (a) Particle size distribution of waste zirconia (b)Waste zirconia, i-block, ii-powder XRD patterns.

3.2. Zeta Potential - Sedimentation Analysis and Preparing Testing Samples

The rheological properties of ceramic slurry depend on its pH, which determines its zeta potential. Zeta potential was measured to find the isoelectric points of SGZ and WZ samples. As a result of zeta potential measurements, it was observed that the IEP points of SGZ zirconia and WZ powders before the addition of dispersant were between pH = 6-7. Zeta potential plots are given in Figures 2a and 2b, respectively. It is seen that both zirconia have negative zeta potential values at pH values above IEP and positive zeta potential values at pH values below IEP. The obtained values agree with the reported values (Schultz and Burckhardt, 1993; Greenwood and Kendall, 1999; Agrafiotis et al., 2000).

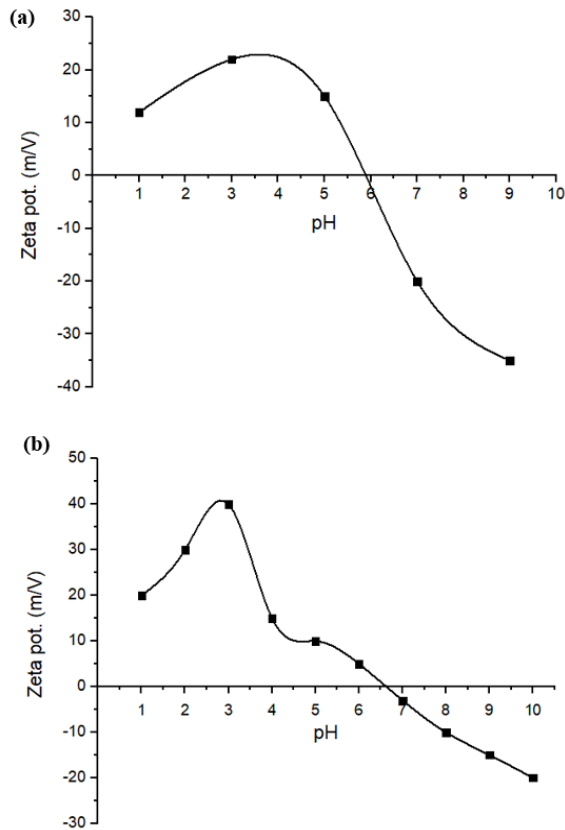


Figure 2. (a) SGZ and (b) WZ zeta potential graphs of zirconia at different pHs.

In the ceramic industry, knowing which dispersant provides the best stability in suspension is important. Determining how much dispersant should be added for economic reasons is vital (Greenwood and Kendall, 1999). For this purpose, Darvan 821-A and Darvan C-N dispersants were added to SGZ and WZ samples at ratios 0-0.2-0.4-0.6-0.8-1 wt% at pH 7, and sedimentation experiments were carried out. Both Darvans belong to the class of ammonium polymeric monomers that can disperse in water. This deflocculant can be used in ceramic dispersions, giving low viscosity slip and low foam production, being proper for extended times of mixture or grinding. Figures 3(a) and (b) show the sedimentation rates varying according to the amount of

Darvan 821-A and Darvan C-N dispersants added to SGZ and WZ, respectively. In both graphs, it is observed that the sedimentation rate decreases as the amount of dispersant increases. Both waste zirconia and commercial zirconia behaved more stable in Darvan C-N dispersant. Since there was no change in sedimentation rate after 0.6%, this rate was chosen for slurry containing 65% solid and 35% water. The same dispersant was used in previous studies on dental zirconia production using the slip casting method (Kim and Lee, 2020).

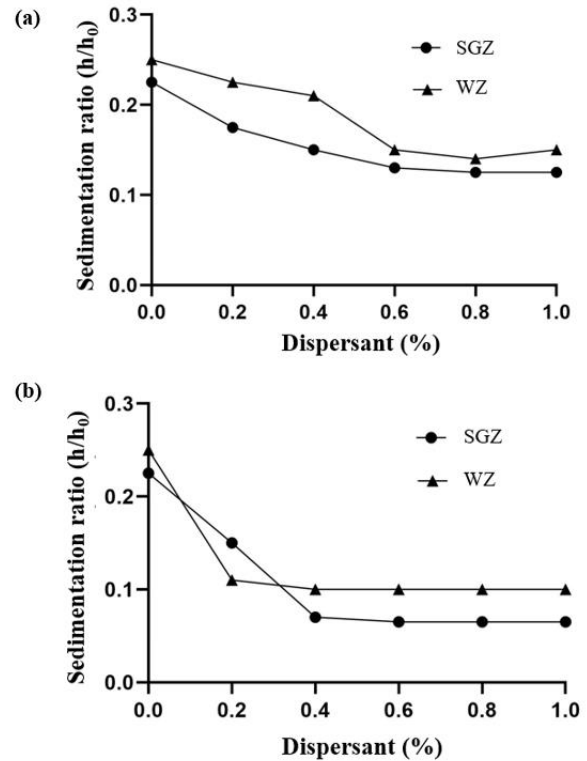


Figure 3. Changing sedimentation rates of waste zirconia and S.G. zirconia at pH7 with increasing rates of (a) Darvan 821A (b) Darvan C-N additive.

After determining the dispersion conditions, the slip-casting masses were prepared and transferred to the plaster mold, as can be seen in Figure 4a. Pre-heat treatment was applied at 1000 °C to ensure condensation after shaping and to smooth the surface. The sample obtained after pre-heat treatment is seen in Figure 4b.

3.3. Characterization of the Sintered Samples

XRD patterns of waste zirconia and commercial zirconia samples sintered at 1450 °C are given in Figure 5. When the XRD patterns are examined, it is seen that there is no change in the crystallographic structure after sintering; waste zirconia is mainly composed of tetragonal zirconia and contains a deficient proportion of monoclinic zirconia phase. In commercial zirconia, slightly higher monoclinic zirconia peaks were observed after sintering than in waste zirconia. Garvie et al. (1990) stated that zirconia can increase both the strength and toughness of ceramics due to the transformation of metastable tetragonal zirconia grains to monoclinic form by the effect of the stress field in front of a crack (Stevens 1986).

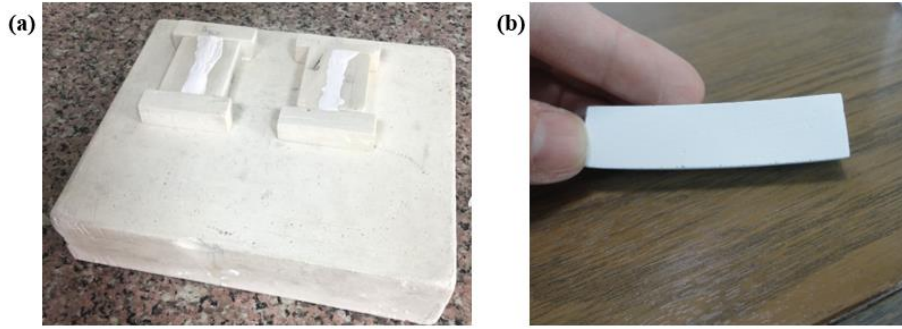


Figure 4. Image of (a) slip casting masses transferred to plaster mold (b) the sample obtained after pre-heat treatment.

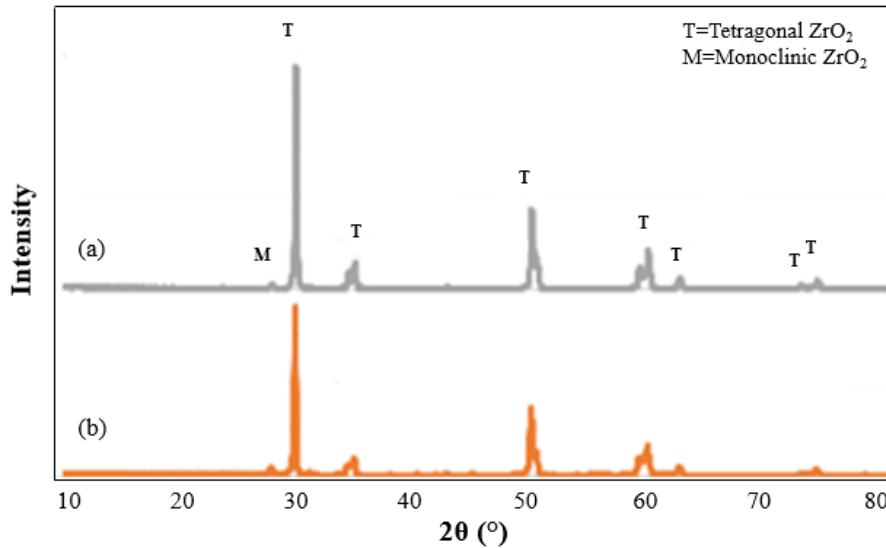


Figure 5. XRD patterns of samples containing 100% waste zirconia (a) and 100% commercial zirconia (b) sintered at 1450 °C.

The tetragonal-monoclinic phase transformation, similar to the martensitic transformation seen in steels, results in a 3 to 5% volume increase in the structure. Thus, in response to the tensile stress caused by the crack, a compressive stress field is formed in the matrix, especially at the crack's tip. This situation prevents crack propagation and increases the toughness of the ceramic (Christel et al., 1989; Piconi and Maccauro, 1999; Grigoriadou, 2006). For this reason, the waste zirconia must have the desired tetragonal structure so that it can be reused, especially in dental applications that require high fracture toughness.

Microstructure and grain size were analyzed by scanning electron microscopy. This analysis mainly aimed to compare waste and commercial zirconia. Figure 6 shows SEM images of waste zirconia sintered at 1400 °C and 1450 °C at high and low magnifications. It is clear from the microstructures that homogeneous and dense structures were obtained. As expected, relatively less porosity and a denser structure were observed in the samples sintered at 1450 °C. As the temperature increased, the crystal structure of zirconia became denser, reducing porosity, defects, and flaws. Figure 7 shows SEM images of commercial zirconia sintered at

1400 °C and 1450 °C at different magnifications. When the images of both samples are compared, it is seen that the microstructure obtained with waste zirconia is very similar to the microstructure of the samples obtained using commercial zirconia.

Figures 8a and 8b show the relative density and porosity values of sintered ceramics of waste and commercial zirconia as a function of temperature, respectively. The density increases, and porosity decreases with increasing temperature. According to Figure 8a, the relative density increased from 0.96 to 0.98 when the temperature was increased from 1400°C to 1450 °C, respectively. In addition, porosity decreased with increasing temperature. Density increases and porosity should decrease with increasing temperature. In Figure 8b, it is also seen that the relative density increases, and porosity decreases with increasing temperature. However, the density increased to 0.98% in waste zirconia and remained around 0.94% in commercial zirconia. The porosity value at 1450 °C was 1.95% in waste zirconia and 5.63% in commercial zirconia. The nearly 3-fold difference in porosity values increases the importance of using waste zirconia.

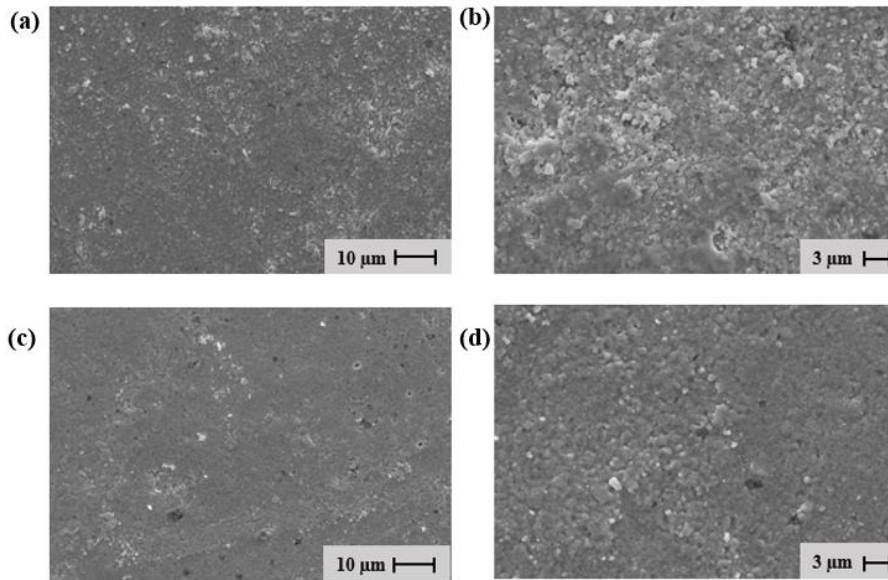


Figure 6. SEM images of waste zirconia samples sintered at different temperatures (a) - (b); 1400 °C, (c) - (d); 1450 °C.

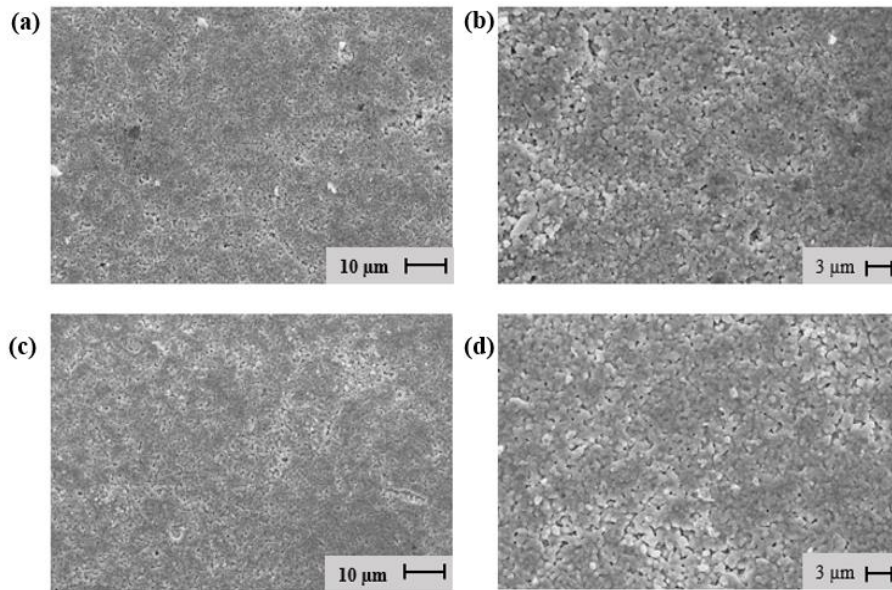


Figure 7. SEM images of commercial zirconia samples sintered at different temperatures (a) - (b); 1400 °C, (c) - (d); 1450 °C.

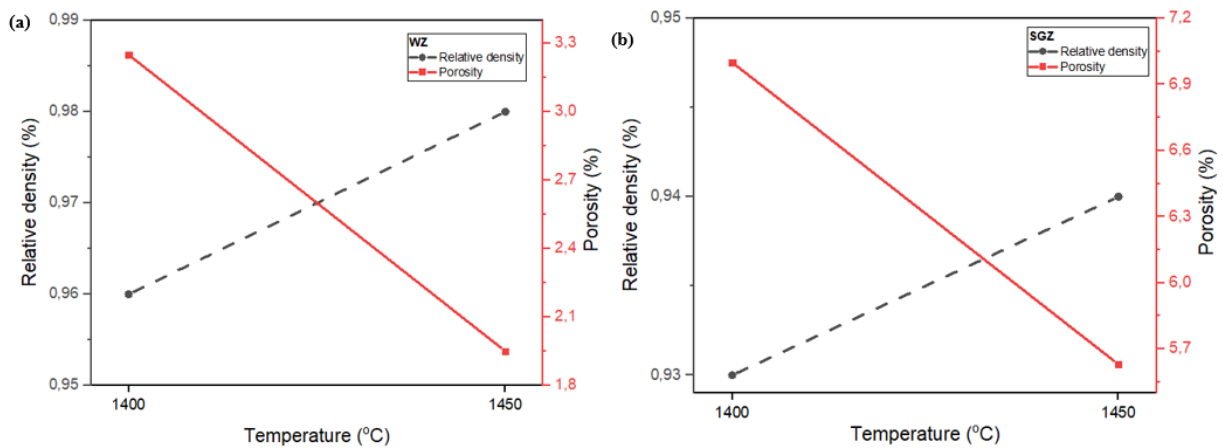


Figure 8. Evolution of relative density and porosity of (a) waste and (b) commercial zirconia as a function of temperature.

Figure 9 shows the 3-point flexural strength test results of waste and commercial zirconia sintered at 1400 and 1450 °C. According to this, it is seen that the bending strength of the samples obtained from waste at both temperatures is higher than the commercially purchased zirconia samples. The surface flaws of the tensile-stressed surface highly influence the 3-point bending strength of dental ceramics. This is because fractures typically initiate from surface defects. Additionally, the flexural strength of dental ceramics can be impacted by the shape and size of the specimens, as well as the test setup conditions (Jin et al., 2004).

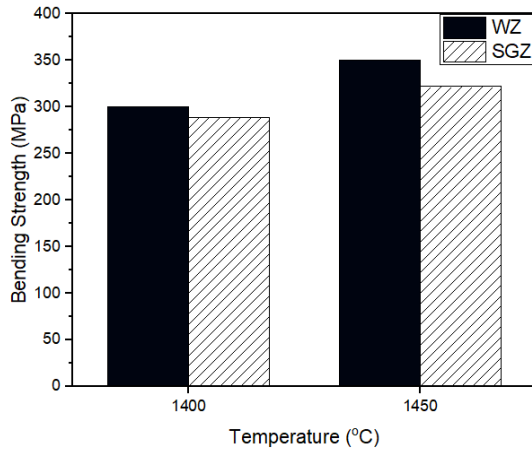


Figure 9. Bending strength of waste and commercial zirconia as a function of temperature.

4. Conclusion

As per the study's findings, the waste zirconia sintered at 1450 °C exhibited superior relative density (0.98%) and bending strength (350 MPa) compared to the commercially available Saint Gobain zirconia. Additionally, the porosity of the former was observed to be lower. These results imply that waste zirconia can be a feasible alternative to Saint Gobain zirconia in specific industrial applications. Based on the study's results, the powdered residues exhibit exceptional properties that make them highly suitable for dental ceramic zirconia. Therefore, it is possible to promote the utilization of waste powder generated from the zirconia CAD/CAM milling process. At the same time, this study has shown that dental ceramics can also be shaped by different methods, thus enabling less material loss. In the continuation of this study, zirconia wastes produced by other companies can be evaluated. The waste method is extremely important for the country's economy. With this study, it has once again shown that waste management is critical in every field.

Author Contributions

The percentage of the author(s) contributions is presented below. All authors reviewed and approved the final version of the manuscript.

	C.B.E.A.	H.Ş.Ç.T.	E.A.
C	100		
D	100		
S	100		
DCP	60		40
DAI	80		20
L	40	30	30
W	50	50	
CR	40	30	30
SR	40	30	30
PM	100		
FA	100		

C=Concept, D= design, S= supervision, DCP= data collection and/or processing, DAI= data analysis and/or interpretation, L= literature search, W= writing, CR= critical review, SR= submission and revision, PM= project management, FA= funding acquisition.

Conflict of Interest

The authors declared that there is no conflict of interest.

Ethical Consideration

Ethics committee approval was not required for this study because of there was no study on animals or humans.

Acknowledgements

The authors would like to gratefully acknowledge that this study has received funding from Afyon Kocatepe University Scientific Projects Commission under the grant number 17.KARİYER.186.

References

- Agrafiotis C, Tsetsekou A, Leon I. 2000. Effect of slurry rheological properties on the coating of ceramic honeycombs with Ytria-Stabilized-Zirconia washcoats. *J American Ceramic Soc*, 83(5): 1033-1038.
- Christel P, Meunier A, Heller M, Torre J, Peille C. 1989. Mechanical properties and short-term in vivo evaluation of yttrium-oxide-partially-stabilized zirconia. *J Biomed Mater Res*, 23(1): 45-61.
- Denry I, Holloway JA. 2010. Ceramics for dental applications: a review. *Materials*, 3(1): 351-368.
- Denry I, Kelly JR. 2008. State of the art of zirconia for dental applications. *Dental Mater*, 24(3): 299-307.
- Denry IL. 1996. Recent advances in ceramics for dentistry. *Crit Rev Oral Biol Medic*, 7(2): 134-143.
- Duraccio D, Mussano F, Faga MG. 2015. Biomaterials for dental implants: current and future trends. *J Mater Sci*, 50: 4779-4812.
- Garvie RC, Hannink R, Pascoe R. 1990. Ceramic steel? In *Sintering Key Papers*: Springer, Berlin, Germany, pp: 253-257.
- Gautam C, Joyner J, Gautam A, Rao J, Vajtai R. 2016. Zirconia based dental ceramics: structure, mechanical properties, biocompatibility and applications. *Dalton Transact*, 45(48):

- 19194-19215.
- Gouveia PF, Schabbach L, Souza J, Henriques B, Labrincha J, Silva F, Fredel M, Mesquita-Guimarães J. 2017. New perspectives for recycling dental zirconia waste resulting from CAD/CAM manufacturing process. *J Clean Product*, 152: 454-463.
- Greenwood R, Kendall K. 1999. Selection of suitable dispersants for aqueous suspensions of zirconia and titania powders using acoustophoresis. *J European Ceramic Soc*, 19(4): 79-488.
- Grigoriadou M. 2006. Fracture resistance of three-unit posterior zirconium dioxide fixed partial dentures: an in vitro study, Freiburg (Breisgau) Univ Diss, Freiburg, Germany, pp: 92.
- Guazzato M, Albakry M, Ringer SP, Swain MV. 2004. Strength, fracture toughness and microstructure of a selection of all-ceramic materials. Part II. Zirconia-based dental ceramics. *Dental Mater*, 20(5): 449-456.
- Jiang L, Liao Y, Wan Q, Li W. 2011. Effects of sintering temperature and particle size on the translucency of zirconium dioxide dental ceramic. *J Mater Sci Mater Medic*, 22: 2429-2435.
- Jin J, Takahashi H, Iwasaki N. 2004. Effect of test method on flexural strength of recent dental ceramics. *Dental Mater*, 23(4): 490-496.
- Kelly JR, Benetti P. 2011. Ceramic materials in dentistry: historical evolution and current practice. *Australian Dental J*, 56: 84-96.
- Kim WC, Lee JK. 2020. Effect of Powder Characteristics on Slip Casting Fabrication of Dental Zirconia Implants. *J Nanosci Nanotechnol*, 20(9): 5385-5389.
- Madfa AA, Al-Sanabani FA, Al-Qudami NH, Al-Sanabani JS, Amran AG. 2014. Use of zirconia in dentistry: An overview. *Open Biomater J*, 5(1): 1-9.
- Mundhe K, Jain V, Pruthi G, Shah N. 2015. Clinical study to evaluate the wear of natural enamel antagonist to zirconia and metal ceramic crowns. *J Prosthetic Dent*, 114(3): 358-363.
- Piconi C, Maccauro G. 1999. Zirconia as a ceramic biomaterial. *Biomaterials*, 20(1): 1-25.
- Pröbster L, Diehl J. 1992. Slip-casting alumina ceramics for crown and bridge restorations. *Quintessence Int*, 23(1): 25-31.
- Roulet JF, Schepker KL, Truco A, Schwarz HC, Rocha MG. 2021. Biaxial flexural strength, crystalline structure, and grain size of new commercially available zirconia-based ceramics for dental appliances produced using a new slip-casting method. *J Mechan Behav Biomed Mater*, 114: 104180.
- Schultz M, Burckhardt W. 1993. The isoelectric point of pure and doped zirconia in relation to the preparation route. *Solid State Ionics*, 63: 18-24.
- Shen J. 2013. *Advanced ceramics for dentistry*. Butterworth-Heinemann, Waltham, US, pp: 391.
- Shenoy A, Shenoy N. 2010. Dental ceramics: An update. *J Conserv Dent*, 13(4): 195.
- Singh BP, Bhattacharjee S, Besra L, Sengupta DK. 2004. Evaluation of dispersibility of aqueous alumina suspension in presence of Darvan C. *Ceramics Int*, 30(6): 939-946.
- Stevens R. 1986. *Zirconia and zirconia ceramics*. Magnesium Elektron Ltd., Twickenham, UK.
- Zhang F, Inokoshi M, Batuk M, Hadermann J, Naert I, Van Meerbeek B, Vleugels J. 2016. Strength, toughness and aging stability of highly-translucent Y-TZP ceramics for dental restorations. *Dental Mater*, 32(12): e327-e337.
- Zhang Y, Lawn BR. 2018. Novel zirconia materials in dentistry. *J Dental Res*, 97(2): 140-147.



INVESTIGATION OF LINEAR AND NONLINEAR BEHAVIOUR OF REINFORCED CONCRETE COLUMN EXPOSED TO CORROSION EFFECT FOR DIFFERENT DAMAGE LIMIT LEVELS

Halit Erdem ÇOLAKOĞLU^{1*}, Muhammed ÖZTEMEL¹


¹Giresun University, Vocational High School of Keşap, Department of Building, 28000, Giresun, Türkiye


Abstract: The high performance of reinforced concrete structural elements under the effects of lateral loads such as earthquakes is of great importance in terms of minimizing the loss of life and property that may occur due to earthquakes. One of the parameters affecting the earthquake behavior of a reinforced concrete structure is the corrosion effect. The aim of this study is to investigate the behavior of reinforced concrete columns exposed to different corrosion levels for different durations within the damage limits. In this direction, it is aimed to perform linear and nonlinear analysis of reinforced concrete columns in 5 different corrosion scenarios. In the study, nonlinear analyzes of the column were made using ANSYS software, the data obtained were determined for different damage limit levels and compared with the section analysis. Because of the study, moment-curvature relations, lateral load-horizontal displacement relations, bending ductility and plastic rotation capacity of the reinforced concrete column were determined for each corrosion scenario.

Keywords: Corrosion, Propagation velocity, Impact time, Plastic rotation, Flexural ductility

*Corresponding author: Giresun University, Vocational High School of Keşap, Department of Building, 28000, Giresun, Türkiye

E mail: haliterdemcolakoglu@gmail.com (H. E. ÇOLAKOĞLU)

Halit Erdem ÇOLAKOĞLU  <https://orcid.org/0000-0002-4498-3569>

Muhammed ÖZTEMEL  <https://orcid.org/0000-0002-6530-0739>

Received: January 24, 2024

Accepted: March 20, 2024

Published: May 15, 2024

Cite as: Çolakoğlu HE, Öztemel M. 2024. Investigation of linear and nonlinear behaviour of reinforced concrete column exposed to corrosion effect for different damage limit levels. BSJ Eng Sci, 7(3): 409-422.

1. Introduction

Reinforcement corrosion occurring in a reinforced concrete structure causes cracking and spalling in the concrete by decreasing the diameter of the reinforcement, loss of adherence between concrete and reinforcement and decrease in the mechanical properties of reinforcing steel, thus decreasing the performance of the carrier system. In reinforced concrete columns and beams exposed to corrosion effect, since volume expansions occur due to excessive corrosion of the reinforcement, corrosion cracks in the longitudinal direction cause the strut layer to break off in time (Figure 1). Reinforced concrete structures subjected to these corrosion effects reach the state of collapse in a much shorter time than normal and in abnormal ways under the effect of earthquake loads.



Figure 1. Reinforced concrete elements subjected to corrosion effect.

When the literature examined, many experimental and numerical studies have carried out on the effects of corrosion on reinforcing steel and the inadequacies in earthquake performance due to the negative effects of corrosion on reinforced concrete structures. In these studies, it has been determined that the failure mode of beams subjected to corrosion under bending effect changes from ductile to brittle (Mangat and Elgarf, 1999; Mohammed et al., 2004). In addition, in these studies, it stated that corrosion of steel reinforcement causes deformation of the entire system, especially the bearing capacity of the structural elements (Yavuz et al., 2019). In studies evaluating the seismic performance of reinforced concrete columns at different corrosion levels and axial load rates, it was determined that the corrosion effect significantly reduces the strength and horizontal displacement capacity of the columns and changes the failure mode from flexural-shear failure to sudden axial failure (Vu and Li, 2018). Palsson and Mirza (2002) subjected reinforcing bar samples taken from reinforced concrete bridges subjected to corrosion to tensile tests and found that the reinforcements fractured brittle. Revathy et al. (2009) concluded that the axial load carrying capacity of column elements subjected to corrosion effect gradually decreases with increasing corrosion effect.

In case of weakening of the adherence bond established



between the reinforcement and concrete in the constituent elements of the reinforced concrete structure, the behavior of the reinforced concrete structure turns into a stressed arch behavior. In stressed arch behavior, since the reinforcement collapses before reaching the yield stress, the relationship between the corrosion level of the reinforcement and the adherence bond strength is extremely important. It was determined that at low corrosion levels, the adherence bond strength increased to a certain extent, but if the corrosion level increased, the adherence bond strength gradually decreased (Chung et al., 2008). This decrease in bond strength causes significant changes in the earthquake performance and target displacements of the structure (Yüksel and Sancaklı, 2018).

In columns where reinforcement losses due to corrosion increase up to 15.1%, the increase in corrosion level impairs the cyclic stability of the reinforced concrete column under cyclic load effects and reduces the ductility of the reinforced concrete column (Ying et al., 2012).

In some studies in the literature, the effect of corrosion on reinforced concrete structures has studied using finite element modeling technique. Dizaj and Kashani (2021) proposed a modeling technique that simulates the regional variability of corrosion and the effects of corrosion damage. Finite element analysis using the proposed modeling approach revealed that corrosion significantly affected the damage states, flexural capacity and energy absorption capacity of reinforced concrete members. In another study by Imperatore et al. (2017), where an experimental study to evaluate the residual flexural capacity of beams was simulated using the finite element method, the relationship between the level of corrosion and the reduction in the flexural strength of the

beam was determined (Bossio et al., 2019). In another study evaluating the seismic behavior of corroded reinforced concrete bridges, the decrease in the bond strength between concrete and reinforcement was modeled using finite element modeling technique. Softening of concrete and reduction in mechanical properties of reinforcement also taken into account in the modeling. Because of the study, it recommended to increase the design PGA from 4.70% to 6.15% for the seismic performance of the bridge considering the reductions due to corrosion effect. (Ou et al., 2013).

In this study, the linear and nonlinear behavior of reinforced concrete column elements under 5 different corrosion scenarios were investigated. In the corrosion scenarios, the adherence losses between reinforcement and concrete and all the consequences of corrosion on concrete and reinforcement elements modelled together depending on the corrosion propagation rate and corrosion duration parameters. In the study, the change in column structural behavior due to corrosion evaluated in terms of damage limits at different corrosion levels using both finite element method and cross-sectional analysis.

2. Materials and Methods

A reinforced concrete column with a rectangular cross-section of 300 x 400 x 2350 mm dimensions determined in accordance with TBDY (2018) used in the study. The concrete strength class of the column element taken as C25/30. The size information of the reinforced concrete column, the layout of the longitudinal and transverse reinforcements used and the variation of the transverse reinforcement spacing are as shown in Figure 2.

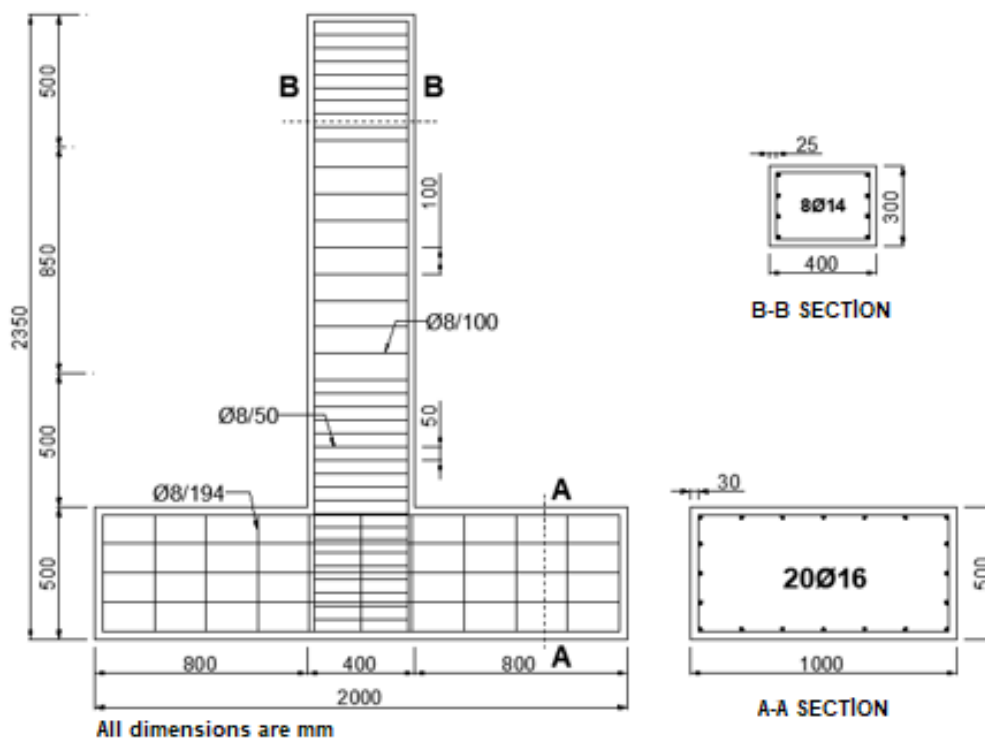


Figure 2. Reinforced concrete column cross-section and reinforcement arrangement.

TBDY, (2018) a 500 mm long formed at the upper and lower ends of the column, and no stirrup with a diameter smaller than Ø8 used as transverse reinforcement in these zones. According to TBDY (2018) the spacing of the transverse reinforcements to be used in the column is arranged so that they are not smaller than 50 mm and not larger than 100 mm. Reinforcement smaller than Ø14 was not used in the reinforced concrete column element, and the longitudinal reinforcement area specified in TBDY (2018) was acted in accordance with the condition that the longitudinal reinforcement area shall not be less than 1% and not greater than 4% of the gross cross section.

According to TBDY (2018) the longitudinal reinforcement ratio in column elements should not be less than 0.01 and not greater than 0.04. In this context, 8Ø14 longitudinal reinforcement used in the reinforced concrete column used in the study and the longitudinal reinforcement ratio calculated as 0.0103. Since the normal force determines the type of fracture in the reinforced concrete column element, the normal force should be limited to prevent brittle fracture (Topçu, 2022). According to TBDY (2018) the maximum axial load that the column element can carry calculated as stated in Equation 1.

$$N_d \leq 0,4f_{ck}A_c \quad (1)$$

According to Equation 1, the maximum axial load value that the reinforced concrete column used in the study can carry calculated as 1200 kN.

In this study, it investigated how the earthquake performance of the reinforced concrete column element, whose dimensional and cross-sectional properties given above, will change if it exposed to corrosion effect. In this context, the reinforced concrete column element was analyzed under 5 different corrosion scenarios. The effect of corrosion on the reinforced concrete column depends on the rate of corrosion spread and the duration of the effect, but it causes the steel reinforcement to expand in volume, soften and reduce its weight. The decrease in the weight and change in the diameter of the steel reinforcement calculated using Equation 2 and Equation 3 as follows (Berto et al., 2008):

$$\% \Delta_w = \frac{\phi_0^2 - \phi(t)^2}{\phi_0^2} \times 100 \quad (2)$$

$$\phi(t) = \phi_0 - 2P_x = \phi_0 - 2i_{corr}k(t - t_{in}) \quad (3)$$

2.1. Evaluation of the Rate of Propagation and Duration of Corrosion

In the literature, a number of formulations based mainly

on empirical expressions have been proposed for the evaluation of corrosion propagation rate (i_{corr}) and weight decrease in reinforcing steel, ranging from a deterministic approach to a probabilistic context (Berto et al., 2009). In particular, the evaluation of corrosion propagation rate (i_{corr}) obtained from laboratory tests and corrosion effects in real structures is shown in Table 1 (Dhir et al., 1994; Brite/Euram, 1995; Middleton and Hogg, 1998).

In this study, $i_{corr}=0.15$ for reinforced concrete columns with low corrosion level and $i_{corr}=0.8$ for reinforced concrete columns with medium corrosion level and $i_{corr}=4$ for reinforced concrete columns with high corrosion level and the current corrosion scenarios are shown in Table 2. In the study, 15 years since the reinforced concrete column was manufactured (t_{in}) was considered as the initial stage of corrosion.

In addition to the weight decrease in the reinforcing bar of a reinforced concrete column subjected to corrosion, some changes occur in the yield and tensile strengths, yield and tensile deformations and elastic modulus of the reinforcement in a corroded reinforcement. These changes calculated using Equation 4, Equation 5, Equation 6 and Equation 7 (Lee and Cho, 2009):

$$\sigma_y = \left(1 - 1,24 \cdot \frac{\Delta_w}{100}\right) \cdot \sigma_{y(initial)} \quad (4)$$

$$\sigma_u = \left(1 - 1,07 \cdot \frac{\Delta_w}{100}\right) \cdot \sigma_{u(initial)} \quad (5)$$

$$E_s = \left(1 - 0,75 \cdot \frac{\Delta_w}{100}\right) \cdot E_{s(initial)} \quad (6)$$

$$\varepsilon_u = \left(1 - 1,95 \cdot \frac{\Delta_w}{100}\right) \cdot \varepsilon_{u(initial)} \quad (7)$$

The effects of corrosion on the bond strength reduction of the steel reinforcement due to corrosion must also take into account. To account for the effects of corrosion on bond strength reduction in the analysis, the concept of equivalent unlimited length was used (Ou et al., 2010). According to this concept, the reduction in bond strength reflected in the models by multiplying the bond reduction coefficient (Φ) defined by Equation 8 by the stress-strain curve of steel.

$$\Phi = \frac{L_{eu}(\text{corrosion free reinforcement})}{L_{eu}(\text{corroded reinforcement})} \quad (8)$$

Here L_{eu} is the equivalent unlimited length derived from Equation 9.

$$L_{eu} = \frac{S_E}{\varepsilon_{sm}} \quad (9)$$

Table 1. Classification of corrosion propagation rate i_{corr} ($\mu A/cm^2$)

Corrosion level	Dhir et al. (1994)	Brite/Euram (1995)	Middleton and Hogg (1998)
Corrosion free	-	$i_{corr} < 0,1$	-
Low	$i_{corr} = 0.1$	$i_{corr} = 0.1 - 0.5$	$i_{corr} = 0.1 - 0.2$
Middle	$i_{corr} = 1$	$i_{corr} = 0.5 - 1$	$i_{corr} = 0.2 - 1$
High	$r > 10$	$i_{corr} > 1.0$	$i_{corr} > 1.0$

Table 2. Corrosion scenarios

Scenario number	Initial diameter (mm)	i_{corr} ($\mu A/cm^2$)	Time t (yil)	t_{in} (yil)	Last diameter (mm)	Weight reduction (%)
1	8	0	0	0	8.00	0.00
	14	0	0	0	14.00	0.00
2	8	4	20	15	7.60	9.75
	14	4	20	15	13.60	5.63
3	8	0.8	50	15	7.44	13.51
	14	0.8	50	15	13.44	7.84
4	8	4	50	15	5.20	57.75
	14	4	50	15	11.20	36.00
5	8	4	35	15	6.40	36.00
	14	4	35	15	12.40	21.55

Where S_E is the slip of a reinforcement in the critical section of a column cross-section ε_{sm} is the maximum strain in the reinforcement and the slip in the reinforcement estimated using Equation 10 and Equation 11 (Sezen and Setzler, 2008):

$$S_E = \frac{\varepsilon_{sm} L_{d1}}{2} \quad (\varepsilon_{sm} \leq \varepsilon_y) \quad (10)$$

$$S_E = \frac{\varepsilon_y L_{d1}}{2} + \frac{(\varepsilon_{sm} + \varepsilon_y) L_{d2}}{2} \quad (\varepsilon_{sm} > \varepsilon_y) \quad (11)$$

Here L_{d1} and L_{d2} is calculated using Equation 12 and Equation 13.

$$L_{d1} = \frac{f_{sm} d_b}{4\tau_{max}} \leq \frac{f_y d_b}{4\tau_{max}} \quad (12)$$

$$L_{d2} = \frac{(f_{sm} - f_y) d_b}{4\tau_f} \quad (13)$$

Where f_{sm} , is the maximum stress in the reinforcement, d_b , is the longitudinal reinforcement diameter, τ_{max} , is the bond strength and τ_f , is the residual friction bond strength. For reinforcement without corrosion effect, τ_{max} and τ_f values can be taken as $\sqrt{f_c}$ and $0.15\tau_{max}$ respectively. When the reduction in reinforcement weight exceeds 1.5%, the corrosion effect calculated according to Equation 14 (Bhargava et al., 2008). When the corrosion level is less than 1.5 %, the bond strength assumed to be equal to the corrosion-free value. Here τ_{maxo} , is the bond strength is assumed to be equal to the corrosion free value.

$$\tau_{max} = 1.346e^{-0.198\Delta_w(\%)} \tau_{maxo} \quad (14)$$

The stress-unit strain curves of the reinforcements in the reinforced concrete column subjected to corrosion effect arranged for each corrosion scenario by considering the decrease in the adherence bond strength (Figure 3).

Cracking and softening effects occurring in the concrete due to corrosion effect should also take into consideration in the reinforced concrete column element exposed to corrosion. The softening effect of concrete due to corrosion expressed by concrete softening coefficient (ζ). Concrete softening coefficient calculated according to Equation 15 (Ou et al., 2013).

$$\zeta = \frac{0.9}{\sqrt{1 + 600\varepsilon_r}} \quad (15)$$

Where ε_r the yield is strain of reinforcement and calculated according to Equation 16. Where b_0 is the perimeter length of the reinforced concrete column cross-section and $\sum w_{cr}$ is the total crack width in the concrete due to corrosion of longitudinal and transverse reinforcement (Ou et al., 2013). Each crack width w_{cr} calculated using Equation 17 (Molina et al., 1993) (Figure 4).

$$\varepsilon_r = \frac{\sum w_{cr}}{b_0} \quad (16)$$

$$w_{cr} = \pi \cdot (V_{rs} - 1) \cdot 2x \quad (17)$$

Here $2x$ is the reduction in the diameter of the steel reinforcement due to corrosion. The volume expansion of steel reinforcement due to corrosion causes softening and weight decrease (Figure 4). V_{rs} is the diameter expansion coefficient of steel reinforcement due to corrosion. For this study, $V_{rs} = 2$ (Ou et al., 2013) (Figure 4).

Considering the effects of cracking and softening of the concrete due to the corrosion effect in the reinforced concrete column element subjected to corrosion, Equation 18 and Equation 19 are used for the increasing and decreasing regions of the stress- strain relationship of concrete, respectively (Hsu, 1993).

$$\sigma = \zeta f'_c \left[2 \left(\frac{\varepsilon}{\zeta \varepsilon_0} \right) - \left(\frac{\varepsilon}{\zeta \varepsilon_0} \right)^2 \right] \quad (18)$$

$$\sigma = \zeta f'_c \left[1 - \left(\frac{\frac{\varepsilon}{\zeta \varepsilon_0} - 1}{\frac{2}{\zeta} - 1} \right)^2 \right] \quad (19)$$

Here, ε_0 is the unit strain value corresponding to the maximum stress in the stress-strain curve of concrete and it accepted as approximately 0.002.

In the study, the stress-strain curve of the concrete material for each corrosion scenario in the reinforced concrete column subjected to corrosion effect was determined by considering the effects of cracking and softening in the concrete (Figure 5).

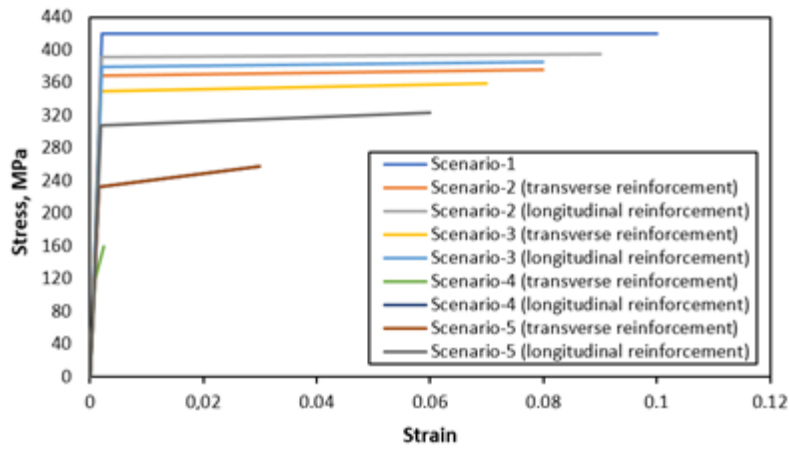


Figure 3. Stress - strain curves of steel according to corrosion scenarios.

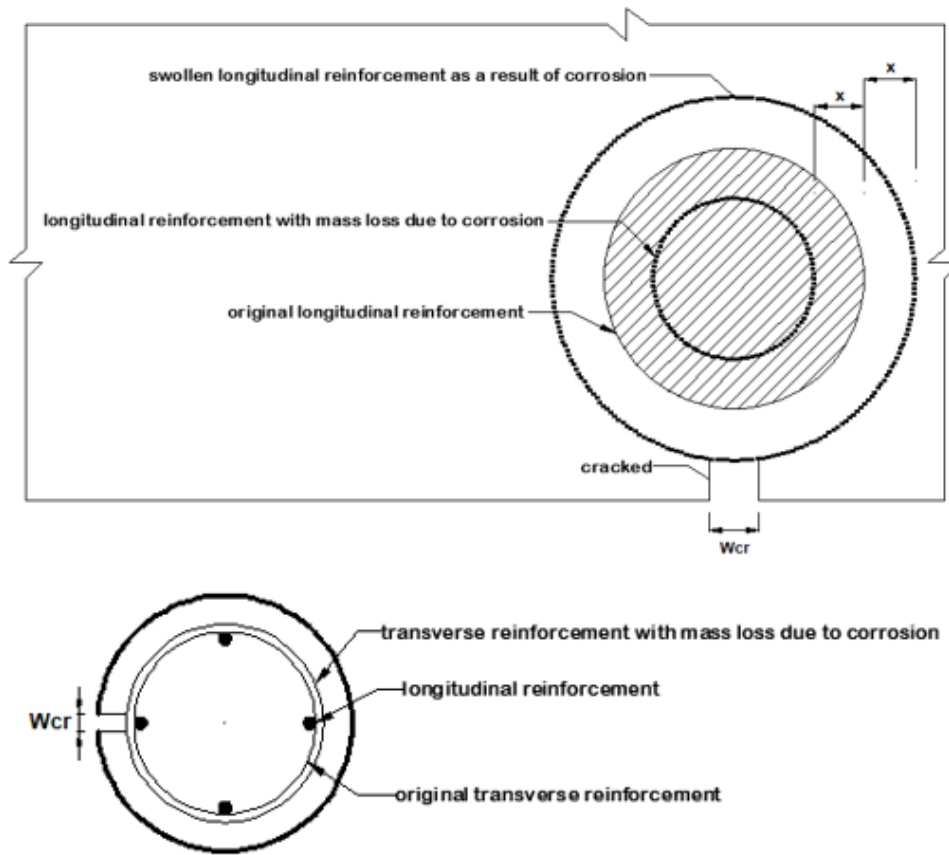


Figure 4. Corrosion cracks in longitudinal and transverse reinforcement.

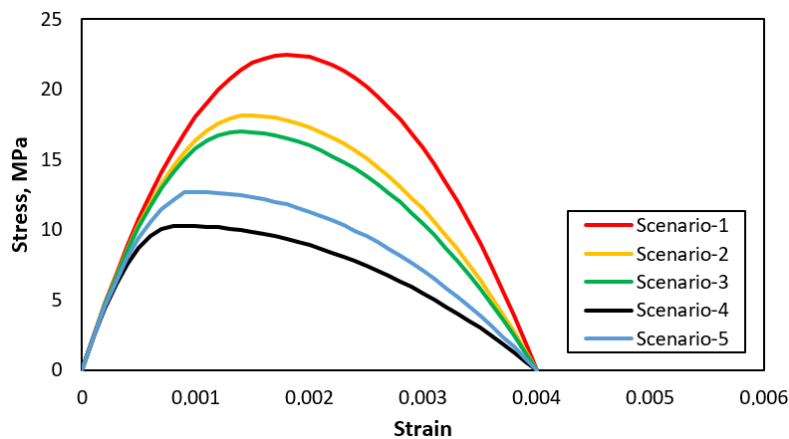


Figure 5. Stress - strain curves of concrete according to corrosion scenarios.

2.2. Creation of Finite Element Model of Reinforced Concrete Column

Finite element model of the reinforced concrete column element to be used in the study was created using ANSYS software. In the finite element model, Solid65, which is a solid element with 8 nodes, was used for concrete and Link180 elements were used for reinforcing steel. The finite element model of the reinforced concrete column shown in Figure 6.

In the finite element model, the foundation of the reinforced concrete column not modelled in order to shorten the analysis time and to create the minimum number of finite elements. Instead, each nodal point at

the lower end of the reinforced concrete column modelled in accordance with the anchored support assumption (Figure 7).

2.3. Determination of Stress-Strain Relationships for Concrete and Steel in Finite Element Model

The stress-strain curves of the concrete used in the finite element model of the reinforced concrete column shown in Figure 8 and the stress-strain curves of the reinforcing steel shown in Figure 3.

Concrete of strength class C25/30 used in the finite element model of the reinforced concrete column. The modulus of elasticity of concrete and steel material for different corrosion scenarios given in Table 3.

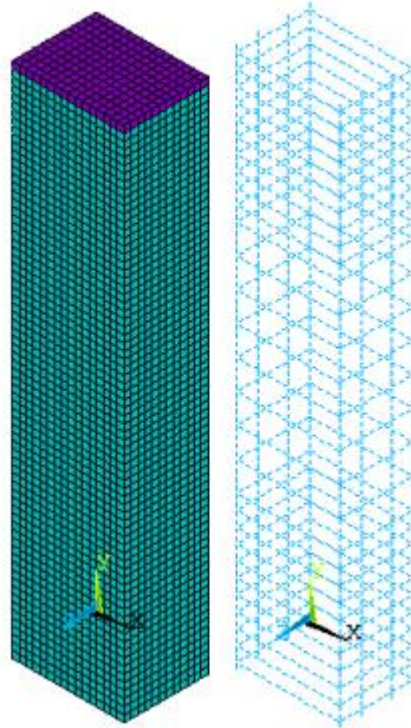


Figure 6. Reinforced concrete column concrete and reinforcement finite element model.

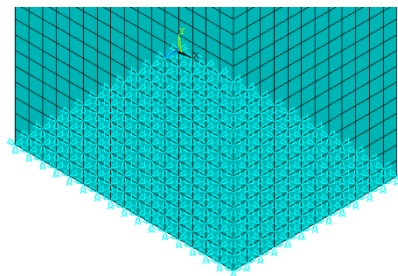


Figure 7. Reinforced concrete column anchored support model.

Table 3. Material properties according to corrosion scenarios (MPa)

Scenario number	Concrete (E_c)	Steel (E_s)	Concrete softening coefficient (α)
1	24306	200000	0.9
2	24139	188465	0.73
3	24080	183988	0.68
4	23483	129688	0.41
5	23767	156838	0.51

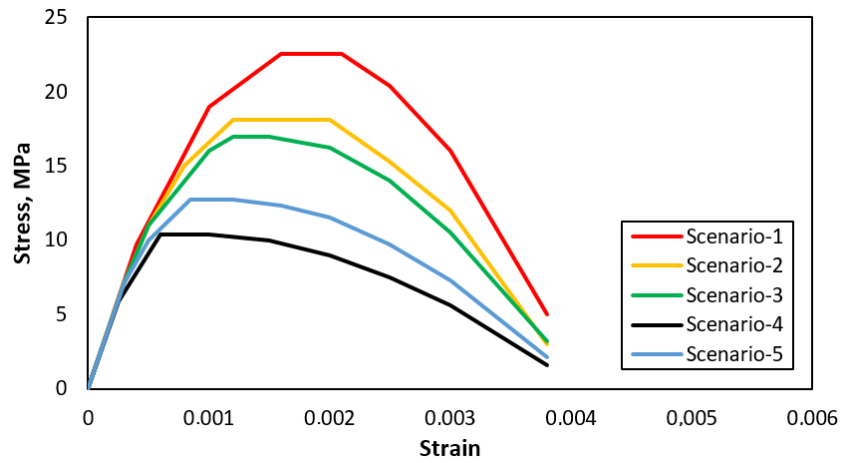


Figure 8. Concrete material models according to corrosion scenarios.

2.4. Application of Axial and Horizontal Load in Finite Element Model

In this study, the nonlinear behavior of a finite element modelled reinforced concrete column subjected to corrosion under axial load and lateral load investigated. For this purpose, 165 nodal points selected at the upper end of the column and the axial load $N_d = 1200\text{ kN}$ equally distributed to each nodal point. In addition, horizontal displacement applied to a node at the upper end of the reinforced concrete column by utilizing the rigid beam feature of the MPC184 compliance element. The rigid beam feature of the MPC184 element utilized in order to distribute the applied lateral load equally and evenly to the reinforced concrete column and to prevent excessive deformation of the concrete particles forming the column nodes (Figure 9).

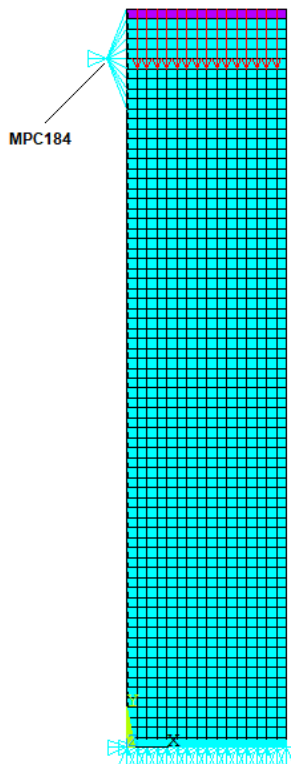


Figure 9. Application of axial load and lateral load.

2.5. Evaluation of the Reliability of the Finite Element Modelling Method Used

The reliability of the finite element modelling software used in the study and the demonstration that the parameters used in the modelling are determined in a way to give the closes results to the actual behavior of the reinforced concrete column are of great importance for the present study.

In the study conducted by Elçi and Göker (2018) the reinforced concrete column whose section geometry and reinforcement plan shown in Figure 10 was experimentally investigated under axial and lateral load. The existing reinforced concrete column was finite element modelled by Çolakoğlu (2020) and subjected to nonlinear analysis under the axial and horizontal load effects in the experimental study by Elçi and Göker (2018). The data obtained were processed and the shear force-horizontal displacement and bending moment-curvature relationships in Figure 11 were drawn.

When Figure 11 examined, it considered that the finite element modelling and nonlinear analysis performed with the ANSYS package are very reliable for reinforced concrete columns and it is important to adjust the modelling parameters to give results close to reality.

3. Results

In this study, nonlinear analysis of a reinforced concrete column whose finite element model produced using ANSYS software performed. In addition, cross-sectional analysis of the reinforced concrete column under corrosion effect performed and the deformation state compared with the nonlinear analysis. Lateral load – horizontal displacement relationship, bending moment-curvature relationship, flexural ductility and plastic rotation capacity evaluated using the obtained data.

3.1. Lateral Load - Horizontal Displacement Relationship

The horizontal load-lateral displacement graph obtained because of the nonlinear analysis of the reinforced concrete column subjected to corrosion effect under axial load and horizontal load shown in Figure 12 for each corrosion scenario.

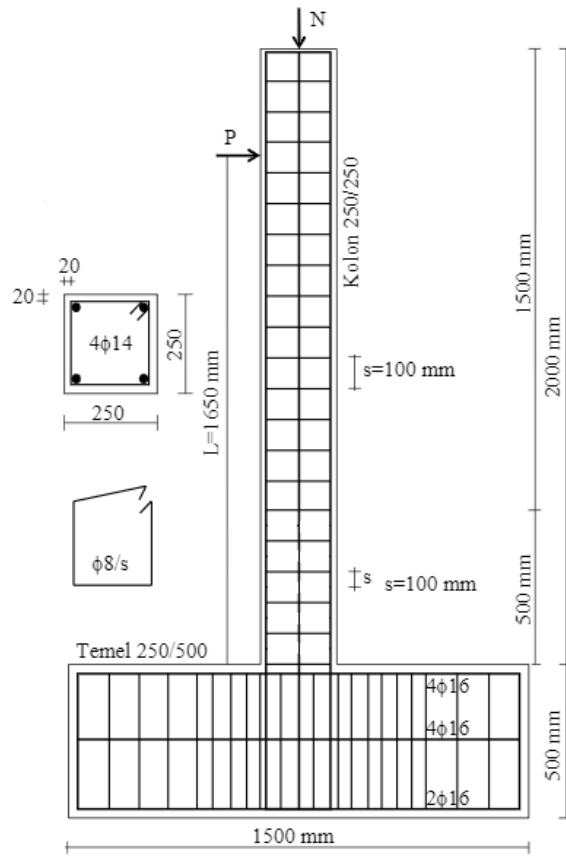


Figure 10. Reinforced concrete column cross-section and reinforcement plan.

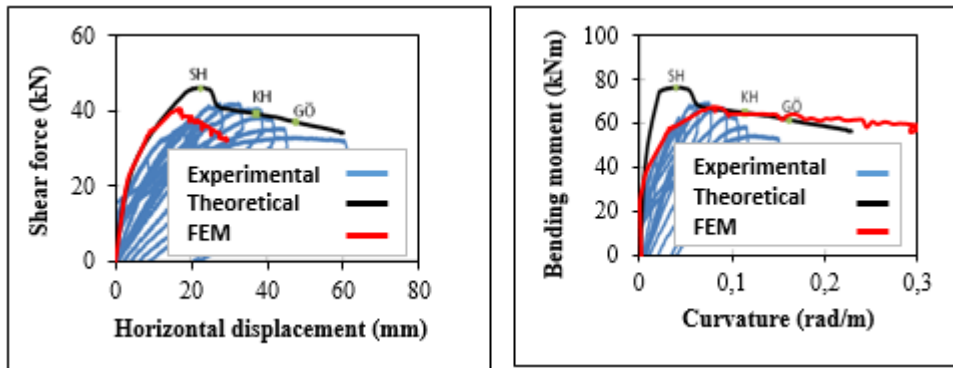


Figure 11. Shear force - horizontal displacement relationship and bending moment - curvature relationship.

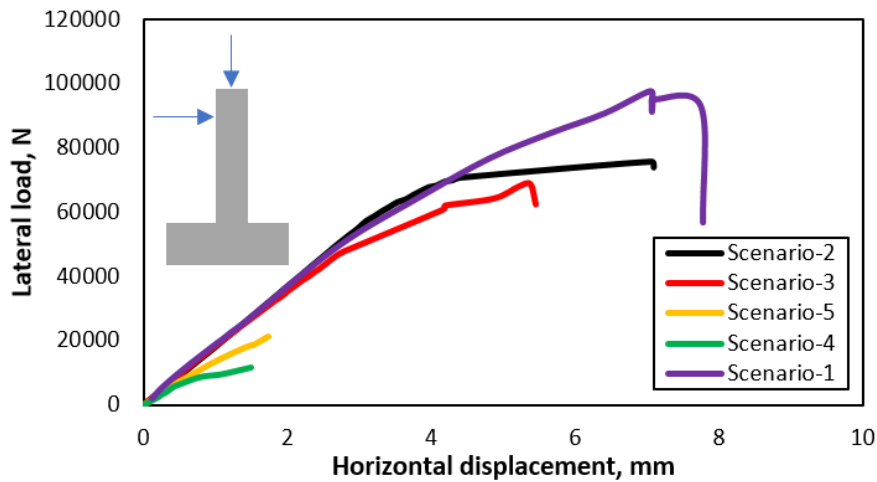


Figure 12. Lateral load - horizontal displacement relationship (ANSYS).

When Figure 12 analyzed, it seen that the lateral load capacity of the reinforced concrete column element exposed to corrosion effect decreases.

3.2. Bending Moment - Curvature Relationship

In order to determine the behavior of a section under the effect of bending and axial force or only bending, the moment-curvature relationship of a modelled element can be obtained based on the actual material behavior (Ersoy and Özcebe, 2018).

In order to calculate the values of M_i and K_i , which constitute the moment-curvature relationship, by iteration method, equations of equilibrium and compatibility are utilised. If a beam section is utilised, assumptions are made for the value of c (neutral axis depth), and the value of c is changed until the balance of forces is achieved. A value is chosen for the unit shortening of concrete at the outermost lift, ϵ_{ci} . Steel unit deformations, ϵ_{si} , are found for known ϵ_{ci} and c . Stresses in the reinforcement and reinforcement forces are determined from the ϵ_{si} values. The concrete compression component F_c is calculated. After equilibrium reached, the moment of internal forces around the centre of gravity is calculated and M_i found. The curvature is determined as given in Equation 20 (Ersoy and Özcebe, 2018).

$$K_i = \frac{\epsilon_{ci}}{c} \quad (20)$$

In the finite element model of the reinforced concrete column, the curvature calculated for each horizontal row of solid elements at the lower end of the column calculated as in Equation 21 by using the unit strains at the beginning and end nodes of each fibre as shown in Figure 13.

$$\phi = (|\epsilon_1| + |\epsilon_2|)/L \quad (21)$$

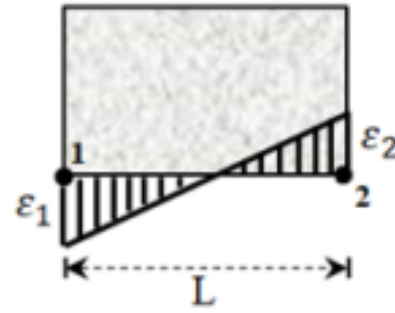


Figure 13. Definition of curvature in finite element modelling.

Figure 14 shows the bending moment-curvature relationship obtained from the nonlinear analysis of the reinforced concrete column subjected to corrosion effect, and Figure 15 shows the bending moment-curvature relationship obtained from the section calculation for each corrosion scenario.

When the lateral load - horizontal displacement relationship and bending moment - curvature relationship obtained from the nonlinear analysis of the reinforced concrete column subjected to corrosion effect were examined, it was determined that the lateral load capacity and moment carrying capacity decreased depending on the duration and rate of propagation of corrosion. This decrease found to be more intense especially in Scenario-4, where the rate of propagation and duration of corrosion was the highest.

When the cross-sectional analysis performed due to the corrosion effects to which the reinforced concrete column element was exposed were examined, it was determined that the moment carrying capacity and cross-sectional ductility decreased depending on the corrosion levels, similar to the results obtained in the nonlinear analysis.

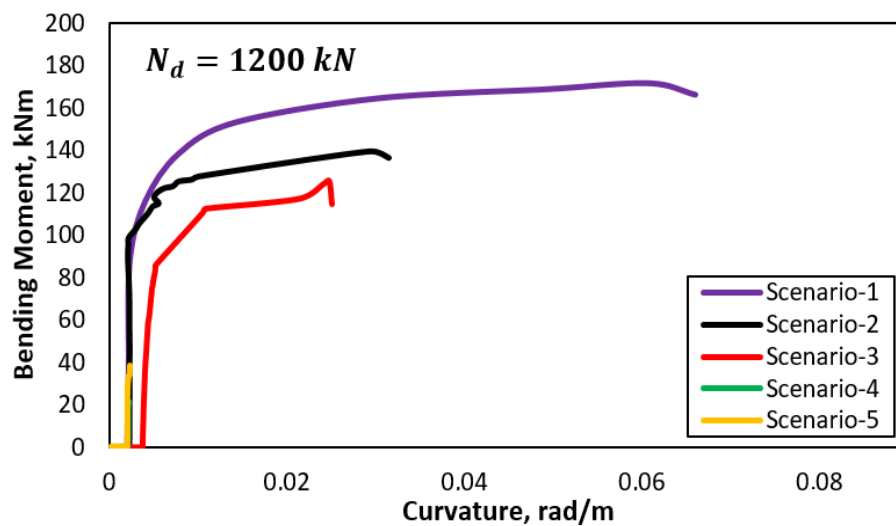


Figure 14. Bending moment - curvature relationship for nonlinear analyses (FEM)

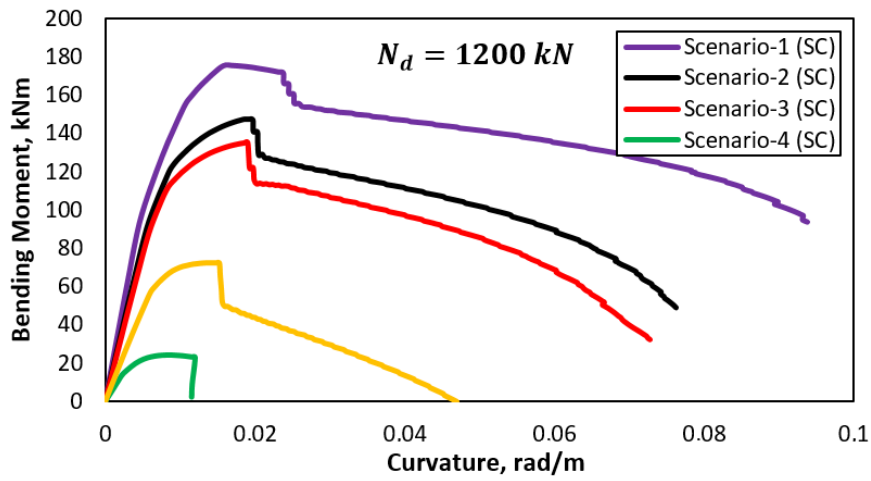


Figure 15. Bending moment – curvature relationship for section calculation (SC).

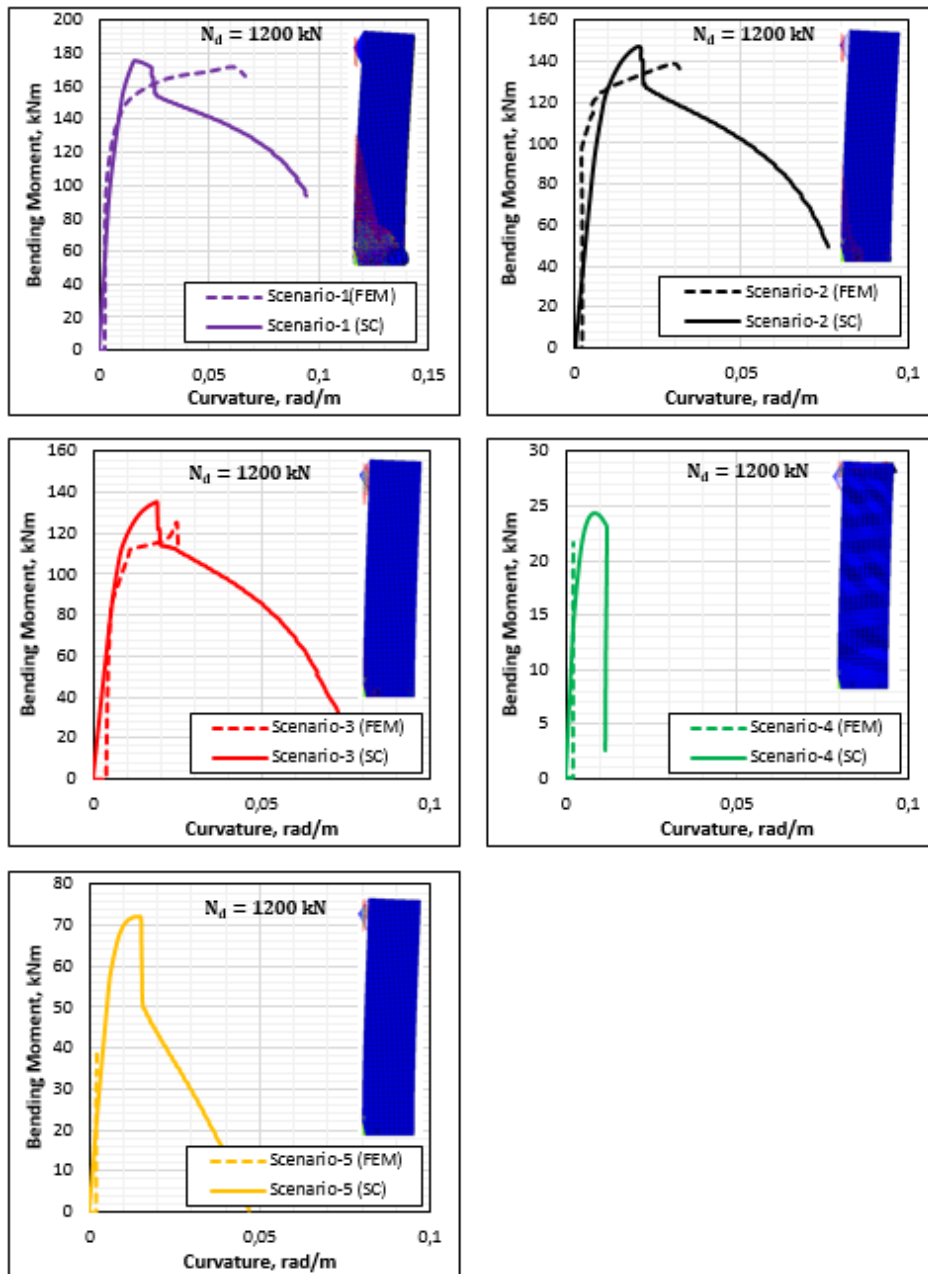


Figure 16. Bending moment – curvature relations for corrosion scenarios.

In Figure 16, the bending moment - curvature relationships of the reinforced concrete column subjected to corrosion effect in different corrosion scenarios compared in terms of nonlinear analysis and cross-sectional analysis, and in Table 4, the reduction in lateral load and bending moment carrying capacity for each corrosion level calculated according to Scenario-1 without corrosion effect.

3.2.1. Flexural ductility of reinforced concrete column

Flexural ductility defined as the ratio of the maximum curvature that can occur in a reinforced concrete element section in bending without a significant reduction in strength to the curvature now when yielding occurs in the tensile reinforcement, which is determined as the end of linear behavior. Flexural ductility calculated as shown in Equation 22 (Celep, 2008).

$$\mu = \frac{\phi_{u(max)}}{\phi_y} \tag{22}$$

The flexural ductility of the reinforced concrete column subjected to corrosion effect obtained because of nonlinear analysis and section analysis shown in Table 5.

3.2.2. Plastic joint yield rotation and plastic rotational capacity

As the reinforced concrete column element translated under the effect of the applied lateral load, the displacements increase at the sections where the moment is the largest at the base of the column. In particular, the displacements, which are zero at the place where the column supported on the foundation, increase smoothly until the plastic hinge occurs, while a sudden increase in curvature occurs in the plastic hinge region. Plastic joint yield rotation (θ_y) determined according to the stacked plastic behaviour model of the reinforced concrete column element is calculated as given in

Equation 23 and plastic rotation capacity (θ_p) is calculated as given in Equation 24, Equation 25 and Equation 26.

$$\theta_y = \frac{\phi_y L_s}{3} + 0.0015\eta \left(1 + 1.5 \frac{h}{L_s}\right) + \frac{\phi_y d_b f_{ye}}{8\sqrt{f_{ce}}} \tag{23}$$

$$\theta_p^{(G\ddot{o})} = \frac{2}{3} \left[(\phi_u - \phi_y) L_p \left(1 - 0.5 \frac{L_p}{L_s}\right) + 4.5 \phi_u d_b \right] \tag{24}$$

$$\theta_p^{(KH)} = 0.75 \theta_p^{(G\ddot{o})} \tag{25}$$

$$\theta_p^{(SH)} = 0 \tag{26}$$

Where ϕ_y the effective is yield curvature and ϕ_u is the total curvature before collapse. For beam and column elements, $\eta = 1$ taken and h is the height of the section. f_{ce} and f_{ye} are the average (expected) compressive strength of concrete and average yield strength of reinforcement, respectively. d_b is the average diameter of the reinforcing steel clamped to the support, while L_s is the shear span.

It assumed that the curvature in the plastic joint regions where linear inelastic deformations are concentrated in the reinforced concrete column subjected to corrosion effect increases abruptly. L_p , which expresses the length of the plastic joint region where the curvature increases rapidly, calculated as given in Equation 27.

$$L_p = 0.5h \tag{27}$$

Table 6 shows the plastic rotation capacities and plastic joint yield rotations of the reinforced concrete column for different corrosion scenarios in the nonlinear analysis and Table 7 shows the plastic rotation capacities and plastic joint yield rotations for Limited Damage (LD), Controlled Damage (CD) and Collapse Prevention (CP) performance levels in the section analysis.

Table 4. Lateral load and bending moment capacity losses

Scenario number	Lateral load (kN)		Bending moment (kNm)	
	FEM	SC	FEM	SC
Scenario -1	0.000		0.000	0.000
Scenario -2	20.99		18.95	15.79
Scenario -3	28.20		27.08	22.73
Scenario -4	87.96		87.37	86.05
Scenario -5	77.83		77.43	57.79

Table 5. Flexural ductility

Scenario number	Yield curvature (ϕ_y)		Maximum curvature ($\phi_{u(max)}$)		Flexural ductility (μ)	
	FEM	SC	FEM	SC	FEM	SC
	Scenario -1	0.0078	0.011	0.060	0.094	7.69
Scenario -2	0.0061	0.0093	0.031	0.076	5.08	8.17
Scenario -3	0.0052	0.0085	0.024	0.073	4.62	8.58
Scenario -4	0.0021	0.0035	0.0022	0.012	1.05	3.43
Scenario -5	0.0022	0.0066	0.0023	0.047	1.05	7.12

Table 6. Plastic joint yield rotation and plastic rotational capacity (FEM)

Scenario number	Plastic rotation capacity			Plastic joint yield rotation
	$\theta_{P(SH)}$	$\theta_{P(KH)}$	$\theta_{P(G\ddot{O})}$	(θ_y)
Scenario -1	0	0.01956	0.026079	0.008399
Scenario -2	0	0.009377	0.012503	0.007422
Scenario -3	0	0.007089	0.009453	0.006904
Scenario -4	0	0.000089	0.000119	0.005121
Scenario -5	0	0.000098	0.000131	0.005178

Table 7. Plastic joint yield rotation and plastic rotation capacity (SC)

Scenario no	Plastic rotation capacity			Plastic joint yield rotation
	$\theta_{P(SH)}$	$\theta_{P(KH)}$	$\theta_{P(G\ddot{O})}$	(θ_y)
Scenario -1	0	0.031056	0.041408	0.010239
Scenario -2	0	0.024903	0.033204	0.009262
Scenario -3	0	0.024041	0.032054	0.008802
Scenario -4	0	0.00318	0.004239	0.005925
Scenario -5	0	0.015033	0.020044	0.007709

4. Discussion and Conclusion

In this study, the deformation of a rectangular reinforced concrete column subjected to corrosion effect under axial and lateral load effects investigated. In the study, the finite element model of the reinforced concrete column produced using ANSYS software and the nonlinear analysis performed. In addition, cross-sectional analysis of the reinforced concrete column under the effect of corrosion carried out and the deformation state compared with nonlinear analysis. The findings of the study draw attention to the losses caused by the corrosion effect on the lateral load carrying capacity and bending moment carrying capacity of the reinforced concrete column. In this context, it thought to be a good guide for the readers in determining the effect of corrosion on structures. The results obtained because of the research explained below.

- The lateral load and bending moment carrying capacities of reinforced concrete structural elements vary depending on the duration of the corrosion effect and the propagation speed parameters. Compared to Scenario-1, where there is no corrosion effect, in Scenario-4, where the corrosion effect is the most intense, the lateral load carrying capacity of the reinforced concrete column decreased by approximately 87.96% and the bending moment carrying capacity decreased by approximately 87.37% in the nonlinear analysis.
- When the Scenario-2 and Scenario-4 cases where the rate of corrosion spread is $i_{corr} = 4$ are examined, it is determined that the loss in the horizontal load and bending moment carrying capacity of the reinforced concrete column increases by an average of 4.4 times in the nonlinear analysis if the corrosion period increases from 20 years to 50 years.
- When Scenario-3 and Scenario-4 cases where the duration of corrosion is $t=50$ years, it is determined

that the loss in the horizontal load and bending moment carrying capacity of the reinforced concrete column increases by an average of 3.2 times in the nonlinear analysis if the corrosion propagation rate increases from 0.8 to 4.

- Ductility of reinforced concrete structural elements is of great importance in terms of earthquake performance. In this study, it was determined that corrosion effect not only reduces the lateral load and bending moment capacity of the reinforced concrete column but also negatively affects the flexural ductility. While the flexural ductility ratio was 7.69 according to the nonlinear analysis in Scenario-1 without corrosion effect, the flexural ductility ratio was determined as 1.05 in Scenario-4 with the highest corrosion effect. When the data obtained from the cross-sectional analysis of the reinforced concrete column are examined, it is determined that the flexural ductility ratio decreases significantly when the mass loss in the reinforcement increases to 35% and above due to the corrosion effect. It was determined that there was no significant change in the flexural ductility ratio as a result of the section analysis at mass losses below 35%. It is thought that this result is due to the fact that the section analysis does not consider the cracking behavior of concrete.
- In the nonlinear analysis of the reinforced concrete column, the plastic rotation capacity decreased by approximately 99.55 % for CD and CP damage limit levels in Scenario-4, where the corrosion effect is the highest, compared to Scenario-1, where there is no corrosion effect. In section analysis, this reduction was calculated as 89.76% for CD and CP damage limit levels in Scenario-4, where the mass loss in the reinforcement was more than 35%.
- In the beyond-linear analysis of the reinforced concrete column, it was determined that a loss of 12% for Scenario-2, 17% for Scenario-3, 17% for

Scenario-4 and 39% for Scenario-5 occurred in the plastic joint yield rotation value compared to Scenario-1 without corrosion effect. In the cross-sectional analysis, it was determined that a loss of 7% for Scenario-2, 11% for Scenario-3, 41% for Scenario-4 and 22% for Scenario-5 occurred in the plastic joint yield rotation value compared to Scenario-1. Accordingly, it can be said that similar losses occur in the plastic joint yield rotation value when the corrosion level is the highest in both nonlinear analysis and cross-sectional analysis.

- The bending moment capacity of the reinforced concrete column subjected to corrosion effect obtained from the nonlinear analysis was lower than the bending moment carrying capacity obtained from the cross-sectional analysis. The cracking property of the Solid65 element used in the finite element modelling under load effect and the cracking behavior of concrete are considered as the reason for this situation.

Author Contributions

The percentage of the author(s) contributions is presented below. All authors reviewed and approved the final version of the manuscript.

	H.E.Ç.	M.Ö.
C	50	50
D	60	40
S	40	60
DCP	50	50
DAI	40	60
L		100
W	100	
CR	40	60
SR	50	50
PM	50	50
FA	50	50

C=Concept, D= design, S= supervision, DCP= data collection and/or processing, DAI= data analysis and/or interpretation, L= literature search, W= writing, CR= critical review, SR= submission and revision, PM= project management, FA= funding acquisition.

Conflict of Interest

The authors declared that there is no conflict of interest.

Ethical Consideration

Ethics committee approval was not required for this study because of there was no study on animals or humans.

References

Berto L, Seatta A, Simioni P, Vitaliani R. 2008. Nonlinear static analyses of RC frame structures: influence of corrosion on seismic response. Proceedings of the 8th World Congress on Computational Mechanics (WCCM8), 23-25 June, Venice, Italy, pp: 25.

Berto L, Vitaliani R, Saetta A. 2009. Seismic assessment of

existing RC structures affected by degradation phenomena. *Struct Safety*, 31(4): 284-297.

Bhargava K, Ghosh AK, Yasuhiro M, Ramanujam S. 2008. Suggested empirical model for corrosion-induced bond degradation in reinforced concrete. *J Struct Eng*, 134(2): 221-230.

Bossio A, Imperatore S, Kioumars M. 2019. Ultimate flexural capacity of reinforced concrete elements damaged by corrosion. *Buildings*, 9(160): 1-13.

BRITE/EURAM. 1995. The residual service life of reinforced concrete structures, Final Technical Report, Report No. BRUE-CT92-0591.

Celep Z. 2008. Betonarme taşıyıcı sistemlerde doğrusal ötesi davranış ve çözümleme. İstanbul Teknik Üniversitesi, İstanbul, Türkiye, pp: 75.

Chung L, Kim JJ, Seong Y. 2008. Bond strength prediction for reinforced concrete members with highly corroded reinforcing bars. *Cement Concrete Compos*, 30 (7): 603-611.

Çolakoglu HE. 2020. Numerical investigation of the effect of transverse reinforcement spacing on earthquake performance of reinforced concrete columns. *Adiyaman Üniv Müh Bil Derg*, 12(7): 1-13.

Dhir RK, Jones MR, McCarthy MJ. 1994. PFA concrete: chloride-induced reinforcement corrosion. *Magazine Concrete Res*, 46(169): 269-277.

Dizaj EA, Kashani MM. 2021. Nonlinear structural performance and seismic fragility of corroded reinforced concrete structures: modelling guidelines, *European J Environ Civil Eng*, 2021: 5374-5403.

Elçi H, Göker KA. 2018. Comparison of earthquake codes (TEC 2007 and TBEC 2018) in terms of seismic performance of RC columns. *Int J Scient Technol Res*, 4(6): 9-21.

Ersoy U, Özcebe G. 2018. Betonarme. Orta Doğu Teknik Üniversitesi, Ankara, Türkiye, pp: 125.

Hsu TTC. 1993. Unified Theory of Reinforced Concrete. CRC-Press Inc., Boca Raton, US.

Imperatore S, Rinaldi Z, Drago C. 2017. Degradation relationships for the mechanical properties of corroded steel rebars. *Construct Build Mater*, 148: 219-230.

Lee HS, Cho YS. 2009. Evaluation of mechanical properties of steel reinforcement embedded in concrete specimen as a function of the degree of reinforced corrosion. *Int J Fracture*, 157(1): 81-88.

Mangat P, Elgarf M. 1999. Flexural strength of concrete beams with corroding reinforcement. *ACI Struct J*, 97(1): 149-59.

Middleton CR, Hogg V. 1998. Review of deterioration models used to predict corrosion in reinforced concrete structures. Cambridge University Engineering Department Technical Report No. CUED/D - STRUCT/TR.173, Cambridge, UK.

Mohammed TU, Hamada H, Yamaji T. 2004. Concrete after 30 years of exposure -Part II: Chloride ingress and corrosion of steel bars. *ACI Mater J*, 101(1): 13-18.

Molina FJ, Alonso C, Andrade C. 1993. Cover cracking as a function of rebar corrosion: part 2- numerical mode. *Mater Struct*, 26: 532-548.

Ou YC, Fan HD, Nguyen ND. 2013. Long-term seismic performance of reinforced concrete bridges under steel reinforcement corrosion due to chloride attack. *Earthquake Eng Struct Dynamics*, 42: 2113-2127.

Ou YC, Tsai MS, Chang KC, Lee G. 2010. Cyclic behavior of precast segmental concrete bridge column with high performance or conventional steel reinforcing bars as energy dissipation bars. *Earthquake Eng Struct Dynamics*, 39(11): 1181-1198.

Palsson R, Mirza MS. 2002. Mechanical response of corroded

- steel reinforcement of abandoned concrete bridge. *ACI Struct J*, 99(2): 157-162.
- Revathy J, Suguna K, Raghunath PN. 2009. Effect of corrosion damage on the ductility performance of concrete columns. *American J Eng Appl Sci*, 2(2): 324-327.
- Sezen H, Setzler EJ. 2008. Reinforcement slip in reinforced concrete columns. *ACI Struct J*, 105(3): 280-289.
- TBDY. 2018. Türkiye bina deprem yönetmeliği. Afet ve Acil Durum Başkanlığı, Ankara, Türkiye.
- Topçu A. 2022. Eskişehir Osmangazi Üniversitesi. URL: <http://mmf2.ogu.edu.tr/atopcu/> (accessed date: August 01, 2019).
- Vu NS, Li B. 2018. Seismic performance of flexural reinforced concrete columns with corroded reinforcement. *ACI Struct J*, 115(5): 1253-1266.
- Yavuz R, Günaydın O, Güçlüer K. 2019. Investigation of corrosion and adherence in reinforced concrete. *Kahramanmaraş Sütçü İmam Univ J Eng Sci*, 22: 12-18.
- Ying M, Yi C, Jinxin G. 2012. Behavior of corrosion damaged circular reinforced concrete columns under cyclic loading. *Construct Build Mater*, 29(1): 548-556.
- Yüksel İ, Sancaklı GB. 2018. Zemin katı korozyona maruz kalmış bir binanın performans değerlendirmesi. *Eskişehir Teknik Üniv Bil Teknol Derg B- Teor Bil*, 6: 152-165.



İÇ LOJİSTİK FAALİYETLERİNDE YALIN TEKNİKLERİN KULLANILMASI VE BİR UYGULAMA

Ayşe UÇAR¹, Betül TURANOĞLU ŞİRİN^{1*}

¹Atatürk University, Faculty of Engineering, Department of Industrial Engineering, 25240, Erzurum, Türkiye

Özet: Yalın kavramı 1950'li yıllarda Japon şirketlerinde ortaya çıkmıştır. Yalın felsefe, iş süreçlerinde verimliliği artırmayı, israfları ortadan kaldırmayı ve müşteri değerine odaklanmayı amaçlayan bir felsefedir. Dünya genelinde yalın felsefe; küresel rekabette avantaj sağlamak, sürdürülebilirlik hedeflerine ulaşmak, hızlı piyasa değişimlerine adapte olmak, müşteri memnuniyetini artırmak gibi önemli amaçlar doğrultusunda birçok işletmeye fayda sağlamıştır. Günümüzde yalınlaşma ve yalın teknikler, imalat sistemleri ile birlikte hizmet sistemlerinde de kullanılmaktadır. Buna; eğitim, tedarik ve lojistik, bilişim ve teknoloji gibi iş kolları örnek olarak gösterilebilir. Bu çalışmada, bir gıda firmasının iç lojistik süreçlerinde yalın teknikler kullanılarak süreç iyileştirme yapılmıştır. Öncelikle, söz konusu sürece değer katmayan işlemleri tespit edip ortadan kaldırmak için Değer Akışı Haritalama (DAH) kullanılmıştır. Bu süreçte manuel yürütülen işlemler elimine edilerek yeni bir sistem oluşturulmuştur. Mevcut durumda toplam 434 dakikada tamamlanan malzeme transfer süreci, yeni sistem önerisi ile 284 dakikaya düşürülmüştür. Daha sonra PUKÖ döngüsü ile yaşanan bazı problemler analiz edilerek çözüm önerileri sunulmuştur. Son olarak, spaghetti diyagramı ve Milk Run taşıma sistemi ile gereksiz taşımalar minimize edilmiştir. Bu sistemin kullanılmasıyla, yıllık ortalama taşımalar için harcanan 470 saatin 50,1 saate düşmesi öngörülmektedir.

Anahtar kelimeler: Yalın iç lojistik, Süreç iyileştirme, Değer akışı haritalama, PUKÖ döngüsü, Spagetti diyagramı, Milk Run

Using Lean Techniques in Internal Logistics Activities and an Application

Abstract: The concept of lean emerged in Japanese companies in the 1950s. Lean philosophy is a mindset aimed at enhancing efficiency in business processes, eliminating waste, and prioritizing customer value. This philosophy has globally benefited numerous businesses for crucial purposes such as gaining a competitive edge in the global market, achieving sustainability goals, adapting to rapid market changes, and enhancing customer satisfaction. Today, simplification and lean techniques are employed not only in manufacturing systems but also in-service systems. Business sectors such as education, supply and logistics, informatics, and technology can be cited as examples. In this study, lean techniques were employed to improve the internal logistics processes of a food company. Initially, Value Stream Mapping (VSM) was utilized to identify and eliminate processes that do not contribute value to the targeted process. In this process, manual procedures were eliminated, and a new system was implemented. The material transfer process, which currently takes 434 minutes in total, has been reduced to 284 minutes with the new system proposal. Subsequently, issues encountered within the PDCA cycle were analysed, and potential solutions were proposed. Finally, unnecessary transportation was minimized through the spaghetti diagram and the implementation of the Milk Run transportation system. By using this system, it is anticipated that the annual average of 470 hours spent on transportation will decrease to 50.1 hours.

Keywords: Lean internal logistics, Process improvement, Value stream mapping, PDCA cycle, Spaghetti diagram, Milk Run

*Sorumlu yazar (Corresponding author): Atatürk University, Faculty of Engineering, Department of Industrial Engineering, 25240, Erzurum, Türkiye

E mail: b.turanoglu@atauni.edu.tr (B. TURANOĞLU ŞİRİN)

Ayşe UÇAR



<https://orcid.org/0000-0002-0680-8137>

Betül TURANOĞLU ŞİRİN



<https://orcid.org/0000-0002-7910-6312>

Gönderi: 14 Şubat 2024

Kabul: 20 Mart 2024

Yayınlanma: 15 Mayıs 2024

Received: February 14, 2024

Accepted: March 20, 2024

Published: May 15, 2024

Cite as: Uçar A, Turanoğlu Şirin B. 2024. Using lean techniques in internal logistics activities and an application. BSJ Eng Sci, 7(3): 423-435.

1. Giriş

Yalın düşünce felsefesi 1950'li yıllarda Toyota Motor İşletmesi tarafından ortaya çıkmıştır. Yalın düşüncedeki temel amaç, değer hammadde mamul oluşuncaya kadar geçen sürede kesintisiz akmasıdır. Bu amaca ulaşmanın temelinde ise israfları öncelikle tespit edip ardından elimine etmek vardır. Az maliyet, az israf, hızlı üretim ve uygun fiyat ile en kaliteli üretimi yapabilmek fikridir (Yangınlar ve Bal, 2019).

Değer katmayan adımlar israf olarak tanımlanmakla beraber, literatürde Taiichi Ohno tarafından 1988 yılında 'Yedi Ölümcül İsrar' başlığı altında "gereksiz üretim, fazla bekleme, üretimde hata, fazla stok, gereksiz taşıma,

gereksiz işler ve gereksiz hareketler" olarak tanımlanmıştır (Topuz, 2021).

Globalleşen dünyada firmalar sektöre tutunabilmek için değişmek ve gelişmek zorunda bırakılmıştır. Bu süreçte işletmeler kaliteli ürünü daha ucuza üretmeyi hedeflemiştir. Hedeflere ulaşma yolunda Yalın araç ve tekniklerden faydalanılmıştır. Yeni yönetim kavramları ve süreç iyileştirmedeki süreklilik yalın felsefenin vurguladığı temel konulardan biri olmuştur.

İşletmeler bünyesinde yalınlaşmaya gidilecek bir konu da lojistik faaliyetlerdir. Fabrika içinde yalın lojistik yaklaşımı üretilen ürünlerin az maliyetle ve kısa sürede işletme içerisinde taşınmasıdır. Bu da iç lojistik kavramı olarak karşımıza çıkmaktadır (Topuz, 2021). Takip



edilebilir ve standart olmayan bir iç lojistik sistemi, işletmelerin stok hareketlerinde dengesizliğe ve katma değer oluşturmayan faaliyetlere neden olmaktadır. Taşıma yapan aracın etkili kullanılmamasından dolayı çalışanların katma değersiz işler yapması, malzemelerin zamanında tedarik edilememesi veya büyük miktarda yarı mamul birikimi gibi durumlar işletmeler için önemli bir maliyet unsurudur (Küçüköğlü ve ark., 2018).

Yalın düşünce kapsamında israfları yok ederken belli başlı araç ve yöntemler kullanılır. Bunlardan bazıları; 5S, SMED, Değer Akışı Haritalama, Spagetti Diyagramı, Milk Run, Hoshin Kanri, Poke-Yoke, A3, PUKÖ, Just in Time, Kök Neden Analizidir.

Literatürde iç lojistik, değer akışı haritalama, PUKÖ döngüsü ve Milk Run ile ilgili birçok uygulama çalışmasına rastlanmıştır. Bunlardan bazıları Tablo 1’de özetlenmiş ve aşağıdaki gibi açıklanmıştır:

Gecü (2008) bir otomotiv firmasının iç lojistiğinde yaptığı çalışmada, her bir çalışan için üretimde lojistik rotalarını çizmiş, verimsizlikleri tespit etmiş ve yeni bir yerleşim planı oluşturmuştur. Zaman etütleri yaparak ihtiyaç duyulan işgücünü tespit etmiştir. Ayrıca, ana montaj hatlarında kit halinde üretime malzeme transferleri yapmış ve hat kenarında izlenebilirliği arttırmıştır. Sol (2011), çalışmada yalın üretim tekniklerinden Kanban, değer akışı haritalama, 5S ve spagetti diyagramını kullanmıştır. Operatör ve malzemelerin katma değer yaratmayan faaliyetlerinin belirlenmesi için süreç akış şemalarından faydalanmıştır. Yapılan analizler sonucunda, set şeklinde sevkiyat sisteminin ara stok miktarlarını azalttığı, malzeme akışları ve hareketlerindeki kontrolleri kolaylaştırdığı ve taşımaları azalttığını tespit etmiştir. Kilic ve ark. (2012)

yaptıkları çalışmada, gerçek bir üretim ortamındaki gözlemlere dayanarak tesislerdeki Milk Run dağıtım problemini kategorize etmiş ve açıklamışlardır. Ana kategorilerden biri için modelleme yapmışlardır. Geliştirilen modellerin amacı, araç sayısını ve kat edilen mesafeyi en aza indirmektir. Çalışmada, modellerin uygulanabilirliğini göstermek için gerçek uygulamalardan esinlenerek sayısal bir örnek sunulmuştur. Koçan (2014) çalışmada, set şeklinde sevkiyat sisteminin hat besleme yöntemleri arasındaki yerini incelemiş ve hangi yöntemle hat kenarına parçaların taşınması gerektiğine karar vermeyi amaçlamıştır. Set şeklinde teslimat için bir süreç yaklaşım metodu geliştirmiştir. Ayrıca; Kanban, 5S ve süreç akış şemaları yalın teknikler olarak kullanılmıştır. Yapılan tüm bu süreç iyileştirme çalışmalarının set şeklinde sevkiyat sisteminin parça akış kontrolünü kolaylaştırdığı, hat kenarı alanlarından tasarruf sağladığı, ara stok miktarlarını azalttığı, daha esnek bir üretim sistemi sağladığı, malzeme ve parça taşımalarını azalttığı, katma değer yaratmayan faaliyetleri yok ederek çevrim süresini düşürdüğü ve üretkenliği artırdığı görülmüştür. Tyagi ve ark. (2015), gaz tribünleri üreten bir fabrikada değer akışı haritalamayı kullanarak ürün geliştirme sürecinin süresinde ortalama %50’lik bir azalma sağlamışlardır. Korytkowski ve Karkoszka (2016), bir montaj hattında Milk Run operatörünün verimliliği ve etkileşimlerini incelemek için simülasyon tabanlı bir model önerisinde bulunmuşlardır. Kuvvetli ve Erol (2017), ağaç ürünleri üreten bir işletmede malzeme taşıma sistemini simülasyonla incelemiş ve alternatif bir çözüm yöntemi sunmuştur.

Tablo 1. Özetlenmiş literatür araştırması

Yazar/lar ve Yayın Yılı	Uygulama Konusu	Kullanılan Teknikler
Gecü, 2008	İç lojistik / Malzeme taşıma	Zaman etütü
Sol, 2011	Malzeme taşıma sistemi	Kanban, 5S, DAH, Spagetti diyagramı
Kilic ve ark., 2012	İç lojistik / Dağıtım problemi	Milk Run
Koçan, 2014	İç lojistik / Sevkiyat sistemi	Kanban, 5S, Süreç akış şemaları
Tyagi ve ark., 2015	Ürün geliştirme süreci	DAH
Korytkowski ve Karkoszka, 2016	Montaj hattı verimliliği	Milk Run, Simülasyon
Kuvvetli ve Erol, 2017	İç lojistik / Malzeme taşıma	Simülasyon, İstatistik
Sangpikul, 2017	Öğrenme ve öğretme problemi	PUKÖ döngüsü
Realyvásquez-Vargas ve ark., 2018	Ürün kusurlarını azaltma	PUKÖ döngüsü
Küçüköğlü ve ark., 2018	İç lojistik / Malzeme taşıma	Matematiksel model
Turan, 2019	Süreç iyileştirme	DAH, AHP
Sevgili ve Antmen, 2019	Süreç iyileştirme	DAH
Patır, 2019	İç lojistik	DAH
Derdiyok, 2019	Kalite güvence sistemleri	PUKÖ döngüsü
Usuk ve Selvi, 2019	İç lojistik / Malzeme taşıma	Otomasyon
Doğan ve Kama, 2021	Tedarik zinciri	DAH
Grzegorz ve ark., 2021	Malzeme taşıma sistemi	Milk Run
Topuz, 2021	İç lojistik / Malzeme taşıma	Kanban, Milk Run, Süpermarket
Gu ve ark., 2021	Yönetim	PUKÖ döngüsü
Kuğu ve Köse, 2021	Süreç iyileştirme	DAH
Lu ve ark., 2021	Süreç iyileştirme	Nesnelerin interneti, DAH
Facchini ve ark., 2024	İç lojistik / Malzeme taşıma	Nesnelerin interneti, Milk Run

Mevcut durumda, vinçler ile çalışılan alanda konveyörlerin kullanılması durumu incelenmiş ve istatistiksel olarak konveyör kullanımının daha anlamlı olduğu tespit edilmiştir. Sangpikul (2017) çalışmasında, PUKÖ döngüsünü kullanarak bir akademik hizmet projesi için bir öğrenme ve öğretme modeli geliştirmiştir. Realyvásquez-Vargas ve ark. (2018), bir imalat işletmesinde ürün kusurlarını azaltmak için PUKÖ döngüsünden faydalanmışlardır. Analiz edilen üç farklı üründe, kusur oranı ortalama %70 oranında azaltılmıştır. Küçüköğlü ve ark. (2018) çalışmasında, bir otomotiv yan sanayi firmasında fabrika içi malzeme tedarik problemini ele almıştır. Fabrika içerisinde hat yanı stoklarını minimuma düşürmek ve daha sağlıklı bir malzeme taşıma süreci sağlamak için iki aşamalı bir çözüm yaklaşımı geliştirmiştir. Turan (2019), bir otomotiv yan sanayi fabrikasında değer akışı haritalama ile analitik hiyerarşi süreci yöntemini birlikte kullanarak iyileştirmeler yapmış ve yaşanan problemlere çözüm önerileri sunmuştur. Sevgili ve Antmen (2019) çalışmalarında, bir metal fabrikasında değer akışı haritalamayı kullanarak süreç iyileştirme yapmışlardır. Çalışmada; toplam üretim süresinde düşüş, üretim miktarında artış ve proses değişkenliğinde azalma sağlanmıştır. Patır (2019), bir otomotiv yan sanayi firmasının üretim lojistiği sürecini incelemiştir. İsrâfları gün yüzüne çıkarmak için değer akışı haritalama yönteminden faydalanmıştır. Bu çalışma sonunda, stoklarda yaklaşık %20 oranında azalma sağlanırken, lojistik maliyeti ve operatör sayısı gibi konularda da iyileştirmeler yapılmıştır. Derdiyok (2019), kalite güvence sistemlerinin üniversitelerde uygulanmasını yaygınlaştırmak amacıyla PUKÖ döngüsünü kullanan bir model önermiştir. Usuk ve Selvi (2019) çalışmasında, kabloşuz acil malzeme istek sistemi oluşturmuştur. Fabrika içi lojistik aksaklıklar nedeniyle malzemelerin sahaya geç teslim edilmesinden kaynaklanan hat duruşları ortadan kaldırılmıştır. Böylece, malzemelere ulaşmak daha kolay hale gelmiş ve taşıma işlemi standartlaştırılmıştır. Ayrıca, taşımalarda gerçekleşen israflar minimize edilmiştir. Doğan ve Kama (2021) çalışmalarında, bir imalat işletmesinin tedarik zincirindeki israfları belirleyip en aza indirmek için değer akışı haritalama yöntemini kullanmışlardır. Çalışma sonunda, bir ürünün hammadde sürecinden alıcıya ulaşmasına kadar geçen sürede %21'lik bir azalma sağlanacağı öngörülmüştür. Grzegorz ve ark. (2021), Milk Run taşıma sistemleri için referans bir model önerisinde bulunmuşlardır. Topuz (2021), beyaz eşya sektöründe yaptığı çalışmada yalın üretim tekniklerinden Kanban, Milk Run ve süpermarket yöntemlerinin kullanıldığı bir metodoloji geliştirmiştir. Sonuç olarak malzeme taşıma, montaj sahasından alınarak bir süpermarket kurulmuştur. Toplam malzeme taşıma mesafesi %79 oranında azaltılmıştır. Gu ve ark. (2021) çalışmalarında, lisansüstü tıp öğrencilerinin yönetiminde yaşanan zorlukları gidermek amacıyla PUKÖ döngüsünden faydalanmışlardır. Kuğu ve Köse (2021), ısı değiştirici

üretim hattında uyguladıkları değer akışı haritalama ile ara stok miktarlarında ortalama %59'luk bir düşüş sağlarken işlem süresinde %31'lik bir azalma elde etmişlerdir. Lu ve ark. (2021), nesnelerin interneti teknolojisini kullanarak küçük ve orta ölçekli işletmeler için dijital ikiz tabanlı bir değer akışı haritalama yöntemi önermişlerdir. Facchini ve ark. (2024), bir otomotiv sanayi işletmesinde nesnelerin interneti tabanlı Milk Run taşıma ve rotalama problemini ele almışlardır. Çalışma sonunda her iş istasyonunun envanteri sağlanmış, çekici tren filosunun ortalama kullanım oranı iyileştirilmiş ve günlük kat edilen mesafe azaltılmıştır.

Bu çalışmada bir gıda işletmesinin iç lojistik süreçleri incelenmiş ve süreçlerde tespit edilen katma değersiz işlemler yalın teknikler olan değer akışı haritalama (DAH), PUKÖ döngüsü, kök neden analizi, Spagetti Diyagramı ve Milk Run kullanılarak minimize edilmiştir. Literatürdeki çalışmalara bakıldığında, bu çalışmanın katkıları aşağıdaki gibi sıralanabilir:

- Bir gıda firmasının iç lojistik faaliyetlerinde süreç iyileştirme üzerine yapılan gerçek bir uygulama çalışmasıdır.
- DAH, PUKÖ döngüsü, kök-neden analizi, spagetti diyagramı ve Milk Run gibi beş farklı teknik kullanılmıştır.
- Firmanın deposunda uygulanan bu çalışma ile toplam işlem süresinde %31'lik bir azalma olmuştur. Ayrıca elde edilen sonuçlar, malzeme taşıma için önerilen Milk Run sisteminin toplam malzeme taşıma süresinde yıllık %89'luk bir düşüş sağlayacağını göstermiştir.
- Çalışma kapsamında yapılan tüm çalışmalar, firma yönetimi tarafından kabul görmüş ve uygulamaya konmuştur.

2. Materyal ve Yöntem

2.1. İç Lojistik Kavramı

Tedarik ve dağıtım lojistiği arasında kalan iç lojistik, bir diğer adı ile üretim lojistiği; hammaddelerin, nihai ürünün, yarı mamullerin tesis içindeki hareketi, stok yönetimi, planlama, depolama ve istiflenme, sipariş toplama ve dağıtım, malzeme taşıma araçlarının seçimi ve hareketlerine ilişkin kurallar gibi süreçleri kapsamaktadır. Bu süreçler aşağıdaki gibi detaylandırılabilir:

- Depolama: Mal kabulü, malzemelerin kayıt altına alınması, istifleme, taşıma, sevkiyat öncesi ürünleri hazırlama ve etiketleme, depolama alanların düzeni ve tertibi işlemlerinden oluşmaktadır (Erturgut, 2021).
- Stok yönetimi: Ürünlerin nerede stoklanacağı, ne kadar sipariş verileceği, siparişin teslim tarihi, ne stoklanacağı ile ilgili soruların cevaplarının arandığı bir yönetimdir.
- Planlama: Planlama aşamasında müşterilerin beklentilerinin karşılanması ve doğru zamanda nihai ürünün müşteriye ulaştırılması hedef alınarak

üretim, tedarikin ve sevkiyat süreçlerinin organize edilmesidir (Erturgut, 2021).

- Malzeme taşıma araçlarının seçimi: Günümüz işletme yapılarında maliyetlerin ve firmalar arası rekabetin artması kaynaklı üretim için harcanan maliyetin ve zamanın önemi ile beraber elleçleme için ayırdığı zamanı da değerli kılmıştır. Elleçleme de çalışma ortamına en uygun aracın seçilmesidir (Dur, 2019).
- Ambalajlama ve etiketleme: Ambalajlar ürünleri dış etkilerden koruyan, ürün tipine göre metal, plastik, cam vb. türevlerden oluşan malzemelerdir. Ambalajlama ve etiketleme gerek depolama esnasında gerek fabrika içi transferlerde güvenli, hatalı işlem yapma ve hasar riskini minimumda tutmaya doğrudan katkısı olan bir süreçtir. (Erturgut, 2021).

2.2. Yalın Üretim Kavramı

Yalın üretim katma değersiz işlemlerin elimine edilerek, tam anlamı ile israfların ortadan kaldırılmasına odaklanan bir sistem bütünüdür. Verimliliği ve esnekliği hedef alır (Mofolasoyoa ve ark., 2022).

Yalın üretim sisteminin tarihi 1950'li yıllara dayanmaktadır. Toyota firmasında Eiji Toyota ve Taiichi Ohno öncülüğünde atılmıştır. Amerika'da yer alan firmalara rakip olacak seviyeye gelebilmeyi hedeflemiş ve yeni bir yönetim biçimi arayışına girmişlerdir. Adım adım ilerleyerek tüm üretim sistemlerini gözden geçirmişlerdir. Seri üretimden ziyade küçük partiler halinde ve çeşitliliği artırarak düşük taleplere de cevap verebilecek bir üretim sistemi geliştirmişlerdir. Başta Japonya olmak üzere zamanla dünyaya yayılmış bir sistem haline gelmiştir (Kocabaş, 2014).

Yalınlaşmanın temelinde israfları yok etmek yatar. Değer ile israfı ayırt ederek odakları değer yaratan işlere yönlendirmeyi hedef alır. Değer müşterinin ödemeye istekli olduğu ürün ve süreçlerdir (Ertürk ve Özçelik, 2008).

Yalın üretim, sürekli iyileştirme ve kaynakları en etkili şekilde kullanma felsefesiyle tanınan bir üretim yaklaşımıdır. Bu yaklaşım, üretim süreçlerindeki israfları belirleyerek ve azaltarak verimliliği artırmayı hedefler.

Yalın üretimde yedi temel israf vardır:

- Fazla üretim: Sipariştten önce, ihtiyaçtan fazla üretimi kapsamaktadır. Fazla üretimler için ek depolama alanları, malzeme akışında dengesizlik gibi problemlere yol açmaktadır.
- Fazla stok: Nihai ürün, hammadde, yarı mamul gibi stok türlerinde fazla tutulan stokları ifade eder. Fazla tutulan stoklar depolama maliyeti oluşturur. Depolardaki hareketin kısıtlanmasına sebep olmakla beraber hatalı işlem yapma oranını arttırmaktadır.
- Gereksiz işlem: Katma değersiz işlemler ile ilgilenmektir. Yalın üretim felsefesi katma değersiz işlemlerin elimine edilmesini hedeflenmektedir. Değer yaratan işlemler üzerinde çalışmaya odaklanmaktadır.

- Gereksiz hareket: Çalışanların, ürüne veya hizmete herhangi bir katkı sağlamayan nedenlerle gereksiz hareket etmeleri sonucu ortaya çıkan israftır. Üretimde kullanılacak malzemelerin hatlardan uzak olması, ergonomik açıdan zorlayan iş ekipmanları, aşırı harekete sebep olan düzenlemeler örnek olarak gösterilebilir.
- Hatalı üretim: Bir ürünü düzeltmek, onarmak ya da yenisi üretmek olarak tanımlanabilir. Bu israf ek hammadde ve işçilik maliyeti doğurmaktadır. Bununla beraber müşteri siparişlerinin teslimatında gecikmeye de sebep olmaktadır.
- Gereksiz bekleme: Personel veya makine, ekipmanların çalışma saatleri içerisinde boşta kalması ve beklemesi olarak tanımlanmaktadır. Makinede bulunan arıza kaynaklı makinenin çalışmadan beklemesi, personelin makine hazırlık sürecinde makinenin hazırlanmasını beklemesi, makinenin personeli beklemesi gibi örnekler verilebilmektedir.
- Gereksiz taşıma: Gereksiz taşıma, ürünlerin bir noktadan diğerine taşınması sırasında oluşan israfı temsil eder. Yalın üretimde, minimum taşıma mesafeleri ve daha etkili lojistik süreçleri üzerinde çalışma önemlidir.

Bu çalışmada kullanılan yalın üretim teknikleri değer akışı haritalama, PUKÖ döngüsü, kök neden analizi, spaghetti diyagramı ve Milk Run taşıma sistemidir.

2.3. Değer Akışı Haritalama

Değer Akışı Haritalama (DAH), yalın felsefede kullanılan en önemli tekniklerden biridir. Üretim ve hizmet sektörlerinde yaygın olarak tercih edilen DAH, hammaddenin firmaya gelişinden ürünün müşteriye teslim edilmesine kadar geçen süreçleri kapsamaktadır (Doğan ve Kama, 2021). Değer akışı, bir ürünü oluşturmak için temel olan ana akışlar boyunca ihtiyaç duyulan faaliyetleri kapsayan bir kavramdır. Bu faaliyetler hem katma değer yaratan hem de yaratmayan unsurları içerir. Eğer her bir ürün için gerekli olan ana akışları sıralarsak; hammaddenin müşteriye üretim akışı ile başlanabilir ve ardından ürün geliştirme süreci, yani tasarım, takip eder (Kuşu ve Köse, 2021).

DAH' da süreçler semboller ile ifade edilir. Sırasıyla, incelenecek ürün ailesinin veya sürecin belirlenmesi ile mevcut durum haritası çizilir. Süreçte yapılabilecek iyileştirmeler planlanarak gelecek durum haritası oluşturulur. İsrافی görselleştiren bir teknik olarak DAH ile gelecek durum haritası çizildikten sonra aktiviteler planlanır ve uygulamalar gerçekleştirilir. Bu süreç, işlemleri daha etkin hale getirerek israfı azaltmayı ve değeri artırmayı amaçlar.

DAH' da bazı veriler önem arz etmektedir. Bunlar; çevrim süresi, katma değer süresi, akış süresi, operatör sayısı, makine hazırlık süreleri, çalışma süreleridir (Birgün ve ark., 2006):

- Çevrim süresi (C/T): Boşaltma, yükleme, hazırlık süreleri dahil bir prosesin tamamlanma sıklığıdır.
- Katma Değer Süresi (V/A): Müşterinin değer olarak

tanımladığı iş elemanlarının süresidir.

- Akış Süresi (L/T): Bir işin başlama ve bitiş zamanları arasında geçen süre akış süresi olarak tanımlanmaktadır.

2.4. PUKÖ Döngüsü

İşletmelerde planlama, araştırma, tasarlama, üretim ve satışın birbirini takip eden bir çevrim olduğunu savunan W. Edward Deming, Deming Döngüsü olarak da anılan PUKÖ döngüsünü literatüre kazandırmıştır. Deming'in bu çevriminden esinlenen Japon yöneticiler, Deming' in bu çevrimini yönetimin tüm aşamalarına uygulayarak buna PUKÖ (Planla-Uygula-Kontrol Et-Önlem Al) döngüsü adını vermişlerdir (Efil, 1994). Mükemmelliği aramayı hedefleyen yalın yönetim sisteminde de PUKÖ döngüsü önemli yer tutar. PUKÖ, iyileştirme ve geliştirme süreçlerinde önemli bir yol gösterici olarak kullanılmaktadır.

PUKÖ döngüsünün dört temel aşaması aşağıdaki gibi açıklanabilir (Realyvásquez-Vargas ve ark., 2018):

- Planla: Bu aşamada, iyileştirme fırsatları belirlenir ve daha sonra bunlara öncelik verilir. Aynı şekilde, analiz edilecek sürecin mevcut durumu tutarlı verilerle tanımlanır, sorunun nedenleri belirlenir ve çözmek için olası çözümler önerilir.
- Uygula: Bu aşamada, eylem planını uygulamak, bilgiyi seçmek ve belgelemek amaçlanır. Ayrıca, beklenmeyen olaylar, öğrenilen dersler ve edinilen bilgi göz önüne alınmalıdır.
- Kontrol Et: Bu adımda, önceki adımda uygulanan eylemlerin sonuçları analiz edilir. İyileştirmelerin olup olmadığı ve belirlenen hedeflere ulaşıp ulaşılmadığı kontrol edilir. Bu amaçla, Pareto çizelgesi veya Ishikawa diyagramı gibi çeşitli grafik destek araçları kullanılabilir.
- Önlem Al: Bu aşama, iyileştirmeleri standartlaştırmaya yönelik yöntemler geliştirmeyi içerir. Ayrıca, iyileştirmeyi tekrar test etmek ve yeni veri elde etmek için tekrar kanıtlanır veya uygulanan eylemlerin etkili iyileştirmeler sağlamadığı durumda proje terk edilir ve yeni bir proje ilk aşamadan başlanır.

2.5. Kök Neden Analizi

Kök neden analizi, bir sorunun temel nedenlerini belirlemek ve bu nedenleri ele alarak tekrarlayan problemleri önlemek amacıyla kullanılan bir analitik yöntemdir. Temelde bir olayın ya da sorunun yüzeydeki belirgin nedenlerinin ötesine geçerek, altında yatan temel nedenleri ortaya çıkarmayı hedefler. Bu analiz, problemlerin sadece semptomları değil, asıl kök nedenleri ele alarak kalıcı çözümler bulmaya odaklanır. Kök neden analizi genellikle "5 Neden" tekniği veya İngilizce adıyla "5 Whys" yöntemi kullanılarak gerçekleştirilir. Bu yöntemde, bir sorunun nedenini bulmak için sıralı olarak beş kez "Neden?" sorusu sorulur. Her soru, önceki cevaptan türetilmiş ve altında yatan temel nedeni daha da açığa çıkarmaya yöneliktir. Bu süreç, sorunun kök nedenine ulaşana kadar devam eder. Kök neden analizi, iş süreçlerindeki iyileştirmeleri,

tekrarlayan problemlerin önlenmesini ve etkili çözümler geliştirmeyi sağlayarak sürdürülebilir başarı için önemli bir araçtır (Dogget, 2006).

2.6. Spagetti Diyagramı

Spagetti diyagramı, bir iş akışı için çalışanın yaptığı tüm hareketleri gösteren ve bu hareketlerden ortaya çıkan israfın anlaşılmasını sağlayan yalın tekniklerden biridir. Spagetti diyagramı ile çalışanların kullandıkları her yol renklendirilerek bir harita oluşturulur. Bu harita üzerinden süreç ya da iş akışı için atılan toplam adım sayısı hesaplanır. Elde edilen toplam adım sayısı ile gerçekleşen hareket israfının azaltılması amaçlanır (Sönmez ve Yağmur, 2021). Spagetti diyagramları genellikle bir işyerindeki fiziksel alanları veya bir sürecin adımlarını temsil eden bir harita üzerinde çizilir. Bu diyagramlar, sürecin karmaşıklığını ve etkileşimlerini daha iyi anlamak için bir araç olarak kullanılır.

Spagetti diyagramının temel amaçları aşağıdaki gibi sıralanabilir:

- İş süreçlerindeki adımların ve aktivitelerin nasıl birbirine bağlı olduğunu gösterir. Bu sayede gereksiz hareketleri ve kayıpları belirleyebilir.
- İş süreçlerindeki fiziksel mesafeleri, hareketleri ve ilişkileri görselleştirerek mevcut durumu anlama ve değerlendirme imkânı sağlar.
- Çizgiler arasındaki karmaşık örüntüler sayesinde, süreçteki olası iyileştirme fırsatları daha net bir şekilde anlaşılabilir.

2.7. Milk Run

Milk Run kavramı, farklı satıcılardan farklı teslimatları maksimum kapasite ve minimum maliyetle gerçekleştirilmesini sağlayan bir teslimat yöntemi olarak açıklanabilir. Milk Run adı, kamyonların günlük süt ihtiyacını mandıra kooperatiflerine ulaştırmak için kullanılan yöntemden türetilmiştir. Milk Run, talep gereksinimini en az maliyetle ve etkili bir şekilde taşımayı karşılamak için minimum mesafe kat edilmesini ve maksimum talebin teslimat aracına taşınmasını sağlar. Bu, yükün birçok farklı yerde ve daha küçük birimlerde dağıldığı durumlarda uygulanır. Böyle bir durumda her merkezden tek tek taşıma çok pahalı olacağından ihtiyaca göre bir şema tasarlanmakta ve buna göre tüm farklı üniteler temin edilip taşınmaktadır.

Milk Run, birkaç iş istasyonunu bir tedarik döngüsüne bağlayan ve bir rota boyunca römorkör treninin çok kez yüklendiği ve boşaltıldığı bir taşıma sistemidir. Son on yılda, malzeme taşımanın yoğun olduğu işlerde artan bir popülerlik kazanmıştır. Forkliftlerin aksine, bir süpermarketi bir taşıma rotası boyunca birden fazla teslimat konumuyla birbirine bağlarlar (Facchini ve ark., 2024). Bu sistemlerin ana avantajı, sabit programlara göre çalışarak değişkenliği azaltmalarıdır. Böylece, bir tedarik ağı içerisinde stok, kapasite ve zaman tamponlarının azaltılmasına olanak tanır (Grzegorz ve ark., 2021).

Milk Run taşıma sistemleri, lojistik maliyetlerini azaltmaya katkısından dolayı işletmelerde tercih edilmektedir. Bu çalışmada, hammadde depodan üretim

cep depolara günlük olarak yapılan transferler ile ilgili Milk Run'dan faydalanılmıştır.

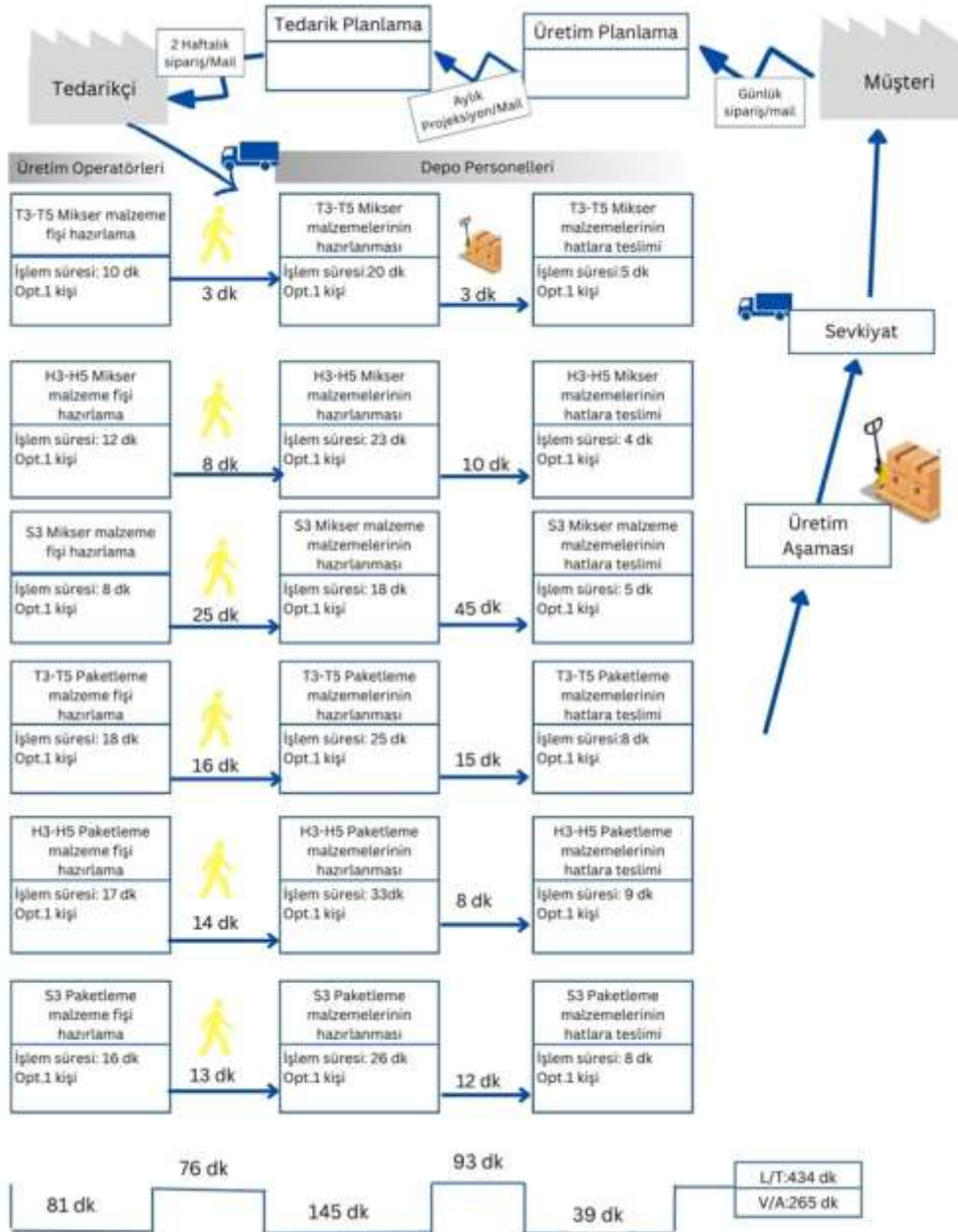
3. Bulgular ve Tartışma

Bu çalışmada, üç vardiya olarak çalışan bir gıda işletmesinde yukarıda açıklanan teknikler uygulanmıştır. Hammadde depodan üretim hatlarına olan transfer süreçleri incelenmiş ve iyileştirmeler yapılmıştır. Mevcut durumda üretim cep depolarına hammadde transferleri 16.00-00.00 vardiyasında gerçekleşmekte olup depo personellerine operatörler tarafından gelen ihtiyaç listelerine göre yapılmaktadır. Her hattın operatörü öncelikle cep depo stoklarını kontrol ederek ihtiyaç listesini oluşturup depoya malzeme fişi götürmektedir. Fişteki malzemeleri hazırlayan depo personeli, ilgili hatlara malzemeleri transpalet yardımı ile transfer etmektedir. Bu süreçte manuel yapılan işlerin ve gereksiz

taşımaların olduğu gözlenmiştir.

Bu esnada, katma değerli faaliyetlerin tespiti için öncelikle değer akışı haritalama yönteminden faydalanılmıştır. Sahada kâğıt üzerinde elle çizilen çalışma, EdrawMax programına aktarılıp haritalandırılmıştır. Mevcut durum değer akışı haritası Şekil 1'deki gibidir.

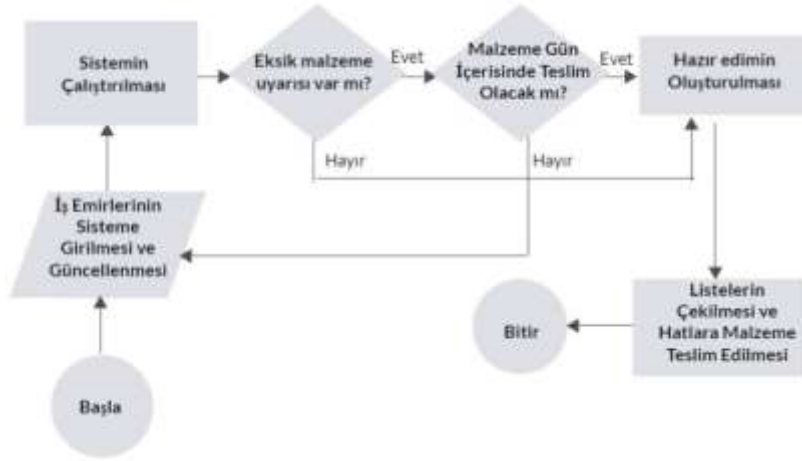
Haritalama ve saha gözlemleri sonucunda operatörlerin manuel olarak fiş hazırlamaya harcadığı zaman ile fişleri depoya teslim ederken harcadığı zamanların minimize edilmesi üzerine odaklanılmıştır. Bu kapsamda, manuel yürütülen işlemlerin SAP ile yürütülmesi ve günlük gelen iş emirlerine göre doğrudan ihtiyaç listelerinin oluşturulması üzerine SAP uzmanları ile çalışılmıştır. Sistemde yapılacak değişikliklerin ilgili birimlere de aktarılması ve sürekliliğin sağlanması yönünde PUKÖ döngüsünden faydalanılmıştır.



Şekil 1. Mevcut durum değer akışı haritası.

Tarih: 4.05.2023			1.05.2023					8.05.2023								
PROJE PLANI			Planlanan Başlangıç	Planlanan Bitiş	Pzt	Sal	Çar	Per	Cum	Cmt	Paz	Pzt	Sal	Çar	Per	Cum
					1	2	3	4	5	6	7	8	9	10	11	12
1.Uygulama Yapılacak Problemlerin Belirlenmesi																
1.Açılış Toplantısı ve Planın Paylaşılması	4.05.2023	4.05.2023														
2.Depo personelleri ve operatörlere eğitim verilmesi	5.05.2023	5.05.2023														
3.Sistemsel hazırlık ve kontroller	6.05.2023	7.05.2023														
4.Pilot hattın seçilerek sayımının alınması	8.05.2023	8.05.2023														
5.Belirlenen pilot hat için hazır edimlerin hazırlanması ve problemlerin incelenmesi	9.05.2023	10.05.2023														
6.Sonuçların değerlendirilmesi ve kapanış	11.05.2023	11.05.2023														

Şekil 2. Plan çizelgesi.



Şekil 3. İş akış şeması.

PUKÖ döngüsünün aşamalarında yapılan işler sırasıyla aşağıda açıklanmıştır:

- “Planla” Aşaması: Bu aşamada, öncelikle problemin tanımlaması yapılmıştır. Problem, hammadde transferi sürecinde manuel yürütülen işlemlerden kaynaklı katma değeri olmayan adımların bulunması olarak tanımlanmıştır. Daha sonra, manuel yürütülen işlemlerin SAP’e entegre edilerek israfların ortadan kaldırılması hedeflenmiştir. Bu hedefe uygun olarak gelecek planların oluşturulmuştur. Plan çizelgesi Şekil 2’de verilmiştir.
- “Uygula” Aşaması: SAP sisteminden yürütülecek olan sistemin sağlıklı ilerleyebilmesi için öncelikli olarak ihtiyaçlar belirlenmiş ve SAP uzmanları ile paylaşılmıştır. SAP sisteminde mevcut bir çalışma olan hazır edim ekranı firma çalışma düzenine entegre edilerek çalışma tamamlanmıştır. İlk olarak, operatörlerin depoya malzeme listelerini ulaştırmak için harcadığı gereksiz işlemlerin ortadan kaldırılmasına odaklanılarak, malzeme listelerinin tamamen SAP üzerinden oluşturulma talebi sunulmuştur. Bu çalışma ile beraber operatörlerin yanlış, eksik veya fazla malzeme talep etmesi problemini önlemek amacıyla açık iş emirleri göz

önünde tutularak tamamen mamul reçetelerinden çekilecek hammadde miktarlarına göre üretim cep depo stokları ile karşılaştırılarak ihtiyaç listelerinin oluşturulması istenmiştir. Bu talep, geçmiş zamanlardan kalan açık iş emirlerinin kapatılma zorunluluğunu beraberinde getirmiştir. Ek olarak, transfer edilen malzemelerin paletli veya koli şeklinde olmasına göre veriler düzenlenmiştir. Örnek olarak; 25 kg’lık çuvallarda gelen bir malzeme için 10 kg ihtiyaç çıkartması durumunda 10 kg’ı 25 kg’ a yuvarlayarak ihtiyaç listesinde gösterme durumu verilebilir. Bu talebin sebebi, gıda güvenliği ve malzeme denkliliğini sağlamak için hammadde depoda açık malzemenin tutulmaması gerekliliğidir. Test sürümünde yapılan denemelerin ardından sistem, canlı sisteme taşınmıştır. Öncelikli olarak ilgili birim yöneticileri ile açılış toplantısı yapılarak süreç tanıtılmış ve sistemdeki kritik noktalar üzerine görüşülmüştür. Planla aşamasında oluşturulmuş olan planlama çizelgesindeki adımlar sırası ile planlanan tarihlerde tamamlanmıştır. Yeni sisteme ait süreç akış şeması oluşturulmuş ve ilgili personeller ile paylaşılmıştır. Her gün 16.00-00.00 vardiyasında bir sonraki güne ait iş emirlerinin gelmesinin ardından sisteme iş emirlerinin girilmesi, akışın ilk adımını oluşturacaktır. Sistemin

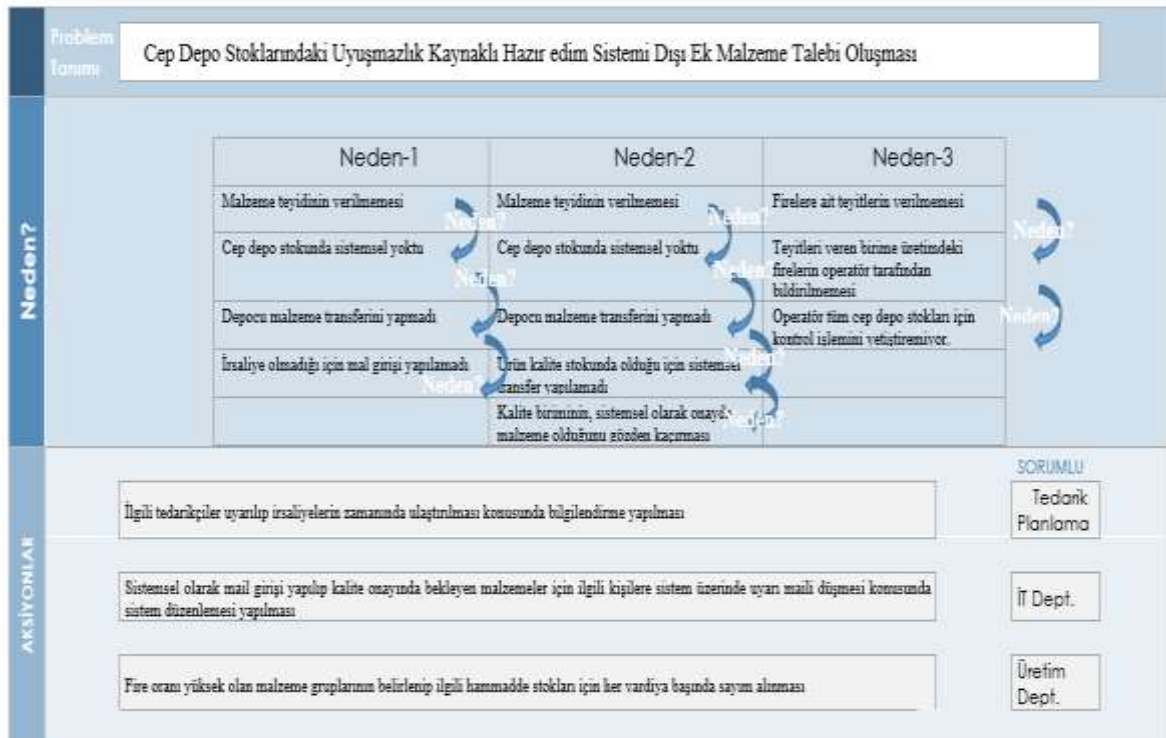
çalıştırılması ve kontrol işlemlerinin ardından hazır edim listeleri oluşturulacaktır. İlgili hatta ait bir günlük ihtiyaç listesi sistem üzerinden çekilip hatlara teslim edilecektir. Bu aşamaya ait iş akış şeması Şekil 3'te verilmiştir.

- “Kontrol Et” Aşaması: “Planla” ve “Uygula” aşamalarında yapılmış olan çalışmaların kontrolleri bu aşamada gerçekleştirilmiştir. Hazır edim sistemi sürecine ait pilot çalışmalar yapılmış ve yaşanan problemler üzerine odaklanılmıştır. Bu kapsamda, karşılaşılan problemlerin kaynağının tespit edilmesinde kök neden analizinden faydalanılmıştır. Kök neden analizi çalışması işletmede depo personeli, operatör, teyit personeli eşliğinde gerçekleştirilerek doğrudan sürecin içinde yer alan kişilerin deneyim ve gözlemlerinden faydalanılmıştır. Sistem iyileştirmesi esnasında karşılaşılan temel problem, sistemsel ve fiziksel cep depo stoklarındaki uyumsuzluk olmuştur. Bunun için ilgili birimler eşliğinde problem sebepleri incelenmiş ve aksiyonlar alınmıştır. Yapılan kök neden analizi Şekil 4'te verilmiştir. Alınan aksiyonların sonuçları yeniden incelenmiş, sistemsel ve fiziksel stoklardaki fark miktarlarında düşüş gözlenmiştir. Aksiyon alınmadan önce hazır edim dışında haftalık depodan manuel olarak talep edilen malzeme kalem sayısı 24 iken aksiyon sonrası bu sayı haftalık 9 kaleme düşmüştür.
- “Önemli Al” Aşaması: Yapılan kontrollerin ve kök-neden analizinin ardından, süreçte yaşanabilecek aksaklıkların önüne geçmek için aşağıdaki önlemler alınmıştır:
 - ✓ Cep depo stoklarındaki uyumsuzluğun önüne

geçmek için fire oranları yüksek olan hammaddeler tespit edilmiş ve her vardiya sonunda sayımları alınıp fire hammadde çıkışları yapılarak sistem stoklarının kontrol altına alınması hedeflenmiştir.

- ✓ Depo tarafından her mal girişi yapıldığında kalite onayı için ilgili birimlere mail düşmesi üzerine çalışma yaparak, kalite onayında uzun süre malzeme kalması önlenerek fiziksel olarak üretim hattında teslim edilen malzemenin sistemsel olarak da hatlara transferleri sağlanmış olup teyit süreçleri daha sağlıklı hale getirilecektir.
- ✓ Tedarikçinin geç irsaliye yönlendirmesinden kaynaklı mal girişinin gecikmesi probleminin önüne geçmek için ilgili tedarikçilerin uyarılacak ve takip sıklaştırılacaktır.

PUKÖ döngüsünden de faydalanılarak adım adım malzeme transfer süreçlerinde iyileştirme üzerine çalışmalar yapılmıştır. Mevcut durum DAH’ da tespit edilen manuel işlemler sistem üzerinden takip edilmeye başlanmış, mevcut sisteme dahil olmak durumunda kalan 6 personel bu süreçte ilgili iş için sistemden çıkarılmıştır. Bu iş yerine sahada bulunan mevcut işlerine ayırarak zamanları artmıştır. 6 personel yerine 1 üretim planlama sorumlusunun sistemsel işlemi ile süreç yönetilmeye başlanmıştır. Girilen iş emirlerine göre sistemde bulunan cep depo stokları ile karşılaştırma yaparak ihtiyaç listeleri dijital ortama taşınmıştır. Daha sonra, değer akışı haritalama Şekil 5'teki gibi tekrar çizilmiştir. Mevcut durumda toplam 434 dakikada yürütülen bu işlem, iyileştirme sonrası 284 dakikaya düşmüştür. Aynı şekilde katma değersiz işlemlerin toplam süresi 265 dakikadan 191 dakikaya düşürülerek bir iyileşme sağlanmıştır.



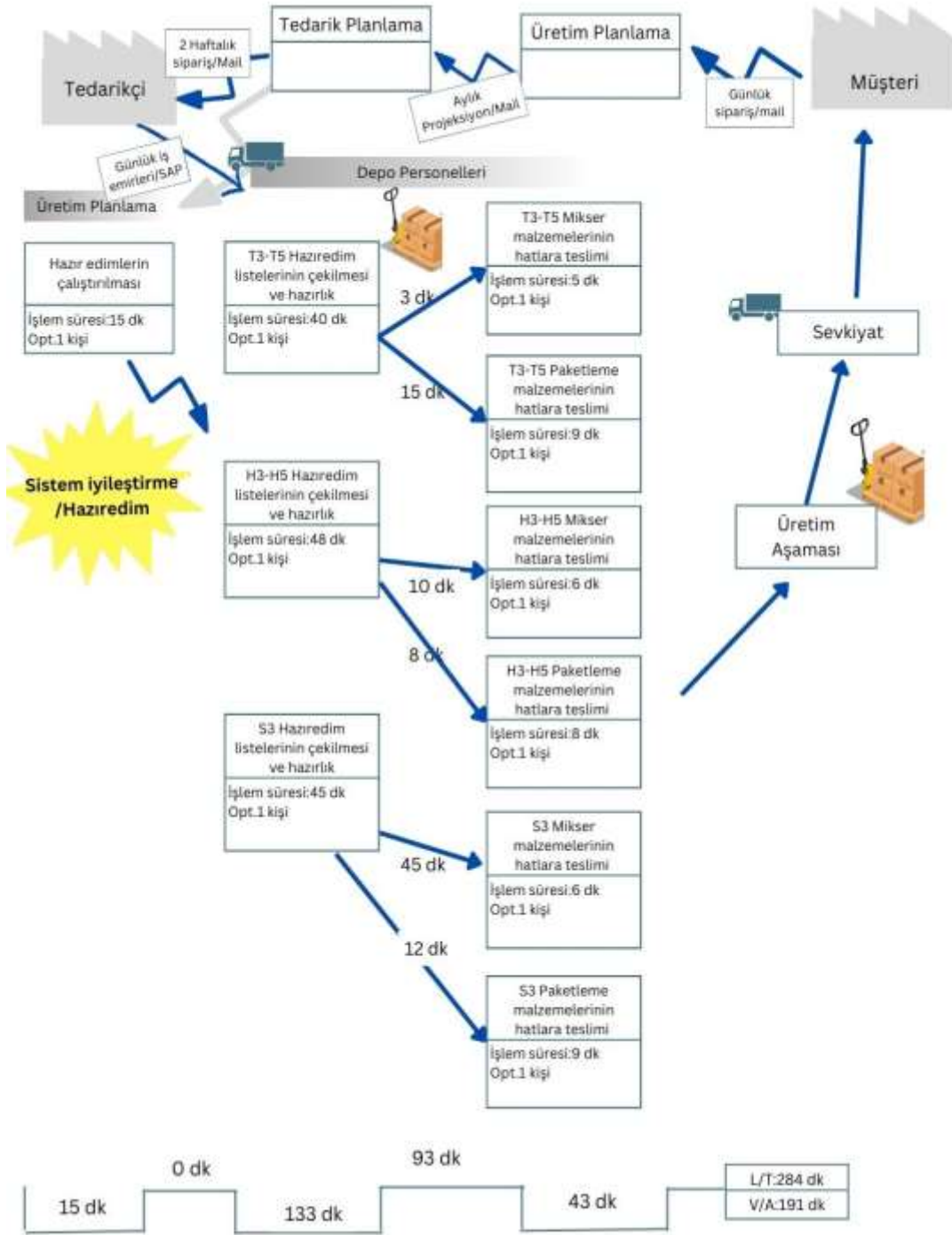
Şekil 4. Kök neden analizi.

Bir diğer iyileştirme çalışması, 7 temel israftan biri olan gereksiz taşımalar üzerine yapılmıştır. Malzeme transfer süreci esnasında günlük kat edilen rota spagetti diyagramından faydalanılarak çizilmiştir. Fabrika bünyesinde depo personellerinin ofislerinin de bulunduğu ve süreci yönettiği ham madde depo ve paketleme malzemelerinin depolandığı ambalaj depo olmak üzere iki ana depo vardır. Kısa ömürlü mamullerin günlük olarak düzenli üretimleri yapıldığı için 5 hat üzerinde çalışma yapılmıştır.

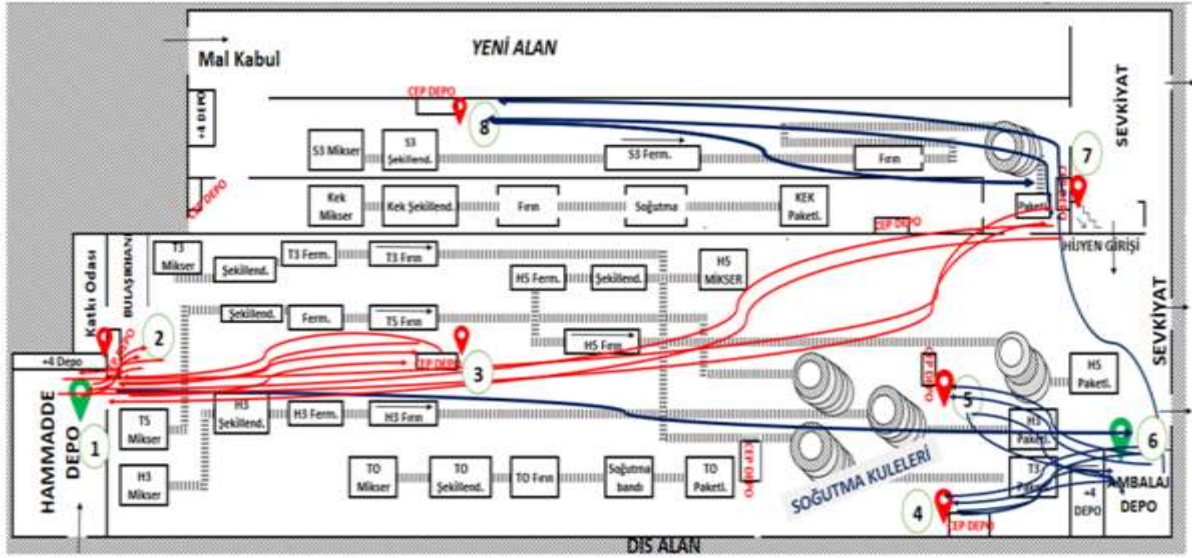
Uzun ömürlü ürün gruplarına ait üretimler dönemsel olduğundan çalışmada kapsam dışı bırakılmıştır. Öncelikle cep depolar ve hammadde depolar harita

üzerinde belirtilerek mesafeler ölçülmüştür. Mevcut durum spagetti diyagramı Şekil 6'daki gibi çizilmiştir. Burada, hammadde ve ambalaj depo dahil tüm uğranan cep depolar numaralandırılmıştır.

Rotalar arası mesafelerin ölçümünde lazer metre ve metre kullanılmıştır. Sürecin dakika cinsinden karşılığına ulaşmak için personellerin ortalama 1 dakikada yüklü transpalet ile kat ettiği yol ölçülmüştür. Sürecin incelemesinin ardından ambalaj depo ve hammadde depo çevresinde yoğunluk olduğu tespit edilmiştir. Mevcut durumda malzemeler plastik paletlere istiflenip hatlara teslim edilmektedir. Taşıma esnasında trans palet kullanılmaktadır.



Şekil 5. İyileştirilmiş durum değer akışı haritası.



Şekil 6. Mevcut durum spagetti diyagramı.

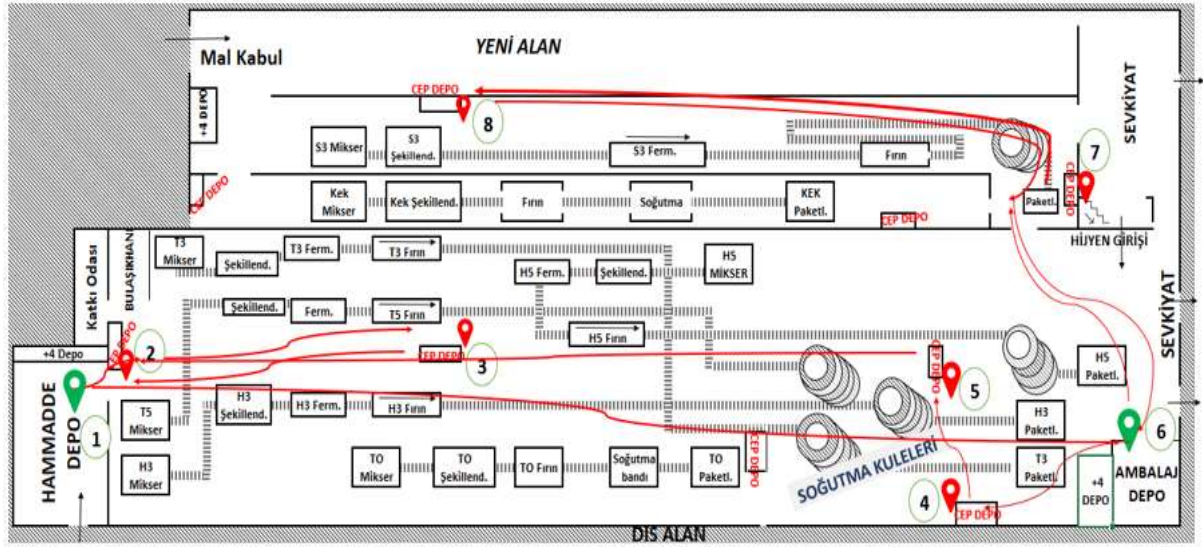
Malzeme transferlerinin zamanında yetişmesi için bu işlem iki personel ile yapılmaktadır. Bir personel tek seferde bir paletlik malzemeyi çekebilmektedir ve ilgili cep depoya teslim ettikten sonra ikinci bir paleti almak için tekrar depoya dönmek zorunda kalmaktadır. Mevcut durum spagetti diyagramında, kırmızı çizgiler kat edilen yolları göstermektedir. Bu yolların oluşturduğu toplam taşıma mesafesini minimuma düşürmek için, işletmeye Milk Run taşıma sistemi önerisi sunulmuştur. Örnek bir Milk Run aracı Şekil 7'de gösterilmiştir. Milk Run taşıma sistemine geçiş için, öncelikle ihtiyaçlar belirlenmiş ve yapılacak yatırımın maliyeti tespit edilmiştir. Her bir cep depoya günlük olarak transfer edilen malzeme miktarının palet cinsinden karşılığı bulunmuştur. Günde 12 palet ve her bir cep depoya 2 paletlik transfer yapıldığı verisine ulaşılmıştır. İşletme için uygun araç özellikleri üzerinde araştırma yapılmış ve fiyat bilgisi toplanmıştır. Ürünler paletli taşındığı için her bir vagon ölçüsünün 100x120 cm ölçülerinde olmasına karar kılınmıştır.



Şekil 7. Örnek bir Milk Run taşıma aracı.

Tedarikçi firmanın saha incelemesi sonrası 4 vagonlu bir çekici önerilmiştir. Personellerin 1 dakikada transpalet ile kat ettiği yol ölçülerek ilgili yolun dakika cinsinden karşılığı 470 saat olarak hesaplanmıştır. Bir personelin ilgili işletmeye saatlik maliyeti 120 TL'dir. Bu işlem yılda 56.400TL'ye mal olmaktadır. Milk Run aracının kapasitesi göz önünde tutularak rota önerisinde bulunulmuş ve günlük 835 metre, yılda toplam 250.500 metreye tekabül eden rota planlanmıştır. Çekicinin teorikte saatlik 5,76 kW yaktığı ve 2023 yılı ağustos ayı ücretlerine göre 1 kW elektrik tutarının 4,6 TL olduğu bilinmektedir. Çekici için önerilen hız sınırı saatte 5 km/saat 'tir. Önerilen rotaya ve hız sınırına göre bu işlem Milk Run aracı ile yıllık 50,1 saate tekabül etmektedir. 50,1 saatte harcadığı elektrik enerjisi maliyeti de 1327,4 TL'dir. 4 adet vagon ve 1 çekicinin maliyeti 349.600,20 TL'dir. Trans paletli taşımadan Milk Run sistemine geçişinde işletmenin yıllık kazancı 49.060,60 TL olacaktır. Son olarak yatırımın geri ödeme süresi yönteminden faydalanılarak proje verileri somutlaştırılmıştır. Geri ödeme süresi; yatırımlarda, toplam yatırım tutarının net kâr üzerinden geri dönüş süresi olarak ifade edilir. Toplam yatırım tutarı kazanca bölünerek sonuca ulaşılır. Çalışma kapsamında önerilen sistemin geri ödeme süresi 7,12 yıl olarak bulunmuştur. Önerilen Milk Run aracının sisteme dahil edilmesiyle spagetti diyagramı Şekil 8'deki gibi olacaktır. Bu diyagrama göre, kırmızı çizgilerin ifade ettiği toplam taşıma mesafesinin mevcut duruma göre azaldığı açıkça gözükmektedir.

Bir gıda firmasının depo bölümünde, yalnız teknikler kullanılarak yapılan tüm bu iyileştirme çalışmalarının öncesi ve sonrası Tablo 2'de özet olarak verilmiştir. Bu tabloya göre; depo personeli sayısında %83'lük, toplam işlem süresinde %31'lik, katma değersiz işlem süresinde %28'lik ve malzeme taşıma süresinde yıllık ortalama %89'luk bir iyileşme sağlanmıştır.



Şekil 8. İyileştirilmiş durum spagetti diyagramı.

Tablo 2. İyileştirme öncesi ve sonrası elde edilen veriler

	İyileştirme Öncesi	İyileştirme Sonrası	% İyileştirme
Depo personeli sayısı	6	1	%83
Toplam işlem süresi (dk.)	434	284	%31
Toplam katma değersiz işlem süresi (dk.)	265	191	%28
Yıllık toplam malzeme taşıma süresi (saat)	470	50,1	%89

4. Sonuç

Bu çalışmada, bir gıda firmasına ait iç lojistik süreçleri incelenmiş ve süreçler yalın teknikler yardımıyla israflardan arındırılmaya çalışılmıştır. Başlangıçta malzeme transferi işlemi için sahada bir değer akışı haritalama yapılmış ve bunun sonucunda manuel yürütülmüş olan işlemlerin SAP üzerinden takip edilmesine karar verilerek bir iyileştirme çalışması yapılmıştır. Bu çalışma sonunda, toplam işlem süresi 434 dakikadan 284 dakikaya düşmüştür. Zaman açısından elde edilen kazancın yanında çalışmanın aşağıdaki faydaları da olmuştur:

- ✓ Üretim cep depo stoklarının düzenli kontrol edilmesi görevi operatörlere verilerek personele sorumluluk bilinci aşılanmıştır.
- ✓ Malzeme teslim süreçlerinde personel kaynaklı hatalı veya eksik malzeme alımının önüne geçilmiştir.
- ✓ Depodan eksik malzeme talep etme kaynaklı ani malzeme ihtiyaçlarının ve bu ihtiyaç kaynaklı üretimde yaşanan aksaklıklar önlenmiştir.
- ✓ Çalışma kapsamında personeller ile yapılan kök-neden analizi çalışması sonucu personeller problem çözme yolunda kendilerini geliştirmiş ve bu çalışmayı sahada kullanmaya başlamışlardır.

Milk Run tasarımı ile işletme içi taşımaların minimize edilmesi hedeflenmiştir. Yapılan hesaplamalara göre iki personel ile toplamda yıllık 470 saati alan malzeme transferi işlemi, tek personel ile yıllık toplam 50,1 saatte yapılabilecektir. Yapılacak olan yatırım sadece bu çalışmada kullanılacağı düşünülerek 7,12 yılda kendini

amorti edebilecektir. Milk Run sistemi işletmeye ek olarak aşağıdaki faydaları sağlayacaktır:

- ✓ Malzeme transferlerinde rol alan depo personelleri taşıma için ayıracağı zamanı mevcut koşullarda yetismeyen işlerine ve depo düzenine ayırabilecektir.
- ✓ Manuel yapılan taşıma işlemi çekici ile taşınacağı için ergonomik açıdan konfor sağlanmış olacaktır.
- ✓ Öneri olarak sunulan Milk Run vagonlarının koruma ekipmanlı olması manuel taşıma esnasında sık karşılaşılan, çuvalı malzemelerin paletten kayıp devrilmesi sonucu oluşacak hasar miktarını en aza düşürerek fayda sağlayacaktır.

İç lojistikte yalın tekniklerin kullanımıyla ilgili gelecekte yapılabilecek çalışmalar için aşağıdaki öneriler verilebilir:

- ✓ Üretim veya hizmet sektörlerinin farklı alanlarında benzer yöntemler kullanılarak süreç iyileştirme çalışmaları yapılabilir.
- ✓ Aynı veya farklı iş kollarında, farklı yalın teknikler kullanılabilir.
- ✓ Milk Run araçlarının seçimi, çok kriterli bir karar verme problemi olarak ele alınıp çözülebilir.
- ✓ Milk Run araçlarının rotalanması için bir matematiksel model ve çözüm önerisi sunulabilir.

Katkı Oranı Beyanı

Yazar(lar)ın katkı yüzdesi aşağıda verilmiştir. Tüm yazarlar makaleyi incelemiş ve onaylamıştır.

	A.U.	B.T.Ş.
K	70	30
T	50	50
Y	20	80
VTI	100	
VAY	80	20
KT	50	50
YZ	50	50
KI	40	60
GR		100
PY	20	80
FA	50	50

K= kavram, T= tasarım, Y= yönetim, VTI= veri toplama ve/veya işleme, VAY= veri analizi ve/veya yorumlama, KT= kaynak tarama, YZ= Yazım, KI= kritik inceleme, GR= gönderim ve revizyon, PY= proje yönetimi, FA= fon alımı.

Çatışma Beyanı

Yazarlar bu çalışmada hiçbir çıkar ilişkisi olmadığını beyan etmektedirler.

Etik Onay Beyanı

Bu çalışmada hayvanlar ve insanlar üzerinde herhangi bir çalışma yapılmadığı için etik kurul onayı alınmamıştır.

Destek ve Teşekkür Beyanı

Bu çalışma, Ayşe UÇAR'ın yüksek lisans tezinden üretilmiştir.

Kaynaklar

Birgün S, Gülen KG, Özkan K. 2006. Yalın üretime geçiş sürecinde değer akışı haritalama tekniğinin kullanılması: İmalat sektöründe bir uygulama. İstanbul Ticaret Üniv Fen Bil Derg, 5(9): 47-59.

Derdiyok, T. 2019. Üniversitelerde kalite güvence sistemi kapsamında PUKÖ yönetim döngüsü uygulamasında bir model önerisi. Ufuk Üniv Sos Bil Enst Derg, 8(15): 173-198.

Dogget M. 2006. Root cause analysis: a framework for tool selection. Quality Manag J, 12(4): 34-45.

Doğan NÖ, Kama A. 2021. Tedarik zincirinde değer katmayan faaliyetlerin ortadan kaldırılması: İmalat sektöründe bir değer akış haritalama uygulaması. Niğde Ömer Halisdemir Üniv Müh Bil Derg, 10(1): 91-99.

Dur Z. 2019. AHP'ye dayalı bulanık Utastar yaklaşımı: malzeme taşıma ekipmanı uygulaması. Yüksek Lisans Tezi, Hacettepe Üniversitesi, Fen Bilimleri Enstitüsü, Ankara, Türkiye, pp: 72.

Efil İ. 1994. Grup halinde problem analizi ve çözümünde iyileştirme çalışmaları. Uludağ Üniv İİBF Derg, 15(2): 139-159.

Erturgut R. 2021. Lojistik ve Tedarik Zinciri Yönetimi. Nobel Yayınevi, İstanbul, Türkiye.

Ertürk, H, Özçelik F. 2008. Yalın üretim uygulayan işletmeler için yalın muhasebe. Uludağ Üniv İİBF Derg, 27(1): 15-45.

Facchini F, Mossa G, Sassanelli C, Digiesi S. 2024. IoT-based milk-run routing for manufacturing system: an application case in an automotive company. Int J Product Res, 62(1-2): 536-555.

Gecü B. 2008. İç lojistik sistemlerinin yalın üretim bakışıyla

yeniden tasarlanması ve otomotiv sektöründe örnek bir uygulama. Yüksek Lisans Tezi, İstanbul Teknik Üniversitesi, Fen Bilimleri Enstitüsü, İstanbul, Türkiye, pp: 117.

Grzegorz B, Izabela N, Arkadiusz G, Zbigniew B. 2021. Reference model of milk-run traffic systems prototyping. Int J Product Res, 59(15): 4495-4512.

Gu S, Zhang A, Huo G, Yuan W, Li Y, Han J, Shen N. 2021. Application of PDCA cycle management for postgraduate medical students during the COVID-19 pandemic. BMC Medic Educ, 21(1): 308.

Kilic HS, Durmusoglu MB, Baskak M. 2012. Classification and modeling for in-plant milk-run distribution systems. The Int J Adv Manufact Technol, 62: 1135-1146.

Kocabaş D. 2014. Yalın lojistik ve değer akışı haritalandırma yöntemi. Yüksek Lisans Tezi, İstanbul Teknik Üniversitesi, Fen Bilimleri Enstitüsü, İstanbul, Türkiye, pp: 115.

Koçan A. 2014. İç lojistikte setleme/sıralama sisteminin tasarımı ve otomotiv sektöründe bir uygulama. Yüksek Lisans Tezi, İstanbul Teknik Üniversitesi, Fen Bilimleri Enstitüsü, İstanbul, Türkiye, pp: 185.

Korytkowski P, Karkoszka R. 2016. Simulation-based efficiency analysis of an in-plant milk-run operator under disturbances. The Int J Adv Manufact Technol, 82: 827-837.

Kuğu S, Köse R. 2021. Isı değiştirici üretim hattında değer akış haritalama uygulamasının etkileri. Kırklareli Univ J Eng Sci, 7(1): 135-146.

Kuvvetli Y, Erol R. 2017. Ağaç ürünleri üreten bir işletmede malzeme taşıma sisteminin ağaç ürünleri üreten bir işletmede malzeme taşıma sisteminin simülasyon yaklaşımı ile iyileştirilmesi. Çukurova Üniv Müh Mim Fak Derg, 32(1): 215-222.

Küçüköğlü İ, Yağmahan B, Çağlıyan MS, Yıldız A, Aktokluk D. 2018. İç lojistik sisteminde malzeme tedariki için geliştirilmiş matematiksel modelleme yaklaşımı: Bir uygulama. Uludağ Üniv Müh Fak Derg, 23(4): 159-176.

Lu Y, Liu Z, Min Q. 2021. A digital twin-enabled value stream mapping approach for production process reengineering in SMEs. Int J Comput Integrated Manufact, 34(7-8): 764-782.

Mofolasayoa A, Young S, Martinez P, Ahmad R. 2022. How to adapt lean practices in SMES to support industry 4.0 in manufacturing. Procedia Comput Sci, 200: 934-943.

Patir E. 2019. Otomotiv yan sanayi firmasında yalın üretim ve yalın lojistik uygulamaları. Yüksek Lisans Tezi, Kocaeli Üniversitesi, Fen Bilimleri Enstitüsü, Kocaeli, Türkiye, pp: 104.

Realyvásquez-Vargas A, Arredondo-Soto KC, Carrillo-Gutiérrez T, Ravelo G. 2018. Applying the Plan-Do-Check-Act (PDCA) cycle to reduce the defects in the manufacturing industry. A case study. Appl Sci, 8(11): 2181.

Sangpikul, A. 2017. Implementing academic service learning and the PDCA cycle in a marketing course: Contributions to three beneficiaries. J Hospit Leisure Sport Tour Educ, 21: 83-87.

Sevgili A, Antmen ZF. 2019. Yalın üretim tekniklerinden değer akış haritalandırmanın bir metal işleme fabrikasında süreç iyileştirme amacıyla uygulanması. Avrupa Bil Teknoloj Derg, 16: 219-228.

Sol E. 2011. Set şeklinde teslimat ile hat kenarı besleme sisteminin karşılaştırılması, yalın lojistik bakışıyla iç lojistik faaliyetlerin tasarlanması ve örnek bir uygulama. Yüksek Lisans Tezi, İstanbul Teknik Üniversitesi, Fen Bilimleri Enstitüsü, İstanbul, Türkiye, pp: 239.

Sönmez V, Yağmur C. 2021. Hastane kan toplama merkezinde yalın üretim uygulaması. Uluslararası Müh Araş Geliş Derg, 13(3): 173-187.

Topuz T. 2021. Üretim sistemlerinde çekme tipi esaslı iç lojistik sistemi tasarımına yönelik bütünlük bir metodoloji önerisi:

- Beyaz eşya sektöründe bir uygulama. Yüksek Lisans Tezi, İstanbul Teknik Üniversitesi, Fen Bilimleri Enstitüsü, İstanbul, Türkiye, pp: 253.
- Turan H. 2019. Bulanık ÇKKV metodu kullanarak değer akış haritalama uygulaması. Uluslararası İİB Derg, 5(1): 77-93.
- Tyagi S, Choudhary A, Cai X, Yang K. 2015. Value stream mapping to reduce the lead-time of a product development process. Int J Product Econ, 160: 202-212.
- Usuk MS, Selvi İH. 2019. Fabrika içi lojistik sürecinde kablosuz acil parça istek sistemi otomasyonu: bir otomotiv fabrikası uygulaması. Acta Infologica, 3(1): 1-12.
- Yangınlar G, Bal N. 2019. Yalın yönetim ve yalın lojistik kavramlarının irdelenmesi. Strat Sos Araşt Derg, 3(1): 151-161.



ROBOTIC ARM TRAJECTORY TRACKING USING IMAGE PROCESSING AND KINEMATIC EQUATIONS

Yusuf Hamida EL NASER^{1*}, Durmuş KARAYEL¹, Mert Süleyman DEMİRSOY¹, Muhammed Salih SARIKAYA¹, Nur Yasin PEKER¹


¹Sakarya Applied Science University, Department of Mechatronics Engineering, 54050, Sakarya, Türkiye


Abstract: This study presents a novel approach for scanning and obtaining object contours within a workspace using a camera and subsequently following these 2-D contours to another region with the assistance of an end effector. The process begins with the determination of boundary lines of object images through advanced image processing methodologies. Subsequently, a conversion from camera pixel coordinates to robot metric coordinates is performed to facilitate trajectory planning for the robotic arm. The trajectory of the robot arm, and consequently, the path followed by the end effector, is determined based on these metric coordinates. The article provides a detailed exposition of the methodology, including the mathematical background and experimental study, showcasing the efficacy and accuracy of the proposed approach in real-world scenarios. This research contributes to the advancement of robotic systems capable of precise trajectory tracking and manipulation tasks in diverse applications. This study involves an innovative approach that combines theoretical and practical methods, including object contour detection using image processing, conversion of pixel coordinates obtained from the camera to robot metric coordinates, robot kinematics, and programming steps.


Keywords: Image processing, Robot arm, Inverse kinematics, Trajectory tracking, Smart servos


*Corresponding author: Sakarya Applied Science University, Department of Mechatronics Engineering, 54050, Sakarya, Türkiye


E mail: yusufelnaser@sakarya.edu.tr (Y. H. EL NASER)

Yusuf Hamida EL NASER  <https://orcid.org/0000-0003-4757-6288>

Durmuş KARAYEL  <https://orcid.org/0000-0001-9326-466X>

Mert Süleyman DEMİRSOY  <https://orcid.org/0000-0002-7905-2254>

Muhammed Salih SARIKAYA  <https://orcid.org/0000-0002-2809-9896>

Nur Yasin PEKER  <https://orcid.org/0000-0003-2468-2627>

Received: March 01, 2024

Accepted: March 27, 2024

Published: May 15, 2024

Cite as: El Naser YH, Karayel D, Demirsoy MS, Sarikaya MS, Peker NY. 2024. Robotic arm trajectory tracking using image processing and kinematic equations. BSJ Eng Sci, 7(3): 436-444.

1. Introduction

Robots can be considered as a complex mechanism consisting of a certain number of limbs, rotating and / or sliding joints, actuators that drive these joints and an end effector attached to the last limb (Sophokleous et al., 2021). In this way, they repeatedly follow the trajectories taught by preprogramming and perform certain processes. Scientific studies in the field of robotics continue their development by integrating with many disciplines such as semiconductors, artificial intelligence, power electronics, computer vision, programming, communication, control, mechatronic systems, material science and such (Romero-Gonzalez et al., 2022). From past to present, robot arms, mobile robots, humanoid robots, spider robots, medical robots, and even robots used for space tasks are being integrated with new technologies every day and are offered for use to make life easier for humanity.

When the studies in the field of robotics are examined in the literature, it can be seen that the studies have increased especially in the last few decades as a natural result of the popularity of the subject. Theoretical studies on robot kinematics and dynamics (El Naser et al., 2020) purposes like pick&place operations (Dixon, 2007), drawing (Cheah et al., 2006), painting and cutting

(Grzelczvk et al., 2019), studies for object recognition, sectors such as health & medicine (Dyck et al., 2013), manufacturing (Luo et al., 2019), entertainment shows that the topic is becoming widespread (Liu et al., 2014). In addition to the industrial examples related to use of robots given above, prototypes of the experimental realization of the studies carried out to shed light on the theoretical background of similar objectives also stand out (He et al., 2021).

Since the subject is quite convenient for multidisciplinary studies, it is possible to come across collaborations with artificial intelligence and optimization, control, image processing and many other research areas (Mahmoodpour et al., 2019; Budivanta et al., 2020; Duque et al., 2022). These collaborations have not only inspired scientific articles, but have also allowed the development of original patent ideas.

The aim of this study can be summarized as follows: to scan and obtain the contours of objects on the workspace using a camera, and then to follow these 2-D contours to another region on the workspace with the help of an end effector. The boundary lines of the object image has determined using image processing methodologies and the conversion from camera pixel coordinates to robot metric coordinates has performed. These metric



coordinates have been used to determine the trajectory of the robot arm, thereby the path followed by the end effector has been obtained. Detailed methodology, mathematical background, and experimental study has been described in the rest of the article.

2. Materials and Methods

In the study, a 4-axis SCARA type robot was prototyped in the PRRR sequence. Unlike the standard SCARA configuration, the sliding joint was used on the first axis in order to compensate the negative torque caused by the motor, limb and tool weights. Dynamixel AX-12A and MX-28T DC smart servo motors were used as robot actuators and TTL communication of the devices was decisive in the selection of these motors. The images of the objects located in the workspace was taken with the help of the Logitech C270 USB camera and the edge detection was performed by isolating them from the environment by means of image processing techniques. Instead of dealing with camera calibration, simple numerical regression method was used in transition from camera pixel coordinates to robot metric coordinates. Similarly, the obtained points, which will determine the trajectory of the robot arm, were reproduced by numerical interpolation and the robot movement was performed much more smoothly (Fang et al., 2022).

Thus, uniqueness was obtained compared to similar studies in the literature (Uk et al., 2020). The designed robot can follow the coordinates of the object with the help of forward and inverse kinematic calculations and perform trajectory tracking by the end effector. At the same time, by utilizing other end effectors, it can transport the lines of the object to another region on the workspace and draw it in 2-D. The forward and inverse kinematic equations of the robot arm are detailed in the rest of the sections (Chen et al., 2007). While forward kinematics equations are expressed using Denavit - Hartenberg approach, inverse kinematics equations has solved by geometric approach and detailed visually (Jiao et al., 2018; Zhang et al., 2022; Jian-Peng et al., 2023). Programming of all these processes including image processing, coordinate transformations and interpolation operations, kinematic calculations and computer - actuator communications had realized using LABVIEW 2016 software via USB2Dynamixel control card hardware. Figure 1 shows the USB camera and USB2Dynamixel control card. Figure 2 shows the flow chart of the system.



Figure 1. USB camera and USB2Dynamixel control card.

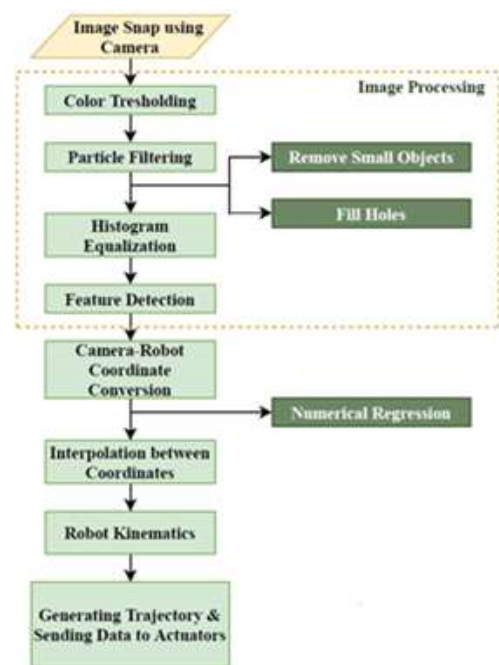


Figure 2. Flowchart of the system.

2.1. Image Processing

A number of image processing steps need to be performed in order to correctly determine the contours of the image taken by camera. These contours will be used to get the trajectory of the end effector driven by the robot arm later on. In this regard, firstly color thresholding procedure was applied to the image taken and the object in the image was tried to be separated from the ground on which it is located (Zhou et al., 2005; Syahrian et al., 2017). Pixel values that are not among the threshold values determined for this are drawn to zero. Thresholding in the HSL (hue-saturation-luminance) color space for the appropriate threshold value was performed according to the following ranges; $0 < \text{hue} < 184$, $0 < \text{sat} < 255$, $0 < \text{lum} < 29$.

Values may vary depending on ambient lightings, the shading, colors and transparency of objects. Since the isolated pixels are still affected by environmental noise, they need to be suppressed. For this purpose, the object in the workspace was completely separated from its background by passing through a series of stages such as particle filtering, hole filling, removal of small objects and histogram equalization. Thanks to this, the image has been made suitable for edge detection. When feature detection algorithms were tested, it was seen that the ideal result for the object in the working space was provided by the Harris algorithm. The determined points were subjected to regression and stored in an array to be converted into metric coordinates. Accordingly, the results obtained are expressed in the following images in Figure 3.

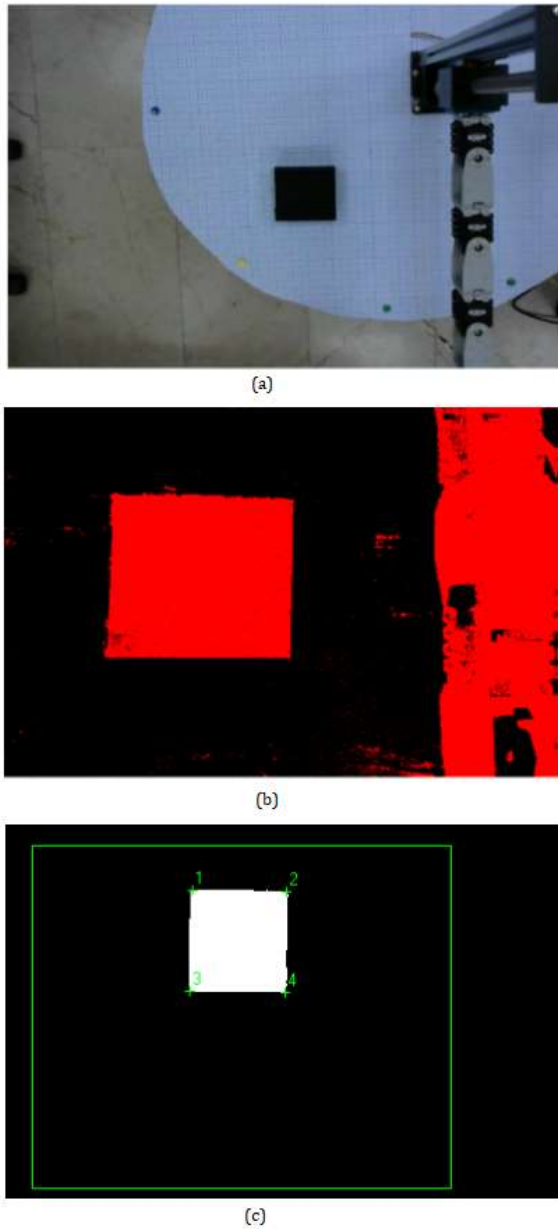


Figure 3. (a) Original image, (b) After color threshold, (c) After edge detection.

2.2. Conversion from Image Pixel to Robot Metric Coordinates

The x-y coordinates obtained from the corner points of the object using edge detection are in pixels and the origin of this coordinate system is the upper left corner of the image. However, the robot arm operates in the metric system and the origin of the coordinate system is located on the first axis of the robot. This should be taken into consideration when converting the found coordinates from pixels to millimeters. In the conversion process, the millimetric coordinates corresponding to the coordinates in pixels found by the feature extraction process were determined by measuring. Accordingly, the pixel coordinates of the points determined as a result of the feature extraction were expressed in pairs $\{x_p, y_p\}$ as the first point $\{651.3, 556.7\}$, second point $\{777.0, 559.0\}$, third point $\{648.2, 680.9\}$ and the fourth point

$\{768.8, 683.8\}$. The corresponding millimetric coordinates are shown in pairs $\{x_m, y_m\}$ respectively, as the first point $\{36, 146\}$, second point $\{36.5, 217\}$, third point $\{106, 146\}$ and the fourth point $\{107, 216.5\}$. Since there is a 90° difference between the pixel and the millimetric coordinates, x_p values should be converted to y_m values and y_p values to x_m . To find the millimetric x-y coordinates, the following equations 1 and 2 can be written;

$$x_m = my_p + n \tag{1}$$

$$y_m = kx_p + l \tag{2}$$

Two cross corner coordinates are substituted in the equations twice and four equations with four unknowns are solved to find m, n, k and l values the formulation is shown in equations 3a, 3b, 3c, 3d and 3e;

$$36 = m.556.7 + n \tag{3a}$$

$$106 = m.680.9 + n \tag{3b}$$

$$146 = k.648.2 + l \tag{3c}$$

$$216.5 = k.768.8 + l \tag{3d}$$

$$m = 0.563607, n = -277.7600, k = 0.584577 \text{ and } l = -232.923 \tag{3e}$$

These values were found using a simple first order regression method. Thus, from pixel to millimeter coordinate transformation operations on both axes were performed with ease. Errors encountered due to the linear approach are discussed in the conclusion section.

2.3. Robot Kinematics

The concept of kinematics can be defined as a discipline that deals with the movements of the systems directly from the geometry, independent of dynamic effects such as force and torque (Tao et al., 2014; Staicu et al., 2018). In mechanisms such as robots, a direct relationship can be established between joint angles and the position of the end effector using kinematic analysis. In this way, trajectory tracking can be performed by modeling the arm movement correctly. Kinematics science is divided into two sub branches as forward kinematics and inverse kinematics (Yanto et al., 2017). Forward kinematics is used to find the end effector position corresponding to certain joint angles (Garriga-Casanovas and Baena, 2019). On the contrary, inverse kinematics is used to determine the joint angles corresponding to the end effector position and orientation (Wang et al., 2015; Nansai et al., 2021). In the study, the forward kinematics of the designed robot were analyzed by Denavit-Hartenberg method and the solutions of the inverse kinematics problem were obtained using geometric approach (Ding and Liu, 2018; Guzman-Gimenez et al., 2020).

2.3.1. Forward kinematics

In Denavit-Hartenberg notation, relationship of two adjacent limbs of the robot with each other and the

characteristic of the joint between these two limbs are expressed with the help of a homogeneous transformation matrix shown in Equation 4 given below:

$${}^{i-1}T_i = \begin{bmatrix} c\theta_i & -s\theta_i & 0 & a_{i-1} \\ s\theta_i c\alpha_{i-1} & c\theta_i c\alpha_{i-1} & -s\alpha_{i-1} & -s\alpha_{i-1}d_i \\ s\theta_i s\alpha_{i-1} & c\theta_i s\alpha_{i-1} & c\alpha_{i-1} & c\alpha_{i-1}d_i \\ 0 & 0 & 0 & 1 \end{bmatrix} \quad (4)$$

Note that $c\theta$ and $s\theta$ represents $\cos\theta$ and $\sin\theta$.

In general, rotation and translation directions of the joints are shown by the z axis, and the directions of the limb perpendicular to movement directions are indicated by an x axis. Then, y axes are determined according to the right hand rule. In Denavit-Hartenberg method, there are 4 joint parameters that constitute the transformation matrix, α_{i-1} , a_{i-1} , d_i and θ_i . The steps to be followed in determining these parameters are as follows:

- α_{i-1} ; distance from z_{i-1} to z_i along x_{i-1} ,
- d_i ; distance from x_{i-1} to x_i along z_i ,
- α_{i-1} ; rotation angle from z_{i-1} ve z_i about x_i ,
- θ_i ; rotation angle from x_{i-1} to x_i about z_i .

By multiplying these matrices respectively, the relationship between the first and the last limb of the robot is obtained. The illustration of the system and the D-H parameters table are given in Figure 4 and Table 1.

The resulting matrix were written in the equation 5:

$${}^0_5T = \begin{bmatrix} r_{11} & r_{12} & r_{13} & p_x \\ r_{21} & r_{22} & r_{23} & p_y \\ r_{31} & r_{32} & r_{33} & p_z \\ 0 & 0 & 0 & 1 \end{bmatrix} \quad (5)$$

where equations 6a - 6l are;

$$r_{11} = c(\theta_2 + \theta_3 + \theta_4) \quad (6a)$$

$$r_{12} = s(\theta_2 + \theta_3 + \theta_4) \quad (6b)$$

$$r_{13} = 0 \quad (6c)$$

$$r_{21} = s(\theta_2 + \theta_3 + \theta_4) \quad (6d)$$

$$r_{22} = c(\theta_2 + \theta_3 + \theta_4) \quad (6e)$$

$$r_{23} = 0 \quad (6f)$$

$$r_{31} = 0 \quad (6g)$$

$$r_{32} = 0 \quad (6h)$$

$$r_{33} = 1 \quad (6i)$$

$$p_x = l_1 + l_2 c\theta_2 + l_3 c(\theta_2 + \theta_3) + l_4 c(\theta_2 + \theta_3 + \theta_4) \quad (6j)$$

$$p_y = l_2 s\theta_2 + l_3 s(\theta_2 + \theta_3) + l_4 s(\theta_2 + \theta_3 + \theta_4) \quad (6k)$$

$$p_z = d_1 \quad (6l)$$

Here, p_x , p_y and p_z denote the position of the end effector in x, y, and z coordinates respectively. The term d_1 refers to the displacement of the sliding joint on the 1st axis in the z direction depending on the motor angle θ_1 . The linear displacement of the linear guide rail in the first axis is 5 mm per revolution. This formulated in equation 7.

$$d_1 = \frac{5}{2\pi} \theta_1 \quad (7)$$

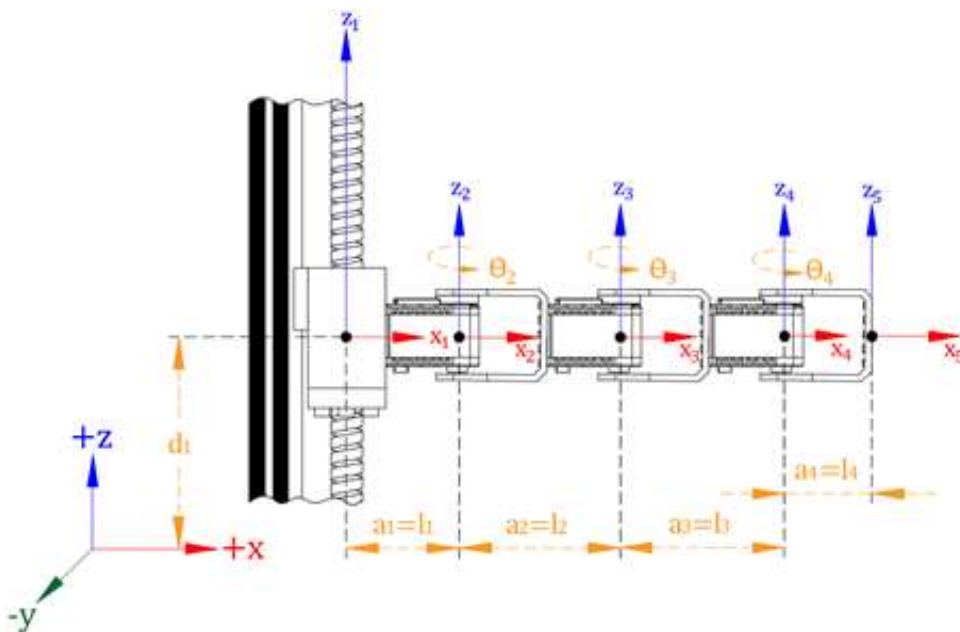


Figure 4. Illustration of D-H parameters of the system.

Table 1. D-H parameters for each axis

	α_{i-1}	a_{i-1}	d_i	θ_i
1 st axis	0	0	d_1	0
2 nd axis	0	a_1	0	θ_2
3 rd axis	0	a_2	0	θ_3
4 th axis	0	a_3	0	θ_4

5 th axis	0	a_4	0	0
----------------------	---	-------	---	---

2.3.2. Inverse kinematics

The inverse kinematics problem is used to determine the joint variables d and θ from the position and configuration of the end effector. The joint variable data are processed in real time and sent to the actuators to ensure continuity of motion. To visualize point coordinates, limb lengths and joint angles used in the solution of inverse kinematics problem, the top view of the system is illustrated in Figure 5.

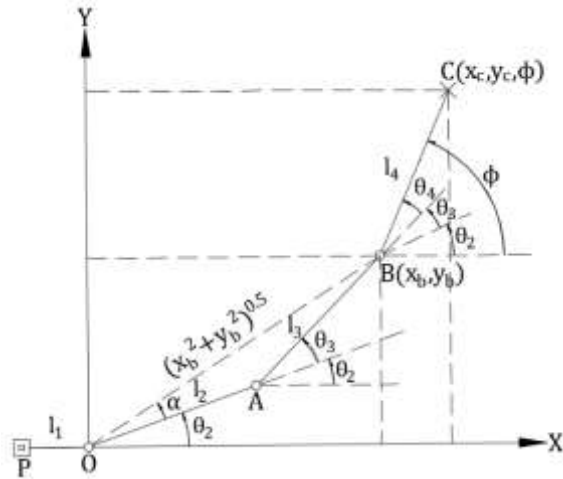


Figure 5. Illustration of inverse kinematics parameters.

The point P here represents linear rail guide on the 1st axis, the line segments |PO|, |OA|, |AB| and |BC| denotes limb lengths bounded by joints, and the point C represents the position of the end effector. For convenience in calculations, the origin of the x-y coordinate system is placed on the 2nd axis. Hence, the joint parameters to be calculated are θ_2 , θ_3 and θ_4 . The position (x_c, y_c) and orientation (ϕ) of the end effector are known and used in determining these parameters. Using the position and orientation of point C, the coordinates of point B are given below. x_b and y_b are formulated in Equations 8 and 9.

$$x_b = x_c - l_4 \cos \phi \tag{8}$$

$$y_b = y_c - l_4 \sin \phi \tag{9}$$

It is clear that the shortest distance between point O and B is equal in Equation 10;

$$|OB| = \sqrt{x_b^2 + y_b^2} = \sqrt{x_c^2 + y_c^2 + l_4^2 - 2l_4(x_c \cos \phi + y_c \sin \phi)} \tag{10}$$

The angle \widehat{OAB} in the figure is the supplementary angle of the angle θ_3 , so it can be shown as $\pi - \theta_3$. Accordingly, the angle θ_3 can be found using the cosine theorem in the triangle of OAB, shown in Equation 11.

$$\theta_3 = \pi - \cos^{-1} \left(\frac{l_2^2 + l_3^2 - x_b^2 - y_b^2}{2l_2 l_3} \right) \tag{11}$$

To find the angle α , the cosine theorem is applied again in

the imaginary triangle AOB, shown in Equation 12.

$$x_b^2 + y_b^2 + l_2^2 - 2\sqrt{x_b^2 + y_b^2} l_2 \cos \alpha = l_3^2 \tag{12}$$

and the angle α equals, shown in Equation 13.

$$\alpha = \cos^{-1} \left(\frac{l_2^2 + x_b^2 + y_b^2 - l_3^2}{2l_2 \sqrt{x_b^2 + y_b^2}} \right) \tag{13}$$

Obviously, the angle $\alpha + \theta_2$ can be represented as the coordinates of point B; formulated in Equations 14 and 15.

$$\alpha + \theta_2 = \tan^{-1} \left(\frac{y_b}{x_b} \right) \tag{14}$$

$$\theta_2 = \tan^{-1} \left(\frac{y_b}{x_b} \right) - \alpha \tag{15}$$

In Figure 5, it can be easily seen that the angle ϕ is equal to the sum of the 2nd, 3rd, and 4th joint angles. That means, shown in Equation 16.

$$\theta_4 = \phi - \theta_2 - \theta_3 \tag{16}$$

and ultimately, the relation between the angle θ_1 and the motion on the z axis were expressed in a linear relation as in Equation 17, and that yields,

$$\theta_1 = \frac{2\pi}{5} d_1 \tag{17}$$

3. Results and Discussion

The following experimental setup has been established to implement the system whose theoretical backgrounds were given in the sections above. Accordingly, the robot arm system, human-PC interface and parts of the program blocks were presented in Figure 6.

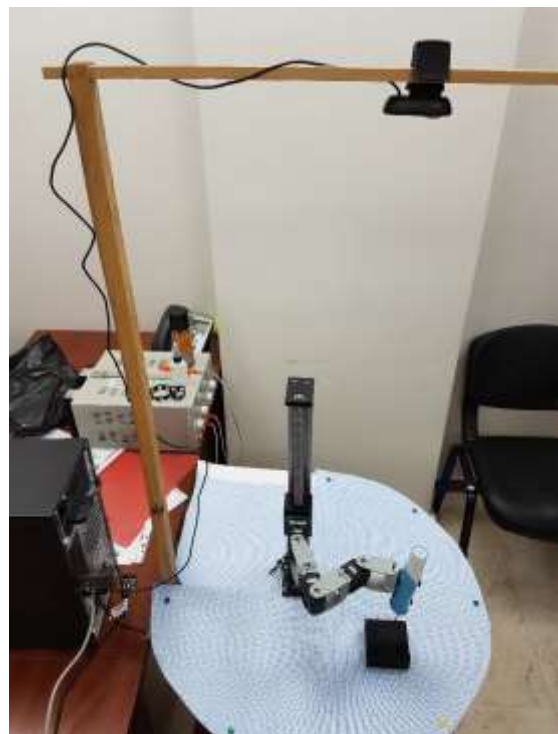


Figure 6. The experimental setup of robot arm system.

The camera was attached on the top of the robot arm to display the object. All actuators used in the system were communicated with each other and the computer via USB2Dynamixel control card. A 0-30V DC power supply were used to energize the motors. Figure 7 and Figure 8 shows the control tools; image, point and angle indicators.

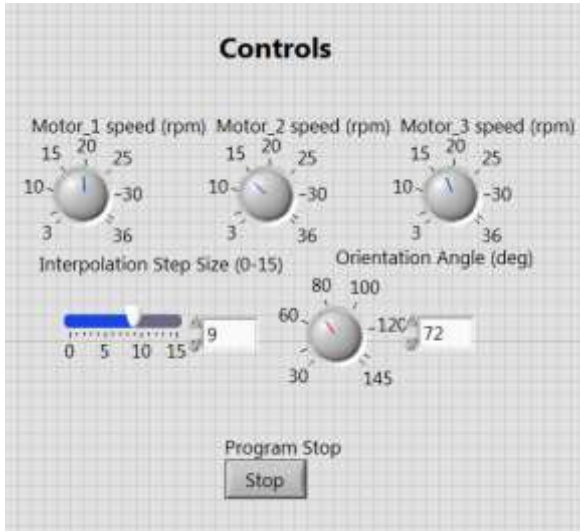


Figure 7. Control tools.

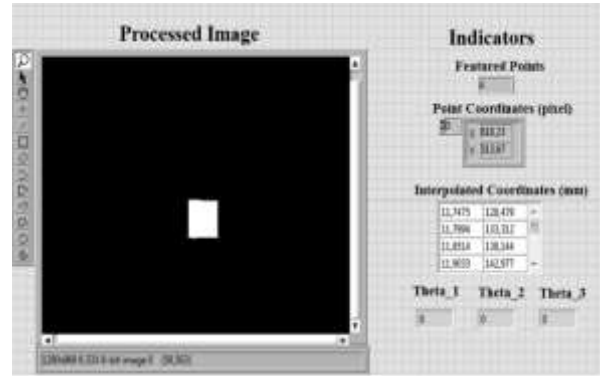


Figure 8. Image, point and angle indicators.

The data I/O on the human-PC interface are shown in the Figure 8. The processed image, feature coordinates, interpolated coordinates and motor angle data were displayed on the screen to inform the user. The user is able to interfere with motor speeds, orientation angle and integration steps in real time.

Sections of the program blocks were given below. In Figure 9, image processing steps were visualized and in Figure 10, interpolation, kinematic calculations and data transmission to actuators were shown.

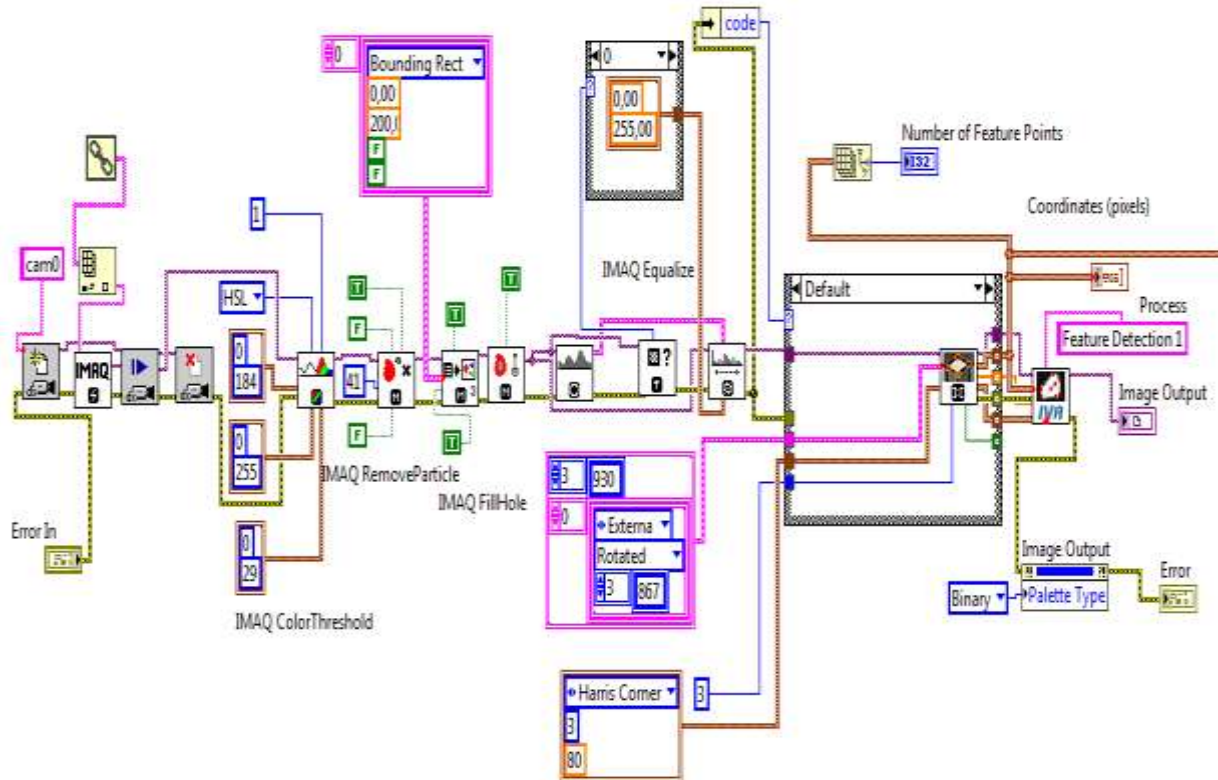


Figure 9. Image processing blocks.

The graph in Figure 11 illustrates the positional error measured in millimeters, between the actual coordinates of the tracked part's geometry and the trajectory coordinates followed by the end effector of the robotic arm.

The illustration above shows the positional errors occurring in the x and y axes along the trajectory of the part geometry during interpolation. These errors primarily result from the resolutions of the camera and servo motors used.

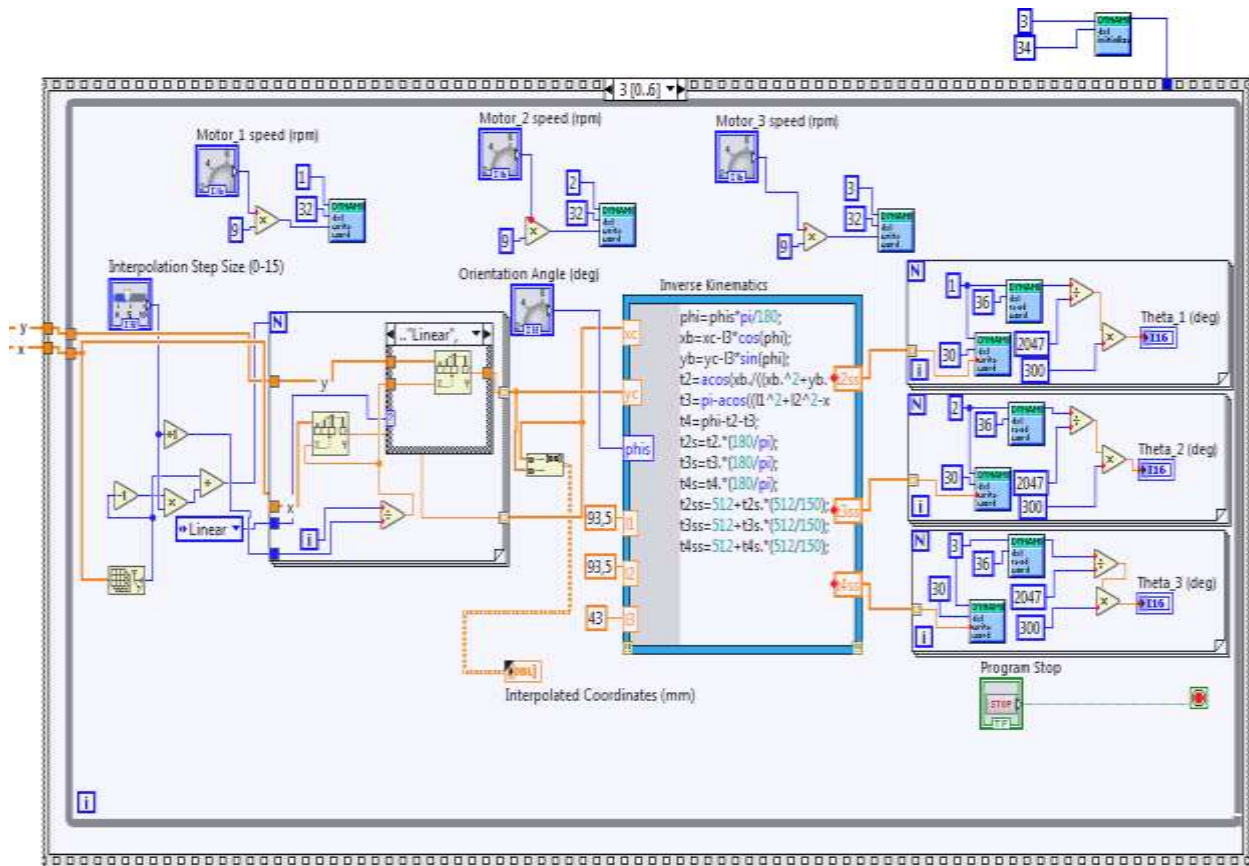


Figure 10. Interpolation, kinematics and data transmission blocks.

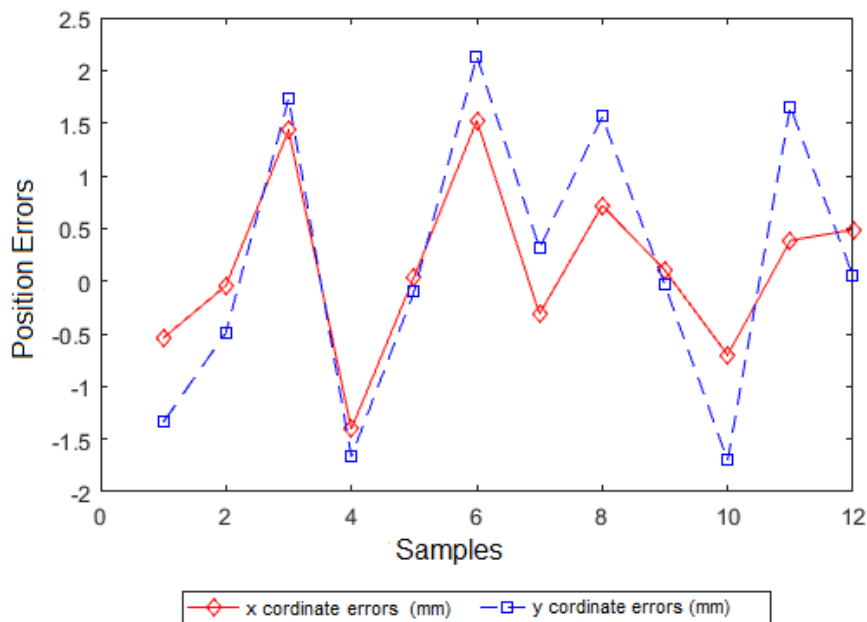


Figure 11. Graphical representation of position errors observed at the interpolation points.

Given that one side of the piece being used is known to be 7 cm, the maximum error rate encountered during advancement along an axis is less than 4% in any cases. As the robotic arm is designed as a SCARA type and exhibits serial manipulator characteristics, positional errors originating from resolution are transferred and

magnified from one axis to another.

4. Conclusion

This study presents the design of a robotic arm that utilizes Dynamixel smart servo motors and connecting elements to track the trajectory of an object captured by a camera in a 2D plane. The trajectory tracking process

was realized through the kinematic equations of the proposed robot arm. Numeric interpolation technique was employed in the transformation of pixel-based coordinates to millimetric coordinates for the feature points extracted through image processing techniques. Errors that occurred along the tracked trajectory were identified through coordinate feedback from the camera. Position accuracy was demonstrated through graphical representations. The established setup is capable of performing operations for various purposes by integrating different end effectors onto it for possible future studies.

Author Contributions

The percentage of the author(s) contributions is presented below. All authors reviewed and approved the final version of the manuscript.

	Y.H.E.N.	D.K.	M.S.D.	M.S.S.	N.Y.P.
C	35	10	25	20	10
D	100				
S	100				
DCP	50		50		
DAI			100		
L	20	20	20	20	20
W	20	20	20	20	20
CR	20	20	20	20	20
SR	20	20	20	20	20
PM	20	20	20	20	20
FA	20	20	20	20	20

C=Concept, D= design, S= supervision, DCP= data collection and/or processing, DAI= data analysis and/or interpretation, L= literature search, W= writing, CR= critical review, SR= submission and revision, PM= project management, FA= funding acquisition.

Conflict of Interest

The authors declared that there is no conflict of interest.

Ethical Consideration

Ethics committee approval was not required for this study because of there was no study on animals or humans.

References

Budiyanta NE, Sereati CO, Lukas L. 2020. PD controller computer vision and robotics integration based for student's programming comprehension improvement. *Telecommun Comput Electron Cont*, 18(2): 899-906.

Cheah CC, Liu C, Slotine JJE. 2006. Adaptive tracking control for robots with unknown kinematic and dynamic properties. *Int J Robot Res*, 25(3): 283-296.

Chen CY, Liao PS, Cheng CC, Jong GF. 2007. Design and implementation of integrated non-uniform rational B-spline and digital differential analyser interpolators for computerized numerical control servocontrollers. *Proceedings of the Institution of Mechanical Engineers, Part C: J Mechan Eng Sci*, 221(9): 1075-1087.

Ding F, Liu C. 2018. Applying coordinate fixed Denavit-Hartenberg method to solve the workspace of drilling robot

arm. *Int J Adv Robot Syst*, 15(4): 1729881418793283.

Dixon WE. 2007. Adaptive regulation of amplitude limited robot manipulators with uncertain kinematics and dynamics. *IEEE Transact Auto Cont*, 52(3): 488-493.

Duque-Suárez N, Amaya-Mejía LM, Martinez C, Jaramillo-Ramirez D. 2022. Deep learning for safe human-robot collaboration. In *advances in automation and robotics research. Proceedings of the 3rd Latin American Congress on Automation and Robotics*, Monterrey, Mexico, May 12-15, pp: 239-251.

Dyck M, Tavakoli M. 2013. Measuring the dynamic impedance of the human arm without a force sensor. *IEEE 13th International Conference on Rehabilitation Robotics (ICORR)*, June 24-26, Seattle, US, pp: 1-8.

El Naser YH, Atalı G, Karayel D, Özkan SS. 2020. Prototyping an industrial robot arm for deburring in machining. *Acad Plat J Eng Sci*, 8(2): 304-309.

Fang L, Liu G, Li Q, Zhang H. 2022. A high-precision non-uniform rational B-spline interpolator based on S-shaped feedrate scheduling. *Int J Adv Manufact Technol*, 121(3-4): 2585-2595.

Garriga-Casanovas A, Baena F. 2019. Kinematics of continuum robots with constant curvature bending and extension capabilities. *J Mechan Robot*, 11(1): 011010.

Grzelczyk D, Szymanowska O, Awrejcewicz J. 2019. Kinematic and dynamic simulation of an octopod robot controlled by different central pattern generators. *Proceedings of the Institution of Mechanical Engineers, Part I: J Syst Cont Eng*, 233(4): 400-417.

Guzmán-Giménez J, Valera Fernández Á, Mata Amela V, Díaz-Rodríguez MÁ. 2020. Synthesis of the Inverse Kinematic Model of non-redundant open-chain robotic systems using Groebner Basis theory. *Appl Sci*, 10(8): 2781.

He B, Xu F, Zhang P. 2021. Kinematics model approach to energy efficiency in sustainable manufacturing. *Res Square*, <https://doi.org/10.21203/rs.3.rs-652070/v1>.

Jian-Peng S, Jin-Gang J, Wei Q, Zhi-Yuan H, Hong-Yuan M, Shan Z. 2023. Digital interactive design and robot-assisted preparation experiment of tooth veneer preparation: An in vitro proof-of-concept. *IEEE Access*, 11: 30292-30307.

Jiao SX, Wang H, Xia LL, Zhang S. 2018. Research on trajectory planning of 6-DOF cutting-robot in machining complex surface. *MATEC Web of Conf*, 220: 06003.

Liu X, Tao R, Tavakoli M. 2014. Adaptive control of uncertain nonlinear teleoperation systems. *Mechatronics*, 24(1): 66-78.

Luo H, Fu J, Jiao L, Liu G, Yu C, Wu T. 2019. Kinematics and dynamics analysis of a new-type friction stir welding robot and its simulation. *Adv Mechan Eng*, 11(7): 1687814019866518.

Mahmoodpour M, Lobov A, Hayati S, Pastukhov A. 2019. An affordable deep learning based solution to support pick and place robotic tasks. In *Instrumentation Engineering, Electronics and Telecommunications-2019: Proceedings of the V International Forum*, November 20-22, Izhevsk, Russian Federation, pp: 66-75.

Nansai S, Ando Y, Itoh H, Kamamichi N. 2021. Design and implementation of a lizard-inspired robot. *Appl Sci*, 11(17): 7898.

Romero-González C, García-Varea I, Martínez-Gómez J. 2022. Shape binary patterns: an efficient local descriptor and keypoint detector for point clouds. *Multimedia Tools Appl*, 81(3): 3577-3601.

Sophokleous A, Christodoulou P, Doitsidis L, Chatzichristofis SA. 2021. Computer vision meets educational robotics. *Electronics*, 10(6): 730.

- Staicu S, Shao Z, Zhang Z, Tang X, Wang L. 2018. Kinematic analysis of the X4 translational–rotational parallel robot. *Int J Adv Robot Syst*, 15(5): 1729881418803849.
- Syahrian NM, Risma P, Dewi T. 2017. Vision-based pipe monitoring robot for crack detection using canny edge detection method as an image processing technique. *Kinetik: Game Technol Info Syst Comput Network Comput Electron Cont*, 2017: 243-250.
- Tao Y, Chen F, Xiong H. 2014. Kinematics and workspace of a 4-DOF hybrid palletizing robot. *Adv Mechan Eng*, 6: 125973.
- Uk ME, Sajjad Ali Shah FB, Soyaslan M, Eldogan O. 2020. Modeling, control, and simulation of a SCARA PRR-type robot manipulator. *Scientia Iranica*, 27(1): 330-340.
- Wang T, Wu Y, Liang J, Han C, Chen J, Zhao Q. 2015. Analysis and experimental kinematics of a skid-steering wheeled robot based on a laser scanner sensor. *Sensors*, 15(5): 9681-9702.
- Yanto L, Dewanto RS, Pramadihanto D, Binugroho EH. 2017. Teen-Size humanoid ‐ œFLoW‐ complete analytical kinematics. *EMITTER Int J Eng Technol*, 5(2): 298-311.
- Zhang T, Cao Y, Ma G. 2022. Trajectory planning of 3-CRU parallel robot with linear kinematics equation. *Proceedings of the Institution of Mechanical Engineers, Part C: J Mechan Eng Sci*, 236(17): 9589-9609.
- Zhou Q, Yuan K, Zou W, Lu P, Hu H. 2005. A multi-scale focus pseudo omni-directional robot vision system with intelligent image grabbers. *IEEE/ASME International Conference on Advanced Intelligent Mechatronics*, July 24-28, Monterey, US, pp: 1563-1568.



USAGE OF WEKA SOFTWARE BASED ON MACHINE LEARNING ALGORITHMS FOR PREDICTION OF LIVER FIBROSIS/CIRRHOSIS

Rukiye UZUN ARSLAN^{1*}, Ziyne PAMUK², Ceren KAYA²

¹Zonguldak Bulent Ecevit University, Faculty of Engineering, Department of Electrical and Electronics Engineering, 67100, Zonguldak, Türkiye


²Zonguldak Bulent Ecevit University, Faculty of Engineering, Department of Biomedical Engineering, 67100, Zonguldak, Türkiye


Abstract: The liver, a life-sustaining organ, plays a substantial role in many body functions. Liver diseases have become an important world health problem in terms of prevalence, incidences, and mortalities. Liver fibrosis/cirrhosis is great of importance, because if not treated in time liver cancer could be occurred and spread to other parts of the body. For this reason, early diagnosis of liver fibrosis/cirrhosis gives significance. Accordingly, this study investigated the performances of different machine learning algorithms for prediction of liver fibrosis/cirrhosis based on demographic and blood values. In this context, random forest, k-nearest neighbour, C4.5 decision tree, K-star, random tree and reduced error pruning tree algorithms were used. Two distinct approaches were employed to evaluate the performances of machine learning algorithms. In the first approach, the entire features of dataset were utilized, while in the second approach, only the features selected through principal component analysis were used. Each approach was rigorously assessed using both 10-fold cross-validation and data splitting (70% train and 30% test) techniques. By conducting separate evaluations for each approach, a comprehensive understanding of the effectiveness of utilizing all features versus extracted features based principal component analysis was attained, providing valuable insights into the impact of feature dimensionality reduction on model performance. In this study, all analyses were implemented on WEKA data mining tool. In the first approach, the classification accuracies of random forest algorithm were 89.72% and 90.75% with the application of data splitting (70%-30%) and cross-validation techniques, respectively. In the second approach, where feature reduction is performed using principal component analysis technique, the accuracy values obtained from data splitting and cross-validation techniques of random forest algorithm were 88.61% and 88.83%, respectively. The obtained results revealed out that random forest algorithm outperformed for both approaches. Besides, the application of principal component analysis technique negatively affected the classification performance of used machine learning algorithms. It is thought that the proposed model will guide specialist physicians in making appropriate treatment decisions for patients with liver fibrosis/cirrhosis, potentially leading to death in its advanced stages.


Keywords: WEKA, Liver fibrosis/cirrhosis, Principal component analysis, Feature selection, Early diagnosis, Machine learning

*Corresponding author: Zonguldak Bulent Ecevit University, Faculty of Engineering, Department of Electrical and Electronics Engineering, 67100, Zonguldak, Türkiye

E mail: rukiyeuzun67@gmail.com (R. UZUN ARSLAN)

Rukiye UZUN ARSLAN  <https://orcid.org/0000-0002-2082-8695>

Ziyne PAMUK  <https://orcid.org/0000-0003-3792-2183>

Ceren KAYA  <https://orcid.org/0000-0002-1970-2833>

Received: August 29, 2023

Accepted: April 02, 2024

Published: May 15, 2024

Cite as: Uzun Arslan R, Pamuk Z, Kaya C. 2024. Usage of weka software based on machine learning algorithms for prediction of liver fibrosis/cirrhosis. BSJ Eng Sci, 7(3): 445-456.

1. Introduction

The liver is a vital organ placed in the upper right side of the abdomen, beneath the diaphragm. It is the largest internal organ in the human body, and its weight is about 1.5 kg, although it differs in men and women. The liver, which can both expand and renew itself, undertakes many important vital functions such as clearing toxic wastes in the blood, storing some important vitamins, storing, and digesting fats in the body, making bile acids usable for our body, balancing hormones. If the liver cannot perform these functions properly, it leads several types of liver diseases like fatty liver, fibrosis, cirrhosis, and liver cancer (Lin, 2009; Acarlı, 2020). These diseases have become a significant global health concern regarding their prevalence, incidences, and mortalities (Asrani et al., 2019; Del Campo et al., 2018; Ramana et al.,

2011). The progression of liver disease is given in Figure 1.

Fibrosis and cirrhosis are conditions involved in scarring of the liver tissue. As seen in Figure 1, since fibrosis/cirrhosis is the previous stage of liver cancer, early diagnosis is of great importance as it can increase the survival rate. Nowadays, liver biopsy accepted as the gold standard test has been used. However, biopsy has many disadvantages such as the risk of complications, being invasive, not being repeated frequently, not providing information about the whole liver, and high cost. Therefore, it is not possible to establish a final diagnosis by liver biopsy. To overcome these disadvantages, alternative methods (biochemical test, biomedical imaging techniques etc.) have been developed. In traditional biomedical tests, many clinical



parameters such as alkaline phosphatase (ALP), Alanine amino-transferase (ALT), Aspartate amino-transferase (AST) are extensively utilized in the diagnosis of the disease and in research studies. On the other hand, the developments in technology have made popular the usage of machine learning (ML), artificial intelligence (AI) and data mining techniques, especially in the field of medicine to diagnose and treat disease. Thanks to these techniques, disease management can be carried out quickly and accurately by a specialist physician. On the other hand, different signs, symptoms, and enzyme levels can be encountered in the diagnosis of liver diseases (Schiff et al., 2017). This situation causes the disease process to be error-prone and complex. Because of this, utilizing ML and data mining algorithms can give support to specialist physicians in diagnosis and prediction of

liver disease. In this context, the performances of six different ML algorithms in classifying healthy and unhealthy (liver fibrosis/cirrhosis) patients were investigated within the scope of this study. This classification study performed in WEKA software was carried out using random forest (RF), C4.5 decision tree (J48), random tree (RT), K-star, reduced error pruning tree (REPTree) and k-nearest neighbour (k-NN, IBk) algorithms. The dataset of 1200 patient collected from Zonguldak Ataturk State Hospital, Türkiye was used in the study, in which all necessary ethics committee permissions were obtained. The dataset consisted of features including age, gender, aspartate aminotransferase (AST), alanine aminotransferase (ALT), Total Bilirubin, Direct Bilirubin, Alkaline Phosphatase (ALP) and Albumin.

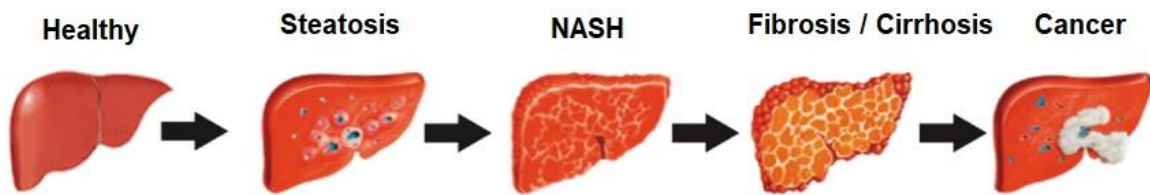


Figure 1. Progression of liver diseases (Xie et. al, 2016).

The remaining parts of this study were formed as follows: In the second part, studies on the prediction of liver diseases used ML methods were given. In the third part, brief information was given about the data set utilized in the study, which pre-processing it has been through, the models created, and the algorithms used in the model. In the fourth part, the performance metrics, complexity matrices and graphs obtained from the algorithms were interpreted. In the last part, the obtained were discussed and future studies were mentioned.

2. Related Works

In literature, many studies-based ML and data mining have been realized to predict liver diseases. Gulia et al. (2014) proposed a hybrid model with (having) three stages (classification, feature selection and comparison of results) to detect potential liver patient using WEKA software. They showed that random forest gives better results (accuracy with 71.87%) than the other methods. Alkuşak and Gök (2014) studied liver failure detection utilizing ML methods on WEKA. Using two different datasets, they evaluated performances of the methods and found that the neural networks' performances were high for both datasets. Pahareeya et al. (2014) carried out four different ML algorithms on Indian Liver Patient Dataset (ILPD) using 10-fold cross-validation technique. They reached 89.11% accuracy value with RF algorithm in liver disease classification. Borulday et al. (2017) investigated the decision tree algorithm's performance to detect different liver diseases such as cirrhosis and acute

hepatitis. In addition, an interface has been developed that includes different demographic data, physical examination, laboratory tests, symptoms, radiological imaging, liver biopsy and unclassified data. Thus, specialist doctors were given the opportunity to select tabs in the interface. Muthuselvan et al. (2018) investigated binary classification performances of Naïve Bayes (NB), K-star, J48 and Random Tree (RT) algorithms by using WEKA software on ILPD dataset. The obtained results demonstrated that RT had superior accuracy (74.2%) with nominal execution time. Alaybeyoğlu and Mulayim (2018) developed a smart model for liver cancer diagnosis based on support vector machine algorithm and reached an accuracy of 78.33%. Ma et al. (2018) utilized diverse ML algorithms to obtain a useful monitoring and optimal predictive model of non-alcoholic fatty liver disease. The algorithms were carried out through WEKA, the classification was implemented by using a 10-fold cross-validation technique and the performances of algorithms were compared. They revealed out that the Bayesian network model (by 83% accuracy) has best performance as compared the other algorithms. Rahman et al. (2019) evaluated the performance of many different ML algorithms to estimate and reduce the cost of diagnosing chronic liver disease. ILPD was used as the data set and the highest performance was obtained in logistic regression (75% accuracy). Keleş et al. (2020) investigated various ML algorithms' performances (like J48, RF, RT) implemented in WEKA to diagnose liver diseases. Using ILPD, the performances of the algorithms were compared

regarding the evaluation metrics. It was obtained from the analysis that the algorithm with the highest performance was RF with 81.9% accuracy. Gaber et al. (2022) proposed a computer-aided decision support model based on ML algorithms and voting classifier to detect fatty and normal livers from ultrasound liver images. The classification performances were obtained 95.71% and 93.12% in voting classifier and J48 algorithm, respectively. Velu et al. (2022) presented a novel classification model on the basis of liver function test results to detect probable liver patients. The model showed a success rate of 98.4% and 99.36% for the test and training phases, respectively. They also designed an interface providing the opportunity to enter patient information for specialist. Dritisas and Trigka (2023) examined the performance of different ML algorithms in the prediction of liver disease at an early stage. The algorithms performances were evaluated regarding accuracy, precision, recall, F-measure and area under the curve (AUC) by 10-fold cross-validation. They revealed out that voting algorithm has higher performance with 80.1% of accuracy in comparison to other algorithms. Mukhyber et al. (2023) investigated the performance of several data mining algorithms in the early diagnosis of liver disease according to parameters such as accuracy, precision, recall and f-measure. In addition, they addressed the comparison of algorithms' performances in accordance with the performance of ILPD.

The above-mentioned studies clearly show that ML algorithms have been widely used in the diagnosis of liver diseases. The models having superior performance had been determined according to different metrics such as accuracy, precision, specificity and F-measure. In this context, accuracy, precision, recall, F-measure and receiver operating characteristic curve (ROC) metrics were used within the scope of this study. Besides, it has been determined that the obtained results in the above-mentioned studies varies depending on many factors like the data set used, evaluation metrics, and the type of liver disease examined.

3. Materials and Methods

This study analyses the individuals' health condition (healthy and unhealthy-suffering from liver fibrosis/cirrhosis) by using 6 different ML algorithms (RF, IBk, k-Star, RT, REPTree and J48) based two different approaches. In the first approach all the features in the dataset were used, while the selected features extracted by PCA were utilized in the second approach. The performances of ML algorithms for each approach were evaluated regarding cross-validation (10-fold) and data splitting (70% train-30% test) techniques separately. General flowchart of proposed model was shown in Figure 2.

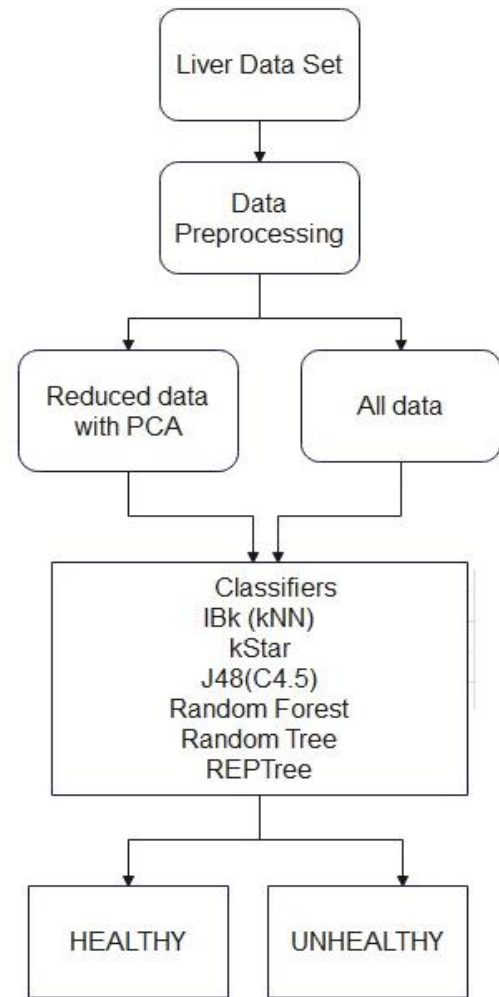


Figure 2. General flowchart of proposed model

3.1. Data Set

This study carried out by using a balanced dataset (600 healthy, 600 with Liver Fibrosis/Cirrhosis) collected from Zonguldak Ataturk State Hospital. The required ethical approval for performing this study was obtained from Zonguldak Bulent Ecevit University, Non-interventional Clinical Research Ethics Committee (Decision no: 2021/05; Date: 10.03.2021). Age, gender, aspartate aminotransferase (AST), alanine aminotransferase (ALT), Total Bilirubin, Direct Bilirubin, Alkaline Phosphatase (ALP) and Albumin features were used to comprise the required dataset. The reference values of these features, which were determined based on the experience of specialist physicians in accordance with ICD-10 K74 standards, were presented in Table 1 with data types.

3.2. Feature Selection

Feature selection indeed plays a crucial role in various machine learning tasks, including classification (Ucar and İncetas, 2022). By identifying and utilizing only the most relevant features, one can improve model performance, reduce computational complexity, and potentially enhance interpretability (Bulut et al, 2023).

On the other hand, principal component analysis (PCA) is a technique used to increase interpretability by reducing

the size of datasets and at the same time minimizing information loss. It minimizes information loss by creating new uncorrelated variables that successively maximize variance. When feature selection and PCA are

used together, better model performance and more effective data analysis can be achieved. In this context, in this study, a dataset with eight features was reduced to six features by PCA.

Table 1. The reference values and data types of features used in dataset

Features	Age	Gender	Reference Value	Data type
Age	-	-	-	Integer
Gender	-	-	-	{ 1, 0 }(Female, Male)
AST	Adult	M	0-35 U/L	Real
		F	0-31 U/L	
ALT	Adult	M	0-45 U/L	Real
		F	0-34 U/L	
T.Bilirubin	-	M/F	0-0.2 mg/dL	Real
D.Bilirubin	Adult	M/F	0.3-1.2 mg/dL	Real
ALP	Adult	M/F	30-120 U/L	Integer
Albumin	Adult	M/F	3.5-5.2 g/dL	Real
	>60		3.2-4.6 g/dL	

3.3. Classification Algorithms

In this study, it was investigated which ML algorithm shows higher performance when making binary classification of patients (healthy and unhealthy-suffering from liver fibrosis/cirrhosis). To that end, RF, IBk, k-Star, RT, REPTree and J48 algorithms were used considering the previous studies in the literature. These algorithms are briefly described below.

RT, an ensemble learning algorithm, generates rules by learning multiple individual rules. It employs a bagging idea to create a decision tree and produce a random dataset. While in a standard decision tree, each node is split using the best split among all variables, in RT algorithm, each node is split using the best split among a randomly selected subset of variables at that node. This approach enables RT to achieve high accuracy results (Işık and Ulusoy, 2021).

RF algorithm is a supervised ensemble learning method developed by Breiman and used to solve classification and/or regression tasks (Breiman, 2001). RF, having common usage, consists of many decision trees. The biggest disadvantage of the decision tree algorithm, one of the classical machine learning methods, is memorizing the data due to excessive learning. In order to overcome this disadvantage, the RO algorithm divides both the data set and its features into a large number of random subsets, trains them, and arrives at a general decision by averaging the answers of each subset generated by the decision tree (Sevli, 2019).

k-NN algorithm is a supervised learning algorithm used for both classification and regression. The working principle of this algorithm is relied on that data points with similar features tend to belong to the same class or have similar output values. Given a new data point, the algorithm finds the k closest data points in the training dataset based on a distance metric and then assigns the class label (in the case of classification) or predicts the value (in the case of regression) based on the majority

vote or average of the labels/values of the k nearest neighbours (Duda et al., 2000; Uzun et. al, 2018; Azam et al., 2020).

K-star algorithm, a classification method in machine learning, relies on the k-nearest neighbor (k-NN) principle but distinguishes itself by employing the Pearson correlation coefficient as the similarity measure rather than traditional distance metrics. It assesses similarities between feature vectors focusing solely on linear relationships, generating a correlation matrix to measure interactions among instances in the training dataset. Utilizing these similarities, it classifies test instances by comparing them with the matrix. K-star can be particularly effective for small-sized datasets and situations where nonlinear relationships are deemed insignificant for classification (Ünal et. al, 2019; Mishra et. al, 2021).

J48, which is an implementation of the C4.5 algorithm, is a popular decision tree algorithm used for classification. It builds a decision tree by applying a recursive binary splitting approach. It uses an attribute selection measure, typically based on information gain or gain ratio, to determine the most informative attribute to divide the data at each node of the tree. The dividing process continues recursively until a stop criterion is met, such as reaching a maximum depth or a minimum number of instances per leaf (Kaya et al., 2017; Muthuselvan et al., 2018).

REPTree is a decision tree learning algorithm designed to minimize variance during tree construction. It operates by iteratively generating multiple decision trees and selecting the best one based on variance reduction. The algorithm employs the square of the average error in predictions as the criterion for pruning the tree, ensuring that the selected tree maintains high accuracy. It builds the decision tree based on information gain as the splitting criterion and utilizes reduced error pruning to streamline the learning process. By employing this

approach, REPTree aims to produce decision trees that are efficient, accurate, and resistant to overfitting, making it a valuable tool in various machine learning applications, particularly in classification tasks (Şenel et. al, 2021).

All these algorithms, implemented on WEKA software, were used for classification of patients as healthy and unhealthy (suffering liver fibrosis/cirrhosis). WEKA is a popular open-source software tool. It comprises many machine learning algorithms, data pre-processing tools, and visualization abilities (Uzun et. al, 2019).

3.4. Evaluation Metrics

The ML algorithms' performances were evaluated by considering the accuracy, specificity, precision, recall and F-measure metrics that are frequently used in the similar studies. Accuracy (equation 1) is the ratio of correctly classified instances out of the total number of instances, whereas precision (equation 2) is the ratio of correctly predicted positive instances to all positive instances. Recall (equation 3) is the rate of the correctly predicted positive instances to all actual positive instances and F-measure (equation 4) is the harmonic mean of sensitivity and precision metrics. The mathematical equations for these metrics were given below. The confusion matrix evaluated the performance of ML algorithms consists of four elements: true positive (TP), true negative (TN), false positive (FP) and false negative (FN). In the confusion matrix, TP, FN, FP and TN correspond to correctly predicted positive class value, incorrectly predicted negative class value, incorrectly predicted positive class value and correctly predicted negative class

value, respectively (Narin et al., 2021; Şenyer Yapıcı, 2021).

$$\text{Accuracy} = \frac{TP + TN}{TP + TN + FP + FN} \quad (1)$$

$$\text{Precision} = \frac{TP}{TP + FP} \quad (2)$$

$$\text{Recall} = \frac{TP}{TP + FN} \quad (3)$$

$$\text{FMeasure} = 2 * \frac{\text{Precision} * \text{Recall}}{\text{Precision} + \text{Recall}} \quad (4)$$

In this study, the performances of ML algorithms were evaluated in accordance with cross-validation (10-fold) and data splitting (70%-30%) techniques. Besides, ROC metric with a value ranging from [0, 1] was given for the ML algorithm with the highest classification performance.

4. Results

In this study, ML algorithms performances was evaluated on a balanced dataset including liver fibrosis/cirrhosis patients (unhealthy, 600) and healthy patients (600) regarding cross-validation (10-fold) and data splitting (70%-30%) techniques separately. The classification performances of these algorithms were calculated based evaluation metrics given above. The dataset consisted of features including age, gender, aspartate aminotransferase (AST), alanine aminotransferase (ALT), Total Bilirubin, Direct Bilirubin, Alkaline Phosphatase (ALP) and Albumin. These eight features were used as input parameters in WEKA (Figure 3).

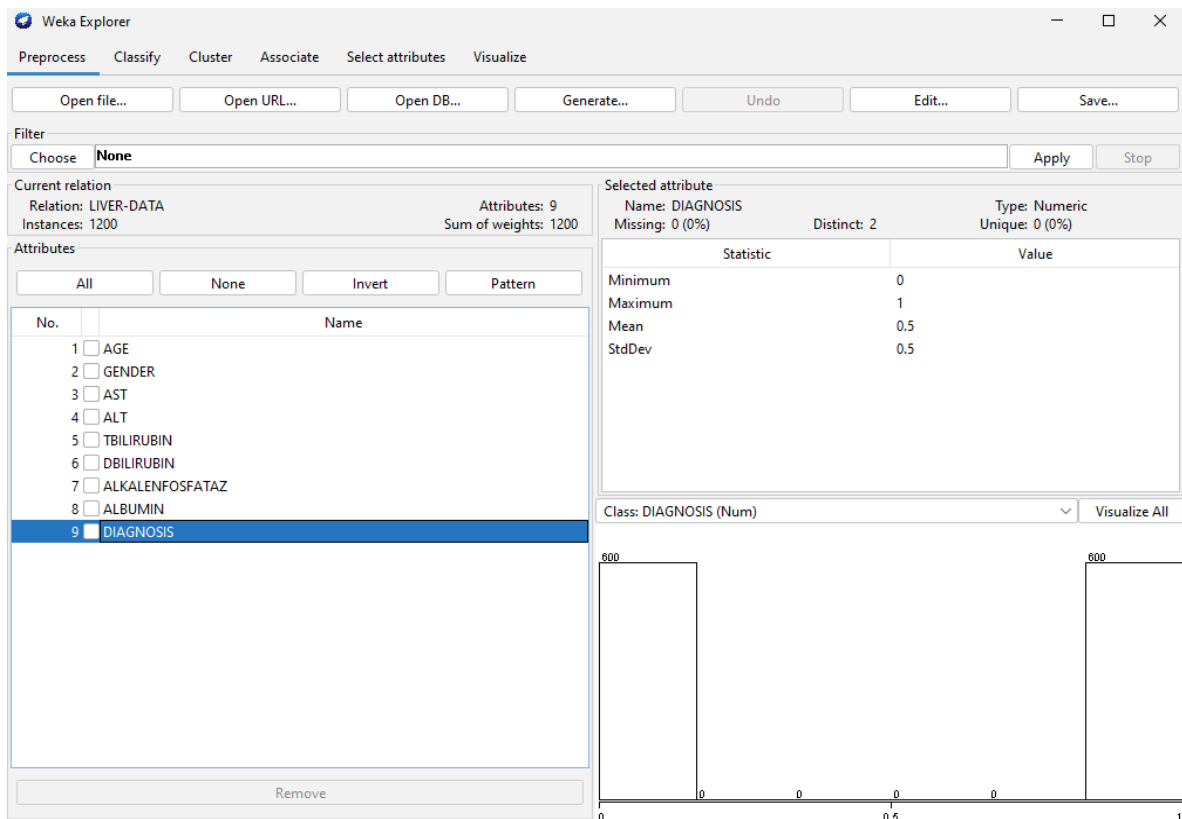


Figure 3. WEKA screenshot with all features given as input.

An example ARFF file of these features was shown in Figure 4. PCA method was used while feature selection. Ranker Search Method was selected when performing this process. The most significant feature was identified as Direct Bilirubin (0.64814) considering rank sorting of all features. The screenshot of ranked features appearing in WEKA after this process was illustrated in Figure 5. As clearly seen in Figure 5, age and ALT features, which their ranks were below 0.1, were not included in the reduced data set (six features).

```
@relation LIVER-DATA

@attribute AGE numeric
@attribute GENDER numeric
@attribute AST numeric
@attribute ALT numeric
@attribute TBILIRUBIN numeric
@attribute DBILIRUBIN numeric
@attribute ALKALENFOSFATAZ numeric
@attribute ALBUMIN numeric
@attribute DIAGNOSIS numeric
@data
63,1,34,31,1.1,0.44,127,4.5,1
60,1,41,20,2.3,1.34,61,4,1
65,1,31,24,1.8,0.61,88,4.6,1
62,1,38,38,1,0.3,91,4.3,1
73,0,67,42,1.1,0.54,66,3.7,1
81,1,15,10,0.6,0.33,141,4,1
81,1,12,6,0.6,0.37,142,3.7,1
46,1,37,29,1.2,0.5,108,3.8,1
46,1,44,30,1.4,0.53,114,3.5,1
46,1,42,22,1.5,0.7,101,3.3,1
46,1,50,76,0.4,0.18,113,4.5,1
44,1,49,31,2.6,1.1,101,3.5,1
47,1,39.5,24.5,1,0.5,293,3.2,1
47,1,25,16,1.4,0.55,124,3.9,1
59,1,32,25,1.2,0.52,91,3.5,1
77,1,15,13,0.4,0.22,63,3.9,1
80,0,36,16,2.56,1.09,124,3.5,1
63,0,50,41,1.3,0.47,85,5.2,1
49,1,34.1,31.1,0.5,0.26,82,4.7,1
69,0,19,13,0.7,0.25,80,4.7,1
72,0,27,14,0.8,0.32,111,4.1,1
85,0,64,13,0.6,0.32,140,2.7,1
```

Figure 4. Example liver ARFF file.

The first step in this study is to compare the performance of the ML algorithms using all features in the dataset. The obtained results for cross-validation (10-fold) and data splitting (70%-30%) techniques were summarized in Table 2 and Table 3, respectively. As seen from Table 2, RF algorithm showed higher classification outperform (with 90.75% accuracy) as compared with other

algorithms as evaluated 10-fold cross validation techniques. J48, RT, K-star, REPTree and IBk algorithms, respectively, having 86%, 85.08%, 88.08%, 84.33% and 83.84% accuracy were followed RF. In addition, as seen in Table 3, the highest classification performance was also obtained for RF algorithm (89.72%) when ML performances were evaluated based data splitting method. The classification accuracies for J48, RT, K-star, REPTree and IBk algorithms were obtained 85.27%, 86.66%, 88.05%, 84.16% and 85%, respectively.

Following the analysis of the performance of ML algorithms based on all features, significant features in the dataset were identified using PCA technique. Afterwards, using these extracted features, the performances of ML algorithms were compared separately according to data data splitting and cross-validation techniques. The obtained results were given in Table 4 and Table 5 for cross-validation (10-fold) and data splitting (%70-%30) techniques, respectively.

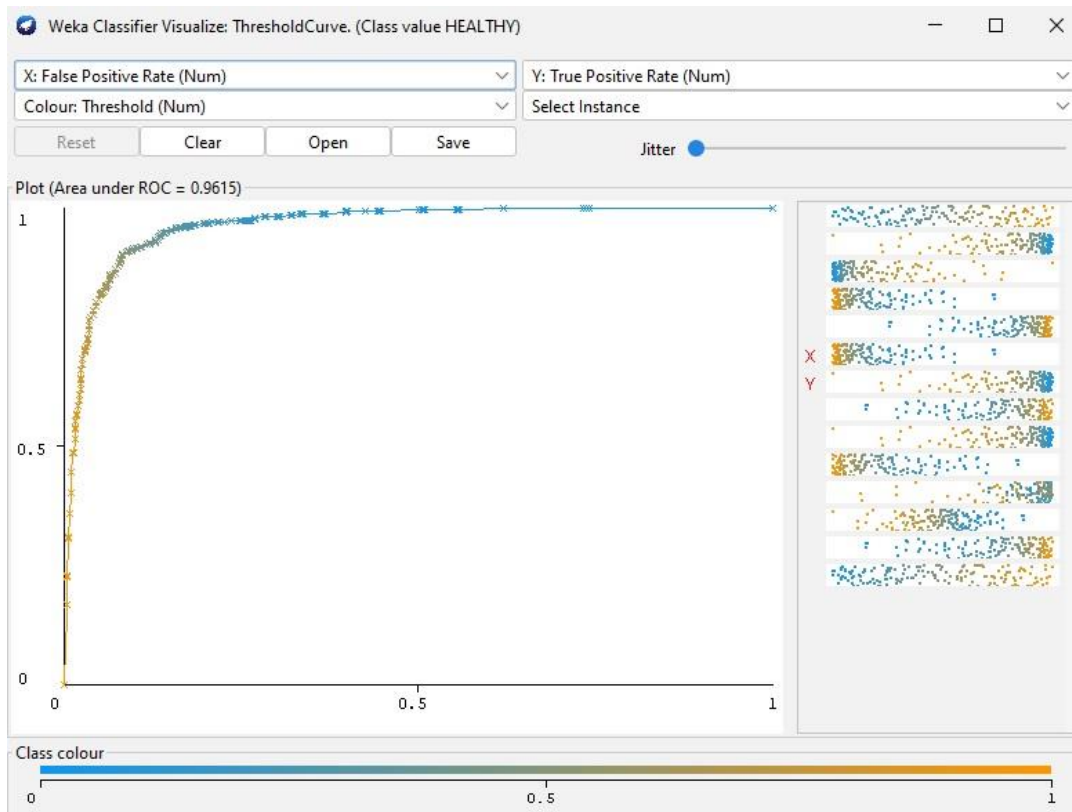
As seen from Table 4, RF algorithm showed higher classification outperform (with 88.83% accuracy) as compared with other algorithms as evaluated 10-fold cross validation techniques. J48, RT, K-star, REPTree and IBk algorithms, respectively, having 85.75%, 84.83%, 87.91%, 84.16% and 83.91% accuracy were followed RF. In addition, as seen in Table 5, the highest classification performance was also obtained for RF algorithm (88.61%) when ML performances were evaluated based data splitting method. The classification accuracies for J48, RT, K-star, REPTree and IBk algorithms were obtained 86.11%, 85.55%, 86.38%, 82.77% and 82.77%, respectively.

At the end of this study, ROC curves were plotted for RF algorithm having the highest classification accuracy for the first approach used all features in the dataset. ROC curves of the algorithm for 10-fold and data splitting were given in Figure 6 and Figure 7, in turn. The ROC curves of the algorithm were exhibited compatibility with the results given in Table 2 and Table 3.

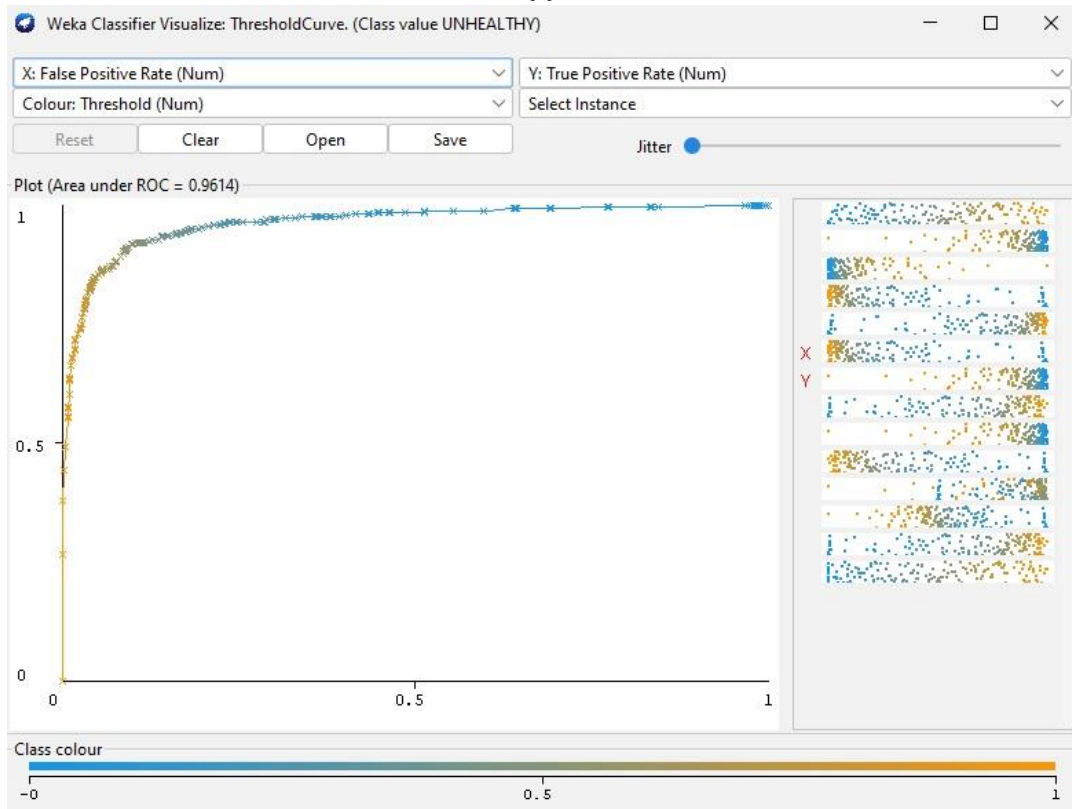
Studies in the literature used ML algorithms conducted on diagnosis of liver diseases were given in Table 6. It is important to compare the results with previous studies and Table 6 summarizes this comparison. It can be clearly seen that the accuracy value obtained with proposed method is higher than other studies. The studies in the literature commonly had been performed on publicly available datasets and had not taken into consideration the specialist physicians' opinions.

```
Ranked attributes:
0.64814 1 0.482DBILIRUBIN+0.468TBILIRUBIN+0.384ALT+0.36 AST+0.327DIAGNOSIS...
0.48636 2 0.694AGE-0.483GENDER-0.456ALBUMIN-0.256ALT+0.075DBILIRUBIN...
0.37525 3 -0.591ALKALENFOSFATAZ+0.467TBILIRUBIN+0.431DBILIRUBIN-0.406DIAGNOSIS+0.219ALBUMIN...
0.27414 4 0.633GENDER-0.482AST-0.429ALBUMIN-0.244ALKALENFOSFATAZ-0.243ALT...
0.18856 5 -0.527AST+0.491ALKALENFOSFATAZ-0.353ALT-0.329AGE-0.306GENDER...
0.11025 6 0.739DIAGNOSIS-0.507ALKALENFOSFATAZ-0.387GENDER+0.111ALT-0.107AGE...
0.05367 7 -0.618AGE-0.609ALBUMIN+0.291AST-0.266ALT-0.209GENDER...
0.00521 8 -0.701ALT+0.516AST+0.301DIAGNOSIS+0.29 ALBUMIN+0.228GENDER...
```

Figure 5. Screenshot obtained by PCA analysis.

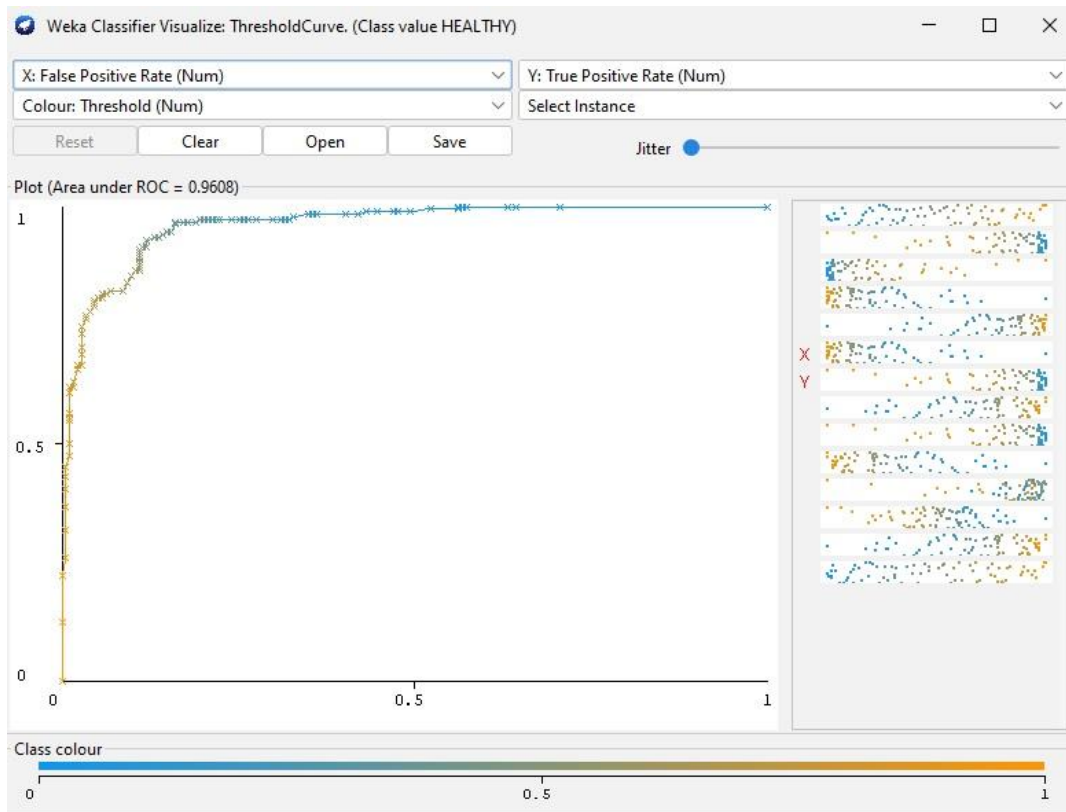


(a)

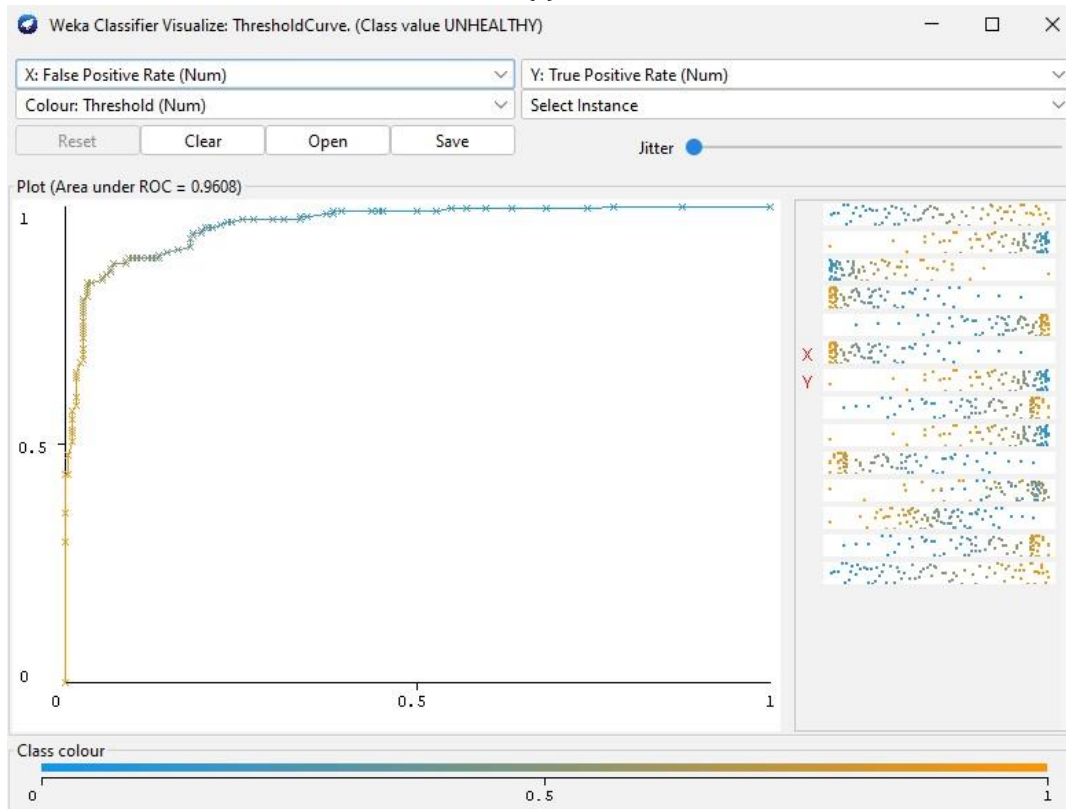


(b)

Figure 6. ROC curves of RF algorithm for whole dataset (10-fold) a) Healthy, b) Unhealthy class.



(a)



(b)

Figure 7. ROC curves of RF algorithm for reduced dataset by applying PCA (70%-30%) a) Healthy, b) Unhealthy class.

Table 2. The performance of algorithms on whole dataset for 10-fold cross validation

ML Algorithms	Accuracy (%)	Precision (%)	Recall (%)	F-Measure	ROC
IBk (k-NN)	86.66	86.80	86.70	86.70	86.50
K-star (K*)	88.08	88.10	88.10	88.10	94.40
J48 (C4.5)	86	86	86	86	86.10
Random Forest (RF)	90.75	90.80	90.80	90.70	96.10
Random Tree (RT)	85.08	85.20	85.10	85.10	84.90
REPTree	84.33	84.40	84.30	84.30	89.40

Table 3. The performance of algorithms on whole dataset for 70%-30% ratio

ML Algorithms	Accuracy (%)	Precision (%)	Recall (%)	F-Measure	ROC
IBk (k-NN)	85	85	85	85	84.40
K-star (K*)	88.05	88.10	88.10	88.10	94.40
J48 (C4.5)	85.27	85.30	85.30	85.30	87.20
Random Forest (RF)	89.72	89.70	89.70	89.70	96.10
Random Tree (RT)	86.66	86.80	86.70	86.70	86.70
REPTree	84.16	84.20	84.20	84.20	88.30

Table 4. The performance of algorithms on reduced dataset by applying PCA for 10-fold cross validation

ML Algorithms	Accuracy (%)	Precision (%)	Recall (%)	F-Measure	ROC
IBk (k-NN)	83.91	84	83.90	83.90	85.10
K-star (K*)	87.91	87.90	87.90	87.90	94.20
J48 (C4.5)	85.75	85.80	85.80	85.70	86
Random Forest (RF)	88.83	88.90	88.88	88.88	95.50
Random Tree (RT)	84.83	84.90	84.80	84.80	85.20
REPTree	84.16	84.20	84.20	84.20	88.50

Table 5. The performance of algorithms on reduced dataset by applying PCA for 70%-30% ratio

ML Algorithms	Accuracy (%)	Precision (%)	Recall (%)	F-Measure	ROC
IBk (k-NN)	82.77	82.90	82.80	82.80	82.90
K-star (K*)	86.38	86.40	86.40	86.40	94
J48 (C4.5)	86.11	86.10	86.10	86.10	87
Random Forest (RF)	88.61	88.60	88.60	88.60	95.30
Random Tree (RT)	85.55	85.60	85.60	85.50	85.90
REPTree	82.77	82.80	82.80	82.80	90

5. Discussion

The aim of this study was to classify patients whose were healthy and suffer from liver fibrosis/cirrhosis (600 healthy, 600 unhealthy) using ML algorithms. The collected data set included demographic and blood values of 1200 patients. To make a binary classification of liver disease; random forest, K-star, REPTree, random tree, k-nearest neighbours and C4.5 decision tree algorithms were utilized. The performance of all ML algorithms was interpreted by applying two diverse approaches. The first approach had been realized by using all features on the dataset, whereas the second approach had been carried out using extracted features through PCA. ML performances had been assessed based on 10-fold cross-validation and data splitting (70%-30% train-test) techniques for each approach. The whole analyses were performed in WEKA. The performances of algorithms were evaluated in terms of various metrics (accuracy, precision, recall, F-measure and ROC). These

metrics were preferred, because they commonly utilized in literature.

In this study, models were established based on two different approaches to diagnosing diabetes, and it was determined that the RF algorithm was the algorithm with high discrimination and the best classification criteria in general in correctly classifying the diagnosis of diabetes for both approaches.

In the light of findings, RF algorithm outperforms with high discrimination and the best classification criteria in general in correctly classifying the diagnosis of liver fibrosis/cirrhosis diseases for both approaches. Therefore, RF algorithm could be preferred to make accurate diagnosis of liver disease on the basis of this promising study results.

The studies in the literature usually aim to determine the ML algorithm with the best performance by using open access datasets. In addition, opinions of the specialist physicians have not been included in these studies. To

the best of our knowledge, no comprehensive comparison of ML algorithms for the diagnosis of liver fibrosis/cirrhosis diseases has been studied on the whole dataset and PCA-reduced dataset together as in this study.

6. Conclusion

As a result, this study is expected to provide guidance in evaluating the performance of several supervised ML algorithms in liver fibrosis/cirrhosis diagnosis classification. In similar studies, if the performance of the models is to be compared, it may be recommended to evaluate them with such approaches to increase the

sensitivity of the study.

In future studies, to obtain higher classification performance, it is thought to increase the dataset, to use different pre-processing techniques and to apply diverse feature selection methods gained increasingly popular recently. Performance evaluations will be investigated using different data mining methods and algorithms. The performance of the proposed model in the detection of different types of liver disease will be examined. In addition, it is planned to develop applications that can be used in the early diagnosis of fibrosis/cirrhosis and support decision-making by healthcare professionals-

Table 6. The comparison with studies-based ML algorithms on liver diseases diagnosis in the literature

Authors	Dataset	Tool	ML Algorithms	Accuracy (%)
Gulia et al. (2014)	Indian Liver Patient Dataset (ILPD)	WEKA	BayesNet, J48, MLP, Random Forest and SVM	MLP: 70.8405%
				SVM: 71.3551%
Muthuselvan et al. (2018)	Indian Liver Patient Dataset (ILPD)	WEKA	Naïve Bayes, k-Star, J48 and Random Tree	J48: 70.669%
				Random Forest: 71.8696%
Keleş et al. (2020)	Indian Liver Patient Dataset (ILPD)	WEKA	J48, LMT, Decision Stump, Hoeffding Tree, REP Tree, Random Forest, Random Tree and IBk	BayesNet: 69.1252% (After Feature Selection)
				Naïve Bayes: 60.6%
Proposed Study	Dataset collected from Zonguldak Ataturk State Hospital	WEKA	J48, IBk, K-star, Random Tree, REPTree and Random Forest (10-fold)	K-star: 67.2%
				J48: 71.2%
Proposed Study	Dataset collected from Zonguldak Ataturk State Hospital	WEKA	J48, IBk, K-star, Random Tree, REPTree and Random Forest (10-fold after PCA Feature Selection)	Random Tree: 74.2%
				J48: 74.40%
Proposed Study	Dataset collected from Zonguldak Ataturk State Hospital	WEKA	J48, IBk, K-star, Random Tree, REPTree and Random Forest (10-fold after PCA Feature Selection)	LMT: 73.80%
				Decision Stump: 67.10%
Proposed Study	Dataset collected from Zonguldak Ataturk State Hospital	WEKA	J48, IBk, K-star, Random Tree, REPTree and Random Forest (10-fold after PCA Feature Selection)	Hoeffding Tree: 69.10%
				REP Tree: 71.30%
Proposed Study	Dataset collected from Zonguldak Ataturk State Hospital	WEKA	J48, IBk, K-star, Random Tree, REPTree and Random Forest (10-fold after PCA Feature Selection)	Random Forest: 81.90%
				Random Tree: 73.80%
Proposed Study	Dataset collected from Zonguldak Ataturk State Hospital	WEKA	J48, IBk, K-star, Random Tree, REPTree and Random Forest (10-fold after PCA Feature Selection)	IBk: 81.60%
				J48: 86%
Proposed Study	Dataset collected from Zonguldak Ataturk State Hospital	WEKA	J48, IBk, K-star, Random Tree, REPTree and Random Forest (10-fold after PCA Feature Selection)	IBk: 86.66%
				K-star: 88.08%
Proposed Study	Dataset collected from Zonguldak Ataturk State Hospital	WEKA	J48, IBk, K-star, Random Tree, REPTree and Random Forest (10-fold after PCA Feature Selection)	Random Tree: 85.08%
				REPTree: 84.33%
Proposed Study	Dataset collected from Zonguldak Ataturk State Hospital	WEKA	J48, IBk, K-star, Random Tree, REPTree and Random Forest (10-fold after PCA Feature Selection)	Random Forest: 90.75%
				J48: 85.75%
Proposed Study	Dataset collected from Zonguldak Ataturk State Hospital	WEKA	J48, IBk, K-star, Random Tree, REPTree and Random Forest (10-fold after PCA Feature Selection)	IBk: 83.91%
				K-star: 87.91%
Proposed Study	Dataset collected from Zonguldak Ataturk State Hospital	WEKA	J48, IBk, K-star, Random Tree, REPTree and Random Forest (10-fold after PCA Feature Selection)	Random Tree: 84.83%
				REPTree: 84.16%
Proposed Study	Dataset collected from Zonguldak Ataturk State Hospital	WEKA	J48, IBk, K-star, Random Tree, REPTree and Random Forest (10-fold after PCA Feature Selection)	Random Forest: 88.83%

Author Contributions

The percentage of the author(s) contributions is presented below. All authors reviewed and approved the final version of the manuscript.

	R.U.A	Z.P.	C.K.
C	25	50	25
D	25	50	25
S	50	20	30
DCP	20	60	20
DAI	20	60	20
L	40	30	30
W	40	30	30
CR	30	30	40
SR	60		40
PM	50	25	25
FA		100	

C=Concept, D= design, S= supervision, DCP= data collection and/or processing, DAI= data analysis and/or interpretation, L= literature search, W= writing, CR= critical review, SR= submission and revision.

Conflict of Interest

The authors declared that there is no conflict of interest.

Ethical Consideration

This research is approved by Non-interventional Clinical Research Ethics Committee of Zonguldak Bulent Ecevit University (approval date: March 10, 2021, protocol code: 2021/05).

References

Acarlı K. 2020. Karaciğer sağlığını koruyan 10 hayati öneri. URL: <https://www.memorial.com.tr/saglik-rehberi/karaciger-sagligini-koruyan-10-hayati-oneri> (accessed date: August 28, 2023).

Alaybeyoğlu A, Mulayim N. 2018. Karaciğer kanseri teşhisinde destek vektör makinesi tabanlı uzman sistem tasarımı. Tıp Teknolojileri Kongresi, 8-10 Kasım, Gazi Magaso, KKTC, ss: 208-210.

Alkuşak E, Gök M. 2014. Karaciğer yetmezliğinin teşhisinde makine öğrenmesi algoritmalarının kullanımı. ISITES 2014, June 8-10, Karabük, Türkiye, pp: 703-707.

Asrani SK, Devarbhavi H, Eaton J, Kamath PS. 2019. Burden of liver diseases in the world. *J Hepatol*, 70(1): 151-171.

Azam MS, Rahman A, Iqbal SHS, Ahmed MT. 2020. Prediction of liver diseases by using few machine learning based approaches. *Aust J Eng Innov Technol*, 2(5): 85-90.

Breiman L. 2001. Random forests. *Machine Learn*, 45: 5-32.

Borulday MG, Yegin EG, Mahouti P, Gunes F. 2017. Diagnosing liver Diseases with decision tree algorithm. *Inter J Tech Phys Problems Engin*, 33: 67-70.

Bulut C, Ballı T, Yetkin EF. 2023. Filtre modeli öznetelik seçim algoritmalarının EEG tabanlı beyin bilgisayar arayüzü sistemindeki karşılaştırmalı sınıflandırma performansları. *Gazi Üniv Müh Mimar Fak Derg* 38(4): 2397-2408.

Del Campo JA, Gallego P, Grande L. 2018. Role of inflammatory response in liver diseases: Therapeutic strategies. *World J*

Hepatol, 10(1): 1.

Dritsas E, Trigka M. 2023. Supervised machine learning models for liver disease risk prediction. *Comput*, 12(1): 19.

Duda RO, Hart PE, Stork DG. 2000. *Pattern classification*. Wiley, New Jersey, USA, 2nd ed., pp: 176-181.

Gaber A, Youness HA, Hamdy A, Abdelaal HM, Hassan AM. 2022. Automatic classification of fatty liver disease based on supervised learning and genetic algorithm. *Applied Sci*, 12(1): 521.

Gulia A, Vohra R, Rani P. 2014. Liver patient classification using intelligent techniques. *Inter J Comput Sci Inform Technol* 5(4): 5110-5115.

Işık K, Ulusoy SK. 2021. Metal Sektöründe üretim sürelerine etki eden faktörlerin veri madenciliği yöntemleriyle tespit edilmesi. *Gazi Üniv Müh Mimar Fak Derg*, 36(4): 1949-1962.

Kaya C, Erkaymaz O, Ayar O, Özer M. 2017 October. Classification of diabetic retinopathy disease from Video-Oculography (VOG): signals with feature selection based on C4. 5 decision tree. *Medical Technologies National Congress (TIPTEKNO)*, 31 October-2 September, Trabzon, Türkiye, pp: 1-4.

Keleş A, Karşlı ÖB, Keleş A. 2020. Makine öğrenme algoritmaları ile karaciğer hastalığının teşhisi. *Turkish Stud Inform Technol Appl Sci*, 15(1): 75-83.

Lin RH. 2009. An intelligent model for liver disease diagnosis. *Artificial Intel Med*, 47(1): 53-62.

Ma H, Xu CF, Shen Z, Yu CH, Li YM. 2018. Application of machine learning techniques for clinical predictive modeling: a cross-sectional study on nonalcoholic fatty liver disease in China. *BioMed Res Inter*, 2018: 4304376.

Mishra S, Tadesse Y, Dash A, Jena L, Ranjan P. 2021. Thyroid disorder analysis using random forest classifier. In *Intelligent and Cloud Computing: Proceedings of ICICC 2019 Volume 2* Springer, Singapore, pp: 385-390.

Mukhyber SJ, Abdulah DA, Majeed AD. 2023. Classification of liver dataset using data mining algorithms. 1st International & 4th Local Conference for Pure Science (ICPS-2021), 26-27 May 2021, Diyala, Iraq, pp: 6.

Muthuselvan S, Rajapraksh S, Somasundaram K, Karthik K. 2018. Classification of liver patient dataset using machine learning algorithms. *Int J Eng Technol*, 7(3): 323.

Narin A, Kaya C, Pamuk Z. 2021. Automatic detection of coronavirus disease (covid-19): using x-ray images and deep convolutional neural networks. *Pattern Anal Applicat*, 24: 1207-1220.

Pahareeya J, Vohra R, Makhijani J, Patsariya S. 2014. Liver patient classification using intelligence techniques. *Inter J Adv Res Comput Sci Software Engin*, 4(2): 295-299.

Rahman AS, Shamrat FJM, Tasnim Z, Roy J, Hossain SA. 2019. A comparative study on liver disease prediction using supervised machine learning algorithms. *Inter J Sci Technol Res*, 8(11): 419-422.

Ramana BV, Babu MSP, Venkateswarlu NB. 2011. A critical study of selected classification algorithms for liver disease diagnosis. *Inter J Database Manage Syst*, 3(2): 101-114.

Schiff ER, Maddrey WC, Reddy KR. 2017. *Schiff's Diseases of the Liver*. John Wiley & Sons, London, UK, pp: 241.

Sevli O. 2019. Performance Comparison of Different Machine Learning Techniques in Diagnosis of Breast Cancer. *Eur J Sci Technol*, 16: 176-185.

Şenel FA, Saygin RR, Saygin M, Öztürk Ö. 2021. Makine Öğrenmesi Algoritmaları Kullanılarak Vücut Analizi ile Uyku Apnesi Teşhisi. *Uyku Bülteni*, 2(1): 6-10.

Ucar M, İncetaş MO. 2022. Classification of brain MRI using Efficientnet CNN model and feature selection method. *İKSAD*

- Publishing House, Ankara, Türkiye, pp: 110.
- Uzun R, İşler Y, Toksan M. 2018 May. Choose of wart treatment method using Naive Bayes and k-nearest neighbors classifiers. 26th Signal Processing and Communications Applications Conference (SIU), 02-05 May 2018, İzmir, Türkiye, pp: 1-4.
- Uzun R, İşler Y, Toksan M. 2019. WEKA yazılım paketinin siğil tedavi yöntemlerinin başarısının tahmininde kullanımı. Düzce Üniv Bilim Teknol Derg, 7(1): 699-708.
- Ünal Y, Sağlam A, Kayhan O. 2019. Improving classification performance for an imbalanced educational dataset example using SMOTE. Avrupa Bilim Teknol Derg, 2019: 485-489.
- Xie G, Wang X, Liu P, Wei R, Chen W, Rajani C, Jia W. 2016. Distinctly altered gut microbiota in the progression of liver disease. Oncotarget 7(15): 19355.
- Velu SR, Ravi V, Tabianan K. 2022. Data mining in predicting liver patients using classification model. Health Technol, 12(6): 1211-1235.
- Yapıcı Şenyar İ. 2021. Obezitenin elektroretinografi (ERG): sinyali üzerindeki etkisi. Doktora Tezi, Zonguldak Bülent Ecevit Üniversitesi, Fen Bilimleri Enstitüsü, Zonguldak, Türkiye, ss: 163.



A GAME-THEORETICAL INTEGRATED APPROACH FOR SUSTAINABLE PORTFOLIO SELECTION: AN APPLICATION ON BIST PARTICIPATION SUSTAINABILITY INDEX STOCKS

Furkan GÖKTAŞ^{1*}

¹Karabük University, Management Faculty, Department of Business Administration, 78050, Karabük, Türkiye

Abstract: Sustainable investment is a hot topic of portfolio selection. This study aims to examine sustainable portfolio selection for conservative investors using the ESG criteria. Thus, we propose a two-stage integrated approach based on two-player zero-sum games. In the first stage, we use a fuzzy multi-criteria decision making (MCDM) approach to calculate the sustainability scores of the stocks based on expert knowledge. In the second stage, we form and solve a linear optimization problem by only adding a sustainability constraint to Young's minimax portfolio selection model. We illustrate the integrated approach using the weekly simple returns of eight stocks. We also compare our results with the results of Young's minimax portfolio selection model. We find that sustainable investment does not necessarily lead to performance loss. Furthermore, it may increase performance in some cases. To the best of our knowledge, this is the first paper on sustainable portfolio selection that depends only on two-player zero-sum games, including the stage of finding sustainability scores.

Keywords: Fuzzy set, Game theory, Multi-criteria decision making, Participation index, Portfolio selection, Sustainability

*Corresponding author: Karabük University, Management Faculty, Department of Business Administration, 78050, Karabük, Türkiye

E mail: furkangoktas@karabuk.edu.tr (F. GÖKTAŞ)

Furkan GÖKTAŞ  <https://orcid.org/0000-0001-9291-3912>

Received: December 12, 2023

Accepted: April 07, 2024

Published: May 01, 2024

Cite as: Göktaş F. 2024. A game-theoretical integrated approach for sustainable portfolio selection: an application on BIST participation sustainability index stocks. *BSJ Eng Sci*, 7(3): 457-464.

1. Introduction

Sustainability is an integrated approach that includes ecological, economic, and social elements (Ok, 2022). It focuses on justice between current and future generations in the consumption of resources. It is defined as the capacity to meet today's needs without compromising the standards of future generations (Mckeown et al., 2002). Sustainable investment is "an investment discipline that considers environmental, social, and governance (ESG) criteria" (Qi and Li, 2020). Markowitz (1952) changes portfolio theory almost entirely by introducing the mean-variance (MV) portfolio selection model. On the other hand, it is not attractive for practitioners due to estimation errors (Goldfarb and Iyengar, 2003). Robust MV models based on the worst-case analysis can be used to overcome this issue (Garlappi et al., 2006; Tütüncü and Koenig, 2004). The models based on expert knowledge can also be used. We give the Bayesian approach introduced by Jorion (1986), the possibilistic MV model introduced by Carlsson et al. (2002), and the minimax model introduced by Ding (2006) as significant examples. The minimax model introduced by Young (1998) is another alternative to Markowitz's MV model. It is based on game theory and only uses historical data.

The models mentioned above are quantitative methods and ignore other criteria such as fundamental analysis,

sustainable investment, etc. On the other hand, Utz et al. (2014), Utz et al. (2015), Gasser et al. (2017), Hilario-Caballero et al. (2020), and Steuer and Utz (2023) modify Markowitz's MV model by adding a third criterion for sustainable investment. Pedersen et al. (2021) analyze the ESG - Sharpe ratio frontier. Ballester et al. (2012) use utility theory under uncertainty to integrate sustainable investment into portfolio selection. Qi and Li (2020) modify Markowitz's MV model by adding three additional constraints on the ESG criteria. There are also many approaches, such as a fuzzy multi-criteria model proposed by Calvo et al. (2016), an extended goal programming model proposed by Bilbao-Terol et al. (2018), an intuitionistic fuzzy MCDM approach proposed by Yadav et al. (2023), an intuitionistic fuzzy multi-objective optimization approach proposed by Hanine et al. (2021), and a multi-objective minimax-based portfolio optimization model proposed by Xidonas and Essner (2022).

The ESG criteria are considered as important indicators in measuring and reporting the sustainability performance of businesses (Şişman and Çankaya, 2021). Their emergence is based on socially responsible investors (Staub-Bisnang, 2012). Clearly, this study is intended for socially responsible investors, and there may be no reason for other investors to consider ESG criteria in portfolio selection. Kalayci et al. (2019) say



that Young’s minimax model is one of the most important deterministic models, which overcomes the shortcomings of Markowitz’s MV model. Thus, we determine it as a basis for this study, which focuses on sustainable investment.

We aim to examine sustainable portfolio selection for conservative investors using the ESG criteria. Our motivation is to achieve this aim with a tractable integrated approach. Thus, we first use a fuzzy MCDM approach, called as Game Theoretical Fuzzy Evaluation System (G-FES), to calculate the sustainability scores of the stocks. G-FES is related to a two-player zero-sum game (Göktaş and Gökerik, 2024). Then, we form and solve a linear optimization problem by only adding a sustainability constraint to Young’s minimax portfolio selection model. Both stages of the integrated approach are worst-case-oriented and suitable for conservative investors. To the best of our knowledge, this is the first paper on sustainable portfolio selection that depends only on two-player zero-sum games, including the stage of finding sustainability scores.

The rest of the paper is organized as follows. Section 2 gives the theories of G-FES and Young’s minimax portfolio selection model. Section 3 illustrates the integrated approach using the weekly simple returns of eight stocks included in the BIST services and BIST participation sustainability indexes. Section 4 concludes the paper.

2. Materials and Methods

2.1. G-FES

If fuzzy numbers form the decision matrix, fuzzy MCDM methods are used (Chu and Lin, 2009). The membership function of the triangular fuzzy number (c, d, e) is as in Equation 1.

$$\mu(t) = \begin{cases} 1 - \frac{d-t}{d-c}, & c \leq t < d \\ 1, & t = d \\ 1 - \frac{t-d}{e-d}, & d < t \leq e \\ 0, & \text{else} \end{cases} \quad (1)$$

The different views of multiple experts are brought together with G-FES. Linguistic variables and their crisp equivalents are shown in Table 1 (Göktaş and Gökerik, 2024).

The steps of G-FES are as follows (Göktaş and Gökerik, 2024).

Step 1: Using the linguistic variables in Table 1, expert views are taken for each alternative-criterion pair. (There are n alternatives and m criteria.)

Step 2: For the i^{th} alternative and j^{th} criterion pair, their minimum rating is assigned as c_{ij} , their median rating is assigned as d_{ij} , their maximum rating is assigned as e_{ij} , and the fuzzy utility is determined as the triangular fuzzy number (c_{ij}, d_{ij}, e_{ij}) . Then, a fuzzy decision matrix $A_{n \times m}$ is formed.

For the i^{th} alternative and j^{th} criterion pair, the utility’s fuzzy mean (m_{ij}) is as in Equation 2, where $E_F()$ is the fuzzy mean operator (Carlsson et al., 2002).

Table 1. Linguistic variables

Linguistic variables	Corresponding crisp number
Extremely good (EG)	1
Very good (VG)	0.75
Good (G)	0.5
A little good (LG)	0.25
Fair (F)	0
A little poor (LP)	-0.25
Poor (P)	-0.5
Very poor (VP)	-0.75
Extremely poor (EP)	-1

$$m_{ij} := E_F \left((c_{ij}, d_{ij}, e_{ij}) \right) = \frac{c_{ij} + 4d_{ij} + e_{ij}}{6} \quad (2)$$

For the i^{th} alternative and j^{th} criterion pair, the utility’s fuzzy standard deviation (s_{ij}) is as in Equation 3, where $STD_F()$ is the fuzzy standard deviation operator (Carlsson et al., 2002).

$$s_{ij} := STD_F \left((c_{ij}, d_{ij}, 1) \right) = \frac{1 - c_{ij}}{2\sqrt{6}} \quad (3)$$

Step 3: Fuzzy mean matrix $M_{n \times m} = (m_{ij})$ is formed using Equation 2.

Step 4: Fuzzy standard deviation matrix $S_{n \times m} = (s_{ij})$ is formed using Equation 3.

Let the decision maker’s two linear objectives maximize the utility’s fuzzy mean and minimize the utility’s fuzzy standard deviation. The payoff matrix (P) is defined as in Equation 4, where the first objective’s weight (w) is in [0,1]. If the decision maker is risk-neutral i.e. the fuzzy mean is maximized, w equals 1. If the decision maker’s risk aversion degree is at the highest level i.e. the fuzzy standard deviation is minimized, w equals 0. If it is at the medium level, w equals 0.5.

$$P := wM - (1-w)S \quad (4)$$

Step 5: Using Equation 4, the payoff matrix (P) is formed for $w \in [0,1]$.

Due to the linearity of the objectives, the weighted objective function equals $x^T P y$, where x and y are the nonnegative weight vectors of the alternatives and criteria, respectively. (The row vector x^T is the transpose of the column vector x.) Then, G-FES is defined with Expression 5, corresponding to a two-player zero-sum game with the payoff matrix $P_{n \times m} = (p_{ij})$ (Göktaş and Gökerik, 2024).

$$\max_x \min_y x^T P y \quad (5)$$

The solution of Expression 5 for the row player (decision-maker) equals the optimal solution of Expression 6, which is a linear optimization problem (Raghavan, 1994; Chen and Larbani, 2006; Sikalo et al.,

2022). Its optimal solution may not be unique, but we assume it is unique in this study.

$$\begin{aligned}
 & \max t \\
 & \text{s.t. } \sum_{i=1}^n p_{ij}x_i \geq t, \text{ for all } j \\
 & \sum_{i=1}^n x_i = 1 \\
 & x_i \geq 0, \text{ for all } i
 \end{aligned} \tag{6}$$

The dual problem of Expression 6 is as in Expression 7. Its optimal solution (y^*) equals the weight vector of the criteria. That is, G-FES objectively determines the criteria weights.

$$\begin{aligned}
 & \min t \\
 & \text{s.t. } \sum_{j=1}^m p_{ij}y_j \leq t, \text{ for all } i \\
 & \sum_{j=1}^m y_j = 1 \\
 & y_j \geq 0, \text{ for all } j
 \end{aligned} \tag{7}$$

Step 6: The alternatives' priority vector (x^*) is found by solving Expression 6. The criteria's weight vector (y^*) is found by solving Expression 7.

Step 7: According to their priority values, alternatives are ranked and/or resources are distributed to the alternatives. In this study, we use them as sustainability scores (ss_i). The stock is more preferable for socially responsible investors if its sustainability score is higher. This study uses the ESG criteria to get the sustainability scores.

2.2. Young's Minimax Portfolio Selection Model and Its Extension

Let $R_{n \times z} = (r_{ik})$ be the simple return matrix for n assets and z periods. Young's minimax portfolio selection model is in Expression 8 (Young, 1998). It gives the solution of a two-player zero-sum game for the row player (investor), where the payoff matrix is $R_{n \times z}$ and the column player is the market (Sikalo et al., 2022). Expression 8 finds the portfolio that maximizes the worst-case return based only on the historical data.

$$\begin{aligned}
 & \max t \\
 & \text{s.t. } \sum_{i=1}^n r_{ik}x_i \geq t, \text{ for all } k \\
 & \sum_{i=1}^n x_i = 1 \\
 & x_i \geq 0, \text{ for all } i
 \end{aligned} \tag{8}$$

In the integrated approach, we use Expression 9 to consider sustainability where $\alpha \in [0,1]$ is a scalar that shows the target level of the portfolio's sustainability score, and ss_i is the sustainability score of the i^{th} stock. Expression 9 finds the portfolio that maximizes the worst-case return based on the historical data and the

sustainability constraint.

$$\begin{aligned}
 & \max t \\
 & \text{s.t. } \sum_{i=1}^n r_{ik}x_i \geq t, \text{ for all } k \\
 & \sum_{i=1}^n x_i = 1 \\
 & \sum_{i=1}^n x_i ss_i \geq \alpha \\
 & x_i \geq 0, \text{ for all } i
 \end{aligned} \tag{9}$$

Remark: Since the sustainability scores depend on the decision maker's (investor's) risk aversion degree (w) due to G-FES, the optimal solution of Expression 9 also depends on it.

3. Results and Discussion

In this section, we illustrate the integrated approach using the weekly simple returns of eight stocks included in the BIST services and BIST participation sustainability indexes. The main limitations of the integrated approach can be listed as follows. The first limitation is that it may not be suitable for non-conservative investors due to the worst-case-orientation. The second limitation is that it cannot be used when short selling is allowed. The third limitation is that historical data may reflect the future poorly. The fourth limitation is that there is no formal procedure to determine the decision-maker's risk aversion degree (w) in G-FES. The fifth limitation is that G-FES can only be used with triangular fuzzy numbers. The sixth limitation is that the experts may poorly evaluate the alternatives' ESG, and the use of expert knowledge may not be practical if the stock number is high.

3.1. G-FES

In this subsection, we use G-FES to calculate the sustainability scores of the eight stocks based on expert knowledge. (Expert knowledge is used by Yadav et al. (2023) to calculate the sustainability scores. But, their intuitionistic fuzzy MCDM approach is not worst-case oriented, unlike G-FES.) These stocks are AKSEN, BIMAS, DOAS, ENJSA, MAVI, MPARK, PGSUS and THYAO. They are evaluated by five experts using publicly available information before 01.01.2023 (the start of the testing period), where the criteria are environmental issues (C1), social issues (C2), and governance issues (C3). See Refinitiv (2023) for detailed information about them.

Step 1: We take five experts' views for each alternative-criterion pair based on the linguistic variables in Table 1. Table 2 shows the first expert's views. (The experts are either the academicians or sector professionals.) For example, the linguistic ratings of AKSEN are poor (P) for C1, good (G) for C2, and extremely good (EG) for C3.

Step 2: Using the minimum, median, and maximum ratings of expert views for each alternative-criterion pair, we form the fuzzy decision matrix (A) as in Table 3. For

example, the minimum rating for the AKSEN - C3 pair is fair (F), the median rating for the AKSEN - C3 pair is a little good (LG), and the maximum rating for the AKSEN - C3 pair is extremely good (EG).

Table 2. The first expert's views

	C1	C2	C3
AKSEN	P	G	EG
BİMAS	LG	G	LG
DOAS	EG	F	LG
ENJSA	LG	P	G
MAVI	LG	F	G
MPARK	LP	F	LG
PGSUS	LP	G	F
THYAO	LG	LG	G

Table 3. The fuzzy decision matrix (A)

	C1	C2	C3
AKSEN	(-0.75, -0.5, 0)	(-0.25, 0, 0.75)	(0, 0.25, 1)
BİMAS	(0, 0.5, 0.75)	(0.25, 0.25, 0.75)	(0, 0.25, 0.75)
DOAS	(0.5, 0.75, 1)	(-0.25, 0, 0.5)	(0.25, 0.25, 0.5)
ENJSA	(0, 0.25, 0.75)	(-0.5, -0.25, 0.5)	(-0.25, 0.5, 1)
MAVI	(0.25, 0.5, 0.75)	(0, 0.25, 1)	(0, 0.5, 0.75)
MPARK	(-0.5, -0.25, 0.5)	(-0.25, 0.25, 0.5)	(0, 0.5, 0.5)
PGSUS	(-0.25, 0.25, 0.5)	(0, 0.5, 0.75)	(0, 0.25, 0.75)
THYAO	(-0.25, 0, 0.5)	(0, 0.25, 0.75)	(0, 0.25, 0.5)

Step 3: We form the fuzzy mean matrix (M) by using Equation 2. Here, $m_{13} = (0+4 \times 0.25+1)/6$.

Table 4. The fuzzy mean matrix (M)

	C1	C2	C3
AKSEN	-0.4583	0.0833	0.3333
BİMAS	0.4583	0.3333	0.2917
DOAS	0.7500	0.0417	0.2917
ENJSA	0.2917	-0.1667	0.4583
MAVI	0.5000	0.3333	0.4583
MPARK	-0.1667	0.2083	0.4167
PGSUS	0.2083	0.4583	0.2917
THYAO	0.0417	0.2917	0.2500

Step 4: We form the fuzzy standard deviation matrix (S) by using Equation 3. Here, $s_{13} = (1-0)/2\sqrt{6}$.

Table 5. The fuzzy standard deviation matrix (S)

	C1	C2	C3
AKSEN	0.3572	0.2552	0.2041
BİMAS	0.2041	0.1531	0.2041
DOAS	0.1021	0.2552	0.1531
ENJSA	0.2041	0.3062	0.2552
MAVI	0.1531	0.2041	0.2041
MPARK	0.3062	0.2552	0.2041
PGSUS	0.2552	0.2041	0.2041
THYAO	0.2552	0.2041	0.2041

Step 5: Using Equation 4, we form the payoff matrix (P) as follows. $P = M$ when $w = 1$, $P = -S$ when $w = 0$, $P = (M-$

$S)/2$ when $w = 0.5$. Clearly, w equals the weight of maximization of fuzzy mean, whereas $1-w$ equals the weight of minimization of fuzzy standard deviation.

Step 6: By solving Expression 6 for different payoff matrices, we uniquely find the priority vectors (x^*) as in Table 6. When $w = 1$, the fuzzy mean (the first moment of the fuzzy utility) is maximized. That is, the focus is to maximize the central tendency. When $w = 0$, the fuzzy standard deviation (the square root of the second moment of the fuzzy utility) is minimized. That is, the focus is to minimize the risk. When $w = 0.5$, there is a balance of these objectives.

Table 6. The priority vectors

	w = 1	w = 0.5	w = 0
AKSEN	0	0	0
BİMAS	0	0.0190	0.6667
DOAS	0	0	0.3333
ENJSA	0	0	0
MAVI	0.6000	0.5666	0
MPARK	0	0	0
PGSUS	0.4000	0.4144	0
THYAO	0	0	0

By solving Expression 7 for different payoff matrices, we uniquely find the criteria's weight vectors (y^*) as in Table 7. y^* leads to the minimum payoff for x^* .

Table 7. The weight vectors of the criteria

	w = 1	w = 0.5	w = 0
C1	0.3000	0.1736	0
C2	0.7000	0.7066	0.3333
C3	0	0.1198	0.6667

Step 7: When the decision maker is risk neutral ($w = 1$), the sustainability scores of MAVI and PGSUS are 0.6000 and 0.4000, respectively. Other scores equal 0. When the decision maker's risk aversion degree is at a medium level ($w = 0.5$), the sustainability scores of MAVI, PGSUS, and BİMAS are 0.5666, 0.4144, and 0.0190, respectively. Other scores equal 0. When the decision maker's risk aversion degree is at the highest level ($w = 0$), the sustainability scores of BİMAS and DOAS are 0.6667 and 0.3333, respectively. Other scores equal 0.

3.2. Young's Minimax Portfolio Selection Model and Its Extension

Table 8 shows the summary statistics for the weekly simple returns of the eight stocks in the training period (2022). We use this data set and the information provided by Section 3.1 in step 7 to derive optimal portfolios. We take the first three quarters of 2023 as the testing period.

Table 9 shows the results when $w = 1$. The weight of MAVI (AKSEN) increases (decreases) with the increase in the target sustainability level (α) of Expression 9. Young's (1998) optimal portfolio has a sustainability score of 0.0358 in this case. When α increases, the relative weight

of the ESG criteria increases with respect to the weight of the absolute value of worst-case return.

Table 10 shows the results when $w = 0.5$. The results are similar to the results in Table 9. The optimal portfolios consist of only MAVI and AKSEN when α equals or

exceeds 0.2. MAVI has the maximum sustainability score when $w = 0.5$ or $w = 1$. 71.41% of Young's (1998) optimal portfolio consists of AKSEN. This portfolio has a sustainability score of 0.0374 in this case.

Table 8. The summary statistics

	Minimum	Maximum	Median	Mean	Standard Dev.
AKSEN	-0.0610	0.2595	0.0170	0.0321	0.0635
BIMAS	-0.0754	0.1860	0.0122	0.0170	0.0550
DOAS	-0.1058	0.2099	0.0239	0.0316	0.0705
ENJSA	-0.1064	0.1419	0.0179	0.0215	0.0562
MAVI	-0.1024	0.1810	0.0105	0.0277	0.0600
MPARK	-0.0947	0.1802	0.0179	0.0230	0.0559
PGSUS	-0.1164	0.1957	0.0419	0.0365	0.0747
THYAO	-0.0733	0.2458	0.0317	0.0402	0.0653

Table 9. The optimal portfolios for risk-neutral investors

	Young (1998)	$\alpha = 0.1$	$\alpha = 0.2$	$\alpha = 0.3$	$\alpha = 0.4$	$\alpha = 0.5$	$\alpha = 0.6$
AKSEN	0.7141	0.7173	0.6667	0.5000	0.3333	0.1667	0
BIMAS	0.0156	0	0	0	0	0	0
DOAS	0	0	0	0	0	0	0
ENJSA	0.0446	0	0	0	0	0	0
MAVI	0	0.1571	0.3333	0.5000	0.6667	0.8333	1.0000
MPARK	0.1362	0.1112	0	0	0	0	0
PGSUS	0.0895	0.0144	0	0	0	0	0
THYAO	0	0	0	0	0	0	0

Table 10. The optimal portfolios when the risk aversion degree is at a medium level

	Young (1998)	$\alpha = 0.1$	$\alpha = 0.2$	$\alpha = 0.3$	$\alpha = 0.4$	$\alpha = 0.5$	$\alpha = 0.6$
AKSEN	0.7141	0.7168	0.6470	0.4705	0.2941	0.1176	
BIMAS	0.0156	0	0	0	0	0	
DOAS	0	0	0	0	0	0	
ENJSA	0.0446	0	0	0	0	0	No feasible solution
MAVI	0	0.1737	0.3530	0.5295	0.7059	0.8824	solution
MPARK	0.1362	0.1057	0	0	0	0	
PGSUS	0.0895	0.0038	0	0	0	0	
THYAO	0	0	0	0	0	0	

Table 11. The optimal portfolios when the risk aversion degree is at the highest level

	Young (1998)	$\alpha = 0.1$	$\alpha = 0.2$	$\alpha = 0.3$	$\alpha = 0.4$	$\alpha = 0.5$	$\alpha = 0.6$
AKSEN	0.7141	0.6448	0.5339	0.3920	0.2419	0.0898	0
BIMAS	0.0156	0.1096	0.2369	0.3847	0.5380	0.6928	0.8742
DOAS	0	0.0808	0.1262	0.1305	0.1239	0.1145	0.0517
ENJSA	0.0446	0	0	0	0	0	0
MAVI	0	0.0176	0.0233	0.0146	0.0020	0	0
MPARK	0.1362	0.0720	0.0125	0	0	0	0
PGSUS	0.0895	0.0752	0.0672	0.0781	0.0941	0.1030	0.0742
THYAO	0	0	0	0	0	0	0

Table 11 shows the results when $w = 0$. The weight of BIMAS (AKSEN) increases (decreases) with the increase in α . Young's (1998) optimal portfolio has a sustainability score of 0.0104 in this case. BIMAS has the maximum sustainability score when $w = 0$. In this case, we derive more diversified optimal portfolios due to fuzzy standard

deviation orientation.

Table 12 shows the results for training and testing periods respectively, when $w = 1$. WCR is the worst-case return, and AR is the average return. Young's portfolio selection model in Expression 8 and its extension in Expression 9 minimize the risk (the absolute value of

WCR) for the training period. AR is the natural return measure. If portfolio A has lower risk and higher return than portfolio B, then we say that A is superior to B, or equivalently B is inferior to A. Table 12 also shows the inferior or superior portfolios to Young's (1998) optimal portfolio when $w = 1$. This portfolio is generally superior to others in the training period. On the other hand, this information is not valid for the testing period.

Table 13 shows the inferior or superior portfolios to

Young's (1998) optimal portfolio when $w = 0.5$. This portfolio is generally superior to others in the training period. On the other hand, this information is not valid for the testing period.

Table 14 shows the inferior or superior portfolios to Young's (1998) optimal portfolio when $w = 0$. This portfolio is generally superior to others in the training period. The opposite is true for the testing period.

Table 12. The risk-return analysis for the risk-neutral investors

	Young (1998)	$\alpha = 0.1$	$\alpha = 0.2$	$\alpha = 0.3$	$\alpha = 0.4$	$\alpha = 0.5$	$\alpha = 0.6$
Tra-WCR	-0.0262	-0.0307	-0.0419	-0.0570	-0.0722	-0.0873	-0.1024
Tra-AR	0.0305	0.0304	0.0306	0.0299	0.0291	0.0284	0.0277
Training P.	N/A	Inferior	N/A	Inferior	Inferior	Inferior	Inferior
Test-WCR	-0.1117	-0.1156	-0.1214	-0.1242	-0.1279	-0.1316	-0.1353
Test-AR	0.0034	0.0035	0.0046	0.0074	0.0103	0.0131	0.0159
Testing P.	N/A	N/A	N/A	N/A	N/A	N/A	N/A

Table 13. The risk-return analysis when the risk aversion degree is at a medium level

	Young (1998)	$\alpha = 0.1$	$\alpha = 0.2$	$\alpha = 0.3$	$\alpha = 0.4$	$\alpha = 0.5$	$\alpha = 0.6$
Tra-WCR	-0.0262	-0.0312	-0.0437	-0.0597	-0.0757	-0.0917	
Tra-AR	0.0305	0.0304	0.0305	0.0297	0.0290	0.0282	
Training P.	N/A	Inferior	Inferior	Inferior	Inferior	Inferior	No feasible solution
Test-WCR	-0.1117	-0.1160	-0.1209	-0.1249	-0.1288	-0.1327	
Test-AR	0.0034	0.0035	0.0049	0.0079	0.0109	0.0139	
Testing P.	N/A	N/A	N/A	N/A	N/A	N/A	

Table 14. The risk-return analysis when the risk aversion degree is at the highest level

	Young (1998)	$\alpha = 0.1$	$\alpha = 0.2$	$\alpha = 0.3$	$\alpha = 0.4$	$\alpha = 0.5$	$\alpha = 0.6$
Tra-WCR	-0.0262	-0.0282	-0.0315	-0.0349	-0.0384	-0.0421	-0.0544
Tra-AR	0.0305	0.0300	0.0285	0.0265	0.0243	0.0220	0.0192
Training P.	N/A	Inferior	Inferior	Inferior	Inferior	Inferior	Inferior
Test-WCR	-0.1117	-0.1057	-0.0985	-0.0901	-0.1041	-0.1372	-0.1758
Test-AR	0.0034	0.0049	0.0073	0.0104	0.0138	0.0172	0.0199
Testing P.	N/A	Superior	Superior	Superior	Superior	N/A	N/A

Since the integrated approach adds a sustainability constraint to Young's minimax portfolio selection model, we expect an inevitable increase in the risk (the absolute value of WCR) and a potential decrease in the return (AR) for the training period due to the nature of the optimization. On the other hand, this expectation is not valid for the future (testing period). That is, sustainable investment does not necessarily lead to performance loss. It is compatible with the results given by Hilario-Caballero et al. (2020), Utz et al. (2014), Utz et al. (2015), and Qi and Li (2020). Furthermore, it may increase performance in some cases, as in this study. It is compatible with the results given by Pedersen et al. (2021) and Xidonas and Essner (2022). On the other hand, Ballesteros et al. (2012) find that sustainable investment increases the risk, whereas Gasser et al. (2017) find that it decreases the return. The models in the studies mentioned above are not intended for conservative investors except for the model proposed by Xidonas and Essner (2022). This information may

increase the relative importance of the integrated approach intended for conservative investors.

4. Conclusion

Game theory is a widely used decision-making tool. Since two-player zero-sum games depend on minimax optimization problems, it is convenient for conservative decision-makers. Sustainability is a nonnegligible concept for socially responsible investors. ESG criteria are accepted as important indicators of sustainability. Thus, this study proposes an integrated approach using ESG criteria and two-player zero-sum games for conservative investors' sustainable portfolio selection. We also illustrate the integrated approach with a real-world example. Our findings show that sustainable investment does not necessarily lead to performance loss than conventional investment. Furthermore, it may result in increased performance in some cases. These results are compatible with the many studies in the literature.

Socially responsible investors can prefer the integrated approach to Young's minimax model, which is one of the key models in deterministic portfolio selection. This is because the integrated approach's second stage is formed by only adding a sustainability constraint to Young's minimax portfolio selection model. The fundamental analysis could be combined into the integrated approach in future research.

Author Contributions

The percentage of the author(s) contributions is presented below. The author reviewed and approved the final version of the manuscript.

	F.G.
C	100
D	100
S	100
DCP	100
DAI	100
L	100
W	100
CR	100
SR	100
PM	100
FA	100

C=Concept, D= design, S= supervision, DCP= data collection and/or processing, DAI= data analysis and/or interpretation, L= literature search, W= writing, CR= critical review, SR= submission and revision, PM= project management, FA= funding acquisition.

Conflict of Interest

The author declared that there is no conflict of interest.

Ethical Consideration

Ethics committee approval was not required for this study because of there was no study on animals or humans.

References

Ballestero E, Bravo M, Pérez-Gladish B, Arenas-Parra M, Pla-Santamaria D. 2012. Socially responsible investment: A multicriteria approach to portfolio selection combining ethical and financial objectives. *Eur J Oper Res*, 216(2): 487-494.

Bilbao-Terol A, Arenas-Parra M, Cañal-Fernández V, Obam-Eyang PN. 2018. Multi-criteria analysis of the GRI sustainability reports: an application to socially responsible investment. *J Oper Res Soc*, 69(10): 1576-1598.

Calvo C, Ivorra C, Liern V. 2016. Fuzzy portfolio selection with non-financial goals: exploring the efficient frontier. *Annals Operat Res*, 245(1-2): 31-46.

Carlsson C, Fullér R, Majlender P. 2002. A possibilistic approach to selecting portfolios with highest utility score. *Fuzzy Sets Syst*, 131(1): 13-21.

Chen YW, Larbani M. 2006. Two-person zero-sum game approach for fuzzy multiple attribute decision making problems. *Fuzzy Sets Syst*, 157(1): 34-51.

Chu TC, Lin Y. 2009. An extension to fuzzy MCDM. *Comput Math with Appl*, 57(3): 445-454.

Ding Y. 2006. Portfolio selection under maximum minimum criterion. *Qual Quant*, 40(3): 457-468.

Garlappi L, Uppal R, Wang T. 2006. Portfolio selection with parameter and model uncertainty: A multi-prior approach. *Rev Financ Stud*, 20(1): 41-81.

Gasser SM, Rammerstorfer M, Weinmayer K. 2017. Markowitz revisited: social portfolio engineering. *Eur J Oper Res*, 258(3): 1181-1190.

Göktaş F, Gökerik M. 2024. Sosyal medya reklam platformu seçimi üzerine yeni bir oyun - teorik yaklaşım. *J Turkish Operat Manage*, in-press.

Goldfarb D, Iyengar G. 2003. Robust portfolio selection problems. *Math Operat Res*, 28(1): 1-38.

Hanine Y, Lamrani Alaoui Y, Tkiouat M, Lahrichi Y. 2021. Socially responsible portfolio selection: an interactive intuitionistic fuzzy approach. *Mathematics*, 9(23): 3023.

Hilario-Caballero A, Garcia-Bernabeu A, Salcedo JV, Vercher M. 2020. Tri-criterion model for constructing low-carbon mutual fund portfolios: A preference-based multi-objective genetic algorithm approach. *Int J Environ Res Public Health*, 17(17): 6324.

Jorion P. 1986. Bayes-Stein estimation for portfolio analysis. *J Financial Quant Anal*, 21(3): 279-292.

Kalayci CB, Ertenlice O, Akbay MA. 2019. A comprehensive review of deterministic models and applications for mean-variance portfolio optimization. *Expert Syst Appl*, 125: 345-368.

Markowitz H. 1952. Portfolio selection. *J Finance*, 7(1): 77-91.

McKeown R, Hopkins C, Rizzi R, Chrystalbride M. 2002. Education for sustainable development toolkit. Knoxville: Energy, Environment and Resources Center, University of Tennessee, Knoxville, US, pp: 1-142.

Ok Ş. 2022. Activity based costing and budgeting based on carbon accounting: Application in a manufacturing business. PhD Thesis, Karabük University, Graduate Education Institute, Karabük, Türkiye, pp: 294.

Pedersen LH, Fitzgibbons S, Pomorski L. 2021. Responsible investing: the ESG-efficient frontier. *J Financ Econ*, 142(2): 572-597.

Qi Y, Li X. 2020. On imposing ESG constraints of portfolio selection for sustainable investment and comparing the efficient frontiers in the weight space. *Sage Open*, 10(4): 2158244020975070.

Raghavan TES. 1994. Zero-sum two-person games. *Handbook Game Theory Econ Appl*, 2: 735-768.

Refinitiv 2023. Environmental, Social and Governance (ESG) scores from LSEG. URL: https://www.lseg.com/content/dam/data-analytics/en_us/documents/methodology/lseg-esg-scores-methodology.pdf (accessed date: Jan 15, 2024).

Sikalo M, Arnaut-Berilo A, Zaimovic A. 2022. Efficient asset allocation: Application of game theory-based model for superior performance. *Int J Finan Stud*, 10(1): 20.

Şişman ME, Çankaya S. 2021. The effect of environmental, social and corporate governance (ESG) data on the financial performance of firms: A study on the airline industry. *Çukurova Üniv İİBF Derg*, 25(1): 73-91.

Staub-Bisnang M. 2012. Sustainable investing for institutional investors - risks, regulations and strategies. John Wiley & Sons, New York, US, pp: 256.

Steuer RE, Utz S. 2023. Non-contour efficient fronts for identifying most preferred portfolios in sustainability investing. *Eur J Oper Res*, 306(2): 742-753.

Tütüncü RH, Koenig M. 2004. Robust asset allocation. *Annals Operat Res*, 132: 157-187.

- Utz S, Wimmer M, Hirschberger M, Steuer RE. 2014. Tri-criterion inverse portfolio optimization with application to socially responsible mutual funds. *Eur J Oper Res*, 234(2): 491-498.
- Utz S, Wimmer M, Steuer RE. 2015. Tri-criterion modeling for constructing more-sustainable mutual funds. *Eur J Oper Res*, 246(1): 331-338
- Xidonas P, Essner E. 2022. On ESG portfolio construction: A multi-objective optimization approach. *Comput Econ*, 2022: 1-25.
- Yadav S, Kumar A, Mehlawat MK, Gupta P, Charles V. 2023. A multi-objective sustainable financial portfolio selection approach under an intuitionistic fuzzy framework. *Inf Sci*, 646: 119379.
- Young MR. 1998. A minimax portfolio selection rule with linear programming solution. *Manage Sci*, 44(5): 673-683.



MODELING CLIMATE CHANGE SCENARIOS FOR SPRING BARLEY IN SOUTHEAST OF ALMATY IN KAZAKHSTAN USING THE LINTUL APPROACH

Aidana SABITOVA¹, Gulnur SULEIMANOVA¹, Tefide KIZILDENİZ^{2*}, Ali Kaan YETİK²

¹Kazakh National Agrarian Research University, Faculty of Agrobiology, Department of Horticulture, Plant Protection and Quarantine, 050000, Almaty, Kazakhstan


²Niğde Ömer Halisdemir University, Faculty of Agricultural Sciences and Technologies, Biosystem Engineering Department, 51240 Niğde, Türkiye


Abstract: Barley stands as a cornerstone in agricultural landscape of Kazakhstan, weaving through diverse climate zones, and annually grazing over 1.5 million hectares. The intricate interplay between climate and food systems necessitates thorough analysis and strategic measures to food safety and nutritional security, as the evolving climate significantly influences both the quantity and quality of our food resources. This study aims to employ the LINTUL-MULTICROP Model to assess how spring barley adapts to both today's climatic conditions and potential climate change scenarios to elevated levels of carbon dioxide and temperature under the specific conditions of southeast of Almaty. Three different global climate change models were studied (GCMs); i) GFDL-ESM2M, ii) HadGEM2-AO, and iii) MPI-ESM-MR for historical period (1986-2005) under RCP 4.5 and RCP 8.5 during the periods of i) 2040-2059 years scenarios, ii) 2060-2079 years scenarios, and iii) 2080-2099 years scenarios. Overall, the HADGEMAO and MPIESMMR models exhibited promising results in simulating yield, projecting an increase in spring barley yield for both RCP4.5 and RCP8.5 scenarios in GFDL-ESM2M model case also demonstrated stable increase in rainfed conditions. In conclusion, it should be noted that in the conditions of Kazakhstan, the cultivation of spring barley tends to change to growth in the southeast of Almaty.


Keywords: Climate change, LINTUL, Spring barley, Yield, Crop modeling


*Corresponding author: Niğde Ömer Halisdemir University, Faculty of Agricultural Sciences and Technologies, Biosystem Engineering Department, 51240 Niğde, Türkiye

E mail: tkizildeniz@ohu.edu.tr (T. KIZILDENİZ)

Aidana SABITOVA  <https://orcid.org/0009-0000-6068-7666>

Gulnur SULEIMANOVA  <https://orcid.org/0000-0002-2322-6155>

Tefide KIZILDENİZ  <https://orcid.org/0000-0002-5627-1307>

Ali Kaan YETİK  <http://orcid.org/0000-0003-1372-8407>

Received: March 05, 2024

Accepted: April 16, 2024

Published: May 15, 2024

Cite as: Sabitova A, Suleimanova G, Kizildeniz T, Yetik AK. 2024. Modeling climate change scenarios for spring barley in Southeast of Almaty in Kazakhstan using the LINTUL approach. *BSJ Eng Sci*, 7(3): 465-472.

1. Introduction

Climate change, a consequence of human activities, unfolds the profound transformation of our planet's climatic dynamics (Gergis, 2023). The existence of radioactively active substances in the atmosphere of the Earth increases the global average outer layer temperature by 30 °C, creating our world livable for life. From the time of the Industrial Revolution, man-made activities have led to a rise in carbon dioxide and other trace gases, ended up in approximately 2 W m⁻² of radiative heating in the troposphere and surface. This warmth is anticipated to be compounded by altering in snow, clouds, water vapor, and sea ice (Gergis, 2023). The elevated concentrations of atmospheric carbon dioxide (CO₂) contribute significantly to the greenhouse gas effect, exerting profound consequences on the Earth's climate and ecosystems. As a major greenhouse gas, increased CO₂ concentrations lead to enhanced heat retention within the atmosphere, contributing to global warming including fluctuations in temperature, alterations in precipitation patterns, and the melting of

glaciers (Van der Werf and Petit, 2002). With temperatures already on the ascent by approximately 1°C, our world is witnessing the repercussions – heightened heat waves, unpredictable floods, and prolonged droughts that pose significant challenges to our collective well-being (Reddy and Reddy, 2015; McMichael, 2017). In this intricate interplay between humanity and the environment, agriculture assumes a pivotal role, grappling with an array of challenges that strain global food security (Van der Werf and Petit, 2002; Gregory et al., 2005).

As per the 2022 IPCC Sixth Assessment Report, there is a strong consensus indicating that climate change, as it stands, has predominantly resulted in adverse effects on both crop yields and crop quality in agriculture. The impact of heightened CO₂ levels extends to terrestrial ecosystems, influencing plant physiology and altering photosynthetic processes (Fleming et al., 2018). While some plants may benefit from increased CO₂ in the short term through enhanced growth (Kizildeniz, 2024; Kizildeniz et al., 2021) and water-use efficiency, the



overall ecological balance is at risk due to potential disruptions in nutrient cycling, changes in species composition, and increased susceptibility to pests and diseases (Kizildeniz et al., 2021). Climate change exerts a multifaceted and severe impact on various crops, with barley being no exception. The influence of weather change impact on barley growth manifests in diverse developmental stages, introducing complexities and challenges for agricultural systems, with differences in temperature impacting tiller number, plant height, and dry aboveground plant parts (Gray and Brady, 2016). Barley plants respond to elevated temperatures by promoting elongation growth and accelerating inflorescence development, which can impact canopy architecture and grain production (Zhu et al., 2021). Elevated temperatures resulting from climate change affect the expansion and development process of barley leads to alterations in morphological and developmental traits (Raza et al., 2019).

Kimball et al. (2002) and Long et al. (2005) were revealed that rising carbon dioxide has been shown to directly alter plant photosynthesis and, as a result, the development of plants. Climate change affects seasonal precipitation patterns and raises mean temperatures, causing a detrimental impact on agricultural output (Meehl et al., 2007). Barley is the 4th foremost crop with regard to worldwide productivity (Giraldo et al., 2019). Photosynthesis of individual barley leaf enhanced with rising CO₂ (Ford and Thorne, 1967; Pettersson et al., 1993), however in various investigations, the processes of photosynthesis was solely intermittently enhanced (Hibberd et al., 1996; Sicher and Bunce, 1997). Barley leaves development responded differently to CO₂ advancement, with an advantageous result (Ford and Thorne, 1967) and a lack of reaction (Bunce, 2004), whereas stem height increased with CO₂ rise (Weigel et al., 1994; Saebo and Mortensen, 1996). Two investigations demonstrated an enhancement in harvest index with CO₂ rise (Pettersson et al., 1993). Nevertheless, in numerous additional studies, an absence or reduction was seen (Weigel et al., 1994). Drought and high temperatures throughout seed formation can diminish productivity and quantity while also affecting seed quality features including dormancy and robustness (Sehgal et al., 2018). Overall, climate change poses challenges to barley crops, but understanding these impacts can inform breeding efforts to develop climate-resilient varieties (Zenda et al., 2021).

Crop models, ranging from empirical to optimizing types, are essential for understanding intricate interactions among atmosphere, crops, and soil. These models, based on physiological knowledge, efficiently simulate various scenarios, aiding agriculture in pest management, breeding, and climate change impact assessment (Boote et al., 2013; Oteng-Darko et al., 2013; Craufurd et al., 2013; Reynolds et al., 2018; Aşık et al., 2021; Akhavadegan et al., 2021; Wajid et al., 2021). Crop models which have been applied in barley include deep

neural network (DNN) and machine learning (ML) regression approaches (Jeong et al., 2022). Models for two- and multi-row spring barley cultivars have been developed, considering factors such as yield structure, plant density, and root characteristics (Newton et al., 2012). However, there are already applied crop models for barley, but they are either tailored for specific environmental conditions or focused on yield components. More to the point, these existing models may not be suitable for application when crop production and quality attributes vary due to unique processes that are not mandated in the model (Tao et al., 2018).

In addition to assessing the adaptability of product to the current climatic conditions, there is a curiosity about its potential yield in the event of climatic changes in the upcoming years. As a result, climate change consequences on altering planting periods and accessibility to water, which may lead to yield decreases, should be examined in order to provide policymakers with credible data in relevant locations. Leveraging the capabilities of the LINTUL model enables the simulation of barley production, allowing for the optimization of land use, streamlining technological operations, and judiciously allocating mineral fertilizers to enhance both yield and profitability. Therefore, beyond evaluating the adaptability of the product to existing climatic conditions, it becomes imperative to ascertain potential yields in the event of climate variations in the upcoming years. Therefore, it is crucial to investigate how climate change may impact shifts in planting seasons and affect water availability, potentially resulting in decreased yields. This research aims to provide policymakers with reliable data in relevant areas. In this research, the LINTUL-MULTICROP Model was employed to scrutinize the habituation of barley to prevailing climatic conditions and anticipated climate change scenarios, elucidating its response to elevated carbon dioxide levels and increased temperatures.

2. Materials and Methods

2.1. Model Explanation

Linus Franke of the University of Bloemfontein adapted the earliest versions of the LINTUL-MULTICROP Model, which had been developed in Fortran, into Microsoft Excel (Franke et al., 2013). Franke et al. (2013) and Haverkort et al. (2013) conducted the initial research study employing this approach. The model demands three major data sets as input: climate, crop and soil data. Spitters (1989) and Spitters and Schapendonk (1990) established a mechanistic model known as LINTUL (Light Interception and Utilization) that calculates dry matter buildup employing solar radiation absorption and radiation addition efficiency ratios. LINTUL is an important tool to evaluate the difference between current and projected crop yield. In addition, by entering precise meteorological factors, the model may compute the amount of grain that could be generated in a particular setting compared to agricultural productivity

under existing ecological conditions (Farré et al., 2000). Farré et al. (2000) examined and validated LINTUL for the forecasting of timing of flowering, leaf area index, and production, and agreed that the model correctly estimated outcomes for all maize characteristics.

LINTUL might be utilized for investigating the effects of various irrigation systems on productivity in diverse regions for crop sustainability. The model is also valuable for researchers in identifying carbon dioxide fixation during photosynthesis (Yetik et al., 2023). LINTUL may evaluate light absorption and utilization rates throughout photosynthetic. It may develop the accumulation of dry mass in the presence of appropriate nutrients and moisture, pest, disease, and without weeds environments, and current weather circumstances (Spitters and Schapendonk, 1990). Dry mass is mostly the result of light interception (Shibu et al., 2010). The versatile LINTUL model not only aids in assessing soil water mechanism like drainage, evapotranspiration, and runoff, but also facilitates the adaptation of cropping patterns and management practices based on the anticipated availability of soil water, generating a diverse set of outputs through its simulation equations (Ahmed et al., 2013). Furthermore, the model's versatility extends to its seamless integration with remote sensing images, facilitating the monitoring of spatiotemporal barley growth patterns and yield dynamics (Gimplinger and Kaul, 2012).

The first of these inputs is climatic data including precipitation (mm), averages of temperature minimum

and maximum (°C), solar radiation ($\text{MJ m}^{-2} \text{ day}^{-1}$) and monthly evapotranspiration values (mm). The additional input agricultural dataset contains the dates of radiation use efficiency (RUE, g MJ^{-1}), sowing and harvest (day), planting, and effective rooting depth (cm), sprout growth rate (Extension of the below ground sprout per day-degree, $\text{mm degree day}^{-1}$), harvest index (%), dry matter concentration (%), effective temperature sum between emergence and 100% ground cover (GC) (0-100% GC, degree day), Lowest and highest temperatures for the photosynthetic as well as optimal photosynthetic (°C). Ultimately, the model provides a default selection for nine distinct kinds of soil with various water capacity, bulk densities, accessible water contents, and wilting points, that the user can simply choose. The LINTUL-MULTICROP Model produces various results. The model might provide climate change adaptation strategies by determining the days between planting and emergence, the duration of growth time (days), the days between 100% GC and harvest and the days between emergence and 100% GC. The model may determine the need for irrigation water using precipitation and ETP data. In addition to that, the model can forecast yield in both irrigated and non-irrigated conditions.

2.2. Study Site

The research was performed in 2023. Field trials were undertaken on the experimental land of for the KazNIIZiR LLP 43°13'10"N 76°41'06"E 803m in southeast of Almaty, located in Kazakhstan (Figure 1).



Figure1. The location of study area

Soil cover of the experimental is represented by irrigated light chestnut soils with deep groundwater (more than 10 meters), characteristic of the foothill plain of the Trans-Ili Alatau. According to the classification principles reported by Dokuchaev (1899), the soil of the stationary site belongs to the light brown subtype. Light-brown and dark chestnut soils of upland agricultural landscapes, developed on loess-like loams of medium loamy mechanical composition, are situated on the foothill-inclined plain of the northern slope of the Trans-Ili Alatau. Generally, the relief of this territory is distinguished by a fairly significant degree of horizontal dissection by a network of branched logs with gentle and sloping slopes used in irrigated agriculture. In general, it

is a moderately arid zone with a pronounced continental climate, with large daily fluctuations in air temperatures and annual precipitation.

The soil is marked by relatively low humus content (2.20-2.45%), due to high carbonation, the response of the soil mixture is almost alkaline 7.5-7.8. The uptake capacity does not exceed 15.5 mg /eq., the main part of the absorbed bases is calcium, the amount of absorbed magnesium is not extremely high. Total nitrogen contains 0.20%, total phosphorus - 0.25%. According to the degree of supply of batteries, the experimental site is characterized as poorly provided with phosphorus and high potassium. Weather conditions of the southeast of Almaty and the mean climate data from 2000 to 2023

and the monthly crop evapotranspiration data (ETP) were calculated as Yagiz et al. (2020) are given in Table 1.

2.3. Plant Material

Barley (*Hordeum vulgare* L. spp vulgare) is vital crop in Kazakhstan’s agriculture, and it grows various climatic areas covering more than 1.5 million hectares every year. At the moment, it is the nation's 2nd most extensively produced grain crop following wheat, yielding a mean of 2.0 million tons each year (Genievskaya et al., 2018). The ultimate outcome of barley in the nation is feed for livestock in Kazakhstan, with a mean output of 1.5 tons per hectare (Genievskaya et al., 2018). Because of the

nation's long, harsh winters and frequently dry summers of Kazakhstan, two-row spring barley is the dominating variety in all major barley growing locations. Summer is a particularly challenging season in two out of three years, with drought and heat resulting in an enormous decline in grain production (Genievskaya et al., 2018).

Spring barely, which is well suited to the ecological environmental circumstances in the area and barley is a strategically important crop for Kazakhstan, was used as plant material. The input crop data of LINTUL-MULTICROP model achieved from various sources was examined and given in Table 2.

Table 1. The long-term annual climate data of Southeast of Almaty from 2000 to 2023

Months	AT min (°C)	AT max (°C)	AT mean (°C)	AP (mm)	R (MJ m ⁻² day ⁻¹)	ETP (mm)
January	-8.20	0.78	-4.57	34.67	5.72	28.6
February	-5.60	3.18	-1.96	42.87	8.67	43.4
March	1.29	12.01	6.15	76.91	12.24	61.2
April	7.69	19.24	13.18	102.73	16.41	82.1
May	12.71	24.68	18.59	95.86	19.29	96.5
June	17.59	29.71	23.60	57.07	21.56	107.1
July	19.96	32.33	26.04	36.92	21.27	106.4
August	18.54	31.30	24.71	33.45	20.05	100.3
September	13.12	25.94	19.27	29.00	16.27	81.4
October	5.82	17.52	11.10	56.91	10.94	54.7
November	-0.74	8.04	2.93	59.19	6.98	34.9
December	-5.92	1.76	-2.85	39.05	4.86	24.3
Average	6.36	17.21	11.35	55.38	13.68	68.4

AT min= average temperature minimum, AT max= average temperature maximum, AT mean= average temperature mean, AP= average precipitation R= radiation ETP= evapotranspiration data.

Table 2. Input parameters of LINTUL Model obtained from the field experiment

Parameters	Values	
Sowing date (days)	14/04	
Planting depth (cm)	5	
Harvest date (days)	5/08	
Effective rooting depth (cm)	7	
Dry matter concentration* (%)	40	
Harvest index (%)	25	
Sprout growth rate (mm degree day ⁻¹)	1.4	
0-100% GC (degree day)	736	
RUE** (g MJ ⁻¹)	1.48	
Temperature for the photosynthesis (°C)	Minimum	5
	Maximum	35
Temperature for the optimum photosynthesis (°C)	Minimum	15
	Maximum	25

*Dry matter concentration (%) of barley data was referred as Stacey et al. (2006). **RUE (g MJ⁻¹) of barley data was referred as Goyné et al. (1993).

2.4. Climate Change Scenarios

In the study, yield calculations for three distinct future periods, namely 2040-2059 (F1), 2060-2079 (F2), and 2080-2099 (F3), were conducted to assess the impacts of climatic variations, excluding the reference period (RF) covering the years 1986-2005. The computed yield values were obtained using climate data from three

different models. In the process of model selection, three widely utilized models in academic literature were chosen: HADGEM-AO, GFDL-ESM2M, and MPI-ESM-MR, each recognized for their accurate and reliable representation of complex climatic processes. To encompass a diversity of potential future emission scenarios, two distinct Representative Concentration

Pathways (RCPs) were considered. RCP 4.5, representing stabilization, and RCP 8.5, representing high emissions, were employed to project potential climate conditions. This approach facilitates a comprehensive examination of comparative future trajectories and allows for an in-depth exploration of potential future scenarios. The climate parameters for the reference and future periods presented in this study were derived from scaled projections obtained from the WorldClim database. These projections utilized Coupled Model Intercomparison Project Phase 5 (CMIP5) models with a resolution of $1.0^\circ \times 1.0^\circ$ (100km x 100km), as documented in WorldClim (2023). These models serve as fundamental tools in simulating future climate conditions based on different greenhouse gas emission scenarios, contributing to the robustness of the study.

3. Results

The simulated barley yield in rainfed agricultural systems exhibited a substantial increase across all climate change scenarios, reflecting an evaluation of climate forecasts for precipitation conditions (Table 3) to gauge their impact on spring barley crop yield. Separate assessments were conducted for four distinct periods (1986-2005, 2040-2059, 2060-2079, and 2080-2099) for two scenarios, namely RCP4.5 and RCP8.5, for each

model. The historical period (1986-2005) simulations using the LINTUL model revealed barley yields of 6.7 t ha^{-1} for HADGEMAO, 3.8 t ha^{-1} for GFDLESM2M, and 3.5 t ha^{-1} for MPIESMMR. Moving into the future under different RCP scenarios, distinct patterns emerged. Under the RCP4.5 scenario for 2040-2059 (F1), HADGEMAO projected an increase to 7.7 t ha^{-1} , while GFDLESM2M and MPIESMMR showed yields of 4.4 and 4.2 t ha^{-1} , respectively. In the same period under the more severe RCP8.5 scenario, HADGEMAO exhibited higher yields at 8.3 t ha^{-1} , while GFDLESM2M and MPIESMMR showed 4.2 and 4.8 t ha^{-1} , respectively. Transitioning to 2060-2079 (F2), HADGEMAO, GFDLESM2M, and MPIESMMR under RCP4.5 yielded 8.1 , 4.3 , and 5.3 t ha^{-1} , respectively. Meanwhile, under RCP8.5, HADGEMAO yielded 7.8 t ha^{-1} , GFDLESM2M yielded 3.9 t ha^{-1} , and MPIESMMR yielded 4.4 t ha^{-1} . In the final projection period (2080-2099, F3), RCP4.5 showed HADGEMAO, GFDLESM2M, and MPIESMMR yields of 8.9 , 4.1 , and 4.4 t ha^{-1} , respectively. Contrastingly, under RCP8.5, the yields were 8.2 t ha^{-1} for HADGEMAO, 4.2 t ha^{-1} for GFDLESM2M, and 3.8 t ha^{-1} for MPIESMMR. The results underscore the variability in simulated barley yields across different climate models, scenarios, and time periods, with RCP8.5 consistently projecting higher yields compared to RCP4.5, and model-specific responses to changing climate conditions.

Table 3. Yields (t ha^{-1}) and yield changes (%) of different scenarios for spring barley

Model	1986-2005 (Historical)	RCP scenarios	2040-2059 (F1)	2060-2079 (F2)	2080-2099 (F3)
HADGEMAO	6.7 ^a	4.5	7.7 (14.9 ^b)	8.1 (20.9)	8.9 (32.8)
		8.5	8.3 (23.9)	7.8 (16.4)	8.2 (22.4)
GFDLESM2M	3.8	4.5	4.4 (15.8)	4.3 (13.2)	4.1 (7.9)
		8.5	4.2 (10.5)	3.9 (2.6)	4.2 (10.5)
MPIESMMR	3.5	4.5	4.2 (20.0)	5.3 (51.4)	4.4 (25.7)
		8.5	4.8 (37.1)	4.4 (25.7)	3.8 (8.6)

^aSimulated yields (t ha^{-1}), ^bYield changes (D, %) $D = [(Yield - Historical \text{ yield}) \div Historical \text{ yield}] \times 100$.

The HADGEMAO model, under the RCP4.5 scenario, demonstrated a consistent upward trend across three future periods. The percentage increase was 14.9% in the 2040-2059 periods, escalating to 20.9% in the 2060-2079 period, and reaching 32.8% in the 2080-2099 periods. In the case of the HADGEMAO RCP8.5 scenario, a projected profitability increase of 23.9%, 16.4%, and 22.4% was forecasted for the respective periods of 2040-2059, 2060-2079, and 2080-2099. The second model, GFDL-ESM2M, with RCP4.5, indicated a 15.8% increase in yield during the 2040-2059 periods. In the middle future period (2060-2079) was observed with an increase of -13.2%. The model projected an increase of -7.9% in the 2080-2099 periods. For the GFDL-ESM2M model with RCP8.5, a mixed trend emerged, showcasing increases of 10.5%, 2.6%, and 10.5% in the periods 2040-2059, 2060-2079, and 2080-2099, respectively. The MPIESMMR model, under the RCP 4.5 scenario, displayed substantial increases in barley yield during the periods 2040-2059

(20.0%) and 2060-2079 (51.4%), with a subsequent increase of 25.7% in 2080-2099. Under the RCP 8.5 scenario, stable percentage was (37.1%), (25.6%), (8.6%) increase in barley yield were observed across the periods 2040-2059, 2060-2079 and 2080-2099.

Overall, the HADGEMAO and MPIESMMR models exhibited promising results in simulating yield, projecting an increase in spring barley yield for both RCP4.5 and RCP8.5 scenarios in GFDL-ESM2M model case also demonstrated stable increase in rainfed conditions.

4. Discussion

Climate change, particularly the rise in ambient temperatures, is anticipated to exert a considerable impact on agricultural yields (Wang et al., 2018). The future yield estimations of barley were conducted through the application of the LINTUL Model to create a strategy to the critical threshold imposed by this

phenomenon. On the other hand, Gardi et al. (2022) utilization of the DSSAT-CERES-Barley model for Ethiopian barley production reveals potential yield increases despite climate change. Projections suggest a consistent temperature rise of up to 5 °C and variable rainfall patterns. Despite a simulated significant decline in production, up to 98 and 63% for Traveller and EH-1493, respectively, adaptation strategies involving early sowing, an increase in both density (25%), and fertilizer rate (50%) counteract these negative effects. The study highlights the efficiency of the model in assessing the influence of climate change on rainfed barley yield in Ethiopia and suggesting measures for adaptation, providing a parallel perspective to our investigation utilizing the LINTUL model. Mirgol et al. (2020) found that, under certain climate scenarios, the irrigation water requirements (IR) for winter wheat and barley in Iran's semi-arid Qazvin Plateau are projected to increase significantly by 38%–79% highlighting the critical importance of water resource management under the climate change conditions. In our study, we focus different point, highlighting that our observed increase in potential yield is attributed to our precise management of irrigation, maintaining soil water level at the optimal threshold for crop needs. Bento et al. (2021) examined the influence of climate change on production of barley in the Iberian Peninsula, revealing a projected increase in the northern regions due to early winter warming stimulating earlier growth, while the southern regions face potential severe yield losses primarily attributed to rising spring maximum temperatures. Ko et al. (2019) assessed geospatial variations in South Korean barley production under climate change scenarios (RCP 4.5 and 8.5) using the CERES-barley model. Projected yields for four barley cultivars demonstrated moderate rises under RCP 4.5 and rapid enhancement under RCP 8.5, revealing notable regional variation. Trnka et al. (2004) demonstrated that the combined effects of direct and indirect impacts of doubled CO₂ on potential yields resulted in a substantial 19-30% increase in barley yields across various localities. The observed increase in barley yields with rising temperatures can be attributed, in part, to the potential enhancement of photosynthetic processes. Warmer temperatures may stimulate enzymatic reactions associated with photosynthesis, leading to increased carbon assimilation and a subsequent positive impact on crop yield. This experience is particularly relevant to C3 crops like barley. However, it is crucial to note that while elevated temperatures may have beneficial effects, the relationship between temperature and yield is nuanced. There exists a threshold beyond which the positive effects may turn detrimental due to heat stress. In regions where water resources are limited, the potential impact of increased temperatures on barley yields should be carefully considered (Al-Bakri et al., 2011).

4. Conclusion

The optimization of yields is the critical determinant the improvement of the quality and economic value of crops. In recent years, the landscape has undergone significant changes to achieve optimal cultivation efficiency, due to alterations in precipitation patterns as an outcome of climate change, as well as an increase in air temperature and atmospheric CO₂ levels. In this current research, the reaction of spring barley harvested in southeast of Almaty to explored various climatic scenarios and assessed optimal growth conditions for adaptation. The analysis of three models of global climate change and various scenarios shows a significant a rise in spring barley yield under different climate change scenarios. Particular emphasis should be given to the positive trends observed in the HADGEMAO and MPIESMMR models predicting an increase in spring barley yield for both RCP 4.5 and RCP 8.5 scenarios. These data open up valuable prospects for making informed decisions that climate change in the southeast of Almaty practically does not threaten the barley harvest, highlighting the critical importance of water resource management in response to the challenges posed by climate shifts. However, it is crucial to note that while elevated temperatures may have beneficial effects, the relationship between temperature and yield is nuanced. There exists a threshold beyond which the positive effects may turn detrimental due to heat stress. In regions where water resources are limited, the potential impact of increased temperatures on barley yields should be carefully considered.

Author Contributions

The percentage of the author(s) contributions is presented below. All authors reviewed and approved the final version of the manuscript.

	A.S.	G.S.	T.K.	A.K.Y.
C	10	20	40	30
D	10	10	40	40
S			80	20
DCP	90	10		
DAI	60		10	30
L	60	10	10	20
W	60	10	10	20
CR		20	40	40
SR			90	10
PM			80	20
FA	40	60	0	0

C=Concept, D= design, S= supervision, DCP= data collection and/or processing, DAI= data analysis and/or interpretation, L= literature search, W= writing, CR= critical review, SR= submission and revision.

Conflict of Interest

The authors declared that there is no conflict of interest.

Ethical Consideration

Ethics committee approval was not required for this study because of there was no study on animals or humans.

References

Ahmed M, Asif M, Hirani AH, Akram MN, Goyal A. 2013. Modeling for agricultural sustainability: a review. Bhullar G, Bhullar NK, editors. Agriculture Sustainability. Elsevier, London, UK, pp: 145.

Akhavizadegan F, Ansarifard J, Wang L, Huber I, Archontoulis SV. 2021. A time-dependent parameter estimation framework for crop modeling. *Sci Rep*, 11(1): 11437.

Al-Bakri J, Suleiman A, Abdulla F, Ayad J. 2011. Potential impact of climate change on rainfed agriculture of a semi-arid basin in Jordan. *Phys Chem Earth A/B/C/*, 36(5-6): 125-134.

Aşık M, Yetik AK, Candoğan BN, Kuşçu H. 2021. Determining the yield responses of maize plant under different irrigation scenarios with AquaCrop model. *Int J Agric Environ Food Sci*, 5(3): 260-270.

Bento VA, Ribeiro AF, Russo A, Gouveia CM, Cardoso RM, Soares PM. 2021. The impact of climate change in wheat and barley yields in the Iberian Peninsula. *Sci Rep*, 11(1): 15484.

Boote KJ, Jones JW, White JW, Asseng S, Lizaso JL. 2013. Putting mechanisms into crop production models. *Plant Cell Environ*, 36(9): 1658-1672.

Bunce JA. 2004. Carbon dioxide effects on stomatal responses to the environment and water use by crops under field conditions. *Oecologia*, 140: 1-10.

Craufurd PQ, Vadez V, Jagadish SK, Prasad PV, Zaman-Allah, M. 2013. Crop science experiments designed to inform crop modeling. *Agric For Meteorol*, 170: 8-18.

Dokuchaev VV. 1899. A contribution to the theory of natural zones: Horizontal and vertical soil zones. Mayor's Office Press, St. Petersburg, Russia, pp: 123.

Farré I, Van Oijen M, Leffelaar PA, Faci JM. 2000. Analysis of maize growth for different irrigation strategies in northeastern Spain. *Eur J Agron*, 12(3-4): 225-238.

Fleming ZL, Doherty RM, Von Schneidemeser E, Malley CS, Cooper OR, Pinto JP, Feng Z. 2018. Tropospheric Ozone Assessment Report: Present-day ozone distribution and trends relevant to human health. *Elem Sci Anth*, 6: 12.

Ford MA, Thorne GN. 1967. Effect of CO₂ concentration on growth of sugar-beet, barley, kale, and maize. *Ann Bot*, 31(4): 629-644.

Franke AC, Haverkort AJ, Steyn JM. 2013. Climate change and potato production in contrasting South African agro-ecosystems 2. Assessing risks and opportunities of adaptation strategies. *Potato Res*, 56: 51-66.

Gardi MW, Memic E, Zewdu E, Graeff-Hönninger S. 2022. Simulating the effect of climate change on barley yield in Ethiopia with the DSSAT-CERES-Barley model. *Agron J*, 114(2): 1128-1145.

Genievskaia Y, Almerikova S, Sariev B, Chudinov V, Tokhetova L, Sereida G, Turuspekoy Y. 2018. Marker-trait associations in two-rowed spring barley accessions from Kazakhstan and the USA. *PLoS one*, 13(10): e0205421.

Gergis J. 2023. Humanity's moment: A climate scientist's case for hope. Island Press, London, UK, pp: 45.

Gimplinger DM, Kaul HP. 2012. Calibration and validation of the crop growth model LINTUL for grain amaranth (*Amaranthus* sp.). *J App Bot Food Qual*, 82(2): 183-192.

Giraldo P, Benavente E, Manzano-Agugliaro F, Gimenez E. 2019. Worldwide research trends on wheat and barley: A

bibliometric comparative analysis. *Agron*, 9(7): 352.

Goyne PJ, Milroy SP, Lilley JM, Hare JM. 1993. Radiation interception, radiation use efficiency and growth of barley cultivars. *Aust J Agric Res*, 44(6): 1351-1366.

Gray SB, Brady SM. 2016. Plant developmental responses to climate change. *Dev Biol*, 419(1): 64-77.

Gregory PJ, Ingram JS, Brklacich M. 2005. Climate change and food security. *Phil Trans R Soc A*, 360(1463): 2139-2148.

Haverkort AJ, Franke AC, Engelbrecht FA, Steyn JM. 2013. Climate change and potato production in contrasting South African agro-ecosystems 1. Effects on land and water use efficiencies. *Potato Res*, 56: 31-50.

Hibberd JM, Richardson P, Whitbread R, Farrar JF. 1996. Effects of leaf age, basal meristem and infection with powdery mildew on photosynthesis in barley grown in 700 μmol mol⁻¹ CO₂. *New Phytol*, 134(2): 317-325.

Jeong S, Ko J, Shin T, Yeom JM. 2022. Incorporation of machine learning and deep neural network approaches into a remote sensing-integrated crop model for the simulation of rice growth. *Sci Rep*, 12(1): 9030.

Kimball BA, Kobayashi K, Bindi M. 2002. Responses of agricultural crops to free-air CO₂ enrichment. *Adv Agron*, 77: 293-368.

Kizildenz T. 2024. Assessing the growth dynamics of alfalfa varieties (*Medicago sativa* cv. Bilensoy 80 and Nimet) response to varied carbon dioxide (CO₂) concentrations. *Heliyon*, DOI:<https://doi.org/10.1016/j.heliyon.2024.e28975>.

Kizildenz T, Pascual I, Irigoyen JJ, Morales F. 2021. Future CO₂, warming and water deficit impact white and red Tempranillo grapevine: Photosynthetic acclimation to elevated CO₂ and biomass allocation. *Physiol Plant*, 172(3): 1779-1794.

Ko J, Ng CT, Jeong S, Kim JH, Lee B, Kim HY. 2019. Impacts of regional climate change on barley yield and its geographical variation in South Korea. *Int Agrophys*, 33(1): :81-96.

Long SP, Ainsworth EA, Leakey AD, Morgan PB. 2005. Global food insecurity. Treatment of major food crops with elevated carbon dioxide or ozone under large-scale fully open-air conditions suggests recent models may have overestimated future yields. *Phil Trans R Soc B*, 360(1463): 2011-2020.

Meehl GA, Stocker TF, Collins WD, Friedlingstein P, Gaye AT, Gregory JM, Zhao ZC. 2007. Global climate projections. Cambridge University Press, Cambridge, UK, pp: 41.

McMichael A. 2017. Climate change and the health of nations: famines, fevers, and the fate of populations. Oxford University Press, Oxford, UK, pp: 28.

Mirgol B, Nazari M, Eteghadipour M. 2020. Modelling climate change impact on irrigation water requirement and yield of winter wheat (*Triticum aestivum* L.), barley (*Hordeum vulgare* L.), and fodder maize (*Zea mays* L.) in the semi-arid Qazvin Plateau, Iran. *Agric*, 10(3): 60.

Newton AC, Guy DC, Bengough AG, Gordon DC, McKenzie BM, Sun B, Hallett PD. 2012. Soil tillage effects on the efficacy of cultivars and their mixtures in winter barley. *Field Crops Res*, 128: 91-100.

Oteng-Darko P, Yeboah S, Addy SNT, Amponsah S, Danquah EO. 2013. Crop modeling: A tool for agricultural research-A review. *J Agri Res Develop*, 2(1): 1-6.

Pettersson R, Lee HSJ, Jarvis PG. 1993. The effect of CO₂ concentration on barley. URL: <https://link.springer.com/article/10.1007/BF00048180> (accessed date: April 14, 2022).

Raza A, Razaq A, Mehmood SS, Zou X, Zhang X, Lv Y, Xu J. 2019. Impact of climate change on crops adaptation and strategies to tackle its outcome: A review. *Plants*, 8(2): 34.

- Reddy PP, Reddy PP. 2015. Impacts of climate change on agriculture. Reddy PP, editor. *Climate resilient agriculture for ensuring food security*. Springer, London, UK, pp: 43-90.
- Reynolds M, Kropff M, Crossa J, Koo J, Kruseman G, Molero Milan A, Vadez V. 2018. Role of modelling in international crop research: overview and some case studies. *Agron*, 8(12): 291.
- Saebo A, Mortensen LM. 1996. Growth, morphology and yield of wheat, barley and oats grown at elevated atmospheric CO₂ concentration in a cool, maritime climate. *Agric Ecosyst Environ*, 57(1): 9-15.
- Sehgal A, Sita K, Siddique KH, Kumar R, Bhogireddy S, Varshney RK, Nayyar H. 2018. Drought or/and heat-stress effects on seed filling in food crops: impacts on functional biochemistry, seed yields, and nutritional quality. *Front Plant Sci*, 9: 1705.
- Shibu ME, Leffelaar PA, Van Keulen H, Aggarwal PK. 2010. LINTUL3, a simulation model for nitrogen-limited situations: Application to rice. *European J Agron*, 32(4): 255-271.
- Sicher RC, Bunce JA. 1997. Relationship of photosynthetic acclimation to changes of Rubisco activity in field-grown winter wheat and barley during growth in elevated carbon dioxide. *Photosynth Res*, 52: 27-38.
- Spitters CJT. 1989. Crop Growth Models: Their usefulness and limitations. *Acta Hort*, 267: 349-368.
- Spitters CJ, Schapendonk AH. 1990. Evaluation of breeding strategies for drought tolerance in potato by means of crop growth simulation. *Gen Aspects Plant Min Nut*, 2: 151-161.
- Stacey P, O'Kiely P, Hackett R, Rice B, O'Mara FP. 2006. Changes in yield and composition of barley, wheat and triticale grains harvested during advancing stages of ripening. *Ir J Agric Food Res*, 2006: 197-209.
- Tao F, Rötter RP, Palosuo T, Gregorio Hernández Díaz-Ambrona C, Mínguez MI, Semenov MA, Schulman AH. 2018. Contribution of crop model structure, parameters and climate projections to uncertainty in climate change impact assessments. *Global Change Biol*, 24(3): 1291-1307.
- Trnka M, Dubrovský M, Žalud Z. 2004. Climate change impacts and adaptation strategies in spring barley production in the Czech Republic. *Clima Change*, 64(1-2): 227-255.
- Van der Werf HM, Petit J. 2002. Evaluation of the environmental impact of agriculture at the farm level: a comparison and analysis of 12 indicator-based methods. *Agric Ecosyst Environ*, 93(1-3): 131-145.
- Wajid A, Hussain K, Ilyas A, Habib-ur-Rahman M, Shakil Q, Hoogenboom G. 2021. Crop models: Important tools in decision support system to manage wheat production under vulnerable environments. *Agric*, 11(11): 1166.
- Wang J, Vanga SK, Saxena R, Orsat V, Raghavan V. 2018. Effect of climate change on the yield of cereal crops: A review. *Clim*, 6(2): 41.
- Weigel HJ, Manderscheid R, Jäger HJ, Mejer GJ. 1994. Effects of season-long CO₂ enrichment on cereals. I. Growth performance and yield. *Agric Ecosyst Environ*, 48(3): 231-240.
- WorldClim. 2023. Climate Data at the National Center for Atmospheric Research. Disponible URL: <http://www.wdi.worldbank.org/> (accessed date: 15 January, 2024).
- Yagiz AK, Cakici M, Aydogan N, Omezli S, Yerlikaya BA, Ayten S, Haverkort AJ. 2020. Exploration of climate change effects on shifting potato seasons, yields, and water use employing NASA and national long-term weather data. *Potato Res*, 63: 565-577.
- Yetik AK, Kızıldeniz T, Ünal Z. 2023. Simulating The Yield Responses of Sugar Beet to Different Climate Change Scenarios by LINTUL-MULTICROP Model. *BSJ Eng Sci*, 6(2): 53-59.
- Zenda T, Liu S, Dong A, Duan H. 2021. Advances in cereal crop genomics for resilience under climate change. *Life*, 11(6): 502.
- Zhu T, Fonseca De Lima CF, De Smet I. 2021. The heat is on: how crop growth, development, and yield respond to high temperature. *J Exp Bot*, 72(21): 7359-7373.



İVESİ KUZULARINDA BÜYÜME ÖZELLİKLERİ İÇİN PRATİK BİR DAMIZLIK SEÇME YÖNTEMİ: KOLAY İNDEKS UYARLAMASI

Yusuf KAPLAN^{1*}, İrfan GÜNGÖR¹, Kürşat ALKOYAK¹, Mustafa TEKERLİ²

¹Republic of Türkiye Ministry of Agriculture and Forestry, General Directorate of Agricultural Research and Policies, Ankara, Türkiye

²Department of Animal Science, Faculty of Veterinary Medicine, Afyon Kocatepe University, Afyonkarahisar, Türkiye

Özet: Hayvan ıslahının en önemli adımlardan biri de damızlık değeri en iyi hayvana üreme şansı verilmesidir. Aynı zamanda küçükbaş hayvancılıkta sürdürülebilirlik için büyüme, üreme ve süt verimi gibi ekonomik özellikler açısından daha verimli hayvanların seçilmesi gereklidir. Hayvanların verimlerine ilişkin damızlık değerlerini tahmin etmek için kullanılan yöntem ve modeller nispeten karmaşık yapıdadır. Çoğu kere yetiştiricilerin kendi başlarına uygulamaları güç olmaktadır. Bu nedenle iyi hayvanların seçimi için basit modellere ve pratik uygulamalara gereksinim duyulmaktadır. Bu çalışmanın amacı, koyun yetiştiricilerinin en iyi kuzularını seçmeleri için pratik bir yöntemi tanıtmak ve bu şekilde kullanılacak damızlıkları belirlemektir. Bu hedefle İvesi kuzularına ait örnek bir veri seti ile "Damızlık Asistanı" adlı bilgisayar yazılımı kullanılmıştır. Veri seti 2016-2018 yılları arasında 49 sürü ve 12 410 baş kuzudan elde edilen doğum ağırlığı (DA), süttten kesim ağırlığı (SKA) ve bu iki özellikten hesaplanan günlük canlı ağırlık artışlarından (GCAA) oluşmaktadır. Damızlık Asistanı ile İvesi kuzularının büyüme özelliklerine önemli çevresel faktörlerin etkisi giderilmiş ve daha sonra kolay indeks yöntemi kullanılarak düzeltilmiş verilerle değerli hayvanlar tespit edilmiştir.


Anahtar kelimeler: Kolay indeks, Pratik seleksiyon, İvesi kuzusu, Büyüme özellikleri


A Practical Selection Method for Growth Traits in Awassi Lambs: Easy Index Implementation


Abstract: One of the most critical steps in animal breeding is that the best animal in terms of breeding value will be given a chance to reproduce. At the same time, for the sustainability of small ruminant industry, the selection of more productive animals is necessary for economic traits such as growth, reproduction and milk yield. The methods and models used to estimate the breeding values of animals related to yields are quite complex. It is often difficult for breeders to implement on their own. Therefore, simple models and practical applications are required for the selection of productive animals. The aim of this study is to demonstrate a simple and practical method for sheep breeders to select their best lambs. Computer software called "Damızlık Asistanı" was used for this purpose with a sample dataset of Awassi lambs. The dataset consists of birth weight, weaning weight and daily live weight gains obtained from 49 herds and 12 410 lambs between 2016-2018. The effects of important environmental factors on the growth traits of Awassi lambs were eliminated by the Damızlık Asistanı and then the easy index method was used to identify valuable animals with the adjusted data.


Keywords: Easy index, Practical selection, Awassi lamb, Growth traits

*Sorumlu yazar (Corresponding author): Republic of Türkiye Ministry of Agriculture and Forestry, General Directorate of Agricultural Research and Policies, Ankara, Türkiye
E mail: yusufkaplan66@gmail.com (Y. KAPLAN)

Yusuf KAPLAN  <https://orcid.org/0000-0001-8853-7686>

İrfan GÜNGÖR  <https://orcid.org/0000-0001-6248-3464>

Kürşat ALKOYAK  <https://orcid.org/0000-0001-6621-6136>

Mustafa TEKERLİ  <https://orcid.org/0000-0002-8634-1193>

Gönderi: 28 Şubat 2024

Kabul: 19 Nisan 2024

Yayınlanma: 15 Mayıs 2024

Received: February 28, 2024

Accepted: April 19, 2024

Published: May 15, 2024

Cite as: Kaplan Y, Güngör I, Alkoyak K, Tekerli M. 2024. A practical selection method for growth traits in Awassi lambs: easy index implementation. *BSJ Eng Sci*, 7(3): 473-477.

1. Giriş

İvesi, yetiştiriciliği Akdeniz'in doğusunda özellikle Mezopotamya bölgesinde yaygın olarak yapılan kurak ve yarı kurak çevre koşullarına uyum sağlayabilen yağlı kuyruklu bir koyun ırkıdır. Bu ırk ekstansif yetiştiricilikten entansif yetiştiriciliğe kadar geniş çevre koşullarına uyum sağlamaktadır. İvesi koyunlarının verim performansı yetiştirildiği çevre ve yetiştirme amacına göre değişiklik göstermektedir. Şekil 1'de görseli yer alan İvesi koyun ırkında yapılan araştırmalar, genellikle büyüme ve süt verimini genetik olarak iyileştirme amacı taşımaktadır (Galal ve ark., 2008).



Şekil 1. İvesi koyunu ve kuzusu.

Bu verimler bakımından damızlık değeri yüksek hayvanların doğru yöntemlerle belirlenmesi, İvesi koyun



yetiştiriciliğinde gelir artışı ve sürdürülebilirliğin sağlanması açısından faydalı olacaktır. Hayvan yetiştirmede gerçek damızlık değerlerinin tahmininde genellikle karma modellerden yararlanılmakta ve bunu çözmeye yönelik farklı yöntem ve programlar kullanılmaktadır (Pollotta ve Gootwineb, 2001; Karabulut ve Tekin 2009; Kaplan ve Tekerli, 2020; Jawasreh ve ark., 2021). Hayvanların verimlere ilişkin damızlık değerlerini tahmin etmek için kullanılan yöntem ve modeller nispeten karmaşık yapıda ve bu konuda uzmanlık gerektirmektedir. Bu nedenle yetiştiriciler kendileri uygulamak istediklerinde bazı güçlüklerle karşılaşmaktadırlar. İvesi koyun ırkını da kapsayan ve Tarımsal Araştırmalar ve Politikalar Genel Müdürlüğü (TAGEM) tarafından 2005 yılından bu yana yürütülen ülkesel hayvan ıslahı projesinde damızlıklar proje liderleri tarafından seçilmektedir. Bu noktada proje liderleri yanında konuya ilgi duyan ziraat mühendisi, veteriner hekim ve yetiştiricilerin koç, koyun ve kuzu seçiminde kullanımı kolay yöntemlere ihtiyaç duydukları görülmektedir (Kaplan ve ark., 2019). Yoğun istatistik bilgisi gerektiren karma modeller kurulmadan da ekonomik özellikleri önemli seviyede etkileyen çevre faktörleri etkisinin tespit edilmesi ve bu etkilerin nasıl elemine edilmesi gerektiği gibi konular bazı araştırmacılar (Harvey 1960; Vanlı ve ark., 2005; Doğan ve ark., 2019) tarafından farklı ırklarda örnekleriyle bildirilmiştir. Bu çalışmanın amacı, Halk Elinde Hayvan Islahı Ülkesel Projesinde kullanılmak üzere geliştirilmekte olan Damızlık Asistanı yazılımı yardımıyla Adıyaman ilinde (Şekil 2) yetiştirilen İvesi ırkı koyunlarda büyüme verilerinde kolay indeks (Arpacık, 1982; Kaplan ve ark., 2019) isimli pratik damızlık seçme yöntemini tanıtmak ve damızlıkların bu yöntemle belirlenebildiğini göstermektir.



Şekil 2. Adıyaman ili.

2. Materyal ve Yöntem

Adıyaman ili, Doğu ve Güneydoğu Anadolu bölgeleri arasında bir köprü vazifesi görmekte aynı zamanda Akdeniz bölgesinin özelliğini de taşımaktadır. Genel olarak kışlar ılık ve yağışlı yazlar ise sıcak ve kurak geçmektedir. Bu nedenle bitki örtüsünde üç bölgenin de özellikleri görülmektedir. İvesi sürüleri, Nisan-Ekim ayları arasında sabahın erken saatlerinden akşama kadar köylere yakın mera ve anızlarda otlatılmaktadır.

Meralarda genellikle çalı tipi ve mevsime bağlı olarak yetişen otlar mevcuttur. Sürüler, kışın hava şartlarının uygun olduğu günlerde dışarıda otlatılmakta ve meraya ek olarak günde yaklaşık 0,5-0,6 kg/baş karma yem (arpa, buğday ve kepek) ve 1-2 kg/baş saman verilmektedir. Hava şartlarının uygun olmadığı günlerde ise ağıllarda barındırılarak; arpa kırması, kuru ot ve buğday samanı ile beslenmeleri ekstansif yetiştirme sistemine örnek teşkil etmektedir. Bu tarz yetiştirme sistemlerinde çeşitli çevre şartlarına maruz kalan İvesi kuzularında verim özellikleri için pratik ve kullanışlı yöntemlerle çevre faktörlerinin etkisini belirlemek ve gidermek, daha sonra yapılacak olan damızlık seçiminin önemini daha da artırmaktadır. Çalışmada 49 farklı sürüde, 2016-2018 yılları arasında 3 yıllık bir sürede doğan ve süttten kesime ulaşabilen 12410 baş kuzunun doğum ağırlığı (DA), süttten kesim ağırlığı (SKA) ve günlük canlı ağırlık artışı (GCAA) verileri kullanılmıştır. Bölgede koç katımı dönemi olan 15 Ağustos ile 15 Ekim tarihleri arasında 20 koyuna 1 koç karşılık gelecek şekilde serbest aşım sistemi uygulanmıştır. Sezonda doğan kuzular 50 kg kapasiteli, 10 gr hassasiyete sahip dijital terazi ile 24 saat içerisinde tartılarak doğum kayıtları kaydedilmiştir. Kuzular geleneksel olarak 90. günde süttten kesilmiş ve bu süre zarfında sabah ve akşam emzirmeleri için analarıyla birlikte tutulmuştur. Süttten kesim ağırlığı belirli günlerde tartıldığı için süttten kesim yaşı 41 ile 136 gün arasında değişmektedir. Bu nedenle hem günlük canlı ağırlık artışı hem de 90 gün ağırlık enterpolasyon metodu kullanılarak hesaplanmıştır. Bu veriler Excel'e aktarıldıktan sonra yapılacak işlem ve analizler için düzenlenmiştir. Şekil 3'te görseli yer alan damızlık asistanı kullanılarak çalışma konusu büyüme özelliklerini etkileyen önemli çevresel faktörler bakımından düzeltilen veriler, kolay indeks adlı yöntemle işlenmiştir. Çalışmada çevresel faktör olarak alınan sürü, yıl, cinsiyet, doğum tipi ve doğum ayı etki payları Damızlık Asistanı kullanılarak yapılan en küçük kareler analizi ile belirlenmiştir. Bu çalışmanın ana fikri gereği modelde sadece bu beş faktör yer alırken hassasiyeti azaltmamak kaydıyla ana yaşı ve benzeri başka faktörlerde modele eklenip çıkarılabilir. Bu durum farklı çalışmalarda araştırmanın hedefine göre değişiklik gösterebilir. Çalışmamızda damızlık asistanıyla yapılan analizler Mitinab istatistik yazılımıyla doğrulanmıştır. Bu çalışmada özellikler için kullanılan istatistik model aşağıdaki gibidir (eşitlik 1).

$$Y_{ijklmn} = \mu + S_i + Y_j + C_k + DT_l + DA_m + e_{ijklmn} \quad (1)$$

Modelde;

Y_{ijklmn} = farklı yaşlarda gözlenen büyüme özelliğini (DA, SKA, GCAA)

μ = popülasyon ortalamasını

S_i = i'inci sürünün etkisini (i = 1'den 49'a; birinci sürü, ikinci sürü, ..., kırk dokuzuncu sürü)

Y_j = j'inci yılın etkisini (j = 1'den 3'e; 2016, 2017, 2018)

C_k = k'inci cinsiyetin etkisini (k = 1'den 2'ye; erkek, dişi)

DT_l = l'inci doğum tipinin etkisini (l = 1'den 2'ye; tekiz,

ikiz)

$DA_m = m$ 'inci doğum ayının etkisini ($m = 1$ 'den 3'e; Ocak, Şubat, Mart)

e_{ijklmn} = her gözlemle ilişkili rastgele hatayı ifade etmektedir.

Şekil 3'te görseli verilen programdaki işlemler dört aşamada özetlenebilir. Birincisi verilerin bulunduğu sekmenin seçilerek onaylanması, ilgili özelliğin veri sayfası sütunundan işaretlenerek seçili özelliği getir düğmesine basılması ve çevre faktörlerinin eklenmesidir. İkinci aşamada ise varyans analiz seçeneği kullanılarak en küçük kareler analizi yapılır. Üçüncü aşamada ise etkisi önemli görülen faktörlerin etki paylarını bulmak için arıtma katsayılarını bul işlemi gerçekleştirilir. Son aşamada ise veriyi çevre etkilerinden arındırmak için en küçük kareler sabitleri, eklemeli düzeltme faktörü olarak kullanılmıştır. Düzeltme faktörünün önündeki artı ya da eksi değere göre toplama ya da çıkartma işlemi damızlık asistanı tarafından otomatik olarak gerçekleştirmiş ve büyüme özellikleri çevre faktörlerine göre sırasıyla düzeltilmiştir (Vanlı ve ark., 2005). Her bir bireyin gözlem değeri ilgili özellik için etkisi önemli görülen çevre faktörlerinden arındırıldıktan sonra Damızlık

Asistanı görevini tamamlamaktadır. Ardından incelenen üç farklı büyüme özelliğinin her birisi için Excel'de bulunan düzeltilmiş veri setinde yukarıda anlatılan işlemler sırasıyla uygulandıktan sonra özellik sütunlarının yanına boş birer sütun daha açılır. Bu sütunların başlığına özellik adı ile birlikte indeks değeri ismi verilir. Düzeltilmiş birinci özellik, yani DA sütunundan başlamak üzere bütün sütun seçilerek büyüme küçüğe sıralanır. Daha sonra boş olan indeks değeri sütununa geçilerek hücreler birden başlamak üzere 1, 2, ... 12 410 olacak şekilde aşağı doğru doldurulur. Aynı işlemler, sırasıyla diğer özellikler (düzeltilmiş SKA ve GCAA) için de uygulanır. Düzeltme ve sıralama işlemi bittikten sonra, aynı veri setinin son sütunu "toplam indeks puanı" başlığıyla isimlendirilir ve tüm özelliklere ait indeks değerleri bu sütuna toplanır. Toplam indeks sütunu Excel'de küçük değerden büyük değere olacak şekilde seçimi genişleterek sıralama işlemi tekrarlanır. (Arpacık, 1982). Bu aşamadan sonra çalışma konusu üç özellik bakımından İvesi kuzularının damızlık değerleri en iyiden en kötüye doğru sıralanmış olur. Yukarıda anlatılan yöntemin nasıl uygulandığına dair kısa bir örnek, Şekil 4'te verilmiştir.

Varyans Analizi		S.D.	K.T.	K.O.	F Değeri	P	R2
Varyasyon Kaynağı		12428	43038392,72				
Genel							
İncelenen Çevre Faktörleri		53	17901167,53	337757,878	166,2774514	0,000	0,415934853
Hata		12375	25137225,19	2031,290925			
Herd	48	5517331,748	114940,2447	56,5848266	0,000	0,128190934	Etkisi Önemli
Year	2	6480045,857	3240022,929	1595,050075	0,000	0,150564309	Etkisi Önemli
BirthMonth	2	5366211,015	2683105,507	1320,886888	0,000	0,12468428	Etkisi Önemli
Sex	1	90872,65645	90872,65645	44,73540646	0,000	0,002111432	Etkisi Önemli

Şekil 3. Damızlık asistanı versiyon 1.0 ile ve varyans analiz sonucu etkisi önemli bulunan çevre faktörleri.

3. Bulgular ve Tartışma

Teknolojinin de gelişmesiyle birlikte, İvesi ırkında damızlık değeri hesaplamak için karma model çözümlerini yapabilen program ve yöntemler kullanılmaktadır (Pollotta ve Gootwineb, 2001; Karabulut ve Tekin 2009; Jawasreh ve ark., 2021). Bu program ve yöntemlerin; hayvan ıslahı, hayvan yetiştirme ve populasyon genetiği alanlarında yeteri kadar uzmanlaşmamış kişiler tarafından uygulanması, damızlık değeri düşük olduğu halde yanlışlıkla seçilen hayvanlarında yetiştirilmede kullanılmasına neden olabilir. Böylece seleksiyonla sağlanacak ilerleme yavaşlayabilir. Bu durumda, özellikle temel yetiştirme bilgisine sahip ve bilgisayar kullanabilen yetiştiriciler, ziraat mühendisleri ve veteriner hekimlerin damızlık hayvanları kolay ve isabetli seçebilmeleri için kullanıcı dostu ve uygulanabilir program ve yöntemler önermek

gerekebilir. Damızlık Asistanı, temel prensipler esas alınarak, damızlık değeri yüksek hayvanların tespiti için gerekli olan istatistik hesaplamaları yapan ve pratik kullanıma sahip henüz yayınlanmamış bir yazılımdır. Bu yazılım Doğan ve arkadaşları (2019) tarafından geliştirilen benzeri LSM-ex (Damızlık Seçimi) yazılımdan ANOVA ve veri düzeltme opsiyonu bakımından yöntem ve kullanım farklılıkları göstermektedir. Ayrıca mevcut çalışmamızda yukarıda ifade edilen kolay indeks yöntemiyle bir hayvanın birden çok özelliğinin katılımıyla oluşturulan indeks değerini hesaplanabilmesidir. Bu yöntemde seleksiyon indeksi oluşturmak için kullanılan karmaşık metotlar yerine excel programının yeteneklerinden yararlanan bir teknik kullanılmıştır. Nitekim seleksiyon indeks yöntemlerinde temel amaç, teksel seleksiyon ve bağımsız ayıklama sınırları yöntemlerinin sakıncalarını ortadan

kaldırmaktır. Her bir İvesi kuzusu için ilgilenilen bütün özellikler ve ekonomik ağırlıkları dikkate alınarak, bir indeks değeri hesaplanması gerekmektedir. Ancak normal indeks yönteminde kuzuların büyüme özellikleriyle bu özelliklere ait kalıtım dereceleri, özellikler arası genetik korelasyonlar ve her bir özelliğin ekonomik önemi dikkate alınarak hesaplanmış ekonomik ağırlık katsayılarının kullanılmasının yararlığı olacağı ifade edilmektedir (Ertuğrul, 1997; Düzgüneş ve ark., 2003). Ancak bunlarında ayrı ve detaylı hesaplama yöntemleri bulunmaktadır. Kolay indeks yöntemi özelliklere eşit ağırlık veren, genetik parametre hesabına gitmeden ve ekonomik ağırlıkların hesaplanmasına da gerek kalmadan pratik damızlık seçimine imkân sağlamaktadır. Çalışmanın metot kısmında açıklanan işlemler tamamlandığında, farklı çağlarda ölçülen büyüme özelliklerini önemli düzeyde etkileyen çevre faktörlerinin etkileri düzeltilmiş ve kolay indeks yöntemi

uygulanarak kuzuların damızlık değeri puanları elde edilmiştir. Bu puanların kullanılmasıyla, büyüme bakımından daha üstün damızlık adaylarının seçimi imkânı ortaya çıkmıştır. Bu çalışmada uygulanan kolay indeks yöntemi sonucunda, üç farklı büyüme özelliği bakımından 12410 baş kuzunun kendi aralarında indeks değerleri belirlenmiştir. İndeks 663 ile 35491 arasında değişen bir skor aralığına sahiptir. Liste 12410 satırdan oluştuğu için ilk 22 kuzuya ait değerler Şekil 5'te verilmiştir. Bu liste kullanılarak basit ve pratik bir şekilde değerli damızlıklar belirlenebilir. Bu çalışma kolay indeks yönteminin, günümüz yetiştiricileri, veteriner hekimleri ve ziraat mühendisleri tarafından rahatlıkla kullanılabilir olduğunu göstermiştir. Söz konusu yöntemin avantajı, yaygın bir şekilde bilinen ofis uygulaması Excel ile kullanılabilir olmasıdır. Diğer önemli bir avantajı ise çok sayıda veri olması durumunda manuel olarak işlem yapmaktan doğabilecek riskleri en aza indirmesidir.

Kolay İndeks Yöntemi:

- Damızlık olacak hayvanlar ilgili karakterler yöntenden karşılaştırılarak bir indeks değeri oluşturulur.
- Örneğin:
Elde 5 baş ivesi kuzusu bulunsun (A,B,C,D,E). Bu beş baş kuzu arasından üç karakter bakımından indeks yöntemi ile en iyi damızlık olabilecek kuzuyu seçmeye çalışalım. Bu üç karakter;
1. Doğum ağırlığı (DA),
2. Sütten kesim ağırlığı (SKA),
3. Doğum ile sütten kesim arası günlük canlı ağırlık artışıdır (GCAA).

Her bir karakterin verim değeri birden beşe kadar (kuzu sayısı kadar) puan verilerek sıralanır ve bu değerler toplam indeks puanı sütununa toplanır.

İvesi Kuzusu	DA (kg)	DA İndeks Değeri	SKA (kg)	SKA İndeks Değeri	GCAA (kg)	GCAA İndeks Değeri	Toplam İndeks Puanı
Kuzu A	4.5	1	33	2	0.40	2	5
Kuzu B	3.9	5	31	3	0.25	4	12
Kuzu C	4.2	3	30	4	0.35	3	10
Kuzu D	4.3	2	35	1	0.50	1	4
Kuzu E	4.1	4	29	5	0.20	5	14

Listede en düşük indeks değerini (4) alan D kuzusu en yüksek damızlık değere sahiptir. En yüksek indeks değerini (14) alan E kuzusu da en düşük damızlık değere sahiptir. İşletme bakımından ekonomik önemi yüksek olan özellikler önemli çevre faktörleri bakımından düzeltildikten sonra basit bir şekilde bu yöntem uygulanabilir.

Şekil 4. Örnek kolay indeks yöntemi.

Kuzu Numarası	Sürü	Yıl	Cinsiyet	Doğum ayı	Doğum tipi	DA (kg)	DA İndeks değeri	SKA (kg)	SKA İndeks değeri	GCAA (kg)	GCAA İndeks değeri	Toplam İndeks Puanı	
1	TRO2000885460	Süleyman Akay	2017	ERKEK	Şubat	TEK	4849.71	305	30821.62	54	281.87	304	663
2	TRO2000995193	Şükriye Kaya	2018	ERKEK	Şubat	TEK	4687.97	638	33967.25	5	359.88	25	668
3	TRO2000995186	Şükriye Kaya	2018	ERKEK	Şubat	TEK	4667.97	666	32867.25	10	338.01	42	718
4	TRO2000995140	Şükriye Kaya	2018	DISI	Şubat	TEK	4767.97	489	31447.75	34	291.98	216	739
5	TRO2000852876	Mehmet Kaya	2017	ERKEK	Ocak	TEK	4880.89	254	30797.32	56	274.55	433	743
6	TRO2000992919	Hüda Ünlü	2018	ERKEK	Şubat	TEK	4656.29	695	32588.57	16	303.57	147	858
7	TRO2001099995	Faruk ERTURK	2018	ERKEK	Şubat	TEK	4662.50	675	32210.61	20	300.12	168	863
8	TRO2000893104	Hanım AVCI	2017	ERKEK	Şubat	TEK	4867.56	276	27209.96	385	290.58	226	887
9	TRO2000991431	Abdurrahman KOYUNCU	2017	ERKEK	Şubat	TEK	4780.30	460	27343.69	367	308.72	125	952
10	TRO2000873939	Sütlük YILMAZ	2017	ERKEK	Şubat	TEK	5155.00	87	26097.17	687	296.16	191	965
11	TRO2000991464	Abdurrahman KOYUNCU	2017	DISI	Ocak	TEK	4780.30	459	27712.98	298	285.47	268	1025
12	TRO2000995223	Sabri Kaya	2018	ERKEK	Şubat	TEK	4467.19	994	35749.57	1	342.81	34	1029
13	TRO2000994824	Mustafa Alakış	2018	ERKEK	Ocak	TEK	4573.99	826	30776.71	58	300.70	164	1048
14	TRO2000995214	Sabri Kaya	2018	ERKEK	Şubat	TEK	4447.19	1015	35549.57	2	340.85	35	1052
15	TRO2000994868	Mustafa Alakış	2018	DISI	Şubat	TEK	4373.99	1086	33168.40	8	358.71	26	1120
16	TRO2000993356	Aziz Gökdemir	2018	DISI	Şubat	TEK	4960.17	174	28884.08	142	259.98	805	1121
17	TRO2000991470	Abdurrahman KOYUNCU	2017	DISI	Ocak	TEK	4680.30	650	27812.98	279	287.54	246	1175
18	TRO2000993356	Aziz Gökdemir	2018	DISI	Ocak	TEK	4860.17	291	29188.51	118	260.62	74	1183
19	TRO2000882564	Sait Ertürk	2017	ERKEK	Ocak	TEK	5248.03	60	27861.78	269	255.51	956	1285
20	TRO2000885895	Fahri DEMİR	2017	ERKEK	Ocak	TEK	4716.07	578	26796.20	492	285.64	265	1335
21	TRO2000798801	Ramazan Koyuncu	2016	ERKEK	Şubat	TEK	5200.03	76	24889.49	1184	321.06	81	1341
22	TRO2000995579	Mehmet Sarımsak	2018	ERKEK	Ocak	TEK	4594.95	800	28665.70	162	274.90	424	1386

Şekil 5. Kolay indeks sonuçlarına ilişkin Excel sıralaması

4. Sonuç

Bu çalışmada açıklanan kolay indeks yöntemi, adından da anlaşılacağı üzere yetiştiriciler, ziraat mühendisleri ve veteriner hekimler tarafından pratik olarak kuzu seçmek amacıyla kullanılabilir. Kaplan ve arkadaşlarının (Kaplan ve ark., 2020) Anadolu mandalarında uyguladıklarını bildirdikleri bu yöntem mevcut çalışmada koyunlara uyarlanmış ve olumlu sonuç elde edilmiştir. Excel'e yönelik görsel ortam aracı eklentisi olarak geliştirilmekte olan Damızlık Asistanı yazılımı da hesabı hızlandırmakta ve basitleştirmektedir. Bu nedenle yöntemin alanın ilgilenenleri tarafından koyun yetiştiriciliğinde bilhassa kalıtım derecesi yüksek karakterlerde kullanışlı olabileceği ve bunun ıslah çalışmalarına ivme kazandıracağı kanaatine varılmıştır.

Katkı Oranı Beyanı

Yazar(lar)ın katkı yüzdesi aşağıda verilmiştir. Tüm yazarlar makaleyi incelemiş ve onaylamıştır.

	Y.K.	İ.G.	K.A.	M.T.
K	40	10	10	40
T	100			
Y	30			70
VTI	50	50		
VAY	70			30
KT	30	30	20	20
YZ	40	15	15	30
KI	30	20	20	30
GR	30	20	20	30
PY	30	20	20	30
FA	25	25	25	25

K= kavram, T= tasarım, Y= yönetim, VTI= veri toplama ve/veya işleme, VAY= veri analizi ve/veya yorumlama, KT= kaynak tarama, YZ= Yazım, KI= kritik inceleme, GR= gönderim ve revizyon, PY= proje yönetimi, FA= fon alımı.

Çatışma Beyanı

Yazarlar bu çalışmada hiçbir çıkar ilişkisi olmadığını beyan etmektedirler.

Etik Onay Beyanı

Bu çalışmada hayvanlar ve insanlar üzerinde herhangi bir çalışma yapılmadığı için etik kurul onayı alınmamıştır. Çalışmada, Adıyaman ilinde TAGEM/02IVES2014-01 numarasıyla yetiştirici şartlarında uygulanan İvesi alt projesinden sağlanan veriler kullanılmıştır.

Destek ve Teşekkür Beyanı

Yazarlar, Halk Elinde Hayvan Islahı Ülkesel Projesine verdikleri destekten dolayı T. C. Tarım ve Orman Bakanlığı Tarımsal Araştırmalar ve Politikalar Genel Müdürlüğü'ne teşekkür eder. Bu çalışma kısmen 2019 yılında Antalya'da gerçekleştirilen 1th International Livestock Science Congress 'de poster olarak sunulmuştur.

Kaynaklar

- Arpacık R. 1982. Sığır Yetiştiriciliği. Endeks yöntemi ile damızlık seçme. Uludağ Üniversitesi Basımevi, Bursa, Türkiye, ss: 163-164.
- Doğan S, Pekgör A, Soysal M. I. 2019. Standardization of environmental factor effecting production traits by least squares methods an examples of application by excel (LSM-ex). 12th World Buffalo Congress, 18-20 Eylül, İstanbul, Türkiye, ss: 42.
- Düzgüneş O, Eliçin A, Akman N. 2003. Hayvan ıslahı kitabı. İndeks denkleminin hesaplanması. Ankara Üniversitesi Ziraat Fakültesi Yayınları, 4. Baskı, Yayın no: 1535, Ankara, Türkiye, ss: 142-148.
- Ertuğrul M. 1997. Hayvan yetiştirme (yetiştiricilik) kitabı. Ankara Üniversitesi Basımevi, Ankara, Türkiye, 2. baskı, ss:65.
- Galal S, Gürsoy O, Shaat I. 2008. Awassi Sheep as a Genetic Resource AND Efforts for their genetic improvement-a review. Small Rumin Res, 79: 99-108.
- Harvey WF. 1960. Least squares analysis of data with unequal subclasses number. USDA Publisher, New York USA, pp: 2-8.
- Jawasreh KI, Haddad N, Lubad AA, Al-Amareen A. 2021. Genome-wide association study for milk production of Awassi sheep in Jordan. J Saudi Soc Agri Sci 21: 302-309. <https://doi.org/10.1016/j.jssas.2021.09.006>.
- Kaplan Y, Tekerli M. 2020. Wombat yazılımı kullanılarak malak doğum ağırlıklarında birey modeli uygulaması. Bahri Dağdaş Hay Araş Derg, 9(2): 105-118.
- Kaplan Y, Cinkaya S, Demirtaş M, Tekerli M. 2019. Application with a practical selection method of buffalo calves. 12th World Buffalo Congress, 18-20 Eylül, İstanbul, Türkiye, ss:59.
- Karabulut O, Tekin M.E. 2009. Damızlık koç seçiminde BLUP metodunun kullanılması. Kafkas Univ Vet Fak Derg, 15(6): 891-896.
- Pollotta G.E, Gootwineb E. 2001. A genetic analysis of complete lactation milk production in Improved Awassi sheep. Livestock Prod Sci, 71: 37-47. [https://doi.org/10.1016/S0301-6226\(01\)00239-1](https://doi.org/10.1016/S0301-6226(01)00239-1).
- Vanlı Y, Özsoy MK, Baş S, Kaygısız A. 2005. Populasyon ve Biyometrik Genetik Kitabı. Kovaryans analizinde düzeltme. Tekirdağ Ziraat Fakültesi, Yayın No: 286, Tekirdağ, Türkiye, ss: 82-83.



SUSTAINABLE AIRPORT MANAGEMENT AND AIRLINE MARKETING

Sevgi AYDIN^{1*}


¹Istanbul Beykent University, Faculty of Economics and Administrative Sciences, Department of Business, 34396, Istanbul, Türkiye

Abstract: The aviation sector comprises every industry that provides direct assistance to mechanical air transportation. The aviation industry includes a variety of institutions, such as military aviation companies, aircraft manufacturers, and various commercial establishments, all of which play important roles. The analysis of airline market shares was carried out within the realm of the aviation industry. Considering the ongoing trajectory of increasing airline market shares, it is crucial for firms to commit resources towards investing in this industry. Furthermore, a thorough evaluation of the existing literature revealed a dearth of research specifically focused on airline marketing. The primary objective of this research was to address the existing gap in the literature. Sustainable airport management and business, the airline industry, business-to-business analytics in the airline sector, customer satisfaction, and customer experience were some of the facets investigated in this study. In addition, the study seeks to provide a SWOT analysis of the airline marketing strategies employed by transportation corporations.

Keywords: Aviation, Airline industry, Airline marketing, Airport management, Customer satisfaction, SWOT Analysis

*Corresponding author: Istanbul Beykent University, Faculty of Economics and Administrative Sciences, Department of Business, 34396, Istanbul, Türkiye

E mail: sevgiaydin@beykent.edu.tr (S. AYDIN)

Sevgi AYDIN  <https://orcid.org/0000-0002-9507-5448>

Received: March 20, 2024

Accepted: April 19, 2024

Published: May 15, 2024

Cite as: Aydın S. 2024. Sustainable airport management and airline marketing. BSJ Eng Sci, 7(3): 478-487.

1. Introduction

Aviation has a pivotal role as the sole worldwide transportation network, serving as a vital catalyst for the advancement of global commerce and the enrichment of tourism. Air transportation plays a pivotal role in providing substantial social and economic advantages. By facilitating tourism and trade, it plays a significant role in fostering economic expansion. Additionally, it contributes to employment creation and augments tax income. The aviation industry plays a crucial role in facilitating the efficient transportation of individuals and goods around the globe. Aviation plays a crucial role in facilitating global commerce and tourism due to its unparalleled ability to create a speedy international transportation network. Facilitating economic progress, especially in emerging nations, is a crucial function that it performs. There are three distinct classifications for the economic impact: direct, indirect, and induced. Primary economic activity conducted by a particular industry within the immediate vicinity results in direct economic impacts. The presence of aviation operations leads to economic activity occurring beyond the immediate vicinity, resulting in indirect impacts. Induced impact refers to the multiplier effects resulting from the augmentation of employment and revenue, which stem from the direct and indirect economic consequences of the aviation industry (Acar and Karabulak, 2015; Vasigh et al., 2018).

Airlines are intricate entities, and the deeply ingrained

production orientation, which originated from monopolistic activities within a regulated sector, presents significant challenges to overcome. However, the airline industry widely recognizes that effective marketing, in its various manifestations, increasingly plays a pivotal role in achieving competitive success. Competition continues to operate within an environmental framework characterized by limited access to transportation channels and the restricted availability of free market alternatives (Driver, 1999).

The correlation between the quality of customer service and the degree of passenger demand is a crucial concern for air carriers, as it empowers airline executives to make strategic determinations on the necessary level of service and associated resources required to attain market share objectives (Suzuki et al., 2001).

Recent research on airports has highlighted the need to consider strategic interactions between airlines and market power when analyzing airport economics and policy. This necessitates a comprehensive assessment of both airports and airline services using an integrated approach. This stands in opposition to the conventional methodology wherein an airport directly encounters the needs of ultimate customers (passengers and shippers), therefore circumventing the involvement of airlines that operate within the airport. Alongside the carrier market structure, the contractual connection between an airport and its airlines is a significant element of the interaction between airports and airlines, wherein airlines, as



downstream customers, possess the ability to impact the operation of the airport (Ha et al., 2013).

The core of contemporary marketing practice revolves around comprehending, generating, conveying, and providing client value and pleasure. In contemporary business philosophy, the focal point is the client, as opposed to marketing, with the primary objective being the attainment of customer service satisfaction. In service-oriented sectors such as the aviation business, it is imperative for managers to possess a comprehensive understanding of customer demands and expectations, as well as to uphold commitments to effectively address the unique characteristics of services (Aksoy et al., 2003).

The prevalence of air travel has increased, leading to a wide range of options for customers and placing considerable strain on airline businesses. In order to thrive in a very competitive industry, the airline firm must comprehend client demands and satisfy them by providing top-notch services (Law et al., 2022). The airline business serves as a catalyst for economic growth, international commerce, tourism, and worldwide investments. Typically, this expansion benefits a range of industries that rely on airplanes, including hotels, retail, and transportation. The method by which airlines provide services to their clients with the aim of enhancing their pleasure has consistently been a critical concern for the organizations. Many authors have proposed a significant correlation between several elements of service quality and customer happiness (Tahanisaz and Shokuhyar, 2020).

There have been very few studies on the aviation market and planning in the literature. Schneider et al. (2013) attempted to improve knowledge of the causes, aspects, and forms of business model innovation, with an emphasis on the aviation sector. They employed an inductive, theory-building methodology that allowed patterns of business model innovation to emerge across several case studies of maintenance, repair, and overhaul (MRO) businesses in the aviation sector. Lytvyn et al. (2019) intended to research aviation aircraft flight planning. Their research topic is the creation of an aviation aircraft planning informational system project. Holland et al. (2020) used market-level data to analyze the relative performance of firms compared to specific competitors. Their demonstration highlighted the capability of utilizing consumer clickstream data, a significant form of big data, to establish a fresh collection of B2B analytical frameworks.

Ciliberto et al. (2021) presented an econometric model that enables the estimation of a game, including simultaneous entrance and price choices, while also accounting for potential correlations between unobservable cost and demand shocks. The researchers employed our framework to incorporate selection in the pricing phase and conducted an estimation of the model using data from the US airline sector. Their findings indicate that failure to consider endogenous entry results in an estimation bias for demand elasticities. Zhang et al.

(2021) obtained data on fly passengers from TravelSky in the Chinese market. In addition to aggregate passenger flow patterns, they investigated changes in airline passenger travel behavior, such as ticket booking time, passenger age distribution, refunds and ticket adjustments, and passenger arrival time at airports. Rizky (2023) aimed to determine whether B2B (Business to Business) and B2C (Business to Customer) marketing strategies affect the way students purchase airline tickets.

In addition, research that has been published in the academic literature and that has an emphasis on digital technology and marketing strategies was also investigated (Karaagaoglu and Cicek, 2019; Stone et al., 2020; Huang and Rust, 2021; Nalbant and Uyanik, 2021; Singh, 2021; Nalbant and Uyanik, 2022; Aydin et al., 2023; Aydin and Nalbant, 2023; Nalbant and Aydin, 2023; Nalbant et al. 2023; Nalbant and Aydin, 2024). These studies have investigated the significance of various digital technologies, such as the metaverse, artificial intelligence, augmented reality, virtual reality, and metahuman, in the context of digital marketing.

2. Materials and Methods

For investigating airline marketing, this study utilized the document analysis methodology. The graphs that were gathered from the different sources pertaining to airline marketing were studied by the researcher. The examination of the graphs reveals that there is a positive influence that airline marketing has on businesses. Document analysis is a research methodology that involves the systematic collection, examination, interrogation, and interpretation of diverse documents as the principal source of empirical data for scholarly investigation.

The acronym SWOT, which stands for "strengths, weaknesses, opportunities, and threats," is a crucial tool in strategic planning that both individuals and organizations can use. A procedure that includes detecting the possible flaws that an organization or corporation may possess is called "weakness identification." By utilizing a SWOT analysis, it is possible to assist in the identification of internal strengths and weaknesses, external opportunities to exploit, and prospective hazards to investigate, which in turn enables the creation of appropriate risk mitigation measures.

Figure 1 illustrates the distribution of marketing budgets dedicated to social media marketing throughout the global airline industry as of September 2017. According to the study findings, a notable proportion of respondents, specifically nine percent, reported allocating almost a quarter of their marketing budget on social media marketing (Statista-1, 2023).

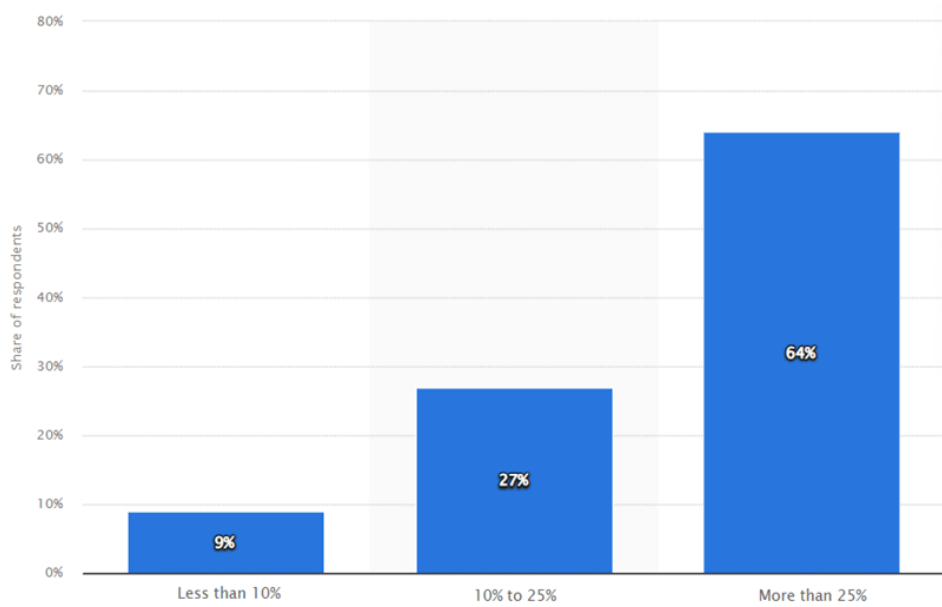


Figure 1. Social media marketing budget share for airlines worldwide in 2017.

The market for passenger air transportation is a thriving sector that transports people to destinations around the world. With operational revenue of approximately 50 billion U.S. dollars in 2022, American Airlines ranked as the second largest airline in North America. Passenger airlines may be subject to significant scrutiny regarding the comfort and satisfaction of their passengers. In terms of domestic market share in 2022, United Airlines, Delta Air Lines, American Airlines, and Southwest Airlines are the top-ranked airlines (Statista-2, 2023). During this era, American Airlines held a dominant position as the primary airline in the United States, commanding a 17.5 percent share of the domestic market. Delta Airlines followed suit with a market share of 17.3 percent (Figure 2).

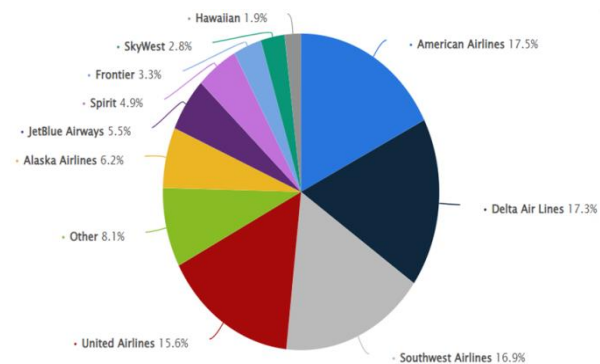


Figure 2. Domestic market share leaders in the United States from February 2022 to January 2023.

Figure 3 indicates that the worldwide aviation analytics market is expected to experience substantial growth, with its value projected to increase from USD 3.5 billion in 2022 to approximately USD 10.75 billion by 2032. Experts anticipate a significant growth in the worldwide aviation analytics market from 2023 to 2032, driven by a notable compound annual growth rate (CAGR) of 11.86%

(Precedence Statistics, 2023).

The exponential expansion of electronic commerce has significantly shifted consumer behavior towards digital platforms. In contemporary times, there is a prevailing expectation among consumers for expedited delivery durations and seamless delivery experiences. To fulfill these requirements, e-commerce enterprises depend on the expeditiousness and effectiveness of cross-border air transportation. Air cargo plays a significant role in facilitating these strategies by effectively facilitating the prompt transportation of products, enabling enterprises to maintain minimal inventory levels while efficiently meeting customer demands. The express air cargo market reached USD 90 billion in 2022 and is projected to grow at a compound annual growth rate (CAGR) of around 5.5% throughout the forecast period (Figure 4). The proliferation of electronic commerce has resulted in a substantial increase in the need for air freight services (Gminsights, 2023).

Based on the evaluation of the papers provided, it can be concluded that airline marketing plays a significant role in the aviation industry. Businesses should invest resources in the aviation industry sector to increase their market shares. Businesses can accomplish this by increasing their market share. It is essential for the company to place a priority on the satisfaction of their customers and to improve the overall quality of the services they provide.

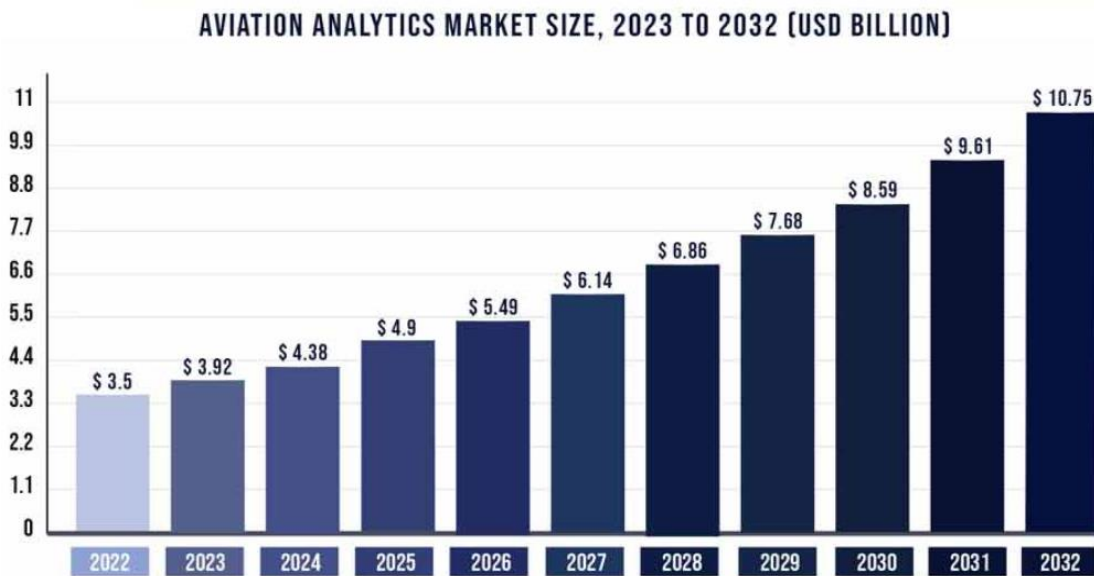


Figure 3. Global aviation analytics market size from 2023 to 2032 (USD billion).

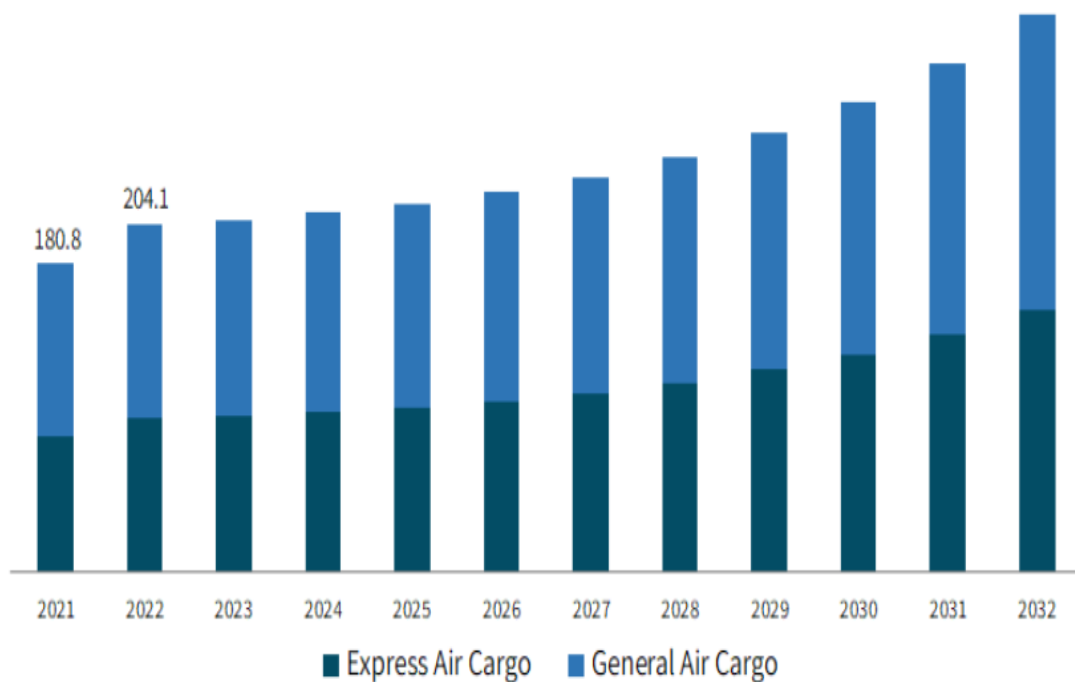


Figure 4. Market Size for Air Cargo Worldwide, By Service Type, 2021-2032 (USD billion).

2.1. Sustainable Airport Management and Business

The air transport industry is a multifaceted macroeconomic sector. In the aviation industry, a diverse range of activities are being carried out by a collaborative network of various entities. These entities include passenger and cargo airlines, integrators, airport authorities, handling agents, in-flight catering firms, general sales agents, car rental companies, air brokers, hardware providers such as aircraft manufacturers and air terminal building firms, as well as tour operators and travel agents. The primary objective of this network is to fulfill, to some extent, the demands of end consumers (Jarach, 2001).

Airports have a crucial role in stimulating the economic

vitality of a certain region. Hence, important performance and economic indicators are indicative of the quality of airport policies, infrastructure, amenities, multi-modal link development, quality assurance, and customer satisfaction. The consortiums accountable for the competitive administration of airports have seen gradual development over the past three decades, with a notable acceleration since 2010. These consortiums demonstrate a commitment to sustainable business practices and contribute to the growth of local economies (Zaharia et al., 2021).

Noncompeting airlines within a network of hub locations successfully transferred costs without facing opposition, despite the expectation of price rivalry among airlines.

The ability to transfer cost increases to non-competing airlines facilitated the management of airports. Established airlines acquired dominance over hub airports by utilizing the slot system due to airports' lack of proactive management and the perception that airlines with higher operating costs provide a more stable and reliable income compared to a landscape of intense competition among airlines and airports. In the realm of non-competing airlines, airport administrators perceived airports as a subsidiary aspect of public service rather than seeing them as a significant component of the burgeoning aviation industry (Barrett, 2000).

The development of airports with a focus on sustainability involves the delicate task of managing and reconciling several aspects of sustainability, including economic, social, environmental, and ecological considerations. The notion aligns with the broader framework of sustainable transportation and may be specifically characterized as the endeavor to fulfill present transportation and mobility requirements while safeguarding the capacity of future generations to fulfill their own demands in this regard. The topic discussed here pertains to the comprehensive management of an airport, which includes finance, operations, human resources, community and investor relations, and environmental considerations, among others. To achieve its objectives, sustainability in transportation must adhere to three fundamental prerequisites: (1) renewable resource consumption should not surpass their generation rates; (2) non-renewable resource consumption should not exceed the rate at which sustainable renewable alternatives are developed; and (3) pollutant emissions should not surpass the environment's capacity for assimilation (Amaeshi and

Crane, 2006; Durmaz, 2011).

2.2. B2B Analytics in the Airline Market

The impact of the pandemic on air freight markets was evident, albeit to a lesser extent. The reduction of passenger flights on international routes has resulted in a decrease in cargo capacity, as belly capacity typically accommodates around 50% of the cargo. Consequently, there has been an increase in demand for freighters. It is probable that this trend will persist in the forthcoming months, mostly attributable to the relaxation of laws governing cargo flights, encompassing cargo-only services operated by passenger aircraft. Nevertheless, it is imperative for airlines to exercise prudence when placing a substantial number of freighter conversion orders, particularly if they have the belief that the revival of passenger flights will eventually lead to an increase in belly capacity. Consequently, airlines may establish competitive pricing strategies for their cargo hold capacity. Furthermore, it is probable that airline bankruptcy and liquidation will lead to a decrease in the price of aircraft capacity in the short term. To make informed decisions on the expansion of freighter capacity, airlines must consider many criteria, such as their financial stability, the cost of freighters, the demand for cargo transportation, and the development of their network (Czerny et al., 2021).

The COVID-19 pandemic has significantly affected airline operations, hence impacting worldwide aviation supply and demand. Airlines themselves or authorities have cancelled numerous flights due to the closure of airports or routes (Mhalla, 2020). Table 1 presents the qualitative relationship between the positioning of each airport and its corresponding key market behaviors (Jarach, 2001).

Table 1. Five distinct airport market positioning strategies (Jarach, 2001)

Type	Market Positioning
Primary hub	The airport serves as a central point for the operations of one or more airlines. Typically constructed in prominent economic hubs that have the potential to independently produce substantial origin and destination (OandD) activities, encompassing both business and tourism sectors,
Secondary hub	As a result of the collaboration between the airport authority and a regional airline, the location has transformed into a central hub for a network of commercial routes characterized by high frequency and low population density. The development of a flag carrier can also be facilitated by the establishment of one or more major hubs that are strategically focused on short-haul operations.
Regional airport	The airport prioritizes point-to-point services, with a particular emphasis on flight segments catering to business-oriented clientele. Within this cluster, city airports can be considered a sub-categorization.
Low-cost airport	The primary objective of the airport is to recruit low-cost carriers, which necessitates a comprehensive reengineering of its whole production chain. This strategic initiative intends to minimize costs across the chain, ultimately resulting in reduced pricing for airline operators.
Cargo airport	The airport primarily focuses on attracting cargo operators and integrators as its primary business segment. The website offers a diverse range of technical infrastructures to support the operational needs of the freight company.

One reason for the growth of global aviation is the increasing ease with which individuals can plan and arrange their trips. Travel agents predominantly

facilitate the distribution of available tickets; however, several airlines have their own specialized city retail locations and are increasingly using direct selling

organizations via telephone. Airlines or groups of airlines play a crucial role in the efficacy of this intricate sales and booking system, particularly through the acquisition of computerized reservation systems (CRS). The proprietors of CRS impose subscription fees for agency utilization and levy booking fees on tickets sold by airlines. These fees eventually contribute to the distribution cost associated with promoting and selling tickets by appearing in the airfares. The reliance of both agencies and airlines on CRS has brought attention to the rising significance of distribution costs, particularly the margins charged for the services provided. Additionally, the utilization of data obtained via this method has become increasingly significant (Driver, 1999).

In the realm of e-commerce marketplaces, where several company rivals and search intermediaries compete for the attention of customers, the search patterns exhibited by consumers who link a price comparison engine with a competitor might serve as an indicator of a business-to-business (B2B) connection. The examination of search flows between two rival firms provides insights into the competitive dynamics and the level of rivalry between the organizations, as shown by the search behaviors exhibited by their respective customer bases. In the context of e-commerce marketplaces, it is crucial to comprehend how customers allocate their attention when navigating between the websites of different commercial organizations. This understanding serves as a significant performance indicator. Hence, the search patterns exhibited by consumers may be utilized to deduce the presence of business-to-business (B2B) connections as well as evaluate the effectiveness of rivals and search intermediaries (Holland et al., 2020).

During the latter part of the 1990s, there was a growing emphasis on B2B e-business as a key component of organizations' strategic initiatives. Concurrently, a notable proliferation of B2B e-marketplaces occurred. One notable recent advancement in the industry is the establishment of strategic alliances, partnerships, and mergers. These initiatives not only facilitate the coordination of schedules and fares but also seek to achieve cost reductions by using joint procurement opportunities. In recent times, airlines have conducted thorough investigations into the possibility of joint procurement opportunities and have implemented strategies to establish consortium-led e-marketplaces as intermediaries for consolidating demand and streamlining transactions. The emergence and development of virtual B2B e-marketplaces, facilitated by Internet-based information and communication technologies (ICT), is a significant innovation that transcends the limits of individual organizations and industries. This innovation generates value by introducing novel exchange mechanisms, distinct transaction techniques, and innovative forms of cooperation among participating firms (Wagner et al., 2004).

2.3. SWOT Analysis of Airline Marketing

Strengths, Weaknesses, Opportunities, and Threats (SWOT) analysis is a strategic framework that is used to identify and evaluate the internal opportunities and threats given by a firm, as well as the internal strengths and weaknesses that are inherent to the organization. This framework is also used to discover and analyze the external strengths and weaknesses that are inherent to the organization. S.W.O.T. statements are another name for this type of analysis.

Table 2. SWOT Analysis of Airline Marketing

Strengths	Weaknesses
<ul style="list-style-type: none"> a) Travel for commercial purposes is in high demand. b) High demand for the service. c) Rapid and secure transportation. d) An enormous number of clients that use the services provided by the aviation sector. e) Operating in markets that are expanding. 	<ul style="list-style-type: none"> a) Insufficient levels of satisfaction among customers. b) Insufficient allocation of resources for commercial strategy and marketing. c) Operating in markets where prices are subject to fluctuation. d) A significant amount of competition is focused on pricing. e) Inadequate participation on social media platforms.
Opportunities	Threats
<ul style="list-style-type: none"> a) Fresh airplanes and emerging markets. b) The tourism industry's continued expansion. c) Achieve the position of the airline brand as the most powerful player in the market. d) The advancement of the current technological status. e) Collaboration with other organizations working to advance economic growth. 	<ul style="list-style-type: none"> a) Increased air services are available at other airports. b) Rise in gasoline surcharges. c) Key competitors are getting a larger proportion of the market. d) Insufficient funding for the airport's construction hinders its upkeep. e) Insufficient compatibility of the brand with the worldwide market.

It is necessary to undertake a comprehensive SWOT analysis to carry out an in-depth examination of the use of airline marketing within the context of digital transformation (Table 2). In recent years, there has been considerable growth in the application of this model in the process of making strategic plans for businesses operating on a local, national, and worldwide scale, as well as for a wide variety of governmental organizations.

2.4. Customer Satisfaction and Experience

The airline sector has long been renowned for its ongoing problems, which encompass cost reduction, the

management of shifting demand, adherence to stringent quality standards, the provision of exceptional services, and the fulfillment of diverse client expectations. The subject of the airline customer experience garners significant attention due to its significance, intricacy, and considerable deficiencies. It is imperative for airlines to prioritize the customer experience and strive for excellence. Since the "customer service revolution" began some decades ago, extensive business research has examined customer satisfaction and the establishment of customer-centric firms. Various stakeholders, including business consultants and companies, have endeavored to ascertain the attributes exhibited by firms that continuously achieve customer pleasure. In addition, they have strived to devise mechanisms for effectively monitoring client contentment and establishing continuous quality improvement systems that are responsive to consumer input (Baker, 2014).

Assessing customer satisfaction serves as a valuable means of gauging if consumers have received service that aligns with their expectations. Building client relationships is a crucial element in business operations. Businesses frequently evaluate customer happiness by comparing their experiences with their pre-existing expectations. To achieve success and generate profitability for a business, it is imperative to effectively meet the needs and expectations of consumers. Airlines are a subset of commercial enterprises that place a significant emphasis on ensuring the contentment and allegiance of their passengers. Numerous airline managers tend to approach passenger requirements primarily from their own subjective standpoint. Nevertheless, the wants and expectations of customers are undergoing transformation in contemporary times. Hence, it is imperative for airlines to consider customer relationship management (CRM) as a strategic investment, yielding substantial advantages via the establishment and maintenance of lucrative, enduring customer relationships. CRM encompasses the process of acquiring and implementing customer knowledge to enhance the airline's ability to offer its services with greater efficiency. Moreover, CRM is a fundamental element of airlines' business strategy, serving to distinguish themselves from other companies. Airlines employ CRM as a strategic approach to personalize services and establish enhanced communication channels with consumers (Ahadmotlaghi and Pawar, 2012; Salah, and Abou-Shouk, 2019).

Now, it has become convenient for all individuals to readily use air transportation services from their designated air terminals. The provision of superior services to consumers within a fiercely competitive landscape is the primary factor that confers a competitive edge, leading to the triumph and enduring expansion of an airline. In response to heightened competition within the air transport industry over the past decade, several airlines have shifted their focus towards enhancing airline service quality as a means of enhancing customer

satisfaction. The competitive advantage of a firm is influenced by the conditions of service quality, since it plays a crucial role in fostering client loyalty and therefore, market share. Ensuring the provision of superior service to customers is crucial for the long-term viability of airlines. Consequently, airlines must consider the preferences and expectations of passengers in relation to their services. Service quality may be defined as the comprehensive perception that a client holds on the relative effectiveness and provision of services by an organization (Agarwal and Gowda, 2021).

Leisure travelers show a strong and positive correlation between customer satisfaction and customer loyalty. However, business travelers do not show increased customer loyalty despite receiving satisfactory service. This finding holds significant implications for airline operators, particularly considering the crucial role of business passengers in contributing to the profitability of airlines. In the examination of factors influencing customer happiness and loyalty, it is imperative to establish clear delineations between business and pleasure travelers. This is due to the evident divergence in their choices pertaining to airfare and service quality. For instance, the study found that the cost of tickets had a statistically significant and positive influence on the overall happiness of leisure travelers. This, in turn, had a reinforcing effect on their loyalty to the airline. However, the research did not find any significant relationship between ticket price and contentment or loyalty among business passengers. The probit models computed indicate that some demographic factors, including gender, income, and education, exhibit statistical significance for one set of passengers but not for another. To enhance consumer loyalty, companies must employ diverse marketing methods tailored to target distinct market groups (Jiang and Zhang, 2016).

3. Results

Industry experts project substantial expansion of the global aviation analytics market between the years 2023 and 2032. Industry experts project that the global aviation analytics market will experience substantial expansion between the years 2023 and 2032, propelled by a noteworthy compound annual growth rate (CAGR) of 11.86%. The rapid growth of electronic commerce has brought about a notable transformation in consumer behavior, leading to a substantial shift towards digital platforms. In the present era, there is a dominant expectation among customers for accelerated delivery timeframes and flawless delivery encounters. To meet these stipulations, e-commerce firms rely on the promptness and efficiency of cross-border air transportation. Air cargo plays a crucial role in supporting these initiatives by successfully facilitating the timely shipment of goods, allowing businesses to maintain low inventory levels while efficiently satisfying consumer requirements.

It has been concluded, based on the findings of the SWOT

analysis, that the selling of airline tickets has a substantial number of prospective advantages and benefits that are due to materialize in the future. The fact that this idea is still in its infancy is given a positive aspect because of this. The area of airline marketing studies, on the other hand, lays a substantial amount of attention on the major contributions that have been made by researcher. In the not-too-distant future, it is anticipated that there will be an increase in the number of individuals who use the airline for the sake of marketing and promotional reasons.

4. Discussion

The allocation of marketing funds specifically designated for social media marketing within the worldwide airline business has significant importance. The passenger air transportation market is a robust industry that facilitates the global movement of individuals to various locations. In the year 2022, investors made significant investments. Experts anticipate considerable growth for this investment in the subsequent years. Industry experts project significant expansion in the global aviation analytics industry.

The process of building airports with a focus on sustainability calls for the meticulous management and coordination of numerous aspects of sustainability. These aspects include economic, social, environmental, and ecological considerations. The COVID-19 pandemic has had a significant impact on the day-to-day operations of airlines, which has had a knock-on effect on the supply and demand dynamics of the aviation sector on a worldwide scale.

When engaging in strategic planning, it is imperative to conduct a comprehensive analysis of the client's requirements and expectations. This is done to ensure the efficacy of the planning process. To successfully formulate a comprehensive strategic plan for a corporation, it is crucial to gather a significant quantity of information. To obtain this information, one can utilize analytical approaches such as SWOT analysis and other similar procedures. Strategic marketing planning empowers organizations to sustain their operations and efficiently handle market risks. As a result, this provides them with a distinct advantage over their competitors. Companies can achieve both of these qualities by implementing strategic marketing planning, which is the main factor responsible for enabling them.

5. Conclusion

The attainment of higher market shares in the civil aviation transportation sector and the formulation of effective competitive strategies are contingent upon a multitude of elements. When competing for a larger piece of the expanding aviation industry, airlines must place a big emphasis on airline marketing if they wish to be successful. Airline firms need to implement successful marketing strategies, precisely segment their customers,

and make good use of marketing mix apps to achieve success and acquire a competitive edge. Airlines must conduct routine reviews and make necessary adjustments to the marketing methods they employ to satisfy the requirements of their clientele. By using this strategy, individuals will have the chance to build a firm foundation, which will enable them to take advantage of a predicted portion of the rising market for air transportation in the years to come. This opportunity will arise because individuals will adopt this technique.

In the context of e-commerce marketplaces, in which different businesses compete with one another for the attention of customers, the search behaviors exhibited by customers who use a price comparison engine in combination with a rival might possibly signal a B2B association. This is because customers in this scenario are more likely to be looking for a better deal. Because of its significance, complexity, and glaring deficiencies, the subject of the airline customer experience has garnered a significant amount of attention in recent years. Airlines are required to place an emphasis on the whole customer experience and strive toward excellence.

Based on an analysis of the available literature, it is possible to deduce that the significance of airline marketing holds considerable weight in the domain of the aviation sector. When considering strategies for market expansion, organizations should prioritize the allocation of resources to the aviation industry sector. One potential strategy for a corporation to attain its objective is by enhancing its market share. Ensuring client satisfaction and enhancing service quality are crucial for the company's success. Furthermore, it is vital for the organization to augment the general caliber of the services they provide.

Author Contributions

The percentage of the author(s) contributions is presented below. The author reviewed and approved the final version of the manuscript.

	S.A.
C	100
D	100
S	100
DCP	100
DAI	100
L	100
W	100
CR	100
SR	100
PM	100
FA	100

C=Concept, D= design, S= supervision, DCP= data collection and/or processing, DAI= data analysis and/or interpretation, L= literature search, W= writing, CR= critical review, SR= submission and revision, PM= project management, FA= funding

acquisition.

Conflict of Interest

The author declared that there is no conflict of interest.

Ethical Consideration

Ethics committee approval was not required for this study because of there was no study on animals or humans.

References

- Acar AZ, Karabulak S. 2015. Competition between full service network carriers and low cost carriers in Turkish airline market. *Procedia Soc Behav Sci*, 207: 642-651.
- Agarwal I, Gowda KR. 2021. The effect of airline service quality on customer satisfaction and loyalty in India. *Mater Today Proc*, 37: 1341-1348.
- Ahadmotlaghi E, Pawar P. 2012. Analysis of CRM programs practiced by passengers'airline industry of India and its impact on customer satisfaction and loyalty. *Res World J Arts Sci Commer*, 3(2 Part 2): 119.
- Aksoy S, Atilgan E, Akinci S. 2003. Airline services marketing by domestic and foreign firms: differences from the customers' viewpoint. *J Air Transp Manag*, 9(6): 343-351.
- Amaeshi KM, Crane A. 2006. Stakeholder engagement: a mechanism for sustainable aviation. *Corp Soc Resp Env Ma*, 13(5): 245-260.
- Aydin S, Nalbant KG, Altuntas C. 2023. Artificial intelligence in digital transformation and sustainable green marketing strategies in the European green consensus process. *İmgelem*, 7(13): 467-492.
- Aydin S, Nalbant KG. 2023. The significance of artificial intelligence in the realms of marketing advertising and branding inside the metaverse. *J Emerg Econ Policy*, 8(2): 301-316.
- Baker D. 2014. Low-cost airlines management model and customer satisfaction. *Int J Econ Commer Manag*, 2(9): 1-17.
- Barrett SD. 2000. Airport competition in the deregulated European aviation market. *J Air Transp Manag*, 6(1): 13-27.
- Ciliberto F, Murry C, Tamer E. 2021. Market structure and competition in airline markets. *J Pol Econ*, 129(11): 2995-3038.
- Czerny AI, Fu X, Lei Z, Oum TH. 2021. Post pandemic aviation market recovery: Experience and lessons from China. *J Air Transp Manag*, 90: 101971.
- Driver JC. 1999. Developments in airline marketing practice. *J Marketing Pract: Appl Mark Sci*, 5(5): 134-150.
- Durmaz V. 2011. Organizational change for the environmentally sustainable airport management. *EMAJ: Emerg Mark J*, 1(2): 13-20.
- Gminsights. 2023. Air cargo market. URL: <https://www.gminsights.com/industry-analysis/air-cargo-market> (accessed date: October 11, 2023).
- Ha HK, Wan Y, Yoshida Y, Zhang A. 2013. Airline market structure and airport efficiency: Evidence from major Northeast Asian airports. *J Air Transp Manag*, 33: 32-42.
- Holland CP, Thornton SC, Naudé P. 2020. B2B analytics in the airline market: Harnessing the power of consumer big data. *Ind Mark Manag*, 86: 52-64.
- Huang MH, Rust RT. 2021. A strategic framework for artificial intelligence in marketing. *J Acad Mark Sci*, 49v 30-50.
- Jarach D. 2001. The evolution of airport management practices: towards a multi-point multi-service marketing-driven firm. *J Air Trans Manag*, 7(2): 119-125.
- Jiang H, Zhang Y. 2016. An investigation of service quality customer satisfaction and loyalty in China's airline market. *J Air Trans Manag*, 57: 80-88.
- Karaagaoglu N, Cicek M. 2019. An evaluation of digital marketing applications in airline sector. *J Hum Sci*, 16(2): 606-619.
- Law CC, Zhang Y, Gow J. 2022. Airline service quality customer satisfaction and repurchase intention: Laotian air passengers' perspective. *Case Stud Transp Pol*, 10(2): 741-750.
- Lytvyn V, Kowalska-Styczen A, Peleshko D, Rak T, Voloshyn V, Noennig JR, Vysotska V, Nykolyshyn L, Pryshchepa H. 2019 September. Aviation Aircraft Planning System Project Development. In: Shakhovska N, Medykovskyy MO editors. *Advances in Intelligent Systems and Computing IV*. CSIT 2019. *Advances in Intelligent Systems and Computing*, Springer, Cham, vol 1080, pp: 315-348. https://doi.org/10.1007/978-3-030-33695-0_23.
- Mhalla M. 2020. The impact of novel coronavirus (COVID-19): on the global oil and aviation markets. *J Asian Sci Res*, 10(2): 96.
- Nalbant KG, Aydin S, Uyanik S. 2023. Generative adversarial network and digital art interactions with metaverse marketing. *Trakya Uni J Soc Sci*, 25(2): 375-396.
- Nalbant KG, Aydin S. 2023. Development and transformation in digital marketing and branding with artificial intelligence and digital technologies dynamics in the metaverse universe. *J Metaverse*, 3(1): 9-18.
- Nalbant KG, Aydin S. 2024. Marketing strategies and benefits in the real estate industry in technologically advancing urban areas. *J Urban Acad*, 17(2): 606-625.
- Nalbant KG, Uyanik S. 2021. Computer vision in the metaverse. *J Metaverse*, 1(1): 9-12.
- Nalbant KG, Uyanik S. 2022. A look at the new humanity: metaverse and metahuman. *Int J Comput*, 2022: 7.
- Precedence Statistics. 2023. Aviation analytics market. URL: <https://www.precedence-research.com/aviation-analytics-market> (accessed date: October 23, 2023).
- Rizky H. 2023. The influence of B2B (Business to Business): and B2C (Business to Customer): Marketing strategies on how to purchase lion group aircraft tickets in the public environment. *J Soc Res*, 2(8): 2688-2697.
- Salah M, Abou-Shouk MA. 2019. The effect of customer relationship management practices on airline customer loyalty. *J Tour Herit Serv Mark*, 5(2): 11-19.
- Schneider S, Spieth P, Clauss T. 2013. Business model innovation in the aviation industry. *Int J Prod Dev*, 18(3-4): 286-310.
- Singh B. 2021. Predicting airline passengers' loyalty using artificial neural network theory. *J Air Transp Manag*, 94 102080.
- Statista-1. 2023. Airline social media marketing budget share. URL: <https://www.statista.com/statistics/368606/airline-social-media-marketing-budget-share/> (accessed date: November 9, 2023).
- Statista-2. 2023. Domestic market share of leading us airlines. URL: <https://www.statista.com/statistics/250577/domestic-market-share-of-leading-us-airlines/> (accessed date: November 15, 2023).
- Stone M, Aravopoulou E, Ekinci Y, Evans G, Hobbs M, Labib A, Laughlin P, Machtynger J, Machtynger L. 2020. Artificial intelligence (AI): in strategic marketing decision-making: a research agenda. *The Bot Lin*, 33(2): 183-200.
- Suzuki Y, Tyworth JE, Novack RA. 2001. Airline market share and customer service quality: a reference-dependent model. *Transp Res Part A: Pol Pract*, 35(9): 773-788.
- Tahanisaz S, Shokuhyar S. 2020. Evaluation of passenger

- satisfaction with service quality: A consecutive method applied to the airline industry. *J Air Trans Manag*, 83: 101764.
- Vasigh B, Fleming K, Tacker T. 2018. *Introduction to air transport economics: from theory to applications*. Routledge.
- Wagner CM, Sweeney E, Smyth A. 2004. A new hub in the aviation industry: towards an integration of B2B e-marketplaces in the airline industry. Working Paper. In *The Purchasing Function: Walking a Tightrope*, Proceedings of the 13th International Purchasing and Supply Education and Research Association (IPSERA) Conference, Catania, Italy, 10-13nApril, pp: 730-741.
- Zaharia SE, Pietreanu CV, Pavel AP, Boc RE. 2021. Globalization of airport management groups. In: Pamfilie R, Dinu V, Tăchiciu L, Pleșea D, Vasiliu C, editors. 2021. 7th BASIQ International Conference on New Trends in Sustainable Business and Consumption, Foggia, Italy, 3-5 June 2021, pp: 698-704
- Zhang L, Yang H, Wang K, Bian L, Zhang X. 2021. The impact of COVID-19 on airline passenger travel behavior: An exploratory analysis on the Chinese aviation market. *J Air Transp Manag*, 95: 102084.



THE IMPACT OF DEVICE TYPE NUMBER ON IOT DEVICE CLASSIFICATION

Ahmet Emre ERGÜN^{1*}, Özgü CAN²

¹*İzmir Katip Çelebi University, Faculty of Engineering and Architecture, Department of Computer Engineering, 35620, İzmir, Türkiye*


²*Ege University, Faculty of Engineering, Department of Computer Engineering, 35100, İzmir, Türkiye*


Abstract: Today, connected systems are widely used with the recent developments in technology. The internet-connected devices create data traffic when communicating with each other. These data may contain extremely confidential information. Observers can obtain confidential information from the traffic when the security of this traffic cannot be adequately ensured. This confidential information can be personal information as well as information about the type of device used by the person. Attackers could use machine learning to analyze encrypted data traffic patterns from IoT devices to infer sensitive information, even without decrypting the actual content. For example, if someone uses IoT devices for health monitoring or smoke detection, attackers could leverage machine learning to discern victims' habits or identify health conditions. An increase in the number of IoT devices may decrease the accuracy of classification when using machine learning. This paper presents the importance of the effect of device type number on the classification of IoT devices. Therefore, inference attacks on privacy with machine learning algorithms, attacks on machine learning models, and the padding method that is commonly used against such attacks are presented. Moreover, experiments are carried out by using the dataset of the traffic generated by the Internet of Things (IoT) devices. For this purpose, Random Forest, Decision Tree, and k-Nearest Neighbors (k-NN) classification algorithms are compared, and the accuracy rate changes according to the number of devices are presented. According to the results, the Random Forest and Decision Tree algorithms are found to be more effective than the k-NN algorithm. When considering a scenario with two device types, the Random Forest and Decision Tree algorithms achieved an accuracy rate of 98%, outperforming the k-NN algorithm, which had an accuracy rate of 95%.

Keywords: Classification, Internet of things (IoT), Machine learning, Padding, Privacy, Trade-off

*Corresponding author: İzmir Katip Çelebi University, Faculty of Engineering and Architecture, Department of Computer Engineering, 35620, İzmir, Türkiye

E mail: ahmetemreergun95@gmail.com (A. E. ERGÜN)

Ahmet Emre ERGÜN  <https://orcid.org/0000-0002-3025-5640>

Özgü CAN  <https://orcid.org/0000-0002-8064-2905>

Received: September 01, 2023

Accepted: April 26, 2024

Published: May 15, 2024

Cite as: Ergün AE, Can Ö. 2024. The impact of device type number on IoT device classification. BŞJ Eng Sci, 7(3): 488-494.

1. Introduction

The use of Internet of Things (IoT) devices is higher than it has ever been, and it is expanding rapidly. The number of cyber threats has increased considerably with the widespread use of these IoT devices. In particular, devices such as cameras, sensors, smartphones, smart clocks, heat meters that are connected to the Internet create various security problems. These devices create data traffic when communicating with each other. If the security and privacy of this data traffic cannot be ensured sufficiently, threats may occur. Attackers who observe data traffic can infer highly confidential information from that traffic (Ergün and Can, 2022a). For this purpose, machine learning algorithms are used to classify the IoT devices and also the type of these devices. Thus, devices that are used in the traffic can be detected and their device models or manufacturer information can be identified. Thereupon, attackers gain large amounts of sensitive information as IoT devices collect significant amount of data. For example, the privacy of personal health information may be violated by detecting wearable devices that measure blood pressure and pacemakers. Also, the location information tracked from

a detected device such as a smartphone or a smartwatch may also result in a privacy violation (Kröger, 2018). Similarly, the smoke sensor information can be used to obtain the smoking habit of the individual.

The machine learning techniques used by the traffic observer extract packet features from encrypted IoT device traffic as input. The encrypted packets' transmission time and packet size characteristics are visible to the observer. Additionally, the observer uses them to categorize IoT devices and anticipates having a high probability of success in accessing accurate data about different device types in the traffic. The fundamental concept behind deploying machine learning is the attacker model's capacity to learn data characteristics like packet size and transmission time, even when the traffic is encrypted. As a result, privacy leakage occurs. Therefore, obfuscating the traffic is needed to falsify the machine learning algorithms. Enhancing communication privacy without degrading network performance is crucial. For this purpose, the padding method is used to prevent traffic classification, to improve the communication privacy and preserve user privacy.



The goal of the packet padding mechanism is to mitigate the challenges in preserving privacy in IoT (Pineiro et al., 2020). Thus, padding is applied to the packet size to disguise the packet size. The goal of this study is to present the privacy threats in IoT traffic, privacy attacks against internet-connected devices, the padding method that is widely used against these attacks, and an evaluation based on Random Forest, Decision Tree and k-NN classification algorithms that are widely used in attacks. For this purpose, the experimental results are compared by the device type number and the related machine learning algorithms that are used for the classification. Thus, the study shows the effect of the number of device types and the chosen machine learning method on the accuracy rates. The organization of this study is as follows: In Section 2, the commonly used machine learning methods, the padding method used to preserve privacy, and attacks on machine learning methods are explained. In Section 3, Random Forest, Decision Tree and k-NN algorithms are evaluated to infer device type. Results and the accuracy rates are presented in Section 4. Finally, Section 4 concludes and outlines the future work.

2. Materials and Methods

2.1. Machine Learning Methods Commonly Used in Attacks

Machine learning methods can be used for inferences made from the traffic of devices connected to the Internet, and the rate of inference can vary according to the selected algorithm. Machine learning algorithms commonly used in attacks on privacy are Random Forest, Decision Tree, and k-NN. Random Forest, as the name

suggests, consists of a large number of individual decision trees that work as a community (Abdulkareem and Abdulazeez, 2021). Each tree in the Random Forest predicts a class and the class with the most votes becomes the model’s prediction. Using the Random Forest algorithm, in the work of (Dogru and Subasi, 2018), they reached 92% accuracy. Decision Tree algorithm deals with developing decision making models based on the true values of data features (Alghuried, 2017). These algorithms work by teaching the system how to classify and predict data (Charbuty and Abdulazeez, 2021). The algorithms look for the tree structure until a selection is made. (Aksoy and Gunes, 2019) used the Decision Tree algorithm to identify 33 IoT devices with a high accuracy of 98%. k-Nearest Neighbor (k-NN) algorithm is a widely used non-parametric classification method (Wang et al., 2021). It is used for classification and regression of data. An important feature of any kNN technique for classification or regression is to find the k-NN that allows us to estimate the value or class for a given point (Gawri et al., 2022). Pineiro et al. (2020) has achieved 94% accuracy rate by using the k-NN algorithm in their studies.

The model in which the traffic observer (attacker) observes the data transmission between the victim and the IoT device and obtains data after taking the resulting data into the machine learning process is shown in Figure 1. The attacker first gathers encrypted data and analyzes traffic using packet sent times and packet sizes. The attacker classifies the data with machine learning algorithms, allowing him/her to infer the types of devices the victim uses.

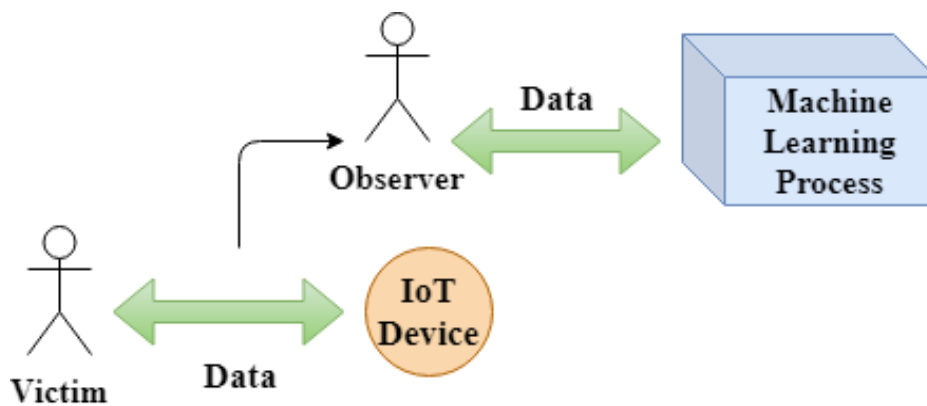


Figure 1. Attack model

2.2. Padding Method

An attacker watching the traffic can make inferences about the traffic even though the traffic is encrypted. This can create serious threats to privacy. The attacker can optimize the packet sizes in the traffic using machine learning algorithms. Packet sizes can cause information leakage about the device type. Therefore, these packets appear as larger bytes than they originally were, thanks to the padding method based on changing traffic packet

sizes. It is a very effective method in reducing the accuracy of the attacker’s machine learning. Adding the least amount of padding while determining the amount of padding is extremely important for the utility of traffic. Therefore, the amount of pad should be the minimum required. Strategies aiming to maintain the privacy-utility trade-off against different scenarios and data types have been discussed in the literature (Ergün and Can, 2022b). But, despite these various strategies aiming to

maintain the privacy-utility trade-off against different scenarios and data types, there is no single optimal padding strategy in the literature that can be applied for every scenario and data type. The visualized version of

the model in which the size of the original packet is increased in the padding method is shown in Figure 2. Packet size may vary depending on the determined padding strategy.

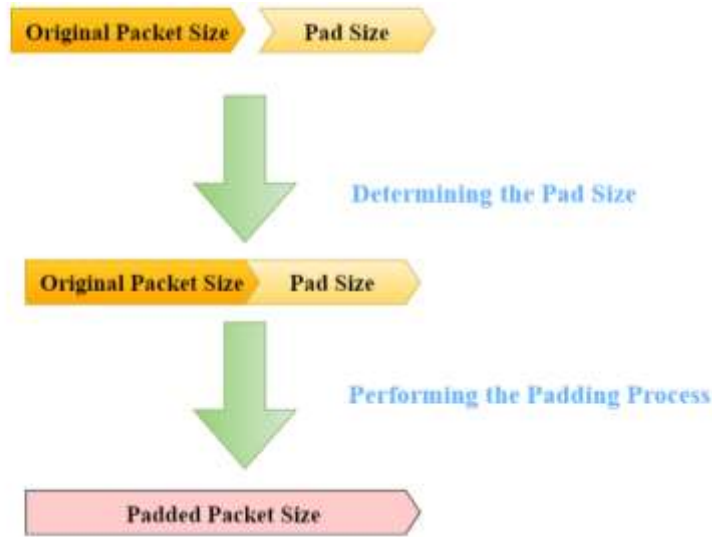


Figure 2. Padding model.

2.3. Attacks against Machine Learning

As the opposite of the scenario in Section 2.1, the roles of attacker and victim are reversed. In this situation, the attacker represents the person owning IoT devices, while the victim is the one aiming to deceive the attacker's machine learning-based classification system. The victim uses techniques to mislead the attacker's model, causing misclassification or a drop in performance. In Adversarial Examples, also known as Evasion Attack, the attacker can mislead the victim's machine learning model with incorrect training data (Kwon et al., 2018). The correct prediction percentage of the machine learning model, which uses adversarial examples in the training data, is reduced. In order to carry out this attack, the attacker trains his own Generative Adversarial Network with the victim's model. It then corrupts the inputs at the time of the test, allowing the victim model to make the wrong decision (Biggio et al., 2013).

Poisoning Attack increases the errors in the testing phase of the machine learning model with the training data produced by the attacker (Biggio et al., 2012). Tolpegin et al. (2020) are used data poisoning attack against federated learning systems. They also proposed defense system against this attack. In the work of Yerlikaya and Bahtiyar (2022), various machine learning algorithm's robustness and performance against adversarial examples are analyzed. In their work, for almost all datasets, some machine learning algorithms exhibit superior robustness and performance results against adversarial attacks.

3. Results

In this section, the findings obtained by using commonly used machine learning algorithms and the dataset of

Sivanathan et al. (2018) are evaluated. In the work of (Alex et al., 2023), it is shown that Sivanathan et al. (2018) dataset large in terms of size, with tens of millions of records, while the others remained in the hundreds of thousands. It was observed in which algorithm the attacker achieved higher results. Experiments were carried out on the data set that Sivanathan et al. (2018) created in his study. From this data set, 3 different experiments were carried out using 2, 4 and 6 IoT devices. 80% of the data was used as training data and 20% as test data. Sivanathan et al. (2018) dataset consists of 10 attributes, one of which is the target attribute. Since encrypted IoT traffic contains only time and packet size features to predict target attribute, our results are lower than those in Sivanathan et al. (2018) work. The test results are shown in Table 1. In the first experiment in which 6 devices were used, 84% accuracy rate was obtained with the Random Forest algorithm, which is widely used in classification, 84% with the Decision Tree algorithm, and 71% with the k-NN algorithm. In the second experiment, 4 devices were used and it was observed that the accuracy rates increased for all 3 algorithms. In the experiment with 4 devices, 88% accuracy rate was obtained with the Random Forest algorithm, 88% with the Decision Tree algorithm, and 85% with the k-NN algorithm. In the third experiment, 2 devices were used. In Random Forest and Decision Tree algorithms, 98% accuracy rate, and 95% accuracy rate in k-NN algorithm has been achieved. The devices used in the experiments are 'Amazon Echo', 'Belkin wemo switch', 'Insteon camera', 'Netatmo welcome', 'Smart things', 'Withings smart baby monitor'.

In Figure 3, the device types and packet numbers in the experiment in which 2 devices were used are shown. The

device types and packet numbers in the experiment in which 4 devices were used are shown in Figure 4. In Figure 5, the types and numbers of devices in the experiment in which 6 devices were used are shown. In three different scenarios, IoT devices with the data numbers closest to each other in Sivanathan et al. (2018) dataset were selected. Having data numbers close to each other during the classification process allows more reliable inferences to be made about the performance and accuracy of machine learning algorithms. The confusion matrices of Random Forest, Decision Tree and k-NN algorithms in experiments using 2, 4 and 6 device types are shown in Figure 6, 7, 8. These matrices showcase the accuracy of each algorithm by showing the

numbers of true and predicted labels for each type of device. The results show that the number of accurate predictions declines with increasing device kinds. In particular, confusion increases with four and six device types, indicating that these circumstances involve more complexity and uncertainty in prediction, but confusion decreases and classification accuracy increases with only two devices.

As seen in Table 1, the accuracy rates of the Random Forest and Decision Tree algorithms are higher than the k-NN algorithm in experiments where 2, 4 and 6 devices are used. As the number of devices increases, accuracy decreases as the diversity in classification increases.

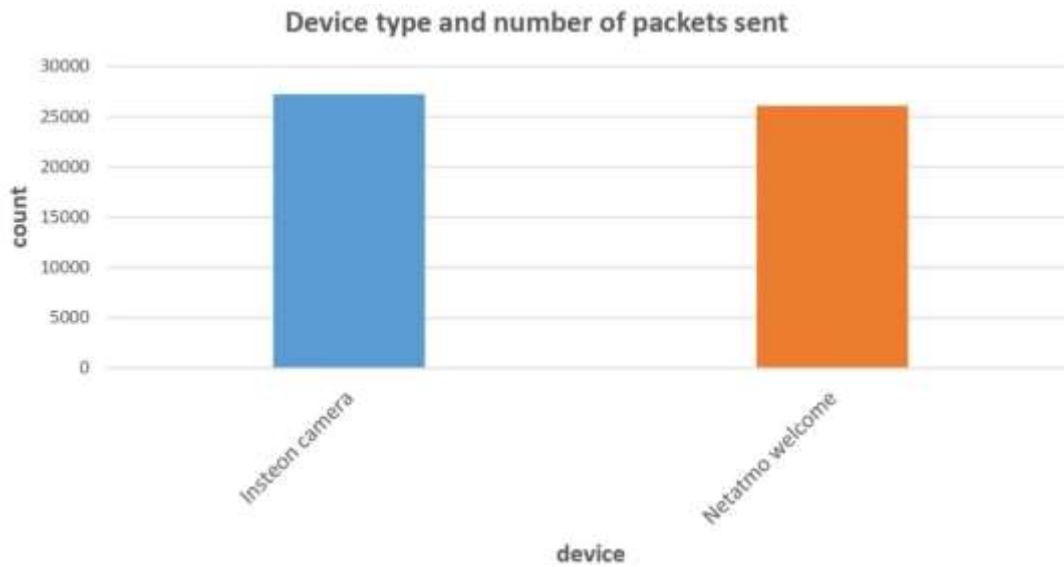


Figure 3. 2 device types and number of packets sent.

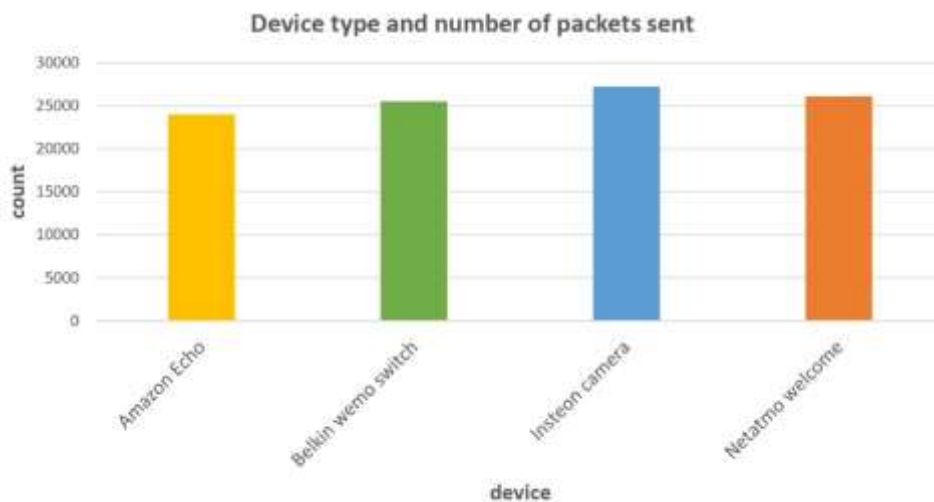


Figure 4. 4 device types and number of packets sent

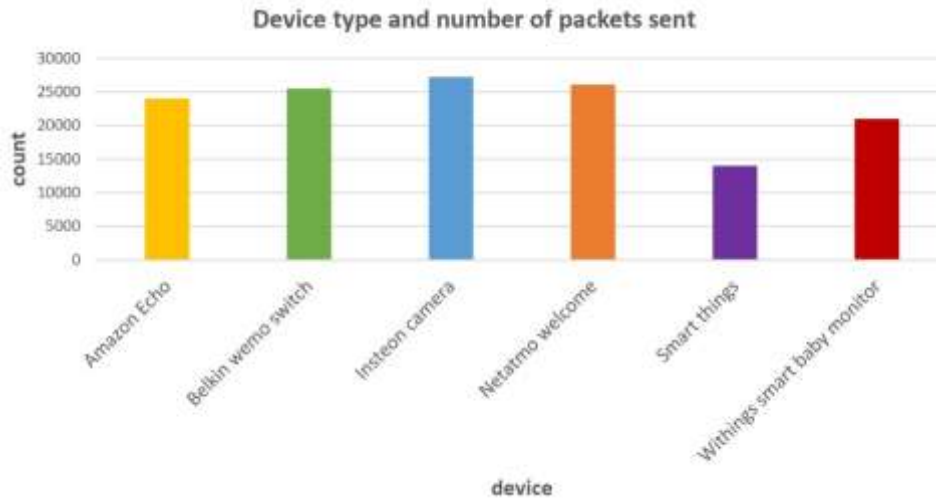


Figure 5. 6 device types and number of packets sent

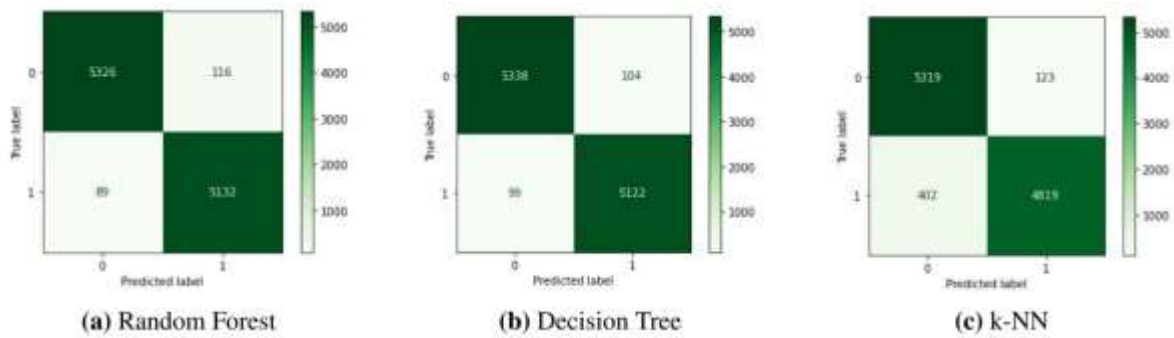


Figure 6. Confusion Matrix for 2 device types

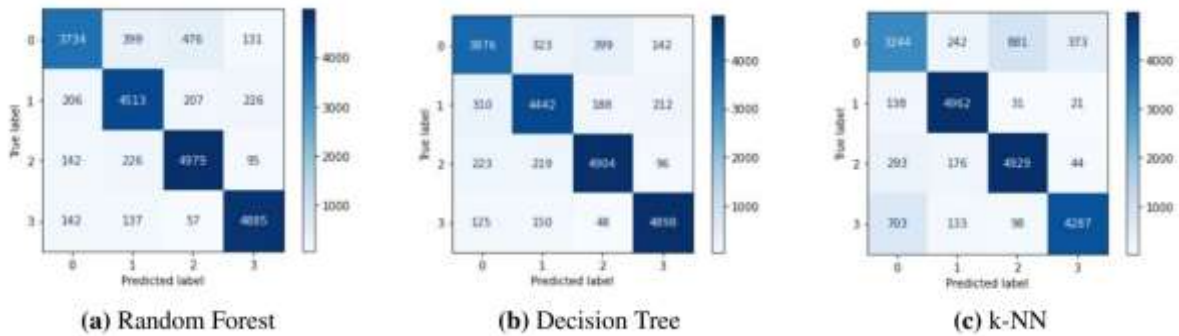


Figure 7. Confusion Matrix for 4 device types

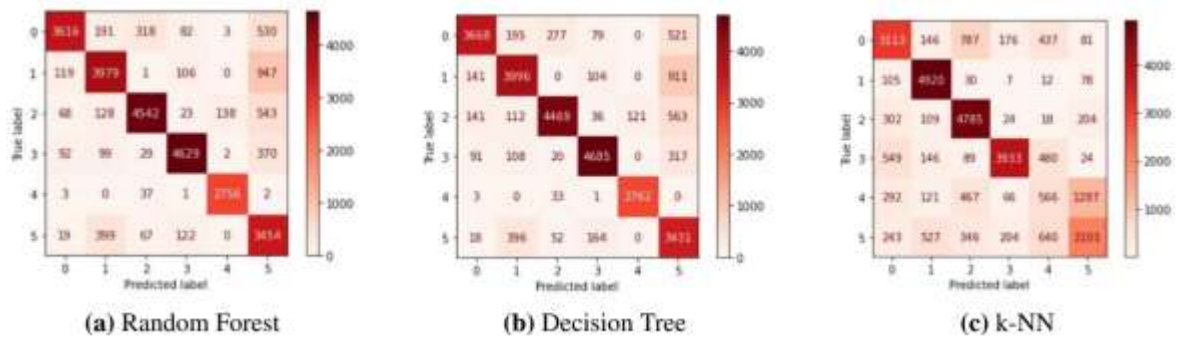


Figure 8. Confusion Matrix for 6 device types

Table 1. Number of device types and accuracy rate of the algorithms

Number of device types	Random Forest	Decision Tree	k-NN
2 devices	98%	98%	95%
4 devices	88%	88%	85%
6 devices	84%	84%	71%

According to the findings obtained from the experiments, it has been observed that the Random Forest and Decision Tree algorithms are more effective than the k-NN algorithm. For all three machine learning algorithms, it has been observed that the accuracy rates increase as the number of device types decreases. In the experiment in which two device types were used, the highest accuracy rate was obtained as 98% with Random Forest and Decision Tree algorithms.

4. Discussion

The use of technological devices in all areas of our lives is increasing and provides convenience to human life. However, these devices bring some risks when communicating with each other. For this reason, it is essential to take security measures while adapting these devices to our lives. It is possible to obtain extremely confidential information from the communication traffic created by the devices. Even if the traffic is encrypted, inferences for the traffic and devices can be made from this data flow. An attacker who observes the traffic can classify these devices using attributes such as time and packet size using machine learning methods. The accuracy of this classification may vary depending on the selected machine learning method and data set. Likewise, this accuracy rate may vary depending on the number of devices in the data set. For attackers, high accuracy rate means self-confidence to classify a device and learn device type of victim uses. That may cause privacy issues for the victim side. As machine learning can be used in attacks, attacks on machine learning models are also discussed in this study. In this study, machine learning algorithms that are widely used to classify devices are explained and experiments are carried out. Padding method, which is widely used to reduce the attacker's accuracy rate and to provide security, is explained. In addition, attacks on machine learning models are mentioned. In the experiment in which six type of devices were used, it was observed that the Random Forest and Decision Tree algorithms, which achieved 84% accuracy, were more effective than the k-NN algorithm, which achieved 71% accuracy. In the experiment where the number of device types was four, it was observed that the Random Forest and Decision Tree algorithms, which achieved 88% accuracy, were more effective than the k-NN algorithm, which achieved 85% accuracy. The highest accuracy was found in experiments using two device types. An accuracy rate of 98% was obtained in the Random Forest and Decision Tree algorithms, and 95%

in the k-NN algorithm. Especially for the k-NN algorithm, it was observed that the accuracy rate increased as the device type decreased. In future studies, it is aimed to develop an effective and optimal defense method for all kinds of machine learning methods used in attacks and to develop a secure framework against attacks on machine learning models.

Author Contributions

The percentage of the author(s) contributions is presented below. All authors reviewed and approved the final version of the manuscript.

	A.E.	Ö.C.
C	50	50
D	50	50
S	50	50
DCP	50	50
DAI	50	50
L	50	50
W	50	50
CR	50	50
SR	50	50
PM	50	50
FA	50	50

C=Concept, D= design, S= supervision, DCP= data collection and/or processing, DAI= data analysis and/or interpretation, L= literature search, W= writing, CR= critical review, SR= submission and revision.

Conflict of Interest

The authors declared that there is no conflict of interest.

Ethical Consideration

Ethics committee approval was not required for this study because of there was no study on animals or humans.

Acknowledgments

This study is supported by Ege University Scientific Research Projects Committee under the grant number FM-HZP-2023-29550.

References

- Abdulkareem NM, Abdulazeez AM. 2021. Machine learning classification based on Random Forest Algorithm: A review. *IJSB*, 5(2): 128-142.
- Aksoy A, Gunes MH. 2019. Automated IoT device identification

- using network traffic. In: ICC 2019 - IEEE International Conference on Communications, 20-24 May, Shanghai, China, pp: 1-7.
- Alex C, Creado G, Almobaideen W, Alghanam OA, Saadeh M. 2023. A Comprehensive survey for IoT security datasets taxonomy classification and machine learning mechanisms. COSE, 134: 103283.
- Alghuried A. 2017. A model for anomalies detection in internet of things (IoT): using inverse weight clustering and decision tree. MSc thesis, Dublin Institute of Technology, Dublin, Ireland, pp: 142.
- Biggio B, Nelson B, Laskov P. 2012. poisoning attacks against support vector machines. arXiv, 1206.6389.
- Biggio B, Corona I, Maiorca D, Nelson B, Šrndić N, Laskov P, Roli F. 2013. Evasion attacks against machine learning at test time. In: Joint European Conference on Machine Learning and Knowledge Discovery in Databases, 23-27 September 2013, Prague, Czech Republic, pp: 387-402.
- Charbuty B, Abdulazeez A. 2021. Classification based on decision tree algorithm for machine learning. JASTT, 2(01): 20-28.
- Dogru N, Subasi A. 2018. Traffic accident detection using random forest classifier. In: 15th Learning and Technology Conference (L&T), 25-27 February 2018, Jeddah, Saudi Arabia, pp: 40-45.
- Ergün A, Can Ö. 2022a. Ensuring IoT Privacy using padding strategies against machine learning approaches. IJMSIT, 6(2): 193-197.
- Ergün A, Can Ö. 2022b. Machine learning attacks against internet of things devices. IJMSIT, 6(1): 23-28.
- Gawri B, Kasturi A, Neti LBM, Hota C. 2022. An efficient approach to kNN algorithm for IoT Devices. In: 2022 14th International Conference on Communication Systems & Networks (COMSNETS), 3-8 January 2022, Bengaluru, India, pp: 734-738.
- Kröger J. 2018. Unexpected inferences from sensor data: a hidden privacy threat in the internet of things. In: IFIP International Internet of Things Conference, 5-8 November 2018, Valencia, Spain, pp: 147-159.
- Kwon H, Kim Y, Park KW, Yoon H, Choi D. 2018. Multi-targeted adversarial example in evasion attack on deep neural network. IEEE Access, 6: 46084-46096.
- Pinheiro AJ, de Araujo-Filho PF, Bezerra JDM, Campelo DR. 2020. Adaptive packet padding approach for smart home networks: a tradeoff between privacy and performance. IEEE IoT-J, 8(5): 3930-3938.
- Sivanathan A, Gharakheili HH, Loi F, Radford A, Wijenayake C, Vishwanath A, Sivaraman V. 2018. Classifying IoT devices in smart environments using network traffic characteristics. IEEE TMC, 18(8): 1745-1759.
- Tolpegin V, Truex S, Gursoy ME, Liu L. 2020. Data poisoning attacks against federated learning systems. In: European Symposium on Research in Computer Security, 14-18 September 2020, Guildford, United Kingdom, pp: 480-501.
- Wang H, Xu P, Zhao J. 2021. Improved KNN algorithm based on preprocessing of center in smart cities. Complexity, 2021: 1-9.
- Yerlikaya FA, Bahtiyar Ş. 2022. Data poisoning attacks against machine learning algorithms. Expert Syst Appl, 208: 118101.



BIODIVERSITY OF *Actinobacteria* FROM KULA GEOPARK IN TÜRKİYE

Betül BAYRAKTAR¹, Kamil IŞIK^{1*}


¹Ondokuz Mayıs University, Faculty of Science, Department of Biology, 55139, Samsun, Türkiye


Abstract: Investigating the microbial diversity of *Actinobacteria* inhabiting the soils of the Kula-Salihli Geopark and identifying species at the genus level using 16S rRNA gene sequences are the primary goals of this work. In the literature review of this geopark located within the borders of Manisa province, no study on actinobacterial biodiversity was found. In this study, 10 different selective isolation media were used to investigate the biodiversity of *Actinobacteria* in the Geopark. A total of 469 *Actinobacteria* strains were isolated using the dilution-plate method. From these 469 strains, 34 strains were selected based on their colony morphology and pigmentation characteristics. The isolates performed phylogenetic analysis based on sequencing of the 16S ribosomal RNA gene region. The isolates were found to belong to nine different genera, including *Actinomadura*, *Amycolatopsis*, *Kribbella*, *Micromonospora*, *Nocardia*, *Nonomuraea*, *Pseudonocardia*, *Saccharothrix* and *Streptomyces*, according to the results of phylogenetic analysis. Five isolates have been identified as novel species as a consequence of our current study.

Keywords: *Actinobacteria*, Geopark soil, 16S rRNA gene, Biodiversity

*Corresponding author: Ondokuz Mayıs University, Faculty of Science, Department of Biology, 55139, Samsun, Türkiye

E mail: kamilis@omu.edu.tr (K. IŞIK)

Betül BAYRAKTAR  <https://orcid.org/0009-0003-8312-5203>

Kamil IŞIK  <https://orcid.org/0000-0003-1764-8113>

Received: March 27, 2024

Accepted: April 29, 2024

Published: May 15, 2024

Cite as: Bayraktar B, Işık K. 2024. Biodiversity of *Actinobacteria* from Kula Geopark in Türkiye. BSJ Eng Sci, 7(3): 495-508.

1. Introduction

The phylum *Actinobacteria*, currently referred to as *Actinomycetota*, is a common group of gram-positive microorganisms found in both terrestrial and aquatic environments. Although *Actinobacteria* are frequently found in both terrestrial and aquatic habitats, they can be found in a variety of harsh environments, including deep seas, deserts, hot springs, salt lakes, and caves (Barka et al., 2016; Hui et al., 2021). *Actinobacteria*, by producing a variety of compounds, play an important role in the bioremediation of pollutants, the degradation of lignocellulosic biomass, and the promotion of plant development (Saini et al., 2015; Mawang et al., 2021; Faddetta et al., 2023).

Actinobacteria's primary and secondary metabolites have been identified as significant industrial compounds. Although rare *Actinobacteria*, which are crucial for the production of novel secondary metabolites, have been discovered in a variety of soil types, volcanic regions are still a relatively unexplored resource for the detection of chemicals with industrial significance (Miao and Davies, 2010; Tiwari and Gupta, 2012).

Geographical areas referred to as UNESCO Global Geoparks are those where landscapes and places of global geological significance are managed using a comprehensive concept of conservation, education, and sustainable development. Currently, there are 213 UNESCO Global Geoparks in 48 countries. Türkiye's first and only UNESCO-registered geopark, Kula-Salihli

UNESCO Global Geopark, is located in Manisa province. The geopark, which has a rich geodiversity, is one of the youngest volcanic areas in Türkiye (UNESCO, 2024). The purpose of this study is to determine the diversity of *Actinobacteria* found in the Kula-Salihli Geopark's soils. Thus, with this study, we aim to both contribute to the biological diversity of our country and contribute to the stock of microorganisms that have the potential to be the source of various metabolites that can be used in biotechnological applications.

2. Materials and Methods

2.1. Collection of Soil Samples

In August 2023, soil samples were collected from four distinct locations inside of Kula Geopark (Figure 1). After being tagged and put in sterile plastic bags, the soil samples were transported to the actinobacterial soil research laboratory and stored there for analysis at 4 °C.



Figure 1. Location of Kula-Salihli Geopark.



2.2. Isolation of Actinobacteria from Geopark Soils

Ten different media were made to isolate the *Actinobacteria* members. Nalidixic acid and cycloheximide were added to each medium to prevent the growth of gram-negative and fungal species. Then, soil samples were first put on a sterile petri plate and allowed to dry at room temperature for 14 days. In a mortar, dried soil samples were pounded into a powder without being mixed. Each of the prepared solutions was then shaken for half an hour. One gram of soil sample was transferred into vials containing 9 milliliters of Ringer's solution and ten-to-one dilution ratio tubes were prepared. Dilutions of 10⁻² and 10⁻³ were obtained via repeated dilution. 200 microliter suspensions were inoculated onto different medium surfaces using an automated pipette, and they were subsequently cultured for 21 days at 28 °C. Table 1 shows the medium used.

2.3. Selection, Purification, and Storage of Strains

Among the incubated colonies, isolates thought to be *Actinobacteria* were selected based on characteristics such as spore production and morphology. These cultures were cultivated on the surface of International *Streptomyces* Project Medium No. 2 (ISP2; Shirling and Gottlieb, 1966) agar using a sterile loop. After incubating at 28 °C for 14 days, pure isolates were obtained from transferred plates. Pure cultures were transferred to 20% v/v glycerol stock solution and stored at -80 °C until use.

2.4. Genomic Extraction of DNA and 16S rRNA Amplification

The PureLink® Genomic DNA Isolation Kit (Invitrogen, USA) was used for obtaining the isolates genomic DNA. Then DNA was detected using 1% agarose gel electrophoresis. Polymerase chain reaction (PCR) amplifications of the 16S rRNA gene region were performed on a MyGenie-96 Gradient Thermal Cycler

(Korea) using universal primers 27F and 1525R (Table 2). A 50-µl reaction mixture was made for the 16S rRNA amplification of each test isolate. This mixture contains deionized water, extracted genomic DNA, 27F and 1525R primers, and Promega's GoTaq® Hot Start Colorless Master mix. There are 22 µl, 1 µl, 1 µl, 1 µl and 25 µl of these compounds in the mixture, in that order. The following parameters are used in PCR amplification (MyGenie-96 Gradient Thermal Cycler, Korea): pre-denaturation for two minutes at 95 °C; denaturation for one minute at 95 °C, comprising thirty cycles; bonding for 1.5 minutes at 55 °C and elongation for three minutes at 72 °C; final stage for ten minutes at 72 °C; and four storage stages at 4 °C. The amplification products were subsequently detected using 1.5% agarose gel electrophoresis (Merck).

2.5. 16S rRNA Gene Analysis

ABI-format chromatogram files resulting from the sequencing of PCR products were examined using the Chromas version 1.7.6 program (C. McCarthy, School of Health Sciences, Griffith University, Queensland, Australia). Each organism's 16S rRNA gene nucleotide sequence was then obtained in FASTA format by overlapping the primer reads. In the EzBioCloud database, every sequence was compared to other sequences (Yoon et al., 2017). ClustalW was used to do multiple sequence alignments in the MEGA 11 software (Tamura et al., 2021). Phylogenetic trees of the alignment sequences were constructed using the neighbor-joining method (Saitou and Nei, 1987), the Jukes-Cantor model (Jukes and Cantor, 1969) and bootstrap analyses based on 1000 resampling (Felsenstein, 1985) using MEGA 11 software. The 16S rRNA gene sequences of the *Actinobacteria* isolates used in this study were stored in the NCBI GenBank database.

Table 1. List of selective media used and antibiotics

Name of medium	Antibiotics	Reference
Actinomycete Isolation Agar	Nalidixic acid (10 µg/ml) and cycloheximide (50 µg/ml)	Kumar et al, 2012
Gause No.1 Agar	Nalidixic acid (10 µg/ml) and cycloheximide (50 µg/ml)	Tan et al., 2006
Nocardia Agar	Nalidixic acid (10 µg/ml) and cycloheximide (50 µg/ml)	Sanglier et al., 1992
Humic Acid Vitamin Agar	Nalidixic acid (10 µg/ml) and cycloheximide (50 µg/ml)	Hayakawa and Nonomuraea, 1987
R2A Agar	Nalidixic acid (10 µg/ml) and cycloheximide (50 µg/ml)	Reasoner and Geldreich, 1985
Oligotrophic Agar	Nalidixic acid (10 µg/ml) and cycloheximide (50 µg/ml)	Jiang et al., 2016
Starch-Casein Agar	Nalidixic acid (10 µg/ml) and cycloheximide (50 µg/ml)	Kuester and Williams, 1964
Hickey-Tresner Agar	Nalidixic acid (10 µg/ml) and cycloheximide (50 µg/ml)	Hickey and Tresner, 1952
Modified Soil Agar	Nalidixic acid (10 µg/ml) and cycloheximide (50 µg/ml)	Sadoway et al., 2013
ISP-2 Agar	Nalidixic acid (10 µg/ml) and cycloheximide (50 µg/ml)	Shirling and Gottlieb, 1966

Table 2. Oligonucleotide primers used for 16S rRNA PCR amplification and sequencing

Primer code	Sequences (5'-3')	Base length	References
27F	AGAGTTTGATCMTGGCTCAG	20	Weisburg, 1991
518F	CCAGCAGCCGCGTAAT	17	Buchholz-Cleven et al, 1997
800R	TACCAGGGTATCTAATCC	18	Chun and Goodfellow, 1995
MG5F	AAACTCAAAGGAATTGACGG	20	Chun and Goodfellow, 1995
1525R	AAGGAGGTGWTCCARCC	17	Lane, 1991

*M= adenine or cytosine, R= adenine or guanine, W= adenine or thymine.

3. Results

3.1. Morphological Analysis of Actinobacteria

In the Kula-Salihli Geopark (2,320 km²), which is located inside the boundaries of the province of Manisa, soil samples were collected using a GPS device at four distinct places (Table 3).

Table 3. Locality and geographical coordinates of soil samples

Soil No.	Locality	Geographical coordinates
1	Kula Fairy Chimneys	38,60760°N 28,80798°E
2	Kula Fairy Chimneys	38,60809°N 28,80753°E
3	Kula Divlit	38,56023°N 28,66096°E
4	Kula	38,56192°N 28,66048°E

By using the dilution plate method for soil isolation, 469 Actinobacteria were isolated in total. A total of 152 different strains, which were selected by eliminating similar ones according to their macroscopic and microscopic images, were divided into 27 color groups according to their colony morphology and pigmentation characteristics (Kelly, 1964). Following color grouping, 34 strains were chosen for 16S rRNA gene region analysis, with consideration given to characteristics such as phylogenetic analyses, ten different selective media, substrate mycelium and air mycelium. When the distribution of actinobacteria according to the media is examined, it is seen that 8 isolates were obtained from starch casein agar, 5 isolates from R2A agar, 9 isolates from humic acid vitamin agar, 1 isolate from Gause agar and 11 isolates from ISP-2. The results showed that ISP-2, starch casein agar and humic acid vitamin agar media were the best media for isolating Actinobacteria from Geopark soil. Figure 2 shows the distribution of the number of isolates according to the media used.

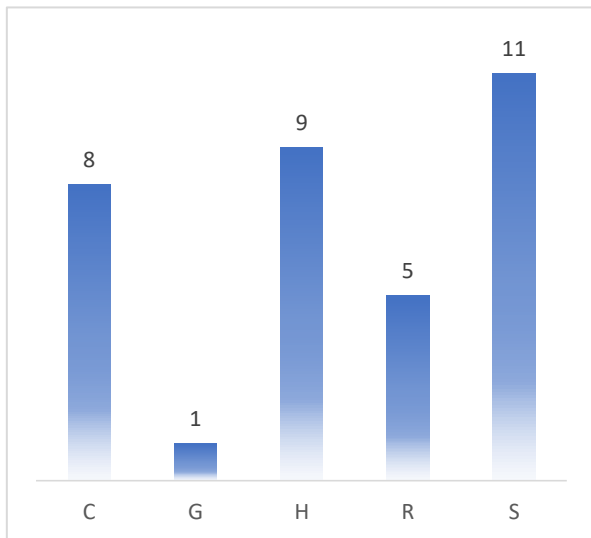


Figure 2. Media distribution of Actinobacteria isolates (C= Starch-Casein agar, G= Gause agar, H= Humic acid vitamin agar, R= R2A agar, S= ISP-2 Agar).

3.2. 16S rRNA Gene Sequence Analysis of Actinobacteria

According to the results of the nucleotide sequence analysis of the 16S rRNA gene region using universal primers (518F, 800R, and MG5F; Table 2), 34 isolates were recognized as members of the Actinobacteria phylum. These isolates were determined to predominantly belong to the genera Amycolatopsis (8 isolates), Kribbella (7 isolates), and Streptomyces (7 isolates). The remaining strains were from the genera Nonomuraea (4 isolates), Micromonospora (2 isolates), Pseudonocardia (2 isolates), Nocardia (2 isolates), Actinomadura (1 isolate), and Saccharothrix (1 isolate). In conclusion, nine different Actinobacteria genera were obtained from Kula-Salihli Geopark in this study. Figure 3 shows the distribution of the genus.

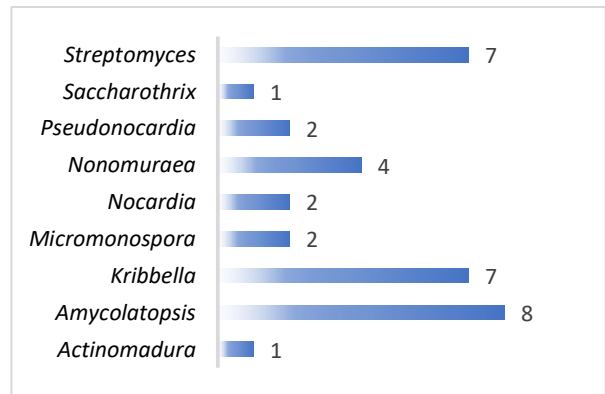


Figure 3. Genus distribution of Actinobacteria isolates.

3.3. Phylogenetic Analysis of the Actinobacteria

To explore the evolutionary links between the Actinobacteria isolates in this study and their closest taxonomic relatives, phylogenetic trees based on 16S rRNA sequences were created. The phylogenetic tree was constructed using the neighbor-joining method. After phylogenetic analysis, the most predominant Actinobacteria genus in this study, members of Amycolatopsis, have a 99.28% similarity with the closest type strain. Kribbella, the other major genus with seven isolates, has a similarity between 99.45% and 99.93% with its closest type strain. Seven isolates of Streptomyces, the other dominant genus, have similarity between 99.17% and 100.0% with their closest type strain. A similarity of the 16S ribosomal RNA gene sequences of each isolate and its closest relatives is shown in Table 4. Phylogenetic trees of the isolates based on the neighbour-joining method are also given in Figure 4-11.

Table 4. Summary of information on 16S rRNA sequence determination of isolated strains

Strain	Closest type strain	Similarity	Nucleotid difference
KC28	<i>Streptomyces thinghirensis</i> DSM 41919 ^T	100.00	0/1449
KC37	<i>Kribbella albertanoniae</i> BC640 ^T	99.79	3/1440
KC40	<i>Micromonospora orduensis</i> S2509 ^T	99.65	5/1437
KC48	<i>Streptomyces xanthophaeus</i> NRRL B-5414 ^T	99.93	1/1447
KC66	<i>Streptomyces cellostaticus</i> DSM 40189 ^T	99.52	7/1448
KC83	<i>Kribbella jejuensis</i> DSM 17305 ^T	99.45	8/1447
KC93	<i>Nocardia</i> sp.	100.00	0/1449
KC97	<i>Micromonospora fulviviridis</i> DSM 43906 ^T	99.44	8/1436
KG3	<i>Amycolatopsis lurida</i> DSM 43134 ^T	99.28	10/1386
KH2	<i>Nonomurea turkmeniaca</i> DSM 43926 ^T	99.01	14/1416
KH8	<i>Amycolatopsis lurida</i> DSM 43134 ^T	99.28	10/1386
KH9	<i>Amycolatopsis lurida</i> DSM 43134 ^T	99.28	10/1386
KH16	<i>Nonomurea polychroma</i> DSM 43925 ^T	98.48	22/1443
KH19	<i>Nonomurea antri</i> NN258 ^T	98.75	18/1441
KH50	<i>Saccharothrix espanaensis</i> DSM 44229 ^T	99.72	4/1438
KH76	<i>Nocardia</i> sp.	100.00	0/1449
KH104	<i>Pseudonocardia cypriaca</i> KT2142 ^T	100.00	0/1442
KH114	<i>Pseudonocardia zijingensis</i> 6330 ^T	99.51	7/1418
KR1	<i>Amycolatopsis lurida</i> DSM 43134 ^T	99.28	10/1386
KR2	<i>Amycolatopsis lurida</i> DSM 43134 ^T	99.28	10/1386
KR3	<i>Amycolatopsis lurida</i> DSM 43134 ^T	99.28	10/1386
KR6	<i>Amycolatopsis lurida</i> DSM 43134 ^T	99.28	10/1386
KR12	<i>Amycolatopsis lurida</i> DSM 43134 ^T	99.28	10/1386
KS12	<i>Streptomyces canus</i> DSM 40017 ^T	100.00	0/1448
KS15	<i>Streptomyces aureocirculatus</i> NRRL ISP-5386 ^T	99.52	7/1450
KS37	<i>Actinomadura hibisca</i> NBRC 15177 ^T	98.96	15/1446
KS52	<i>Kribbella karoonensis</i> Q41 ^T	99.93	1/1447
KS86	<i>Kribbella karoonensis</i> Q41 ^T	99.93	1/1447
KS88	<i>Kribbella karoonensis</i> Q41 ^T	99.86	2/1447
KS95	<i>Kribbella speibonae</i> YM55 ^T	99.72	4/1447
KS96	<i>Kribbella karoonensis</i> Q41 ^T	99.86	2/1447
KS97	<i>Streptomyces canus</i> DSM 40017 ^T	100.00	0/1448
KS108	<i>Nonomurea helvata</i> IFO 14681 ^T	99.43	8/1409
KS109	<i>Streptomyces pseudovenezuelae</i> DSM 40212 ^T	99.52	7/1450

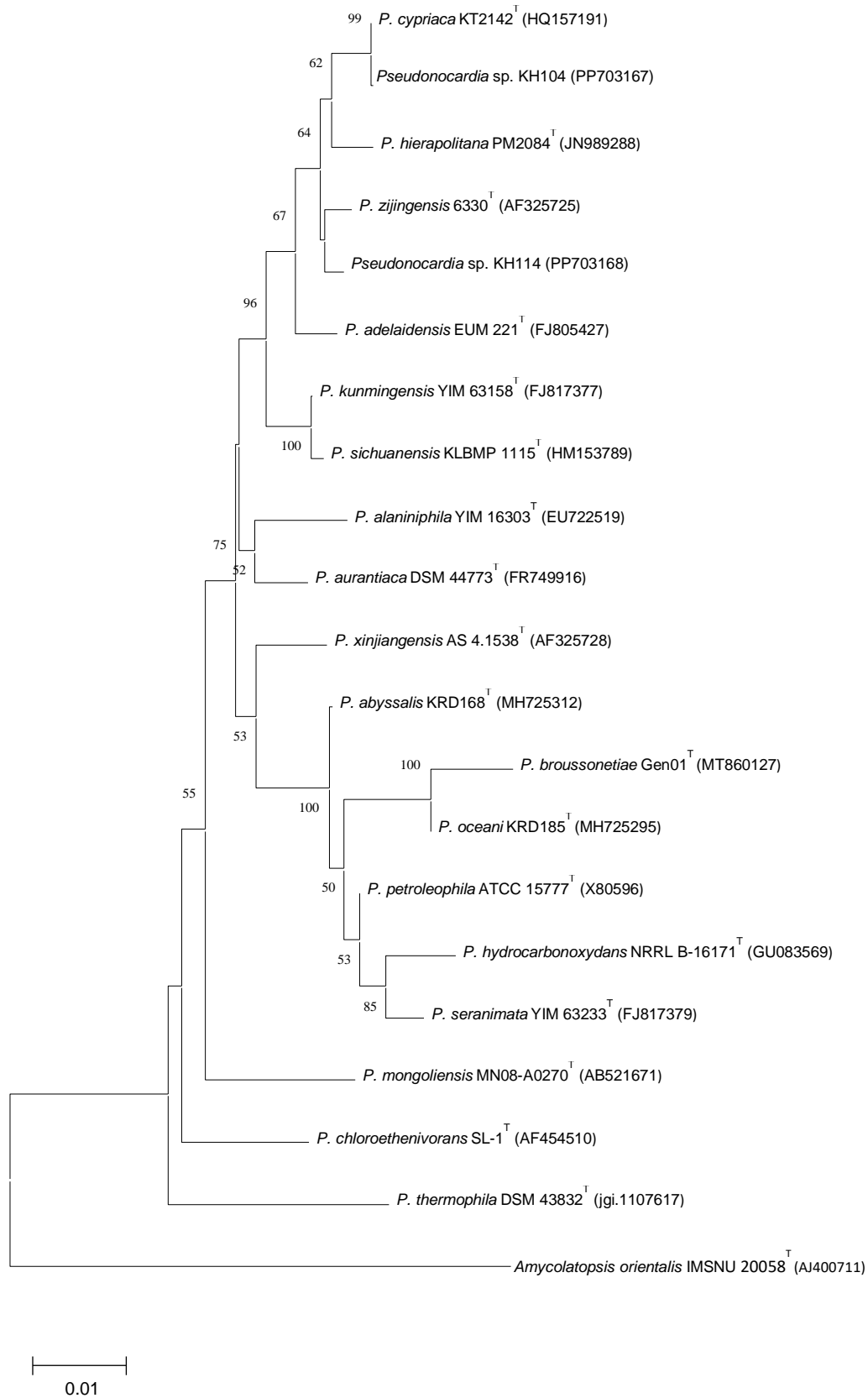


Figure 4. Phylogenetic tree showing the relationship of the actinobacterial isolates in group *Pseudonocardia* and related type strains. Phylogenetic tree was based on the Neighbor-joining method using MEGA 11 software. Bootstrap values above 50% (for 1000 replications) are shown. The scale bar indicates 0.01 substitutions per nucleotide position.

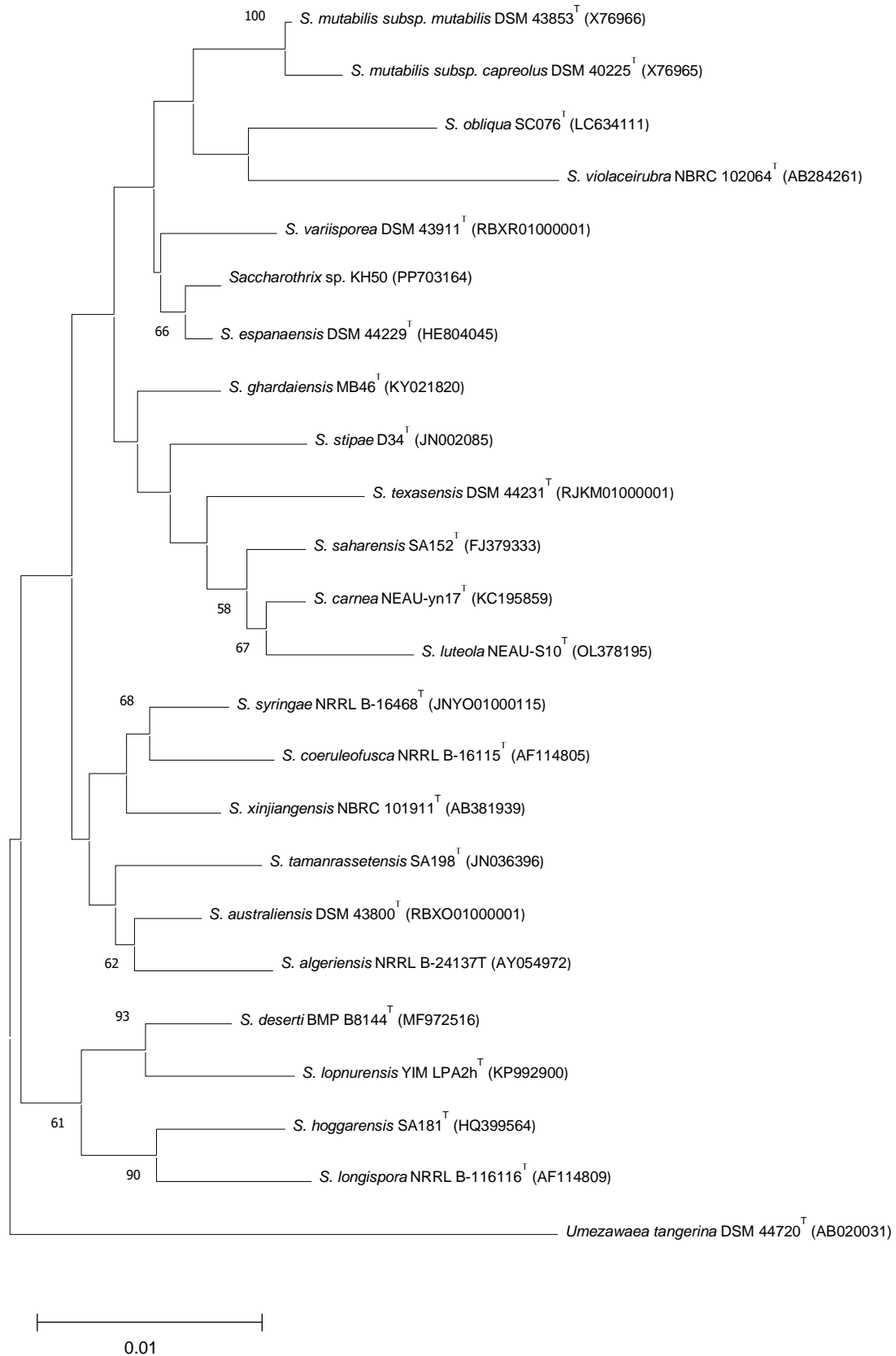


Figure 5. Phylogenetic tree showing the relationship of the actinobacterial isolates in group *Saccharothrix* and related type strains. Phylogenetic tree was based on the Neighbor-joining method using MEGA 11 software. Bootstrap values above 50% (for 1000 replications) are shown. The scale bar indicates 0.01 substitutions per nucleotide position.

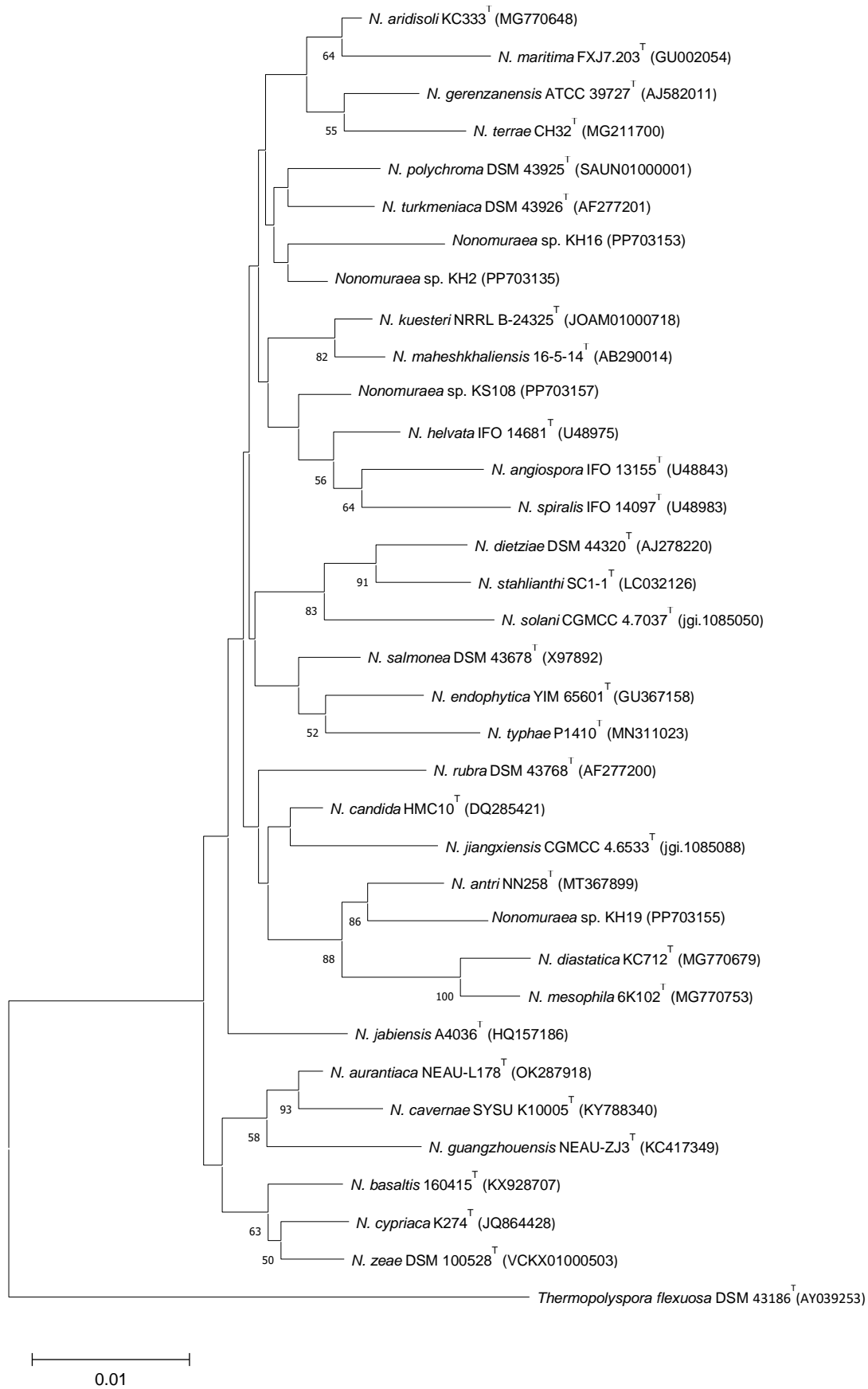


Figure 6. Phylogenetic tree showing the relationship of the actinobacterial isolates in group *Nonomuraea* and related type strains. Phylogenetic tree was based on the Neighbor-joining method using MEGA 11 software. Bootstrap values above 50% (for 1000 replications) are shown. The scale bar indicates 0.01 substitutions per nucleotide position.

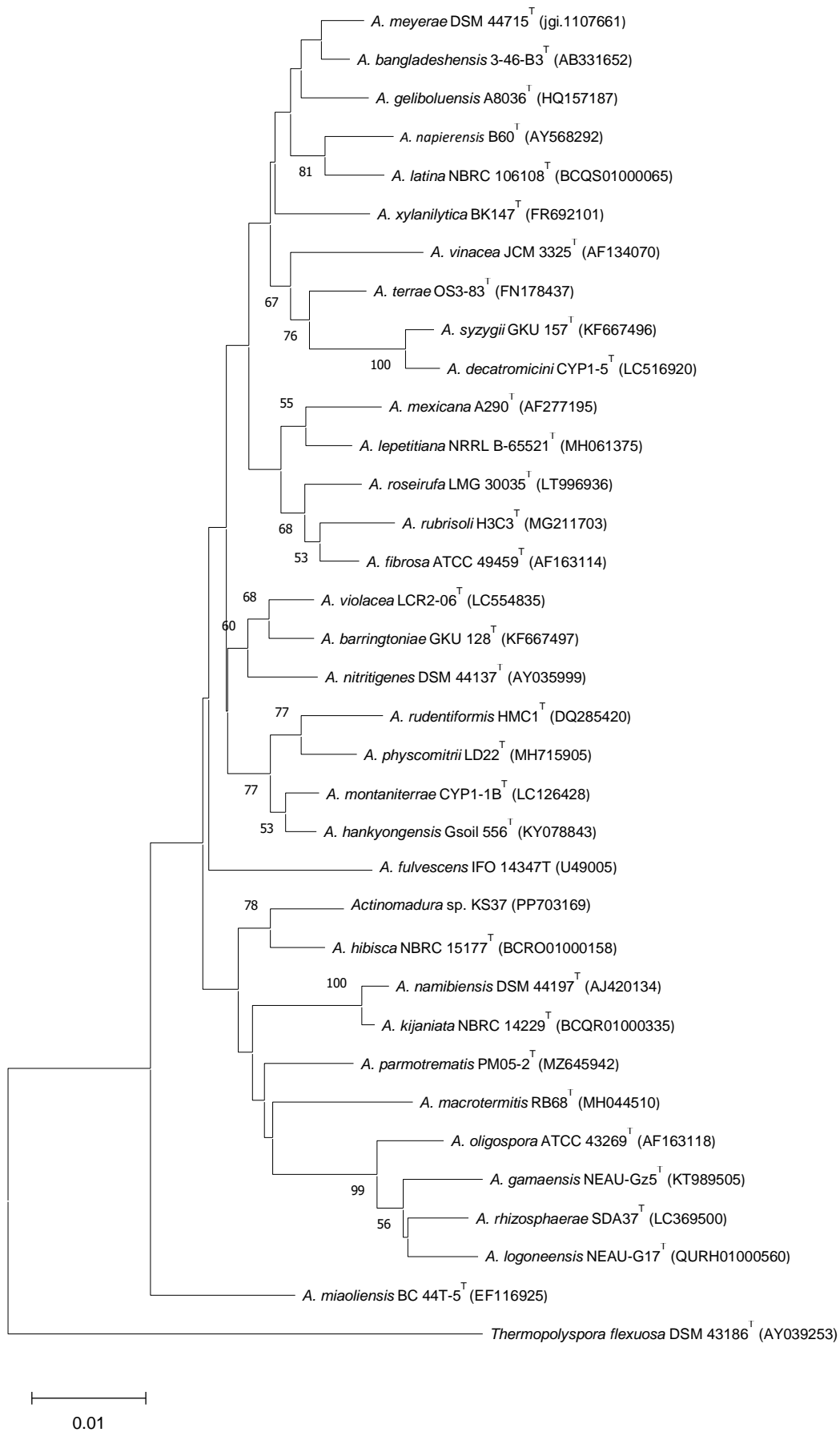


Figure 7. Phylogenetic tree showing the relationship of the actinobacterial isolates in group *Actinomadura* and related type strains. Phylogenetic tree was based on the Neighbor-joining method using MEGA 11 software. Bootstrap values above 50% (for 1000 replications) are shown. The scale bar indicates 0.01 substitutions per nucleotide position.

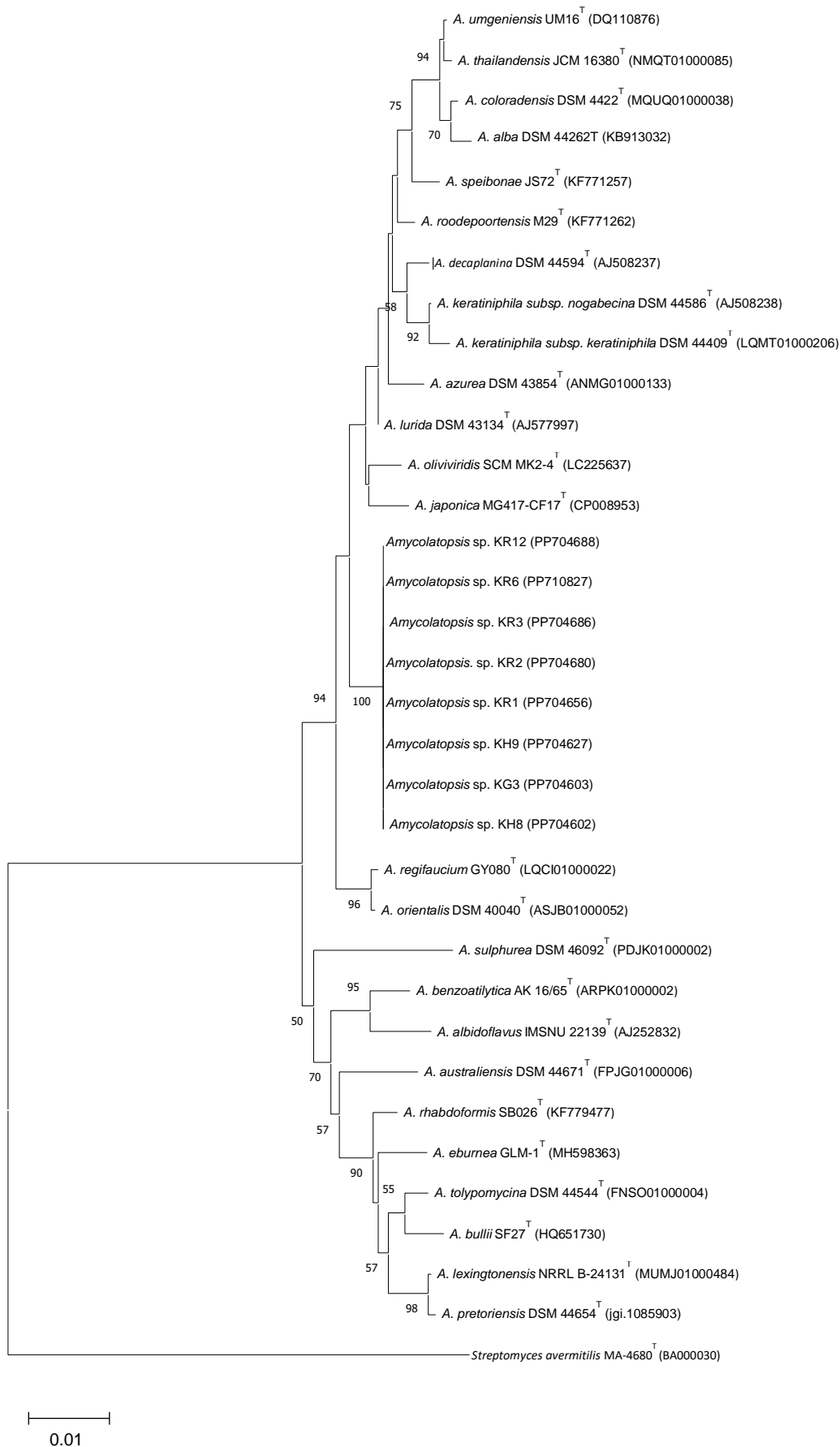
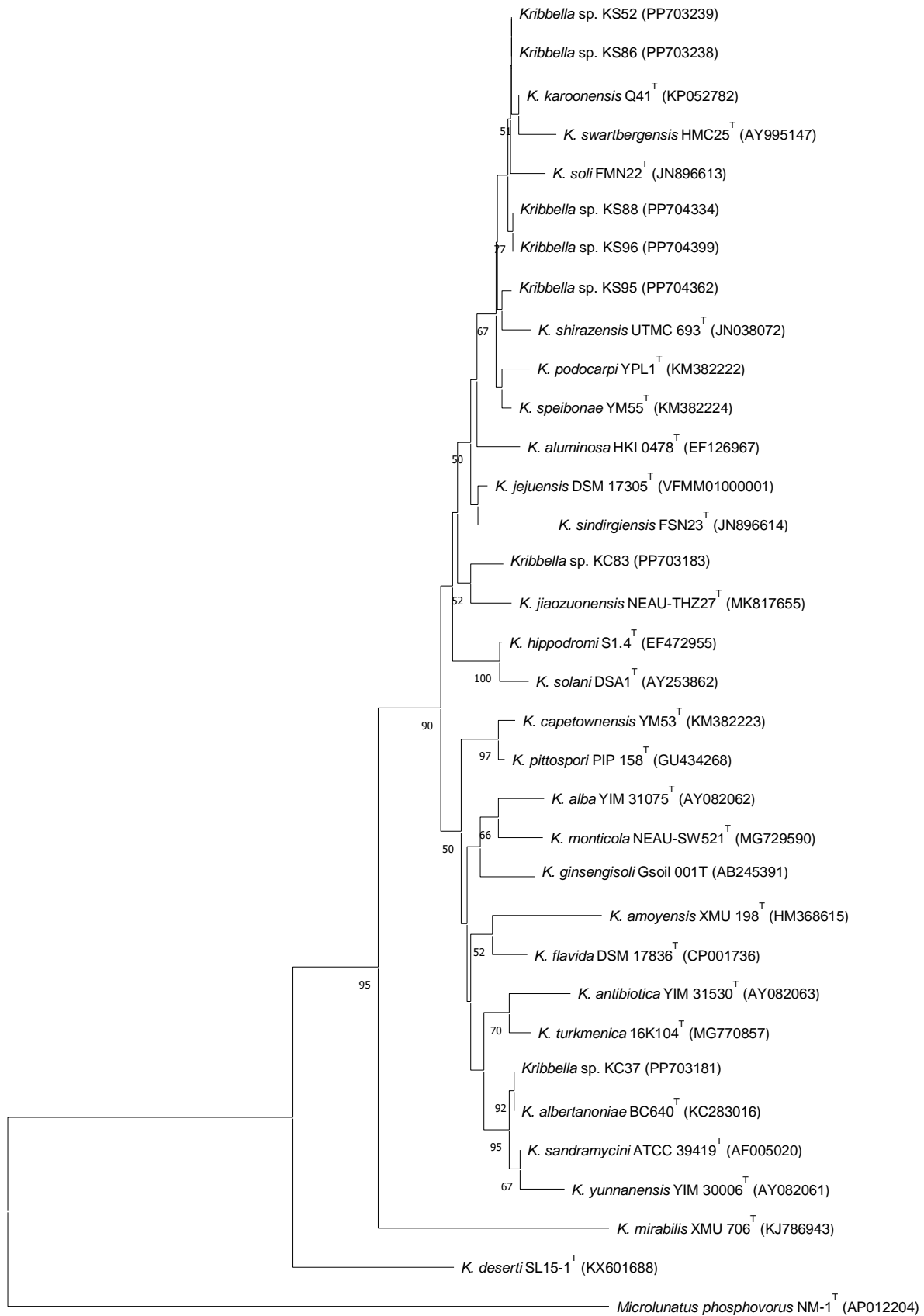
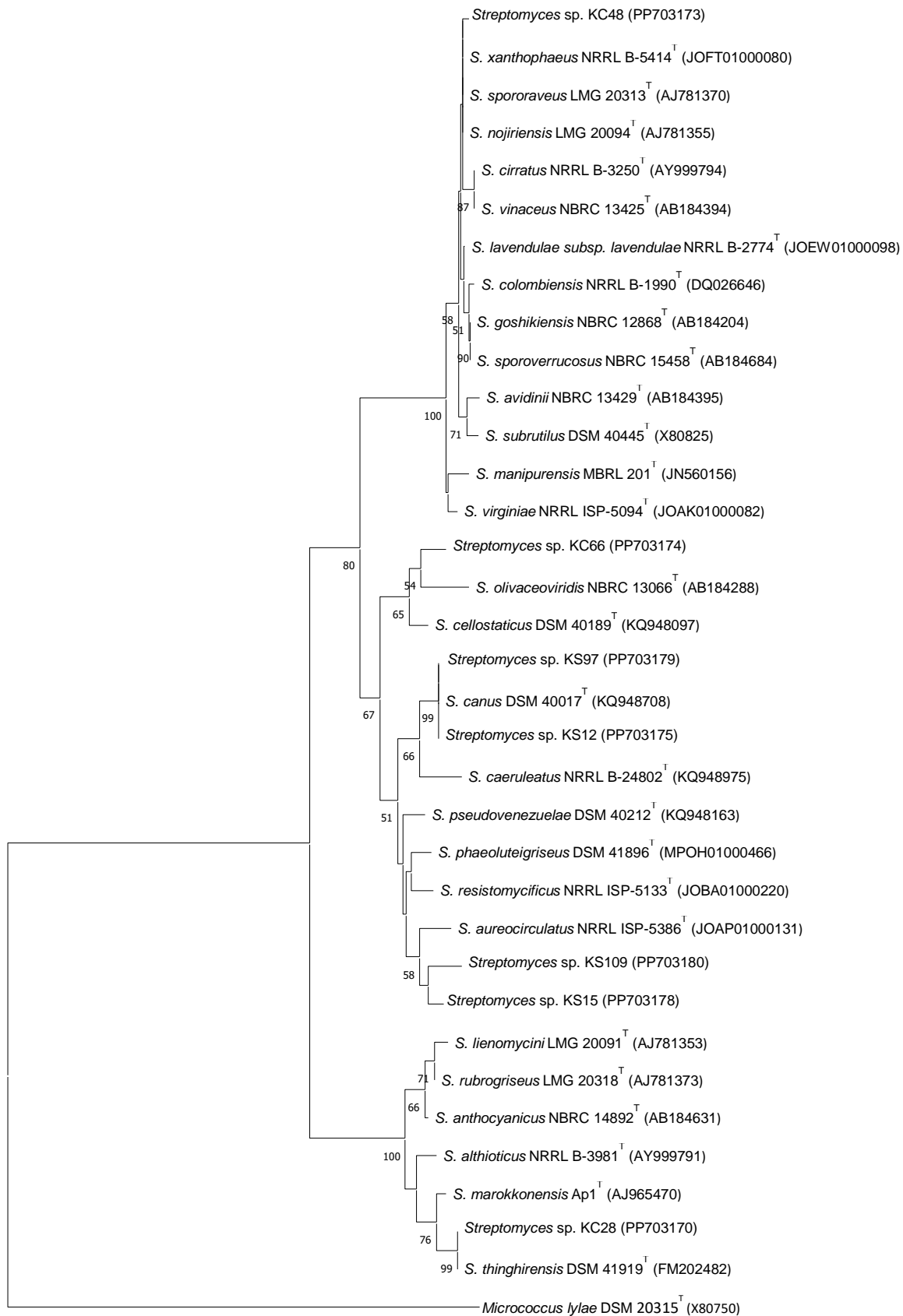


Figure 8. Phylogenetic tree showing the relationship of the actinobacterial isolates in group *Amycolatopsis* and related type strains. Phylogenetic tree was based on the Neighbor-joining method using MEGA 11 software. Bootstrap values above 50% (for 1000 replications) are shown. The scale bar indicates 0.01 substitutions per nucleotide position.



0.01

Figure 9. Phylogenetic tree showing the relationship of the actinobacterial isolates in group *Kribbella* and related type strains. Phylogenetic tree was based on the Neighbor-joining method using MEGA 11 software. Bootstrap values above 50% (for 1000 replications) are shown. The scale bar indicates 0.01 substitutions per nucleotide position.



0.01

Figure 10. Phylogenetic tree showing the relationship of the actinobacterial isolates in group *Streptomyces* and related type strains. Phylogenetic tree was based on the Neighbor-joining method using MEGA 11 software. Bootstrap values above 50% (for 1000 replications) are shown. The scale bar indicates 0.01 substitutions per nucleotide position.

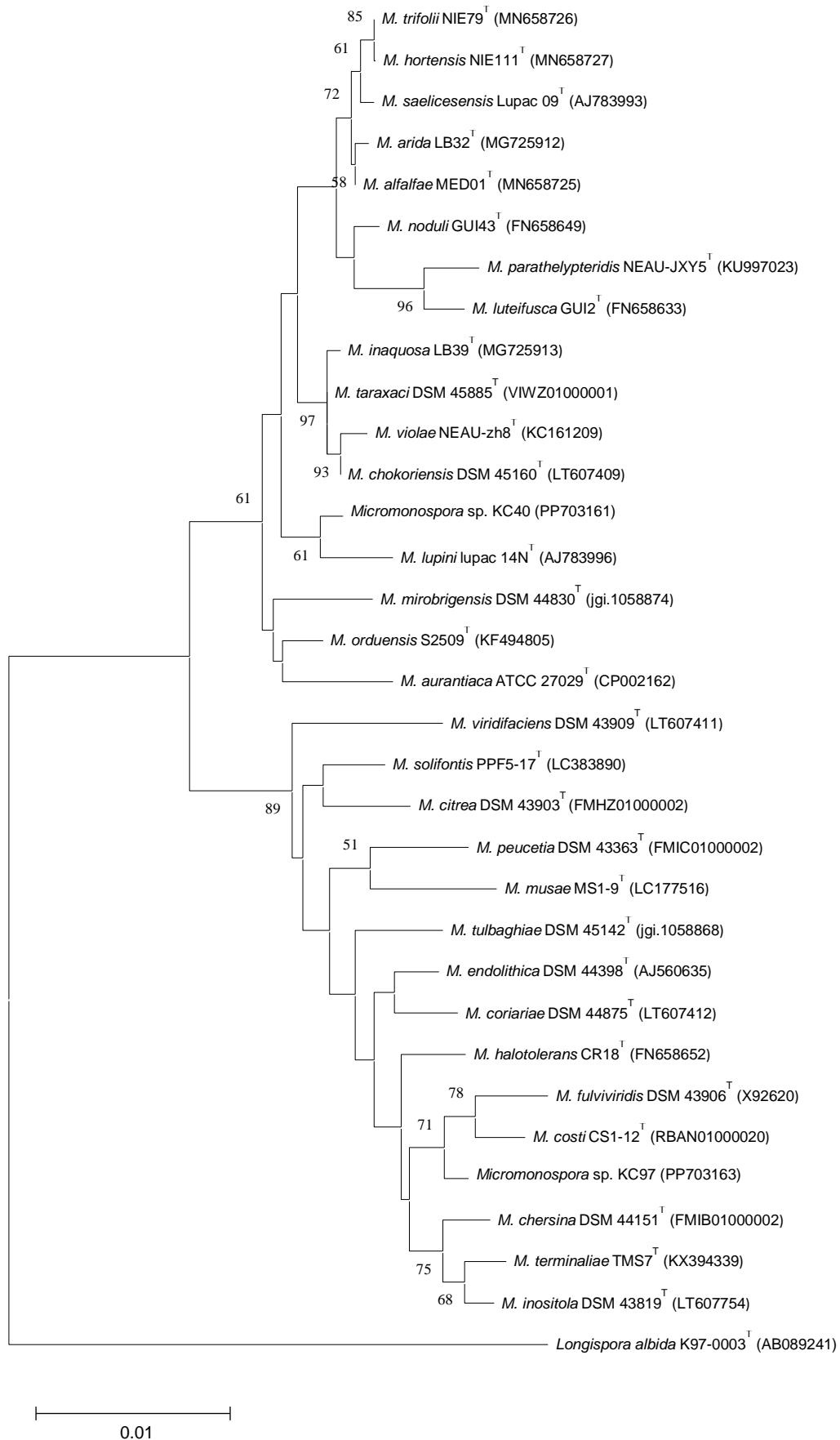


Figure 11. Phylogenetic tree showing the relationship of the actinobacterial isolates in group *Micromonospora* and related type strains. Phylogenetic tree was based on the Neighbor-joining method using MEGA 11 software. Bootstrap values above 50% (for 1000 replications) are shown. The scale bar indicates 0.01 substitutions per nucleotide position.

4. Discussion

To date, *Actinobacteria* members have been found in a wide variety of environments. Among these environments, extreme habitats such as hot springs, volcanic areas, deserts, deep-sea sediments, caves and salt lakes are particularly important. Following a literature review, actinobacteria have also been found in different volcanic regions of the world. These include lava tubes, lakes, caves, sediments, rocks and soils. Studies in volcanic regions have shown the presence of actinobacteria belonging to the following genera: *Brevibacterium*, *Dietzia*, *Micromonospora*, *Nocardia*, *Nocardioopsis*, *Rhodococcus*, *Saccharomonospora*, *Saccharopolyspora*, *Salinospira*, *Streptomyces*, etc. (Riquelme et al., 2015; Meena et al, 2019; Sottorff et al., 2019).

Meena et al. reported in their study in 2019 that deep-sea sediment samples were collected from Barren Island, Andaman and Nicobar Islands. A total of 123 cultivable marine actinobacteria were isolated and identified. Isolates were categorized under 10 genera, of which *Brevibacterium*, *Dietzia* and *Streptomyces* are the dominant genera (Meena et al., 2019).

In another study conducted by Sottorff et al. (2019), it was determined that most of the species isolated from volcanic Easter Island were actinobacteria belonging to the *Dietzia*, *Micromonospora*, *Salinispora* and *Streptomyces* genera, according to the 16S ribosomal RNA gene sequence analysis.

Phylogenetic analysis of 34 isolates obtained in this study revealed that they belong to nine different genera. Five of these isolates are thought to be new species when the nucleotide similarity rates of the 16S rRNA gene region of the closest type strains are compared. The five isolates belong to *Actinomadura*, *Amycolatopsis* and *Nonomuraea* genera known as rare actinobacteria.

According to a study conducted by Penkhrue et al. in 2018, *Amycolatopsis oliviridis* SCM_MK2-4^T strain showed the highest sequence similarity with the closest species, *Amycolatopsis azurea* JCM 3275^T with 99.4%, according to 16S rRNA gene sequence analysis results (Penkhrue et al., 2018). Strains KG3, KH8, KH9, KR1, KR2, KR3, KR6, and KR12 obtained from this study show 99.28% sequence similarity with *Amycolatopsis lurida* DSM 43134^T, the closest species according to 16S rRNA gene sequence analysis results. Based on this information, KG3, KH8, KH9, KR1, KR2, KR3, KR6, and KR12 strains are thought to be new species. Representing *Amycolatopsis lurida* strains, isolate KH8 was selected as a strain with high potential to become a novel species.

In the research of Saricaoglu et al. in 2020 based on phylogenetic analysis of 16S rRNA gene sequences revealed that *Nonomuraea basaltis* 160415^T has 99.1% similarity with the closest type species *Nonomuraea zea* NEAU-ND5^T (Saricaoglu et al., 2020). The KH2, KH16 and KH19 strains isolated in our study have 99.01, 98.48 and 98.75 similarity with the closest type strains, respectively. According to this information, KH2, KH16 and KH19 may be new species.

In accordance with the results of phylogenetic analysis of the 16S rRNA gene sequence in the study conducted by Songsumanus et al. in 2021, *Actinomadura decatromicini* CYP1-5^T showed 99.5% similarity with *Actinomadura syzygii* GKU157^T, the closest type species (Songsumanus et al., 2021). According to the 16 rRNA sequence analysis of the KS37 strain obtained in this study, it was determined that it showed 98.96 similarity with *Actinomadura hibisca* NBRC 15177^T, the closest type species. In the light of this information, KS37 strain is thought to be a novel species.

5. Conclusion

To date, no study has been conducted on the actinobacterial diversity of Kula-Salihli Geopark, one of the youngest volcanic regions in Türkiye. Our research focused on the diversity of actinobacteria found in the soil of Kula-Salihli Geopark in Manisa. A total of 34 isolates were determined to belong to nine genus, including *Actinomadura*, *Amycolatopsis*, *Kribbella*, *Micromonospora*, *Nocardia*, *Nonomuraea*, *Pseudonocardia*, *Saccharothrix* and *Streptomyces* by phylogenetic analysis based on 16S rRNA gene sequencing. Based on the nucleotide difference and percentage similarity of the 16S rRNA gene region, it is probable that the isolates of *Actinomadura* sp. KS37, *Amycolatopsis* sp. KH8, *Nonomuraea* sp. KH2, *Nonomuraea* sp. KH16, and *Nonomuraea* sp. KH19 represent novel species. With this study, in addition to determining the new species potential of the Kula Geopark, we contribute to the biodiversity of our country and the stock of microorganisms that have the potential to be a source of various metabolites that can be used in biotechnological applications.

Author Contributions

The percentage of the author(s) contributions is presented below. All authors reviewed and approved the final version of the manuscript.

	B.B.	K.I.
C	50	50
D	50	50
S	50	50
DCP	50	50
DAI	50	50
L	50	50
W	50	50
CR	50	50
SR	50	50
PM	50	50
FA	50	50

C=Concept, D= design, S= supervision, DCP= data collection and/or processing, DAI= data analysis and/or interpretation, L= literature search, W= writing, CR= critical review, SR= submission and revision, PM= project management, FA= funding acquisition.

Conflict of Interest

The authors declared that there is no conflict of interest.

Ethical Consideration

Ethics committee approval was not required for this study because of there was no study on animals or humans.

Acknowledgements

This study was supported by Ondokuz Mayıs University Scientific Research Projects Coordination Unit (BAPKOB) under the project number PYO.FEN.1904.23.008.

References

Barka EA, Vatsa P, Sanchez L, Gaveau-Vaillant N, Jacquard C, Klenk HP, Meier-Kolthoff JP, Clément C, Ouhdouch Y, van Wezel GP. 2016. Taxonomy, physiology, and natural products of Actinobacteria. *Microbiol Mol Biol Rev*, 80(1): 1-43.

Buchholz-Cleven BEE, Rattunde B, Straub KL. 1997. Screening for genetic diversity of isolates of anaerobic Fe(II)-oxidizing bacteria using DGGE and whole-cell hybridization. *Syst Appl Microbiol*, 20(2): 301-309.

Chun J, Goodfellow MA. 1995. Phylogenetic analysis of the genus *Nocardia* with 16S rRNA gene sequences. *Int J Syst Bacteriol*, 45(2): 240-245.

Faddetta T, Polito G, Abbate L, Alibrandi P, Zerbo M, Caldiero C, Reina C, Puccio G, Vaccaro E, Abenavoli MR, Cavaliere V, Mercati F, Piccionello AP, Gallo G. 2023. Bioactive metabolite survey of Actinobacteria showing plant growth promoting traits to develop novel biofertilizers. *Metabolites*, 13(3): 374.

Felsenstein J. 1985. Phylogenies and the comparative method. *Am Nat*, 125(1): 1-15.

Hayakawa M, Nonomura H. 1987. Humic acid-vitamin agar, a new medium for the selective isolation of soil actinomycetes. *J Ferment Technol*, 65(5): 501-509.

Hickey RJ, Tresner HD. 1952. A cobalt-containing medium for sporulation of *Streptomyces* species. *J Bacteriol*, 64(6): 891.

Hui MLY, Tan LTH, Letchumanan V, He YW, Fang CM, Chan KG, Law JWF, Lee LH. 2021. The extremophilic actinobacteria: From microbes to medicine. *Antibiotics*, 10(6): 682.

Jiang Y, Li Q, Chen X. 2016. Isolation and cultivation methods of actinobacteria. In: Dhanasekaran D, editor. *Actinobacteria-basics and biotechnological application*, IntechOpen, London, UK, pp: 39-57.

Jukes TH, Cantor CR. 1969. Evolution of protein molecules. *Mammal Prot Metabol*, 3(24): 21-132.

Kelly KL. 1964. Color-name charts illustrated with centroid colors. Inter-Society Color Council-National Bureau of Standards, Supplement to NBS Circ. 533, Standard sample No. 2106, Chicago, US.

Kuester E, Williams ST. 1964. Selection of media for isolation of streptomycetes. *Nature*, 202: 928-929.

Kumar A, Gupta R, Shrivastava B, Khasa YP, Kuhad RC. 2012. Xylanase production from an alkalophilic actinomycete isolate *Streptomyces* sp. RCK-2010, its characterization and application in saccharification of second generation biomass. *J Mol Catal B Enzym*, 74(3-4): 170-177.

Lane DJ. 1991. 16S/23S rRNA sequencing. In: Stackebrandt E, Goodfellow M. *Nucleic acid techniques in bacterial systematics*, Wiley, New York, US, pp: 115-175.

Mawang CI, Azman AS, Fuad ASM, Ahamad M. 2021. Actinobacteria: An eco-friendly and promising technology for the bioaugmentation of contaminants. *Biotechnol Rep*, 32: e00679.

Meena B, Anburajan L, Vinithkumar NV, Kirubakaran R, Dharani G. 2019. Biodiversity and antibacterial potential of cultivable halophilic actinobacteria from the deep sea sediments of active volcanic Barren Island. *Microb Pathog*, 132: 129-136.

Miao V, Davies J. 2010. Actinobacteria: the good, the bad, and the ugly. *Antonie Van Leeuwenhoek*, 98: 143-150.

Penkhrue W, Sujarit K, Kudo T, Ohkuma M, Masaki K, Aizawa T, Pathom-Aree W, Khanongnuch C, Lumyong S. 2018. *Amycolatopsis oliviviridis* sp. nov., a novel poly(lactic acid)-bioplastic-degrading actinomycete isolated from paddy soil. *Int J Syst Evol Microbiol*, 68(5): 1448-1454.

Reasoner DJ, Geldreich EE. 1985. A new medium for the enumeration and subculture of bacteria from potable water. *Appl Environ Microbiol*, 49(1): 1-7.

Riquelme C, Rigal F, Hathaway JJ, Northup DE, Spilde MN, Borges PAV, Gabriel R, Amorim IR, Dapkevicius MDLNE. 2015. Cave microbial community composition in oceanic islands: disentangling the effect of different colored mats in diversity patterns of Azorean lava caves. *FEMS Microbiol Ecol*, 91(12): fiv141.

Sadoway T, Rule D, Watson K, Moote P, Soliman LC, Azad N, Donkor K, Cheeptham N, Horne D. 2013. Cure from the cave: volcanic cave actinomycetes and their potential in drug discovery. *Int J Speleol*, 42(1): 5.

Saini A, Aggarwal NK, Sharma A, Yadav A. 2015. Actinomycetes: a source of lignocellulolytic enzymes. *Enzyme Res*, 2015: 279381. <https://doi.org/10.1155/2015/279381>.

Saitou N, Nei M. 1987. The neighbor-joining method: a new method for. *Mol Biol Evol*, 4(4): 406-425.

Sanglier, JJ, Whitehead, D, Saddler, GS, Ferguson, EV and Goodfellow, M. 1992. Pyrolysis mass spectrometry as a method for the classification, identification and selection of actinomycetes. *Gene*, 115(1-2): 235-242.

Saricaoglu S, Saygin H, Topkara AR, Gencbay T, Guven K, Cetin D, Sahin N, Isik K. 2020. *Nonomuraea basaltis* sp. nov., a siderophore-producing actinobacteria isolated from surface soil of basaltic parent material. *Arch Microbiol*, 202: 1535-1543.

Shirling EB, Gottlieb D. 1966. Methods for characterization of *Streptomyces* species. *Int J Syst Bacteriol*, 16(3): 313-340.

Songsumanus A, Kuncharoen N, Kudo T, Yuki M, Ohkuma M, Igarashi Y, Tanasupawat S. 2021. *Actinomadura decatromicini* sp. nov., isolated from mountain soil in Thailand. *J Antibiot*, 74(1): 51-58.

Sottorff I, Wiese J, Imhoff JF. 2019. High diversity and novelty of Actinobacteria isolated from the coastal zone of the geographically remote young volcanic Easter Island, Chile. *Int Microbiol*, 22(3): 377-390.

Tamura K, Stecher G, Kumar S. 2021. MEGA11: molecular evolutionary genetics analysis version 11. *Mol Biol Evol*, 38(7): 3022-3027.

Tan GYA, Ward AC, Goodfellow M. 2006. Exploration of *Amycolatopsis* diversity in soil using genus-specific primers and novel selective media. *Syst Appl Microbiol*. 29(7): 557-569.

Tiwari K, Gupta, RK. 2012. Rare actinomycetes: a potential storehouse for novel antibiotics. *Crit Rev Biotechnol*, 32(2): 108-132.

UNESCO. 2024. List of UNESCO Global Geoparks and Regional Networks. URL: <https://www.unesco.org/en/igpp/geoparks> (accessed date: March 1, 2024).

Weisburg WG, Barns SM, Pelletier DA. 1991. 16S ribosomal DNA amplification for phylogenetic study. *J Bacteriol*, 173(2): 697-703.

Yoon SH, Ha SM, Kwon S, Lim J, Kim Y, Seo H, Chun J. 2017. Introducing EzBioCloud: a taxonomically united database of 16S rRNA gene sequences and whole-genome assemblies. *Int J Syst Evol Microbiol*, 67(5): 1613-1617.



Open Access Journal
e-ISSN: 2619 – 8991

Araştırma Makalesi (Research Article)

Cilt 7 - Sayı 3: 509-520 / Mayıs 2024
(Volume 7 - Issue 3: 509-520 / May 2024)

GEBELİKTE ANNE SAĞLIĞI RİSK GRUPLARININ TAHMİNİNE YÖNELİK MAKİNE ÖĞRENMESİ TABANLI BİR KARAR DESTEK SİSTEM TASARIMI

İrem ŞENYER YAPICI^{1*}, Rukiye UZUN ARSLAN²

¹Zonguldak Bülent Ecevit University, Faculty of Engineering, Department of Computer Engineering, 67100, Zonguldak, Türkiye

²Zonguldak Bülent Ecevit University, Faculty of Engineering, Department of Electrical and Electronics, 67100, Zonguldak, Türkiye

Özet: Gebelik döneminde anne sağlığı risklerinin erken tespiti ve uygun müdahalelerin yapılması, anne ve bebek sağlığı açısından hayati bir önem taşımaktadır. Bu süreçte, büyük veri kümelerinden elde edilen karmaşık ilişkileri ve desenleri otomatik olarak analiz edebilen makine öğrenme (MÖ) algoritmalarının kullanımı son derece kritik bir rol oynamaktadır. MÖ algoritmaları, büyük veri setlerindeki gizli bilgileri açığa çıkararak, gebelikle ilişkili risk faktörlerini daha doğru bir şekilde belirleme imkanı sunmaktadır. Bu bağlamda gerçekleştirilen bu çalışmada, gebelik sürecinde anne sağlığı risk seviyelerinin özellikle yüksek riskli hamileliklerin tahmininde başarının artırılmasına odaklanılmıştır. Bunun için öncelikle başarıyı artıracak önemli (kritik) özellikler belirlenmiş ve altı farklı makine öğrenme algoritması kullanılarak etkili bilgisayar temelli karar destek sistemi tasarlanmaya çalışılmıştır. Ki-Kare testi SelectKBest yöntemiyle birlikte uygulanarak, veri setindeki en kritik özelliklerin yaş, sistolik kan basıncı ve diyastolik kan basıncı olduğu tespit edilmiştir. Yanı sıra veri setindeki dengesizliği gidermek için sentetik azınlık aşırı örnekleme tekniğinden (SMOTE) yararlanılmıştır. Önerilen modelde kullanılan MÖ algoritmalarının başarımları hold-out performans değerlendirme yöntemiyle analiz edilmiştir. Elde edilen bulgular ışığında, SMOTE tekniğinin kullanılmasının gebelikteki risk seviyelerinin tahmininde model başarımlarını artırmada olumlu bir etkiye sahip olduğu belirlenmiştir. Önerilen modelde her bir sınıflandırma algoritması için en yüksek sınıflandırma başarımları yüksek risk sınıfı için elde edilmiştir. Kullanılan algoritmalar arasında, %97 başarı oranıyla en üstün performansa sahip olanın ekstrem gradyan artırma algoritması olduğu tespit edilmiştir. Genel olarak elde edilen sonuçlar, önerilen modelin yüksek risk taşıyan gebeliklerin tespitinde son derece etkili olduğunu doğrulamaktadır. Bu bulgu, önerilen MÖ temelli karar destek sisteminin uzman hekimlere gebelik sürecinde daha doğru teşhisler koyma ve gerekli müdahaleleri daha hızlı bir şekilde gerçekleştirme konusunda önemli bir destek sağlama potansiyeline sahip olduğunu göstermektedir.

Anahtar kelimeler: Gebelik risk sınıfları, Anne sağlığı, Makine öğrenmesi, Özellik seçimi, SMOTE


A Machine Learning-Based Decision Support System Design to Predict Maternal Health Risk Groups during Pregnancy


Abstract: Early detection of maternal health risks during pregnancy and appropriate interventions are vital for maternal and infant health. In this process, the use of machine learning (ML) algorithms that can automatically analyze complex relationships and patterns from large datasets plays a critical role. By revealing hidden information in large data sets, ML algorithms offer the opportunity to more accurately identify pregnancy-related risk factors. In this context, this study focuses on increasing the success of predicting maternal health risk levels during pregnancy, especially in high-risk pregnancies. For this purpose, firstly, important (critical) features that will increase the success are identified and the most effective computer-based decision support system is designed by using six different machine learning algorithms. By applying the Chi-Square test in combination with the SelectKBest method, it was determined that the most critical characteristics in the dataset were age, systolic blood pressure and diastolic blood pressure. In addition, synthetic minority oversampling technique (SMOTE) was utilized to address the imbalance in the dataset. The performance of the ML algorithms used in the proposed model is analyzed by hold-out performance evaluation method. In the light of the findings, it was determined that the use of the SMOTE technique has a positive effect on improving model performance in predicting risk levels in pregnancy. In the proposed model, the highest classification performance for each classification algorithm was obtained for the high risk class. Among the algorithms used, the extreme gradient boosting algorithm was found to have the best performance with a 97% success rate. Overall, the results confirm that the proposed model is highly effective in detecting high-risk pregnancies. This finding shows that the proposed ML-based decision support system has the potential to provide significant support to specialist physicians in making more accurate diagnoses and performing the necessary interventions more quickly during pregnancy.

Keywords: Pregnancy risk classes, Maternal health, Machine learning, Feature selection, SMOTE

*Sorumlu yazar (Corresponding author): Zonguldak Bülent Ecevit University, Faculty of Engineering, Department of Computer Engineering, 67100, Zonguldak, Türkiye

E mail: senyerirem@gmail.com (İ. ŞENYER YAPICI)

İrem ŞENYER YAPICI  <https://orcid.org/0000-0003-0655-340X>

Rukiye UZUN ARSLAN  <https://orcid.org/0000-0002-2082-8695>

Gönderi: 19 Mart 2024

Kabul: 29 Nisan 2024

Yayınlanma: 15 Mayıs 2024

Received: March 19, 2024

Accepted: April 29, 2024

Published: May 15, 2024

Cite as: Şenyler Yapıcı İ, Uzun Arslan R. 2024. A machine learning-based decision support system design to predict maternal health risk groups during pregnancy. BSJ Eng Sci, 7(3): 509-520.



1. Giriş

Günümüzde tıp ve sağlık alanında sağlık hizmetlerinin hastalık önleme konusunda kişi merkezli bir yaklaşım benimsemesi gerektiği kabul edilmektedir. Bu bağlamda, hastalık risklerinin daha hassas bir şekilde değerlendirilmesine olanak tanıyan makine öğrenimi (MÖ) tekniklerinin tıp ve sağlık alanındaki kullanımı giderek artmaktadır. MÖ'nin temel amacı, insan müdahalesinin minimum düzeyde olduğu ya da hiç olmadığı mevcut verilerden öğrenmeyi otomatik olarak gerçekleştiren öğrenme algoritmalarının geliştirilmesidir (Diamantoulaki ve ark., 2022). Literatürde, tıbbi tanı süreçlerinde uzman hekimlere yardımcı olmak amacıyla geliştirilen çok sayıda MÖ temelli karar destek sistemleri bulunmaktadır. Anne sağlığının izlenmesi ve geliştirilmesinde karar destek sistemlerinin kullanımı; hamilelik, doğum ve doğum sonrası dönemlerde annenin ve bebeğin sağlığını korumak adına oldukça önem arz etmektedir. Anne sağlığı, hamilelik, doğum ve doğum sonrası dönemde annenin fiziksel ve psikolojik sağlığını kapsayan bir kavramken; anne sağlığı riski ise bu süreçlerde anne ve bebeğin sağlığını olumsuz etkileyebilecek potansiyel riskleri ifade etmektedir. Bu riskler, anne adayının veya bebeğin sağlığını olumsuz yönde etkileyebilecek çeşitli durumları içermekte olup, gebelik sürecinde veya doğum sonrası dönemde ortaya çıkabilmektedir. Örneğin, yüksek tansiyon, diyabet, enfeksiyonlar, gebelik zehirlenmesi gibi sağlık sorunları anne sağlığı riski olarak değerlendirilmektedir. Ayrıca, gebelik komplikasyonları, doğum sonrası depresyon, doğum sonrası kanamalar gibi durumlar da anne sağlığı riski olarak kabul edilmektedir. Bu bağlamda gebelik sürecinde yüksek riskli gebeliklerin saptanması anne ve fetus sağlığının korunması açısından hayati bir rol oynamaktadır. Bu riskler öngörüldüğü veya teşhis edilebildiği takdirde gerekli önlemler alınabilmekte ve uygun tedavi yöntemleri planlanabilmektedir. Böylelikle anne ve fetus ölümleri kısmen engellenebilmektedir. Gebelikteki risk faktörlerine göre gebelik süreci düşük, orta ve yüksek risk düzeyi olmak üzere üç sınıfa ayrılmaktadır. MÖ algoritmaları sayesinde, geniş veri setleri üzerinde analizler yaparak gebelik sürecinde etkili olan risk faktörleri tanımlanabilmekte ve bu bilgiler kullanarak da gebeliğin risk düzeyleri sınıflandırılabilir. Böylelikle, uzmanlara gebelik sürecini daha yakından takip ederek olası riskleri daha erken aşamada teşhis etmelerinde ve uygun tedavi süreçlerini planlamalarında destek olunmaktadır. Bu bağlamda literatürdeki çalışmalar incelendiğinde, MÖ algoritmalarının gebelikteki risk faktörlerinin belirlenmesinde ve risk düzeylerinin sınıflandırılmasında oldukça başarılı olduğu görülmektedir (Al-Hindi ve ark., 2020; Finlayson ve ark., 2020; Macrohon ve ark., 2022; Togunwa ve Babatunde, 2023; Tokmak, 2023). Örneğin, Rai ve arkadaşları (2018), gebelik komplikasyonları sonucu artan anne ve bebek ölüm risk seviyelerinin parametrelerini değerlendirmek amacıyla anketler aracılığıyla uzmanlardan alınan bilgilere dayanarak yeni

bir model geliştirmişlerdir. Geliştirilen modelin başarımı 117 hamile kadından alınan verilerden 14 özellik seçilerek, yapay sinir ağı (YSA) ve Naive Bayes (NB) algoritmaları kullanılarak analiz edilmiştir. Analizler sonucunda YSA ile %80'lik bir başarımla elde edilirken, NB ile %70 doğruluk oranına ulaşılmıştır. Ahmed ve ark. (2020) tarafından anne sağlık risk faktörlerini tespit etmek için bulut tabanlı bir anne sağlık sistemi önerilmiştir. Önerilen sistemde risk faktörlerinin analizinde, riskin yoğunluğuna göre kategorize etme ve sınıflandırma yaklaşımları kullanılmıştır. Farklı MÖ algoritmaları arasında yapılan karşılaştırmalar sonucunda, gebelik risk seviyesinin sınıflandırılması ve tahmin edilmesi durumunda modifiye karar ağacı (KA) algoritmasının en yüksek doğruluğu verdiği tespit edilmiştir. Ahmed ve Kasem (2020) çalışmalarında risk faktörlerine dayalı olarak gebelikteki risk düzeyini keşfetmek için MÖ algoritmalarından yararlanmışlardır. Çalışmada Pima-Indian-diyabet veri seti kullanılarak risk faktörleri analiz edilmiş ve çeşitli MÖ algoritmaları karşılaştırılmıştır. Yapılan analizler sonucunda gebelik risk seviyesini sınıflandırılmasında ve tahmininde lojistik model ağacı algoritmasının en yüksek doğruluğu verdiği tespit edilmiştir. Buna ek olarak, seçilen birkaç gebe kadının verileri IoT (nesnelerin interneti) özellikli cihazlar aracılığıyla toplanarak, aynı işlemler bu veri kümesine de uygulanmıştır. Karşılaştırmalar sonucunda, risk tahmininin mevcut Pima-Hint diyabet veri kümesi ve gerçek veri kümesi için aynı olduğu gösterilmiştir. 2022 yılında yapılan bir çalışmada, hamilelik sırasında anne sağlığında ortaya çıkabilecek riskleri erken evrede teşhis etmek için rasgele orman (RO) algoritması kullanılmıştır. KA, k-en yakın komşu (KNN), NB gibi algoritmaların da karşılaştırıldığı makalede, RO algoritması %73,37'lük doğruluk oranı ile en yüksek başarımla verdiği tespit edilmiştir. Ayrıca çalışmada modelin genetik algoritmayla optimize edilmesi durumunda başarımın daha da yükseldiği gösterilmiştir (Ramdhani ve ark., 2022). 2022 yılında yapılan başka bir çalışmada özyinelemeli özellik seçimi yapılarak hamilelik dönemindeki risk faktörlerinin sınıflandırılmasında lojistik regresyon (LR), NB ve RO algoritmalarının aynı başarımla verdiği gösterilmiştir (Edayath, 2022). Umoren ve ark. (2022) anne ölümlerine dair risk tahmin modellerini inceleyerek, risk tahminlerini uygulanabilir hale getirmek için KA algoritmasına dayalı bir model geliştirmişlerdir. Geliştirdikleri modelin başarımı, destek vektör makineleri (DVM) dayalı modelle kıyaslanmış ve KA yaklaşımının daha yüksek bir başarımla sahip olduğu ortaya koyulmuştur. Pawar ve ark. (2022) çalışmalarında anne sağlığı risk tahmini için sekiz farklı MÖ algoritması kullanmışlardır. Özellik seçiminin Gini indeksine göre yapıldığı çalışmada en yüksek başarımla RO (%70,21) algoritmasıyla elde edilmiştir. Mutlu ve ark. (2023) IoT tabanlı risk izleme sistemleri aracılığıyla toplanan bir veri seti üzerinde anne sağlığı riskini belirlemek için altı farklı MÖ algoritması kullanmışlardır. Yaş, sistolik kan basıncı, diyastolik kan basıncı, solunum hızı ve kalp atışı

hızı gibi özellikler göz önünde tutularak geliştirdikleri modelin başarımını farklı performans metriklerine göre değerlendirmişlerdir. Yapılan analizler sonucunda en yüksek başarıma KA algoritmasıyla (%89,16) ulaşılmıştır. Şahin ve ark. (2023) anne sağlığı riski tahmininde sekiz farklı MÖ algoritmasının başarımı temel bileşenler analizi (PCA) ve lineer diskriminant analizi (LDA) uygulanması durumları için analiz edilmiştir. Yapılan analizler sonucunda LDA'nın sınıflandırıcı başarımları pozitif yönde etkilediği gösterilmiştir.

Yukarıda bahsedilen çalışmalar, hamilelik sırasında anne sağlığı risklerinin tahmin edilmesinde MÖ ve yapay zekâ tekniklerinin etkin bir şekilde uygulanabileceğini göstermektedir. Ancak, hangi tekniğin daha etkili olduğu konusunda kesin bir cevap bulunmamaktadır. Çünkü her bir tekniğin avantajları ve dezavantajları bulunmakla birlikte, sonuçlar birçok faktöre bağlı olarak değişebilmektedir. Örneğin, bazı durumlarda bir tekniğin başarısı veri setinin özelliklerine, boyutuna ve kalitesine bağlıken, diğer durumlarda kullanılan öznelik seçimi, model hiperparametrelerinin ayarlanması veya eğitim sürecindeki diğer faktörler belirleyici olabilmektedir. Dolayısıyla, en etkili tekniği belirlemek için daha fazla araştırma yapılması ve farklı yöntemlerin kapsamlı bir şekilde karşılaştırılması gerekmektedir. Bu bağlamda gerçekleştirilen bu çalışmada altı farklı MÖ algoritmalarını kullanarak gebelik sırasında oluşabilecek riskler sınıflandırılmıştır. Çalışmanın temel

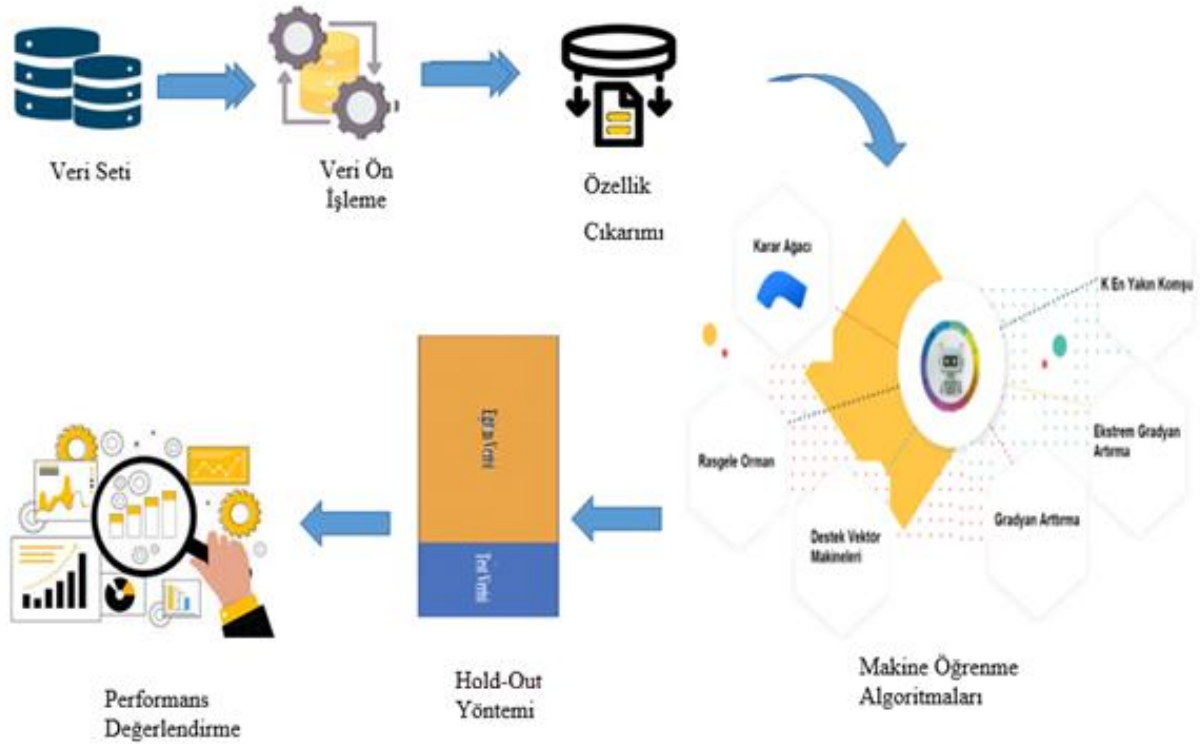
hedefi, yüksek riskli gebeliklerin tespitinde MÖ algoritmalarının ne kadar etkili olduğunu değerlendirmek ve en uygun modeli belirlemektir. Bu çalışmanın, anne sağlığı risklerinin özellikle yüksek gebelik risk seviyesinin erken teşhisinde ve uygun önlemlerin alınmasında uzman hekimlere ve anne adaylarına önemli bir katkı sağlayacağı düşünülmektedir.

2. Materyal ve Yöntem

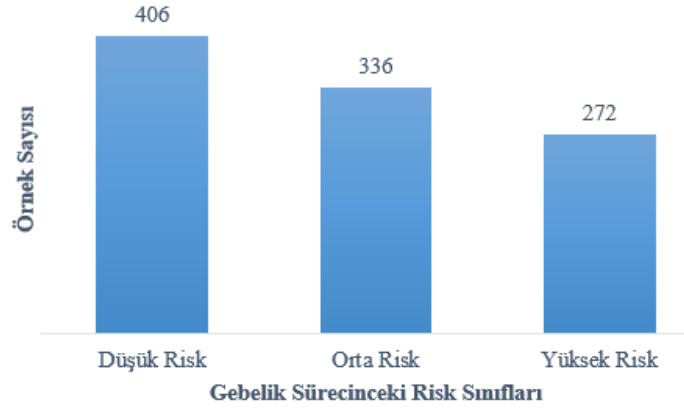
Bu bölümde, gebelik sürecinde anne sağlığı risk seviyesinin tahmine yönelik önerilen bilgisayara destekli karar destek sisteminde kullanılan veri seti, ön işleme, özellik çıkarma yöntemleri ve kullanılan MÖ algoritmaları detaylı bir şekilde açıklanmıştır. Önerilen sistemin genel blok diyagramı Şekil 1'de gösterilmiştir.

2.1. Veri Seti

Çalışmada, açık erişimli UCI Machine Learning Repository veri tabanında yer alan "Maternal Health Risk" başlıklı veri seti kullanılmıştır (Ahmed, 2023). Bangladeş'in farklı bölgelerindeki sağlık kuruluşlarından toplanan veri seti, IoT tabanlı bir risk izleme sistemi aracılığıyla elde edilmiş olup, 1014 örnek ve 7 özellik içermektedir. Tablo 1'de veri setindeki özellikler ve bunların açıklamaları detaylarıyla sunulmuştur. Veri seti, Şekil 2'de gösterildiği gibi 272 yüksek risk (%26,82), 336 orta risk (%33,14) ve 406 düşük risk (%40,04) sınıflarına ait örnekler içermektedir. Tablo 2' de veri setine ait örnek bir görünüm verilmiştir.



Şekil 1. Önerilen modelin blok diyagramı.



Şekil 2. Kullanılan veri setindeki örneklerin risk sınıflarına göre dağılımı.

Tablo 1. Veri setinde yer alan özelliklerinin tanımı ve ölçü birimleri

Özellik	Tanımı	Ölçü Birimi
Yaş	Anne hamilelik yaşı	Nümerik (Yıl)
Sistolik Kan Basıncı	Kalbin kasılması sırasında arterlerdeki maksimum basınç	Nümerik (mmHg)
Diastolik Kan Basıncı	Kalbin gevşemesi sırasında arterlerdeki minimum basınç	Nümerik (mmHg)
Kan Şekeri	Kandaki glukoz miktarı	Nümerik (mmol/L)
Vücut Sıcaklığı	Annenin vücut sıcaklığı	Nümerik (°F)
Kalp Atış Hızı	Normal dinlenme durumunda dakikadaki kalp atış hızı	Nümerik (BPM)
Risk Seviyesi	Hamilelik risk düzeyi	Kategorik

Tablo 2. Kullanılan veri setindeki gebelik döneminde anne sağlığı risk sınıflarına ait örnek

Yaş	Sistolik Kan Basıncı	Diastolik Kan Basıncı	Kan Şekeri	Vücut Sıcaklığı	Kalp Atış Hızı	Risk Seviyesi
48	120	80	11	98	88	Yüksek Risk
17	90	63	6.9	101	70	Orta Risk
33	120	75	10	98	70	Yüksek Risk
30	120	80	7.8	98	70	Düşük Risk
40	140	100	13	101	66	Yüksek Risk
20	120	75	7.5	98	70	Düşük Risk
17	110	75	12	101	76	Yüksek Risk
34	120	75	8	98	70	Düşük Risk
25	140	100	7.01	98	80	Yüksek Risk

2.2. Özellik Seçimi

Öngörücü bir modelin geliştirilmesinde özellik seçimi, veri kümesinden tahmin değişkenine veya çıktısına en çok katkı sağlayan özelliklerin belirlenmesi sürecidir. Veri setindeki özelliklerin doğru seçimi modelin daha hızlı ve daha doğru sonuçlar üretmesine yardımcı olurken, gereksiz veya gürültülü özelliklerin çıkarılmasıyla modelin genelleme yeteneğini arttırmaktadır. Böylelikle daha etkili ve güvenilir bir öğrenme süreci sağlanmaktadır (Selvakuberan ve ark., 2008; Jahan ve ark., 2021). Sınıflandırma tekniklerinde uygulanan farklı özellik seçim yöntemleri bulunmaktadır. Bunlardan biri olan Ki-kare yöntemi, kategorik değişkenler arasındaki ilişkiyi istatistiksel açıdan değerlendirmektedir. Bu yöntemde özelliklerin hedef değişkenle bağımsızlığını incelenerek, değişkenler arasındaki ilişkinin anlamlı olup olmadığını belirlemektedir. Uygulamalarda genellikle, Ki-kare,

SelectKBest veya benzeri bir yöntemle birlikte kullanılmaktadır (Kırlı ve ark., 2023). Bu bağlamda gerçekleştirilen bu çalışmada Ki-Kare SelectKBest yöntemiyle birlikte kullanılarak uygulanmıştır. SelectKBest, bir sınıflandırıcı için veri setindeki en anlamlı ve etkili olan özellikleri seçmek için kullanılmaktadır. Yöntem veri setindeki her bir özelliğin sınıflandırıcıdaki önemini belirlemek için Ki-kare testini kullanarak, en yüksek skora sahip olan özellikleri seçmektedir. Böylelikle, verilerin sınıflandırılmasında gereksiz veya az katkı sağlayan özellikler elimine edilerek sınıflandırma doğruluğu artırılmaktadır.

2.3. Sentetik Azınlık Aşırı Örnekleme Tekniği (SMOTE)

Sentetik Azınlık Aşırı Örnekleme Tekniği (SMOTE), dengesiz veri setlerinde sınıf dengesini sağlamak için kullanılan bir yöntemdir. Bu teknik, azınlık sınıfına ait örneklerin sentetik olarak oluşturulmasını sağlayarak,

veri setindeki sınıflar arasındaki dengesizliği azaltmaktadır. SMOTE, azınlık sınıfındaki örnekler arasında benzerlik ölçüsüne dayalı olarak yeni sentetik örnekler oluşturmaktadır. Bu şekilde, azınlık sınıfı daha dengeli bir şekilde temsil edilerek, sınıflandırma performansları artırılmaktadır (Abacı ve Yıldız, 2023).

2.4. Sınıflandırma Algoritmaları

Sınıflandırma; veri noktalarının belirli özelliklerine göre analiz edilerek, bunları önceden tanımlanmış sınıflara veya kategorilere atama sürecidir. Bu süreç, MÖ algoritmaları kullanılarak gerçekleştirilmekte ve genellikle bir modelin eğitilmesiyle sağlanmaktadır. Çalışma kapsamında hamilelik sürecinde anne sağlığı risklerinin sınıflandırılmasında altı farklı MÖ algoritması kullanılmıştır (Şekil 3).



Şekil 3. Kullanılan makine öğrenme algoritmaları.

k en yakın komşu (KNN) algoritması, sınıflandırma ve regresyon problemleri için kullanılan popüler bir denetimli MÖ algoritmasıdır. Özellikle küçük boyutlu veri kümelerinde ve sınıflar arasındaki ayrımın belirgin olduğu durumlarda etkili bir şekilde çalışmaktadır. Bu algortmada yeni bir veri noktası sınıflandırılırken, k en yakın komşusu dikkate alınmaktadır. Bunun için genellikle Öklid, Manhattan veya Minkowski gibi uzaklık ölçümleri kullanılarak yeni veri noktası ile en yakın k komşuları arasındaki mesafeler hesaplanmaktadır. Hesaplama işleminden sonra k komşunun etiketlerine göre test örneğinin sınıfını belirlemektedir (Hacıbeyoğlu ve ark., 2023).

Karar ağacı (KA), bir veri kümesindeki özelliklerin değerlerine göre sınıflandırma veya regresyon yapmak için kullanılan bir algortmadır. Algortmada veri kümesini en iyi şekilde bölmek için bir dizi karar kuralı oluşturulmakta ve bu kurallar kullanılarak veri daha homojen alt kümelere ayırmaktadır. Böylelikle, basit kararlarla karmaşık ilişkileri açıklama ve yorumlama kolaylığı sağlanmaktadır (Yakut ve Bolat, 2020).

Rasgele Orman (RO), birçok karar ağacının bir araya gelerek oluşturduğu bir ensemble (topluluk) öğrenme algoritmasıdır. Algortmada her bir karar ağacı, rastgele özellikler kullanılarak eğitilmekte ve ardından bunların sonuçlarını bir araya getirilerek hem daha kararlı hem de

genelleştirilebilir bir tahmin yapılmaktadır (Yıldız ve ark., 2023).

Destek vektör makineleri (DVM), veri noktalarını sınıflandırmak veya regresyon yapmak için kullanılan parametrik olmayan güçlü bir denetimli MÖ algoritmasıdır. Algortma; veri noktalarını ayıran en iyi hiperdüzlemi bulmaya çalışarak, sınıflandırma problemlerinde optimum ayrımı sağlamaktadır (Elen ve ark., 2022).

Gradyan arttırma (Gradient Boosting, GB) zayıf tahminicileri (genellikle karar ağaçları) bir araya getirerek güçlü bir tahminci oluşturan MÖ algoritmasıdır. Bu algortma, tahmin edilen ve gerçek değer arasındaki hatayı en aza indirmek için ardışık öğrenme adımları kullanmaktadır. Her adımda, önceki modelin hatalarına odaklanarak yeni bir tahminci ekleyerek modelin performansını arttırmaktadır. Algortmanın temel prensibi, modelin doğru tahmin edemediği veya tahminde zorlanılan örnekler üzerine odaklanarak performansı iyileştirmektir (Friedman, 2002).

Ekstremler gradyan arttırma (Extreme Gradient Boosting, XGBoost), GB algoritmasının optimize edilmiş ve performansı artırılmış bir versiyonudur. Büyük veri kümeleriyle etkili bir şekilde çalışabilen bu algortma, paralel hesaplama yetenekleri ve düşük bellek kullanımıyla öne çıkmaktadır. Ayrıca özelleştirilebilir kayıp fonksiyonları ve düzenleme teknikleri gibi gelişmiş özelliklere sahip olması, modelin performansını artırırken aşırı uyumu azaltmaktadır (Gündoğdu, 2023).

2.5. Performans Metrikleri

Karmaşıklık matrisi (confusion matrix), bir sınıflandırma modelinin performansının değerlendirilmesinde sıklıkla kullanılan bir yöntemdir. Karmaşıklık matrisi, bir sınıflandırıcının bazı test verilerine göre sınıflandırma performansını tanımlayan $N \times N$ boyutlu bir matristir. Bu matris gerçek ve tahmin edilen sınıflar arasındaki ilişkiyi göstermektedir. Bu matris modelin tahminlerinin gerçek sınıflarla karşılaştırılmasını vermekte olup, genellikle dört ana kategoriye içermektedir: Doğru pozitif (DP), Doğru negatif (DN), Yanlış pozitif (YP), Yanlış negatif (YN). Bu kategoriler; modelin doğruluğunu, hassasiyetini, geri çağırma, F1 puanını ve diğer performans metriklerini hesaplamak için kullanılmaktadır. Çalışmada gebelik sürecinde anne sağlığı risk seviyesinin sınıflandırılması amacıyla önerilen MÖ temelli modelin performansı aşağıda verilen denklemlere göre hesaplanan doğruluk, kesinlik, geri çağırma ve F1 skor metriklerine göre değerlendirilmiştir (Eşitlik 1-4).

$$\text{Doğruluk (Accuracy, ACC)} = \frac{DP + DN}{DP + DN + YP + YN} \quad (1)$$

$$\text{Kesinlik (Precision, Prec)} = \frac{DP}{DP + YP} \quad (2)$$

$$\text{Geri çağırma (Recall)} = \frac{DP}{DP + YN} \quad (3)$$

$$F1 - \text{Skor} = 2 * \frac{\text{Recall} * \text{Prec}}{\text{Recall} + \text{Prec}} \quad (4)$$

3. Bulgular ve Tartışma

Yapılan bu çalışmada, MÖ algoritmalarının gebelik sürecinde anne sağlığı risk durumlarının (özellikle yüksek riskli hamilelik geçiren annelerin) tespitindeki başarımları ele alınmıştır. Bunun için 406 "düşük risk", 336 "orta risk" ve 272 "yüksek risk" olmak üzere toplam 1014 örnek içeren bir veri seti kullanılarak altı farklı MÖ algoritmasının başarımları araştırılmıştır. Bu doğrultuda çalışmada ilk olarak, algoritmaların sınıflandırma başarımlarını artırmak amacıyla gebelik sürecinde etkili olan majör risk faktörleri tespit edilmiştir. Bu amaç doğrultusunda Ki-Kare testi SelectKBest yöntemiyle uygulanarak, veri setindeki gereksiz bilgi içeren (etkisiz, anlamsız) özellikler çıkartılmıştır. Analizler sonucunda gebelik sürecinde anne sağlığı risk durumlarının tespitinde yaş, sistolik kan basıncı ve diyastolik kan basıncının daha belirleyici (etkili) olduğu tespit edilmiştir. Daha sonra bu üç özellik kullanılarak altı farklı MÖ algoritmasının sınıflandırma başarımları hold-out performans değerlendirme yöntemiyle analiz edilmiştir. Bununla birlikte çalışma kapsamında MÖ algoritmalarının başarımları, hold-out yönteminin veri setindeki dengesizlikleri elimine etmek amacıyla SMOTE tabanlı örnekleme yöntemiyle birlikte uygulanması durumu için de değerlendirilmiş ve sonuçlar karşılaştırmalı olarak verilmiştir. Hold-out yönteminde

veri seti %80'i eğitim %20'si test verisi olacak şekilde bölünmüştür. Çalışmada kullanılan MÖ algoritmaları, literatürde gebelik sürecinde anne sağlığı risk durumlarının tespitine yönelik yapılan çalışmalar incelenerek seçilmiştir. Bu doğrultuda, K-en yakın komşu (KNN), karar ağacı (KA), rasgele orman (RO) , gradyan arttırma (GB), ekstrem gradyan arttırma (XGBoost) ve destek vektör makineleri (DVM) algoritmaları kullanılmıştır. Phyton programında yapılan analizlerin sonuçları karmaşıklık matrisiyle incelenerek, modellerin performanslarını karşılaştırmak adına karmaşıklık matrisi ile hesaplanan doğruluk, duyarlılık, özgülük ve F-skoru değerleri birlikte sunulmuştur. Bu bağlamda çalışmada ilk olarak KNN algoritmasına ait performans metrikleri elde edilerek, Tablo 3' de verilmiştir.

Tablo 3 incelendiğinde; SMOTE uygulanmayan veri setinde en yüksek doğruluk oranı %92 ile "yüksek risk" seviyesinde, en düşük doğruluk oranı ise %70 ile "orta risk" seviyesinde elde edilmiştir. Veri setine SMOTE uygulanması durumunda da benzer şekilde en yüksek (%93) ve en düşük (%72) doğruluk oranları sırasıyla "yüksek risk" ve "orta risk" seviyelerinde elde edilmiştir. Elde edilen sonuçlar içerisinden en yüksek sınıflandırma oranının elde edildiği yani hold-out yönteminin SMOTE ile birlikte uygulanması durumu için KNN algoritmasına ait karmaşıklık matrisi Şekil 4'de verilmiştir.

Tablo 3. KNN algoritmasına ait performans metrikleri

	Risk Sınıfı	Risk Sınıfı			
		(%)	Düşük	Orta	Yüksek
Hold-out	ACC		73	70	92
	Prec		89	38	79
	Recall		61	69	84
	F1-skor		72	49	81
Hold-out & SMOTE	ACC		80	78	93
	Prec		77	72	78
	Recall		70	66	98
	F1-skor		73	69	87

Gerçek Sınıf	Tahmini Sınıf		
	Düşük risk	Orta risk	Yüksek risk
Düşük risk	67	20	
Orta risk	22	58	1
Yüksek risk	7	10	59

Şekil 4. KNN algoritmasına ait karmaşıklık matrisi.

Şekil 4'de verilen KNN algoritmasına ait karışıklık matrisi incelendiğinde, test verilerinin sınıflandırılmasında %75.41'lik bir doğruluk oranı elde edilmiştir. Yani KNN algoritmasıyla 244 adet test verisinin 184'ü doğru 60 tanesi yanlış sınıflandırılmış olup, en yüksek sınıflandırma başarımı "yüksek risk" sınıfı için elde edilmiştir. Tablo 4'de KA algoritmasına ait performans metrikleri verilmiştir.

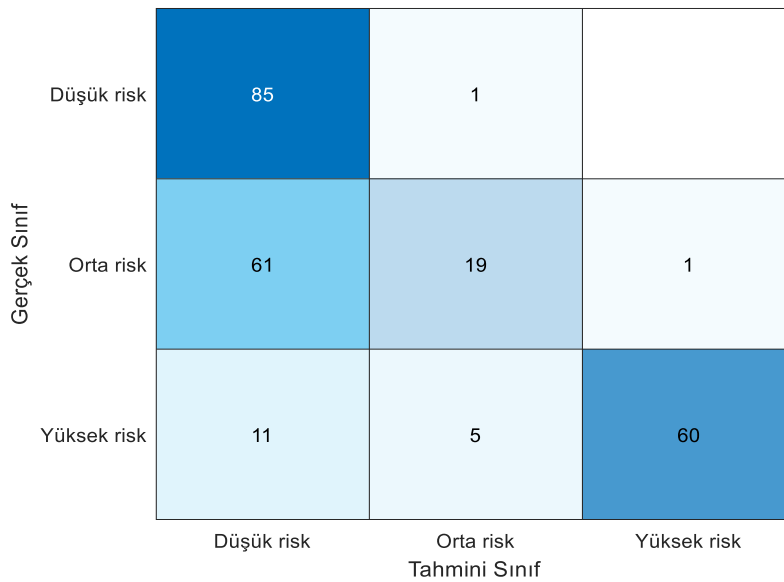
Tablo 4'de sunulan KA algoritmasına ait performans metriklerine göre; SMOTE uygulanmayan veri seti için en yüksek sınıflandırma başarım oranı %93 ile "yüksek risk" seviyesinde, en düşük sınıflandırma başarım oranı ise %67 ile "orta risk" seviyesinde tespit edilmiştir. Veri setine SMOTE uygulandığında ise; en yüksek sınıflandırma başarımına %93'lük bir oranla "yüksek risk" seviyesinde, en düşük sınıflandırma başarımına da %70'lik bir oranla "düşük risk" seviyesinde ulaşılmıştır. Her iki durum için de en yüksek sınıflandırma başarımlarının eşit olduğu ve bunların "yüksek risk" seviyesinde elde edildiği tespit edilmiştir. Buna dayanarak Şekil 5'de her iki durum için ayrı ayrı KA algoritmasına ait karmaşıklık matrisleri verilmiştir.

Şekil 5'den de açıkça görüldüğü üzere, veri setine SMOTE uygulanmadığında 244 tane test verisinin 173'ü doğru 71'i yanlış sınıflandırılırken; SMOTE uygulanmasını durumda ise 165 tanesi doğru ve 79 tanesi yanlış sınıflandırılmıştır. Veri setine SMOTE uygulanmaması durumunda %71'lik, SMOTE uygulanması durumunda ise %68'lik bir başarıma ulaşılmıştır. En yüksek sınıflandırma başarımları her iki durum içinde "yüksek risk" sınıfında edilmiştir. Tablo 5'de DVM algoritmasına ait performans metrikleri verilmiştir.

DVM algoritmasına ait sınıflandırma performans metrikleri incelendiğinde, veri setine SMOTE uygulanmaması halinde en yüksek doğruluk oranı %92 ile "yüksek risk" seviyesinde, en düşük doğruluk oranı ise %67 ile "orta risk" seviyesinde elde edilmiştir. Veri setine SMOTE uygulanması durumunda ise en yüksek doğruluk değeri %93 ile "yüksek risk" seviyesinde iken, en düşük doğruluk oranı %73 ile "düşük risk" seviyesindedir. En yüksek sınıflandırma oranının elde edildiği durum (yani hold-out yönteminin SMOTE ile birlikte uygulanması durumu) için algoritmaya ait karışıklık matrisi Şekil 6'da verilmiştir.

Tablo 4. KA algoritmasına ait performans metrikleri

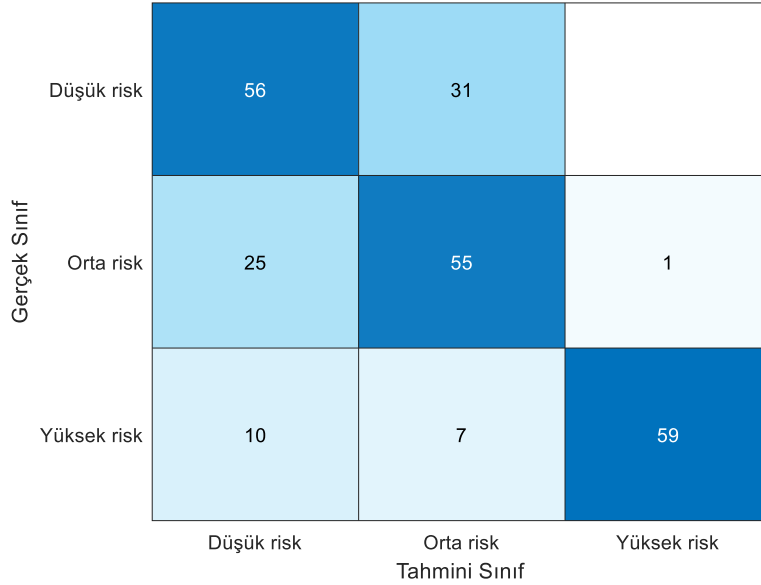
	Risk Sınıfı	Risk Sınıfı			
		(%)	Düşük	Orta	Yüksek
Hold-out	ACC		70	67	93
	Prec		50	70	83
	Recall		67	55	85
	F1-skor		67	55	85
Hold-out & SMOTE	ACC		70	72	93
	Prec		99,4	23	79
	Recall		54	76	98
	F1-skor		70	36	88



Şekil 5. KA ait karmaşıklık matrisi (a) Hold-Out, (b) Hold-out+SMOTE.

Tablo 5. DVM algoritmasına ait performans metrikleri

	Risk Sınıfı			
		(%)	Düşük	Orta
Hold-out	ACC	68	67	92
	Prec	95	21	79
	Recall	55	70	86
	F1-skor	70	32	82
Hold-out & SMOTE	ACC	73	74	93
	Prec	64	68	78
	Recall	62	59	98
	F1-skor	63	63	87



Şekil 6. DVM algoritmasına ait karmaşıklık matrisi.

Şekil 6’de gösterilen DVM algoritmasına ait karmaşıklık matrisi incelendiğinde test verilerinin sınıflandırılmasında %70’lik doğruluk oranı elde edilmiştir. Yani DVM algoritmasıyla 244 tane test verininin 170’i doğru, 74’ü yanlış tahmin edilmiş olup, en yüksek sınıflandırma başarımı “yüksek risk” sınıfı için elde edilmiştir. Tablo 6’da RO algoritmasına ait performans metrikleri sunulmuştur.

RO algoritmasına ait sınıflandırma performans metrikleri incelendiğinde, veri setine SMOTE uygulanması halinde en yüksek doğruluk oranı %93 ile “yüksek risk” seviyesinde, en düşük doğruluk oranı ise %83 ile “orta risk” seviyesinde elde edilmiştir. Veri setine SMOTE uygulanması durumunda ise en yüksek doğruluk değeri %95 ile “yüksek risk” seviyesinde iken, en düşük doğruluk oranı %87 ile “düşük risk” ve “orta risk” seviyelerindedir. Analizlerde en yüksek sınıflandırma oranının elde edildiği durum (yani hold-out+SMOTE durumu) için RO algoritmasına ait karmaşıklık matrisi Şekil 7’de verilmiştir.

Şekil 7’de verilen karmaşıklık matrisi incelendiğinde; RO algoritmasıyla test verilerinin sınıflandırılmasında %85’lik bir sınıflandırma başarımı elde edilmiştir. Yani test için ayrılan 244 verinin 207’si doğru tahmin

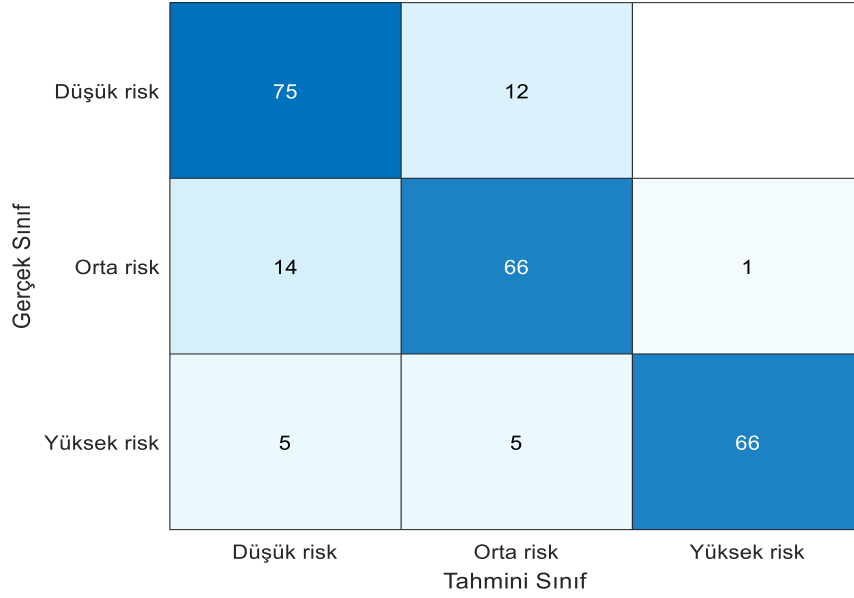
edilirken, 37’si yanlış tahmin edilmiştir. En yüksek sınıflandırma başarımına “yüksek risk” sınıfında ulaşılmıştır. Tablo 7’de GB algoritmasına ait performans metrikleri sunulmuştur.

Tablo 7’de sunulan GB algoritmasına ait sınıflandırma performans metrikleri incelendiğinde, veri setine SMOTE uygulanmaması halinde en yüksek doğruluk oranı %93 ile “yüksek risk” seviyesinde, en düşük doğruluk oranı ise %78 ile “orta risk” seviyesinde olduğu görülmektedir. Veri setine SMOTE uygulanması durumunda en yüksek doğruluk değeri %95 ile “yüksek risk” seviyesinde, en düşük doğruluk değeri ise %82 ile “düşük risk” ve “orta risk” seviyelerindedir. En yüksek sınıflandırma oranının elde edildiği durum (yani hold-out+SMOTE durumu) için algoritmaya ait karmaşıklık matrisi Şekil 8’de verilmiştir.

Şekil 8’deki GB algoritmasına ait karmaşıklık matrisi incelendiğinde, test verilerinin sınıflandırılmasında %79’luk bir doğruluk oranı elde edilmiştir. Yani GB algoritmasıyla 244 tane test verisinin 193’ü doğru, 51’i yanlış sınıflandırılmış olup, en yüksek sınıflandırma başarımı “yüksek risk” sınıfı için elde edilmiştir.

Tablo 6. RO algoritmasına ait performans metrikleri

	Risk Sınıfı			
		(%)	Düşük	Orta
Hold-out	ACC	85	83	93
	Prec	85	76	79
	Recall	78	78	88
	F1-skor	81	77	83
Hold-out & SMOTE	ACC	87	87	95
	Prec	86	81	87
	Recall	80	80	99
	F1-skor	83	80	92



Şekil 7. RO algoritmasına ait karmaşıklık matrisi.

Tablo 7. GB algoritmasına ait performans metrikleri

	Risk Sınıfı			
		(%)	Düşük	Orta
Hold-out	ACC	80	78	93
	Prec	75	72	81
	Recall	74	70	88
	F1-skor	75	71	84
Hold-out & SMOTE	ACC	82	82	95
	Prec	75	77	87
	Recall	75	70	96
	F1-skor	75	73	91

Tablo 8. XGB algoritmasına ait performans metrikleri

	Risk Sınıfı			
		(%)	Düşük	Orta
Hold-out	ACC	88	85	95
	Prec	86	79	87
	Recall	83	81	89
	F1-skor	85	80	88
Hold-out & SMOTE	ACC	89	88	97
	Prec	85	85	91
	Recall	84	80	99
	F1-skor	84	83	95

Gerçek Sınıf	Düşük risk	65	22	
	Orta risk	16	62	3
	Yüksek risk	6	4	66
		Düşük risk	Orta risk	Yüksek risk
		Tahmini Sınıf		

Şekil 8. GB algoritmasına ait karmaşıklık matrisi.

Gerçek Sınıf	Düşük risk	74	13	
	Orta risk	11	69	1
	Yüksek risk	3	4	69
		Düşük risk	Orta risk	Yüksek risk
		Tahmini Sınıf		

Şekil 9. XGB algoritmasına ait karmaşıklık matrisi.

XGB algoritmasına ait performans metrikleri Tablo 8’de verilmiştir. Tablodan da açıkça görüldüğü üzere, veri setine SMOTE uygulanmaması halinde en yüksek doğruluk oranı %95 ile “yüksek risk” seviyelerinde, en düşük doğruluk oranı ise %85 ile “orta risk” seviyesinde elde edilmiştir. Veri setine SMOTE uygulanması durumunda ise en yüksek doğruluk değeri %97 ile “yüksek risk” seviyelerinde iken, en düşük doğruluk değeri %88 ile “orta risk” seviyesindedir. Analizler sonucunda en yüksek sınıflandırma oranının elde edildiği durum (yani hold-out+SMOTE) için algoritmaya ait karmaşıklık matrisi Şekil 9’da verilmiştir.

Şekil 9’deki XGB algoritmasına ait karmaşıklık matrisi incelendiğinde test verilerinin sınıflandırılmasında %87’lik doğruluk oranı elde edilmiştir. XGB algoritmasıyla test için ayrılan 244 verinin 212’si doğru, 32’si yanlış tahmin edilmiştir. En yüksek sınıflandırma

başarımı “yüksek risk” sınıfı için elde edilmiştir.

Elde edilen bulgulara dayanarak genel anlamda gebelik sürecinde anne sağlığı risk tahmininde SMOTE örnekleme tekniğinin kullanımı önerilen modelin başarımını önemli ölçüde arttırdığı belirlenmiştir. Bu bağlamda anne sağlığı risk veri setinden elde edilen üç farklı koşulun (düşük, orta ve yüksek) sınıflandırma sürecinde, kullanılan MÖ algoritmaları arasından en yüksek başarımları %87 ile XGB algoritmasıyla elde edilmiştir. Bu sınıflandırma başarımını sırasıyla %85 ile RO, %79 ile GB, %75 ile KNN, %70 ile DVM ve %68 ile KA sınıflandırıcısı takip etmiştir. Bununla birlikte önerilen modelde risk grupları arasında en yüksek sınıflandırma başarımı her bir algoritma için yüksek risk sınıfında elde edilmiştir. Bu bağlamda, elde edilen yüksek risk grubuna ait sınıflandırma başarımları kNN, KA ve DVM algoritmaları için %93 iken, RO ve GB algoritmaları içinse %95 olarak

hesaplanmıştır. Bu gruba ait en yüksek başarı oranı ise %97 ile XGB algoritmasıyla elde edilmiştir.

4. Sonuç

Gebelik, anne ve bebeğin sağlığı üzerinde önemli etkilere sahip olan karmaşık bir süreçtir. Anne adayının gebelik sürecinde karşılaşılabileceği çeşitli sağlık riskleri, hem anne hem de bebeğin sağlığı açısından ciddi sonuçlar doğurabilmektedir. Bu nedenle, gebelik sürecindeki risklerin erken aşamada tanınması ve etkili bir şekilde yönetilmesi büyük önem taşımaktadır. Ancak, gebelik sırasında ortaya çıkabilecek potansiyel sağlık risklerinin erken aşamada teşhis edilmesi ve etkin bir şekilde yönetilmesi, birçok sağlık sistemi için hala bir zorluktur. Bu bağlamda son yıllarda, gebelik sürecinde uzman hekimlerin karar alma sürecine yardımcı olmak için bilgisayar tabanlı karar destek sistemlerinin geliştirilmesine verilen önem giderek artmaktadır. Gebelik sırasında ortaya çıkabilecek çeşitli risk faktörlerini değerlendirmek ve sınıflandırmak, uzman hekimlerin erken müdahalelerde bulunmasını sağlayarak olası komplikasyonları en aza indirebilir.

Bu çalışmada, gebelik sürecinde anne sağlığı risk seviyelerinin sınıflandırılmasında farklı MÖ algoritmalarının başarımları analiz edilmiştir. Bunun için K-NN, G-NB, KA, RO, LR, XGBoost ve GB algoritmaları kullanılmıştır. Algoritmalarının başarımları hold-out performans değerlendirme kriterine göre elde edilmiştir. Yanı sıra MÖ algoritmalarının başarımları aynı performans değerlendirme kriterine göre veri setindeki dengesizlikler SMOTE örnekleme tekniğiyle giderilmesi durumu için de incelenmiştir. Bununla birlikte çalışmada Chi-kare testi SelectBest özellik seçim yöntemlerine dayanarak gebelik sürecinde anne sağlığı üzerinde etkili (anlamlı) özelliklerin yaş, sistolik kan basıncı ve diyastolik kan basıncı olduğu tespit edilmiştir. Bu özelliklere dayalı önerilen modelin başarımları, tüm özelliklerin kullanıldığı duruma karşılaştırıldığında daha yüksek bulunmuştur. Elde edilen bulgular ışığında hem özellik seçiminin hem de SMOTE tekniğinin gebelik sürecinde anne sağlığı risk seviyesinin (özellikle yüksek risk grubunun) tahmininde sınıflandırıcıların performanslarını önemli ölçüde arttırdığı tespit edilmiştir. Literatürde aynı veri setini kullanılarak daha yüksek başarımların elde edildiği çalışmalar mevcuttur. Bunun temel nedeni eğitim ve test verilerinin bölünmesindeki ayrımların yanı sıra, sınıflandırıcı performans değerlendirme yöntemlerindeki farklılıklarından kaynaklanmaktadır.

Ancak, bu çalışmanın bazı sınırlamaları bulunmaktadır. Örneğin, veri setimizdeki eksiklikler ve kısıtlamalar, makine öğrenmesi algoritmalarının genelleştirilebilirliğini etkileyebilmektedir. Bu bağlamda gelecekte daha geniş ve çeşitli veri setleri kullanılarak, modelin performansını arttırmaya yönelik çalışmaların yapılması planlanmaktadır. Bununla birlikte, daha karmaşık MÖ tekniklerinin yanı sıra, modelin klinik uygulamalarda kullanılabilirliğini artırmak için

anlaşılabilirlik açısından daha şeffaf yaklaşımlar araştırılacaktır.

Katkı Oranı Beyanı

Yazar(lar)ın katkı yüzdesi aşağıda verilmiştir. Tüm yazarlar makaleyi incelemiş ve onaylamıştır.

	İ.Ş.Y.	R.U.A.
K	50	50
T	50	50
Y	30	70
VTI	60	40
VAY	60	40
KT	60	40
YZ	50	50
KI	50	50
GR	100	
PY	40	60

K= kavram, T= tasarım, Y= yönetim, VTI= veri toplama ve/veya işleme, VAY= veri analizi ve/veya yorumlama, KT= kaynak tarama, YZ= Yazım, KI= kritik inceleme, GR= gönderim ve revizyon, PY= proje yönetimi.

Çatışma Beyanı

Yazarlar bu çalışmada hiçbir çıkar ilişkisi olmadığını beyan etmektedirler.

Etik Onay Beyanı

Bu çalışmada hayvanlar ve insanlar üzerinde herhangi bir çalışma yapılmadığı için etik kurul onayı alınmamıştır.

Kaynaklar

- Abacı İ, Yıldız K. 2023. SMOTE vs. KNNOR: An evaluation of oversampling techniques in machine learning. *Gümüşhane Üniv Fen Bil Derg*, 13(3): 767-779.
- Ahmed M, Kashem MA, Rahman M, Khatun S. 2020. Review and analysis of risk factor of maternal health in remote area using the Internet of Things (IoT). 5th International Conference on Electrical, Control & Computer Engineering, July 29, Kuantan, Pahang, Malaysia, pp: 357-365.
- Ahmed M, Kashem MA. 2020. IoT based risk level prediction model for maternal health care in the context of Bangladesh. 2nd International Conference on Sustainable Technologies for Industry 4.0, December 19-20, Dhaka, Bangladesh, pp: 1-6.
- Ahmed M. 2023. Maternal health risk. UCI Machine Learning Repository. DOI: <https://doi.org/10.24432/C5DP5D> (erişim tarihi: 2 Şubat 2023).
- Al-Hindi MY, Al Sayari TA, Al Solami R, Baiti AKA, Alnemri JA, Mirza IM, Faden YA. 2020. Association of antenatal risk score with maternal and neonatal mortality and morbidity. *Cureus*, 12(12): e12230.
- Diamantoulaki I, Diamantoulakis PD, Bouzinis PS, Sarigiannidis P, Karagiannidis GK. 2022. Health risk assessment with federated learning. International Balkan Conference on Communications and Networking, Aug. 22-24, Sarajevo · Bosnia and Herzegovina, pp: 57-61.
- Edayath P. 2022. Analysis of factors affecting maternal health using data mining techniques. Doctoral dissertation, The University of Texas at El Paso, US.
- Elen A, Baş S, Közkurt C. 2022. An adaptive gaussian kernel for support vector machine. *Arabian J Sci Eng*, 47(8): 10579-

- 10588.
- Finlayson K, Crossland N, Bonet M, Downe S. 2020. What matters to women in the postnatal period: A meta-synthesis of qualitative studies. *PloS One*, 15(4): e0231415.
- Friedman JH. 2002. Stochastic gradient boosting. *Comput Stat Data Anal*, 38(4): 367-378.
- Gündoğdu S. 2023. Efficient prediction of early-stage diabetes using XGBoost classifier with random forest feature selection technique. *Multim Tools Appl*, 82(22): 34163-34181.
- Hacıbeyoğlu M, Çelik M, Çiçek ÖE. 2023. K en yakın komşu algoritması ile binalarda enerji verimliliği tahmini. *Necmettin Erbakan Üniv Fen Müh Bil Derg*, 5(2): 28-37.
- Jahan S, Islam MS, Islam L, Rashme TY, Prova AA, Paul BK, Mosharof MK. 2021. Automated invasive cervical cancer disease detection at early stage through suitable machine learning model. *SN Appl Sci*, 3: 1-17.
- Kırlı OA, Sansarcı M, Özkaraca O, Çetin G. 2023. Manyetik rezonans görüntülerinden beyin tümörü tespitinde sınıflandırma algoritmalarının karşılaştırmalı analizi. *Türk Müh Araş Eğit Derg*, 2(2): 113-122.
- Macrohon JJE, Villavicencio CN, Inbaraj XA, Jeng JH. 2022. A semi-supervised machine learning approach in predicting high-risk pregnancies in the Philippines. *Diagnostics*, 12(11): 2782.
- Mutlu HB, Durmaz F, Yücel N, Cengil E, Yildirim M. 2023. Prediction of maternal health risk with traditional machine learning methods. *Naturengs*, 4(1): 16-23.
- Pawar L, Malhotra J, Sharma A, Arora D, Vaidya D. 2022. A robust machine learning predictive model for maternal health risk. 3rd International Conference on Electronics and Sustainable Communication Systems, August 17-19, Coimbatore, India, pp: 882-888.
- Rai SK, Sowmya K. 2018. A review on use of machine learning techniques in diagnostic health-care. *AI Syst Mach Learn*, 10(4): 102-107.
- Ramdhani Y, Maulidia D, Setiadi A, Alamsyah DP. 2022. Feature weighting optimization: Genetic algorithms and random forest for classification of pregnant potential risk. *International Conference on Information Technology Research and Innovation*, November 10, Virtual, pp: 95-100.
- Selvakuberan K, Indradevi M, Rajaram R. 2008. Combined feature Selection and classification-A novel approach for the categorization of web pages. *J Info Comput Sc*, 3(2): 083-089.
- Şahin F, Tulum G, Karaca Ş. 2023. Anne sağlığı riski için makine öğrenmesi modellerinin performans karşılaştırması. *Dicle Üniv Müh Fak Müh Derg*, 14(4): 547-553.
- Togunwa TO, Babatunde AO. 2023. Deep hybrid model for maternal health risk classification in pregnancy: synergy of ANN and random forest. *Front AI*, 6: 1213436.
- Tokmak M. 2023. Anne sağlık durumu riskinin makine öğrenmesi yöntemleri ile belirlenmesi1. In: Bozdemir M, uzun Arslan R, editörler. *Müh Alanında Akademik Analiz ve Tartışmalar*, Editörler, Özgür Yayınları, Gaziantep, Türkiye, pp: 75.
- Umoren I, Chigozirim F, Silas A, Ekong B. 2022. Modeling and prediction of pregnancy risk for efficient birth outcomes using decision tree classification and regression model. URL: https://www.researchgate.net/profile/Imeh-Umoren/publication/359742528_Modeling_and_Prediction_of_Pregnancy_Risk_for_Efficient_Birth_Outcomes_Using_Decision_Tree_Classification_and_Regression_model/links/624c5b31ef01342066596129/Modeling-and-Prediction-of-Pregnancy-Risk-for-Efficient-Birth-Outcomes-Using-Decision-Tree-Classification-and-Regression-model.pdf (erişim tarihi: 15 Ocak 2024)
- Yakut Ö, Bolat E. 2020. Arrhythmia diagnosis from ECG signal using tree-based machine learning methods. *Int J Math Eng Nat Sci*, 4(16): 954-964.
- Yıldız İ, Kotan AE, Altınel AB. 2023. Türkçe faturaların sınıflandırılmasında farklı öznelik seçimi yöntemleri ile topluluk öğrenme algoritmalarının etkilerinin incelenmesi. *Avrupa Bil Teknol Derg*, (52): 272-278.



ADSORPTION OF THE ANTIBIOTIC ROXITHROMYCIN ON LOW-COST FOOD WASTE MATERIALS: BATCH AND COLUMN STUDIES

İlknur TOSUN SATIR¹, Bediha AKMEŞE^{2*}

¹Hitit University, Faculty of Arts and Sciences, Department of Chemistry, 19040, Çorum, Türkiye


²Hitit University, Faculty of Vocational School of Health Services, Department of Pharmacy Services, 19030, Çorum, Türkiye


Abstract: Antibiotics are widely utilized for a variety of medical conditions. Antibiotic residues in wastewater are dangerous to all living beings. Antibiotics remain in the wastewater environment when general treatment plant technologies are employed. The literature has numerous techniques for getting rid of antibiotics. Compared to other techniques for removing contaminants in the solution environment, the adsorption method is preferred due to its benefits, such as ease of use, high efficiency, and low cost. The study investigated using the green walnut shell (GWS), a natural sorbent, as an adsorbent to discharge roxithromycin (ROX) antibiotics from the solution medium. Adsorption conditions were studied in batch and continuous systems. pH, adsorbent amount, interaction time, sorbate concentration, and salt effect parameters were investigated in the batch system. The data obtained were calculated with kinetic and isotherm models. The adsorption process has been based on the so-called pseudo-second-order kinetic model. GWS was characterized using SEM and FTIR techniques. The amount of adsorbent, flow rate, and breakdown in the continuous system were explored. In the batch system, the adsorption equilibrium was set up at the solution's original pH with 0.1 g of adsorbent in 40 minutes, and 79% ROX removal was achieved. The optimum flow rate and adsorbent amount in the continuous system were determined as 0.1 mL/min and 0.3 g, respectively.

Keywords: Wastewater, Adsorption, Roxithromycin, Green walnut shell, Removal, Antibiotic

*Corresponding author: Hitit University, Faculty of Vocational School of Health Services, Department of Pharmacy Services, 19030, Çorum, Türkiye

E mail: bedihaakmese@hitit.edu.tr (B. AKMEŞE)

İlknur TOSUN SATIR  <https://orcid.org/0000-0003-3769-8767>

Bediha AKMEŞE  <https://orcid.org/0000-0002-6652-4574>

Received: March 29, 2024

Accepted: May 03, 2024

Published: May 15, 2024

Cite as: Tosun Satır İ, Akmeşe B. 2024. Adsorption of the antibiotic roxithromycin on low-cost food waste materials: batch and column studies. BSJ Eng Sci, 7(3): 521-528.

1. Introduction

Antimicrobial treatment studies started in the late 19th century. Since the first day of its production, antibiotics have attracted a lot of attention all over the World (Li et al., 2019). Antibiotics are widely used in a wide variety of treatment modalities in humans and animals. Antibiotics are excreted through the feces and urine; 50-80% of them are not metabolized after being taken into the body (Yang et al., 2016). Therefore, antibiotics pollute the environment by mixing into municipal wastewaters in unchanged form or using animal fertilizers as fertilizers. Contamination of wastewater with antibiotics poses a problem and poses a significant risk for all living things (Bai et al., 2015; Yin et al., 2016).

Recently, increased medication and especially antibiotic consumption has been a concern for both environmental protection and human health (Sharma et al., 2019). Since antibiotics cannot be removed with conventional aerobic sludge systems, the treatment plant is located in the outlet waters and receiving environments. Therefore, permanent concentrations of therapeutic antibiotics exist in the environment. High antibiotic concentration in the ecosystem creates toxicity for organisms and disrupts ecological balance (Topal et al., 2013).

Antibiotics contained in waste from animals or humans can be mixed into the environment through municipal wastewater treatment or land irrigation with recycled water. Similarly, animal and poultry manure may contain antibiotics that remain mostly unchanged. Antibiotics in these fertilizers have the potential to switch to the adjacent surfaces of the application point and application point to agricultural lands or to shallow groundwater (Topp et al., 2016). In these ways, antibiotics can reach the surface and groundwater (Rivera-Utrilla et al., 2013). Macrolide group antibiotics are broad-spectrum synthetic antibiotics that are widely used in medicine to treat humans and animals. Macrolide antibiotics have low water solubility. These reasons are found in low concentrations in the aqueous solution medium (Yang and Carlson, 2004). Roxithromycin (ROX), one of the macrolide antibiotics, is widely used in treatments and is produced in large quantities. It also has a long half-life. Considering all these reasons, their concentration in wastewater sources is significant, and treatment should be provided (Liu, 2018).

Various methods such as chemical precipitation, ultrafiltration, reverse osmosis, ion exchange, adsorption, solvent extraction and biological processes are applied to



remove pollutants in water (Mahmoud et al., 2012; Mitrogiannis et al., 2015). Since many of these methods have disadvantages, such as high investment, operating cost, high energy consumption, complex process steps and ineffectiveness, more economical methods should be designed to remove pollutants from water (Salazar-Rabago et al., 2017; Tunali Akar et al., 2021). Among the methods used for treatment processes, adsorption has recently been preferred because of its high removal efficiency and usefulness compared to other methods. In addition, with the adsorption method, it is possible to use adsorbents, which are abundant and waste in nature (Zafarani et al., 2015; Tunali Akar et al., 2021).

A limited number of studies were found in the literature review on the discharge of ROX from the wastewater environment by adsorption method. In a study in which lake sediments were used as adsorbents, the adsorption efficiency with ROX of samples taken from 12 different lake regions was investigated (Huang et al., 2020). According to the results obtained, the adsorption efficiency was found to be low in the removal of ROX from the solution medium. In another study encountered in the literature, porous boron-nitride-carbon nanosheets were used as an adsorbent in the removal of ROX. Two types of porous boron-nitride-carbon nanoplates (BCN and MBCN) with different pore distributions were synthesized, and their adsorption efficiencies were compared. The maximum adsorption capacity for ROX was 575.78 mg/g (Wang et al., 2020).

In this work, the removal of ROX, which is one of the macrolide group antibiotics, from the adsorption method from the wastewater environment, was investigated. For this purpose, Green walnut shell (GWS), an agricultural waste, was determined as an adsorbent. Adsorption studies were applied in batch and column systems. In the batch system; solution pH, adsorbent amount, interaction time, adsorbate concentration, and adsorption-desorption cycle tests were performed. Flow rate, adsorbent amount, and breaking point were investigated in the column system.

GWS is waste biomass that is abundant in nature and is not used in any process. Due to these properties, it is very economical to use in the adsorption process. In addition, according to the results obtained, high adsorption efficiency was obtained in the discharge of ROX from aqueous solutions with a short contact time and low adsorbent amount. According to all these results, we can say that it is a highly efficient and low-cost adsorbent in removing ROX with GWS.

2. Materials and Methods

2.1. Preparation of GWS

The green walnut shells used were taken from Bafra/Samsun/Türkiye province. The GWS was rinsed with distilled water to remove impurities and then oven-dried at 50 °C. Then, GWS was ground with a laboratory grinder and sieved to obtain a particle size of 150 µm (Zafarani et al., 2015).

2.2. Preparation of Roxithromycin Solution

ROX (Figure1) was purchased from Sigma-Aldrich and prepared by dissolving a 100 mg/L stock solution in methanol. The stock solution was stored at + 4 °C in a refrigerator. To be used in the adsorption study, 4 mg/L of ROX solutions were prepared.

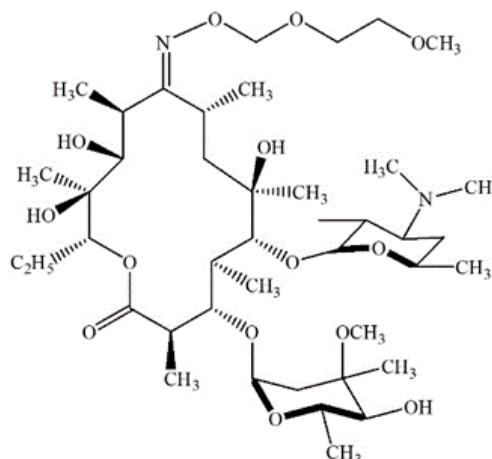


Figure 1. Molecule structure of ROX.

2.3. Instrumentation

Shimadzu model HPLC was used for the quantitative analysis of Roxithromycin. The system includes a system control unit (CBM 20A), pump (LC 20 AD), detector (SPDM 20A Photodiode Array), column oven (CTO 20 AC), and degassing unit (DGU 20 A). In the study, an Intertsil® ODS-4V (5µm, 4.60 x 250 mm) column was selected, and the temperature of the column was adjusted to 35 °C. The wavelength in the detector was chosen as 210 nm.

Human Corp. Zeneer Power I brand device was used for the ultrapure water required during the preparation of the solutions. Adsorption studies were carried out with Ismatec (Wertheim, Germany) brand peristaltic pump, WiseClean brand ultrasonicator, Memmert UN110 model oven, Retsch MM 400 model grinder, Hettich Rotofix 32 A model centrifuge, and Bio RS-24 model rotator.

The surface morphology of GWS was examined using Carl Zeiss AG - EVO® 50 Series, Germany brand SEM. With the help of double-sided carbon tape, GWS was placed on the SEM sample holder surface. It was then coated with a thin layer of gold under a vacuum and examined for surface morphology. The chemical structure analysis of GWS was performed using an FTIR spectrometer (Thermo Nicolet iS10 FTIR Spectrometer, USA).

2.4. Chromatographic Conditions

The mobile phase was prepared as a 40-60% (v/v) acetonitrile-water mixture (20 mM ortho-phosphoric acid), and the pH of the mobile phase was adjusted to pH 2.8 with 1 M NaOH solution (Prats et al., 2002; Zhang et al., 2019). The mobile phase's flow rate in the HPLC system was 1 mL/min, and the column temperature was set at 35 °C. The mobile phase was prepared daily and degassed by an ultrasonicator before each use. The

injection volume was determined as 20 µL.

2.5. Adsorption Experiments

Adsorption conditions in batch and column systems were studied. In the batch system, 10 mL antibiotic solutions and GWS adsorbents were mixed with Bio RS-24 model rotator in the falcon tube. The pH of the ROX solutions was adapted with 0.1 M NaOH and 0.1 M HCl solutions. The kinetic studies were performed using 6 mg/L ROX solution at 25 °C. To determine the batch system conditions in the adsorption of GWS and ROX the effects of pH adsorbent amount, interruption time, adsorbate concentration ad, salt effect. In the continuous (column) system, flow rate, adsorbent amount, and breaking point were determined. Continuous system adsorption studies were prepared by filling GWS between two glass cotton in 5 mL injectors. The amount of biosorbent filled in the column was 0.30 g. The solution flow direction was adjusted from bottom to top. ROX solutions at a concentration of 6 mg/L and a volume of 10 mL were passed through the column at the adjusted flow rate through the prepared column system. ROX solutions were passed through the column designed with the flow direction upwards with a peristaltic pump (Akar et al, 2009).

The adsorption performance (q) of the adsorbent is expressed as the amount of antibiotic adsorbed (mg) per unit mass (g) of the GWS. q is calculated with Equation1.

$$q = \frac{C_0 - C_e}{m} \times V \quad (1)$$

here, q= adsorption capacity (mg/g), C₀= concentration of antibiotic ion (mg/L), C_e= concentration of antibiotic ions remaining in the equilibrium solution (mg/L), m= adsorbent dose (m), and V= solution volume (L).

3. Results and Discussion

3.1. Characterization of GWS

FT-IR spectra of the GWS before and after adsorption were taken to determine the functional groups of GWS. Figure 2 and Figure 3 show the spectra of GWS before and after adsorption, respectively. It belongs to the peak O-H stretch vibration observed at 3335 cm⁻¹ in both spectra. The peak at 2916 cm⁻¹ and 2850 cm⁻¹ is for the aliphatic C-H stretching, which shows that CH₂ and or CH₃ group may involve in ROX adsorption as peak shifts to 2920 cm⁻¹. In addition, the increase in peak intensity at 2850 cm⁻¹ may indicate the presence of adsorption. The peak at 1236 cm⁻¹ is for C-O stretching, which suggests the ester group's presence and shifts to 1234 cm⁻¹ after adsorption. A sharp peak at 1027 cm⁻¹, showing the glycosidic link between cellulose and glucose, belongs to the glycosidic C-H deformation with ring vibration and OH bending (Banerjee et al, 2018).

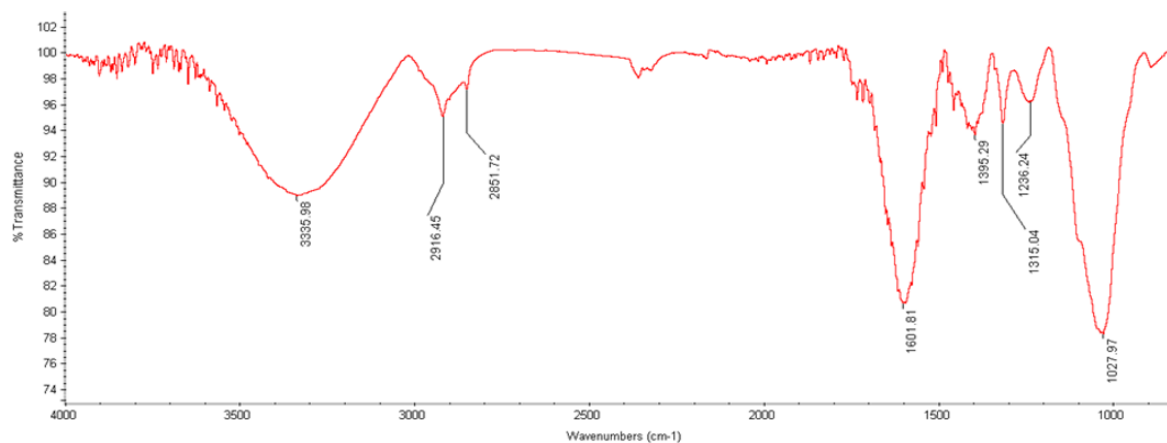


Figure 2. FTIR spectrum of GWS before adsorption.

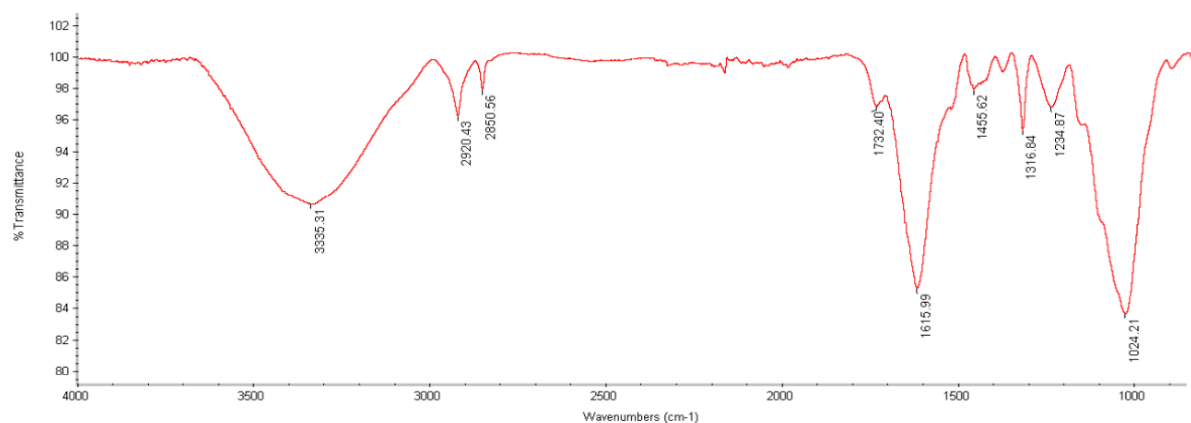


Figure 3. FTIR spectrum of GWS after adsorption.

The surface morphology of GWS (Figure 4 a and b) was detected using SEM techniques. When the figures were examined, it was seen that there were rough and porous areas on the surface of KWH to which ROX molecules could bind. After ROX adsorption on GWS, it was seen that the binding sites were coated with ROX molecules. The surface area (BET multipoint surface area - m²/g) of the GWS is 10.82 m²/g.

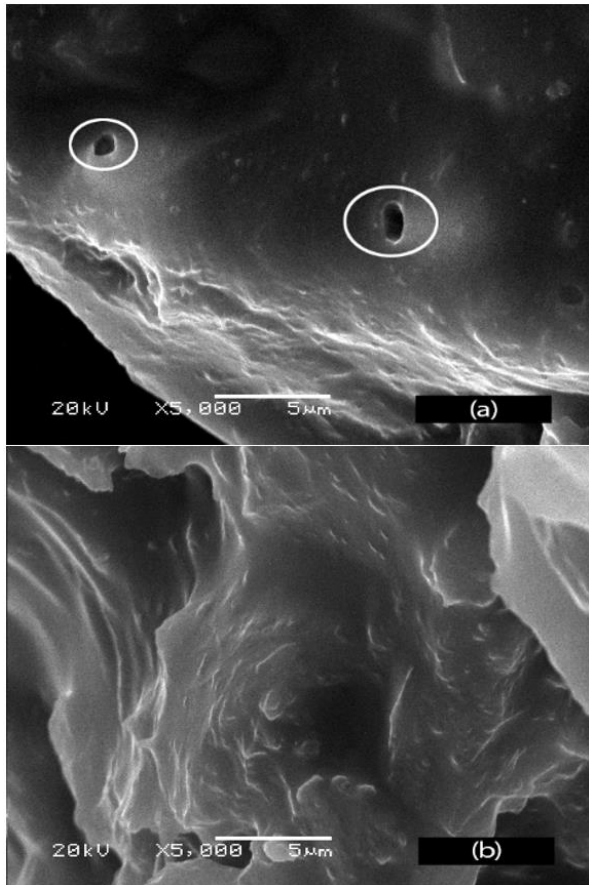


Figure 4. SEM pictogram of GWS a) before adsorption (scale bar-5 μm, X 5.000) b) after adsorption (scale bar-5 μm, X 5.000).

3.2. Batch System Studies

The effect of the pH of the ROX was analyzed. pH-dependent variation of the adsorption efficiency was investigated in the range of pH 2.5-3.5. The pH-dependent change of the adsorption efficiency for the ROX discharge by GWS was given in Figure 5. The figure shows that the adsorption capacity increased to pH 5.5, but there was no significant change at higher pH values.

The dose of GWS was explored at the optimum pH and in the range 0.02-0.20 g (Figure 6). As the amount of GWS increased, the adsorption efficiency increased. The adsorption efficiency remained constant after 0.1 g of the adsorbent amount. The optimum adsorbent amount was determined as 0.1 g.

Interaction time is an important parameter that should be examined in adsorption studies. Therefore, it was studied at a time interval of 5-90 minutes and at room temperature. As seen in Figure 7, the adsorption

efficiency increased until 40 minutes, and no change was seen after this time point. The equilibrium time was determined as 40 minutes, and subsequent studies continued using this time point.

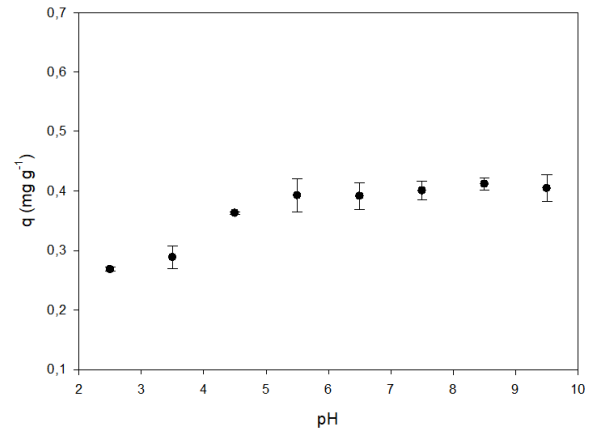


Figure 5. Effect of initial pH.

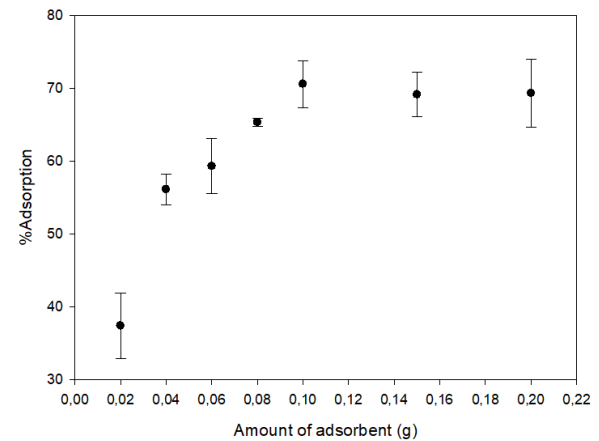


Figure 6. Effect of adsorbent dose.

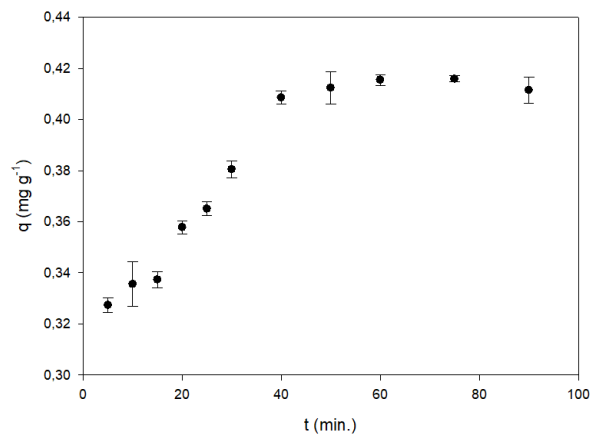


Figure 7. Effect of interaction time.

The effect of ionic strength (salt effect) on distillation water by GWS was realized in the batch system under optimum operating conditions determined by previous studies. For this purpose, NaCl was added to the medium at concentrations ranging from 0.01-0.15 M. ROX removal decreased from 79.79% to 54.80% when the NaCl concentration in the environment was increased from 0.01 to 0.1 M (Figure 8). According to these data, it is

seen that ionic strength slightly decreases the adsorption performance of GWS. Based on these data, it can be said that the ion exchange mechanism may be slightly effective in the adsorption of ROX dye to the GWS surface. In other words, the ionic strength in the concentration range studied did not dramatically affect the adsorption performance of ROX. Considering the high salt content of actual wastewater environments, this is an advantage.

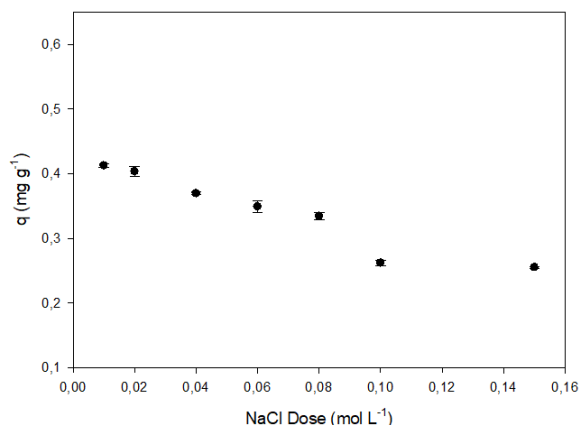


Figure 8. Salt effect.

3.3. Kinetic Parameters

Experimental data obtained from the interaction time study were evaluated using 3 kinetic models. The equation was first assessed with the first-order kinetic model equation (Equation 2) (Lagergren, 1898).

$$\ln(q_e - q_t) = \ln q_e - k_1 t \quad (2)$$

here; q_e = amount of substance adsorbed in equilibrium (mg g^{-1}), q_t = adsorption capacity at time t (mg/g), t = time (min.), k_1 = pseudo-first-order rate constant ($1/\text{min}$).

The data obtained from the experimental study were applied to the so-called first-order kinetic model, and the results were presented in Table 1. The value of r^2 was found to be 0.780. It was seen that the change in this result was not linear. Also, it was determined that the q_e values calculated using the cut-off points were not within acceptable limits. These data showed that the adsorption process did not occur with a so-called first-order reaction.

Table 1. Kinetic parameters

Pseudo-first-order		Pseudo-second-order		Intraparticle diffusion	
q_e (mg g^{-1})	0.205	q_e (mg g^{-1})	0.423	C (mg g^{-1})	0.295
k_1 (min^{-1})	7.9×10^{-2}	k_2 ($\text{g mg}^{-1} \text{min}^{-1}$)	0.346	K_p ($\text{mg g}^{-1} \cdot \text{min}^{-1/2}$)	1.44×10^{-2}
r^2	0.780	r^2	0.991	r^2	0.881

Table 2. Isotherm parameters

Langmuir		Freundlich		D-R	
q_{\max} (mol g^{-1})	9.206×10^{-7}	n	3.23	q_{\max} (mol g^{-1})	3.786×10^{-6}
q_{\max} (mg g^{-1})	0.443	K_F (L g^{-1})	2.247×10^{-5}	β ($\text{mol}^2 \text{kJ}^{-2}$)	2.65×10^{-9}
K_L (L mol^{-1})	3.62×10^5	r^2	0.768	E (kJ mol^{-1})	1.337×10^4
r^2	0.987			r^2	0.810

The pseudo-second-order kinetic model equation (Ho and McKay, 1999) is expressed by Equation 3.

$$\frac{1}{q_t} = \frac{1}{k_2 q_e^2} + \frac{1}{q_e} t \quad (3)$$

here; q_e = amount of substance adsorbed in equilibrium (mg g^{-1}), q_t = adsorption capacity at time t (mg/g), t = time (min.), k_2 = pseudo-second-order rate constant (g/mg min).

In the graph of t vs t / q_t , according to Equation 3, the slope is $1 / q_e$, and the ordinate axis cut-off point is $1/k_2 q_e^2$. The pseudo-second-order kinetic model plot is given in Fig.9. When the data in Figure 9 and Table 2 ($r^2 = 0.991$) were examined, linearity was observed. Also, the q_e value calculated from the kinetic model was in agreement with the experimental data.

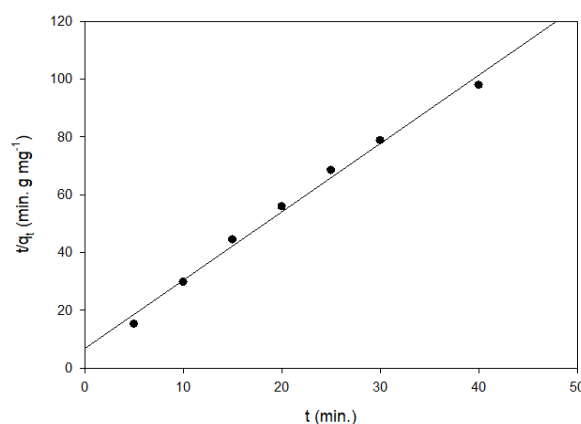


Figure 9. Pseudo-second-order model graphics.

The intraparticle diffusion model proposed by Weber and Morris (Weber and Morris, 1963) is expressed by Equation 4. The r^2 value of the intraparticle diffusion model was calculated as 0.881. When all results were evaluated, it was seen that chemical adsorption was effective.

$$q_t = k_p t^{1/2} + C \quad (4)$$

here; q_t = adsorption capacity at time t (mg/g), t = time (min.), k_p = Intraparticuler diffusion rate constant (mg/g min), and C = constant value.

3.4. Isotherm Parameters

The equation showing the relation of the amount of a substance bound to the adsorbent surface at a constant temperature with its concentration in solution is called the adsorption isotherm. In this study, the initial adsorbate concentration experiment data were investigated with 3 different isotherm models.

The Langmuir adsorption isotherm refers to single-layer homogeneous adsorption. Each molecule has a fixed enthalpy and absorption energy. Langmuir adsorption isotherm is given in Equation 5 (Langmuir, 1916).

$$\frac{1}{q_e} = \frac{1}{q_{max}} + \left(\frac{1}{q_{max} K_L}\right) \frac{1}{C_e} \quad (5)$$

Figure 10 shows the Langmuir isotherm plot of the ROX molecule adsorbed on the GWS adsorbent. When the isotherm data given in Table 2 were examined, the r^2 value of this isotherm was 0,987. Also, the theoretically calculated q_{max} value was 0.443 mg g^{-1} , and it was similar to the experimentally obtained q value. When all results were evaluated, it was seen that the adsorption data fit the Langmuir isotherm model.

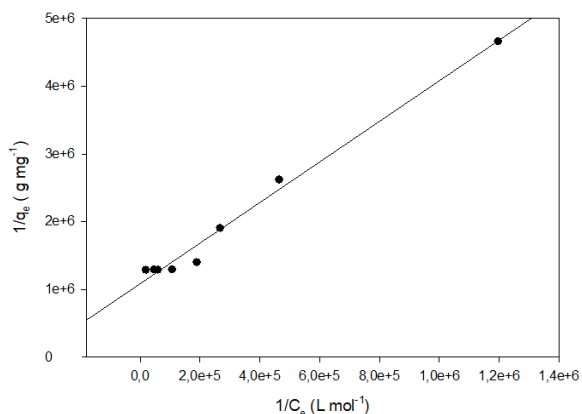


Figure 10. Langmuir isotherm model graphics.

Freundlich isotherm model explains multi-layer, irregularly distributed adsorption on a heterogeneous surface (Freundlich, 1906). The adsorbed amount is the sum of the adsorption in all regions, and when the adsorption is completed, the adsorption energy decreases exponentially (Roginsky and Zeldovich, 1934). This isotherm model is expressed by Equation 6.

$$\ln q_e = \ln K_F + \frac{1}{n} \ln C_e \quad (6)$$

The D-R adsorption isotherm is an isotherm model developed by Dubinin (Misra, 1969) for the interpretation of the adsorption equilibrium of organic compounds in the gas phase in mostly porous solids. However, it has also been applied for adsorption from the solution phase in many studies. In this isotherm model, it gives information about the binding pattern for the adsorption mechanism.

Isotherm was given in Equation 7:

$$\ln q_e = \ln q_m - \beta \varepsilon^2 \quad (7)$$

here: q_e = Amount of substance adsorbed on unit adsorbent at equilibrium (mol/g), q_{max} = Maximum adsorption capacity (mol/g), C_e = The molarity of the substance remaining in solution at equilibrium (mol/L), K_L = Langmuir isotherm constant (L/mol), K_F = Freundlich isotherm constant (L/g), n = Freundlich isotherm constant (unitless), ε = Polanyi potential, and β = Constant related to the mean free energy of adsorption per 1 mole of adsorbate (mol^2/J^2).

The r^2 values of Freundlich and D-R isotherm equations (Table 2) were calculated as 0.768 and 0.810, respectively. The order of suitability for the isotherm models was obtained in Langmuir/ D-R / Freundlich. It was seen from these data that ROX adsorption on GWS was realized in a single layer.

3.5. Column Adsorption Studies

Continuous system adsorption studies were carried out with GWS filled between two glass cotton in 2.5 ml injectors. The solution inlet was adjusted to the bottom of the column and was studied with ROX solution at a volume of 10 mL and a concentration of 6 mg/L.

The sorbate solution's flow rate is a necessary parameter affecting the adsorption performance in continuous system adsorption studies. For this purpose, 5 different flow rates were investigated. It was observed that the adsorption capacity decreased at speeds higher than 0.50 mg/min (Figure 11). The optimum flow rate was determined to be 0.5 ml min.

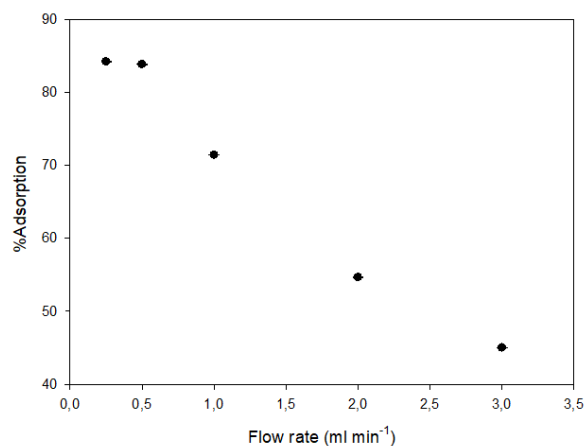


Figure 11. Effect of flow rate in a column system.

The amount of adsorbent filled in the column was changed in the range of 0.025-0.4 g, and ROX adsorption was investigated in the continuous system. The study was carried out with 6 mg/L ROX solutions at a 0.5 mL/min flow rate. The data obtained were given in Figure 12. As the GWS amount increased, the bed height of the column increased, so the contact time with the ROX solution increased, and thus the adsorption efficiency increased. The adsorption yield is fixed after 0.30 g.

A breakthrough was determined in the continuous system. Continuous monitoring of the output ROX ion concentration is given in Figure 13. In this figure, a characteristic S shape curve was observed, which is

favourable for continuous mode sorption applications. The breakthrough was determined around 20 minutes, and almost 87% of the ROX has been removed by this point. These results revealed that ROX adsorption with GWS could be a potential alternative for continuous system processing applications.

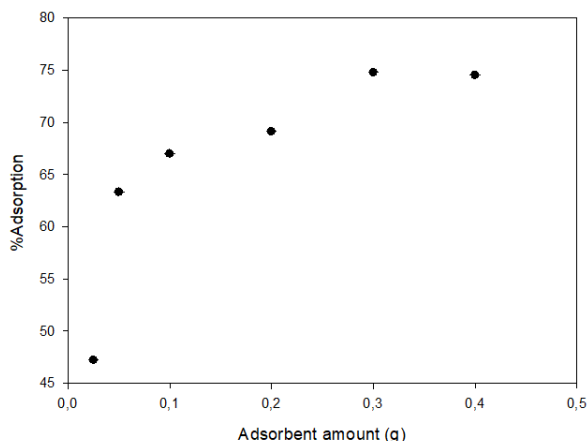


Figure 12. Effect of adsorbent dose in a column system.

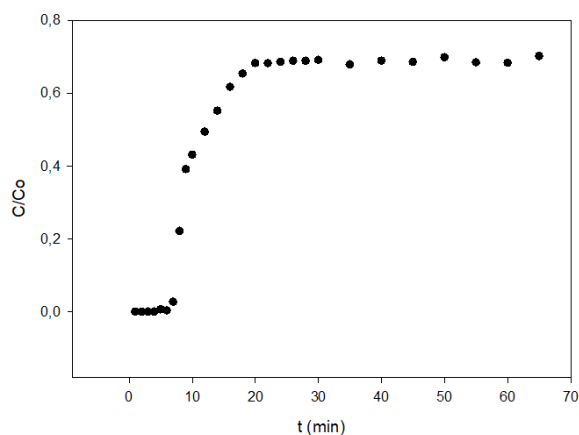


Figure 13. Breakthrough curve for ROX onto GWS.

4. Conclusion

In this study, the removal of green walnut shells, a natural adsorbent, and roxithromycin, one of the macrolide group antibiotics, by adsorption method was investigated. For this purpose, in the batch system, starting solution pH, amount of adsorbent, temperature, time, initial antibiotic concentration, ionic strength; solution flow rate, adsorbent amount, and breakthrough parameters in the column system was examined. It was observed that when the pH of the ROX solution changed in the range of 5.5-9.5, it did not cause a significant change in the adsorption efficiency. According to these results, the optimum pH was determined as the original pH (pH 6.26) of the ROX solution. It is very advantageous not to adjust the pH in the removal of antibiotics from the wastewater environment by the adsorption method. In the batch system, the adsorption equilibrium was established in the amount of 0.1 g adsorbent and in a short time, like 40 minutes. Maximum adsorption efficiency was obtained in the column system at a flow

rate of 0.5 mL/min and an amount of 0.3 g adsorbent. In the batch system optimum conditions, 79% removal was achieved, and 87% removal was completed in the column system.

ROX adsorption by GWS was studied with pseudo-first-order, pseudo-second-order, and intraparticle diffusion models, and the data were found to fit the pseudo-second-order kinetic model. Also, adsorption data were examined with the Langmuir, Freundlich, and D-R isotherm models, and the most suitable model was determined as the Langmuir isotherm model. As a result, the green walnut shell, which is abundant in our country, has a natural adsorbent potential that is highly effective, highly efficient, economical, and easily obtainable for ROX removal from the wastewater environment.

Author Contributions

The percentage of the author(s) contributions is presented below. All authors reviewed and approved the final version of the manuscript.

	İ.T.S.	B.A.
C	50	50
D	60	40
S	50	50
DCP	50	50
DAI	50	50
L	40	60
W	60	40
CR	50	50
SR	40	60

C=Concept, D= design, S= supervision, DCP= data collection and/or processing, DAI= data analysis and/or interpretation, L= literature search, W= writing, CR= critical review, SR= submission and revision.

Conflict of Interest

The authors declared that there is no conflict of interest.

Ethical Consideration

Ethics committee approval was not required for this study because of there was no study on animals or humans.

References

- Akar ST, Gorgulu A, Anilan B, Kaynak Z, Akar T. 2009. Investigation of the biosorption characteristics of lead (II) ions onto *Symphoricarpos albus*: batch and dynamic flow studies. *J Hazard Mater*, 165(1-3): 126-133.
- Bai X, Ma X, Xu F, Li J, Zhang H, Xiao X. 2015. The drinking water treatment process as a potential source of affecting the bacterial antibiotic resistance. *Sci Total Environ*, 533: 24-31.
- Banerjee M, Basu RK, Das SK. 2018. Cr (VI) adsorption by a green adsorbent walnut shell: Adsorption studies, regeneration studies, scale-up design and economic feasibility. *Process Saf Environ Prot*, 116: 693-702.
- Freundlich H. 1906. Freundlich's Adsorption Isotherm. *Phys Chem*, 57: 384.
- Ho YSI, McKay G. 1999. Pseudo-second order model for sorption processes. *Process Biochem*, 34(5): 451-465.

- Huang Y, Wang Y, Huang Y, Zhang L, Ye F, Wang J, Shang J, Liao Q. 2020. Impact of sediment characteristics on adsorption behavior of typical antibiotics in Lake Taihu, China. *Sci Total Environ*, 718: 137329.
- Lagergren S, Lagergren S, Lagergren SY, Sven K. 1898. Zurtheorie der sogenannten adsorption gelösterstoffe. *Zeitschr f Chem und Ind der Kolloide*, 2: 15.
- Langmuir I. 1916. The constitution and fundamental properties of solids and liquids. Part I. Solids. *J Am Chem Soc*, 38(11): 2221-2295.
- Li Z, Li M, Zheng T, Li Y, Liu X. 2019. Removal of tylosin and copper from aqueous solution by biochar stabilized nano-hydroxyapatite. *Chemosphere*, 235: 136-142.
- Liu Z. 2018. Adsorption performance of roxithromycin on multi-walled carbon nanotubes in water. 7th International Conference on Energy and Environmental Protection, July 14-15, Shenzhen, China, pp: 880-886.
- Mahmoud DK, Salleh MAM, Karim WAWA, Idris A, Abidin ZZ. 2012. Batch adsorption of basic dye using acid treated kenaf fibre char: equilibrium, kinetic and thermodynamic studies. *J Chem Eng*, 181: 449-457.
- Misra DN. 1969. Adsorption on heterogeneous surfaces: A dubinin-radushkevich equation. *Surf Sci*, 18(2): 367-372.
- Mitrogiannis D, Markou G, Çelekli A, Bozkurt H. 2015. Biosorption of methylene blue onto *Arthrospira platensis* biomass: kinetic, equilibrium and thermodynamic studies. *J Environ Chem Eng*, 3(2): 670-680.
- Prats C, Francesch R, Arboix M, Pérez B. 2002. Determination of tylosin residues in different animal tissues by high performance liquid chromatography. *J Chromatogr B Analyt Technol Biomed Life Sci*, 766(1): 57-65.
- Rivera-Utrilla J, Sánchez-Polo M, Ferro-García MÁ, Prados-Joya G, Ocampo-Pérez R. 2013. Pharmaceuticals as emerging contaminants and their removal from water. A review. *Chemosphere*, 93(7): 1268-1287.
- Roginsky S, Zeldovich YB. 1934. The catalytic oxidation of carbon monoxide on manganese dioxide. *Acta Phys Chem USSR*, 1(554): 2019.
- Salazar-Rabago JJ, Leyva-Ramos R, Rivera-Utrilla J, Ocampo-Perez R, Cerino-Cordova FJ. 2017. Biosorption mechanism of Methylene Blue from aqueous solution onto White Pine (*Pinus durangensis*) sawdust: Effect of operating conditions. *Sustain Environ Res*, 27: 32-40.
- Sharma BM, Bečanová J, Scheringer M, Sharma A, Bharat GK, Whitehead PG, Klánová J, Nizzetto L. 2019. Health and ecological risk assessment of emerging contaminants (pharmaceuticals, personal care products, and artificial sweeteners) in surface and groundwater (drinking water) in the Ganges River Basin, India. *Sci Total Environ*, 646: 1459-1467.
- Topal M, Uslu G, Arslan Topal EI, Öbek E. 2013. Antibiyotiklerin tespiti ve arıtılması. *Erciyes Üniv Fen Bil Enst Fen Bil Derg*, 29(2): 185-199.
- Topp E, Renaud J, Sumarah M, Sabourin L. 2016. Reduced persistence of the macrolide antibiotics erythromycin, clarithromycin and azithromycin in agricultural soil following several years of exposure in the field. *Sci Total Environ*, 562: 136-144.
- Tunali Akar S, Ozdemir I, Sayin F, Akar T. 2021. Adsorption of diazo dye from aqueous solutions by magnetic montmorillonite composite. *CLEAN-Soil Air Water*, 49(2): 2000165.
- Wang G, Zhang Y, Wang S, Wang Y, Song H, Lv S, Li C. 2020. Adsorption performance and mechanism of antibiotics from aqueous solutions on porous boron nitride-carbon nanosheets. *Environ Sci Water Res Technol*, 6(6): 1568-1575.
- Weber WJ, Morris JC. 1963. Kinetics of adsorption on carbon from solution. *J Sanit Eng Div*, 89(2): 31-60.
- Yang S, Carlson KH. 2004. Solid-phase extraction-high-performance liquid chromatography-ion trap mass spectrometry for analysis of trace concentrations of macrolide antibiotics in natural and waste water matrices. *J Chromatogr A*, 1038(1-2): 141-155.
- Yang Z, Ren K, Guibal E, Jia S, Shen J, Zhang X, Yang W. 2016. Removal of trace nonylphenol from water in the coexistence of suspended inorganic particles and NOMs by using a cellulose-based flocculant. *Chemosphere*, 161: 482-490.
- Yin Y, Guo X, Yang C, Gao L, Hu Y. 2016. An efficient method for tylosin removal from an aqueous solution by goethite modified straw mass. *RSC advances*, 6(98): 95425-95434.
- Zafarani HR, Bahrololoom ME, Noubactep C, Tashkhourian J. 2015. Green walnut shell as a new material for removal of Cr (VI) ions from aqueous solutions. *Desalin Water Treat*, 55(2): 431-439.
- Zhang Y, Pan Z, Rong C, Shao Y, Wang Y, Yu K. 2019. Transformation of antibacterial agent roxithromycin in sodium hypochlorite disinfection process of different water matrices. *Sep Purif Technol*, 212: 528-535.



Open Access Journal
e-ISSN: 2619 – 8991

Araştırma Makalesi (Research Article)

Cilt 7 - Sayı 3: 529-538 / Mayıs 2024
(Volume 7 - Issue 3: 529-538 / May 2024)

HANÖNÜ (KASTAMONU) GÜNEŞ ENERJİSİ SANTRALİNİN FARKLI SİMÜLASYON PROGRAMLARI İLE TASARIMI VE ELEKTRİK ENERJİSİ ÜRETİM SONUÇLARININ DEĞERLENDİRİLMESİ

Sefa KIRNAPCI¹, Nihat PAMUK^{2*}

¹Bulent Ecevit University, Graduate School of Natural and Applied Sciences, Department of Electrical and Electronics Engineering, 67100, Zonguldak, Türkiye

²Bulent Ecevit University, Faculty of Engineering, Department of Electrical and Electronics Engineering, 67100, Zonguldak, Türkiye

Özet: Elektrik üretimi için kullanılan fosil yakıtların çevreye olan olumsuz etkilerinden dolayı son dönemlerde yenilenebilir enerji kaynaklarının kullanımında hızla artış yaşanmaktadır. 2015 yılında Paris'te düzenlenen BM İklim Değişikliği Zirvesi'nde alınan en önemli kararlardan biri olarak küresel ısınmanın 2 °C'nin altında tutulmasına yönelik bir eylem planının uygulanması konusu görüşülmüş olup bu konuda ülkeler arasında mutabakata varılmıştır. Bu bağlamda dünya genelinde yenilenebilir enerji üretiminde kapsamlı çalışmalar yapılmaktadır. Ülkemizde Enerji ve Tabii Kaynaklar Bakanlığı tarafından yürütülen çalışmalar neticesinde 2011 yılında Enerji Piyasası Düzenleme Kurulu (EPDK) tarafından yayımlanan yönetmelik ile küçük ölçekli üretim tesislerinin lisans alma ve şirket kurma yükümlülüğü ortadan kaldırılmıştır. Lisanssız elektrik üretim yönetmeliğinin uygulanmaya başlamasıyla birlikte ülkemizde güneş enerjisinden fotovoltaik sistemler ile elektrik üretimi hız kazanmıştır. Güneş enerjisi santrallerinin kurulduğundan önceki tetkik ve fizibilite çalışmalarının yanı sıra simülasyon programlarından elde edilen detaylı analiz raporları sayesinde sağlıklı veriler elde edilebilmektedir. Fotovoltaik sistem simülasyonu üzerine PVsyst ve PV*SOL programları detaylı veri girişi olanağı sunması ve bu veriler üzerinden olumlu analizler yapabilmesi nedeniyle benzetim programları arasında ön plana çıkmaktadır. Bu çalışmada Hanönü (Kastamonu) Belediyesine ait 2021 yılında kurulumu yapılmış 276 kWp gücünde fotovoltaik güneş enerji santralinin PVsyst ve PV*SOL programları kullanılarak simülasyonları oluşturulmuş ve performans analizleri gerçekleştirilmiştir. Tesisin işletmeye alındığı tarihten itibaren ürettiği elektrik enerjisi miktarı benzetim sonuçları ile karşılaştırılarak benzetim programlarının doğrulukları ve performansları değerlendirilmiştir.

Anahtar kelimeler: Fotovoltaik, Güneş enerjisi, Simülasyon programları, PVsyst, PV*SOL


Design of Hanönü (Kastamonu) Solar Power Plant with Different Simulation Programs and Evaluation of Electrical Energy Production Results


Abstract: Due to the negative environmental impacts of fossil fuels used for electricity generation, renewable energy sources have increased rapidly in recent years. In 2015, the implementation of an action plan to keep global warming below 2 degrees Celsius, which was one of the most important decisions taken at the UN Climate Change Summit held in Paris, was discussed and an agreement was reached between countries on this issue. In this context, extensive studies have been carried out in renewable energy production worldwide. As a result of the efforts carried out by the Ministry of Energy and Natural Resources in our country, the obligation to obtain a license and establish a company for small-scale generation facilities was eliminated with the regulation published by the Energy Market Regulatory Board in 2011. With the implementation of the unlicensed electricity generation regulation, electricity generation from solar energy with photovoltaic systems has gained momentum in our country. Before installing solar power plants, reliable data can be obtained through detailed analysis reports obtained from simulation programs as well as on-site surveys and feasibility studies. PVsyst and PV*SOL programs on photovoltaic simulation stand out among simulation programs because they offer detailed data entry and can perform positive analysis on the data. In this study, the performance analysis of the 276 kWp photovoltaic solar power plant of Hanönü (Kastamonu) Municipality, which was installed in 2021, was simulated with PVsyst and PV*SOL programs. The performance of the simulation programs was also evaluated by comparing the amount of electricity generated by the plant since its commissioning with the simulation results.

Keywords: Photovoltaics, Solar energy, Simulation programs, PVsyst, PV*SOL

*Sorumlu yazar (Corresponding author): Bulent Ecevit University, Faculty of Engineering, Department of Electrical and Electronics Engineering, 67100, Zonguldak, Türkiye

E mail: nihattamuk@gmail.com (N. PAMUK)

Sefa KIRNAPCI  <https://orcid.org/0000-0003-2236-4713>

Nihat PAMUK  <https://orcid.org/0000-0001-8980-6913>

Gönderi: 28 Mart 2024

Kabul: 03 Mayıs 2024

Yayınlanma: 15 Mayıs 2024

Received: March 28, 2024

Accepted: May 03, 2024

Published: May 15, 2024

Cite as: Kirnapci S, Pamuk N. 2024. Design of Hanönü (Kastamonu) solar power plant with different simulation programs and evaluation of electrical energy production results. BSJ Eng Sci, 7(3): 529-538.

1. Giriş

Enerji kaynakları ülkeler açısından ekonomide ve sosyal kalkınmada çok önemli bir rol oynamaktadır. Sanayi

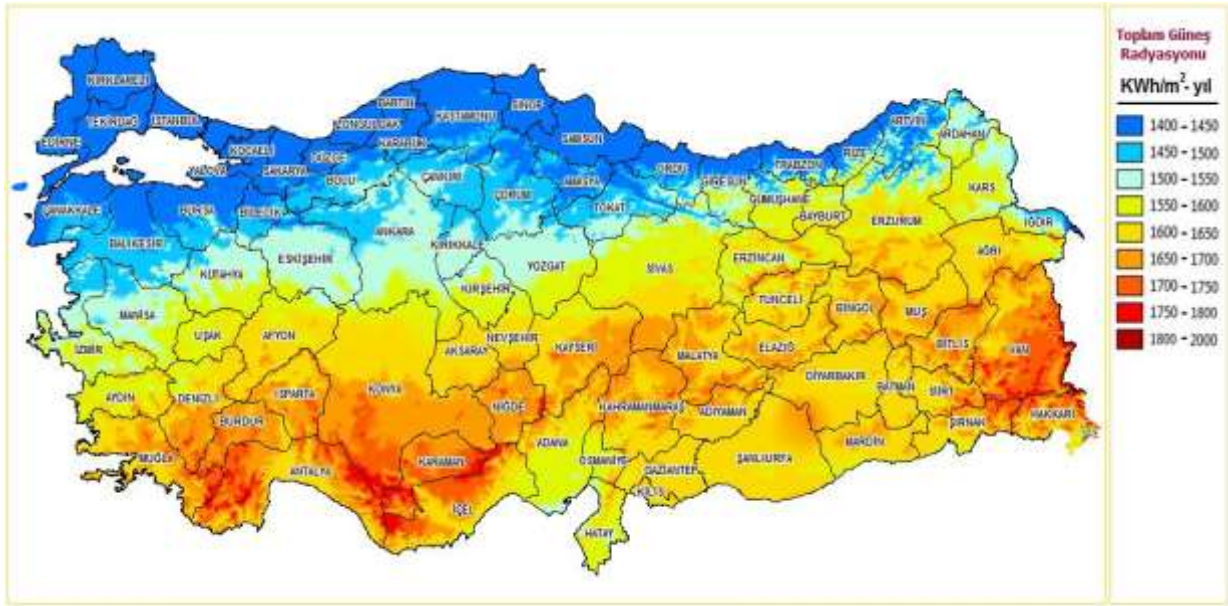
devriminden sonra dünya genelinde yükselen enerji talebi; gelişen teknoloji, ağır sanayi ve artan dünya nüfusu sebebiyle ortaya çıkan enerji ihtiyaçlarından



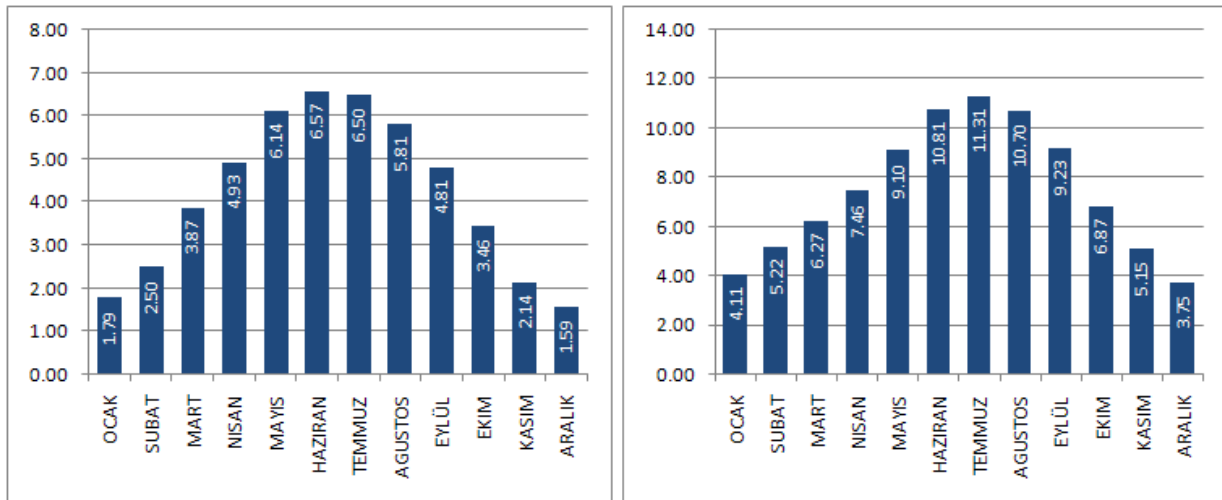
dolayı her geçen gün daha da artmaktadır. Dünya üzerinde ihtiyaç duyulan enerjinin büyük bir kısmı fosil kaynaklardan (kömür, petrol ve doğal gaz) sağlanmaktadır (Aktacı ve Yeşilata, 2011). Fosil yakıtların çevreye vermiş olduğu zararlar ve tükenen bir enerji türü olması sebebiyle kullanımı her geçen gün azalmaktadır. Fosil yakıtların kullanımının azalması ile ortaya çıkan enerji üretim açığı temiz ve yenilenebilir enerji kaynakları ile kapatılmıştır. Fosil kaynaklar bakımından fakir olan Avrupa Birliği ülkeleri ve Uzak Doğu'nun sanayileşmiş ülkeleri ile enerji tüketimi çok yüksek olan Amerika Birleşik Devletleri yenilenebilir enerji kaynaklarının geliştirilmesinde ve yaygınlaştırılmasında öncülük etmişlerdir. Aralık 2015'te Fransa'nın başkenti Paris'te düzenlenen B.M. İklim Değişikliği Zirvesi'nde küresel sıcaklık artışının 2 °C sınırının altında kalınması amaçlanarak ülkelerin stratejik çalışmalar ışığında geliştirici politikalar izlemesi genel anlamda kabul edilmiştir (UNFCCC Conference of

the Parties (COP) (Bali, 2015). Bu çerçevede birçok ülke yenilenebilir enerji alanında iyileştirici ve yapıcı politikalar izlemeye başlamıştır.

Türkiye yenilenebilir enerji kaynakları açısından zengin bir coğrafyaya sahiptir. Dünya üzerinde bulunduğu jeopolitik konumundan ve ülkenin coğrafik yapısından dolayı Türkiye sürdürülebilir enerji türlerinden güneş enerjisi ve rüzgâr enerjisinde ön plana çıkmaktadır. Türkiye coğrafi olarak 36°-42° kuzey enlemleri ile 26°-45° doğu boylamları arasında bulunmaktadır. Türkiye Güneş Enerjisi Potansiyeli Atlasından (GEPA) yapılmış olan çalışmalar neticesinde Türkiye'nin ortalama yıllık toplam güneşlenme süresi 2.741 saat olarak elde edilmiş, ortalama yıllık toplam ışınım değeri ise 1.527,46 kWh/m² olarak değerlendirilmiştir (ETKB - Bilgi Merkezi, 2023). Şekil 1'de Türkiye'nin güneş enerjisi potansiyel haritası gösterilmiştir. Şekil 2'de Türkiye'nin global radyasyon verileri ve güneşlenme periyot süreleri gösterilmiştir. (GEPA – Güneş Enerjisi Potansiyel Atlası, 2023).



Şekil 1. Türkiye güneş enerjisi potansiyeli haritası.



Şekil 2. Türkiye global radyasyon verileri (KWh/m²*gün) ve güneşlenme periyotları (saat).

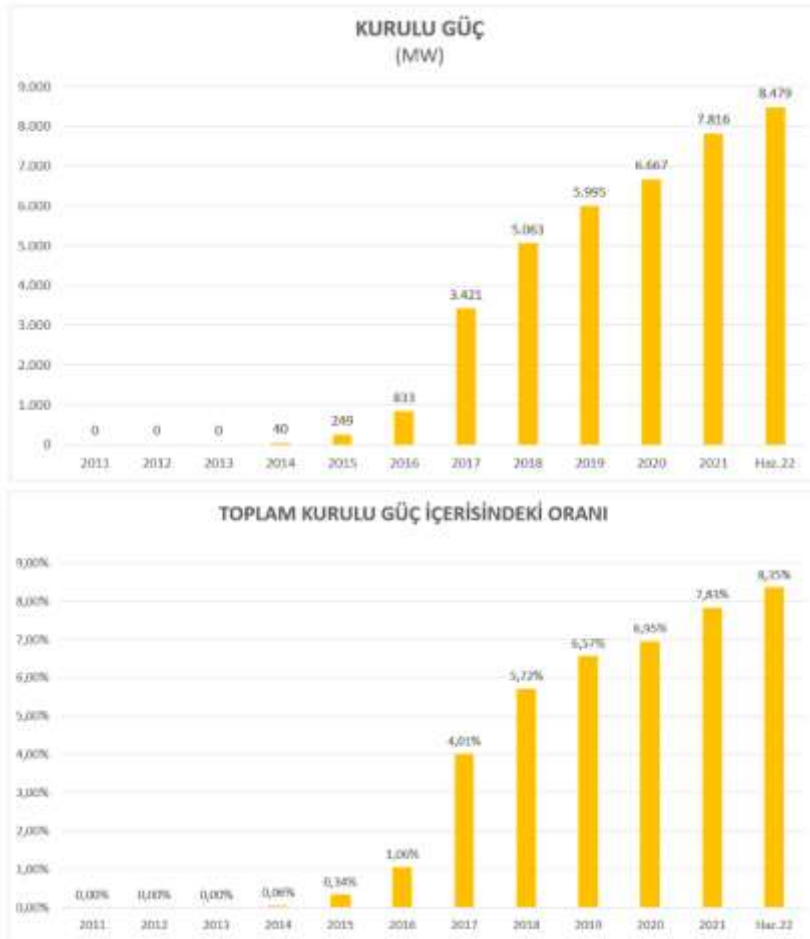
Ülkemizde oldukça iyi seviyede bulunan güneş enerjisi potansiyelinin değerlendirilmesi için Bakanlık düzeyinde yürütülen çalışmalar son yıllarda giderek artmıştır. Bu kapsamda ülke genelinde özel şirketler, kamu kurumları, Belediyeler, küçük-orta-büyük işletmeler güneş enerjisinden elektrik üretimi konusunda bilinçlendirilerek maddi destek (kredi, hibe) sağlanmıştır. Ayrıca güneş enerjisinden elektrik üretiminin küçük ölçekte bile olsa yararlanılabilmesi amacıyla 2013 yılında “Yenilenebilir Enerji Kaynakları Kanunu” kapsamında “Elektrik Piyasasında Lisanssız Elektrik Üretimine İlişkin Yönetmelik” yürürlüğe girmiştir. Bu yönetmelik ile güneş enerjisinden elektrik üreten santrallerin sayısı hızla artmıştır.

Haziran 2022 sonunda, güneş enerji sistemlerine bağlı elektrik kurulu gücümüz 8,479 MW'tır ve toplam kurulu gücün %8,35'ini oluşturmaktadır. Şekil 3'te yıllara göre kurulu güç değerleri ve toplam kurulu gücün yüzdesel karşılıkları gösterilmiştir. (EİGM – Enerji İşleri Genel Müdürlüğü, 2023).

Dünyada güneş enerjisinden elektrik üretimi gerçekleştirebilmek için fotovoltaik sistemler geliştirilmiştir. Güneş panelleri, Fotovoltaik sistemlerin merkezi olmasına rağmen, çalışma düzeni içerisinde başka bileşenlere de ihtiyaç duyulmaktadır. Fotovoltaik sistemler güneş panelleri ile akü, solar invertör, şarj regülatörü gibi başka bileşenlerden de oluşmaktadır.

Fotovoltaik sistemler elektrik şebekesine bağlı olup olmamasına veya bağımsız bir sistem olarak tasarlanıp tasarlanmamasına bağlı olarak farklılıklar göstermektedir. Fotovoltaik sistemlerin başlıca temel bileşenleri ve görevleri aşağıda verilmiştir.

- Fotovoltaik sistemlerde PV modüllerini sabitlemek ve güneşi doğru yönlendirmek amacıyla montaj yapıları kullanılmaktadır.
- Enerji depolama, bağımsız sistemler için kritik bir bileşen olarak kabul edilmektedir. Çünkü bu yapı, fotovoltaik sistemin gece saatlerinde ve kötü hava koşullarında dahi elektrik sağlayabilmesini mümkün kılmaktadır. Aküler enerji depolama birimleri olarak tercih edilmektedir.
- DC-DC dönüştürücüler, modül çıkışının zamana ve hava koşullarına bağlı olarak değişecek gerilim seviyelerinde olmasını sağlamaktadır.
- Şebekeye bağlı sistemlerde, PV modüllerinden elde edilen doğru akım elektrik enerjisini, alternatif akım elektrik enerjisine dönüştürmek için invertörler veya DC-AC dönüştürücüler kullanılmaktadır.
- Kablolar, fotovoltaik sistemlerin farklı bileşenlerini birbirine veya elektrik yüküne bağlamak için kullanılmaktadır. Direnç kayıplarını en aza indirmek için uygun kalınlıkta kabloların seçilmesi son derece önemlidir.



Şekil 3. Türkiye'nin yıllara göre kurulu güç değerleri ve yüzde değişimleri.

Güneş enerjisi santrallerinin amortisman sürelerini belirlemek için, kurulum öncesi detaylı fizibilite çalışmalarının yapılması gerekmektedir. Yatırım öncesinde gerçekleştirilen bu çalışma, yatırımın uygulanabilirliğini değerlendirmek ve projenin ekonomik açıdan başarılı olup olmadığını belirlemek adına büyük bir öneme sahiptir.

Bu çerçevede, yatırımcılar, yapılması düşünülen güneş enerjisi sisteminin masraf analizini, üretim-verim kapasitesini ve amortisman süresini analiz etmektedirler. Bu analizler gerçekleştirilirken çeşitli benzetim programlarından faydalanılmaktadır. Bu programlar, sistemin kurulum maliyetini, enerji üretim potansiyelini ve amortisman süresini hesaplamak için kullanılır. Bu analizler, gerçekleştirilecek olan yatırımın ne kadar sürede geri ödeneceğini ve projeden ne kadar sürede kar sağlanacağını belirlemek açısından oldukça önemlidir.

Bu benzetim programları, yatırımcıların doğru kararlar alabilmeleri için güçlü bir veri analizi sunmaktadır. Ayrıca farklı senaryoları değerlendirmek ve projenin çeşitli değişkenlere nasıl tepki vereceğini anlamak için kullanılabilirler. Fotovoltaik sistemlerin enerji üretim değerlerini etkili bir şekilde tahmin edebilmenin yanı sıra, sistemlerin çalışma davranışını öngörebilme konusunda da önemli bir rol oynamaktadır. 3D sistem tasarımını benzetim programları üzerinde gerçekleştirerek güneş panellerine düşen gölgelenmeleri gerçek zamanlı olarak gözlemlenebilir. Benzetim programları, fotovoltaik sistem tasarımcılarına kurulumun yapılacağı coğrafi bölgeye, enerji talebine ve sistem güvenilirliği gibi parametrelerle uyumlu çalışacak farklı bileşenleri en uygun şekilde seçme özgürlüğü sağlamaktadır (Kıyanççek, 2013). PVsyst ve PV*SOL benzetim programları fotovoltaik sistem tasarımcılarına, sistem bileşenlerini en uygun şekilde seçme ve enerji üretimi tahminlerini yapma konusunda gelişmiş araçlar sunmaktadır.

Her iki program da coğrafi bölgeye özgü parametrelerle çalışabilme yeteneğine sahiptir, bu da sistemin kurulacağı konumun iklim koşullarını ve güneş ışınımını dikkate alarak daha gerçekçi benzetim sonuçları elde etmeyi sağlamaktadır. PVsyst ve PV*SOL'un detaylı analiz özellikleri, sistem tasarımcılarına enerji talebine, güvenilirliğe ve bölgesel özelliklere bağlı olarak en uygun bileşenleri seçme konusunda önemli bir rehberlik sunmaktadır (Ay ve Pamuk, 2023).

Bu benzetimler, sistemin kurulumu sırasında olası maliyetleri minimize etmeye ve enerji üretimini optimize etmeye yönelik stratejiler geliştirmeye olanak tanımaktadır. Ayrıca, gerçek ortam verilerine daha yakın benzetim sonuçları elde etmek için programların güncel tutulması ve teknik özelliklerinin laboratuvar testlerine dayandırılması gibi faktörlere dikkat edilmesi, sistemin performansını iyileştirmeye yönelik daha kesin bilgiler sağlanmasına olanak tanımaktadır. Akademik alanda, güneş enerji santralleriyle ilgili yapılan çalışmalar genellikle çevresel ve/veya maliyet analizlerine odaklanmaktadır.

Bu araştırma, 276 kWp kurulu gücüne sahip güneş enerjisi santralının faaliyete alınması sonrası elde edilen üretim değerlerini benzetim programlarından elde edilen veri analizleri ile karşılaştırmayı amaçlamaktadır. Bu çerçevede, üretim gücü, yapılan tesislerin etkinliği, verimliliği ve maliyet analizi gibi konulara odaklanan çalışmalar incelenmiştir. Bu konuda daha önceden yapılmış bilimsel ve akademik çalışmaların bazıları aşağıda tarihsel sıra ile sunulmuştur.

(Çelebi, 2002), "Bina Düşey Kabuğunda Fotovoltaik Panellerin Kullanım İlkeleri" başlıklı çalışmada, güneş enerjisi sistemlerinde kullanılan fotovoltaik panellerin önemi üzerinde durmuş olup fotovoltaik sistemleri tercih edecek kullanıcıların panellerin yerleştirilmesindeki eğim açısı ve güneş ışınlarının en elverişli şekilde kullanılmasının önemi vurgulanmaktadır. (Tozlu, 2004), tarafından gerçekleştirilen çalışma kapsamında Muğla Sıtkı Koçman Üniversitesi bünyesinde kurularak faaliyete geçen güneş enerji sisteminin gerçek üretim verileri ile benzetim programından elde edilen benzetim sonuçları karşılaştırmıştır. Ortaya çıkan veriler, benzetim programının sunduğu değerlere yakınlık göstermektedir, bu durum benzetim programının tutarlılığını ortaya koymaktadır. (Lalwani, ve ark., 2010) tarafından gerçekleştirilen çalışmada ise, güneş enerji sistemlerinde fizibilite amacıyla kullanılan fotovoltaik sistem benzetim programlarından RET Screen, PV F-Chart, Solar Design Tool, INSEL, TRNSYS, NREL Solar Advisor Model, ESP-r 11.5, PVSYST 4.33, Solar Pro, PV Design Pro-G, PV*SOL Expert, HOMER gibi 12 farklı benzetim programı, işletim maliyeti, kolay kullanım, platform uyumluluğu, verimlilik, içerik ve güncellenebilirlik kriterleri açısından incelenmiştir.

Keskin (2012) tarafından yapılan çalışma ile şebekeden bağımsız (Off Grid) 5 kW kapasiteli bir fotovoltaik sistem modellemesi oluşturmuştur. Çalışma kapsamında yürütülen model PYSyst programı ile oluşturularak panel türlerinden monokristal modüllerden daha fazla verimlilik elde edilebileceği tespit edilmiştir. (Sekçuloğlu, 2012) tarafından gerçekleştirilen çalışma ile yenilenebilir enerji türlerinden olan güneş enerjisi sistemi, rüzgâr enerjisi sistemi ve hibrit sistemlerden elektrik enerjisinin üretimi detaylı olarak incelenmiş, sistemlerin tasarımları HOMER Pro (Pamuk, 2024) ve PVsyst benzetim programları ile gerçekleştirilerek türler arasında elde edilen veriler karşılaştırılmış ve ekonomik parametreler çerçevesinde incelenmiştir. (Haydaroglu, 2017) tarafından gerçekleştirilen çalışmada, Dicle Üniversitesi tarafından kurulumu yapılarak enerji üretimine başlayan 250 kWp kurulu gücüne sahip güneş enerjisi santralının PVsyst benzetim programı ile benzetimi gerçekleştirilmiştir. Santralin uluslararası standart olan IEC 61724 (Fotovoltaik Enerji Sistemleri Performansı Monitörleme - Genel Prensipler ve Ölçümler) kapsamında belirtilen performans kriterlerine uygun olup olmadığı incelenmiştir. Santralin gerçek üretim değerleri ile benzetim sonuçları karşılaştırıldığında Aralık ve Ocak aylarında uyumsuzluk

görülmüştür. Ancak finansal inceleme kapsamında kar/yatırım dengesinin olumlu sonuç vermesi söz konusu projenin ekonomik açıdan uygulanabilirliğini desteklemektedir.

Çiftçi (2016) tarafından yapılan çalışmada, fotovoltaik sistemlerin en önemli parametrelerinden santral gücü, maliyet analizi ve sistem tasarımı üzerine farklı senaryolar kurulmuş ve elde edilen sonuçlar karşılaştırılmıştır. Tasarım aşamasındaki önemli verilerin santral kurulmadan elde edilebildiği ve öngörü oluşturabildiği kanıtlanmıştır. Bu çalışmada PVSOL programı ile tasarımların analizi gerçekleştirilmiştir. Aldudak (2018) tarafından gerçekleştirilen çalışmada ise, PVsyst benzetim programı ile çeşitli illerde faaliyet gösteren güneş enerjisi santrallerinin reel üretim değerleri incelemiştir. Benzetim sonuçları ile gerçek üretim sonuçları karşılaştırıldığında önemli ölçüde birbirine yakın değerler elde edilmiştir.

Şimşek (2018), tarafından yapılan çalışmada, Ankara'nın Gölbaşı ilçesinde ve İzmir'in Torbalı ilçesinde kurulan Güneş Enerji Santralleri için PVsyst benzetim programı aracılığı ile hazırlanan benzetim sonuçları gerçek değerler ile karşılaştırılmıştır. Benzetim sonuçlarının gerçek üretim değerlerine yakın sonuçlar verdiği gösterilmiştir. (Bolat ve ark., 2020) tarafından yapılan çalışmada ise, Lebit Güneş Enerji Santralinin benzetim programlarından elde edilen benzetim sonuçları ile gerçek santral enerji üretim değerleri karşılaştırılmıştır. PVsyst program sonuçlarının uygunluk değerlendirilmesi yapılmıştır. Benzetim sonuçları ile elde edilen üretim değerleri arasında neredeyse hiçbir fark oluşmadığı gösterilmiştir. Bu bağlamda, PVsyst programından gerçeğe yakın veriler elde edildiği kanıtlanmıştır.

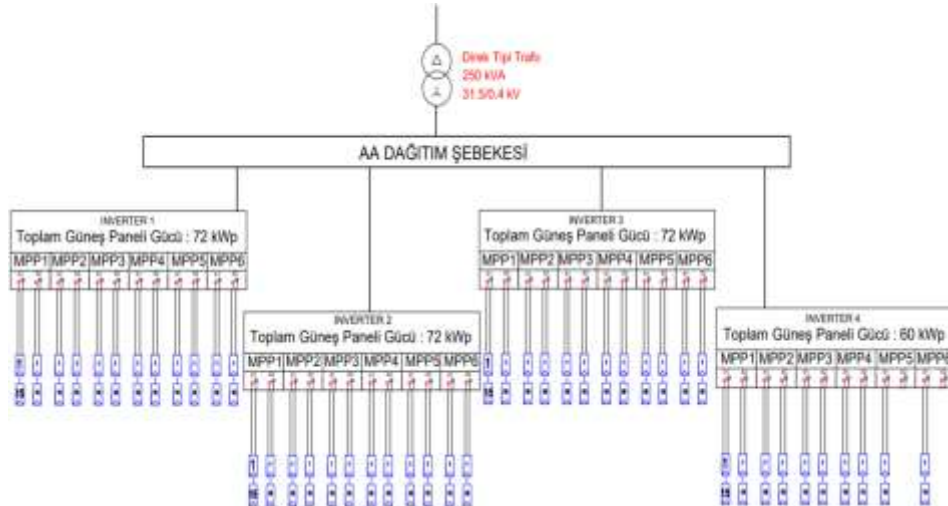
Bu çalışmada, Hanönü (Kastamonu) Belediyesine ait Güneş Enerjisi Santralinin fotovoltaik sistem tasarımı, PVsyst ve PV*SOL benzetim programları kullanılarak analiz edilmiştir. Benzetim sonuçları, Hanönü güneş enerjisi santralinin işletmeye başlayarak üretim yaptığı 2021, 2022, 2023 yıllarına ait üretim verileri ile karşılaştırılmış, her iki programın gerçek üretim verilerine yaklaşımları karşılaştırılmıştır. Tüm bu

analizler ışığında, Hanönü (Kastamonu) Belediyesine ait Güneş Enerji Santralinin performans değerleri incelenmiştir.

2. Hanönü (Kastamonu) Belediyesi Güneş Enerji Santrali'nin PV*SOL ve PVsyst Benzetim Programları ile Enerji Analizi

Güneş enerjisi santrali Hanönü (Kastamonu) Belediyesinin elektrik ihtiyacının karşılanması amacıyla, Kastamonu ili, Hanönü ilçesi Bağdere Mevkii 262 ada 1 parsel 41.6197° enlem, 34.4710° boylam coğrafi koordinatlarında kurularak faaliyete geçirilmiştir. Tesisin maksimum güç üretim kapasitesi 276 kWp'dir. Üretim santralinin kurulu olmuş olduğu bölgede yıllık en düşük ve en yüksek hava sıcaklığı ortalamaları 28.1 °C ile - 4.5 °C arasında değişmektedir (ÇŞİDB - Meteoroloji Genel Müdürlüğü, 2023).

Santralde 690 adet yerli üretim yapan Alfa Solar firmasına ait A3S72M400 marka monokristal güneş panelleri tercih edilmiştir. 400 Wp gücünde 690 adet panel içeren bu fotovoltaik sistem 30° eğim açısı ile güney yönünde konumlandırılarak imalatı yapılmıştır. Santral 3 tane 72 kWp ve 1 tane 60 kWp güçlerinde 4 diziden oluşmaktadır. 72 kWp gücündeki dizilerde 12 adet panel dizisi bulunmaktadır. Her iki dize 72 kWp'lık inverterlerin maksimum güç noktası takip girişine bağlıdır. 60 kWp'lik dizide ise 10 adet panel dizisi bulunmaktadır. Bu dizilerin de her biri 60 kWp'lık inverterlerin maksimum güç noktası takip girişine bağlıdır. Her dizide 15 adet fotovoltaik modül seri şekilde bağlanmıştır. Santralde Growatt New Energy firmasının MAX 60KTL3 LV modeli kullanılmıştır. Hanönü (Kastamonu) Belediyesi Güneş Enerji Santrali 31,5 kV hat gerilimine sahip şebeke hattı ile enterkonnekte sisteme irtibatlandırılmıştır. İnverter çıkışlarındaki alçak gerilim, üç fazlı 0,4/31,5 Kv 50 Hz, 250 kVA'lık direk tipi transformatör aracılığıyla orta gerilim dağıtım şebekesine bağlanmıştır. Şekil 4'te Hanönü (Kastamonu) Belediyesi Güneş Enerji Santralinin tek hat şeması gösterilmiştir.



Şekil 4. Hanönü (Kastamonu) güneş enerji santralinin tek hat bağlantı şeması.

2.1 PV*SOL Benzetim Programı

PV*SOL benzetim programı yardımıyla 5000 adet fotovoltaik modül içerecek şekilde sistem tasarımları gölgelenme biçimleri de dikkate alınmak kaydıyla hesaplanabilmektedir. Program sayesinde güneş enerjisi sistemlerinin tasarımı, optimize edilmesi ve ekonomik değerlendirme sağlanması olmak üzere birçok çalışma yapılabilmektedir. Detaylı analiz yapabilme yeteneği programın veri tabanı genişliği ile ilgilidir. PV*SOL benzetim programı güneş ışığı açıları ve süresi, iklim verileri, gölgelenme durumları, modül, inverter ve diğer montaj ekipmanlarına ait geniş bir veri tabanına sahiptir. Bu durum program kapasitesini ve verimini arttırmaktadır. Çalışmada iklim veri tabanı olarak MeteoSyn ile entegre olacak şekilde çalışma yapılmış olup, analizler detaylı olarak gerçekleştirilmiştir.

PV*SOL programı, güneş ışınımı, sıcaklık ve gölgelenme etkileri gibi değişkenleri dikkate alarak fotovoltaik sistemin çıkış gücünü ve enerji verimini tahmin etmektedir. Program, tasarımcılara PV sistemlerinin beklenen performansını farklı iklim koşulları ve coğrafi konumlarda değerlendirme imkânı sağlamaktadır (Dondariya ve ark., 2018; Milosavljević ve ark., 2022). PV*SOL programı, fotovoltaik sistemin en uygun tasarımını ve konfigürasyonunu gerçekleştirmektedir. Bu durum, panel modüllerinin boyutlandırılması, seçimi, inverterler, bataryalar ve diğer bileşenlerin seçimi gibi unsurları içermektedir (Mohanty ve ark., 2016; Alsadi ve Khatib, 2018; Abo-Khalil ve ark., 2023).

PVSOL, dünya çapında mühendisler, planlamacılar, mimarlar, montaj uzmanları ve nitelikli teknisyenler tarafından yaygın olarak kullanılan bir yazılımdır. PVSOL Premium ile fotovoltaik performans üzerindeki gölgeleme etkilerini doğru bir şekilde değerlendirmek için 3D nesnelere yerleştirmek ve tahmin etmek mümkündür (Cavalcante ve ark., 2019). PV*SOL sayesinde, birkaç modülden oluşan küçük çatı sistemlerinden ticari çatılardaki orta ölçekli sistemlere ve 100.000 modüle kadar olan büyük güneş parklarına kadar farklı büyüklükteki modern güneş enerjisi sistemleri tasarlanabilmekte ve simüle edilebilmektedir.

2.2 PVsyst Benzetim Programı

PVsyst, İsviçre'nin Cenevre Üniversitesi tarafından geliştirilen bir fotovoltaik sistem benzetim programıdır. Bu program, şebekeye bağlantılı veya şebekeden bağımsız fotovoltaik sistem tasarımlarının sonuçlarını üretmeye ve incelemeye yardımcı olmaktadır. Bu program, On Grid (şebeke bağlantılı) veya Off Grid (şebekeden bağımsız) güneş enerjisi sistemleri ve güneş enerjili sulama sistemlerinin tasarımını gerçekleştirmek için kullanılmaktadır (Yadav, 2015). PVsyst güneş enerjisi benzetim programı, 3 boyutlu modellemeler oluşturarak gölgelenme durumlarını analiz etme imkânı sunmaktadır. Tasarlanan güneş enerji sisteminde, güneş panellerine düşen gölgeleri gerçek zamanlı olarak gözleme olanağı sağlamaktadır. Ayrıca, çeşitli güç, gerilim ve markalardaki inverterler ile panel bilgilerini ara yüzünde bulundurarak kurulması planlanan sistemin yıl içerisindeki ortalama performans çıkarımını gerçekleştirmektedir. (Bouzuenda ve ark., 2014; Freeman ve ark., 2014; Fisher ve ark., 2014).

PVsyst, benzer programlardan daha detaylı hesaplamalara ve farklı parametrelerin kullanımına imkân tanımaktadır. PVsyst, iklim verilerini bir düzine farklı kaynaktan ve kişisel verilerden içerebilir (Azam ve ark., 2024).

3. Bulgular

Hanönü (Kastamonu) Belediyesi Güneş Enerjisi Santralini uygulama projesi Haziran 2021 yılında tamamlanmıştır. Santralde kullanılan tüm ekipmanların teknik ve fiziki özelliklerine bağlı olarak PVSOL ile PVsyst programlarında modellemesi yapılarak sistem simüle edilmiştir. Benzetim sonuçlarından sisteme ait elektrik enerjisi üretim değerleri, enerji kayıp değerleri ve bu sonuçlara bağlı olarak performans parametreleri elde edilmiştir. Şekil 5'te Hanönü (Kastamonu) güneş enerjisi santralini kurulduğu alan gösterilmiştir. Şekil 6'da Hanönü (Kastamonu) güneş enerjisi santralini kurulu hali gösterilmiştir. Tablo 1'de Hanönü (Kastamonu) güneş enerjisi santraline ait aylık elektrik enerjisi üretim değerleri gösterilmiştir.



Şekil 5. Hanönü (Kastamonu) güneş enerjisi santralini kurulduğu alan.



Şekil 6. Hanönü (Kastamonu) güneş enerjisi santrali kurulu hali.

Tablo 1. Hanönü güneş enerji santralinde üretilen elektrik enerjisinin aylık dağılımı

Dönem	Üretim Değeri (kWh)
Ocak	10.122
Şubat	15.362
Mart	24.096
Nisan	30.286
Mayıs	33.205
Haziran	36.914
Temmuz	38.711
Ağustos	33.266
Eylül	31.175
Ekim	31.868
Kasım	15.637
Aralık	11.301

Proje kapsamında her iki benzetim programında sahada imalatı tamamlanarak geçici kabulü gerçekleştirilmiş olan ekipmanların marka, model ve teknik verileri aynı olan malzemeler tercih edilmiştir. Böylelikle ekipman özellikleri ve üretim kalitesinden doğabilecek olan verim kayıpları ve oluşacak olan farklar ortadan kaldırılmıştır (Pamuk, 2023).

Pvsyst 7.4.4 programında yapılan benzetim çalışması kapsamında;

- Program içerisinde bulunan harita veri tabanından projenin koordinatlandırılması yapılarak hem lokasyon seçimi hem de lokasyona ait yıllık hava durumu verileri (Meteonorm) seçilmiştir.
- 276 kWp kurulu gücü kapsamında 690 adet monokristal panel kullanılmıştır.
- Hanönü (Kastamonu) Güneş Enerjisi Santralinin uygulamasında kullanılan Alfa Solar firmasına ait A3S72M400 modeli program veri tabanında mevcut olmadığından aynı teknik özelliklere sahip CW Enerji firmasına ait 400 Wp gücünde CWT400 model 690 adet monokristal FV panel kullanılmıştır.
- Sistemde Growatt New Energy markasına ait 60 kW nominal güce sahip MAX 60KTL3 LV model 4 adet invertör kullanılmıştır.

- Fotovoltaik panellerin montajı zemine sabit montajlı olacak şekilde 30° montaj eğimi ve 0° yatay azimut açısı ile tam güney yönünde konumlandırılmıştır.

Tablo 2’te Hanönü (Kastamonu) güneş enerjisi santralinin Pvsyst programı yardımıyla simüle edilen aylık elektrik enerjisi üretim değerleri gösterilmiştir.

Tablo 2. Pvsyst programı üzerinde üretilen elektrik enerjisinin aylık dağılımı

Dönem	Üretim Değeri (kWh)
Ocak	22.199
Şubat	23.923
Mart	30.204
Nisan	35.308
Mayıs	39.249
Haziran	39.779
Temmuz	37.569
Ağustos	38.136
Eylül	36.285
Ekim	28.284
Kasım	21.321
Aralık	19.908

PVSOL programında yapılan benzetim çalışması kapsamında;

- Program içerisinde bulunan harita veri tabanından projenin koordinatlandırılması yapılarak hem lokasyon seçimi hem de lokasyona ait yıllık hava durumu verileri (Meteonorm) seçilmiştir.
- 3D görselleştirme özelliği sayesinde sistemin planlanması gerçekleştirilmiş ve güneş santralinin 3 boyutlu tasarımı yapılmıştır.
- 276 kWp kurulu güç kapsamında 690 adet monokristal panel kullanılmıştır.
- Hanönü (Kastamonu) Güneş Enerjisi Santralinin uygulamasında kullanılan Alfa Solar firmasına ait A3S72M400 modeli program veri tabanında mevcut olmadığından aynı teknik özelliklere sahip CW Enerji firmasına ait 400 Wp gücünde CWT400 model 690 adet monokristal panel kullanılmıştır.

- Sistemde Growatt New Energy markasına ait 60 kW nominal güce sahip MAX 60KTL3 LV model 4 adet invertör kullanılmıştır.
- Fotovoltaik panellerin montajı zemine sabit montajlı olarak 30° montaj eğimi ve 0° yatay azimut açısı ile tam güney yönünde konumlandırılmıştır.

Tablo 3'te Hanönü (Kastamonu) güneş enerjisi santralının PVSOL programı yardımıyla simüle edilen aylık elektrik enerjisi üretim değerleri gösterilmiştir.

Tablo 3. PVSOL programı üzerinde üretilen elektrik enerjisinin aylık dağılımı

Dönem	Üretim Değeri (kWh)
Ocak	11.658
Şubat	15.744
Mart	21.741
Nisan	26.484
Mayıs	36.520
Haziran	40.003
Temmuz	40.669
Ağustos	35.011
Eylül	25.081
Ekim	18.466
Kasım	12.822
Aralık	8.584

4. Sonuçlar ve Öneriler

Bu araştırma kapsamında güneş enerjisi ile enerji üretimi kapsamında projelendirilmiş ve devreye alınmış olan bir santralin gerçek verileri ile benzetim programlarından elde edilen sonuçlar değerlendirilmiştir. Hanönü (Kastamonu) Güneş Enerji Santrali'nin üretime başladığı tarih olan Temmuz 2021 ile Ekim 2023 yılları arasındaki üretim verileri aylık bazda kayıt altına alınmıştır. Söz

konusu aylık üretim verilerinin aynı dönemlerdeki üretim değerlerinin ortalaması alınarak benzetim sonuçları ile karşılaştırılması yapılmıştır.

Aylık üretilen enerji miktarları karşılaştırıldığında direkt güneş açısının azaldığı ve güneşlenme süresinin kısaldığı kış ve sonbahar dönemlerinde PVsyst benzetim programının sonuçları gerçeğe uzak, PV*SOL benzetim programının sonuçları gerçeğe daha yakın olduğu görülmektedir. Güneş açısının ve güneşlenme süresinin arttığı yaz dönemlerinde ise her iki benzetim programının gerçek üretim değerlerine daha yakın sonuç verdiği tespit edilmiştir. Tablo 4'te Hanönü (Kastamonu) güneş enerjisi santralının gerçek, PVSOL ve PVsyst programları yardımıyla simüle edilen aylık elektrik enerjisi üretim değerleri karşılaştırılmıştır.

Tablo 5'te Hanönü (Kastamonu) güneş enerjisi santralının gerçek, PVSOL ve PVsyst programları yardımıyla simüle edilen yıllık elektrik enerjisi üretim değerleri gösterilmiştir.

Benzetim programlarından elde edilen yıllık toplam enerji üretim değerleri ile gerçek üretim değerleri karşılaştırıldığında % 6.15 sapma oranı ile PV*SOL gerçek üretim değerine daha yakın sonuçlar vermiştir. PVsyst programında ise %19,3 sapma oranı ile gerçek değerlere uzak sonuçlar elde edilmiştir.

Güneş enerji sistemlerinin planlanması ve değerlendirilmesinde benzetim programlarının kullanımı büyük bir öneme sahiptir. Fotovoltaik sistem tasarımcıları, coğrafi bölge, enerji talebi ve sistem güvenilirliği gibi faktörlere bağlı olarak, sistem bileşenlerini en uygun şekilde seçmek için benzetim programlarından faydalanabilirler. Bu yaklaşım, maliyetleri düşürerek fazla masraftan kaçınmayı ve sistem tasarımını optimize etmeyi mümkün kılmaktadır (Raj ve ark., 2016).

Tablo 4. Aylık bazda toplam enerji üretim miktarları

Dönem	Hanönü GES Üretim Değeri (kWh)	PVsyst Programı Benzetim Değeri (kWh)	PVSOL Programı Benzetim Değeri (kWh)
Ocak	10.122	22.199	11.658
Şubat	15.362	23.923	15.744
Mart	24.096	30.204	21.741
Nisan	30.286	35.308	26.484
Mayıs	33.205	39.249	36.520
Haziran	36.914	39.779	40.003
Temmuz	38.711	37.569	40.669
Ağustos	33.266	38.136	35.011
Eylül	31.175	36.285	25.081
Ekim	31.868	28.284	18.466
Kasım	15.637	21.321	12.822
Aralık	11.301	19.908	8.584

Tablo 5. Yıl boyunca üretilen toplam enerji üretim miktarları

	Hanönü GES Üretim Değeri (kWh)	PVsyst Programı Benzetim Değeri (kWh)	PVSOL Programı Benzetim Değeri (kWh)
Toplam	311.943	372.165	292.783

Ayrıca, benzetim programlarının detaylı analiz yetenekleri sayesinde sonraki bilimsel çalışmalar detaylandırılabilir. Gerçekleştirilen analizler ile, seçilen parametrelerin enerji üretimi üzerindeki etkisini incelenerek, sistem performansı artırılabilir. Aynı zamanda, benzetim programlarının gerçek ortam verilerine daha yakın sonuçlar üretebilmesi için, enerji üretimi sapma oranları azaltılabilir. Bu bağlamda, benzetim programlarındaki parametre seçenekleri arasında, güneş enerjisi sisteminin haftalık, aylık ve yıllık bakımlarını doğrudan etkileyen sekmelerin bulunması, harita veri tabanlarının sürekli gelişim içinde tutulması ve fotovoltaik sistem ekipmanlarının laboratuvar testlerine tabi tutularak teknik özelliklerinin sağlanması gibi detaylar, gerçek ortam enerji üretimi verilerine daha yakın benzetim sonuçları elde etmede yardımcı olacaktır.

Katkı Oranı Beyanı

Yazar(lar)ın katkı yüzdesi aşağıda verilmiştir. Tüm yazarlar makaleyi incelemiş ve onaylamıştır.

	S.K.	N.P.
K	50	50
T	50	50
Y	50	50
VTI	50	50
VAY	50	50
KT	50	50
YZ	50	50
KI	50	50
GR	50	50
PY	50	50
FA	50	50

K= kavram, T= tasarım, Y= yönetim, VTI= veri toplama ve/veya işleme, VAY= veri analizi ve/veya yorumlama, KT= kaynak tarama, YZ= Yazım, KI= kritik inceleme, GR= gönderim ve revizyon, PY= proje yönetimi, FA= fon alımı.

Çatışma Beyanı

Yazarlar bu çalışmada hiçbir çıkar ilişkisi olmadığını beyan etmektedirler.

Etik Onay Beyanı

Bu çalışmada hayvanlar ve insanlar üzerinde herhangi bir çalışma yapılmadığı için etik kurul onayı alınmamıştır.

Kaynaklar

- Abo-Khalil AG, Sayed K, Radwan A, El-Sharkawy IA. 2023. Analysis of the PV system sizing and economic feasibility study in a grid-connected PV system. *Case Stud Thermal Eng*, 45: 102903.
- Aktacir MA, Yeşilata B. 2011. Harran Üniversitesi kampüsü için fotovoltaik sistem uygulamaları. *Tesisat Müh*, 111: 41-46.
- Aldudak M. 2018. Türkiye'nin farklı şehirlerinde pv sistemlerinin ekonomik analizi ve verimliliği değerlendirmesi. Yüksek Lisans Tezi, Bahçeşehir Üniversitesi, Fen Bilimleri Enstitüsü, İstanbul, Türkiye, pp: 94.
- Alsadi S, Khatib T. 2018. Photovoltaic power systems optimization research status: A review of criteria, constrains,

- models, techniques, and software tools. *Appl Sci*, 8(10): 10. <https://doi.org/10.3390/app8101761>.
- Ay E, Pamuk N. 2023. Zonguldak Bülent Ecevit Üniversitesi Farabi yerleşkesindeki elektrik enerjisi ihtiyacının güneş enerjisi santralleri kurularak elde edilmesi ve ekonomik analizi. *BSJ Eng Sci*, 6(3): 173-184.
- Azam MS, Bhattacharjee A, Hassan M, Rahaman M, Aziz S, Shaikh MAA, Islam MS. 2024. Performance enhancement of solar PV system introducing semi-continuous tracking algorithm based solar tracker. *Energy*, 289: 129989.
- Bali S. 2015. Güneş enerjisi sektöründe kullanılan bilgisayar destekli benzetim programları; PV*SOL Expert programı incelemesi. VIII. Yenilebilir Enerji Kaynakları Sempozyumu, 15-16 Ekim, Adana, Türkiye, pp: 127-132.
- Bolat M, Arifoğlu U, Demiryürek H. 2020. Lebit enerji güneş santralinin Pvsyst programı ile analizi. *Bitlis Eren Üniv Fen Bil Derg*, 9(3): 1351-1363. <https://doi.org/10.17798/bitlisfen.650786>.
- Bouzguenda M, Al Omair A, Al Naeem A, Al Muthaffar M, Ba Wazir O. 2014. Design of an off-grid 2 kW solar PV system. 9th International Conference on Ecological Vehicles and Renewable Energies, March 25-27, Monte-Carlo, Monaco, pp:1-6.
- Cavalcante MM, De Souza Silva JL, Villalva MG, Lins MPF. 2019. Performance analysis of a Solar Photovoltaic Power Plant. IEEE PES Innovative Smart Grid Technologies Conference-Latin America (ISGT Latin America), September 15-18, Gramado, Brazil, pp: 1-5, <https://doi.org/10.1109/ISGT-LA.2019.8894937>.
- Çelebi G. 2002. Bina düzeyi kabuğunda fotovoltaik panellerin kullanım ilkeleri. *Gazi Üniv Müh Mim Fak Derg*, 17(3): 17-33.
- Çiftçi F. 2016. Güneş enerji sistemlerinde farklı cins panellerle maliyet ve güç analizinin yapılması. Yüksek Lisans Tezi, Bahçeşehir Üniversitesi, Fen Bilimleri Enstitüsü, İstanbul, Türkiye, pp: 96.
- ÇŞİDB. 2023. T.C. Çevre, Şehircilik ve İklim Değişikliği Bakanlığı Meteoroloji Genel Müdürlüğü İstatistik Verileri URL: <https://www.mgm.gov.tr/veridegerlendirme/il-ve-ilceler-istatistik.aspx?k=undefined&m=KASTAMONU> (erişim tarihi: 01 Aralık 2023).
- Dondariya C, Porwal D, Awasthi A, Shukla AK, Sudhakar K, Bhimta A. 2018. Performance simulation of grid-connected rooftop solar PV system for small households: A case study of Ujjain, India. *Energy Rep*, 4: 546-553. <https://doi.org/10.1016/j.egy.2018.08.002>.
- EİGM. 2023. T.C. Enerji ve Tabii Kaynaklar Bakanlığı Enerji İşleri Genel Müdürlüğü URL: <https://enerji.gov.tr/eigm-yenilenebilir-enerji-kaynaklar-gunes> (erişim tarihi: 19 Aralık 2023).
- ETKB. 2023. T.C. Enerji ve Tabii Kaynaklar Bakanlığı Bilgi Merkezi URL: <https://enerji.gov.tr/bilgi-merkezi-enerji-gunes> (erişim tarihi: 19 Aralık 2023).
- Fisher B, Ghosal K, Riley D, Hansen C, King B, Burroughs S. 2014. Field performance modeling of Semprius CPV systems. 2014 IEEE 40th Photovoltaic Specialist Conf., June 8-13, Denver, US, pp: 759-765.
- Freeman J, Whitmore J, Blair N, Dobos AP. 2014. Validation of multiple tools for flat plate photovoltaic modeling against measured data. IEEE 40th Photovoltaic Specialist Conference, June 8-13, Denver, US, pp: 1932-1937.
- GEPA. 2023. T.C. Enerji ve Tabii Kaynaklar Bakanlığı Enerji İşleri Genel Müdürlüğü, Güneş Enerjisi Potansiyel Atlası URL: <https://gepa.enerji.gov.tr/MyCalculator/> (erişim tarihi: 19 Aralık 2023).
- Haydaroglu C. 2017. Dicle Üniversitesi güneş enerjisi santralının

- performans analizi. Yüksek Lisans Tezi, Dicle Üniversitesi, Fen Bilimleri Enstitüsü, Diyarbakır, Türkiye, pp: 109.
- Keskin E. 2012. Türkiye iklim koşullarında fotovoltaik güç sistemlerinin tasarımı ve maliyet analizi. Yüksek Lisans Tezi, Hacettepe Üniversitesi Fen Bilimleri Enstitüsü, Ankara, Türkiye, pp: 114.
- Kıyanççek E. 2013. Fotovoltaik sistemlerin boyutlandırılması için pvs2 paket programının gerçekleştirilmesi. Yüksek Lisans Tezi, Selçuk Üniversitesi, Fen Bilimleri Enstitüsü, Konya, Türkiye, pp: 75.
- Lalwani M, Kothari DP, Singh M. 2010. Investigation of solar photovoltaic simulation softwares. *Int J Appl Eng Res Dindigul*, 3(1): 87-92.
- Milosavljević DD, Kevkić TS, Jovanović SJ. 2022. Review and validation of photovoltaic solar simulation tools/ software based on case study. *Open Physics*, 20(1): 431-451. <https://doi.org/10.1515/phys-2022-0042>.
- Mohanty P, Muneer T, Gago EJ, Kotak Y. 2016. Solar radiation fundamentals and PV system components. In P. Mohanty, T. Muneer, & M. Kolhe (Eds.), *Solar Photovoltaic System Applications: A Guidebook for OffGrid Electrification*, Springer, Berlin, Germany, pp: 7-47. https://doi.org/10.1007/978-3-319-14663-8_2.
- Pamuk N. 2023. Performance analysis of different optimization algorithms for MPPT control techniques under complex partial shading conditions in PV systems. *Energies*, 16(8): 3358.
- Pamuk N. 2024. Techno-economic feasibility analysis of grid configuration sizing for hybrid renewable energy system in Turkey using different optimization techniques. *Ain Shams Eng J*, 15(3): 102474.
- Raj A, Gupta M, Panda S. 2016. Design simulation and performance assessment of yield and loss forecasting for 100 Kw grid connected solar PV system. *Next Gener Comput Technol*, 3(5): 528-533.
- Sekçuloğlu SA. 2012. Fotovoltaik (PV), rüzgâr ve hibrit sistemlerin tasarımı ve ekonomik analizi. Yüksek Lisans Tezi, Karadeniz Teknik Üniversitesi Üniversitesi, Fen Bilimleri Enstitüsü, Trabzon, Türkiye, pp: 120.
- Şimşek S. 2018. Fotovoltaik sistemlerde verimliliği etkileyen faktörlerin incelenmesi. Yüksek Lisans Tezi, Hacettepe Üniversitesi, Fen Bilimleri Enstitüsü, Ankara, Türkiye, pp: 147.
- Tozlu C. 2004. Muğla Üniversitesinde kurulu şebekeye bağlı fotovoltaik güç sistemlerinin performans analizi. Yüksek Lisans Tezi, Muğla Üniversitesi, Fen Bilimleri Enstitüsü, Muğla, Türkiye, pp: 114.
- Yadav P. 2015. Simulation and performance analysis of a 1 kWp photovoltaic system using PVsyst. 2015 International Conference on Computation of Power, Energy, Information and Communication (ICCPEIC), April 22-23, Melmaruvathur, India, pp: 358-363.



ELECTROCHEMICAL HYDROGEN PEROXIDE GENERATION AND REMOVAL OF MOXIFLOXACIN BY ELECTRO-FENTON PROCESS

Gökçe Didar DEĞERMENCİ^{1*}, Nejdet DEĞERMENCİ¹


¹Kastamonu University, Faculty of Architecture and Engineering, Department of Environmental Engineering, 37150, Kastamonu, Türkiye


Abstract: In this study, the removal of moxifloxacin, an antibiotic of the fluoroquinolone group, from aqueous solutions was investigated using the electro-Fenton process. As the efficiency of the electro-Fenton process is highly dependent on the amount of H₂O₂ produced during process, the formation of H₂O₂ under acidic conditions was also investigated. In this context, the effects of applied current, cathode type and O₂ flow rate on H₂O₂ production were investigated using boron-doped diamond anode. The highest H₂O₂ production was achieved using the boron-doped diamond anode and the graphite felt cathode. In addition, the optimum conditions for the applied current and oxygen flow rate for H₂O₂ production were determined to be 0.25 A and 0.1 L min⁻¹, respectively. The effects of applied current and Fe²⁺ concentration in the electro-Fenton process on the removal of moxifloxacin were investigated. It was found that the moxifloxacin removal rate increased with increasing applied current. The highest H₂O₂ accumulation was observed at 0.25 A applied current, and moxifloxacin removal also reached 93.6% after 60 min. The moxifloxacin removal rate reached the highest value at Fe²⁺ concentration of 0.01 mM. This study provides promising results for the efficient treatment of moxifloxacin-containing wastewater by the electro-Fenton process without the addition of H₂O₂ using boron-doped diamond anode and graphite felt cathode.

Keywords: Electro-Fenton, Electro-generated H₂O₂, Moxifloxacin, Boron-doped diamond anode, Graphite felt cathode

*Corresponding author: Kastamonu University, Faculty of Architecture and Engineering, Department of Environmental Engineering, 37150, Kastamonu, Türkiye

E mail: gdegermenci@kastamonu.edu.tr (G. D. DEĞERMENCİ)

Gökçe Didar DEĞERMENCİ  <https://orcid.org/0000-0002-4533-9273>

Nejdet DEĞERMENCİ  <https://orcid.org/0000-0003-3135-1471>

Received: March 31, 2024

Accepted: May 04, 2024

Published: May 15, 2024

Cite as: Değermenci GD, Değermenci N. 2024. Electrochemical hydrogen peroxide generation and removal of moxifloxacin by electro-Fenton process. BSJ Eng Sci, 7(3): 539-546.

1. Introduction

Antibiotics, which have a wide range of uses, are drugs used in the treatment of infectious diseases caused by microorganisms and improve the quality of life (Kovalakova et al., 2020; Phoon et al., 2020). Considerable quantities (30 to 90 %) of the antibiotics used to enter the waste stream together with their metabolic products without being metabolized in the body (Carvalho and Santos, 2016). It can be found in surface waters and groundwater due to the widespread use of antibiotics and their inadequate removal in conventional wastewater treatment plants (Kümmerer, 2009; Li et al., 2015; Ngigi et al., 2020; Anh et al., 2021). Therefore, the presence of antibiotics in the aquatic environment leads to a disturbance of flora and fauna and risks to human health (Tiwari et al., 2017). Moxifloxacin (MOX), a third-generation fluoroquinolone, belongs to a group of antimicrobial agents with a broad spectrum of activity and increasing consumption (Van Doorslaer et al., 2011). MOX is widely used against both gram-positive and gram-negative bacteria by inhibiting DNA activity and for the treatment of skin infections (Guay, 2006; Nguyen et al., 2023). However, due to its low biodegradability, it is constantly discharged into the

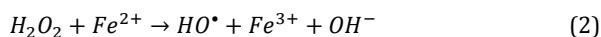
natural environment from conventional wastewater treatment plants (Van Doorslaer et al., 2015).

Antibiotics, which have high production and consumption rates, are not easily biodegradable. Therefore, cost-efficient methods are needed to effectively remove antibiotics from wastewater (Shoorangiz et al., 2019). As conventional treatment processes are not sufficient to remove wastewater containing antibiotics, advanced oxidation processes (AOPs) should be preferred to support them or be used as an alternative (Oturán and Aaron, 2014; Ganzenko et al., 2020; Taoufik et al., 2021). AOPs are methods of great interest for the removal of recalcitrant organics and toxic compounds (such as diclofenac and levofloxacin) (Jia et al., 2024; Qiu et al., 2024). AOPs such as Fenton, ozonation, photocatalysis, activated persulfate, and electrochemical processes have been used to remove toxic and/or recalcitrant organic pollutants (Değermenci et al., 2014; Çobanoğlu and Değermenci, 2022; Li et al., 2023). Among AOPs, Fenton oxidation attracts attention due to its simplicity, which does not require special equipment, and its high efficiency in removing organic pollutants (Arnold et al., 1995; Değermenci, 2023). To avoid disadvantages such as potential risks and loss of



reactive activity during transportation and storage of H₂O₂ used in Fenton oxidation, the electro-Fenton process was developed in combination with Fe²⁺ addition and in situ electro-generated H₂O₂ (Zhou et al., 2007).

The electro-Fenton process is considered an environmentally friendly and promising method for the effective removal of target pollutants from water (Olvera-Vargas et al., 2021; Liu et al., 2022; Yang et al., 2023; de Oliveira Santiago Santos et al., 2023). In the electro-Fenton process, H₂O₂ production is based on the electrochemical reduction of molecular oxygen (O₂) at the cathode (Equation 1) by introducing air or high-purity O₂ into the electrolysis cell, and hydroxyl radicals are formed by the electrochemically assisted Fenton reaction (Equation 2) (Brillas et al., 2009). This process, hydrogen peroxide is continuously generated in situ, which allows better control of the oxidation process (Garcia-Segura et al., 2011; Bensalah et al., 2013). The hydroxyl radical and the hydrogen peroxide produced in the process have a strong oxidative potential (E₀=2.80 V and 1.78 V) (Lucas and Peres, 2006). Non-selective hydroxyl radicals are responsible for the oxidation/mineralization of persistent organic substances that are in the same environment (Olvera-Vargas et al., 2021).



The performance of the electro-Fenton process depends largely on the electrode materials used during electrolysis (Guinea et al., 2010; Bensalah et al., 2013; Midassi et al., 2020). The type of cathode used influences the amount of H₂O₂ produced by the reduction of molecular oxygen (Brillas et al., 2009; Olvera-Vargas et al., 2021). Materials such as carbon brush, carbon felt, stainless steel, carbon sponge etc. were used as cathodes (Sopaj et al., 2020; Olvera-Vargas et al., 2021). Although H₂O₂ production in the electro-Fenton process depends on the cathode type, the structure of the anode material also plays an important role in the overall performance (Sopaj et al., 2016; Yang et al., 2020). Depending on the anode type, heterogeneous hydroxyl radicals are formed

on the anode surface by the oxidation of water (Titchou et al., 2021; Yang et al., 2023). The use of different types of anodes such as Pt, Ti/RuO₂-IrO₂, Ti₄O₇, boron doped diamond (BDD), and graphite felt (GF) in the electro-Fenton process has been investigated in the literature (Sopaj et al., 2016; Zwane et al., 2021). This increases the overall efficiency of the electro-Fenton process, as both the cathodic and anodic reactions contribute to the degradation/mineralization of the organic pollutants (Oturán et al., 2012; Olvera-Vargas et al., 2021). The BDD anode is characterized by a high O₂ evolution overvoltage (around 2.2 V vs SHE for BDD). BDD has proven to be the most effective material for the anodic oxidation of refractory organic pollutants (Panizza and Cerisola, 2009; Olvera-Vargas et al., 2021; Oturan, 2021), and the use of BDD as an anode in the electro-Fenton process has been shown to significantly improve the efficiency of the process (Oturán et al., 2012; Ridruejo et al., 2018; Olvera-Vargas et al., 2021).

In the first part of the study, the effects of different operating variables, such as cathode type, O₂ flow rate, and applied current on H₂O₂ accumulation were discussed. In the second part, the removal of MOX by the electro-Fenton process using a BDD anode and a GF cathode was investigated. The effects of current intensity and Fe²⁺ concentration, which are among the parameters affecting the electro-Fenton process, on MOX removal were investigated.

2. Materials and Methods

2.1. Chemicals

All chemicals and reagents used in this study were used without further purification. Moxifloxacin hydrochloride, potassium hydrogen phthalate, potassium iodide, sodium sulfate, hydrogen peroxide, ammonium heptamolybdate tetrahydrate, sodium hydroxide, and sulphuric acid were purchased from the Merck. All solutions were prepared with distilled water at room temperature.

2.2. Experimental Setup

A scheme of the electrochemical cell used is presented in Figure 1.

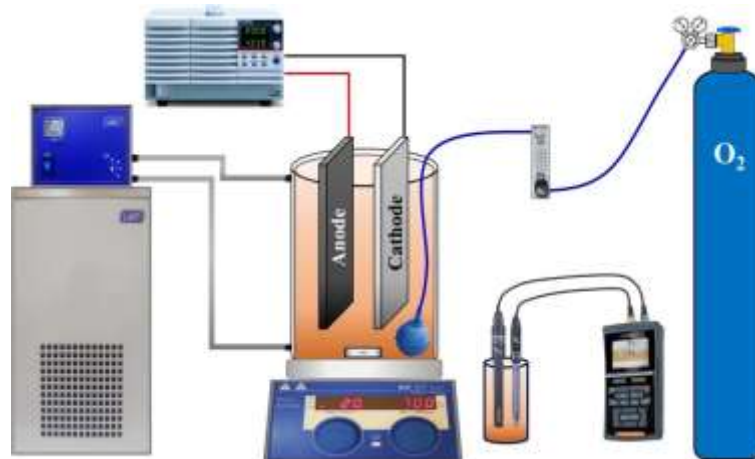


Figure 1. Schematic diagram of electrochemical cell.

Electrochemical H_2O_2 production and MOX removal by the electro-Fenton process were carried out in an undivided cylindrical glass reactor with a diameter of 7.5 cm and a solution capacity of 400 mL. BDD electrode (DiaCCon GmbH, Germany) was used as an anode for H_2O_2 production and the electro-Fenton process. GF, BDD, stainless steel (SS), and graphite plate (GP) electrodes were used as cathodes. All electrodes are 5 cm \times 10 cm in size. The wall thickness is 3 mm for BDD, SS and GP and 12 mm for GF. The temperature of the solution was kept constant at 20°C using a temperature-controlled cooling/heated circulator (LABO, C200-H13). Sodium sulfate (Na_2SO_4) was used as a supporting electrolyte to increase the conductivity of the solution. The aqueous solution was stirred continuously at 700 rpm with a magnetic stirrer (IKA, RCT basic). A power supply unit (GW Instek, PSW 80-40.5) was used in all experiments to ensure constant current operation. This device also displayed the cell voltage during the treatments. Without adding a buffer solution, the pH of the solution was adjusted to the desired value only once at the beginning of the experiment with 1 M H_2SO_4 . The pH value of the solution was measured using the portable WTW Multi-Parameter meter (Xylem Analytics, MultiLine® Multi 3620 IDS).

2.3. Analytical Procedures

The H_2O_2 and MOX concentration were measured using a UV-Vis spectrophotometer (HachLange, DR 6000). The H_2O_2 concentration was measured at 352 nm by the iodometric method (Klassen et al., 1994). To measure the MOX concentration, a MOX stock solution was prepared and known MOX concentrations were determined by dilution. These solutions were used to create a calibration curve at 290 nm, and the unknown MOX concentrations were measured by prepared calibration curve. The MOX removal efficiency and energy consumption were calculated using Equation 3 and Equation 4, respectively:

$$\text{MOX removal, (\%)} = (1 - C_t/C_0) \times 100 \quad (3)$$

$$W, (\text{kWh m}^{-3}) = V \times I \times t/V_S \quad (4)$$

where C_0 is the initial MOX concentration (mg L^{-1}), C_t is the MOX concentration at given time t (mg L^{-1}), V is mean cell voltage (V), I is electrolysis current (A), t is electrolysis duration (h), and V_S is solution volume (L).

3. Results and Discussion

3.1. Electrochemical H_2O_2 Production

The reactant required for the Fenton reaction to form strong oxidative free radicals is H_2O_2 (Değermenci et al., 2019). The efficiency of the electro-Fenton process depends largely on the amount of H_2O_2 produced in the system (Zhao et al., 2018). In the electro-Fenton process, H_2O_2 can be formed under acidic conditions by the electrochemical reduction of oxygen at the cathode (Equation 1) (Brillas et al., 2009; Midassi et al., 2020). In this context, the effects of current intensity, cathode type,

and O_2 flow rate, which are among the parameters affecting electrochemical H_2O_2 production, were examined using the BDD anode.

3.1.1. Effect of cathode type on H_2O_2 production

H_2O_2 production varies depending on the cathode material (Oturán et al., 2021). Therefore, the H_2O_2 production performance of different cathode types using BDD as anode material was investigated. H_2O_2 formation in the experimental system was measured in a solution saturated with O_2 under acidic conditions ($\text{pH} = 3$) and in the absence of pollutants and Fe^{2+} . H_2O_2 production was monitored for 60 min by continuously supplying O_2 to the cathode; the results are shown in Figure 2. The H_2O_2 production during 60 min electrolysis is 42.7, 28.1, 15.4, and 11.1 mg L^{-1} for GF, BDD, SS, and GP, respectively. The highest H_2O_2 production was achieved with GF. The H_2O_2 production during 30 min electrolysis is 36.4, 20, 14.1 and 10.0 mg L^{-1} for GF, BDD, SS and GP, respectively. These results show that the H_2O_2 production rate depends significantly on the cathode type. However, it can be said that the electrochemical reduction of molecular oxygen (Equation 1) occurs faster when GF is used as the cathode. The type of cathode promotes oxygen adsorption and transfer, electron transfer and provides more active sites, thereby promoting the production of H_2O_2 (Feng et al., 2021). Since the highest H_2O_2 production was obtained with GF, it was used as the cathode in the following studies.

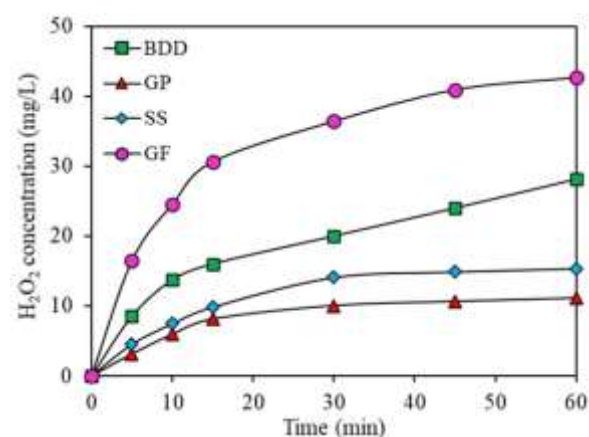


Figure 2. Effect of cathode type on the H_2O_2 generation (Conditions: Current intensity= 1 A, Na_2SO_4 = 50 mM, T= 20°C, initial solution pH= 3, and O_2 flow rate= 1 L min^{-1}).

3.1.2. Effect of applied current on H_2O_2 production

The applied current is one of the most important parameters for electrochemical H_2O_2 production (Köktaş and Gökkuş, 2022). The cathodic production of H_2O_2 via the reaction given in Equation 1 drives the production of hydroxyl radicals in the electro-Fenton process via the reaction given in Equation 2. Therefore, the H_2O_2 accumulation in the electrolysis reactor with BDD anode and GF cathode was investigated. Figure 3 shows the H_2O_2 accumulation at different current values during the 60 min electrolysis at an initial solution pH of 3, an electrolyte concentration of 50 mM Na_2SO_4 and an

oxygen flow rate of 1 L min^{-1} . The H_2O_2 concentration is 23.6 mg L^{-1} after 60 min of electrolysis at a current of 0.05 A. When the current was raised from 0.10 to 0.25 A, the H_2O_2 concentration increased from 53.8 to 95.7 mg L^{-1} . The reason for this increase is that an increase in the applied current supports the oxygen reduction reaction specified in equation 1. However, a further increase in the applied current led to a decrease in H_2O_2 accumulation. H_2O_2 concentration decreased from 66.8 to 42.7 mg L^{-1} when the current was increased from 0.50 to 1.00 A, respectively. This is because the competitive reactions increase with increasing applied current, which leads to a depletion of H_2O_2 . These are explained by the reduction of H_2O_2 to H_2O at the cathode (Equation 5) and the oxidation of H_2O_2 at the anode (Equation 6). Similar results have been reported regarding the effect of applied current on H_2O_2 production (Zhou et al., 2019; Midassi et al., 2020; Olvera-Vargas et al., 2021). Subsequent experiments were carried out at 0.10 A in order to determine the effect of other operating parameters and for cost effectiveness.

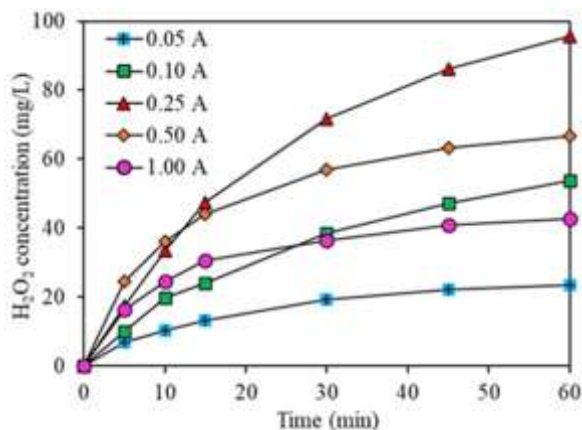


Figure 3. Effect of applied current on the H_2O_2 generation (Conditions: $\text{Na}_2\text{SO}_4 = 50 \text{ mM}$, $T = 20^\circ\text{C}$, initial solution $\text{pH} = 3$, and O_2 flow rate = 1 L min^{-1}).

3.1.3. Effect of O_2 flow rate on H_2O_2 production

The O_2 flow rate supplied to the system is one of the parameters that influence electrochemical H_2O_2 production (Midassi et al., 2020). Figure 4 shows the effects of O_2 flow rate on H_2O_2 production when using a BDD anode and a GF cathode. In the experiments, the effect of different O_2 flow rates ($0\text{--}1 \text{ L min}^{-1}$) on H_2O_2 production was studied for electrolysis time of 60 min. While H_2O_2 production is 14.9 mg L^{-1} when no gas is added to the reactor, H_2O_2 production increases when O_2 is introduced. At an O_2 flow rate of 0.1 L min^{-1} , H_2O_2 accumulation reached the highest value of 61.3 mg L^{-1} in 60 min. A further increase in the gas flow rate reduced H_2O_2 production to 53.9 mg L^{-1} at 0.2 L min^{-1} and 53.8 mg L^{-1} at 1.0 L min^{-1} . Increasing the O_2 flow rate can

increase the concentration of dissolved O_2 and promote the mass transfer rate of dissolved O_2 in the solution, which supports electro-generated H_2O_2 production. At flow rates greater than 0.1 L min^{-1} , excessively large bubbles covering the surface of the gas diffusion electrode lead to reduced H_2O_2 production. Similar results regarding the effect of O_2 flow rate on H_2O_2 production have been reported in some studies (Xia et al., 2019; Köktaş and Gökkuş, 2022). A flow rate of 0.1 L min^{-1} O_2 is sufficient to generate a high H_2O_2 concentration. These results show that adjusting the optimal O_2 flow rate in the system can not only promote H_2O_2 production but also reduce costs (Zhou et al., 2013).

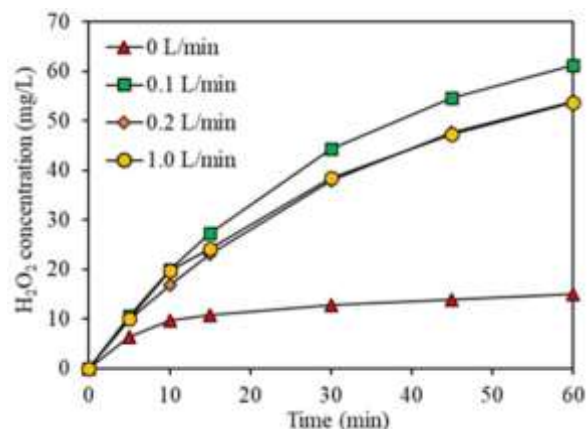


Figure 4. Effect of the O_2 flow rate on the H_2O_2 generation (Conditions: $\text{Na}_2\text{SO}_4 = 50 \text{ mM}$, $T = 20^\circ\text{C}$, initial solution $\text{pH} = 3$, and current intensity = 0.10 A).

3.2. Effect of Different Processes on MOX Removal

In the system in which the highest H_2O_2 production was achieved, graphite felt was used as the cathode and BDD as the anode. In the electrolytic cell, MOX can be removed by adsorption and anodic oxidation together with the electro-Fenton process. A comparison of the MOX removals achieved with these treatment methods is shown in Figure 5. In the experiment to determine the amount of MOX adsorbed on the anode and cathode in the electrolytic cell, no current was applied to the cell and O_2 and Fe^{2+} were not supplied. It was determined that the removal of MOX by adsorption was 11.7% in 10 min and 27.5% in 60 min. Then the removal of MOX by anodic oxidation was determined by applying current (0.10 A) to the electrolytic cell without O_2 and Fe^{2+} . While MOX removal by anodic oxidation was 30.9% at the 10 min electrolysis, it increased to 87.7% after 60 min. Finally, MOX removal was determined by the electro-Fenton process by adding O_2 and Fe^{2+} to the electrolytic cell at a certain current value (0.10 A). MOX removal by the electro-Fenton process increased from 67.3% in 10 min to 89.0% after 60 min. From these results, it was concluded that the electro-Fenton process is the treatment process with the highest removal rate.

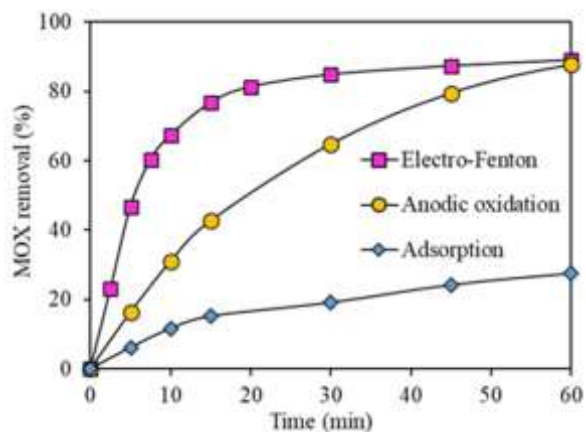


Figure 5. Comparison between electro-Fenton, anodic oxidation and adsorption (Conditions: MOX= 5 mg L⁻¹, Na₂SO₄= 50 mM, initial solution pH= 3, T= 20°C, current intensity= 0.10 A, O₂ flow rate= 0.1 L min⁻¹, Fe²⁺= 0.01mM).

3.2.1. Effect of applied current on MOX removal in the electro-Fenton process

The applied current considerably influences on the electro-Fenton process and is the most important parameter for controlling the reaction rate (Görmez et al., 2022). The effect of the applied current on the removal of MOX by the electro-Fenton process using a GF cathode and a BDD anode is shown in Figure 6. In the electro-Fenton process, MOX removal efficiencies at 60 min electrolysis time were 86.4%, 89.0%, 93.6%, 95.2% and 95.6% at applied currents of 0.05, 0.10, 0.25, 0.50 and 0.75 A, respectively. During the 10 min electrolysis time, MOX removal was 59.6%, 67.3%, 78.5%, 84.6% and 88.5%, respectively, depending on the increasing current value applied. From these results, it can be concluded that the MOX removal rate increases with the increase of the applied current. Comparing these results with H₂O₂ production, the highest H₂O₂ accumulation was obtained at 0.25 A (Figure 3), which does not correspond to the optimum current value for MOX removal. The decreasing H₂O₂ accumulation at high current values does not mean that H₂O₂ production is low. It means that the rate of competitive reactions (Equations 5 and 6) leading to H₂O₂ depletion is high, so the rate of H₂O₂ decomposition is faster than the formation of H₂O₂ (Olvera-Vargas et al., 2021). The H₂O₂ produced in the electrolytic cell reacted with Fe²⁺ via the Fenton reaction (equation 2) before being destroyed via equations 5 and 6. It should be noted that increasing the applied current value increases electrical energy consumption and operating costs.

The change in energy consumption in the experiments conducted at different current values was calculated using equation 4, and the results are shown in Figure 7. As the current value applied to the system increases, the energy consumption increases along with the increase in voltage. The energy consumption for currents of 0.05, 0.10, 0.25, 0.50 and 0.75 A was calculated to be 0.38, 0.86, 2.53, 6.59 and 12.0 kWh m⁻³, at the end of 60 min,

respectively. Increasing the applied current can lead to chemical changes on the electrode surface and shorten the service life of the electrode (GilPavas et al., 2017). However, a further increase in the applied current can have a negative effect on MOX removal due to side reactions (hydrogen evolution and water electrolysis) (Qiu et al., 2024).

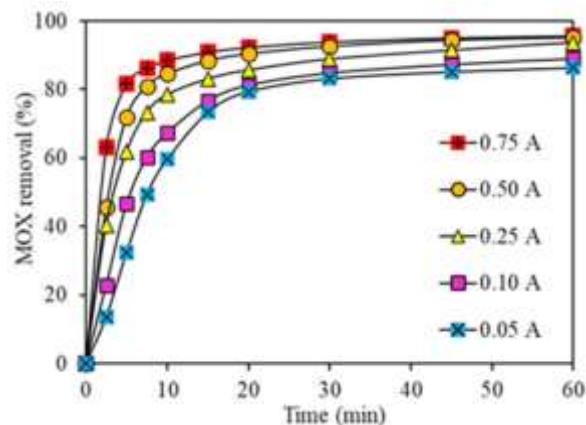


Figure 6. Effect of applied current on the MOX removal in the electro-Fenton process (Conditions: MOX= 5 mg L⁻¹, Na₂SO₄= 50 mM, initial solution pH= 3, T= 20°C, O₂ flow rate= 0.1 L min⁻¹, Fe²⁺= 0.01mM).

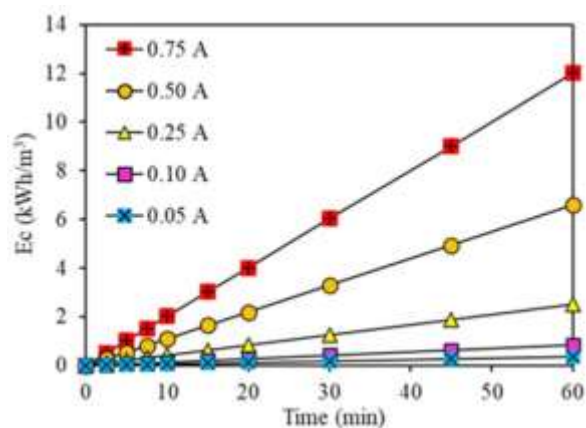


Figure 7. Variation of energy consumption with applied current (Conditions: MOX= 5 mg L⁻¹, Na₂SO₄= 50 mM, initial solution pH= 3, T= 20°C, O₂ flow rate= 0.1 L min⁻¹, Fe²⁺= 0.01mM).

3.2.2. Effect of Fe²⁺ concentration on MOX removal in the electro-Fenton process

The catalyst concentration is one of the important parameters affecting the removal of pollutants in the electro-Fenton process (Wang et al., 2021; Karatas et al., 2022). The effect of Fe²⁺ concentration on MOX removal is shown in Figure 8. While in the absence of Fe²⁺ ions the MOX removal in 10 min was about 30.9 %, a significant increase in MOX removal was observed with the addition of Fe²⁺ ions. At an electrolysis time of 10 min, the Fe²⁺ concentration for MOX removal increased to 63.4 % at 0.005 mM and to 67.3 % at 0.010 mM. This increase in MOX removal can be explained by the contribution of the generated hydroxyl radicals (Equation 2). Increasing the

Fe²⁺ concentration to 0.020 mM led to a slight decrease in MOX removal. This negative effect of the high Fe²⁺ concentration can be explained by the increased rate of the parasitic reaction (Equation 7) that occurs between hydroxyl radicals and excess Fe²⁺ (Özdemir et al., 2011; Xia et al., 2019).

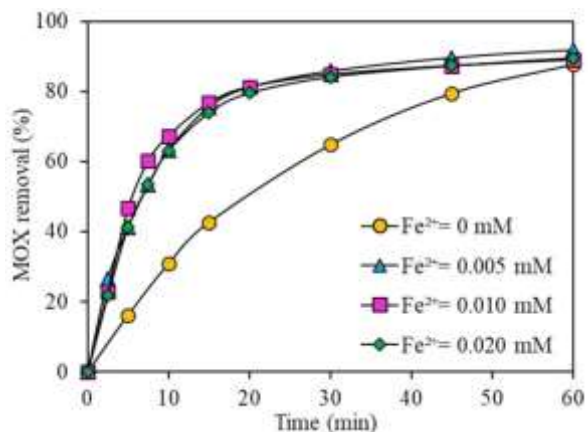


Figure 8. Effect of Fe²⁺ concentration on MOX removal in the electro-Fenton process (Conditions: MOX= 5 mg L⁻¹, Na₂SO₄= 50 mM, initial solution pH= 3, T= 20°C, current intensity= 0.10 A, O₂ flow rate= 0.1 L min⁻¹).

4. Conclusion

In this study, electrochemical H₂O₂ production and MOX removal were successfully performed with a BDD anode. It was found that the electrochemical H₂O₂ production rate was significantly dependent on the cathode type. H₂O₂ production increased with the use of a GF cathode, it was also observed that the applied current and oxygen flow rate also had significant effects on H₂O₂ production. The effects of applied current and Fe²⁺ concentration on MOX removal in the electro-Fenton process were investigated. It was found that the MOX removal rate in the process with BDD anode and GF cathode increased with the increase of the applied current. However, it was found that increasing current was accompanied by a corresponding increase in energy consumption due to the increased voltage. From the findings, it was concluded that the electro-Fenton process could be an effective method for reducing antibiotic contamination in wastewater.

Author Contributions

The percentage of the author(s) contributions is presented below. The author reviewed and approved the final version of the manuscript.

	G.D.D.	N.D.
C	70	30
D	70	30
S	100	
DCP	50	50
DAI	50	50
L	80	20
W	100	
CR	80	20
SR	100	
PM	80	20
FA	100	

C=Concept, D= design, S= supervision, DCP= data collection and/or processing, DAI= data analysis and/or interpretation, L= literature search, W= writing, CR= critical review, SR= submission and revision, PM= project management, FA= funding acquisition.

Conflict of Interest

The author declared that there is no conflict of interest.

Ethical Consideration

Ethics committee approval was not required for this study because of there was no study on animals or humans.

Acknowledgements

This research has been supported by Kastamonu University Scientific Research Projects Coordination Department (Project Number: KÜ-BAP01/2018-97).

References

- Anh HQ, Le TPQ, Le ND, Lu XX, Duong TT, Garnier J, Rochelle-Newall E, Zhang S, Oh N-H, Oeurng C, Ekkawatpanit C, Nguyen TD, Nguyen QT, Nguyen TD, Nguyen TN, Tran TL, Kunisue T, Tanoue R, Takahashi S, Minh TB, Le TL, Pham TNM, Nguyen TAH. 2021. Antibiotics in surface water of East and Southeast Asian countries: A focused review on contamination status, pollution sources, potential risks, and future perspectives. *Sci Total Environ*, 764: 142865.
- Arnold SM, Hickey WJ, Harris RF. 1995. Degradation of atrazine by Fenton's reagent: Condition optimization and product quantification. *Environ Sci Technol*, 29: 2083-2089.
- Bensalah N, Bedoui A, Chellam S, Abdel-Wahab A. 2013. Electro-Fenton treatment of photographic processing wastewater. *Clean (Weinh)*, 41: 635-644.
- Brillas E, Sirés I, Oturan MA. 2009. Electro-fenton process and related electrochemical technologies based on fenton's reaction chemistry. *Chem Rev*, 109: 6570-6631.
- Carvalho IT, Santos L. 2016. Antibiotics in the aquatic environments: A review of the European scenario. *Environ Int*, 94: 736-757.
- Çobanoğlu K, Değermenci N. 2022. Comparison of reactive azo dye removal with UV/H₂O₂, UV/S₂O₈²⁻ and UV/H₂O₂/S₂O₈²⁻ processes in aqueous solutions. *Environ Monit Assess*, 194: 302.

- De Oliveira Santiago Santos G, Athie Goulart L, Sánchez-Montes I, Da Silva RS, De Vasconcelos Lanza MR. 2023. Electrochemically enhanced iron oxide-modified carbon cathode toward improved heterogeneous electro-Fenton reaction for the degradation of norfloxacin. *Environ Sci Pollut Res Int*, 30: 118736-118753.
- Değermenci GD, Bayhan YK, Değermenci N. 2014. Investigation of treatability of industrial wastewater containing high organic matter by Fenton process. *J Inst Sci Technol*, 4(2): 17-22.
- Değermenci GD. 2023. Decolorization of reactive azo dye by fenton and photo-fenton processes in aqueous solution: The influence of operating conditions, kinetics study, and performance comparison. *Bull Chem Soc Ethiop*, 37: 197-210.
- Değermenci N, Değermenci GD, Ulu HB. 2019. Decolorization of reactive azo dye from aqueous solutions with Fenton oxidation process: effect of system parameters and kinetic study. *Desalin Water Treat*, 169: 363-371.
- Feng Y, Li W, An J, Zhao Q, Wang X, Liu J, He W, Li N. 2021. Graphene family for hydrogen peroxide production in electrochemical system. *Sci Total Environ*, 769: 144491.
- Ganzenko O, Trelu C, Oturan N, Huguenot D, Péchaud Y, Van Hullebusch ED, Oturan MA. 2020. Electro-Fenton treatment of a complex pharmaceutical mixture: Mineralization efficiency and biodegradability enhancement. *Chemosphere*, 253: 126659.
- Garcia-Segura S, Centellas F, Arias C, Garrido JA, Rodríguez RM, Cabot PL, Brillas E. 2011. Comparative decolorization of monoazo, diazo and triazo dyes by electro-Fenton process. *Electrochim Acta*, 58: 303-311.
- GilPavas E, Arbeláez-Castaño P, Medina J, Acosta DA. 2017. Combined electrocoagulation and electro-oxidation of industrial textile wastewater treatment in a continuous multi-stage reactor. *Water Sci Technol*, 76: 2515-2525.
- Görmez Ö, Akay S, Gözmen B, Kayan B, Kaldersı D. 2022. Degradation of emerging contaminant coumarin based on anodic oxidation, electro-Fenton and subcritical water oxidation processes. *Environ Res*, 208: 112736.
- Guay DRP. 2006. Moxifloxacin in the treatment of skin and skin structure infections. *Ther Clin Risk Manag*, 2: 417-434.
- Guinea E, Garrido JA, Rodríguez RM, Cabot P-L, Arias C, Centellas F, Brillas E. 2010. Degradation of the fluoroquinolone enrofloxacin by electrochemical advanced oxidation processes based on hydrogen peroxide electrogeneration. *Electrochim Acta*, 55: 2101-2115.
- Jia X, Huang J, Zhao X, Wu T, Wang C, He H. 2024. Levofloxacin degradation in a heterogeneous electro-Fenton system with an FeOCl/MoS₂ composite catalyst. *React Chem Eng*, 9: 1127-1139. <https://doi.org/10.1039/d3re00548h>.
- Karatas O, Gengec NA, Gengec E, Khataee A, Kobya M. 2022. High-performance carbon black electrode for oxygen reduction reaction and oxidation of atrazine by electro-Fenton process. *Chemosphere*, 287: 132370.
- Klassen N V, Marchington D, McGowan HCE. 1994. H₂O₂ Determination by the I₃- Method and by KMnO₄ Titration. *Anal Chem*, 66: 2921-2925.
- Köktaş İY, Gökkuş Ö. 2022. Removal of salicylic acid by electrochemical processes using stainless steel and platinum anodes. *Chemosphere*, 293: 133566.
- Kovalakova P, Cizmas L, McDonald TJ, Marsalek B, Feng M, Sharma VK. 2020. Occurrence and toxicity of antibiotics in the aquatic environment: A review. *Chemosphere*, 251: 126351.
- Kümmerer K. 2009. Antibiotics in the aquatic environment - A review - Part I. *Chemosphere*, 75: 417-434.
- Li S, Wu Y, Zheng H, Li H, Zheng Y, Nan J, Ma J, Nagarajan D, Chang J-S. 2023. Antibiotics degradation by advanced oxidation process (AOPs): Recent advances in ecotoxicity and antibiotic-resistance genes induction of degradation products. *Chemosphere*, 311: 136977.
- Li W, Gao L, Shi Y, Liu J, Cai Y. 2015. Occurrence, distribution and risks of antibiotics in urban surface water in Beijing, China. *Environ Sci Process Impacts*, 17: 1611-1619.
- Liu Z-j, Wan J-q, Yan Z-c, Wang Y, Ma Y-w. 2022. Efficient removal of ciprofloxacin by heterogeneous electro-Fenton using natural air-cathode. *Chem Eng J*, 433: 133767.
- Lucas MS, Peres JA. 2006. Decolorization of the azo dye Reactive Black 5 by Fenton and photo-Fenton oxidation. *Dye Pigment*, 71: 236-244.
- Midassi S, Bedoui A, Bensalah N. 2020. Efficient degradation of chloroquine drug by electro-Fenton oxidation: Effects of operating conditions and degradation mechanism. *Chemosphere*, 260: 127558.
- Ngigi AN, Magu MM, Muendo BM. 2020. Occurrence of antibiotics residues in hospital wastewater, wastewater treatment plant, and in surface water in Nairobi County, Kenya. *Environ Monit Assess*, 192: 18.
- Nguyen TH, Nguyen XH, Do TG, Nguyen LH. 2023. Development of biochar supported NiFe₂O₄ composite for peroxydisulfate (PDS) activation to effectively remove moxifloxacin from wastewater. *Chem Eng J Adv*, 16: 100550.
- Olvera-Vargas H, Gore-Datar N, Garcia-Rodriguez O, Mutnuri S, Lefebvre O. 2021. Electro-Fenton treatment of real pharmaceutical wastewater paired with a BDD anode: Reaction mechanisms and respective contribution of homogeneous and heterogeneous OH. *Chem Eng J*, 404: 126524.
- Oturan MA, Aaron JJ. 2014. Advanced oxidation processes in water/wastewater treatment: Principles and applications. A review. *Crit Rev Environ Sci Technol*, 44: 2577-2641.
- Oturan MA. 2021. Outstanding performances of the BDD film anode in electro-Fenton process: Applications and comparative performance. *Curr Opin Solid State Mater Sci*, 25: 100925.
- Oturan N, Bo J, Trelu C, Oturan MA. 2021. Comparative Performance of Ten Electrodes in Electro-Fenton Process for Removal of Organic Pollutants from Water. *ChemElectroChem*, 8: 3294-3303.
- Oturan N, Brillas E, Oturan MA. 2012. Unprecedented total mineralization of atrazine and cyanuric acid by anodic oxidation and electro-Fenton with a boron-doped diamond anode. *Environ Chem Lett*, 10: 165-170.
- Özdemir C, Öden MK, Şahinkaya S, Kalipçi E. 2011. Color Removal from Synthetic Textile Wastewater by Sono-Fenton Process. *Clean (Weinh)*, 39: 60-67.
- Panizza M, Cerisola G. 2009. Direct and mediated anodic oxidation of organic pollutants. *Chem Rev*, 109: 6541-6569.
- Phoon BL, Ong CC, Mohamed Saheed MS, Show P-L, Chang J-S, Ling TC, Lam SS, Juan JC. 2020. Conventional and emerging technologies for removal of antibiotics from wastewater. *J Hazard Mater*, 400: 122961.
- Qiu B, Zhou X, Li W, Hhu H, Yu L, Yuan C, Dou R, Sun M, Wang S. 2024. A magnetically induced self-assembly of Ru@Fe₃O₄/rGO cathode for diclofenac degradation in electro-Fenton process. *Environ Res*, 242: 117781.
- Ridruejo C, Centellas F, Cabot PL, Sirés I, Brillas E. 2018. Electrochemical Fenton-based treatment of tetracaine in synthetic and urban wastewater using active and non-active anodes. *Water Res*, 128: 71-81.
- Shoorangiz M, Nikoo MR, Salari M, Rakhshandehroo GR, Sadegh

- M. 2019. Optimized electro-Fenton process with sacrificial stainless steel anode for degradation/mineralization of ciprofloxacin. *Process Saf Environ Prot*, 132: 340-350.
- Sopaj F, Oturan N, Pinson J, Podvorica F, Oturan MA. 2016. Effect of the anode materials on the efficiency of the electro-Fenton process for the mineralization of the antibiotic sulfamethazine. *Appl Catal B Environ*, 199: 331-341.
- Sopaj F, Oturan N, Pinson J, Podvorica FI, Oturan MA. 2020. Effect of cathode material on electro-Fenton process efficiency for electrocatalytic mineralization of the antibiotic sulfamethazine. *Chem Eng J*, 384: 123249.
- Taoufik N, Boumya W, Achak M, Sillanpää M, Barka N. 2021. Comparative overview of advanced oxidation processes and biological approaches for the removal pharmaceuticals. *J Environ Manage*, 288: 112404.
- Titchou FE, Zazou H, Afanga H, Gaayda JE, Akbour RA, Hamdani M, Oturan MA. 2021. Electro-Fenton process for the removal of Direct Red 23 using BDD anode in chloride and sulfate media. *J Electroanal Chem*, 897: 115560.
- Tiwari B, Sellamuthu B, Ouarda Y, Drogui P, Tyagi RD, Buelna G. 2017. Review on fate and mechanism of removal of pharmaceutical pollutants from wastewater using biological approach. *Bioresour Technol*, 224: 1-12.
- Van Doorslaer X, Demeestere K, Heynderickx PM, Van Langenhove H, Dewulf J. 2011. UV-A and UV-C induced photolytic and photocatalytic degradation of aqueous ciprofloxacin and moxifloxacin: Reaction kinetics and role of adsorption. *Appl Catal B Environ*, 101: 540-547.
- Van Doorslaer X, Dewulf J, De Maerschalk J, Van Langenhove H, Demeestere D. 2015. Heterogeneous photocatalysis of moxifloxacin in hospital effluent: Effect of selected matrix constituents. *Chem Eng J*, 261: 9-16.
- Wang Y, Chen J, Gao J, Meng H, Chai S, Jian Y, Shi L, Wang Y, He C. 2021. Selective electrochemical H₂O₂ generation on the graphene aerogel for efficient electro-Fenton degradation of ciprofloxacin. *Sep Purif Technol*, 272: 118884.
- Xia Y, Shang H, Zhang Q, Zhou Y, Hu X. 2019. Electrogeneration of hydrogen peroxide using phosphorus-doped carbon nanotubes gas diffusion electrodes and its application in electro-Fenton. *J Electroanal Chem*, 840: 400-408.
- Yang W, Oturan N, Liang J, Oturan MA. 2023. Synergistic mineralization of ofloxacin in electro-Fenton process with BDD anode: Reactivity and mechanism. *Sep Purif Technol*, 319: 124039.
- Yang W, Oturan N, Raffy S, Zhou M, Oturan MA. 2020. Electrocatalytic generation of homogeneous and heterogeneous hydroxyl radicals for cold mineralization of anti-cancer drug Imatinib. *Chem Eng J*, 383: 123155.
- Zhao K, Quan X, Chen S, Yu H, Zhang Y, Zhao H. 2018. Enhanced electro-Fenton performance by fluorine-doped porous carbon for removal of organic pollutants in wastewater. *Chem Eng J*, 354: 606-615.
- Zhou L, Hu Z, Zhang C, Bi Z, Jin T, Zhou M. 2013. Electrogeneration of hydrogen peroxide for electro-Fenton system by oxygen reduction using chemically modified graphite felt cathode. *Sep Purif Technol*, 111: 131-136.
- Zhou M, Yu Q, Lei L, Barton G. 2007. Electro-Fenton method for the removal of methyl red in an efficient electrochemical system. *Sep Purif Technol*, 57: 380-387.
- Zhou W, Rajic L, Meng X, Nazari R, Zhao Y, Wang Y, Gao J, Qin Y, Alshwabkeh AN. 2019. Efficient H₂O₂ electrogeneration at graphite felt modified via electrode polarity reversal: Utilization for organic pollutants degradation. *Chem Eng J*, 364: 428-439.
- Zwane BN, Orimolade BO, Koiki BA, Mabuba N, Gomri C, Petit E, Bonniol V, Lesage G, Rivallin M, Cretin M, Arotiba OA. 2021. Combined electro-fenton and anodic oxidation processes at a sub-stoichiometric titanium oxide (Ti₄O₇) ceramic electrode for the degradation of tetracycline in water. *Water (Basel)*, 13: 2772.



NATURE INSPIRED PRACTICES IN SUPER TALL BUILDING DESIGNS: SIMILARITIES OF FORM

Aslı YILDIZ^{1*}, Güneş Mutlu AVİNÇ²

¹Nevşehir Hacı Bektaş Veli University, Faculty of Engineering and Architecture, Department of Architecture, 50300, Nevşehir, Türkiye

²Muş Alparslan University, Faculty of Engineering and Architecture, Department of Architecture, 49250, Muş, Türkiye

Abstract: Nowadays, competition between cities for super tall buildings is increasing. These buildings exceed the 300-meter height threshold, reaching enormous dimensions and playing a decisive role in the iconic character, visual impact, and prestige, and economic growth, technological and architectural progress of cities. In this context, the aim of the study is to formally analyze super tall buildings inspired by nature. In the study, which is evaluated according to two variables, super tall buildings are analyzed within the scope of the search for inspiration from nature in their form and interior formations. The study involves a content analysis of the ten tallest buildings in the Council on Tall Buildings and Urban Habitat (CTBUH) database. The formal analysis of the buildings revealed that the nature-inspired approach significantly influenced the design of the super tall buildings. This study emphasizes that combining super-tall designs with nature-inspired principles can create a new paradigm in architectural design. This combination improves the quality of life of individuals living in urban areas by enabling them to establish a closer relationship with nature. In this context, nature-inspired super tall buildings promote physical and mental well-being and create spaces that enhance indoor comfort.

Keywords: Super tall building, High-rise building, Nature inspired design, Formal analyses

*Corresponding author: Nevşehir Hacı Bektaş Veli University, Faculty of Engineering and Architecture, Department of Architecture, 50300, Nevşehir, Türkiye

E mail: aslydz@gmail.com (A. YILDIZ)

Aslı YILDIZ



<https://orcid.org/0000-0003-0408-1533>

Güneş Mutlu AVİNÇ



<https://orcid.org/0000-0003-1049-2689>

Received: March 19, 2024

Accepted: May 06, 2024

Published: May 15, 2024

Cite as: Yıldız A, Avinç GM. 2024. Nature inspired practices in super tall building designs: similarities of form. BSJ Eng Sci, 7(3): 547-559.

1. Introduction

There is no universally valid definition for tall buildings (Yıldız and Kalaycı, 2022). Definitions and height limits vary across countries, cities, specializations, regulations, relevant legislation and standards. The Council on Tall Buildings and Urban Habitat (CTBUH) has proposed a methodology and classification to establish a standard definition for tall buildings. According to this proposal, contextual data determines whether a building can be classified as a tall building.

A building is considered a tall building if it meets one or more of the criteria of context, proportion and technological sophistication (Figure 1). While the number of storeys is a poor indicator to identify a building due to varying height, a building over 14 storeys and 50 meters high is used as the threshold for a tall building. Furthermore, the CTBUH has created two categories for structures that reach significant heights: mega and super tall buildings. A super tall building is a structure with a height of 300 meters or more. A mega-tall building is used to characterize buildings with a height of 600 meters or more. In this context, since there are only four mega-tall buildings in the world (Burj Khalifa, Merdeka 118, Shanghai Tower and Mecca Royal Clock Tower) (CTBUH, 2023), the scope of the study is limited to super-tall buildings. The design of tall buildings draws inspiration from a variety of sources and

processes. Nature-inspired approach is frequently preferred in tall building design. This is the process of transferring biological knowledge from nature to different disciplines through analysis, interpretation and abstraction (Mutlu Avinç, 2023). The systems in nature offer many strategies, systems and mechanisms that can be transferred to nature-inspired design (Badarnah and Kadri, 2015). This approach includes significant opportunities in terms of structural durability, high-quality indoor environment, resource-energy efficiency and morphology (Cruz et al., 2021).

The nature-inspired approach is applied in building design at three levels: organism, behavior and ecosystem. The organism level refers to imitating part or all of an organism/phenomenon such as an animal or plant. The behavior level involves being inspired by the behavior of an organism/phenomenon. Finally, the ecosystem level refers to transferring the ecosystem process and its logic as a solution to the problem. Each level has five possible imitation dimensions: form, material, construction, process and function (Zari, 2007). In this study, super tall buildings are analyzed in the context of form. In other words, the formal similarities with nature in the form formations and interior designs of the buildings were investigated. In this way, the study evaluates morphological approaches as well as natural elements such as plants, natural light and water in interior and exterior spaces.



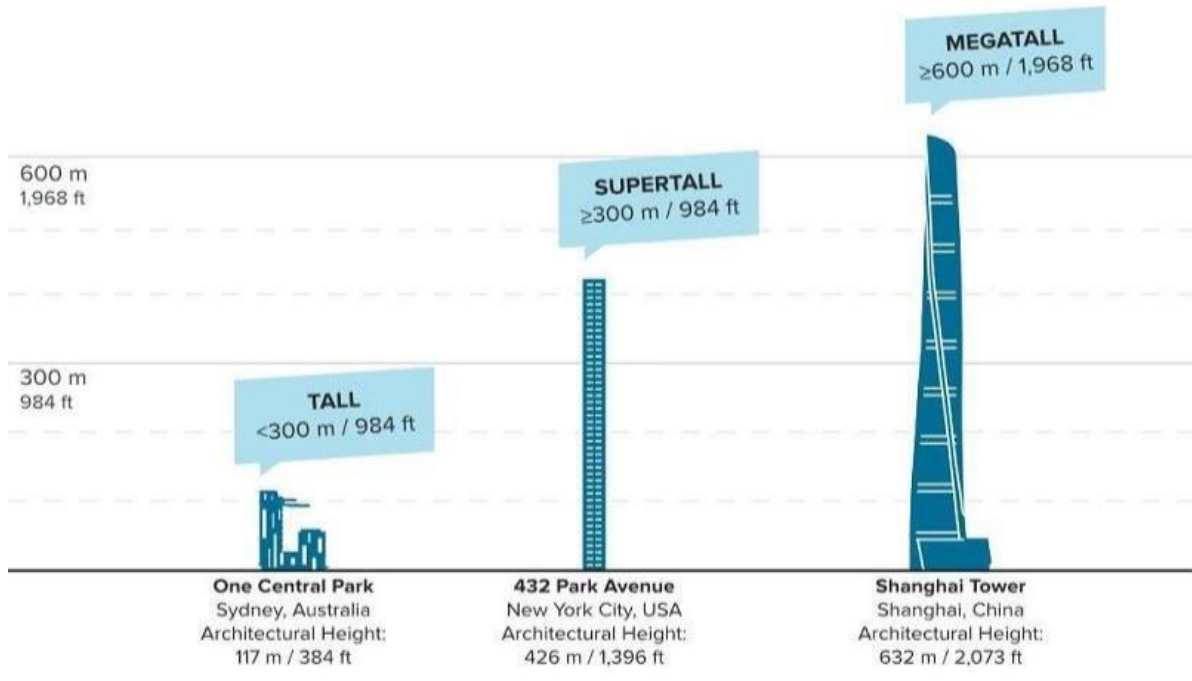


Figure 1. Types of tall buildings according to their height (CTBUH, 2023)

When the studies conducted so far with the keywords "tall building" and "nature-inspired building" are searched in the literature, it is seen that there is a limited number of studies on the subject. In the study by Altınöz et al. (2017), tall buildings designed with a biomimetic approach were analyzed. In the study, the energy consumption of the buildings was analyzed and the energy gains obtained were investigated (Altınöz et al., 2017). In Al-Sehail's (2017) study, "Biomimetic Structural Form" was developed as a sustainable paradigm. The design of a sustainable super high-rise building is examined as an application example of "Biomimetic Structural Form" (Al-Sehail, 2017). Mirniazmandan and Rahimianzarif (2018) examined different approaches and levels of biomimicry in tall buildings. In this study, it is discussed that the use of different biomimicry principles can lead to different results regarding the sustainability of tall buildings (Mirniazmandan & Rahimianzarif, 2018). In a study conducted in 2018, Al-Kodmany evaluated 30 tall buildings in different parts of the world in terms of sustainable design features and strategies (Al-Kodmany, 2018). The study identified design approaches that can bring sustainability and iconicity together. In the study conducted by Yetkin in 2020, the ecological gains provided by the biomimicry approach in architecture to tall buildings were classified (Yetkin, 2020). In another study by Contreras et al. (2023), the effects of biomimicry and biophilic design approaches in tall buildings were examined. It was determined that these concepts are very important in achieving a sustainable and healthy built environment (Contreras et al., 2023). Although there are many studies in the literature on the use of nature-inspired approaches in tall buildings, there is no research examining the relationship between nature-

inspired design and super tall buildings. In this context, the study investigates the phenomenon of being inspired by nature in the form of super tall buildings. By their very nature, super-tall buildings stand out with their technological sophistication, construction systems, earthquake and wind resistance, and functionality. This study contributes to the related literature by evaluating super tall buildings in terms of their relationship with nature.

2. Materials and Methods

In this study, super tall buildings in the CTBUH (2023) database are analyzed within the scope of nature-inspired design approaches. The study was limited to 10 buildings whose construction was completed until 2024. General information about the buildings (building name, city, and year of construction, height, number of floors, material and function) is presented in Table 1.

The super tall buildings are evaluated according to the relationships they establish with nature in their building form and interior design. The design inputs of the buildings were obtained from literature studies and websites sharing information about the buildings and the formal similarities with nature were analyzed. Formal similarities consist of plant and animal morphologies as well as various sources of inspiration that can be associated with nature. In the interiors, the use of natural elements such as materials, plants, trees and water, as well as the use of parameters such as color, texture and form that emulate nature were also taken into consideration. In this way, it has been revealed how the buildings establish a connection with nature both in their form shaping and interior design. Figure 2 shows the flow chart of the study.

Phytomorphic approach means having or being

represented by the qualities of a plant that give information about its anatomy, forms and structure (Merriam-Webster, 2023). While the zoomorphic approach is the transfer of animal characteristics to inanimate beings, the anthropomorphic approach is the transfer of human characteristics to inanimate beings (Suyabatmaz and Sever, 2023). Abiotic embodiment, on

the other hand, is defined as being influenced by non-living features that are part of the physical or chemical environment that affect the functioning of living things and ecosystems (Chapin, et al., 2002). Therefore, ten super-high structures with zoomorphic, anthropomorphic, phytomorphic and abiotic morphology were analyzed in this study.

Table 1. List of super tall buildings

Building Name	City	Year	Height	Floor	Malzeme	Function
Burj Khalifa	Dubai	2010	828 m	163	Steel + Concrete	Office+Residence+Hotel
Merdeka 118	Kuala Lumpur	2023	678 m	118	Concrete+Steel+Composite	Office+Residence+Hotel
Shanghai Tower	Shanghai	2015	632 m	128	Concrete+Steel+Composite	Office+Hotel
Ping An IFC	Shenkron	2017	599 m	115	Concrete+Steel+Composite	Office
Tianjin CTF	Tianjin	2019	530 m	97	Concrete+Steel+Composite	Office+Residence+Hotel
Taipei 101	Taipei	2004	508 m	101	Composite	Office
Lakhta Center	St. Petersburg	2019	462 m	87	Concrete+Steel+Composite	Office
Vincom Landmark 81	Ho Chi Minh	2018	461 m	81	Concrete+Steel+Composite	Hotel+Residence
Suzhou IFS	Suzhou	2019	450 m	95	Concrete+Steel+Composite	Office+Residence+Hotel
Al Hamra Tower	Kuveyt	2011	413 m	80	Concrete	Office

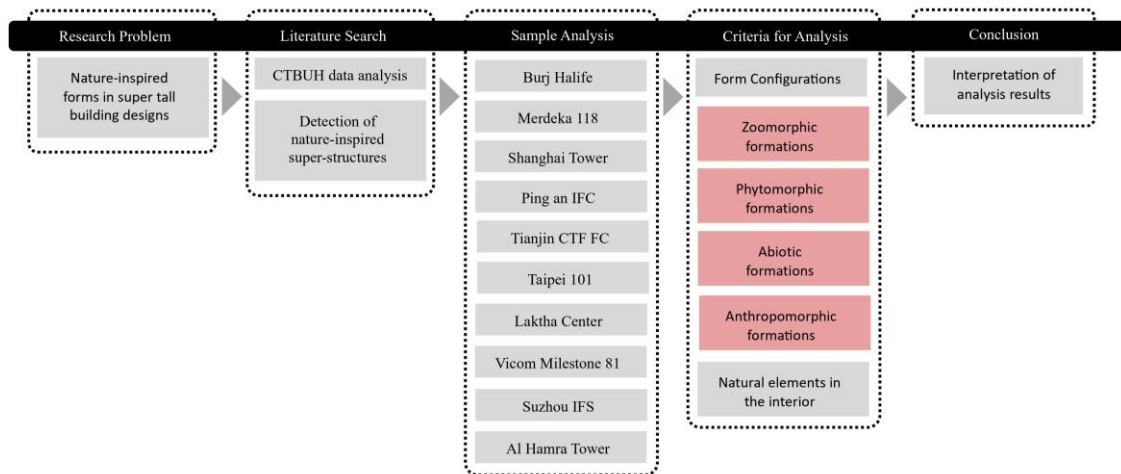


Figure 2. Method flowchart

3. Results

In this part of the study, descriptive information about each building is presented regarding the interiors' nature-inspired design approach and biophilic features.

The buildings were analyzed from the highest to the least high building.

3.1. Burj Khalifa

The building, completed in 2010, is 828 meters high with 163 floors and currently holds the title of the tallest

building in the world. The architectural and structural design of the building in Dubai was carried out by Skidmore Owings and Merrill. The structure generally consists of a hexagonal core in the center and units connected to it. The starting point of the design is the Spider Lily (Hymenocallis), a flower that grows in the desert. The flower's tri-axial structure and spiral growth pattern have been crucial in shaping the tower's form. In addition, traditional Islamic forms and intertwined geometries are other references used to enrich the design. As the building gets higher, its narrower form both emphasizes the height effect of the building and reduces the effect of wind loads. The building's facades are intentionally designed with non-planar surfaces, specifically avoiding flat surfaces and employing circular corners to minimize wind loads on the building's exterior (Figure 3) (Ilgın and Günel, 2008).

This desert flower-shaped triaxial plan has many advantages for the building. The first advantage is that it

offers an ideal solution for residential units. It provides both privacy and access to the panorama between the units. Another advantage is that it allows the building to be designed with a buttressed core system. The decreasing profile of the building's plan section along its height accentuates the tower's ascent to the sky, giving the impression of a structure perpetually rising with increasing momentum. This phenomenon highlights the tower's height, simultaneously reducing the wind load on the upper levels of the building. As the tower ascends, the variation in the plan section minimizes the impact of wind forces. The distinct design of each new layer prevents the formation of wind vortices (Weismantle et al., 2007).

Biophilic elements are also included in the interior design of the building. More bright and spacious interiors were obtained with perennial trees in the lobby spaces. Natural elements were used in the offices to comfort the employees, especially in the resting areas (Figure 4).



Figure 3. Burj Khalifa design (URL-1), Hymenocallis flower (URL-2).



Figure 4. Burj Khalifa office designs (URL-3); (URL-4)

3.2. Merdeka 118

The building, completed in 2023, is 678 meters high and has 118 floors. The civil and structural engineer of this building is Arup. The building serves as a hotel, residence, and office. It is the tallest building in Malaysia and Southeast Asia and the second tallest in the world. The form of the building is based on the posture of Tunku Abdul Rahman's speech on 31 August 1957 when he declared Malaysia's independence (Arup, 2023) (Figure 5).

The design of the building incorporates biophilic elements in its overall design and interior spatial composition. In order to break the cold and hard appearance of concrete curtain walls and beams in semi-open spaces, the spaces are enriched with soft floors and landscape elements that emulate nature (Figure 6). In the

landscape design of the building, interaction with nature is strengthened with water and green elements.

3.3. Shanghai Tower

The building, completed in 2015, is 632 meters high and has 128 floors. The building serves as a hotel and office. Shanghai Tower is located in Pudong, the business and commercial center along the east bank of the Huangpu River on the Lujiazui peninsula, the financial center of Shanghai. It is the second-tallest building in the world and the tallest building in China. The decisive factors in the design of the structure include its location in an area with strong air flows, its positioning in an active seismic zone, its foundation on weak soil, and its candidacy for LEED Gold certification. The spiral transparent form of the tower serves as a showcase for the latest technologies and exemplifies targeted sustainability

strategies and emerging standards in public spaces (Xia et al., 2010). Additionally, rainwater harvesting has been considered in the Shanghai Tower (Lau, 2015). The building's form was inspired by the spiral movement of the wind, and the form was shaped with vertically displaced sky gardens (Xia et al., 2010; Ali and Kodmany, 2012). Analyses conducted on wind and airflow patterns led to the preference for a form that offers optimal

resilience and resistance against the prevailing winds (Figure 7).

Biophilic elements are included in the interior landscape designs of the building. The building, which consists of two shell surfaces, is enriched with natural landscape elements to break the cold and soulless effect between the glass spaces (Figure 8).



Figure 5. Merdeka 118 Design Concept (URL-5).



Figure 6. Merdeka 118 interior and exterior designs (URL-6), (URL-7).

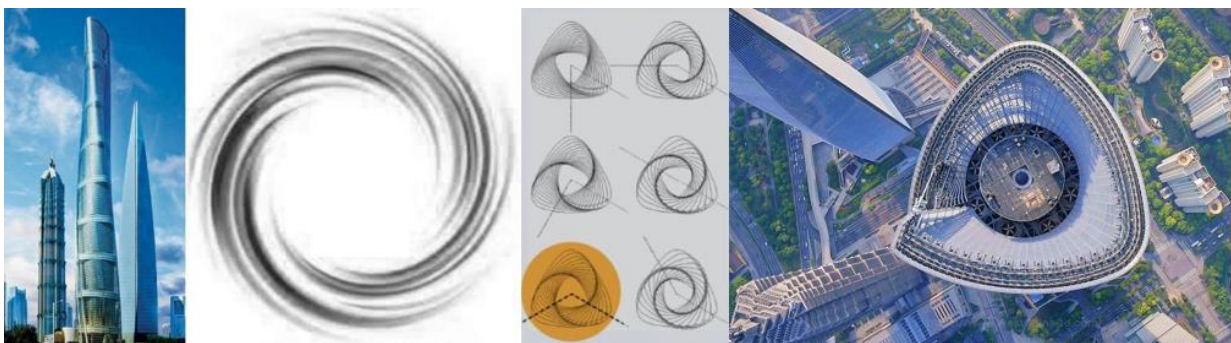


Figure 7. Shanghai Tower Design Concept (URL-8), (URL-9), (URL-10).



Figure 8. Shanghai Tower interior design (URL-11).

3.4. Ping An International Finance Centre

The building, completed in 2017, is 599 meters high and has 115 floors. Designed by Kohn Pedersen Fox, the building serves as offices. The tower has a distinctive, futuristic design that combines various sustainable features such as a double skin facade, rainwater harvesting system, and energy-efficient HVAC system. The building has a square plan and is designed considering earthquake and wind loads (Poon et al., 2011). The building form resembles a stretched cable. With its sharp corner lines and pointed endpoint design, the building resembles precious stones (diamonds, etc.) that are rare in nature (Figure 9).

Biophilic elements are included in the interior design of the building. Nature-inspired design elements are frequently used in the shared areas of the building to enrich the interiors. The roof gardens of the building also feature natural elements (Figure 10).

3.5. Tianjin CTF Finance Centre

The building, completed in 2019, is 530 meters high and has 97 floors. The convex and concave surfaces of the

structure, along with its conical form, are designed to reduce wind loads. The architectural form of the building exhibits biomorphic characteristics, resembling the pistils of greenhouse flowers. The building combines residence, office, and hotel programs under a single roof and is an important center at the intersection of transportation axes (Lee et al., 2016) (Figure 11).

Green elements are included in the interior design of the building. More interesting and spacious interiors have been obtained by breaking the monotony of the corridor spaces with live plant walls. Natural wood surfaces and wave-shaped lighting elements in the corridor spaces have a biophilic character (Figure 12). In addition to the interior spaces, the building establishes a visual connection with the natural landscape in the exterior spaces.

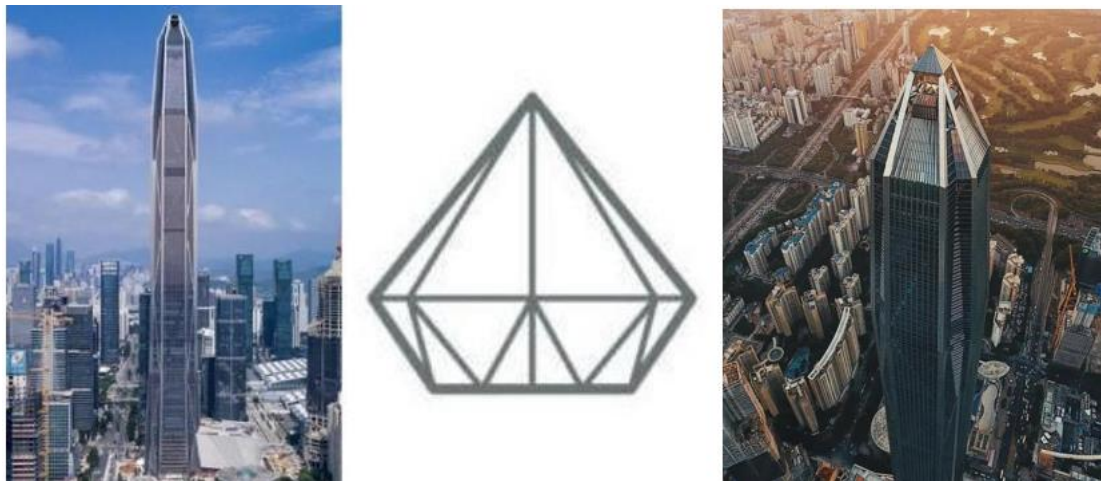


Figure 9. Ping An IFC design concept (URL-12) <https://thetowerinfo.com/visit-ping-an-finance-center-observatory/>.



Figure 10. Ping An IFC Indoor and Outdoor Spaces (URL-13), (URL-14)



Figure 11. Tianjin CTF Design Concept (URL-15), (URL-16)



Figure 12. Tianjin CTF Indoor and Outdoor Spaces (URL-17), (URL-18), (URL-19)

3.6. Taipei 101

The building, completed in 2004, is 508 meters high, 101 stories, and is used as offices. The design of the building is based on wind and earthquake loads. It is risky to build high-rise buildings in the Taipei region, which is shaken by earthquakes twice a year. Therefore, the building has a flexible design (Chang, 2012). From the main façade, the eight-section building resembles a Chinese or Japanese Pagoda (Buddhist temple). The form of the pagoda, inspired by the pagoda flower, and the thin and delicate cross-section of the bamboo plant have shaped the design of the building. The division of the structure into eight segments is rooted in the Chinese belief that the number 8 brings good luck. The windows of the building are blue-green, and motifs found in Chinese temples are placed at all corners of the façade. The building forms an inverted cone by narrowing 5 degrees in the first 25 stories. Afterward, it widens by 7 degrees in every nine stories upwards. The mobility in the form and the high rate of delicacy reveal the elegance of the building (Figure 13).

The building overlooks the natural landscape of Taipei City and has Biophilic features in its interior design.

Artificial and natural landscape elements and water pools in the atrium spaces create warmer and more spacious interiors (Figure 14).

3.7. Lakhta Center

Lakhta Centre is 462 meters high and has a total rotation angle of 90 degrees. The rotation angle for each floor is 1 degree. A circular form at the center and five additional conical volumes surrounds this central form in a spiral movement. Built-in 2019, the building has 87 floors and is used as an office. It has a five-pointed star-like floor arrangement and a conical twisted form. While the conical form contributes positively to its aerodynamic performance, the twisted form reduces the wind load on the structure (Askarinejad, 2014). The form of the Lakhta Centre is inspired by the geometry of the ice crystal (Figure 15).

The building is located on the shore of the Baltic Sea, and biophilic elements are prominent in landscape and interior design. The atrium spaces are enriched with perennial trees, shrubs, and grasses. In addition to landscape elements, flexible and fluid spaces were achieved with natural and organic forms (Figure 16).



Figure 13. Taipei 101 Design Concept (URL-20), (URL-21).



Figure 14. Taipei 101 indoor and outdoor spaces (URL-22).

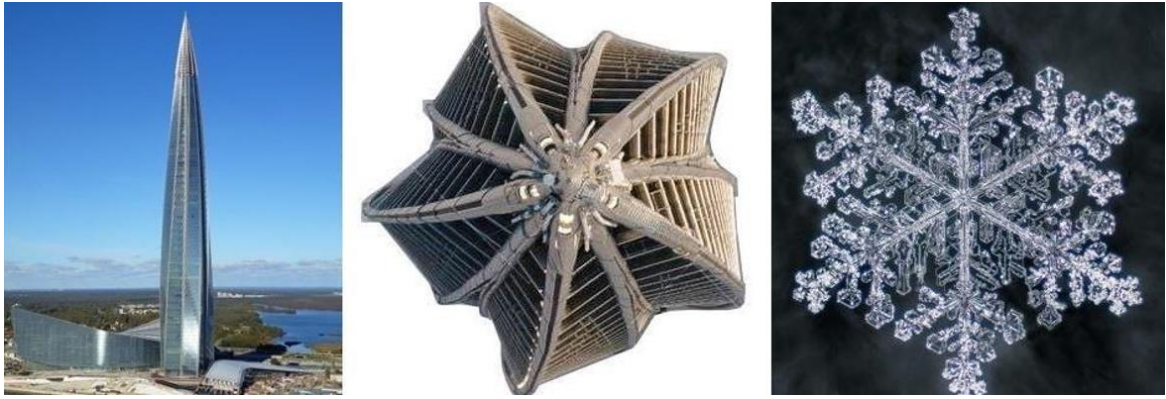


Figure 15. Laktha Center design concept (URL-23).



Figure 16. Laktha Center indoor and outdoor spaces (URL-24; URL-25; URL-26).

3.8. Vincom Landmark 81

Completed in 2018 in Ho Chi Minh City, Vietnam, the 461m high Vincom Landmark 81 is a hotel and residential building. It is the tallest building in Vietnam. The shape of the building is inspired by the traditional bamboo bundle, representing strength and unity in Vietnamese culture (Truong et al., 2020). The blue glass façade of the building is covered with colored lights to make it stand out both day and night (Figure 17).



Figure 17. Vincom Landmark 81 design concept (URL-27).

Located on the periphery of Vinhomes Central Park, the building establishes a panoramic visual connection with the Saigon River. The building has biophilic features in its interior and landscape designs. Natural elements are frequently used in the interiors, semi-open, and open spaces to break the hard and cold glass-steel material effect. The use of water and plant elements together in

the landscape design of the building emphasizes the integrity of natural and built elements (Figure 18).

3.9. Suzhou IFS

Suzhou IFS is 450 meters high and functions as a hotel, office, and apartment building. The form of the tower is designed inspired by a fish. The tower is planned to interact with the surrounding bodies of water. The tower form and orientation reduce heat and glare while bringing more natural daylight into the interior spaces (Bao et al., 2015) (Figure 19).

The tower moves towards Lake Jinji, opening up towards the water. More than a mere architectural ornament, it maximizes the water view for the serviced apartments within the expanded base. Natural elements and vegetal forms are indirectly included in the interior design of the building. Natural materials and textures are preferred in the living areas, and warmer, more comfortable spaces have been created (Figure 20).

3.10. Al Hamra Tower

The building, also known as Firdous Tower, is the tallest in Kuwait. The building, completed in 2011, was designed by Skidmore, Owings and Merrill (SOM). The 80-storey, 413m (371m used) tall Al Hamra Tower is an example of a helix-shaped super-tall building with an office function. Since the office tenants wanted to see the golf view, the architects designed the building so that they could see the golf as they went up to the upper floors. The north, west, and east sides of the building form are transparent, while the south side is opaque against the harsh desert sun. The building form resembles a curved metal plate as a source of inspiration (Figure 21).

Biophilic elements such as natural landscapes, geometric patterns, and plants are used in the interior design of the

building. Nature-inspired elements are frequently used in workspaces and offices to create spacious and comfortable spaces for employees. The building also has a natural sea view. The large glass windows provide a direct visual connection with the sea view. The natural light coming in through the large glass windows creates a dynamic and diffused light effect (Figure 22).

The nature-inspired approaches seen in the form and interior design of ten (10) super tall buildings are

presented in Table 2. Accordingly, formal similarities are established with biotic and abiotic natural concepts such as desert flower, human pose, wind vortex, precious stones, greenhouse flower, bamboo plant, snow crystal, and fish. In addition, in the interior spaces of these buildings, recreation areas, visual connection with the landscape, the use of live plants and trees in the atrium and corridor spaces, and the use of natural materials are observed.



Figure 18. Vincom Landmark 81 design concept (URL-28; URL-29).



Figure 19. Suzhou IFS concept design (URL-30).



Figure 20. Suzhou IFS indoor and outdoor spaces (URL-31; URL-32; URL-33).



Figure 21. Al Hamra Tower (URL-34; URL-35).

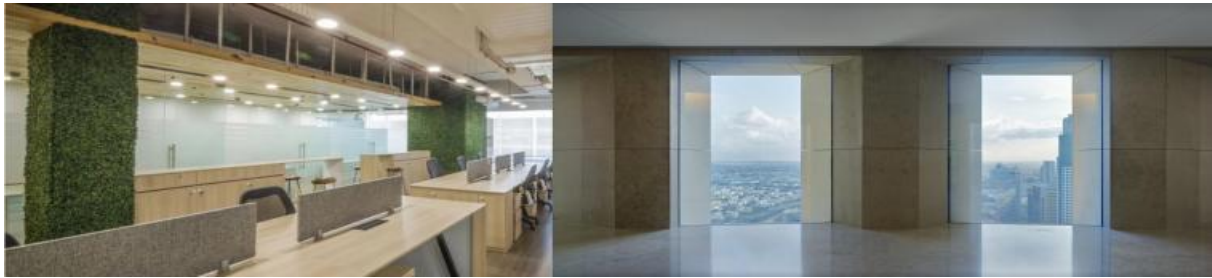


Figure 22. Al Hamra Tower indoor and outdoor spaces (URL-36; URL-37).











4. Discussion

In super tall buildings, design inspirations are partially in the background compared to low-rise buildings due to structural system requirements and height limits. In the examples, the focus is on super tall buildings that are inspired by nature. In this way, the potentials of super tall buildings in terms of design are revealed. The search for inspiration from nature has been identified in both the interior design and the form shaping of the buildings. At the same time, while the examples have natural inspirations in terms of form, there are also forms of learning from nature such as collecting rainwater, shaping the form against wind and earthquake loads. Integrating nature-inspired elements into tall building designs has positive effects on the physical and mental well-being of the occupants. The buildings analysed in this study have integrated principles and elements from nature into their design. In the analysed examples, organic and inorganic natural forms such as bamboo plant and bundle, wind vortex, diamond, desert flower, human posture, ice crystal, pagoda flower, greenhouse flower and fish were found to be the inspiration for super tall building designs. In addition, it has been found that all the buildings analysed have given elements such as landscape, plant and water elements, natural patterns in their interior and exterior designs. In general, common areas such as atriums, lobbies, corridors, seating and resting areas are the spaces where nature-inspired approaches come to the fore. These spaces create larger, spacious and comfortable areas for the building users.

5. Conclusion

In conclusion, super tall buildings by their very nature are characterised by technological sophistication, construction systems, earthquake and wind resistance, and functionality. This study contributes to the related literature by evaluating super tall buildings in terms of their relationship with nature, which is often ignored. As super tall buildings get higher, their connection with nature and the ground decrease. On the other hand, in order to re-establish interaction with nature, natural elements are used more in the interior spaces. Analogical inspirations from nature are widely used in the interior and exterior designs of the super tall buildings. This study is limited only to the form and interior design of the buildings in their relationship with nature. However, nature-inspired design is also used as a data source in many aspects such as structural lightness, durability, responsiveness, adaptability and sustainability. In future studies, the scope of the study can be expanded by adding these criteria.

Table 2. Nature-inspired approaches to super tall buildings

No	Image	Connection with nature in the formation of the building	Connection with nature in the interior	No	Image	Connection with nature in the formation of the building	Connection with nature in the interior
1		Inspired by the desert flower Phytomorphic formations	Use of nature-inspired elements in offices, recreation areas, and outdoor spaces Visual connection with the view/landscape	6		Inspired by the bamboo plant Phytomorphic formations	Use of nature-inspired elements in atrium spaces and outdoor spaces Visual connection with the view/landscape
2		Inspired by human posture Anthropomorphic formations	Use of nature-inspired elements in semi-open spaces and outdoor areas Visual connection with the view/landscape	7		Inspired by snowflakes Abiotic formations	Use of nature-inspired elements in atrium spaces and outdoor spaces Visual connection with the view/landscape
3		Inspired by the wind vortex Abiotic formations	The use of nature-inspired elements in atrium spaces on the floors and outdoor spaces Visual connection with the view/landscape	8		Inspired by the bamboo bunch Phytomorphic formations	Use of nature-inspired elements in semi-open spaces and outdoor areas Visual connection with the view/landscape
4		Inspired by precious stones in nature Abiotic formations	Use of nature-inspired elements in shared areas and outdoor spaces Visual connection with the view/landscape	9		Inspired by the fish figure Zoomorphic formations	Use of nature-inspired elements in living spaces and outdoor areas Visual connection with the view/landscape
5		Influenced by greenhouse flowers Phytomorphic formations	Use of nature-inspired elements in the corridor areas on the floors and outdoor spaces Visual connection with the view/landscape	10		Inspired by curled metal plate or paper Abiotic formations	Use of nature-inspired elements in offices, workspaces, and outdoor spaces Visual connection with the view/landscape

Author Contributions

The percentage of the author(s) contributions is presented below. All authors reviewed and approved the final version of the manuscript.

	A.Y.	G.M.A.
C	50	50
D	50	50
S	50	50
DCP	50	50
DAI	50	50
L	50	50
W	50	50
CR	50	50
SR	50	50
PM	50	50
FA	50	50

C=Concept, D= design, S= supervision, DCP= data collection and/or processing, DAI= data analysis and/or interpretation, L= literature search, W= writing, CR= critical review, SR= submission and revision, PM= project management, FA= funding acquisition.

Conflict of Interest

The authors declared that there is no conflict of interest.

Ethical Consideration

Ethics committee approval was not required for this study because of there was no study on animals or humans.

References

Ali MM, Al-Kodmany K. 2012. Tall buildings and urban habitat of the 21st century. *Buildings*, 2(4): 408-411.

Al-Kodmany K. 2018. Sustainability and the 21st century vertical city: a review of design approaches of tall buildings. *Buildings*, 8(8): 1-40.

Al-Sehail O. 2017. A biomimetic structural form: developing a paradigm to attain vital sustainability in tall architecture. *Inter J Civil Environ Struct Construct Architect Engin*, 11(3): 322-332.

Altınöz M, Mihlayanlar E, Yardımlı S. 2017. Analyzing energy and biomimesis concepts in the context of sustainability on building envelope. *A+Arch Design Inter J Architect Design*, 3(2): 1-14.

Arup. 2023. Set to be one of the world's tallest buildings in 2022. www.arup.com (accessed date: March 23, 2024).

Askarinejad P. 2014. Structural design of Shanghai tower for wind loads. *CTBUH 2014 Shanghai Conference Proceedings*, 16-19 September, Shanghai, China, 14: 556-562.

Badarnah L, Kadri U. 2015. A methodology for the generation of biomimetic design concepts. *Architect Sci Rev*, 58(2): 120-133.

Bao L, Chen J, Qian P, Huang Y, Tong J, Wang D. 2015. The new structural design process of super-tall buildings in China. *Inter J High-Rise Buildings*, 4(3): 219-226.

Chang CC. 2012. Structural design of Taipei 101 Tower. <http://www.sefindia.org/rangarajan/Taipie101BuildingAnalysis>. (accessed date: March 21, 2024).

Chapin FS, Matson PA, Mooney HA, Vitousek PM. 2002. *Principles of terrestrial ecosystem ecology*. Springer, New York, USA, pp: 35.

Contreras GS, Lezcano RAG, Fernandez EJJ, Gutierrez MCP. 2023. Architecture learns from nature. The influence of biomimicry and biophilic design in building. *Modern Applied Sci*, 17(1): 58-70.

Cruz E, Hubert T, Chancoco G, Naim O, Chayaamor-Heil N, Cornette R, ... & Aujard F. 2021. Design processes and multi-regulation of biomimetic building skins: a comparative analysis. *Ener Buildings*, 246: 111034.

İlgin HE, Günel MH. 2008. Ne zamana kadar en yüksek. *Ege Mimarlık Derg*, 67: 26-27.

Lau GL. 2015. Sustainable high-rise construction in Shanghai: case study – Shanghai Tower. Master thesis, *Universidade de Lisboa, Institute of Science, Lisbon, Portugal*, pp: 152.

Lee B, Baker W, Johnson R, Rhee I. 2016. Next-generation super-tall tower form determinants: a study of the Tianjin CTF Finance Center. *CTBUH J*, 2016: 1256-1263.

Merriam-Webster (2023). Accessed from: <https://www.merriam-webster.com/dictionary/phytomorphic#:~:text=phy%C2%B7E2%80%8Bto%C2%B7E2%80%8Bmor,the%20attribut%20of%20a%20plant> (accessed date: March 23, 2024).

Mirniazmandan S, Rahimianzarif E. 2018. Biomimicry, an approach toward sustainability of high-rise buildings. *Iranian J Sci Technol Transact A: Sci*, 42(4): 3-7.

Mutlu Avinç G. 2023. Bio-informed design thinking through problem-based approach: an architectural point of view. In *Contemporary Manifests on Design Thinking and Practice IGI Global, Shanghai, China*, pp: 48-70.

Poon D, Hsiao L, Yi Z, Zuo S, Pacitto S, Gottlebe T, Liang J. 2011. Finite element analyses of super composite column and its connections for Ping an International Finance Center Tower. *Structures Congress*, 2011, New York, USA, pp: 24.

Suyabatmaz E, Sever İA. 2023. İç mekanlarda biyomorfik yaklaşımlarla parametrik tasarım. *Yapı Bilgi Model*, 5(1): 26-38.

The Council on Tall Buildings and Urban Habitat (CTBUH). 2023. <https://www.ctbuh.org/resource/height#tab-tall-supertall-and-megatall-buildings> (accessed date: March 23, 2024).

Truong Q, Pham TH, Pham QD, Pham HN. 2020. Design and construction solution of foundation for landmark 18-The Tallest Tower in Vietnam. *Geo-Congress 2020: Foundations, Soil Improvement, and Erosion*, pp: 123.

URL 1: <https://www.burjkhalifa.ae/en/the-tower/design-construction/> (accessed date: March 21, 2024).

URL 10: <https://parametric-architecture.com/everything-you-need-to-know-about-bionic-architecture/> (accessed date: March 20, 2024).

URL 11: <https://img.designswan.com/2017/02/shanghaiTower/7.jpg> (accessed date: March 19, 2024).

URL 12: <https://www.skyscrapercenter.com/building/ping-an-finance-center/54> (accessed date: March 23, 2024).

URL 13: https://www.iskydance.com/uploads/kindeditor417/image/20210122/20210122070617_33334.jpg (accessed date: March 19, 2024).

URL 14: <https://www.skyscrapercenter.com/building/ping-an-finance-center-south/5207> (accessed date: March 23, 2024).

URL 15: <https://www.skyscrapercenter.com/building/tianjin-ctf-finance-centre/310> (accessed date: March 23, 2024).

URL 16: <https://www.som.com/news/tianjin-ctf-finance-centre-meets-the-breeze-with-a-biomorphic-form/> (accessed date: March 19, 2024).

URL 17:

- <https://www.thebeijinger.com/sites/default/files/styles/large/public/7e1d5743a64247352ce0b6ebb951754.jpg> (accessed date: March 19, 2024).
- URL 18: <https://twitter.com/MakeArchitects/status/1380455558579425280> (accessed date: March 23, 2024).
- URL 19: <https://www.behance.net/gallery/100838049/Tianjin-CTF-Finance-Center-SOM> (accessed date: March 21, 2024).
- URL 2: <https://www.skyscrapercenter.com/building/burj-khalifa/3> (accessed date: March 19, 2024).
- URL 20: <https://www.skyscrapercenter.com/building/taipei-101/117> (accessed date: March 19, 2024).
- URL 21: <https://prezi.com/spm6z3sdfif9/nature-as-an-inventor/> (accessed date: March 21, 2024).
- URL 22: <https://pixabay.com/de/photos/shopping-mall-taipei-einkaufszentrum-1416500/> (accessed date: March 19, 2024).
- URL 23: <https://www.skyscrapercenter.com/building/lakhta-center/12575> (accessed date: March 23, 2024).
- URL 24: <https://fabiomazzeoarchitects.com/wp-content/uploads/2020/05/06-fabio-mazzeo-architects-lakhta-center-1200x700-1.jpg> (accessed date: March 19, 2024).
- URL 25: <https://www.worldconstructionnetwork.com/projects/lakhta-center-primorsky-district-saint-petersburg/?cf-view> (accessed date: March 20, 2024).
- URL 26: <https://www.arup.com/projects/lakhta-centre> (accessed date: March 20, 2024).
- URL 27: <https://www.skyscrapercenter.com/building/vincom-landmark-81/18192> (accessed date: March 19, 2024).
- URL 28: <https://cf.bstatic.com/xdata/images/hotel/max1280x900/487320542.jpg?k=e8d4cc19185a04960e948a9b4c44fb10a651536f30afadaacd740294e00003f9&o=&hp=1> (accessed date: March 19, 2024).
- URL 29: <https://landezine-award.com/vincom-landmark-81/> (accessed date: March 19, 2024).
- URL 3: <https://www.commercialinteriordesign.com/insight/48570-unmissable-examples-of-biophilic-design-weve-spotted-around-dubai> (accessed date: March 21, 2024).
- URL 30: <https://www.skyscrapercenter.com/building/suzhou-ifs/196> (accessed date: March 23, 2024).
- URL 31: <https://www.kpf.com/project/suzhou-international-finance-square> (accessed date: March 19, 2024).
- URL 32: <https://www.sldgroup.com/en/residential-detail.aspx?id=31> (accessed date: March 19, 2024).
- URL 33: <https://www.wongtung.com/en/projects/suzhou-ifs/> (accessed date: March 25, 2024).
- URL 34: <https://www.skyscrapercenter.com/building/al-hamra-tower/208> (accessed date: March 20, 2024).
- URL 35: <https://www.worldconstructionnetwork.com/projects/al-hamra/?cf-view> (accessed date: March 19, 2024).
- URL 36: <https://imageproxy-v2.services.lokalebasen.dk/h1080/lb-images-eu/kw/6519870/4105761-al-hamra-tower-35th-floor-east-maqwa.jpg?v=m1702526005> (accessed date: March 19, 2024).
- URL 37: <https://archello.com/project/al-hamra-tower> (accessed date: March 20, 2024).
- URL 4: https://assets.iwgplc.com/image/upload/f_auto,q_auto,w_834,h_522,c_fill/CentreImagery/2766/2766_2.jpg (accessed date: March 19, 2024).
- URL 5: <https://www.skyscrapercenter.com/building/merdeka-118/10115> (accessed date: March 23, 2024).
- URL 6: <https://cf.bstatic.com/xdata/images/hotel/max1024x768/428453964.jpg?k=38813698ba9f1e5303cee9929a34c5fd20553068eacc0acb781138639dc86eb4&o=&hp=1> (accessed date: March 23, 2024).
- URL 7: <https://en.wikiarquitectura.com/merdeka-118-11-2/> (accessed date: March 19, 2024).
- URL 8: <https://www.skyscrapercenter.com/building/shanghai-tower/56> (accessed date: March 19, 2024).
- URL 9: <https://du.gensler.com/vol6/shanghai-tower-zh/#/why-this-shape> (accessed date: March 20, 2024).
- Weismantle PA, Smith GL, Sheriff M. 2007. Burj Dubai: an architectural technical design case study. *Struct Design Tall Special Buildings*, 16: 335–360.
- Xia J, Poon D, Mass CD. 2010. Case study: Shanghai tower. *CTBUH J*, (2): 12-18.
- Yetkin EG. 2020. Effects of biomimicry on architecture. *European J Nat Scis Med*, 3(2): 106-120.
- Yıldız A, Kalaycı PD. 2022. Fractal change of facades of high-rise buildings according to architectural periods. *Uluslararası Hakemli Tasarım ve Mimarlık Dergisi*, 26: 220-243.
- Zari MP. 2007. Biomimetic approaches to architectural design for increased sustainability. <http://103.62.146.201:8081/xmlui/bitstream/handle/1/1127/033PEDERSENZARI.pdf?sequence=1&isAllowed=y> (accessed date: March 19, 2024).



FLUOKSETİN VE NORFLUOKSETİNİN SENTEZİ ÜZERİNE ÇALIŞMALAR VE ANTİOKSİDANT ÖZELLİĞİNİN ARAŞTIRILMASI

Nesimi ULUDAĞ^{1*}

¹Tekirdağ Namık Kemal University, Faculty of Arts and Sciences, Department of Chemistry, 59030, Tekirdağ, Türkiye

Özet: İki halkalı antidepresan ilaç olan norfluoksetin ve fluoksetinin sentezi için, başlangıç materyali olarak kolayca bulunabilen sirenlerin epoksidasyonunun kullanılmasını içeren yeni, pratik ve kısa bir yöntem geliştirilmiştir. Bu çalışma, norfluoksetin ve fluoksetinin kısa bir yolla yeni yöntemlerin yapımında, ticari olarak ilgi gören bu bileşiklerin sentezinde uygulama alanı bulmuştur. Ayrıca, başlıkta verilen bu iki bileşiğin antioksidan aktivitesi CUPRAC (bakır indirgeyici antioksidan kapasite yöntemi) yöntemi ve fluoksetin ve norfluoksetinin TEAC (Trolox-Eşdeğer Antioksidan Kapasite) katsayısı ile değerlendirilmiştir. Bu çalışmada antioksidan özelliğinin araştırılması literatürde ilk defa yapılmıştır. Aynı zamanda, Bu metot ile yüzde verim, reaksiyon şartları ve reaksiyon basamağının kısıklığı ile de avantajlar sağlamaktadır. Sentezlenen bileşiklerin karakterizasyonu ¹H-NMR, ¹³C-NMR IR ve MS-kütle spektroskopisi ile yapılmıştır.

Anahtar kelimeler: Prozac, Antidepresan, Antioksidanlar, Fluoksetin, Epoksidasyon

Studies on the Synthesis of Fluoxetine and Norfluoxetine and Investigation of their Antioxidant Properties

Abstract: A new, practical and short method has been developed for the synthesis of bicyclic antidepressant drugs norfluoxetine and fluoxetine, which involves the use of epoxidation of easily available sirens as starting materials. This study has found application in the synthesis of these compounds of commercial interest, in the construction of new methods of norfluoxetine and fluoxetine in a short way. Additionally, the antioxidant activity of these two compounds given in the title was evaluated by the CUPRAC (copper-reducing antioxidant capacity method) method and the TEAC (Trolox-Equivalent Antioxidant Capacity) coefficient of fluoxetine and norfluoxetine. In this study, the antioxidant properties were investigated for the first time in the literature. At the same time, this method provides advantages in terms of percentage yield, reaction conditions and shortness of the reaction step. Characterization of the synthesized compounds was made by ¹H-NMR, ¹³C-NMR IR and MS-mass spectroscopy.

Keywords: Prozac, Antidepressant, Antioxidants, Fluoxetine, Epoxidation

*Sorumlu yazar (Corresponding author): Tekirdağ Namık Kemal University, Faculty of Arts and Sciences, Department of Chemistry, 59030, Tekirdağ, Türkiye

E mail: uludag99@yahoo.com (N. ULUDAĞ)

Nesimi ULUDAĞ  <https://orcid.org/0000-0002-2819-3612>

Gönderi: 26 Mart 2024

Kabul: 06 Mayıs 2024

Yayınlanma: 15 Mayıs 2024

Received: March 26, 2024

Accepted: May 06, 2024

Published: May 15, 2024

Cite as: Uludağ N. 2024. Studies on the synthesis of fluoxetine and norfluoxetine and investigation of their antioxidant properties. BSJ Eng Sci, 7(3): 560-565.

1. Giriş

Yüksek talep nedeniyle antidepresan ilaç bileşikleri sentetik organik kimyacıların büyük ilgisini çekmiştir. Fluoksetin ve analogları, ilk seçici inhibitörlerden biri olarak ortaya çıkan ve psikiyatrik bozuklukların tedavisinde kullanılan bir ilaçtır (Rossi ve ark., 2004; Lapis ve ark., 2005). Fluoksetin ve benzerleri, norfluoksetin ilk olarak Wonh ve meslektaşları tarafından ilk serotonin inhibitörü olarak ortaya çıkmıştır (Wirth ve ark., 1995; Wong ve ark., 1995). Temsil edici biyolojik özellikleri, anksiyete ve depresyon tedavisinde büyük özelliklere sahip olmalarını sağlamış, sonuçta psikiyatrik bozuklukların tedavisinde kullanılması nedeniyle, hazırlanmaları için yeni sentetik yöntemlerin geliştirilmesinde sürekli çabalara neden olmuştur. Fluoksetin (Prozac), norfluoksetin, nisoksetin, tomoksetin içeren bu ilaç grubu, genellikle depresyon ve anksiyete bozukluklarının tedavisinde ilk tercihtir (Şekil 1).

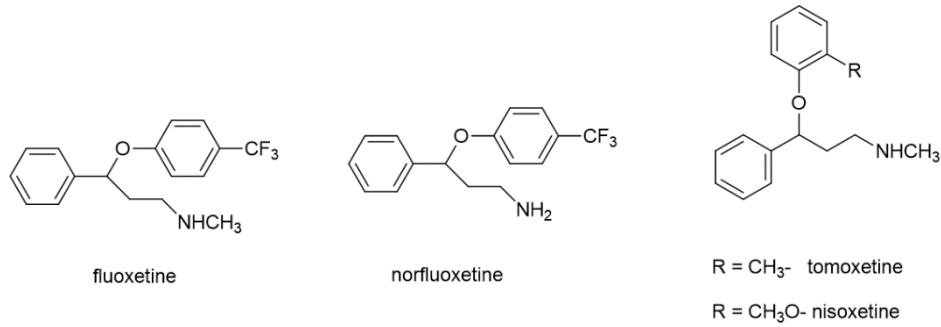
Farmakolojik özellikleri göz önüne alındığında, fluoksetin ve ticari adıyla prozac şu anda rasemik formda pazarlanmaktadır, insan metabolizması üzerinde farklı etkileri vardır (Robertson ve ark., 1988a; Robertson ve ark., 1988b) ve anti inflamatuvar ve ağrı kesici etkileri olduğu gösterilmiştir (Bianchi ve ark., 1994; Bianchi ve ark., 1995). Ketonların enzimatik indirgenmesi (Kumar ve ark., 1991), α - ve β -Hidroksi Amidler (Kakeive ark., 2005), epoksidatin reaktinler [Gao ve ark., 1988] ile kimyasal ve enzimatik reaksiyonlar dahil olmak üzere birçok sentetik yaklaşım denenmiştir (Bracher ve ark., 1996; Korey ve ark., 1989; Caiaffo ve ark., 2016). Farmakolojik potansiyelleri göz önüne alındığında ve yeni yöntemden cesaret alarak, rasemik fluoksetin ve norfluoksetin için stiren epoksidasyonunu içeren ve bileşen olarak ucuz olan yeni ve kısa bir sentetik yol öneriyoruz (Şekil 1) ve etkinliğini gösteriyoruz. Fluoksetin ve rasemik formunun metabolik davranışta yüksek oranda arzu edilir olduğu ve rasemik fluoksetinin



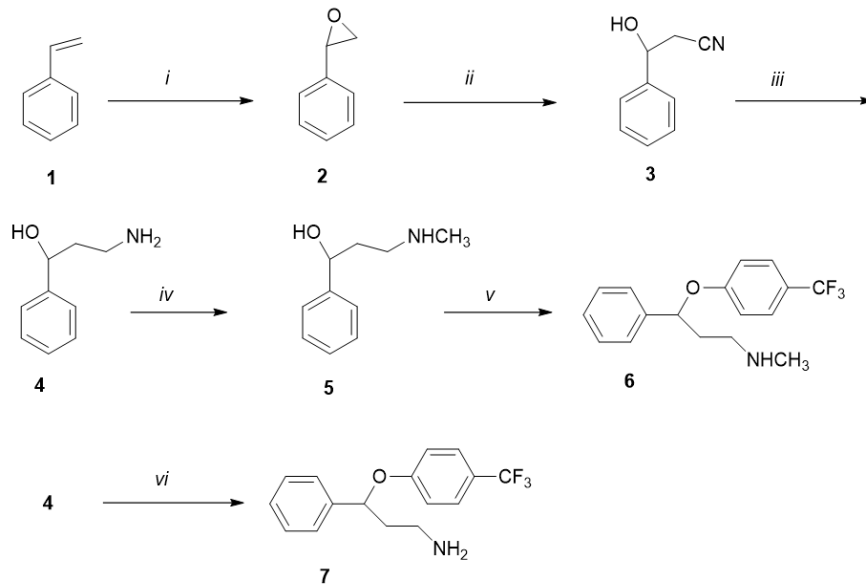
etkinliği iyi belgelenmiş bir antidepresan, depresyon, alkolizm, depresyon, obezite ve bulimia olduğu genel olarak kabul edilmektedir (Stark ve ark., 1985; Zerbe ve ark., 1985). Bilindiği üzere, fluoksetin ve türevlerinin antioksidan enzimler üzerindeki etkisinin yanı sıra sıçan karaciğer mitokondrisindeki enerji metabolizması üzerinde potansiyel olarak toksik çoklu etkileri olduğuna dair bilgiler de mevcuttur (Djordjevic ve ark., 2011). Fluoksetinin antioksidan üzerindeki bir diğer etkisi, fluoksetinin karaciğerdeki antioksidan kapasiteyi geri kazanmasıdır (Zafir ve Banu, 2007). Bu nedenle, CUPRAC yöntemini kullanarak bileşiklerin antioksidan kapasitesini belirlemeyi amaçladık. Norfluoksetin ve fluoksetin için belirlenen antioksidan özellikler Tablo 1'de sunulmuştur. Mevcut araştırma sonuçları,

antioksidan çalışmalarda güçlü olan yeni ilaç sınıfının tasarlanması için düşünülebilir ve fluoksetin ve norfluoksetinin antioksidan potansiyeli de ilgi konusu olmuştur (Kohen ve Nyska, 2002; Serdaroglu ve ark., 2021; Uludag ve Metin, 2021; Uludag, 2023).

Bu nedenle, fluoksetin ve norfluoksetin bileşiklerinin her iki enantiyomerinin asimetrik sentezi son yıllarda artan bir ilgi görmüştür (Piparaki ve , Parissi-Poulou, 1993; Kumar ve ark., 2004). Tıp ve ilaç alanında büyük bir yere sahip olan bu yapılar, fluoksetin ve norfluoksetinin sentezine Şema 1'de gösterildiği gibi ticari olarak temin edilebilen stiren 1'den başlanmıştır. Stiren, ilaç endüstrisi ve polimer teknolojisinde giderek genişleyen bir uygulama yelpazesinde en önemli yapılardan biridir (Gruttes ve ark., 2006; 2006; Wang ve ark., 2009).



Şekil 1. Fluoksetin, norfluoksetinin, tomoksetin ve nisoksetinin kimyasal yapısı.



Şekil 2. Reaktifler ve koşullar: i. Bisdioksomolibden, TBHP, oda sıcaklığı, ii. KCN, rt, iii. BH₃.Me₂S, 0 °C, iv. Metil kloroformat, LiAlH₄, 0 °C, v. NaH, 4-klorobenzotriflorür, vi. NaH, 4-klorobenzotriflorür.

Tablo 1. Test edilen bileşiklerin doğrusal kalibrasyon denklemleri, doğrusal aralıkları ve TEAC katsayıları ile CUPRAC yöntemine göre toplam antioksidan kapasitesi

Bileşikler	Molekül Ağırlığı(Mw) (g/mol)	Doğrusal kalibrasyon Eşitliği	Doğrusal Çalışma Aralığı (M)	TEAC
Fluoksetin (6)	309.13	A=27658 c + 0.045	1.77x10 ⁻⁵ - 6.28x10 ⁻⁵	1.91
Norfluoksetin (7)	295.12	A=679 c + 0.05	3.13x10 ⁻⁴ - 12.43x10 ⁻⁴	1.24

DCM de trolüksun doğrusal eşitliği A=16300 c + 0.02. A= absorpsan, C= konsantrasyon.

2. Materyal ve Yöntem

¹H ve ¹³C NMR spektrumları bir Bruker cihazı DPX-400 MHz Yüksek Performanslı Dijital FT-NMR spektrometresi CDCl₃ ile tetrametilsilan (sırasıyla ¹H ve ¹³C için 400 ve 101 MHz) kaydedilmiştir. IR spektrumları 1000 FT-IR spektrometresinde ve KBr pellet tekniği ile kaydedilmiştir. Kütle spektrumları GEC-21 100B Finnigan Mat 1210 kütle spektrometresinde kaydedilmiştir. İnce tabaka kromatografisi (silika jel 60 F254) tekniği. Bileşikler izole etmek ve saflaştırmak için silika jel 60 (230-400 mesh, Merck) kullanılmıştır. Deneylerde kullanılan çözücüler uluslararası standartlara göre saflaştırılmıştır.

2.1. Materyal

2.1.1. 2-Feniloksiran (2)

Bis(asetilasetonato)dioksomolibden(VI)'nın (4,0 g, 12,2 mmol) 30 ml CH₂Cl₂ içindeki manyetik olarak karıştırılan bir çözeltisi stiren (1,2 g, 12,2 mmol) ve di-tert-butil peroksit (TBHP) (1,6 g, 12,2 mmol) ile muamele edildi ve ardından karışım 12 saat boyunca oda sıcaklığında karıştırıldı. Çözücü buharlaştırıldı ve ardından ürün kolon kromatografisi (hekzan) ile saflaştırılarak renksiz bir yağ olarak 2-feniloksiran (2) (1,2 g, %87) elde edildi. ¹H NMR (CDCl₃), δ: 2,81 (dd, 1H, CH, J = 7,2, 3,6 Hz), 3,17 (dd, 1H, J = 6,8, 5,6 Hz, CH), 3,89 (t, 1H, J = 4,4 Hz, CH), 7,32-7,40 (m, 5H, ArH). ¹³C NMR (CDCl₃), δ: 51,3 (CH₂), 58,1 (CH), 96,2 (CH), 128,3 (Ar C), 130,1 (Ar C), 130,8 (Ar C), 138,3 (Cq). IR (KBr), ν/cm⁻¹: 3089, 2937, 2914, 1497, 1466, 1452, 1381, 1254, 1202, 983, 874, 755, 695, 573. MS (m/z, bağıl yoğunluk): 120 (M⁺, 100), 91 (100), 65 (18), 51 (12), 39 (14).

2.1.2. 3-Hidroksi-3-Fenilpropanenitril (3)

Manyetik olarak karıştırılan 2-feniloksiran'ın (1,0 g, 8,3 mmol) 30 mL etanol içindeki çözeltisine 30 mL su ilave edildi ve ardından potasyum siyanür (1,6 g, 24,9 mmol) ile tek parçada eklendi. Karışım oda sıcaklığında azot atmosferi altında 24 saat karıştırıldı. Reaksiyon tamamlandıktan sonra TLC kontrol edilerek EtOAc ekstrakte edildi ve organik tabaka MgSO₄ üzerinde kurutulularak süzülde. Çözücü buharlaştırıldı ve kalıntı silika jel (hekzan-aseton, 4:1) kullanılarak kromatografide 3-hidroksi-3-fenilpropanenitril 3 (1,0 g, %83) soluk sarı olarak elde edildi. ¹H NMR (CDCl₃), δ: 2,48 (br s, 1H, OH), 2,73-2,80 (m, 2H, CH₂CN), 5,11 (t, 1H, J = 6,2 Hz, CHOH), 7,23-7,51 (m, 5H, ArH). ¹³C NMR (CDCl₃), δ: 26,9, 68,3, 116,8, 125,3, 128,9, 129,2, 175,3. IR (KBr), ν/cm⁻¹: 3432, 3043, 2951, 2927, 2817, 2234, 1604, 1493, 1458, 1412, 1223, 1078, 1053. MS (m/z, bağıl yoğunluk): 147 (M⁺, 100), 147 (0,8), 121 (11), 107 (24), 105 (100), 91 (14), 77 (36).

2.1.3. 3-amino-1-Phenylpropan-1-ol (4)

BH₃.Me₂S kompleksinin (1,1 g, 1,4 mL 13,6 mmol) 20 mL susuz THF içindeki manyetik olarak karıştırılmış bir çözeltisi, 3-hidroksi-3-fenilpropanenitril 3'ün (1,0 g, 6,8 mmol) kuru 20 mL THF içindeki çözeltisine °C'de 3 saat boyunca damla damla ilave edildi. Reaksiyon karışımı 80 °C'de 6 saat boyunca ısıtıldı. 0 °C'ye soğutulduktan sonra, reaksiyonu söndürmek için 30 mL su ilave edildi. EtOAc

(3 x 20 mL) ile ekstraksiyondan sonra, birleştirilmiş organik faz MgSO₄ üzerinde kurutuldu, süzülde ve çözücü beyaz bir katı (966 mg %94) vermek üzere vakumda uzaklaştırıldı, erime noktası 55-57 °C ((Keoning ve ark., 1994) 56 °C). ¹H NMR(CDCl₃), δ: 1,71-1,83 (m, 2H, CH₂NH₂), 2,88-3,11 (m, 2H, CH₂CH), 5,06 (dd, 1H, J = 8,5, 3,0 Hz, CHOH), 7,29-7,63 (m, 5H, ArH). ¹³C NMR (CDCl₃), δ: 40,4, 40,8, 73,8, 124,7, 127,3, 128,1, 146,2. IR (KBr), ν/cm⁻¹: 3342, 3278, 3155, 2931, 2866, 1552, 1467, 1429, 1317, 1044. MS (m/z, relative intensity): 152 (M⁺, 100), 151 (14), 132 (0,8), 115 (34), 106 (11), 84 (54), 77 (100).

2.1.5. 3-(Metilamino)-1-fenilpropan-1-ol (5)

4 numaralı bileşik (500 mg, 3,3 mmol) ve metilkloroformatın (500 mg, 5,0 mmol) 20 mL CH₂Cl₂ içindeki çözeltisine 20 mL H₂O içinde K₂CO₃ (1,8 g, 13,2 mmol) 0 °C'de 2 saat karıştırılarak ilave edildi. Reaksiyon tamamlandıktan sonra TLC kontrol edilerek 20 mL su ilave edildi, EtOAc ekstrakte edildi ve organik tabaka MgSO₄ üzerinde kurutuldu ve süzülde. Çözücü buharlaştırıldı ve kalıntı 20 mL susuz THF içinde çözüldü. Elde edilen çözelti 0 °C'de 500 mg (13,5 mmol) LiAlH₄ ile birkaç porsiyon halinde muamele edildi ve ardından reaksiyon karışımı 12 saat boyunca ısıtıldı. 0 °C'ye soğutulduktan sonra, reaksiyona 3 mL su ilave edildi. Elde edilen süzülde ve organik tabaka ayrıldı ve süzülde, MgSO₄ üzerinde kurutuldu. Çözücü buharlaştırıldı ve kalan kısım silika jel (EtOAc-CH₂Cl₂, 4:1) kullanılarak kromatografi yapıldı ve renksiz bir yağ olarak 5 (433 mg, %87) elde edildi. ¹H NMR (CDCl₃), δ: 1,87-1,96 (m, 2H, CH₂NH), 2,38 (s, 3H, CH₃), 2,85-2,94 (m, 2H, CH₂CH), 4,93 (dd, 1H, J = 8,3, 3,1 Hz, CHOH), 7,34-7,46 (m, 5H, ArH). ¹³C NMR (CDCl₃), δ: 33,7, 36,2, 47,2, 70,3, 124,7 (2C), 126,3, 128,1 (2C), 144,5. IR (KBr), ν/cm⁻¹: 3431, 2934, 1657, 1593, 1451, 1244, 1089, 788, 693, 524. MS (m/z, bağıl yoğunluk): 165 (M⁺, 100), 133(11), 133 (28), 117 (56), 104 (68), 91 (14), 77 (100), 43 (14).

2.1.6. Fluoksetin (N-Metil-3-fenil-3-(4-(triflorometil)fenoksi)propan-1-amin) (6) Sentezi

3-(metilamino)-1-fenilpropan-1-ol 5'in (200 mg, 1,2 mmol) 30 mL DMF içindeki çözeltisine sodyum hidrür (267 mg, %60 dispersiyon yağı, 6,0 mmol), azot atmosferi altında birkaç porsiyon halinde ilave edildi, karışım 3-(metilamino)-1-fenilpropan-1-ol (5) anyonunu oluşturmak için 0 °C'de 1 saat karıştırıldı. Daha sonra 393 mg (2,4 mmol) 4-klorobenzotriflorür şırınga ile eklenerek karışım 4 saat boyunca kaynatıldı kuvvetli karıştırma ile ısıtıldı. Reaksiyon tamamlandıktan sonra TLC kontrol edilerek oda sıcaklığına soğutuldu ve suya döküldü, EtOAc (3 x 25 mL) ile ekstrakte edildi ve organik tabaka toplandı ve magnezyum sülfat üzerinde kurutuldu, filtre edildi ve çözücü indirgenmiş basınç altında uzaklaştırıldı. Ham yağ, saf fluoksetin elde etmek için eluent olarak kolon kromatografisi (EtOAc-n-hekzan, 5: 1) ile saflaştırıldı ve daha sonra çözücü çıkarıldıktan sonra elde edilen ürün, beyaz bir katı olarak 326 mg (%88) elde etmek için dietil eterden yeniden kristalleştirildi, fluoksetinin erime noktası 158-160 °C'dir

((Wei ve ark., 2018)157-159 °C). ¹H NMR (CDCl₃), δ: 2,24 (d, 1H, J = 6,3 Hz, CH), 2,38 (dd, J = 13,4, 6,1 Hz, CH), 2,54 (s, 3H, CH₃), 2,91 (s, 2H, CH₂), 5,73 (s, 1H, CH), 6,81 (d, 2H, J = 8,6 Hz, ArH), 7,19-7,22 (m, 1H, ArH), 7,29-7,33 (m, 4H, ArH), 7,41 (d, 2H, J = 8,5 Hz, ArH). ¹³C NMR (CDCl₃), δ: 161,3, 142,2, 128,9 (2C), 127,4, 126,8 (2C), 125,3, 124,7 (2C), 121,8 (2C), 115,4, 78,9, 47,6, 38,7, 36,2). IR (KBr), ν/cm⁻¹: 3334,3021, 2964,2937, 2781, 2735, 2444, 1617, 1523, 1324, 1235, 1159, 1101, 1061. MS (m/z, bağlı yoğunluk): 309 (M⁺), 164 (12), 162 (0,6), 148 (20), 104 (18), 91 (32), 77 (100).

2.1.7. Norfluoksetin (3-fenil-3-(4-(triflorometil)fenoksi)propan-1-amin) (7) sentezi

Benzer şekilde, 3-amino-1-fenilpropan-1-ol'ün (4) (200 mg, 1,3 mmol) arilasyonu, yukarıdaki prosedür kullanılarak sarı bir yağ olarak norfluoksetin 7 %91 (390 mg) elde etmek için DMF içinde baz olarak NaH ve 4-klorobenzotriflorür kullanılarak nükleofilik aromatik yer değiştirme ile gerçekleştirilmiştir. ¹H NMR (CDCl₃), δ: 1,58 (bs, 2H, NH₂), 1,92-2,01 (m, 1H, CH), 2,11-2,23 (m,1H, CH), 2,78-2,91 (m, 2H, CH₂), 5,29 (dd, 1H, J = 8,6, 4,8 Hz, CH), 6,87 (d, 2H, J = 8,7 Hz, ArH), 7,21-7,27 (m, 1H, ArH), 7,31-7,38 (m, 4H, ArH), 7,41 (d, 2H, J = 8,7 Hz, ArH). ¹³C NMR (CDCl₃), δ: 161,8, 142,3, 129,3, 128,7, 127,4, 126,5, 124,9, 121,5, 117,2, 77,3, 41,2, 37,5. IR (KBr), ν/cm⁻¹: 3328, 2971, 2834, 1617, 1523, 1344, 1231, 1143, 1113, 1058. MS (m/z, bağlı yoğunluk): 295 (M⁺, 100), 278 (0,3), 251 (2), 197 (22), 162 (15), 134 (100).

3. Bulgular ve Tartışma

Sentetik yaklaşımlarda, başlangıç materyalinin hazırlanması, stiren oksit 2 literatüre göre sentezlendi, ilk adımda epoksidasyon yoluyla fluoksetin ve norfluoksetin sentezleme prosedürü (Wang ve ark., 2009). Bunun nedeni, stirenden 3-hidroksi-3-fenilpropanenitril 3 üretmek için nükleofilik atakların oluşumunda stiren oksidin büyük önem taşımasıdır. Bu nedenle, bu çalışmada stiren oksidasyonu için oksidant olarak TBHP (tert-Bütül hidroperoksit) kullandık. Şekil 1'de gösterildiği gibi, oda sıcaklığında potasyum siyanür varlığında siyanürün 1,2-epoksitlere 2 eklenmesi için çok basit ve verimli bir yöntem rapor ederek %83 gibi yüksek bir verimle 2-feniloksiran 3'ü elde ettik. Ürün 3, siyanürün daha az sübstitüe karbon atomuna saldırmasından elde edilmiştir. KCN ile gerçekleştirilen açılma reaksiyonu, epoksitlere eklenerek reaksiyon koşulu hafif ve verim yüksektir (Chini ve ark., 1991). Daha sonra bileşik 3, kuru THF içinde BH₃.Me₂S ile indirgenmeye tabi tutularak %94 verimle amino alkol 4 elde edilmiş, bu da metil kloro format ve indirgenmiş lityum alüminyum hidrür ile ardışık işleme N-metillenmiş 5'e dönüştürülmüştür [Li ve ark., 2005]. Son olarak, N-metilamino alkolün arilasyonu 120 °C'de DMSO içinde NaH ve 4-klorobenzotriflorür ile muamele edilmiştir (Koenig ve ark., 1994; Hilborn et al., 2001). Bu prosedürle, rasemik fluoksetin (5) beş adımda %60 toplam verimle katı olarak elde edilmiştir. Öte yandan, rasemik norfluoksetin sentezi için, amino alkol 4, DMSO

inde 120 °C'de 4-klorobenzotriflorür ile muamele edildi ve sarı bir yağ olarak %62 verimle karşılık gelen rasemik norfluoksetine 7 dönüştürülebildi.

Sonuç olarak, epoksidasyon yoluyla yeni farklı bir yolla rasemik fluoksetin ve norfluoksetin için kısa ve operasyonel olarak basit bir yöntem geliştirilmiştir. Bu yöntem diğer ilaç endüstrisinin sentezine genişletilebilir.

4. Antioksidan Araştırmaları

Serbest radikaller, eşleşmemiş elektronlara sahip oldukça reaktif yapılardır. Bu kararsız yapılar -OH ve -NO ile temsil edilir. Bunlar canlı organizmaları etkileyen bazı oksidatif stresler olarak bilinir. Bu süreç normal hücre metabolizmasını değiştirir ve hatta hücre ölümüne yol açabilir. Bu nedenle, radikal inhibitörleri sağlık için önemlidir. Bu amaçla yeni bileşiklerin araştırılması önemlidir. Devam etmekte olan çalışmalarımızın devamı olarak, burada fluoksetin ve norfluoksetinin sentez antioksidan potansiyelini araştırdık.

Fluoksetin ve norfluoksetinin antioksidan aktivitelerinin değerlendirilmesi metanolde TEAK "Trolox equivalent antioxidant capacity" ile gerçekleştirilmiştir. Fluoksetin ve norfluoksetinin kalibrasyon eğrileri CUPRAC yöntemine göre oluşturulmuş ve doğrusal kotasyonlar elde edilmiştir. Antioksidan potansiyelin genel sonuçları Tablo 1'de özetlenmiştir. Sonuçlar, fluoksetinin norfluoksetin antioksidan aktivitesinden daha yüksek bir antioksidan aktiviteye sahip olduğunu ortaya koymuştur. Fluoksetinin antioksidan aktivitesi, nitrojenin metil grubuna bağlı olarak varlığından kaynaklanmaktadır. NCH₃ sübstitüent grubunun varlığından farklı olarak. Diğer bir etki antioksidan aktivite, (4-(triflorometil)fenil)-1-oksitan fragmanlarının varlığından kaynaklanmaktadır (Kolla ve ark., 2005; Juarez-Luna ve ark., 2019).

5. Sonuç

Bu çalışmada fluoksetin ve norfluoksetinin sentezi farklı bir yöntemle gerçekleştirilmiştir. Sentezlenen iki bileşiğin antioksidan özelliği de araştırıldı bu yöntem ile literatürde ilk defa bu özelliği de araştırıldı. Sentez yöntemi ile uygulanabilir bir yöntem olarak ilaç sanayisi için farklı bir akışı geliştirilmiştir. Ara basamakta uygulanan sentez yöntemleriyle diğer buna benzer çalışmalar için farklı bir bakış açısı getirmiştir.

Katkı Oranı Beyanı

Yazar(lar)ın katkı yüzdesi aşağıda verilmiştir. Yazar makaleyi incelemiş ve onaylamıştır.

	N.U.
K	100
T	100
Y	100
VTI	100
VAY	100
KT	100
YZ	100
KI	100
GR	100
PY	100
FA	100

K= kavram, T= tasarım, Y= yönetim, VTI= veri toplama ve/veya işleme, VAY= veri analizi ve/veya yorumlama, KT= kaynak tarama, YZ= Yazım, KI= kritik inceleme, GR= gönderim ve revizyon, PY= proje yönetimi, FA= fon alımı.

Çatışma Beyanı

Yazar bu çalışmada hiçbir çıkar ilişkisi olmadığını beyan etmektedirler.

Etik Onay Beyanı

Bu çalışmada hayvanlar ve insanlar üzerinde herhangi bir çalışma yapılmadığı için etik kurul onayı alınmamıştır.

Destek ve Teşekkür Beyanı

Çalışma Tekirdağ Namık Kemal Üniversitesi, Kimya Bölümü, Organik Kimya Araştırma Laboratuvarı'nda yapılmış olup, mevcut olanakları sağlayan Tekirdağ Namık Kemal Üniversitesi'ne teşekkürü borç bilirim.

Kaynaklar

Bianchi M, Rossoni G, Sacerdote P, Panerai AE, Berti F. 1995. Effects of clomipramine and fluoxetine on subcutaneous carrageenin-induced inflammation in the rat. *Inflamm Res*, 44: 466-469.

Bianchi M, Sacerdote P, Panerai AE. 1994. Fluoxetine reduces inflammatory edema in the rat: involvement of the pituitary-adrenal axis. *Eur j Pharmacol*, 263: 81-84.

Bracher F, Litz T. 1996. An efficient chemoenzymatic route to the antidepressants (R)-fluoxetine and (R)-tomoxetine. *Bioorg Med Chem*, 4: 877-880.

Caiaffo V, Oliveira BDR, Se SA FB, Evencio Neto J. 2016. Anti-inflammatory, antiapoptotic, and antioxidant activity of fluoxetine. *Pharmacol Res Perspect*, 4: e00231.

Chini M, Crotti P, Favero L, Macchia F. 1991. Easy direct stereo- and regioselective formation of β -hydroxy nitriles by reaction of 1, 2-epoxides with potassium cyanide in the presence of metal salts. *Tetrahedron Lett*, 32: 4775-4778.

Djordjevic J, Djordjevic A, Adzic M, Elaković I, Matić G, Radojčić MB. 2011. Fluoxetine affects antioxidant system and promotes apoptotic signaling in Wistar rat liver. *Eur J Pharmacol*, 659: 61-66.

Gao Y, Sharpless KB. 1988. Asymmetric Synthesis of both enantiomers of tomoxetine and fluoxetine. Selective reduction of 2,3-epoxycinnamyl alcohol with Red-Al. *J Org Chem*, 53:

4081-4084.

Grutters MM, Müller C, Vogt D. 2006. Highly selective cobalt-catalyzed hydrovinylation of styrene. *J Am Chem Soc*, 128: 7414-7415.

Hilborn JW, Lu ZH, Jurgens AR, Fang Q K, Byers P, Wald SA, Senanayake CH. 2001. A practical asymmetric synthesis of (R)-fluoxetine and its major metabolite (R)-norfluoxetine. *Tetrahedron Lett*, 42: 8919-8921.

Juarez-Luna PJ, Mendoza S, Cardenas A. 2019. Comparison of electrochemical methods using CUPRAC, DPPH, and carbon paste electrodes for the quantification of antioxidants in food oils. *Analytical Methods*, 11: 5755-5760.

Kakei HT, Ohshima N, Shibasaki TM. 2005. Efficient synthesis of chiral α - and β -hydroxy amides: Application to the synthesis of (R)-fluoxetine. *Angew Chem Int Ed*, 43: 317-320.

Koenig TM, Mitchell D. 1994. A convenient method for preparing enantiomerically pure norfluoxetine, fluoxetine and tomoxetine. *Tetrahedron Lett*, 35: 1339-1342.

Kohen R, Nyska A. 2002. Invited review: oxidation of biological systems: oxidative stress phenomena, antioxidants, redox reactions, and methods for their quantification. *Toxicol Pathol*, 30: 620-650.

Kolla N, Wei Z, Richardson JS, Li XM. 2005. Amitriptyline and fluoxetine protect PC12 cells from cell death induced by hydrogen peroxide. *J. Psychiatry Neurosci*, 30: 196-201.

Korey EJ, Reichhard GA. 1989. Enantioselective and practical syntheses of R- and S-fluoxetines. *Tetrahedron Lett*, 30: 5207-5210.

Kumar A, Ner DH, Dike SY. 1991. A new chemoenzymatic enantioselective synthesis of R-(-)-tomoxetine, (R)- and (S)-fluoxetine. *Tetrahedron Lett*, 32: 1901-1904.

Kumar P, Upadhyay RK, Pandey RK. 2004. Asymmetric dihydroxylation route to (R)-isoprenaline, (R)-norfluoxetine and (R)-fluoxetine. *Tetrahedron Asymmetry*, 15: 3955-3959.

Lapis AAM, De Fatima A, Martis JED, Costa VEU, Pilli RA. 2005. Asymmetric reduction of prochiral ketones using in situ generated oxazaborolidine derived from (1S,2S,3R,4R)-3-amino-7,7-dimethoxynorbornan-2-ol. An efficient synthesis of enantiopure (R)-tomoxetine. 2005. *Tetrahedron Lett*, 46: 495-498.

Li Y, Li Z, Li F, Wang Q, Tao F. 2005. Preparation of polymer-supported Ru-TsDPEN catalysts and use for enantioselective synthesis of (S)-fluoxetine. *Org Biomol Chem*, 3: 2513-2518.

Piparaki S, Parissi-Poulou M. 1993. Use of Cyclodextrins as chiral selectors for direct resolution of the enantiomers of fluoxetine and its metabolite norfluoxetine by HPLC Chirality, 5: 258-266.

Robertson DW, Jones ND, Swartzendruber JK, Wong DT. 1988b. Molecular structure of fluoxetine hydrochloride, a highly selective serotonin-uptake inhibitor. *J Med Chem*, 31: 185-189.

Robertson DW, Krushinski JH, Fuller RW, Leander JD. 1988a. Absolute configurations and pharmacological activities of the optical isomers of fluoxetine, a selective serotonin-uptake inhibitor. *J Med Chem*, 31: 1412-1417.

Rossi A, Barraco A, Donda P. 2004. Fluoxetine: a review on evidence based medicine. *Ann Gen Hosp Psychiatry*, 3: 1-8.

Serdaroğlu G, Uludag N, Sagumar P, Rajkumar P. 2021. (-)-Tubifolidine as strychnos indole alkaloid: Spectroscopic characterization (FT-IR, NMR, UV-Vis), antioxidant activity, molecular docking, and DFT studies. *J Mol Struct*, 1244: 130978.

Stark P, Hardison CD. 1985. A review of multicenter controlled studies of fluoxetine vs. imipramine and placebo in outpatients with major depressive disorder. *J Clin Psychiatry*, 46: 53-58.

- Uludag N, Serdaroğlu G. 2021. An efficient studies on C-2 cyanomethylation of the indole synthesis: The electronic and spectroscopic characterization (FT-IR, NMR, UV-Vis), antioxidant activity, and theoretical calculations] Mol Struct, 1247: 131416.
- Uludag N. 2023. Çinko-triflat katalizörü kullanılarak farklı süstitüye izokumarin türevlerinin sentezi. BSJ Eng Sci, 6: 127-131.
- Wang Y, Wu Z, Li Z, Zhou XG. 2009. Asymmetric epoxidation of styrenes catalyzed by molybdenum complexes with amino alcohol ligands. Tetrahedron Lett, 50: 2509-2511.
- Wei Y, Xuan Q, Zhou Y, Song Q. 2018. Reductive N-alkylation of primary and secondary amines using carboxylic acids and borazane under mild conditions. Org. Chem. Front, 5: 3510-3514.
- Wirth DD, Baertschi SW, Johnson RA, Maple SR, Miller MS, Hallenback DK, Gregg SM. 1995. Maillard reaction of lactose and fluoxetine hydrochloride, a secondary amine. J Pharm Sci, 87: 31-39.
- Wong DT, Bymaster FP, Engelman EA. 1995. Prozac (fluoxetine, lilly 110140), the first selective serotonin uptake inhibitor and an antidepressant drug: Twenty years since its first publication. Life Sci, 57: 411-441.
- Zafir A, Banu N. 2007. Antioxidant potential of fluoxetine in comparison to curcuma longa in restraint-stressed rats. Eur J Pharmacol, 572: 23-31.
- Zerbe RL, Rowe H, Enas GG, Wong D, Farid N, Lemberger L. 1985. Clinical pharmacology of tomoxetine, a potential antidepressant. J Pharmacol Exp Ther, 232: 139-143.



EVALUATION OF AGING EFFECTS OF ZINC OXIDE ON THE OPTICAL PROPERTIES OF POROUS SILICON-ZINC OXIDE HETEROJUNCTION PHOTODETECTOR DEVICE

Safiye KARAÇAM¹, Meltem GÖR BÖLEN^{1*}


¹Erzurum Technical University, Faculty of Engineering and Architecture, 25100, Erzurum, Türkiye


Abstract: Porous silicon is very important for integrated technology because of its many superior properties, such as suitability for mass production, easy and controlled production, and adjustable electrical and optical properties. Semiconductors with metal oxides, such as indium oxide, indium tin oxide, tin oxide, and zinc oxide, are highly preferred in optical devices. Among these metal oxides, zinc oxide is preferred for photodetectors because of its stable crystal structure and large exciton binding energy of 60 meV. Researchers have conducted studies on photodetectors with porous silicon-zinc oxide heterojunction structures. The importance of the stable operation of devices has been emphasized. Therefore, in this study, a porous silicon-based zinc oxide heterojunction structure suitable for photodetector production was formed, and the effect of aging on zinc oxide was investigated over time. As a result of the investigation, it was observed that the intensity decreased approximately 2.5 times at the end of 365 days owing to the aging of zinc oxide. In addition, UV spectroscopy measurements were performed to investigate the optical properties that affect their operation as photodetectors. Because the PS-ZnO heterojunction functions as a detector in the UV region, the absorption and reflectivity of the PS-ZnO heterojunction were investigated, especially in the UV region. From the measurements, it was observed that aging decreased absorption and increased reflectance. These findings underscore the negative impact of aging on photodetector performance.

Keywords: Porous silicon, Zinc oxide, Photodetector, Aging

*Corresponding author: Erzurum Technical University, Faculty of Engineering and Architecture, 25100, Erzurum, Türkiye

E mail: meltem.gor@erzurum.edu.tr (M. GÖR BÖLEN)

Safiye KARAÇAM  <https://orcid.org/0009-0005-1236-2169>

Meltem GÖR BÖLEN  <https://orcid.org/0000-0002-5340-6026>

Received: February 19, 2024

Accepted: May 08, 2024

Published: May 15, 2024

Cite as: Karaçam S, Gör Bölen M. 2024. Evaluation of aging effects of zinc oxide on the optical properties of porous silicon-zinc oxide heterojunction photodetector device. BSJ Eng Sci, 7(3): 566-574.

1. Introduction

Silicon plays a central role in integrated circuit technologies and informatics, and serves as a primary material extensively employed for the production of various devices. These devices range from complex integrated circuits to economical solar cells. Silicon forms the basis of integrated circuits found in electronic devices. As complementary metal-oxide semiconductor (CMOS) production lines enable large-scale manufacturing, silicon-on-insulator (SOI) technology has emerged as a crucial platform for integrated photonics (Bloem, 1979; Mayer, 1984; Sieval et al, 2000; Guo et al., 2002; Shuchen et al., 2008; Cui et al., 2009; Westerveld et al., 2012; Garvey et al., 2020; De Matteis et al., 2020).

Silicon has a wide range of applications in integrated technology. They are utilized in the fabrication of thin-film transistors (TFTs), solar photovoltaic (PV) cells, peripheral circuits of liquid crystal displays (LCDs), and electrodes in Si integrated circuits (Periasamy et al., 2017). In contemporary settings, silicon plays a crucial role in various device applications and remains an integral component of the silicon integrated circuit technology (Lioudakis et al, 2008).

Photonics based on silicon and silicon nitride (Si₃N₄) are

now employed for sensing assignments, encompassing tasks ranging from refractive index measurements to spectroscopic sensing (Subramanian et al., 2015). Silicon-on-insulator-based devices continue to be utilized in niche market applications, including high-temperature and radiation-hard integrated circuits (Colinge, 1998; Won et al., 2007; Zhong and Bernasek, 2011)

Silicon has been extensively incorporated into Application-Specific Integrated Circuit (ASIC) technology, particularly in designing readout electronics for silicon sensors in particle physics experiments (Won et al., 2007). The use of silicon-integrated circuits and micromachining technology enables the creation of microelectrode arrays and intricate electrical systems.

There are several reasons for using silicon as a substrate in integrated technology. Silicon is a well-known and mature technology that is widely used in industry, making it a cost-effective option (Yusoff et al., 2012). Second, silicon has a low thermal expansion coefficient, which makes it a suitable substrate for high-temperature applications (Gomes et al., 2011). Third, silicon has a high level of compatibility with other materials, such as III-V materials, making it a suitable substrate for hybrid integration (Gomes et al., 2011). Fourth, silicon-on-



insulator (SOI) wafer technology, which uses a layered silicon-insulator-silicon substrate, can reduce parasitic capacitance and improve performance (Bacquian and Gomez, 2019). Fifth, the tight regulation of the size and chemical composition of III-V nanowires has the potential to be used in upcoming silicon technologies and employed as the active element in optoelectronic devices (Bakkers et al., 2007). Sixth, the use of a high-resistivity silicon substrate along with a grounded Faraday cage can suppress substrate coupling in high-frequency applications (Sharifi and Mohammadi, 2008; Peng et al., 2010). Finally, the development of silicon carbide substrates has allowed the organization of integrated group production of devices, making it a suitable substrate for electronic components.

Zinc oxide (ZnO) has various properties that make it useful in a wide range of applications. It has antimicrobial, anti-inflammatory, wound healing, catalytic, magnetic, optical, and electronic properties (Kaningini et al., 2022). ZnO is also used in piezoelectric gadgets, semiconductors, sensors, and for antimicrobial functions (Wasim et al., 2020). It has extraordinary physical and chemical properties that make it an important material for electrical, optical, mechanical, and scientific research. ZnO thin films have emerged as new and interesting materials owing to their electrical, optical, and piezoelectric properties (Rodríguez-Báez et al., 2007). Owing to their remarkable characteristics and unique physical and chemical properties, including remarkable chemical stability, anti-corrosiveness, low electron conductivity, broad radiation absorption, high photostability, and tremendous heat resistance, ZnO and metal-doped oxides are widely employed in the Nano World. (Mishra et al., 2022).

ZnO has good optical properties with respect to UV absorption (Weichelt et al., 2010; Zuo and Erbe, 2010). ZnO exhibits an optical transmittance of greater than 70% in the visible region. The optical band gap of ZnO is around 3.7 eV (Czekalla et al., 2010). The optical properties of ZnO nanoparticles have also been studied, and they were found to exhibit nonlinear optical properties. The structural, morphological, and optical features of the ZnO nanoparticles were determined using X-ray diffraction, scanning electron microscopy, and ultraviolet-visible spectroscopy.

Properties of ZnO UV photodetectors include: - Wide bandgap of approximately 3.37 eV [34] - High radiation durability (Tian et al., 2014) - Low visible absorption (Guo et al., 2023) - High transmittance in the ultraviolet (UV) region (Guo et al., 2023) - Excellent environmental stability (Guo et al., 2023) - Excellent photoresponse in the UV regime (Gebrehiwot, 2017) - Can be synthesized using a room ambient sonochemical process (Nayak et al., 2012)- Can be synthesized using a UV-assisted photochemical synthesis method (Chen et al., 2018) - Can be synthesized as a composite with reduced graphene oxide (rGO) (Chen et al., 2018; An et al., 2018) - Can be synthesized as a composite with single-walled carbon

nanotube (SWNT) thin films (Ates et al., 2012) - Can be synthesized as a composite with zinc gallium oxide ($ZnGa_2O_4$) for deep-ultraviolet (DUV) photodetectors (Gebrehiwot, 2017) - Can be used to construct flexible and wearable photodetectors (An et al., 2018) - Can be integrated with other materials, such as lead sulfide (PbS) quantum dots, to induce a photoconductive gain (Dong et al., 2014) - Can be used in outdoor applications, such as wood coatings (Boruah et al., 2015) - ZnO nanowires (ZNWs) have a weak photon absorption and high recombination rate of electron-hole pairs, which limits their application in UV photodetection (Chen et al., 2018). However, this limitation can be overcome by using ZnO in composites with other substances, such as graphene (Yedurkar et al., 2016).

ZnO finds a wide range of applications across various fields. In electronics, it is used in piezoelectric devices, UV absorbers, and sensors. Additionally, it plays a role in communication, solar panel devices, and environmental protection. In the medical industry, ZnO is employed in drug delivery, nanomedicine, and gene delivery. Notably, ZnO nanoparticles show promise in biological sensing, biological labeling, and as antibacterial agents. In cosmetics, ZnO is utilized in sunscreens, whereas it serves as a food additive in the food industry. ZnO also contributes to biosensors, material sciences, and environmental remediation.

The synthesis of ZnO employs various methods, including chemical approaches, such as the sol-gel method, solvothermal and hydrothermal methods, and emulsion and microemulsion environment methods. Despite their potential applications, a significant hurdle in the development and utilization of ZnO-based materials for electrical and photonic purposes is the complexity of the carrier doping. The introduction of extra zinc or doping ZnO with elements like Al, Ga, or In simplifies the creation of ZnO (Piticescu et al., 2006; Amara et al., 2014; Mohsenzadeh and Moosavian, 2017; Nazir et al., 2018; Chikkanna et al., 2019; Dheivamalar and Banu, 2019; Khan et al., 2018).

Aging in ZnO thin films refers to the changes occurring in the properties of the films over time due to exposure to environmental factors such as humidity and temperature (Yaklin et al., 2010). This process can lead to the formation of surface films primarily composed of hydrated tin and zinc oxy-hydroxide (Hanawa et al., 1987). The key characteristics of ZnO thin films include low electrical resistivity, excellent thermal stability, high optical transparency in the visible spectrum, and nontoxicity (Devasia et al., 2021; Amudhavalli et al., 2023). Defect sites in the microstructure, such as oxygen vacancies or zinc interstitials, play a crucial role in controlling the charge carrier mobility in thin-film transistor devices (Matysiak et al., 2018; Hoffman et al., 2021). Prolonged soft annealing times can induce an increase in the oxygen vacancy concentration in zinc tin oxide thin-film transistors. Additionally, when heated to 350 °C, the electrical conductivity of ZnO thin films doped

with aluminum deteriorates rapidly and unevenly. ZnO thin films are renowned for their advantageous characteristics, including low electrical resistivity, excellent thermal stability, great optical transparency in the visible spectrum, and non-toxicity (Konstantinidis et al., 2007; Huang et al., 2011; Nayak et al., 2013; Widyastuti, et al., 2022).

According to the available literature, there is no specific information on the causes of aging in ZnO UV photodetectors. However, some studies have mentioned that the high radiation endurance and low visible absorption of ZnO make it a promising material for UV photodetector applications. Moreover, some commercial UV photodetectors made of silicon or gallium arsenide semiconductors require a filter to block visible and infrared light, and they may also be harmed by strong UV light because of aging faults that are created. (Sirkeci et al., 2018). Therefore, it can be inferred that aging of ZnO UV photodetectors may be related to the intensity and duration of UV radiation exposure. However, further research is required to determine the specific causes of aging in ZnO UV photodetectors.

There are several advantages and disadvantages to aging ZnO thin films. They are also non-toxic, inexpensive, and abundant in materials (Sellers et al., 2000). In addition, thin films of ZnO exhibit piezoelectric capabilities (Kuo et al., 2009). Thus, the use of ZnO thin films is growing in fields such as photovoltaic cells, photocatalytic materials, and poisonous gas sensors (Konstantinidis et al., 2007). However, there are also some disadvantages to aging ZnO thin films. For example, the concentration of mercury in a thin surface film is depleted after aging (Amudhavalli et al., 2023). Overall, the advantages and disadvantages of aging in ZnO thin films depend on their specific applications and desired properties.

There is limited information on how the aging of ZnO thin films affects UV photodetector performance. However, several studies have investigated the performance of ZnO thin film-based UV photodetectors. For example, one study reported the use of solution-based synthesis to create transparent and flexible ZnO nanowire UV photodetectors (Chen et al., 2018). Another study reported the performance enhancement of ZnO UV photodetectors using surface plasmons (Gebrehiwot, 2017). Additionally, UV photodetectors using thin sheets of indium ZnO with a binary cation exhibited a significant improvement in performance over their single-cation equivalents (He et al., 2022). Other studies have investigated the use of amorphous indium gallium ZnO film transistors for UV photodetector applications (Chang et al., 2012), p-n junctions of NiO thin films for UV photodiode characteristics, and the effect of the oxygen vacancy ratio on GaZTO solar-blind photodetectors. Furthermore, the thermal stability of the aluminum-doped ZnO thin films was found to be significantly improved when exposed to UV ozone for a short time before heating. The oxygen plasma surface activation of electron-depleted ZnO nanoparticle films was also found

to enhance the performance of the UV photodetectors. Finally, slightly doped ZnO films with manganese were found to exhibit increased photocatalytic performance compared to pure ZnO semiconductor thin films. Overall, although there is limited information on how aging specifically affects UV photodetector performance, several studies have investigated the performance of UV photodetectors based on ZnO thin films (Habibi and Askari, 2011; Tyagi et al., 2012; Liu et al., 2017; Syu et al., 2018).

These studies provide information on various aspects of ZnO thin films, but only one study (Yaklin et al., 2010) has specifically noted accelerated aging studies. A prior study (Yaklin et al., 2010) investigated the effects of humidity and temperature on the performance of transparent conducting ZnO and included accelerated aging studies to determine the reliability factors and kinetic parameters.

ZnO thin films have been extensively studied because of their advantageous characteristics, which include their lack of toxicity, low electrical resistivity, high thermal stability, and high optical transparency. However, aging of ZnO thin films has been a topic of interest in recent studies. Yaklin et al. (2010) observed the electrical characteristics of conducting ZnO using an in situ electroanalytical technique under controlled air conditions, and discovered that one of the main causes of cell/module failure is water seeping into the modules in the field. Amudhavalli et al. (2023) studied the conduction mechanism of ZnO nanoparticles deposited using a low-cost nebulizer spray method. Kim et al. (2009) examined the optical and electrical properties of amorphous hafnium-indium-ZnO semiconductor thin-film transistors for thin-film transistor applications. Kappertz et al. (2002) investigated the correlation between the structure, stress, and deposition parameters of direct-current sputtered ZnO films. Indluru and Alford (2009) investigated how the thickness of Ag affects the optical and electrical characteristics of indium tin oxide–Ag–indium tin oxide multilayers. Park et al. (2021) investigated the antimicrobial effect of ZnO thin films formed by atomic layer deposition and evaluated their applicability to membrane surfaces. Konstantinidis et al. (2007) studied the deposition of ZnO layers using high-power impulse magnetron sputtering. Overall, the literature suggests that aging of ZnO thin films can affect their electrical, optical, and structural properties, and further research is needed to fully understand the aging mechanisms and develop strategies to mitigate their effects.

The integration of ZnO thin film-silicon heterojunctions has been a topic of interest in recent years owing to its potential applications in various electronic devices. A heterojunction is formed by combining two different materials with different electronic properties, which can lead to unique electronic properties at the interface. In this essay, we discuss the development of ZnO thin film-silicon heterojunctions and their potential applications.

One approach to forming a ZnO thin film-silicon heterojunction is by depositing indium tin oxide (ITO) and indium zinc oxide (IZO) thin films on vertically aligned silicon nanowire (SiNW) arrays (Chang et al., 2016). Another method involves depositing an IZO thin film on a p-type porous silicon (PS) substrate to obtain an n-IZO/PS/p-Si heterojunction diode (Belaid et al., 2015). To create a heterojunction interface structure, reactively sputtered transparent and conductive Al-doped ZnO (AZO) films can be deposited on a macroporous silicon (MPS) substrate (Mendoza-Aguero et al., 2015). These methods demonstrate the potential of ZnO thin films in combination with silicon to create heterojunctions with unique electronic properties. ZnO thin film-silicon heterojunctions have potential applications in various electronic devices. For example, in photovoltaics, if titanium oxide is produced using a metal-organic chemical vapor deposition technique at substrate temperatures of only 80–100°C, a wide-bandgap heterojunction between crystalline silicon and titanium oxide can be employed (Avasthi et al., 2013). ZnO thin film-silicon heterojunctions can also be used in the production of thin metal oxide films by spray pyrolysis using supercritical CO₂-assisted nebulization of aqueous solutions (Sellers et al., 2000). In conclusion, the integration of ZnO thin film-silicon heterojunctions has shown potential for unique electronic properties and applications in various electronic devices. These heterojunctions have been developed through various methods, including depositing ITO and IZO thin films on vertically aligned SiNW arrays, depositing IZO thin films on p-type PS substrates, and reactively sputtering AZO films onto MPS substrates. The potential applications of ZnO thin film-silicon heterojunctions include tuning the accumulated electron concentration in TFTs, photovoltaics, and the production of thin metal oxide films. Further research is required to explore the full potential of ZnO thin film-silicon heterojunctions in electronic devices.

Competing evidence for an integrated technology composed of ZnO thin films and silicon heterojunctions has been found in various studies. For instance, Schlupp et al. (2013) suggested that, unlike the well-studied indium gallium ZnO, zinc-tin oxide is a promising n-type channel material for thin-film transistors and is composed solely of many components. Similarly, Masaud et al. (2011) proposed that materials suitable for the silicon process, such as thin-film ZnO, are still largely unexplored despite their potential to enhance the functioning of integrated silicon photonic devices. In addition, Ciolan and Motrescu (2022) claimed that as a first step toward creating an n-ZnO/p-Si heterojunction, ZnO thin films were produced at a comparatively low deposition temperature using pulsed laser ablation, a straightforward and non-toxic technique. Furthermore, Lee et al. (2016) suggested that because of its high mobility value, zinc oxynitride, a mixture of ZnO and zinc nitride, has been acknowledged as a potent replacement

for traditional semiconductor films such as silicon and indium gallium ZnO. Finally, amorphous indium-gallium-ZnO thin-film transistors (a-IGZO TFTs) can be viewed as a replacement for amorphous silicon and low-temperature polycrystalline silicon in high-resolution liquid crystal displays for mobile applications and in organic light-emitting diode TVs in the display industry.

2. Materials and Methods

2.1. Formation of Porous Silicon

Boron-doped p-type silicon with a resistivity of 0.001–0.005 Ωcm and thickness of 200 μm was preferred as a silicon wafer. Electrochemical anodic etching was performed using a double-tank Teflon cell to create pores in silicon (Gör and Karacali, 2017). The solution was prepared as (1:2 (v / v) HF (40%) / EtOH (99%)) because the most controlled and smooth pore formation was observed in this ratio (Karacali, 2003). In the electrochemical anodization method, a current density of 10 mA/cm² was applied to the silicon for 5 min. The structure proposed in this study is suitable for use in photodetectors. For this reason, a 650 nm PS layer was formed to reduce the recombination risk of the electron-hole pair. A scanning electron microscopy (SEM) image of porous silicon is shown in Figure 1.

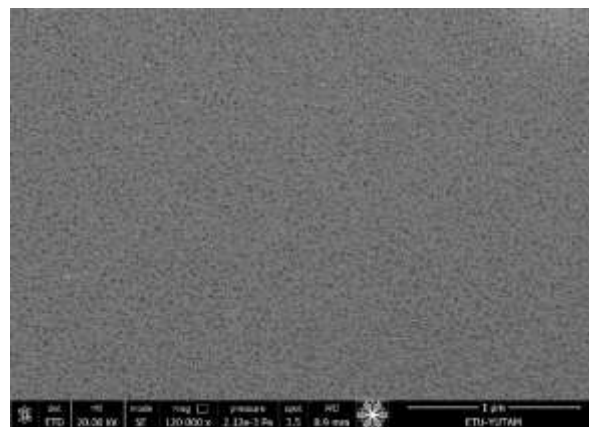


Figure 1. SEM image of the pores obtained by applying 10 mA/cm² current density for 5 min.

2.2. Synthesis of ZnO

During the preparation of the ZnO solution, zinc acetate dihydrate [Zn(CH₃COO)₂·2H₂O] was used as the starting material. In addition, monoethanolamine (C₂H₇NO, MEA) and 2-methoxyethanol (C₃H₈O₂) were used as the stabilizer and solvent, respectively. The solution was stirred at 60 °C for 2 hours to obtain a homogeneous and clear solution (Keskenler et al., 2017).

2.3. The Deposition of ZnO Thin Film

ZnO thin films were produced on the PS using the spin coater technique. For this process, the PS to be used as a substrate was first placed in a rotary coating device (Laurell WS-650MZ-23NPPB) and the prepared ZnO solution was applied to the surface. The sample was then rotated at 3000 rpm for 25 seconds and the coating was applied. The coated film was sintered at 250 °C for 10

minutes to evaporate the solvent. This process was repeated nine times. Finally, the sample was annealed in air at 500 °C for 30 minutes (Keskenler et al., 2017).

3. Results and Discussion

3.1. Thin Film Characterization

As a result of this process, we observed the production of 130 nm thick ZnO thin films through the SEM images presented in Figure 2(a). Additionally, we performed energy-dispersive spectroscopy (EDS) using a Quanta FEG 250 and X-ray diffraction (XRD) measurements for characterization after producing the thin film on PS. It was confirmed that the ZnO thin film was successfully coated onto the silicon. The EDS and SEM results are shown in Figure 2(b), and Figure 3, respectively.

The SEM image of the ZnO thin film heterostructure on PS is shown in Figure 2. a. When the porous layer thickness was ~650 nm, the thickness of the ZnO thin film was measured to be ~136 nm. Figure 2.b shows the EDS results of the ZnO thin-film heterostructure on the PS. In the EDS results, in addition to the Zn and O peaks of ZnO, peaks of B-doped Si were also observed. As shown in Figure 3, several characteristic peaks can be observed in the XRD spectrum of ZnO. The most prominent peak is typically located at approximately $2\theta = 34.4^\circ$, corresponding to the (002) crystal plane of the hexagonal wurtzite ZnO. Other peaks can be observed at different 2θ angles, representing different crystal planes

and orientations of ZnO. By analyzing the positions, intensities, and shapes of these peaks, valuable information regarding the crystal structure, phase purity, and crystallinity of the ZnO sample can be obtained.

When comparing the results obtained in Figure 3 with the data from the literature presented in Figure 4, the dominant peak observed is identified as (002), and it is evident that the ZnO peaks are aligned. In Figure 4, the XRD results of thin films produced with 0.5, 1 and 1.5 M ZnO solutions prepared in the study conducted by (Keskenler et al., 2017) are presented.

The ZnO thin film prepared on PS was stored in a climate room where special conditions were provided in a dark environment at 23.4 °C and 55% humidity for one year. The ambient conditions, including humidity and temperature, are shown in Figure 5.

The XRD measurement results of the sample kept in a dark environment at 23.4 °C and 55% humidity for 365 days are shown in Figure 6. As shown in Figure 6, the dominant peak is (002), and it is observed that the ZnO peaks match. However, according to the measurement results shown in Figure 3, the intensity decreased considerably. While the ZnO peak is dominant in the unaged sample shown in Figure 3, it is weakened in the aged sample, as shown in Figure 6. Therefore, while the ZnO peak is dominant in the unaged sample, the Si peak is more dominant in the aged sample.

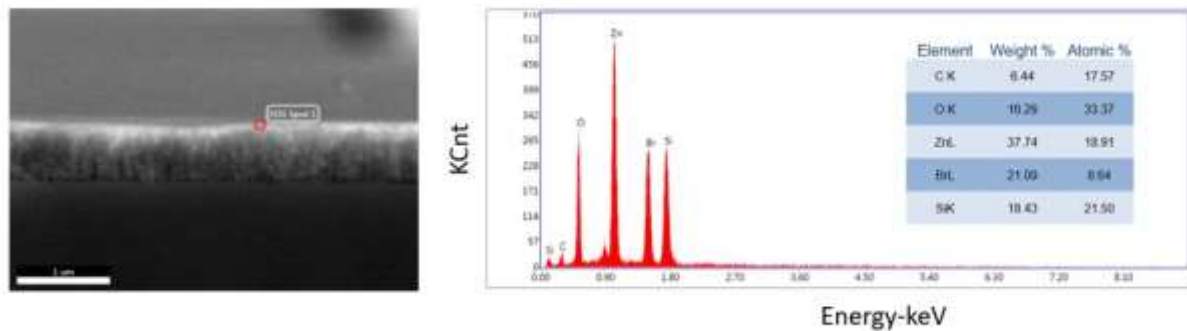


Figure 2. EDS and SEM results of ZnO thin film on PS.

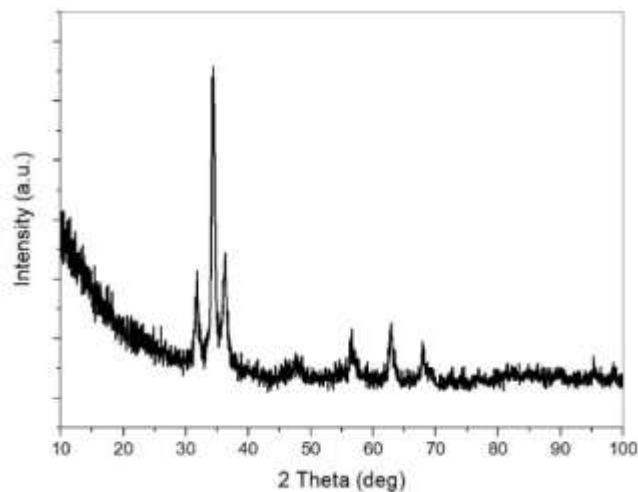


Figure 3. XRD results of ZnO thin film on PS.

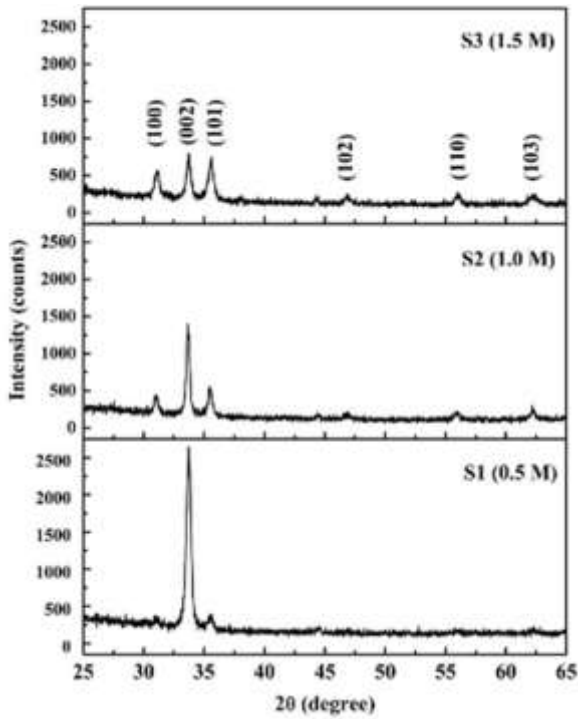


Figure 4. XRD result of ZnO thin film coating taken from the literature.



Figure 5. Device showing the ambient conditions under which the PS-ZnO heterostructure is left to age.

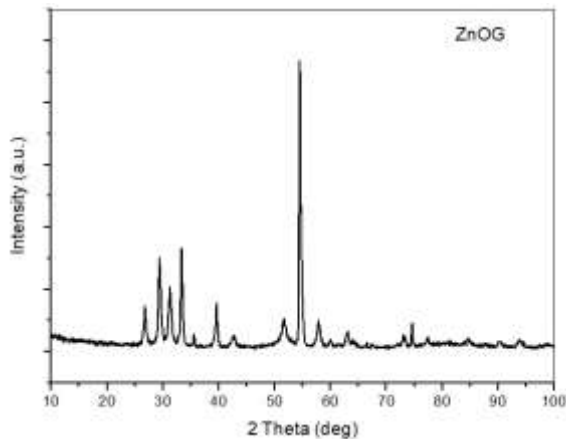


Figure 6. XRD results of PS-ZnO heterojunction kept in dark environment at 23.4 °C and 55% humidity for 1 year.

Figure 7 illustrates the absorption and reflectance graphs of a 1-year aged and unaged PS-ZnO heterojunction, measured using a Shimadzu UV-3600 Plus UV-VIS-NIR Spectroscopy device. In Figure 7(a), the absorption percentage (~12%) of the unaged sample is higher than the absorption percentage (~8%) of the 1-year aged sample, whereas the reflectivity shows the opposite trend. The reflection percentage (~4%) of the unaged sample is smaller than that (~6%) of the 1-year aged sample, as shown in Figure 7(b).

For optimal photodetector performance, high absorption and low reflectivity are desirable. Efficient operation relies on capturing light at a high rate, while minimizing the rate of reflection. As shown in Figure 7, aging adversely affects the optical performance of the photodetector. Given that PS-ZnO heterojunction photodetectors operate in the UV region, particular attention was paid to investigating the UV region.

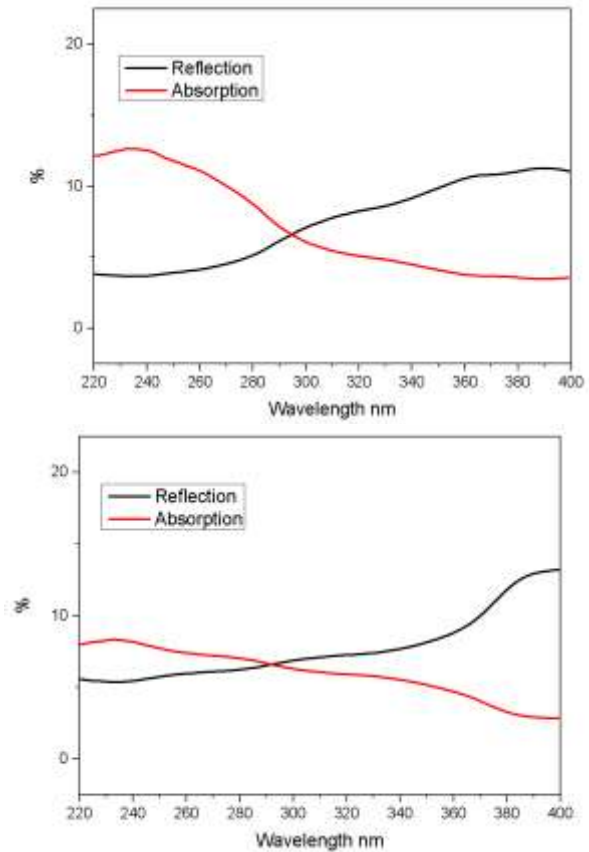


Figure 7. Absorption and reflectance graphs of PS-ZnO heterojunction (a) unaged PS-ZnO heterojunction (b) aged for 1 year at 23.4 °C and 55% humidity in the dark.

4. Conclusion

While the ZnO peaks dominate in Figure 3, it is evident that the PS peak becomes more prominent, as shown in Figure 6. This indicates a transition in the crystal structures of the films from a single to polycrystalline nature over time (Keskenler et al., 2017). In other words, time-dependent depressions and agglomerations manifest in the structure, leading to a decrease in the intensity over time (Wojtasik et al., 2023). This results in

deterioration of the homogeneity within the structure. For semiconductor devices, maintaining homogeneity is crucial for a stable operation.

As shown in Figure 7, UV measurements were conducted to investigate the effect of aging on the optical properties of the photodetector in the PS-ZnO heterojunction. The measurements revealed that aging decreased the optical performance of the photodetector.

Considering these observations, studies focusing on delaying aging, which is a critical factor in determining the working life of devices, hold promise.

Author Contributions

The percentage of the author(s) contributions is presented below. All authors reviewed and approved the final version of the manuscript.

	S.K.	M.G.B.
C		100
D		100
S		100
DCP	100	
DAI	100	
L		100
W		100
CR		100
SR		100
PM		100
FA		100

C=Concept, D= design, S= supervision, DCP= data collection and/or processing, DAI= data analysis and/or interpretation, L= literature search, W= writing, CR= critical review, SR= submission and revision, PM= project management, FA= funding acquisition.

Conflict of Interest

The authors declared that there is no conflict of interest.

Ethical Consideration

Ethics committee approval was not required for this study because of there was no study on animals or humans.

Acknowledgements

This work was supported by 2211-A Tübitak and Erzurum Technical University 2021/017 BAP. The authors thank Kamer Özge Erişmiş for her assistance during the earlier stages of this study.

References

Amara S, Slama IB, Mrad I, Rihane N, Khemissi W, El Mir L, Sakly M. 2014. Effects of zinc oxide nanoparticles and/or zinc chloride on biochemical parameters and mineral levels in rat liver and kidney. *Human Exp Toxicol*, 33(11): 1150-1157.

Amudhavalli B, Mariappan R, Prasath M. 2023. Low-cost nebulizer spray deposited conduction mechanism of thin film ZnO nanoparticles. *J Ovonic Res*, 19(1): 53-63.

An J, Le TSD, Lim CHJ, Tran VT, Zhan Z, Gao Y, Kim YJ. 2018. Single-step selective laser writing of flexible photodetectors for wearable optoelectronics. *Adv Sci*, 5(8): 1800496.

Ates ES, Kucukyildiz S, Unalan HE. 2012. Zinc oxide nanowire photodetectors with single-walled carbon nanotube thin-film electrodes. *ACS Appl Mater Interfaces*, 4(10): 5142-5146.

Avasthi S, McClain WE, Man G, Kahn A, Schwartz J, Sturm JC. 2013. Hole-blocking titanium-oxide/silicon heterojunction and its application to photovoltaics. *Appl Physics Lett*, 102: 203901.

Bacquian BCS, Gomez FRI. 2019. A study of wafer backgrinding tape selection for SOI wafers. *J Eng Res Rep*, 6(2): 1-6.

Bakkars EP, Borgström MT, Verheijen MA. 2007. Epitaxial growth of III-V nanowires on group IV substrates. *Mrs Bull*, 32(2): 117-122.

Belaid H, Nouiri M, Sayari A, Ben Ayadi Z, Djessas K, El Mir L. 2015. Structural and electrical characterizations of ZnO: In/PS/Si heterojunction deposited by rf-magnetron sputtering. *J Electroceramics*, 35: 141-147.

Bloem J. 1979. Gas phase diffusion and surface reactions in the chemical vapour deposition of silicon. Pergamon, 1979: 435-447.

Boruah BD, Ferry DB, Mukherjee A, Misra A. 2015. Few-layer graphene/ZnO nanowires based high performance UV photodetector. *Nanotechnol*, 26(23): 235703.

Chang S, Ju BK, Yakuphanoglu F. 2012. Ultraviolet and visible light detection characteristics of amorphous indium gallium zinc oxide thin film transistor for photodetector applications. *Int J Adv Smart Converg*, 1: 61-64.

Chang WC, Su SC, Wu, CC. 2016. The development of high-density vertical silicon nanowires and their application in a heterojunction diode. *Materials*, 9(7): 534.

Chen C, Zhou P, Wang N, Ma Y, San H. 2018. UV-assisted photochemical synthesis of reduced graphene oxide/ZnO nanowires composite for photoresponse enhancement in UV photodetectors. *Nanomaterials*, 8(1): 26.

Chikkanna MM, Neelagund SE, Rajashekarappa KK. 2019. Green synthesis of zinc oxide nanoparticles (ZnO NPs) and their biological activity. *SN Appl Sci*, 1: 1-10.

Ciolan MA, Motrescu I. 2022. Pulsed laser ablation: A facile and low-temperature fabrication of highly oriented n-type zinc oxide thin films. *App Sci*, 12(2): 917.

Colinge JP. 1998. Silicon-on-Insulator Technology: Past Achievements and Future Prospects. *MRS Bull*, 23(12): 16-19.

Cui LF, Ruffo R, Chan CK, Peng H, Cui Y. 2009. Crystalline-amorphous core-shell silicon nanowires for high capacity and high current battery electrodes. *Nano Lett*, 9(1): 491-495.

Czekalla C, Nobis T, Rahm A, Cao B, Zúñiga-Pérez J, Sturm C, Grundmann M. 2010. Whispering gallery modes in zinc oxide micro-and nanowires. *Physica Status Solidi (b)*, 247(6): 1282-1293.

De Matteis D, De Luca M, Fadaly EM, Verheijen MA, López-Suárez M, Rurali R, Zardo I. 2020. Probing lattice dynamics and electronic resonances in hexagonal Ge and Si x Ge1-x alloys in nanowires by raman spectroscopy. *ACS Nano*, 14(6): 6845-6856.

Devasia S, Athma PV, Raphael R, Jose A, Anila EI. 2021. Effect of source-substrate distance on transparent electrode properties of the spray-cast aluminium doped zinc oxide thin films. *Res Square*, <https://doi.org/10.21203/rs.3.rs-230292/v1>

Dheivamalar S, Banu KB. 2019. A DFT study on functionalization of acrolein on Ni-doped (ZnO) 6 nanocluster in dye-sensitized solar cells. *Heliyon*, 5(12): e02903.

Dong R, Bi C, Dong Q, Guo F, Yuan Y, Fang Y, Huang J. 2014. An ultraviolet-to-NIR broad spectral nanocomposite photodetector with gain. *Adv Optical Mater*, 2(6): 549-554.

- Garvey S, Holmes JD, Kim YS, Long B. 2020. Vapor-phase passivation of chlorine-terminated Ge (100) using self-assembled monolayers of hexanethiol. *ACS Appl Mater Interfaces*, 12(26): 29899-29907.
- Gebrehiwot K. 2017. Synthesis and characterization of zinc cobalt sulphide (Zn_xCo_{1-x}S) by chemical bath deposition method from acidic bath. PhD thesis, Hawassa University, Addis Ababa, Ethiopia, pp: 148.
- Gomes UP, Kuldeep RK, Rathi S, Biswas D. 2011. A strategic review on growth of InP on silicon substrate for applications in high frequency RF devices. *Int J Electron*, 1: 1-6.
- Gör M, Karacalı T. 2017. Porous Silicon Based Membrane Fabrication for Proton Transportation. 13th Nanoscience & Nanotechnology Conference; Antalya, Türkiye, pp: 52.
- Guo A, Zhang L, Cao N, Lu T, Zhu Y, Tian D, Zhao F. 2023. Pulsed laser deposition of ZnGa₂O₄ thin films on Al₂O₃ and Si substrates for deep optoelectronic devices applications. *Appl Physics Express*, 16(2): 021004.
- Guo TF, Chang SC, Pyo S, Yang. 2002. Vertically integrated electronic circuits via a combination of self-assembled polyelectrolytes, ink-jet printing, and electroless metal plating processes. *Langmuir*, 18(21): 8142-8147.
- Habibi MH, Askari E. 2011. The effect of operational parameters on the photocatalytic degradation of CI reactive yellow 86 textile dye using manganese zinc oxide nanocomposite thin films. *J Adv Oxidat Technol*, 14(2): 190-195.
- Hanawa T, Takahashi H, Ota M, Pinizzotto RF, Ferracane JL, Okabe T. 1987. Surface characterization of amalgams using X-ray photoelectron spectroscopy. *J Dental Res*, 66(9): 1470-1478.
- He J, Xu P, Zhou R, Li H, Zu H, Zhang J, Wang F. 2022. Combustion synthesized electrospun InZnO nanowires for ultraviolet photodetectors. *Adv Electronic Mater*, 8(4): 2100997.
- Hoffmann RC, Sanctis S, Liedke MO, Butterling M, Wagner A, Njel C, Schneider JJ. 2021. Zinc oxide defect microstructure and surface chemistry derived from oxidation of metallic zinc. Thin film transistor and sensoric behaviour of zno films and rods. *Chemistry–A Eur J*, 27(17): 5312-5312.
- Huang JH, Tan RQ, Li J, Zhang YL, Yang Y, Song WJ. 2011. Thermal stability of aluminum doped zinc oxide thin films. *Mater Sci Forum*, 685: 147-151.
- Indluru A, Alford TL. 2009. Effect of Ag thickness on electrical transport and optical properties of indium tin oxide–Ag–indium tin oxide multilayers. *J Appl Physics*, 105(12): 123528.
- Kaningini AG, Azizi S, Sintwa N, Mokalane K, Mohale KC, Mudau FN, Maaza M. 2022. Effect of optimized precursor concentration, temperature, and doping on optical properties of ZnO nanoparticles synthesized via a green route using bush tea (*Athrixia phylicoides* DC.) leaf extracts. *ACS Omega*, 7(36): 31658-31666.
- Kappertz O, Drese R, Wuttig M. 2002. Correlation between structure, stress and deposition parameters in direct current sputtered zinc oxide films. *J Vacuum Sci Technol A: Vacuum Surf Films*, 20(6): 2084-2095.
- Karacalı T. 2003. Darbeli anodizasyon tekniği ile gözenekli ve Si tabanlı fabry-perot yapılarının üretimi: Yapısal ve optik özelliklerinin incelenmesi. Doktora Tezi, Atatürk Üniversitesi. Fen Bilimleri Enstitüsü, Erzurum, Türkiye: ss: 129.
- Keskenler EF, Turgut G, Keskenler MF. 2017. Characterization of ZnO thin films grown by sol-gel spin coating technique regarding precursor solution. *Turkish J Mater*, 2(1): 25-30.
- Khan R, Inam MA, Iqbal MM, Shoaib M, Park DR, Lee KH, Yeom IT. 2018. Removal of ZnO nanoparticles from natural waters by coagulation-flocculation process: influence of surfactant type on aggregation, dissolution and colloidal stability. *Sustainability*, 11(1): 17.
- Kim CJ, Kim S, Lee JH, Park JS, Kim S, Park J, Chung UI. 2009. Amorphous hafnium-indium-zinc oxide semiconductor thin film transistors. *Appl Physics Lett*, 95: 252103.
- Konstantinidis S, Hemberg A, Dauchot JP, Hecq M. 2007. Deposition of zinc oxide layers by high-power impulse magnetron sputtering. *J Vacuum Sci Technol B: Microelectroni Nanometer Struct Proces Measur Phenomena*, 25(3): L19-L21.
- Kuo SY, Lin WT, Chang LB, Jeng MJ, Lu YT, Hu SC. 2009. Effects of growth parameters on surface-morphological, structural, electrical and optical properties of AZO films by RF magnetron sputtering. *MRS Online Proc Library*, 1201: H05.
- Lee E, Kim DH, Kim HW, Denlinger JD, Kim H, Kim J, Kang JS. 2016. The 7× 1 Fermi surface reconstruction in a two-dimensional f-electron charge density wave system: PrTe₃. *Sci Rep*, 6(1): 30318.
- Lioudakis E, Othonos A, Lioutas CB, Vouroutzis N. 2008. Transient photoinduced absorption in ultrathin as-grown nanocrystalline silicon films. *Nanoscale Res Lett*, 3: 1-5.
- Liu Q, Gong M, Cook B, Thapa P, Ewing D, Casper M, Wu J. 2017. Oxygen plasma surface activation of electron-depleted ZnO nanoparticle films for performance-enhanced ultraviolet photodetectors. *Physica Status Solidi (a)*, 214(11): 1700176.
- Masaud TB, Jaberansary E, Bagnall DM, Chong HMH. 2011. Silicon electro-optic switch based on n-ZnO/p-Si heterojunction structure. 8th IEEE International Conference on Group IV Photonics, September 14-16, London, UK, pp: 136-138.
- Matysiak W, Tański T, Zaborowska M. 2018. Manufacturing process and optical properties of zinc oxide thin films as photoanode in DSSC. *J Achiev Mater Manufact Eng*, 86(1): 33-40.
- Mayer JW. 1984. Gold contacts to semiconductor devices. *Gold Bull*, 17: 18-26.
- Mendoza-Aguero N, Agarwal V, Villafan-Vidales HI, Campos-Alvarez J, Sebastian PJ. 2015. A heterojunction based on macro-porous silicon and zinc oxide for solar cell application. *J New Mater Electrochem Syst*, 18(4): 225.
- Mishra PN, Pathak D, Mishra PK, Kumar V. 2022. Low-cost processing of pure and Al-doped capped ZnO nano powder for industry scale applications. *Chalcogenide Lett*, 19(1): 19-31.
- Mohsenzadeh S, Moosavian SS. 2017. Zinc sulphate and nano-zinc oxide effects on some physiological parameters of *Rosmarinus officinalis*. *Amer J Plant Sci*, 8(11): 2635-2649.
- Nayak AP, Lin TC, Islam MS. 2012. UV and oxygen sensing properties of ZnO nanowires grown on glass using ultrasound. *Nanosci Nanotechnol Lett*, 4: 977-982.
- Nayak PK, Hedhili MN, Cha D, Alshareef HN. 2013. Impact of soft annealing on the performance of solution-processed amorphous zinc tin oxide thin-film transistors. *ACS Appl Mater Interf*, 5(9): 3587-3590.
- Nazir S, Zaka M, Adil M, Abbasi BH, Hano C. 2018. Synthesis, characterisation and bactericidal effect of ZnO nanoparticles via chemical and bio-assisted (*Silybum marianum* in vitro plantlets and callus extract) methods: a comparative study. *IET Nanobiotechnol*, 12(5): 604-608.
- Park KH, Sun PF, Kang EH, Han GD, Kim BJ, Jang Y, Park HD. 2021. Photocatalytic anti-biofouling performance of nanoporous ceramic membranes treated by atomic layer deposited ZnO. *Separ Purificat Technol*, 272: 118935.
- Peng YY, Lu KJ, Sui WQ. 2010. A 7-to 14-GHz GaAs pHEMT LNA with 1.1 dB noise figure and 26 dB gain. *Microw Optic Technol Lett*, 52(11): 2615-2617.

- Periasamy S, Venkidusamy S, Venkatesan R, Mayandi J, Pearce J, Selj JH, Veerabahu R. 2017. Micro-Raman scattering of nanoscale silicon in amorphous and porous silicon. *Zeitschrift für Physikalische Chemie*, 231(9): 1585-1598.
- Piticescu RR, Piticescu RM, Monty CJ. 2006. Synthesis of Al-doped ZnO nanomaterials with controlled luminescence. *J Eur Ceramic Soc*, 26(14): 2979-2983.
- Rodríguez-Báez J, Maldonado A, Castañeda L, Delgado GT, Castanedo-Pérez R, Olvera MDLL. 2007. On the effect of acetic acid on physical properties of chemically sprayed fluorine-doped ZnO thin films. *Thin Solid Films*, 515(24): 8689-8694.
- Schlupp P, Von Wenckstern H, Grundmann M. 2013. Amorphous zinc-tin oxide thin films fabricated by pulsed laser deposition at room temperature. *MRS Online Proc Library*, 1633: 101-104.
- Sellers SP, Miles BA, Sievers RE, Halverson W. 2000. The production of thin metal oxide films by spray pyrolysis using supercritical CO₂-assisted aerosolization of aqueous solutions. *KONA Powder Part J*, 18: 74-80.
- Sharifi H, Mohammadi S. 2008. Self-aligned wafer-level integration technology with an embedded faraday cage for substrate crosstalk suppression. *Microw Optical Technol Lett*, 50(3): 829-832.
- Shuchen H, Liu GF, Koel BE. 2008. Real-time scanning tunneling microscopy observations of the oxidation of a Ti/Pt (111)-(2x2) surface alloy using O (sub 2) and NO (sub 2). *J Vacuum Sci Technol A, Int J Devoted Vacuum Surfaces Films*, 26(5): 21192429.
- Sieval AB, Opitz R, Maas HP, Schoeman MG, Meijer G, Vergeldt FJ, Sudhölter EJ. 2000. Monolayers of 1-alkynes on the H-terminated Si (100) surface. *Langmuir*, 16(26): 10359-10368.
- Sirkeli VP, Yilmazoglu O, Hajo AS, Nedeoglo ND, Nedeoglo DD, Preu S, Hartnagel HL. 2018. Enhanced Responsivity of ZnSe-Based Metal-Semiconductor-Metal Near-Ultraviolet Photodetector via Impact Ionization (Phys. Status Solidi RRL 2/2018). *Physica Status Solidi*, 12(2): 1870305.
- Subramanian AZ, Ryckeboer E, Dhakal A, Peyskens F, Malik A, Kuyken B, Baets R. 2015. Silicon and silicon nitride photonic circuits for spectroscopic sensing on-a-chip. *Photonics Res*, 3(5): B47-B59.
- Syu JC, Hsu MH, Chang SP, Chang SJ, Lu L. 2018. Effect of oxygen vacancy ratio on a GaZTO solar-blind photodetector. *Coatings*, 8(9): 293.
- Tian C, Jiang D, Li B, Lin J, Zhao Y, Yuan W, Qin J. 2014. Performance enhancement of ZnO UV photodetectors by surface plasmons. *ACS Appl Mater Interf*, 6(3): 2162-2166.
- Tyagi M, Tomar M, Gupta V. 2012. PN junction of NiO thin film for photonic devices. *IEEE Electron Device Lett*, 34(1): 81-83.
- Wasim M, Khan MR, Mushtaq M, Naeem A, Han M, Wei Q. 2020. Surface modification of bacterial cellulose by copper and zinc oxide sputter coating for UV-resistance/antistatic/antibacterial characteristics. *Coatings*, 10(4): 364.
- Weichelt F, Emmeler R, Flyunt R, Beyer E, Buchmeiser MR, Beyer M. 2010. ZnO-Based UV nanocomposites for wood coatings in outdoor applications. *Macromol Mater Eng*, 295(2): 130-136.
- Westerveld WJ, Pozo J, Harmsma PJ, Schmits R, Tabak E, van den Dool TC, Yousefi M. 2012. Characterization of a photonic strain sensor in silicon-on-insulator technology. *Optics Lett*, 37(4): 479-481.
- Widyastuti E, Hsu JL, Lee YC. 2022. Insight on photocatalytic and photoinduced antimicrobial properties of ZnO thin films deposited by HiPIMS through thermal oxidation. *Nanomater*, 12(3): 463.
- Wojtasik K, Zięba M, Tyszkiewicz C, Pakieła W, Żak G, Jeremiasz O, Karasiński P. 2023 Zinc oxide films fabricated via sol-gel method and dip-coating technique-effect of sol aging on optical properties, morphology and photocatalytic activity. *Materials*, 16(5): 1898.
- Won E, Choi JH, Ha H, Hyun HJ, Kim HJ, Park H. 2007. Fabrication of analog electronics for serial readout of silicon strip sensors. *ArXiv*, 0704.1334.
- Yaklin MA, Schneider DA, Norman K, Granata JE, Staiger CL. 2010. Impacts of humidity and temperature on the performance of transparent conducting zinc oxide. 35th IEEE Photovoltaic Specialists Conference, June 20-25, Honolulu, US, pp: 002493-002496.
- Yedurkar S, Maurya C, Mahanwar P. 2016. Biosynthesis of zinc oxide nanoparticles using ixora coccinea leaf extract-A green approach. *Open J Synthes Theory Appl*, 5: 1-14.
- Yusoff MZM, Hassan Z, Woei CC, Ahmad A, Yusof Y, Abd Rahim AF. 2012. The study of GaN pn-junction grown on Si substrate by MBE with Ni/Ag as ohmic contact. *IEEE Symposium on Business, Engineering and Industrial Applications*, September 23-26, Bandung, Indonesia, pp: 37-39.
- Zhong YL, Bernasek SL. 2011. Mild and efficient functionalization of hydrogen-terminated Si (111) via sonochemical activated hydrosilylation. *J Amer Chem Soc*, 133(21): 8118-8121.
- Zuo J, Erbe A. 2010. Optical and electronic properties of native zinc oxide films on polycrystalline Zn. *Physical Chem Chem Physics*, 12(37): 11467-11476.



PROTEİN KAYNAKLARININ İN VİTRO OLGUNLAŞTIRILMIŞ SIĞIR OOSİTLERİNİN GLUTATYON PEROKSİDAZ ENZİM AKTİVİTESİ ÜZERİNE ETKİSİ

Nisa Nur YILMAZ^{1*}

¹Ondokuz Mayıs University, Agricultural Faculty, Department of Agricultural Biotechnology, 55139, Samsun, Türkiye

Özet: Bu çalışma, siğir oositlerinin in vitro olgunlaştırma (IVO)'sında kültür medyumuna ilave edilen protein kaynaklarının glutatyon peroksidaz (GPx) enzim aktivitesi üzerine etkisinin belirlenmesi amacıyla yapılmıştır. Siğir ovaryumlarından elde edilen oositler %10 fetal buzağı serum (FBS), 4 mg/mL siğir serum albümin (SSA), 1 mg/mL polivinil alkol (PVA) içeren ve protein kaynağı içermeyen bikarbonat tamponlu doku kültür medyumlarında (TCM-199) 38,5 °C sıcaklıkta ve %5 CO₂ içeren nemlendirilmiş ortamda 22 saat IVO'ya alınmıştır. Olgunlaşma süresi sonunda elde edilen kumulus-oosit kompleksleri (KOK'ler), kumulus hücrelerinden ayırmak için işleme tabi tutulmuştur. Kumulus hücrelerinden ayrılan oositler, polivinil alkol içeren ve Ca²⁺ ve Mg²⁺ içermeyen fosfat tamponlu tuz çözeltisi (PBS) ile yıkanmıştır. Daha sonra, oositler belirlenmiş örnek boyutlarına bölünerek mikrotüplerde saklanmıştır. IVO kültürü sonrasında oositlerdeki glutatyon peroksidaz (GPx) enzim aktivitesi için ticari kit kullanarak 340 nm dalga boyunda spektrofotometrik olarak belirlenmiştir. Çalışmada, her bir deneme grubundaki oositlerden izole edilen hücre ekstraktlarındaki GPx enzim aktivitesinin seviyelerinin zamanla değişmediği, kültür medyumuna PVA eklenmiş oositlerinde GPx enzim aktivitesinin diğer deneme gruplarındaki oositlerden daha düşük olduğu tespit edilmiştir (P>0,05). Bu çalışma sonucunda farklı protein kaynaklarının antioksidan aktivitenin göstergelerinden biri olan GPx enzim seviyelerinin siğir oositlerinde üzerine etkileri belirlenmiş ve FBS ve BSA'nın protein kaynağı olarak siğir oosit gelişimi üzerine daha etkili olabileceği tespit edilmiştir.

Anahtar kelimeler: Oosit, Siğir, Antioksidan aktivitesi, Protein, Olgunlaşma


Effect of Protein Sources on Glutathione Peroxidase Enzyme Activity of In Vitro Matured Bovine Oocytes

Abstract: This study was conducted to determine the effect of protein sources added to the culture media during in vitro maturation (IVM) on the glutathione peroxidase (GPx) enzyme activity of bovine oocytes. Oocytes obtained from bovine ovaries were IVM cultured in bicarbonate buffered tissue culture media (TCM-199) containing 10% fetal calf serum (FBS), 4 mg/mL bovine serum albumin (SSA), 1 mg/mL polyvinyl alcohol (PVA) and without protein source for 22 hours in a humidified environment containing 38.5 °C and 5% CO₂. Following the maturation period, cumulus-oocyte complexes (COCs) obtained were subjected to a procedure to separate the cumulus cells from the oocytes. The oocytes separated from the cumulus cells were washed with phosphate-buffered saline (PBS) containing polyvinyl alcohol and devoid of Ca²⁺ and Mg²⁺. Subsequently, the oocytes were divided into predetermined sample sizes and stored in microtubes for further processing. After IVM culture, using a commercial kit, glutathione peroxidase (GPx) enzyme activity in oocytes was determined spectrophotometrically at a wavelength of 340 nm. In the study, the levels of GPx enzyme activity in the cell extracts isolated from the oocytes in each experimental group did not change over time, and the GPx enzyme activity in the oocytes with PVA added to the culture medium was lower than the oocytes in the other experimental groups (P>0.05). As a result of this study, the effects of different protein sources on GPx enzyme levels, one of the indicators of antioxidant activity in bovine oocytes, were determined, and FBS and BSA, as protein sources, could be more effective on bovine oocyte development.

Keywords: Oocyte, Bovine, Antioxidant activity, Protein, Maturation

*Sorumlu yazar (Corresponding author): Ondokuz Mayıs University, Agricultural Faculty, Department of Agricultural Biotechnology, 55139, Samsun, Türkiye

E mail: nisanyilmaz06@gmail.com (N. N. YILMAZ)

Nisa Nur YILMAZ  <https://orcid.org/0000-0002-8675-9709>

Gönderi: 19 Şubat 2024

Kabul: 08 Mayıs 2024

Yayınlanma: 15 Mayıs 2024

Received: February 19, 2024

Accepted: May 08, 2024

Published: May 15, 2024

Cite as: Yılmaz NN. 2024. Effect of protein sources on glutathione peroxidase enzyme activity of in vitro matured bovine oocytes. *BSJ Eng Sci*, 7(3): 575-579.

1. Giriş

Hücre için ATP üretimi, oksidatif metabolizmanın bir yan ürünü olarak gerçekleşir; ancak bu metabolik aktivitenin bir sonucu olarak istenmeyen serbest oksijen radikalleri (SOR) de üretilir (Sen ve Kuran, 2018; Sen, 2021; Sen ve ark., 2022). SOR üretimi, oksidatif metabolizma hızına bağlı olarak değişebilir ve yüksek metabolik aktivite, SOR üretimini artırabilir (Sturmey ve ark., 2009). Yüksek SOR miktarları, hücresel enzimlerin etkisiz hale gelmesine, membran lipid peroksidasyonuna ve embriyo

hücrelerinde DNA hasarına yol açabilir (Halliwell, 1996). Hücresel hasar, metabolik aktivitenin artmasına ve daha fazla besin tüketimi ile daha fazla SOR üretimine neden olarak apoptoza yol açabilmektedir (Sturmey ve ark., 2009). Oositlerin in vitro olgunlaştırılması sırasında kullanılan medyumların çoğu, olgunlaşmayı desteklemek için bir protein kaynağı içerir. Örneğin, siğir oositlerin in vitro olgunlaşmasında siğir serum albümin, fetal buzağı serumu ve gibi çeşitli protein kaynaklarının eklenmesi neredeyse zorunlu olarak bildirilmiştir (Sen, 2015;



Kocyyigit ve ark., 2015). Yapılan çalıřmalar, in vitro kùltür ortamına eklenen protein kaynaklarının oosit ve embriyo üzerinde toksik etkisi olan maddelerin olumsuz etkilerini azaltabileceğini, SOR'lara karşı bir savunma oluşturarak hücrel bileřenleri koruyabileceğini ve redoks potansiyelini düzenleyebileceğini göstermiştir (Flood ve Shirley, 1991; Koçyigit ve ark., 2015). Protein ilavesinin aynı zamanda oosit olgunlaşmasını destekleyen büyüme faktörlerini sağlayabileceğini bildirilmiştir (Koçyigit ve ark., 2015). Dolayısıyla bu çalıřma, farklı protein kaynaklarının in vitro oosit olgunlaşma kùltürlerine eklenmesinin, hücrel antioksidan aktivitenin bir göstergesi olan glutasyon peroksidaz enzim seviyelerini nasıl etkileyebileceğini anlamayı amaçlamaktadır. Ayrıca, hangi protein kaynağının sığır oositlerinin olgunlaşmasında daha etkili bir antioksidan aktivite sağlayabileceğini belirlemeye yardımcı olacaktır.

2. Materyal ve Yöntem

2.1. Kumulus-Oosit Komplekslerinin (KOK) Elde Edilmesi

Sığır ovaryumları, yerel bir mezbahadan (Florya A.Ş.) kesim sonrasında temin edildi. Çalıřma süresince toplam 50 ovaryumdan 200 oosit elde edildi. Ovaryumlar, kesimden sonra yaklaşık 2 ila 3 saat içinde, 35-37 °C sıcaklıkta 0,9% NaCl (S5886; w/v) içeren ve 0,1% v/v antibiyotik çözeltisi (A5955; mL başına 10.000 IU penisilin, 10 mg streptomisin ve 25 µg amfoterisin B) eklenmiş bir ortamda laboratuvara nakledildi. 2 ila 8 mm çapındaki follüküllerden 18 gauge iğneye baėlı 10 mL'lik tek kullanımlık bir şırınga kullanılarak kumulus-oosit kompleksleri (KOK'ler) elde edildi (Şekil 1). KOK'ler, %1 v/v antibiyotik-antimikotik çözeltisi ile 100 µg/mL L-glutamin ilave edilen Hepes-modifiye ticari kùltür medyumu (H-TCM-199; M7528) içinde birkaç kez yıkandı. KOK'ler morfolojik olarak incelendi ve sadece atretik olmayan kümüslü yapısına, kompakt ve düzenli granüle edilmiş sitoplazmaya sahip olanlar IVO için seçildi (Şekil 1) (Sen, 2022).

2.2. İn Vitro Oosit Olgunlaştırması

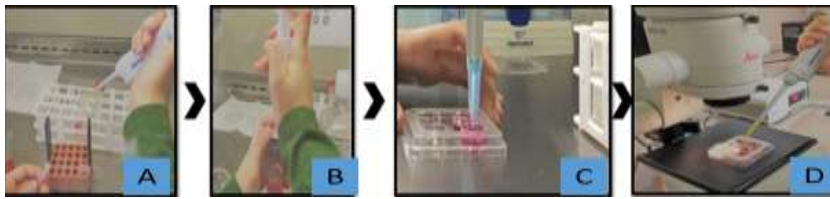
Sığır oositlerinin IVO kùltürü Sen (2021)'in önerdiği şekilde gerçekleştirilmiştir (Şekil 2). IVO kùltür medyumu, Earle tuzları ve L-glutamin takviyeli, 5,5 µg/mL sodyum piruvat, %1 v/v antibiyotik-antimikotik solüsyon içeren ve sodyum bikarbonat tamponlu ticari doku kùltürü medyumundan (TCM-199; M4530) hazırlandı. Seçilen KOK'lar, üç kez H-TCM-199 kùltür medyumunda yıkandı ve ardından rastgele sığır oositi olgunlaştırma kùltür gruplarına dağıtıldı. Sığır oositi olgunlaştırma kùltür grupları; (a) IVO + 4 mg/mL BSA , (b) IVO + %10 FCS , (c) IVO + 1 mg/mL PVA ve (d) makromolekül takviyesi olmayan şekilde oluşturulmuştur. Kùltürde olgunlaştırma medyumundan dört göznlü petrinin (Nunc, Roskilde, Danimarka) her bir kuyucuğuna 500 mL aktarılmış ve üzeri 300 mL mineral yaė (Sigma M-5904) ile kapatılıp ısınması ve gazlanması için inkübatöre bırakılmıştır. Her bir ortam grubundaki KOK'lar 38,5 °C'de, %5 CO₂ ve %95 oranında nem içeren atmosferde 22 saat süreyle kùltüre alınmışlardır (Cevik ve ark., 2011; Sen ve Kuran, 2018).

2.3. Glutasyon Peroksidaz (GPx) Enzim Aktivitesi

Olgunlaşma süresi sonunda KOK'lar, 2 defa H-TCM-199'da yıkandıktan sonra 1,5 ml'lik endorf tüplerin içerisine alınıp etrafını saran kumulus hücrelerinden ayırmak için 5 dakika vortekslenmişlerdir (Labart Multi-Mixer). Kumulus hücrelerinden ayrılan ve çıplak kalan oositler 1 mg/ml polivinil alkol ilaveli Ca²⁺ ve Mg²⁺ içermeyen fostat tamponlu tuz çözeltisi (PBS) içerisinde 3 kez yıkandı ve 10 µl PBS içinde 25 adet oosit olacak şekilde GPx enzim aktivite analizine kadar -80°C'de mikrotüplerde depolanmıştır. Analiz güzünü çözdürülen örnekler enzimatik ekstraksiyon için 50W'de 2 dakika süreyle sonikasyona tabi tutulmuştur (Sen ve ark., 2022). Daha sonra örneklerin her birinden 50 µl alınmış ve 2M 1X Assay Buffer (50 mM Tris-HCl, pH 7,6, 5 mM EDTA) ve 2 µl DTT solüsyonunda 15 dakika boyunca buz içerisinde inkübe edilmiştir. Her bir numune 3 tekrarlamalı olarak 30 saniye aralıklarla vorteks edilmiştir. Numuneler 4°C'de 15 dakika boyunca 10.000 x g' de santrifüj edilmiştir.



Şekil 1. Oositlerin enjektör yardımı ile aspire edilmesi ve değerlendirilmesi.



Şekil 2. A) Olgunlaşma medyumuna protein kaynaklarının eklenmesi. B) Olgunlaşma medyumunun filtre edilmesi. C) Olgunlaşma medyumunun dört göznlü petri kutusuna alınması. D) Olgunlaşmaya bırakılacak oositlerin dört göznlü petriye alınıp inkübasyona bırakılması.

Süpernantlar pipet yardımı ile alınmıştır. Oositlerin GPx aktivitesi, ticari kit (GSH-Px Assay, Northwest Life Science Specialities, LLC ve Vancouver, WA ABD) kullanılarak üreticinin önerdiği şekilde spektrofotometrik olarak belirlenmiştir. GPx enziminin aktivite tayini UV spektrofotometre (Shimadzu UV-1800) kullanılarak glutasyon dönüşümüne bağlı olarak absorbans artışı 340 nm'de gözlemlenmiştir. Spektrofotometrik yöntemler, Kinatics rate ayarında 340 nm'de ve 3 dakika boyunca yapılmıştır (Sen, 2022).

2.4. İstatistik Analiz

Çalışma boyunca elde edilen veriler Ondokuz Mayıs Üniversitesi lisansı ile kullanılan SPSS 20,0 (2014) paket programı kullanılarak analiz edilmiştir. Farklı protein kaynağı içeren kültür medyumlarında olgunlaştırmaya alınmış sığır oositlerinin GPx enzim aktivitelerine ait verilerinin normallik varsayımı Shapiro Wilk testi ile belirlenmiş ve normal dağılım sergilediği tespit edilmiştir. Ayrıca Verilerin varyans analizine uygunluğu Levente varyans homojenlik testi değerlendirilmiş olup varyansların homojen olduğu (P<0,05) tespit edilmiştir. Deneme gruplarından elde edilen ortalamaların önem seviyesinin karşılaştırılması 0,05 önem düzeyinde Duncan Çoklu Karşılaştırma Testi kullanılarak yapılmıştır (Genç ve Soysal, 2018).

3. Bulgular

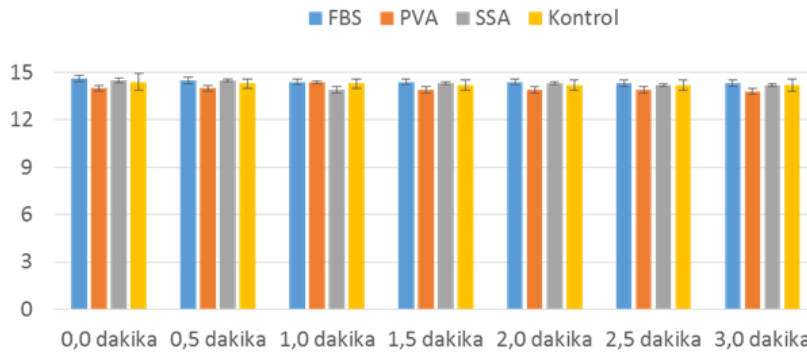
Çalışmada kullanılmak üzere mezbahaneye kesim için getirilen 53 baş sığırdan elde edilen toplam 106 adet ovaryum laboratuvara getirilmiştir. Protein kaynağı olarak fetal buzağı serumu (FBS), sığır serum albumini (SSA) ve polivinil alkol (PVA) eklenmiş kültür medyumlarında in vitro olgunlaştırılan sığır oositlerinin farklı ölçüm zamanlarındaki ve ortalama Glutasyon peroksidaz (GPx) enzim aktiviteleri (nmol/dakika/ml)

sırasıyla Şekil 3 ve Tablo 1'de sunulmuştur. Çalışmada, her bir deneme grubundaki oositlerden izole edilen hücre ekstraktlarındaki GPx enzim aktivitesinin seviyelerinin zamanla değişmediği, fakat kültür medyumuna PVA eklenmiş oositlerinde GPx enzim aktivitesinin diğer deneme gruplarındaki oositlerden daha düşük olduğu tespit edilmiştir (P>0,05).

Olgunlaştırma ortamına eklenen farklı protein kaynaklarının GPx enzim aktivitesi üzerine etkisinin incelenmesi amacıyla farklı protein kaynaklarında olgunlaştırılmaya alınan oosit hücreleri depolanarak numuneler elde edilmiştir. Elde edilen bu numunelerin farklı protein kaynakları üzerine etkisi araştırılmıştır. Yapılan aktivite tayinleri sonucunda elde edilen veriler aşağıdaki şekil 3'te gösterilmiştir.

4. Tartışma ve Sonuç

Sığır oositlerinin in vitro olgunlaşması, embriyo üretimi süreçlerinde kritik bir aşamayı temsil eder ve bu süreç, elde edilen embriyo kalitesi ve üretim verimliliği üzerinde önemli etkilere sahiptir. İn vitro koşullarda oosit olgunlaşması, oositlerin fizyolojik ve biyokimyasal özelliklerini dikkate alan uygun bir çevrenin sağlanmasını gerektirir (Brackett ve Zuelke, 1993; Gordon, 1994). Modern embriyo üretimi süreçlerinde, kültür ortamının bileşimi, oositlerin ve embriyonun gelişimini doğrudan etkileyebilmektedir. Protein kaynaklarının türü, besin madde içeriği ve diğer katkı maddeleri, bu süreçte belirleyici faktörlerdir. Bu süreç, oositlerin ve embriyonun adaptif yanıtlarını tetikleyebilir; çünkü in vitro koşulları, oositlerin doğal çevresinden belirgin şekillerde farklılık gösterebilir ve bu da hücreyel yanıtları etkileyebilir (Sturmey ve ark., 2009).



Şekil 3. İn vitro olgunlaştırma medyumuna farklı protein kaynaklarının eklenen sığır oositlerinin farklı ölçüm zamanlarındaki GPx enzim aktivitesi seviyeleri (nmol/dakika/ml). FBS= fetal buzağı serumu, SSA= sığır serum albumini, PVA= polivinil alkol.

Tablo 1. İn vitro olgunlaştırma medyumuna farklı protein kaynaklarının eklenen sığır oositlerinin ortalama GPx enzim aktivitesi (nmol/dakika/ml). ^{a,b} (P<0,05).

	SSA	FCS	PVA	Control
GPx EA	14,362±0,18 ^a	14,414±0,21 ^a	13,932±0,1 ^b	14,061±0,2 ^{ab}

^{a,b}Aynı satırda farklı harfler ile gösterilen ortalamalar arasındaki fark istatistik olarak önemlidir (P<0,05). GPx EA= glutasyon peroksidaz enzim aktivitesi, FBS= fetal buzağı serumu, SSA= sığır serum albumini, PVA= polivinil alkol.

Oositlerin ve embriyonun biyokimyasal dengesini desteklemek ve olgunlaşma sürecini optimize etmek amacıyla, in vitro embriyo üretimi sürecinde farklı katkı maddelerinin kullanımı yaygın bir yaklaşımdır. Bu bağlamda, FBS, BSA ve PVA gibi protein kaynakları önemli bir rol oynamaktadır. Bu katkı maddeleri, embriyo kültür ortamının besin içeriğini artırabilmekte ve oositlerin metabolik ihtiyaçlarını karşılamaya yardımcı olabilmektedir. Önceki çalışmalar, bu tür protein ilavelerinin, özellikle pronükleus oluşumu gibi kritik evreleri hızlandırma yeteneğine sahip olduğunu ortaya koymuştur. Ayrıca, FBS, BSA ve PVA'nın in vitro kültür sırasında gen transkript düzeylerini etkileyebildiği ve bu da embriyo gelişim hızı ve kalitesi üzerinde olumlu etkiler yaratabileceği belirtilmiştir (Ali ve Sirard, 2002). Mevcut çalışmada farklı protein kaynaklarının sığır oositlerinde glutatyon peroksidaz (GPx) enzim aktivitesi üzerine etkisinin araştırılmasıdır. GPx, antioksidan savunmanın kritik bir bileşenidir ve hücrelerde reaktif oksijen türlerine (ROS) karşı koruma sağlar. Sığır oositlerinde glutatyon peroksidaz (GPx) enzim aktivitesinin incelenmesi, in vitro embriyo üretimi sürecindeki önemli bir parametreyi değerlendirmeyi amaçlar. GPx enzimi, antioksidan savunmanın kritik bir bileşenidir ve hücrelerde reaktif oksijen türlerine (ROS) karşı koruma sağlar. Oositlerin antioksidan kapasitesi, embriyo kalitesi üzerinde belirleyici bir faktördür çünkü ROS, oositlerin sağlığını, genetik bütünlüğünü ve gelişim potansiyelini olumsuz yönde etkileyebilir. İn vitro koşullarda oosit olgunlaşması süreci, oositlerin döllenmeye hazır hale gelmesini sağlar ve bu süreçte oositlerin çevresel stres faktörlerine karşı direnci önemlidir. Oositler, doğal olarak antioksidan enzimlerle donatılmış olmasına rağmen, in vitro ortamda maruz kalınan stres ve oksidatif hasar, bu antioksidan savunmanın etkinliğini azaltabilir. Bu nedenle, oositlerin antioksidan kapasitesini değerlendirmek ve optimize etmek, başarılı bir in vitro embriyo üretimi süreci için kritik öneme sahiptir. GPx enzim aktivitesinin incelenmesi, kullanılan kültür ortamının ve protein kaynaklarının oositlerin antioksidan savunmasını nasıl etkilediğini anlamamıza yardımcı olmaktadır (Cetica ve ark., 2001). Bu çalışmanın sonuçları, farklı protein kaynaklarının medyum içeriğine eklenmesinin oositlerin antioksidan kapasitesini nasıl etkileyebileceğine dair önemli bir içgörü sunmaktadır. Elde edilen sonuçlar, her bir deneme grubundan elde edilen oositlerin hücre ekstraktlarında GPx enzim aktivitesinin zaman içinde anlamlı bir değişiklik göstermediğini göstermektedir. Bununla birlikte, PVA eklenmiş medyumlarda yetiştirilen oositlerde GPx enzim aktivitesinin diğer deneme gruplarına kıyasla istatistiksel olarak anlamlı bir şekilde daha düşük olduğu tespit edilmiştir. Bu bulgular, farklı protein kaynaklarının oositlerin in vitro olgunlaşma işlemleri sırasındaki antioksidan kapasitesini etkileyebileceğini göstermektedir. Daha düşük GPx aktivitesi, olgunlaşma ortamına PVA eklenmiş oositlerde gözlenirken, diğer protein kaynaklarının oositlerin

antioksidan savunmasını daha etkili bir şekilde artırabileceği düşünülebilir.

Sonuç olarak, bu çalışma farklı protein kaynaklarının sığır oositlerinin in vitro olgunlaşma süreçlerindeki antioksidan kapasite üzerindeki etkilerini aydınlatarak, in vitro embriyo üretimi süreçlerinin optimize edilmesine ve embriyo kalitesinin artırılmasına yönelik stratejiler geliştirilmesine katkı sağlamaktadır.

Katkı Oranı Beyanı

Yazar(lar)ın katkı yüzdesi aşağıda verilmiştir. Yazar makaleyi incelemiş ve onaylamıştır.

	N.N.Y.
K	100
T	100
Y	100
VTI	100
VAY	100
KT	100
YZ	100
KI	100
GR	100
PY	100
FA	100

K= kavram, T= tasarım, Y= yönetim, VTI= veri toplama ve/veya işleme, VAY= veri analizi ve/veya yorumlama, KT= kaynak tarama, YZ= Yazım, KI= kritik inceleme, GR= gönderim ve revizyon, PY= proje yönetimi, FA= fon alımı.

Çatışma Beyanı

Yazar bu çalışmada hiçbir çıkar ilişkisi olmadığını beyan etmektedirler.

Etik Onay Beyanı

Bu çalışmada hayvanlar ve insanlar üzerinde herhangi bir çalışma yapılmadığı için etik kurul onayı alınmamıştır.

Destek ve Teşekkür Beyanı

Bu çalışma TÜBİTAK 2209/A Üniversite Öğrencileri Araştırma Projeleri Destek Programı kapsamında desteklenmiştir.

Kaynaklar

- Ali A, Sirard MA. 2002. Effect of the absence or presence of various protein supplements on further development of bovine oocytes during in vitro maturation. *Biol Reprod*, 66(4): 901-905.
- Brackett B, Zuelke K. 1993. Analysis of factors involved in the in vitro production of bovine embryos. *Theriogenology*, 39(1): 43-64.
- Cetica PD, Pintos LN, Dalvit GC, Beconi MT. 2001. Antioxidant enzyme activity and oxidative stress in bovine oocyte in vitro maturation. *IUBMB Life*, 51(1): 57-64.
- Cevik M, Kocyigit A, Sen U, Kuran M. 2014. Can commercial human embryo culture media be used in bovine embryo culture? *J Fac Vet Med, Univ Kafkas*, 20(1): 149-153.
- Cevik M, Sen U, Kocyigit A, Soydan E, Kuran M. 2011. Effects of serum, gonadotropins, epidermal growth factor and estradiol

- 17-Beta on cumulus expansion and nuclear maturation of bovine oocytes. *J Fac Vet Med, Univ Kafkas*, 17(6): 1009-1014.
- Flood L, Shirley B. 1991. Reduction of embryotoxicity by protein in embryo culture media. *Molec Reprod Develop*, 30: 226-231.
- Genç S, Soysal Mİ. 2018. Parametric and nonparametric post hoc tests. *BSJ Eng Sci*, 1(1): 18-27.
- Gordon I. 1994. Laboratory production of cattle embryo. Wallingford: CAB International, Newyork, USA, pp: 30-142.
- Halliwell B, Gutteridge J. 1990. Role of free radicals and catalytic metal ions in human disease. An overview *Methods Enzymol*, 186: 1-8.
- Halliwell B. 1996. Antioxidants in human health and disease. *Annu Rev Nutr*, 16: 33-50.
- Kocyigit A, Cevik M, Sen U, Kuran M. 2015. The effect of macromolecule and growth factors combinations on in vitro development of bovine embryos. *Turkish J Vet Anim Sci*, 39: 308-313.
- Sen U, Kuran M. 2018. Low incubation temperature successfully supports the in vitro bovine oocyte maturation and subsequent development of embryos. *Asian-Australas J Anim Sci*, 31(6): 827-834.
- Sen U, Şirin E, Onder H, Özyürek S, Kolenda M, Sitkowska B. 2022. Macromolecules Influence Cellular Competence and Expression Level of IGFs Genes in Bovine Oocytes In Vitro. *Animals*, 12(19), 2604.
- Sen U. 2015. Effects of sperm from different bulls on developmental competence, blastosist quality and cell number of bovine embryos in vitro. *J Fac Vet Med, Univ Kafkas*, 21(3): 339-344.
- Sen U. 2021. Maturation of bovine oocytes under low culture temperature decreased glutathione peroxidase activity of both oocytes and blastocysts. *Polish J Vet Sci*, 24: 93-99.
- Sen U. 2022. In vitro maturation culture temperature alters the enzymatic antioxidant activity of bovine oocytes and embryos. 37th International Conference on "Chemical, Agriculture, Biological & Environmental Sciences", December 12-14, Lisbon, Portugal, pp: 1-4.
- Sturmey RG, Hawkhead JA, Barker EA, Leese HJ. 2009. DNA damage and metabolic activity in the preimplantation embryo. *Hum Reprod*, 24: 81-91.



FORECASTING ROAD FREIGHT AND PASSENGER TRANSPORT DEMANDS IN TÜRKİYE USING THE EXPONENTIAL SMOOTHING

Hümeýra BOLAKAR TOSUN^{1*}


¹Aksaray University, Faculty of Engineering, Department of Civil Engineering, 68100, Aksaray, Türkiye

Abstract: Exponential smoothing is a popular technique used to analyze and forecast trends in various industries such as road transportation and passenger transportation. This method is used to calculate weighted averages using historical data and adjust forecasts based on recent trends. In the Turkish context, forecasting transportation demands using exponential smoothing provides valuable information for transportation planning and resource allocation. The increasing number of vehicles has caused many negative environmental consequences. This study analyzed ten years of data on road freight and passenger transportation on a regional scale in order to make future predictions. In the study, solution suggestions are presented based on the findings and the policies that should be implemented to solve the problem are evaluated.

Keywords: Transportation, Transport demands, Exponential smoothing method, Forecasting

*Corresponding author: Aksaray University, Faculty of Engineering, Department of Civil Engineering, 68100, Aksaray, Türkiye

E mail: bolakarhumeýra@gmail.com (H. BOLAKAR TOSUN)

Hümeýra BOLAKAR TOSUN  <https://orcid.org/0000-0002-6710-2277>

Received: March 06, 2024

Accepted: May 08, 2024

Published: May 15, 2024

Cite as: Bolakar Tosun H. 2024. Forecasting road freight and passenger transport demands in Türkiye using the exponential smoothing. BSJ Eng Sci, 7(3): 580-586.

1. Introduction

Transporting goods and people from one place to another via road vehicles is known as road transport. It is an essential component of the global logistics industry, responsible for moving around 70% of all world trade. The road transport process can be divided into four stages: planning, loading, transportation, and delivery. The planning stage involves taking into account factors such as the quantity and nature of the load, the transport distance, and the delivery date. The type of transport vehicle, cargo packaging, and palletizing are also determined during this stage. Loading is the process of securely placing the load onto the transport vehicle, carried out by loading personnel. Transporting the load from one point to another is then done by the driver. Finally, delivery involves handing over the cargo to the buyer, which is done by the loading personnel. The benefits of road transportation include its convenience, safety, speed, punctuality, and affordability. The advantages of road transportation are:

- Flexibility: Road transportation is more flexible than other types of transportation. Different vehicle types can be used depending on the amount and nature of the load.
- Speed: Road transportation is faster than other types of transportation.
- Cost: Road transportation is cheaper than other types of transportation.
- The disadvantages of road transport are:
- Capacity: Road transportation has less capacity than

other types of transportation.

- Safety: Road transportation can be more dangerous than other types of transportation.
- Environmental impact: Road transportation may create more environmental impact than other types of transportation.

Road transportation is the most widely used type of transportation today because of those advantages (URL1). The transportation sector is the second largest energy consumer sector worldwide and makes a profound contribution to the economy, more obviously in developing countries (He et al., 2020) and (Sharif et al., 2019). The transportation sector around the world also causes an increase in the release of hazardous gases, such as CO₂ emissions in the air, and manufacturers are working to make the transportation sector more sustainable, which will give an alarming signal to this policy (Amin et.al., 2020). The increase and continuous growth of carbon emissions from the transportation sector attract the attention of politicians for sustainable transportation. A sustainable transport system is a key component of sustainable economic growth, providing its citizens with accessibility and mobility in safe and environmentally friendly transport modes (Alshehrya and Belloumia, 2016) and (Özkan et al., 2019). The energy used in road transportation can provide social and economic development, but it can have a negative impact on the environment and cause climate changes on a global scale (Figueroa and Ribeiro, 2013). Many recent studies emphasize that policies that direct transport



towards a low-carbon path should be aligned with sustainable development goals and principles (Amekudzi, 2011). The energy used in road transportation can provide social and economic development, but it is thought to have a negative impact on the environment and cause climate change on a global scale (Edenhofer, 2015). According to the report published by the Organization of Petroleum Exporting Countries, the number of private vehicles used in 2009 is expected to increase from approximately 870 million to 1.76 billion in 2035 (Kahn et al., 2007). According to the same report, this rate in OECD countries will be four times higher than in countries that are still industrializing modeled regional and global car ownership for the year 2100 (Meyer et al., 2012) Global results give a range of 1.4-2.0 billion cars for 2035 and 1.7-2.8 billion cars for 2050. According to studies, making significant transportation policy changes that reduce passenger travel levels themselves is the most effective way to timely and profoundly reduce transportation emissions in existing economies. This study utilized ten-year regional data on road freight and passenger transportation to make future predictions and discuss the results.

2. Materials and Methods

SPSS 21.0 and Eviews 9 software were used to analyze the data. Exponential correction methods were used in the 2023-2025 estimates of vehicle-km, passenger-km and ton-km data obtained from the General Directorate of Highways (KGM). Exponential correction methods are one of the most widely used methods in science. Series that have components that vary over time and that can be expressed with more than one regression curve since there is no regression curve are called stochastic trend series. The exponential smoothing method is known as a method suitable for all series with stochastic and deterministic trends (Yağimli and Ergin, 2017). This trend can create future predictions using historical data with error and seasonality components (Bowerman at al., 1979). Exponentially decreasing data, but predominantly moving average data, are used. As a result of these ideas, the exponential smoothing method produces modeling of different components. Among these components, seasonal changes, trends, and overlapping components in the series at specified intervals are included (Yağimli and Ergin, 2017). Exponential smoothing trend method is known as a minor method of feasible prediction. It is an important way to make predictions when there are only a few observations to base it on. In contrast to constant coefficient regression model predictions, exponential smoothing trend method predictions are adjusted based on past prediction errors (Bowerman at al., 1979). Since annual data between 2013 and 2022 were used in this study, that is, there was no seasonal data, the Holt-Winters exponential smoothing method was used. The method used is suitable for series with no seasonal changes. Additionally, the method used is like the double smoothing method in that it does not include a seasonal

component and produces linearly trending forecasts. The method called the double smoothing method is more discriminative because it uses only one parameter, but this method is a two-parameter method. The smoothed \hat{y}_t series is expressed by the following formula (equation 1):

$$\hat{y}_{t+k} = a + bk \quad (1)$$

In this formula, a and b are defined as the permanent component and the trend. These two coefficients are defined as follows (Equation 2-3):

$$a(t) = \alpha y_t + (1 - \alpha)(a(t - 1) + b(t - 1)) \quad (2)$$

$$b(t) = \beta(a(t) - a(t - 1)) + 1 - \beta b(t - 1) \quad (3)$$

where $0 < \alpha, \beta, \gamma < 1$ are the damping factors. This is a two-parameter exponential smoothing method. Estimates are calculated as given in Equation 4:

$$\hat{y}_{T+k} = a(T) + b(T)k \quad (4)$$

The predictions expressed here lie in the linear trend intersected by the slope. Holt-Winters exponential smoothing model can be applied when both trend and seasonality are present, with the two components being either additive or multiplicative. Winters additive and multiplicative models was extremely high and both additive and multiplicative models (Djakaria and Saleh, 2021; Konarasinghe, 2021). T Non-Seasonal Two-Parameter Holt-Winters are not by addition with or multiplication by $\gamma = 0$. The condition $\gamma = 0$ only restricts the temporal variation of seasonal factors (Bergmeir et al., 2016).

3. Results and Discussion

3.1. Findings Regarding Vehicle-Km Data

Table 1 includes the vehicle-km data of the highways between 2013 and 2022.

According to analyzing the vehicle-km data from Table 1, it is evident that the vehicle-km values have increased between 2013 and 2022. The 1st Region had the highest vehicle-km values in 2013 and 2022, whereas the 6th Region had the lowest vehicle-km values in 2013 and the 9th Region had the lowest values in 2022. Figure 1 depicts the regional level of vehicle-km values on highways from 2013 to 2022.

The data in Table 2 indicates that the largest proportional increase compared to the previous year happened in 2021 with a 17.4% increase. Based on the data from 2013, the total change in vehicle-km in 2022 is a 60% increase. At a regional level, the 6th Region had the highest proportional increase compared to the previous year with 103% in 2021, while the 14th Region had the highest increase in 2017 with 82.9%. Based on the 2013 data, the 14th Region saw the highest increase in vehicle-km on highways with 497% and the 6th Region with 258% in 2022. Figure 2 displays the regional level of proportional increase in vehicle-km on highways between 2013 and 2022.

Table 1. 2013-2022 vehicle-km values of highways (x1000)

Region	2013	2014	2015	2016	2017	2018	2019	2020	2021	2022
1	9,373,246	9,615,197	10,048,391	10,057,524	10,754,897	11,016,764	11,567,943	9,472,109	10,871,917	11,620,266
2	1,840,373	2,108,009	2,389,097	2,548,834	2,781,404	2,880,849	3,782,512	3,239,337	3,741,236	4,120,231
4	2,554,100	2,690,956	3,042,077	3,282,559	3,420,856	3,460,344	3,671,414	3,453,687	4,135,131	4,121,714
5	3,211,085	3,313,686	3,891,533	4,124,861	4,365,945	4,202,703	4,579,920	4,346,316	4,987,506	5,041,811
6	239,218	264,644	306,561	326,778	347,780	299,392	370,926	362,289	735,459	855,702
9	320,001	318,510	335,246	331,349	361,571	349,807	379,961	335,151	436,891	429,682
14	426,807	448,667	568,299	671,541	1,227,961	1,405,242	1,953,121	2,089,794	2,439,661	2,549,440
Total	17,964,830	18,759,669	20,581,204	21,343,446	23,260,414	23,615,101	26,305,797	23,298,683	27,347,801	28,738,846

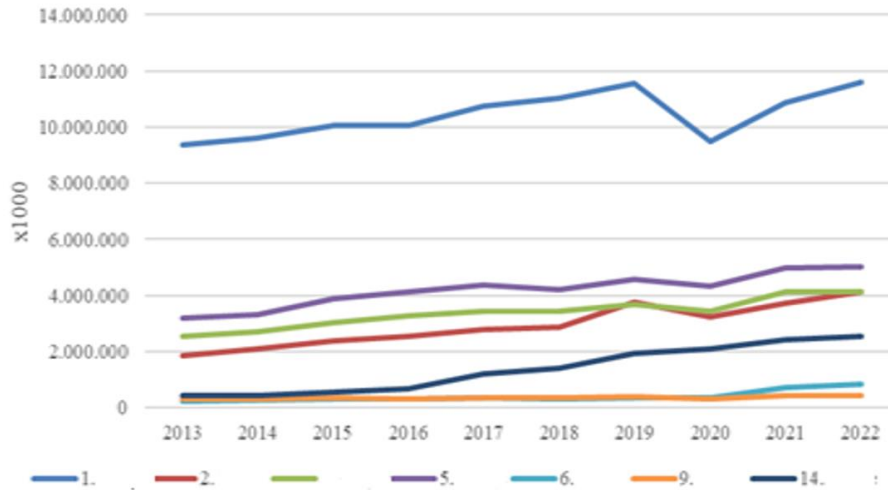


Figure 1. 2013-2022 vehicle-km values of highways (x1000).

Table 2. 2013-2022 vehicle-km change rates of highways (%)

Area	2014	2015	2016	2017	2018	2019	2020	2021	2022	2013-2022
1	2.6	4.5	0.1	6.9	2.4	5.0	-18.1	14.8	6.9	24.0
2	14.5	13.3	6.7	9.1	3.6	31.3	-14.4	15.5	10.1	123.9
4	5.4	13.0	7.9	4.2	1.2	6.1	-5.9	19.7	-0.3	61.4
5	3.2	17.4	6.0	5.8	-3.7	9.0	-5.1	14.8	1.1	57.0
6	10.6	15.8	6.6	6.4	-13.9	23.9	-2.3	103.0	16.3	257.7
9	-0.5	5.3	-1.2	9.1	-3.3	8.6	-11.8	30.4	-1.7	34.3
14	5.1	26.7	18.2	82.9	14.4	39.0	7.0	16.7	4.5	497.3
Total	4.4	9.7	3.7	9.0	1.5	11.4	-11.4	17.4	5.1	60.0

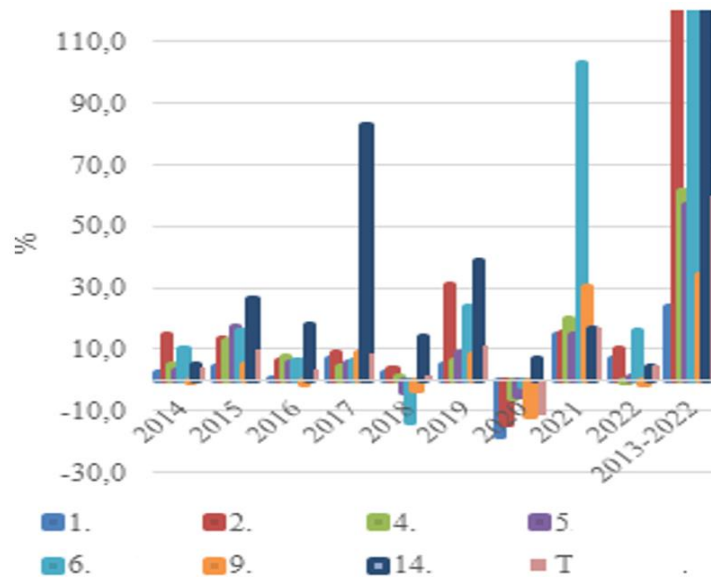


Figure 2. 2013-2022 vehicle-km change rates of highways compared to the previous year (y axis %).

According to Figure 2, it is evident that there was a rapid change in vehicle-km rates, especially in a negative direction, in all regions in 2020 and in a positive direction in all regions in 2021.

Table 3 includes the vehicle-km 2023-2025 forecast results of highways. The non-seasonal Holt-Winters (No Seasonal) method was used as the forecasting method.

Table 3. Vehicle-km 2023-2025 estimation results of highways (x1000)

Area	2023	2024	2025
1	11,530,467	11,593,445	11,656,422
2	4,272,927	4,535,987	4,799,047
4	4,366,588	4,547,836	4,729,085
5	5,256,279	5,454,603	5,652,926
6	1,102,829	1,344,886	1,586,943
9	425,104	445,773	466,442
14	2,752,738	2,948,425	3,144,112
Total	29,265,372	30,395,426	31,525,480

Based on the Holt-Winters non-seasonal double-parameter exponential correction, the prediction results show that the total vehicle kilometers traveled on highways will reach 31,525,480,000 by 2025. Additionally, when examining these results at the regional level, it is observed that the 1st Region will continue to have the highest vehicle-kilometer value in 2025.

3.2. Findings on Passenger-Km Data

Table 4 shows the passenger-km data of the highways between 2013 and 2022.

According to Table 4, it is seen that the passenger-km values increased between 2013 and 2022. In 2013, the highest passenger-km values were in the 1st Region, the lowest passenger-km values were in the 6th Region, in

Table 4. 2013-2022 passenger-km values of highways (x1000)

Region	2013	2014	2015	2016	2017	2018	2019	2020	2021	2022
1	30,281,515	30,468,944	30,311,035	29,670,496	30,079,065	30,955,116	32,274,161	24,492,245	28,817,243	31,494,552
2	5,431,719	6,083,866	6,674,117	7,038,355	7,450,457	7,768,206	10,251,643	8,222,334	9,725,348	10,943,829
4	8,363,070	8,618,078	9,229,735	9,715,846	9,825,595	9,656,624	10,192,313	8,865,138	10,864,595	11,067,571
5	11,431,733	11,484,347	12,447,559	12,759,908	12,578,186	12,189,180	13,240,113	11,382,607	13,375,120	14,061,621
6	828,337	891,645	977,804	1,018,416	999,488	869,660	1,068,726	950,408	1,950,905	2,363,647
9	1,244,230	1,198,777	1,151,487	1,083,682	1,086,683	1,053,790	1,141,543	885,952	1,185,690	1,227,453
14	1,413,706	1,545,180	1,730,390	1,987,997	3,392,382	3,896,897	5,333,551	5,306,587	6,337,051	6,788,729
Total	58,994,310	60,290,837	62,522,127	63,274,700	65,411,856	66,389,473	72,502,050	60,105,271	72,255,952	77,947,402

Table 5. 2013-2022 passenger-km change rates of highways (%)

Area	2014	2015	2016	2017	2018	2019	2020	2021	2022	2013-2022
1	0.6	-0.5	-2.1	1.4	2.9	4.3	-24.1	17.7	9.3	4.0
2	12.0	9.7	5.5	5.9	4.3	32.0	-19.8	18.3	12.5	101.5
4	3.0	7.1	5.3	1.1	-1.7	5.5	-13.0	22.6	1.9	32.3
5	0.5	8.4	2.5	-1.4	-3.1	8.6	-14.0	17.5	5.1	23.0
6	7.6	9.7	4.2	-1.9	-13.0	22.9	-11.1	105.3	21.2	185.3
9	-3.7	-3.9	-5.9	0.3	-3.0	8.3	-22.4	33.8	3.5	-1.3
14	9.3	12.0	14.9	70.6	14.9	36.9	-0.5	19.4	7.1	380.2
Total	2.2	3.7	1.2	3.4	1.5	10.7	-18.2	20.2	7.9	32.1

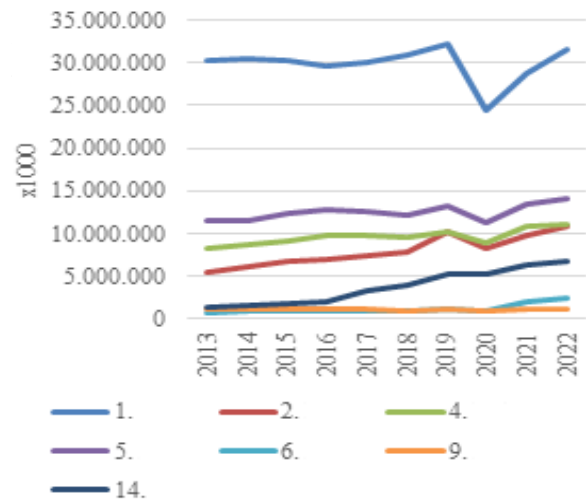


Figure 3. 2013-2022 passenger-km values of highways (x1000).

Based on Table 5, the year with the highest proportional increase, compared to the previous year, was 2020 with a 20.2% rise. In 2022, the total passenger-km change is expected to increase by 32% when compared to the figures from 2013. At a regional level, the greatest proportional increase compared to the previous year occurred in the 6th Region in 2021 (105%), and in the 14th Region in 2017 (71%). Based on 2013 data, it is noteworthy that the highest increase in passenger-km values on highways in 2022 took place in the 14th Region (380%) and in the 6th Region (185%). Figure 4 illustrates the regional level of the proportional increase in passenger-km values on highways between 2013 and 2022. Figure 4 shows that there has been a significant change in passenger-km rates, especially negative in 2020 and positive in 2021, across all regions.

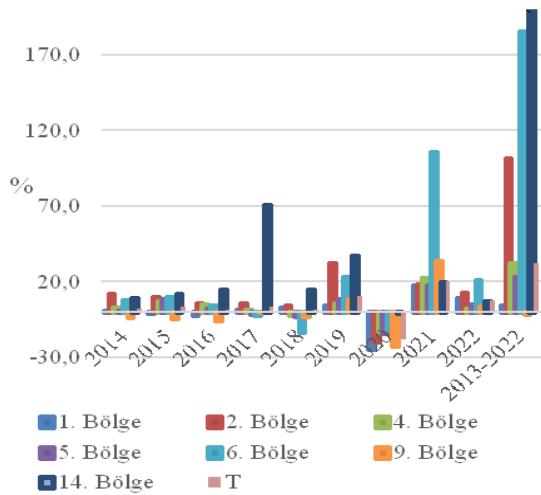


Figure 4. 2013-2022 passenger-km change rates of highways compared to the previous year (%).

Figure 4 illustrates the regional level of the proportional increase in passenger-km values on highways between 2013 and 2022. Figure 4 shows that there has been a significant change in passenger-km rates across all regions, especially negative in 2020 and positive in 2021. Table 6 shows the passenger-km 2023-2025 forecast results of highways. The non-seasonal Holt-Winters (No Seasonal) method was used as the forecasting method.

According to Table 5, the year that had the highest proportional increase in passenger-km compared to the previous year was 2020, with a rise of 20.2%. It is expected that in 2022, the total passenger-km change will increase by 32% compared to the numbers from 2013. At a regional level, the 6th Region had the greatest proportional increase compared to the previous year in 2021 (105%), and the 14th Region had the highest in 2017 (71%). It is worth noting that based on 2013 data, the highest increase in passenger-km values on highways

in 2022 took place in the 14th Region (380%) and the 6th Region (185%).

Table 6. Passenger-km 2023-2025 forecast results of highways (x1000)

Area	2023	2024	2025
1	29,743,093	29,499,958	29,256,823
2	10,947,954	11,564,872	12,181,789
4	10,950,178	11,208,889	11,467,600
5	13,483,068	13,712,212	13,941,355
6	3,044,552	3,746,889	4,449,226
9	1,193,327	1,274,302	1,355,277
14	7,276,967	7,773,605	8,270,243
Total	73,784,36	75,263,668	76,742,701

3.3. Findings on Ton-Km Data

Table 7 includes ton-km data of highways between 2013 and 2022.

Table 7 data reveals that the ton-km values on highways have increased between 2013 and 2022. In 2013, the 1st Region had the highest ton-km values, while the 6th Region had the lowest. Similarly, in 2022, the 1st Region had the highest ton-km values, but the lowest were recorded in the 9th Region. Regional level ton-km values on highways between 2013 and 2022 are displayed in Figure 5.

Table 8 shows the change in ton-km data of highways at the regional level.

As Table 8, the highest proportional increase in ton-km values when compared to the previous year was recorded in 2021 at 17.9%. When compared to 2013, the total ton-km change in 2022 recorded an increase of 54.7%. The 6th Region recorded the highest proportional increase compared to the previous year in 2021 at 64.3% and the 14th Region recorded the same in 2017 at 53.9%.

Table 7. 2013-2022 ton-km values of highways (x1000)

Region	2013	2014	2015	2016	2017	2018	2019	2020	2021	2022
1	24,841,564	25,978,351	26,667,732	26,605,152	27,684,119	28,836,103	28,591,508	27,075,092	31,640,354	31,655,989
2	3,013,552	3,287,588	3,603,833	3,915,975	4,311,525	4,783,947	6,852,455	6,021,556	7,189,090	8,335,133
4	7,171,248	7,637,588	8,347,276	8,870,871	8,472,227	8,499,779	8,729,400	8,506,144	10,188,632	9,881,511
5	12,347,585	12,927,194	13,969,457	14,385,420	14,427,253	14,217,564	15,425,187	15,460,914	17,503,573	18,873,952
6	835,350	929,246	1,086,233	1,185,431	1,128,446	1,024,494	1,216,286	1,320,837	2,169,578	2,908,691
9	1,611,370	1,625,944	1,610,179	1,499,090	1,586,260	1,513,559	1,648,895	1,368,370	1,808,203	1,986,114
14	1,257,564	1,343,215	1,591,018	1,817,677	2,796,703	3,242,044	3,883,990	3,932,667	4,601,682	5,379,799
Total	51,078,233	53,729,126	56,875,728	58,279,616	60,406,533	62,117,490	66,347,721	63,685,580	75,101,112	79,021,189

Table 8. shows the change in ton-km data of highways at the regional level

Area	2014	2015	2016	2017	2018	2019	2020	2021	2022	2013-2022
1	4.6	2.7	-0.2	4.1	4.2	-0.8	-5.3	16.9	0.0	27.4
2	9.1	9.6	8.7	10.1	11.0	43.2	-12.1	19.4	15.9	176.6
4	6.5	9.3	6.3	-4.5	0.3	2.7	-2.6	19.8	-3.0	37.8
5	4.7	8.1	3.0	0.3	-1.5	8.5	0.2	13.2	7.8	52.9
6	11.2	16.9	9.1	-4.8	-9.2	18.7	8.6	64.3	34.1	248.2
9	0.9	-1.0	-6.9	5.8	-4.6	8.9	-17.0	32.1	9.8	23.3
14	6.8	18.4	14.2	53.9	15.9	19.8	1.3	17.0	16.9	327.8
Total	5.2	5.9	2.5	3.6	2.8	6.8	-4.0	17.9	5.2	54.7

Based on 2013, the highest increase in ton-km values on highways in 2022 was recorded in the 14th Region at 327.8%, followed by the 6th Region at 248.2%, and the 2nd Region at 176.6%. Figure 6 shows the regional level of the proportional increase in ton-km values on highways between 2013 and 2022. According to Figure 6, it is evident that there was a rapid change in ton-km rates, especially in a negative direction, in all regions in 2020. However, in 2021, there was a positive change in all regions.

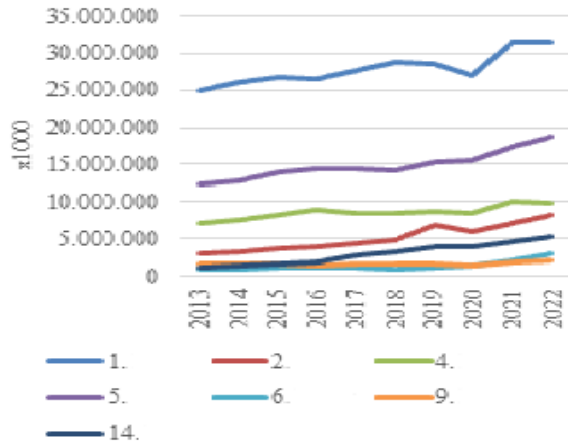


Figure 5. The course of ton-km values of highways in 2013-2022 (x1000).

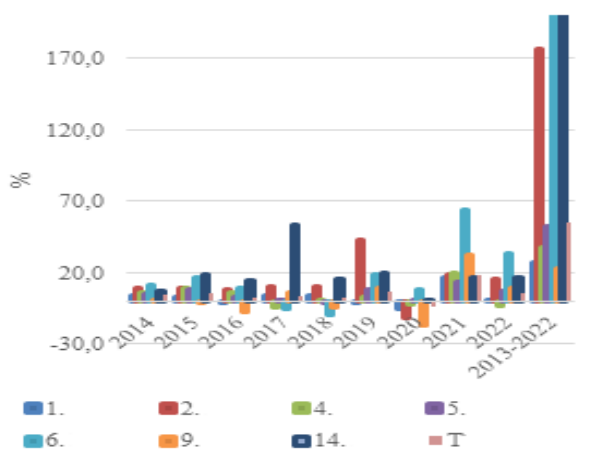


Figure 6. 2013-2022 ton-km change rates of highways compared to the previous year (%).

Table 9 shows the ton-km 2023-2025 forecast results of highways. The non-seasonal Holt-Winters (No Seasonal) method was used as the forecasting method.

Table 9. Ton-km 2023-2025 forecast results of highways (x1000)

Area	2023	2024	2025
1	32,375,088	33,173,996	33,972,904
2	8,973,032	9,892,933	10,812,833
4	10,080,944	10,368,802	10,656,660
5	19,669,503	20,479,463	21,289,423
6	3,715,267	4,527,095	5,338,924
9	1,983,754	2,181,963	2,380,172
14	5,736,174	6,133,070	6,529,966
Total	76,230,983	79,413,384	82,595,784

According to the Holt-Winters non-seasonal double-parameter exponential correction, the prediction results in Table 9 reveal that the total tonne-kilometers (ton-km) on highways will reach 82,595,784,000 by 2025. Additionally, when analyzed at a regional level, it is observed that the 1st Region will continue to have the highest ton-km value in 2025.

4. Conclusion

Upon examining the study results, it has been determined that passenger and cargo carrying capacity has increased in certain regions over the years and is predicted to continue to increase in the future. However, these increases in road transportation have negative impacts such as environmental pollution, climate change, and traffic accidents. Therefore, it is crucial to reduce transportation where possible. To achieve this, the following measures can be taken:

- Encourage the use of public transportation by prioritizing information and awareness-raising campaigns.
- Promote environmentally friendly transportation methods like walking and cycling.
- Implement deterrent measures to encourage people to reduce their daily travel distances.
- Increase public awareness through commercial approaches such as electronic shopping, and reduce people's need for physical shopping.
- Develop smart transportation systems to optimize traffic flow.

Transportation-related greenhouse gas emissions make up a significant portion of Türkiye's total emissions. To reduce these emissions, we can take measures such as changing transportation preferences and improving transportation infrastructure. Additionally, we need to ensure that the transportation system promotes sustainable development by meeting basic accessibility needs that are consistent with human and ecosystem health, producing limited amounts of greenhouse gas emissions, and paying attention to the affordability, equity, and efficiency of the system.

Author Contributions

The percentage of the author(s) contributions is presented below. The author reviewed and approved the final version of the manuscript.

	H.B.T.
C	100
D	100
S	100
DCP	100
DAI	100
L	100
W	100
CR	100
SR	100
PM	100
FA	100

C=Concept, D= design, S= supervision, DCP= data collection and/or processing, DAI= data analysis and/or interpretation, L= literature search, W= writing, CR= critical review, SR= submission and revision, PM= project management, FA= funding acquisition.

Conflict of Interest

The author declared that there is no conflict of interest.

Ethical Consideration

Ethics committee approval was not required for this study because of there was no study on animals or humans.

References

Alshehrya AS, Belloumia M. 2016. Study of the environmental Kuznets curve for transport carbon dioxide emissions in Saudi Arabia. *Renew Sustain Energy Rev*, 75: 1339-1347. <https://doi.org/10.1016/j.rser.2016.11.122>.

Amekudzi A. 2011. Placing carbon reduction in the context of sustainable development priorities: a global perspective. *Carbon Manag*, 2(4): 413-423.

Amin A, Altinoz B, Dogan E. 2020. Analyzing the determinants of carbon emissions from transportation in European countries: the role of renewable energy and urbanization. *Clean Technol Environ Pol*, 22(8): 1725-1734. <https://doi.org/10.1007/s10098-020-01910-2>.

Bergmeir C, Hyndman RJ, Benítez JM. 2016. Bagging exponential smoothing methods using STL decomposition and Box-Cox transformation. *Int J Forecast*, 32: 303-312.

Bowerman Bruce L, Richard TO. 1979. *Time series and forecasting: An applied approach*. Duxbury Press, New York, US, pp: 36.

Djakaria I, Saleh S. 2021. Covid-19 forecast using Holt-Winters exponential smoothing. *J Physics*, 2021: 012033.

Edenhofer O. 2015. *Climate change 2014: mitigation of climate change (Vol. 3)*. Cambridge University Press, Cambridge, UK, pp: 147.

Figueroa MJ, Ribeiro SK. 2013. Energy for road passenger transport and sustainable development: assessing policies and goals interactions. *Curr Opin Environ Sustain*, 5(2): 152-162.

He F, Chang KC, Li M, Li X, Li F. 2020. Bootstrap ARDL test on the relationship among trade, FDI, and CO2 emissions: based on the experience of BRICS countries. *Sustainability*, 12(3): 1060.

Kahn Ribeiro S, Kobayashi S, Beuthe M, Gasca J, Greene D, Lee DS, Zhou PJ. 2007. *Transport and its infrastructure. Climate change 2007: mitigation. contribution of working group III to the fourth assessment report of the intergovernmental panel on climate change*. Cambridge University Press, Cambridge, UK, pp: 65.

Konarasinghe K. 2021. Forecasting COVID-19 outbreak in the Philippines and Indonesia. *J New Front Healthcare Biol Sci*, 2: 1-19.

Meyer, B. D., & Sullivan, J. X. (2012). Identifying the disadvantaged: Official poverty, consumption poverty, and the new supplemental poverty measure. *Journal of Economic Perspectives*, 26(3), 111-136.

Ozkan T, Yanginlar G, Kalayci S. 2019. Testing the transportation-induced environmental Kuznets curve hypothesis: evidence from eight developed and developing countries. *Int J Energy Econ Pol*, 9(1): 174-183.

Sharif A, Raza SA, Ozturk I, Afshan S. 2019. The dynamic relationship of renewable and nonrenewable energy consumption with carbon emission: A global study with the application of heterogeneous panel estimations. *Renew Energy*, 133: 685-691. <https://doi.org/10.1016/j.renene.2018.10.052>.

URL1: <http://www.kgm.gov.tr> (accessed date: March 5, 2023).

Yağımılı M, Ergin H. 2017. Türkiye’de iş kazalarının üstel düzette metodu ile tahmin edilmesi. *Marmara Fen Bil Derg*, 4: 118-123.



A COMPACT GAN POWER AMPLIFIER MODULE FOR NEW GENERATION CELLULAR BASESTATIONS

Burak Berk TÜRK¹, Furkan HÜRÇAN², Hüseyin Şerif SAVCI^{2*}, Hakan DOĞAN²


¹Istanbul Technical University, Faculty of Electrical Engineering, Department of Electronics and Communication Engineering, 34810, İstanbul, Türkiye


²Istanbul Medipol University, Faculty of Engineering and Natural Sciences, Department of Electrical and Electronics Engineering, 34810, İstanbul, Türkiye


Abstract: This paper presents a compact class-AB Power Amplifier Module (PAM) designed for new generation massive Multiple Input Multiple Output (MiMo) cellular base stations. The module is designed at the center frequency of 3.5GHz targeting Long Term Evolution (LTE) and 5G New Radio (NR) bands. The module is a hybrid design that incorporates a Gallium Nitride (GaN) High Mobility-Electron Transistor (HEMT) die, discrete components-based input, and output matching networks. The entire design is realized on an 8.5 x 5.2 mm, 2-layer Rogers4003C substrate. The module is assembled on a PCB as an open-top for post-characterization tuning. The small signal and large signal measurements are in quite good agreement. The measurement results show that the amplifier is unconditionally stable, the input return loss is 12.2 dB, the output return loss is 7.7 dB, and the small signal gain is 13.4 dB. The saturated output power is 33.3 dBm with a Power Added Efficiency of 20.1%. The small signal gain drops to 11.2 dB at around 22 dBm of input power due to GaN technology's intrinsic soft compression characteristics.


Keywords: Power amplifier module, Gallium nitride HEMT, 5G n78, LTE band 42

*Corresponding author: Istanbul Medipol University, Faculty of Engineering and Natural Sciences, Department of Electrical and Electronics Engineering, 34810, İstanbul, Türkiye
E mail: hsavci@medipol.edu.tr (H. Ş. SAVCI)

Burak Berk TÜRK  <https://orcid.org/0009-0005-7378-3960>

Furkan HÜRÇAN  <https://orcid.org/0009-0009-7245-1410>

Hüseyin Şerif SAVCI  <https://orcid.org/0000-0002-5881-1557>

Hakan DOĞAN  <https://orcid.org/0000-0001-5716-5488>

Received: March 19, 2024

Accepted: May 10, 2024

Published: May 15, 2024

Cite as: Türk BB, Hürçan F, Savcı HŞ, Doğan H. 2024. A compact GaN power amplifier module for new generation cellular basestations. BSJ Eng Sci, 7(3): 587-593.

1. Introduction

The new generation of mobile services requires several different bands both at sub-6GHz and millimeter wave frequencies. Some of them are re-allocations of intrinsic cellular bands while others are newly assigned. These new frequency bands are there to handle more data traffic with complex modulations resulting in more demanding system requirements. Such high demands from the system increased the number of base stations with higher performance but smaller coverage in a typical cell. Small-cell base stations such as Microcells, Picocells, and Femtocells, therefore, gained attraction over macro cells as they are smaller in size, emit less power, are easier on thermal control, and are more environmentally friendly (Hsu et al., 2017). The sub-6 GHz bands are expected to operate with higher consumer demand than mm-wave ones (Li et al., 2018). Regardless of the frequency band, power amplifiers are one of the key RF elements in the entire cellular transceiver design. As the generation of cellular system increase, the requirements of micro or macro base-station power amplifiers evolve to be more stringent. The transmitter of microcells, picocells, and femtocells are compact for frequent placement in indoor or outdoor locations. As part of a small transmitter, the PAs need to be designed

more compact and more power efficient in order to have a thermally stable operation. GaN devices have a higher energy gap than GaAs devices which enable them to have higher breakdown voltage and power density (Colantonio et al., 2009). The higher breakdown also allows large voltage swings and high power output. With the high output power handling capability, GaN PAs are commonly used in small cell applications. In this work, a class-AB GaN HEMT PAM is designed for new-generation cellular networks. This paper is organized as follows: The design procedure is explained in section 2 whereas the implementation and measurements are detailed in section 3 followed by a conclusion.

2. Material and Methods

The purpose of any amplifier is to produce an output that follows the characteristics of the input signal but with higher voltage or power. One of the most important blocks of wireless communication systems is RF power amplifiers. RF Power amplifier design entails multiple design challenges such as linearity, gain, stability, output power, input and output matching, and thermal (Ozalas, 2021). The topology and transistor selection play a critical role in overcoming all these challenges. The PAM is realized on a 8.5x5.2mm sized 20-mil thick Rogers



4350C low-loss RF substrate with 1oz copper on both sides. A 8W GaN HEMT transistor (Cree’s CGH60008D) and 0603 sized discrete components are used. GaN technology is chosen for its higher breakdown voltage, larger power density, and broader bandwidth. The PAM is designed in Class AB mode operation to optimize between Power Added Efficiency (PAE) and linearity (Monprasert et al., 2010). The quiescent operating drain current I_{ds} is 134 mA for the drain voltage V_{ds} of 28 V, which corresponds to the gate voltage $V_{gs} = -2.7$ V where the performance optimization for the desired linearity at the highest efficiency is obtained (Iqbal and Piacibello, 2016). The HEMT die is attached to the laminate using the 25 μ m gold bond wires for the gate and the drain connections. The effects of wirebonds were included in the design process with the proper EM-based model where the mutual inductance and capacitance among multiple wires and the ground plane is included (Nazarian et al., 2012). Figure 1 shows the simplified schematic of the proposed PAM.

The design is optimized through the simulations using vendor-supplied component models and EM simulations of laminate layout and bond wires. The HEMT device model includes large signal behavior which enables harmonic balance simulations. Therefore, besides small-signal characterization, the load pull simulations were done to optimize the output matching network based on the AM-to-AM and AM-to-PM nonlinearities of the transistor. The output matching network is designed using iterative load-pull and source-pull simulations to ensure optimum performance of the PAE and the 3rd order output Intercept Point (OIP3) for targeted power delivery (Tao et al., 2015). The source and load impedances for the maximum gain, the optimum OIP3 and the PAE for the transistor were $3.2-j*7.7 \Omega$ and $24.5+j*12.9 \Omega$ respectively at the center frequency between the 3.4 GHz and 3.6 GHz frequency bands. The

input and output matching circuits were realized with lumped elements. The input matching network was designed with a high-pass T-type topology where the effects of gate bias and stability networks are embedded in the matching. The output network is designed with a DC-blocked low-pass L topology where the supply network is used for 2nd harmonic optimization. The supply decoupling capacitors were also added at both the gate and the drain bias lines. The proper stability network consists of a shunt series RC network at the input of the PAM. The design is optimized using parametric schematic and EM simulations. The topology and final component values are given in Figure 1.

Figure 2 shows the simulated performance. The saturated output power is 37.1 dBm for an input power of 24.75 dBm which corresponds to 12.35 dB gain 39% and power-added efficiency at about 1dB compression point. A 100 Ω resistor was used as the stability network. Figure 3 shows the result of a parametric study of the stability resistor over the input and the output return loss. Small signal stability analysis is a common method used in the design of RF amplifiers. In an amplifier, the closed loop gain of a classical feedback system shown in Equation (1) should satisfy the stability condition for each feedback loop including the ones caused by the parasitic electric and magnetic couplings. Here, A presents the open loop gain of the amplifier, and β presents the feedback network transfer function. If the $A\beta$ which is the loop gain, has the amplitude of 1 with the phase of π the amplifier becomes unstable (Sedra et al., 2021).

This approach has been widely used in the design of power amplifiers to analyze the stability (Zhao et al., 2022). Besides many parasitic feedback loops, the parasitic effects coming from the finite impedance ground connection at the source of the active device can be considered the strongest feedback path in the system.

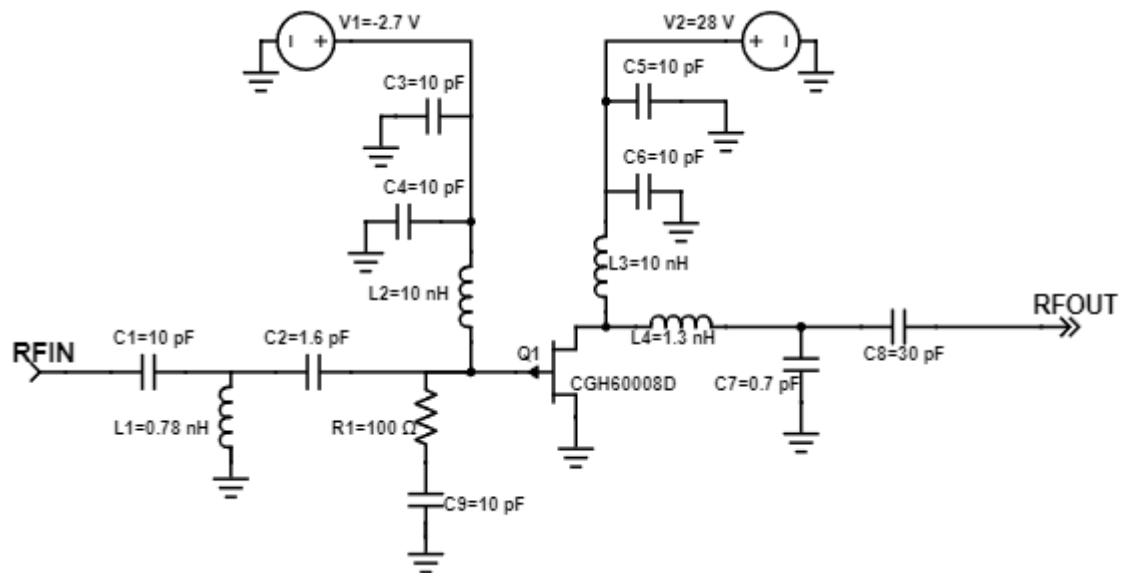


Figure 1. Schematic of proposed module design.

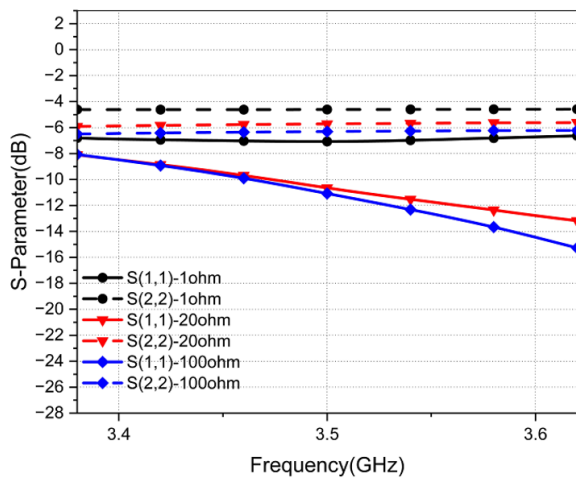


Figure 3. Parametric study of stability resistor values.

$$A_f = \frac{A}{1 + A\beta} \quad (1)$$

The stability condition was simulated for the input power of 24.75 dBm which corresponds to 5W output power. Figure 5 shows the loop gain from DC to 10 GHz at the drain and the gate nodes. It is observed that the circuit is stable as the loop gains for both cases are below -15 dB. Although small signal stability is a commonly checked one, power amplifiers are typically used under large signal conditions. In addition to small signal stability analysis, the stability conditions under large signal presence should also be checked. In this work, the large signal stability analysis was done and a test setup was constructed to simulate the large signal conditions. In addition to the loop-gain-based stability criteria, another method, which is based on the driving point impedance technique, was used to check stability (Bode, 1945). The driving point impedance is the network determinant divided by the same determinant with the node that is selected, discarded from the network matrix. Same condition can be considered for the admittance. Figure 4 shows the network built with admittance nodes.

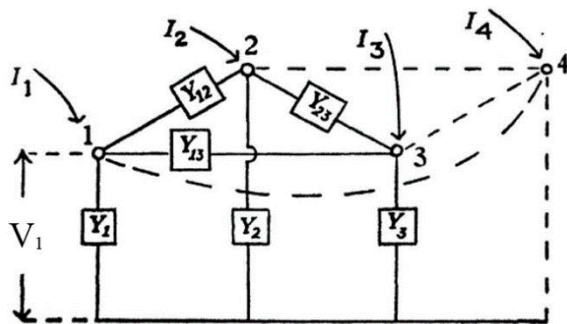


Figure 4. Admittance network.

Considering the current flow and node voltages driving point admittance can be calculated. Y-matrix is built with a set of nodal equations. The nodal equation in Equation (2) is an example of current equation at node 1 where \$Y_{11}\$ can be written as Equation (3). Just like \$Y_{11}, Y_{22}\$ or any \$Y_{nn}\$ can be written in this form. Thereon, Equation (4) is

created with the admittance of the nodes. Discarding the node from the matrix means the column and row which contains the node is removed from the matrix. This means that in Equation (4), the determinant of the matrix with the removal of node 2, discards \$Y_{22}\$ along with the \$Y_{21}\$ and \$Y_{12}\$ from the matrix and only \$Y_{11}\$ remains. Normally the matrix determinant of the admittance network is \$Y_{11}Y_{22} - Y_{21}Y_{12}\$; however, removal of the node 2 divides the determinant with the remaining \$Y_{11}\$ and driving point admittance of node 2 becomes Equation (5).

$$Y_{11}V_1 - Y_{12}V_2 - \dots - Y_{1n}V_n = I_1 \quad (2)$$

$$Y_{11} = Y_1 + Y_{12} + \dots + Y_{1n} \quad (3)$$

$$\begin{bmatrix} Y_{11} & Y_{12} \\ Y_{21} & Y_{22} \end{bmatrix} \quad (4)$$

$$\frac{\Delta'}{\Delta'_{22}} = \frac{Y_{11}Y_{22} - Y_{21}Y_{12}}{Y_{11}} \quad (5)$$

In other words, the driving point admittance of a node is the ratio between the driving current entering the node and the node voltage that results in. If the node self-oscillates, the response of the network may give unexpected results (Ozalas, 2021). Moreover, Kurokawa (1969) also checks the stability with the impedance response. If the real part of the impedance is either zero or negative, while the slope of the imaginary part increases with the frequency increase, the self-oscillation condition occurs. Figure 6 points out the real value of driving point admittance for the gate and drain nodes of PAM from DC to 10 GHz. It is observed that the minimum value is 0.011 which concludes that the PAM is stable for the entire frequency range. Kurokawa condition was also checked with driving point admittance. Since the sign of the impedance is crucial for Kurokawa condition driving point admittance result can be used. It assured the PAM's unconditional stability as well.

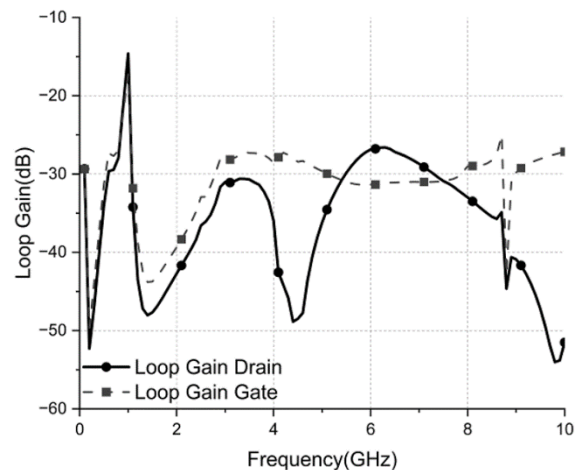


Figure 5. Logarithmic loop gain of PA.

An evaluation board was designed as a connectorized testing vehicle for small signal and large signal measurements of the PAM. The Figure 7 shows the die

picture and the evaluation board. The board includes 2 input and output SMA connectors, 2 DC bias pins, and 2 extra pins for merging the ground connections of the

supplies. A finned aluminum plate is attached to the back of the board for proper heat dissipation. The size of the evaluation board is 26 x 21 mm².

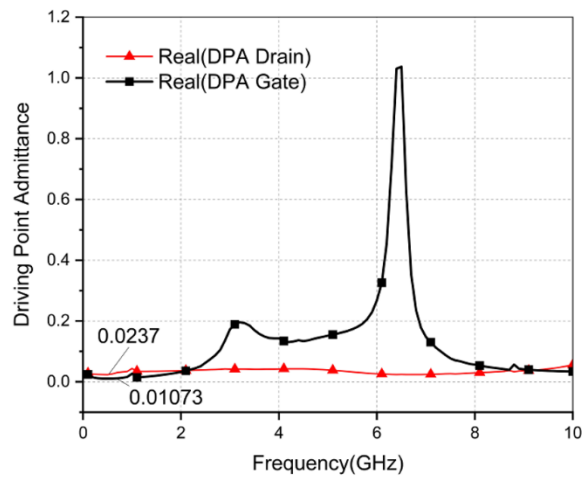


Figure 6. Driving point admittance of PA.

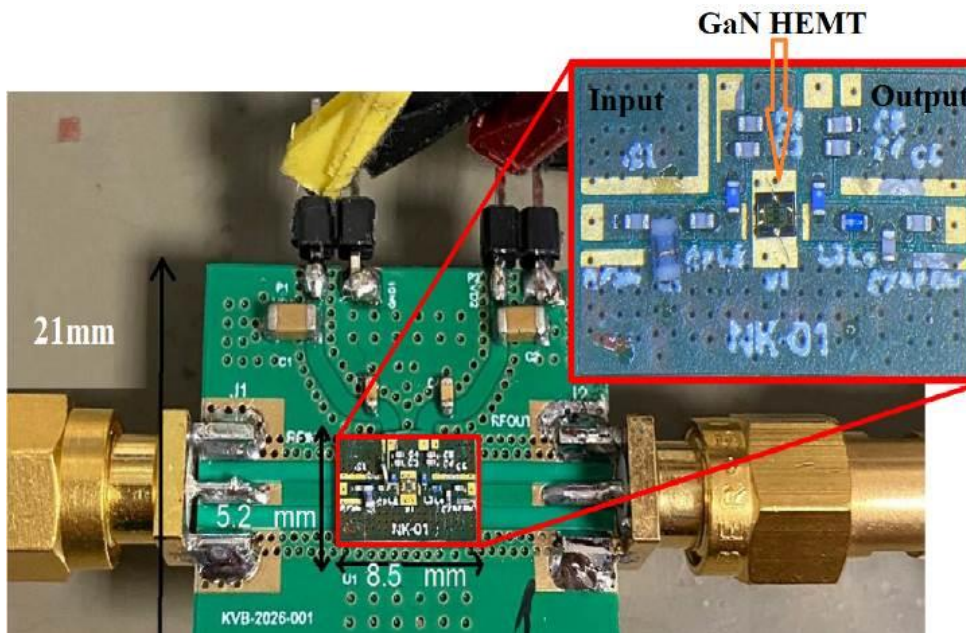


Figure 7. The assembled power amplifier module.

3. Results and Discussion

The laminate is manufactured with solder mask and silkscreen. Die placement, component assembly and wire bondings are manually done. The GaN HEMT die has gold back plate. Therefore, electrically conductive Epotek H20e silver epoxy was used for die bonding. 25 μ m gold wirebonds are for gate and drain connections. Although there is thru-wafer-via in the GaN die extra downbonds are added for RF grounding. The board was characterized for both small signal and large signal performance at Istanbul Medipol University RF Laboratory.

3.1. Small Signal Measurements

The small signal response of the PAM was measured by Rohde&Schwarz ZNB8 model Vector Network Analyzer. Figure 8 shows the simulation and measurement results for small signal gain, input return loss and output return loss. At 3.5 GHz the gain was measured as 13.4 dB, the

output return loss was measured as -7.7 dB and the input return loss was measured as -12.2 dB. The small signal stability indicators of μ and μ' values were calculated from the measured S-parameters (Colantonio et al., 2009). As both the μ and μ' are greater than 1 across a broad frequency range, the PAM was unconditionally stable under small-signal conditions.

3.2. Large Signal Measurements

The large signal response of the PAM was tested with a 3.4 GHz single tone supplied by the Rohde&Schwarz SMB100A signal generator and a Mini Circuits ZHL-5W-63-S+ driver amplifier, and the output of PAM was monitored with the Rohde&Schwarz FSH8 spectrum analyzer. The block diagram of the test setup is shown in Figure 9. A 30 dB attenuator was used for protection of the spectrum analyzer from the incidence of high-power signal. Likewise, two 10 dB attenuators in the setup were

used for protection of DUT, preamplifier and the signal generator from the incidence or reflectance of high-power signals under high VSWR conditions (Mini-Circuits, 2020). To measure the large signal response of PAM, the signal generator was swept in the range of -30 dBm to -8 dBm, so that the preamplifier can drive the DUT with signal levels between 0 dBm to 22 dBm. The measurements were performed in short periods and with a running cooler fan in order to thermally stress the PAM. The output power and supply currents were recorded for each input power value and post-measurement calculations were done.

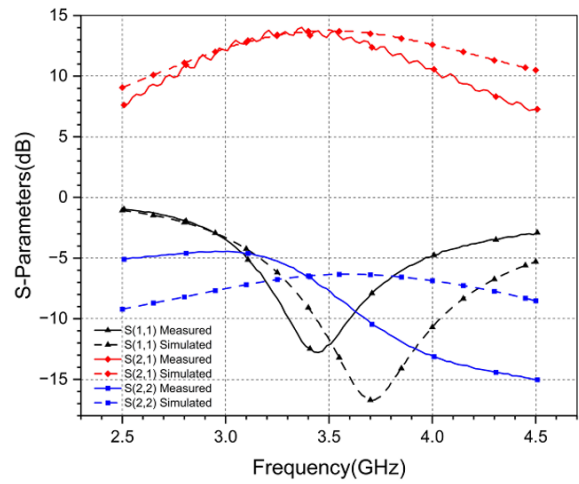


Figure 8. S-parameter vs frequency for measurement and simulation.

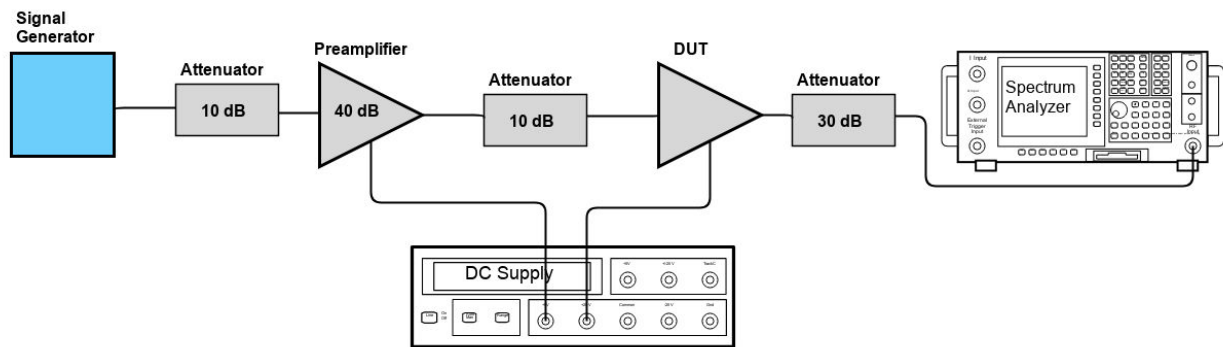


Figure 9. The block diagram of the proposed large signal test.

Figure 10 shows the output power and transducer power gain at 3.4 GHz. The cable losses and test setup losses were de-embedded from the large signal measurements. The measurement was done only up to the output of 33.2 dBm due to the driving power limitations in our measurement setup. The maximum output power was measured as 33.3 dBm without any compression. The gain was flat for the input power range from 17 to 22 dBm. The transducer power gain is greatly affected by the mismatches at both input and output. Figure 10. Measurement of output power, gain at 3.4 GHz. Table 1 shows the comparison of similar hybrid power amplifier module studies in the literature. The measured PAE was only reported up to a power output of 33.2dBm due to the driving power limitations in our measurement setup. For this output power, PAE was 20 % and we expect the peak PAE to be closer to 39 % for an output power of 37dBm as shown in Figure 2. Our work is the smallest one among the referenced works. The output power is average and output matching network needs more adjustment to increase efficiency. This work targets small cell base station applications.

The development phase requires a low-cost solution for small quantities. The hybrid PA Module comes forward as a strong solution due to its easy-post-production-tuning feature and ultra-low-cost nature when compared to the other custom MMIC based solutions.

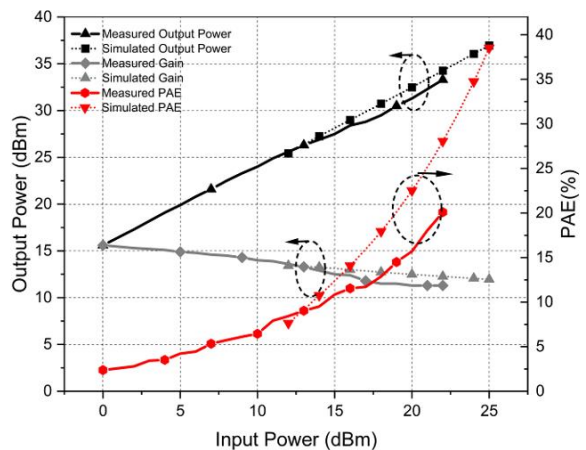


Figure 10. Measurement of output power, gain at 3.4 GHz.

Table 1. Comparison with reference products

References	Frequency (GHz)	Gain (dB)	Output Power (dBm)	Efficiency	Size (mm)
Inoue and Ebihara (2016)	3.6	24	40/32	40%/20%	8x8
Saad et al. (2010)	1.9-4.3	10	40.5	50%@3.5 GHz	65x65
Komatsuzaki et al. (2017)	3.0-3.6	12	34.2@3.5 GHz	45.9%-50.2%	78x60
Sakata et al. (2020)	3.6	30	37.3	44.7%	10x6
Barisich et al. (2015)	1.0-11.5	4	35@3.0 GHz	30%	76.2x25.4
Crescenzi et al. (2005)	1.96	27.5	44.8	45%	15.2x25.4
This work	3.4-3.6	11.3	33.2	20%	8.5x5.2

4. Conclusion

In this article, detailed design steps of a class-AB PAM are explained. The Power Amplifier Module is constructed on an 8.46 x 5.22 mm Rogers4003C laminate as a hybrid design using a GaN HEMT transistor die and 0603 sized discrete resistor, capacitor and inductors. For the design simulations, the vendor supplied compact model of CGH6008D, vendor supplied S-parameter data for the inductor, and resistor and capacitors, along with the bond wire model obtained from full-wave 3D EM simulations to account for parasitic effects of the 25 μm gold wire are used. An evaluation board was designed and fabricated along with the PA Module. Initial measurements show that more than 2W saturated output power was obtained from the PA with 11.2 dB gain and 20.1 % PAE at 3.4 GHz. S11 and S22 were measured as -12.2 dB and -7.7 dB respectively. S21 was measured as 13.4 dB at 3.5 GHz. The shunt resistor used as the stability network ensured unconditional stability of the PAM. It was verified using both small signal and large signal stability analyses.

Author Contributions

The percentage of the author(s) contributions is presented below. All authors reviewed and approved the final version of the manuscript.

	H.Ş.S.	B.B.T.	F.H.	H.D.
C	70			30
D	15	50	30	5
S	70			30
DCP	10	90		
DAI	20	70	5	5
L	10	70	20	
W	20	80		
CR	80	20		
SR	70	30		
PM	50	35	5	10
FA	40	20		40

C=Concept, D= design, S= supervision, DCP= data collection and/or processing, DAI= data analysis and/or interpretation, L= literature search, W= writing, CR= critical review, SR= submission and revision, PM= project management, FA= funding acquisition.

Conflict of Interest

The authors declared that there is no conflict of interest.

Ethical Consideration

Ethics committee approval was not required for this study because of there was no study on animals or humans.

Acknowledgements

This study was supported by Nero Industries Co. The authors would acknowledge the financial support of the company.

References

- Barisich GC, Ulusoy AC, Gebara E, Papapolymerou J. 2015. A reactively matched 1.0–11.5 GHz hybrid packaged gan high power amplifier. *IEEE Microw Wirel Compon Lett*, 25(12): 811-813. <https://doi.org/10.1109/lmwc.2015.2495195>.
- Bode HW. 1945. *Network analysis and feedback amplifier design*. D. Van Nostrand Company, New Jersey, US, pp: 54.
- Colantonio P, Giannini F, Limiti E. 2009. *Power amplifier fundamentals. High Efficiency RF and Microwave Solid State Power Amplifiers*, Wiley, London, UK, pp: 1-47. <https://doi.org/10.1002/9780470746547.ch1>.
- Crescenzi EJ, Pengelly RS, Wood SM, Buss RE. 2005. 60 watt doherty amplifiers using high gain 2-stage hybrid amplifier modules. *IEEE MTT-S International Microwave Symposium Digest*, June 17, Long Beach, US. <https://doi.org/10.1109/mwsym.2005.1516941>.
- Hsu YC, Li JY, Wu LK. 2017. High reliable Doherty power amplifier module for LTE Small Cell Base Station. *IEEE CPMT Symposium*, November 20-22, Kyoto, Japan. <https://doi.org/10.1109/icsj.2017.8240083>.
- Inoue S, Ebihara K. 2016. Broadband 2-stage gan power amplifier in an 8x8mm package. *11th European Microwave Integrated Circuits Conference*, October 3-4, London, UK. <https://doi.org/10.1109/eumic.2016.7777532>.
- Iqbal M, Piacibello A. 2016. A 5W class-AB power amplifier based on a Gan HEMT for LTE Communication Band. *16th Mediterranean Microwave Symposium*, November 14-16, Abu Dhabi, United Arab Emirates. <https://doi.org/10.1109/mms.2016.7803827>.
- Komatsuzaki Y, Nakatani K, Shinjo S, Miwa S, Ma R, Yamanaka K. 2017. 3.0–3.6 GHz wideband, over 46% average efficiency Gan Doherty power amplifier with frequency dependency compensating circuits. *EEE Topical Conference on RF/Microwave Power Amplifiers for Radio and Wireless Applications*, January 15-18, Phoenix, US. <https://doi.org/10.1109/pawr.2017.7875563>.
- Kurokawa K. 1969. Some basic characteristics of broadband negative resistance oscillator circuits. *Bell Syst Tech J*, 48(6): 1937-1955. <https://doi.org/10.1002/j.1538-7305.1969.tb01158.x>.
- Li SH, Hsu SS, Zhang J, Huang KC. 2018. A sub-6 ghz compact

- Gan Mmic Doherty pa with a 49.5% 6 DB back-off PAE for 5G communications. IEEE/MTT-S International Microwave Symposium, June 10-15, Philadelphia, US. <https://doi.org/10.1109/mwsym.2018.8439474>.
- Mini-Circuits. 2020. ZHL-5W-63-S+ Amplifier. URL: <https://www.minicircuits.com/WebStore/dashboard.html?model=ZHL-5W-63-S> (accessed date: January 15, 2024).
- Monprasert G, Suebsombut P, Pongthavornkamol T, Chalermwisutkul S. 2010. 2.45 GHz GaN HEMT Class-AB RF power amplifier design for wireless communication systems. ECTI International Conference on Electrical Engineering/Electronics, Computer, Telecommunications and Information Technology, May 19-21, Chiang Mai, Thailand, pp: 566-569.
- Nazarian AL, Tiemeijer LF, John DL, van Steenwijk JA, de Langen M, Pijper RM. 2012. A physics-based causal bond-wire model for RF Applications. IEEE Transact Microw Theory Techniq, 60(12): 3683-3692. <https://doi.org/10.1109/tmtt.2012.2217983>.
- Ozalas M. 2021. Designing for stability in high frequency circuits, Keysight. URL: <https://www.keysight.com/us/en/assets/3121-1255/application-notes/Designing-for-Stability-in-High-Frequency-Circuits.pdf> (accessed date: January 15, 2024).
- Saad P, Fager C, Haiying Cao Zirath H, Andersson K. 2010. Design of a highly efficient 2–4-GHz octave bandwidth Gan-HEMT power amplifier. IEEE Transact Microw Theory Techniq, 58(7): 1677–1685. <https://doi.org/10.1109/tmtt.2010.2049770>.
- Sakata S, Kato K, Teranishi E, Sugitani T, Ma R, Chuang K, Shinjo S. 2020. A fully-integrated GAN doherty power amplifier module with a compact frequency-dependent compensation circuit for 5G massive MIMO base stations. IEEE/MTT-S International Microwave Symposium, August 4-6, Los Angeles, US, pp: 711-714. <https://doi.org/10.1109/ims30576.2020.9223897>.
- Sedra AS, Smith KC, Carusone CT, Gaudet V. 2021. Microelectronic circuits. Oxford University Press, New York, US, pp: 1264.
- Tao Y, Ishikawa R, Honjo K. 2015. Optimum load impedance estimation for high-efficiency microwave power amplifier based on low-frequency active multi-harmonic load-pull measurement. Asia-Pacific Microwave Conference, December 6-9, Nanjing, China, pp: 1-3. <https://doi.org/10.1109/apmc.2015.7411814>.
- Zhao B, Sanabria C, Hon T. 2022. A 2-stage S-band 2W CW GAN MMIC Power Amplifier in an Overmold QFN package. IEEE Texas Symposium on Wireless and Microwave Circuits and Systems, April 19-20, Waco, US, pp: 1-5. <https://doi.org/10.1109/wmcs55582.2022.9866273>.



MEETING THE ENERGY NEEDS OF POULTRY HOUSES WITH WIND TURBINE SYSTEM UNDER TEKİRDAĞ CONDITIONS AND ITS ENVIRONMENTAL EFFECTS

Elif TÜRKBOYLARI^{1*}, Ahmet Nedim YÜKSEL²

¹Tekirdağ Namık Kemal University, Vocational School of Technical Sciences, Department of Plant and Animal Production, 59030, Tekirdağ, Türkiye


²Tekirdağ Namık Kemal University, Faculty of Agriculture, Department of Biosystem Engineering, 59030, Tekirdağ, Türkiye (Retired)


Abstract: Türkiye has a favorable geographical location for renewable energy sources such as wind and solar. Accordingly, renewable energy sources can be used in the fast-growing bovine, ovine, and poultry farms that perform plant and animal production. Marmara Region is the leading production center of the Turkish poultry production industry. However, there are problems in maintaining environmental conditions in poultry houses. The fan-pad system plays an essential role in maintaining environmental conditions in the poultry houses. For this reason, the fan-pad system required for evaporative cooling in the poultry houses in Tekirdağ region was designed. The project was carried out in poultry houses with 6000 chickens and the dimension of the poultry house is 14 x 30 (420 m²). In the poultry house, a 16.8 m² pad is needed for cooling, and a circulation pump with 0.2 kWh power is required for water circulation in the system. For mechanical ventilation, 11 units of aspirators with a diameter of 60 cm a power of 0.75 kWh, and a flow rate of 9500 m³h⁻¹ will be sufficient for the system. For the ventilation and cooling system, an 8.45 kWh wind turbine system will supply the required energy. However, due to the variability of wind power, a turbine system larger than 8.45 kWh, such as 10 kWh, should be used. The cost of the cooling system planned with the wind turbine energy system reaches 35953 \$. The use of wind turbine systems to generate electricity in agriculture will significantly reduce CO₂ emissions to nature. In Tekirdağ conditions, 18250 kWh of electricity can be produced annually with a 10-kWh wind turbine system. With eco-friendly energy generation, it can play a major role in preventing climate change by avoiding the emission of 17155 kg of CO₂ which is equivalent to the annual electricity production.

Keywords: Wind turbine system, Poultry houses, Ventilation, Pad system, CO₂ emission

*Corresponding author: Tekirdağ Namık Kemal University, Vocational School of Technical Sciences, Department of Plant and Animal Production, 59030, Tekirdağ, Türkiye

E mail: eyuksel@nku.edu.tr (E. TÜRKBOYLARI)

Elif TÜRKBOYLARI  <https://orcid.org/0000-0003-4658-8068>

Ahmet Nedim YÜKSEL  <https://orcid.org/0000-0002-0278-7498>

Received: March 13, 2024

Accepted: May 10, 2024

Published: May 15, 2024

Cite as: Türkboyları E, Yüksel AN. 2024. Meeting the energy needs of poultry houses with wind turbine system under Tekirdağ conditions and its environmental effects. BSJ Eng Sci, 7(3): 594-600.

1. Introduction

The increase in the world population, developments aimed at increasing the comfort of human life, particularly in the last century, and the industrial activities carried out have led to a great increase in the consumption of fossil resources. The use of these resources leads to imbalances in the gas composition present in the atmospheric layer and, in particular, to an increase in the CO₂ gas that retains heat. As a result, the greenhouse gas emission into the atmosphere is increased and this creates a greenhouse effect triggering global warming on our planet. Global warming is the increase in the long-term average temperature of the earth (Kurucu, 2015). The effects of global warming can be listed as temperature increase, drought, desertification, soil erosion and salinization, deterioration in soil structure, changes in underground and surface water resources, melting of glaciers, increase in ocean and sea water levels, deterioration of the global economy and socio-economic structure (Doğan, 2005). To cope with the negative effects of global warming

countries have been shifting towards renewable energy sources as healthy, clean, and sustainable energy sources (Karık et al., 2017). Although there are several definitions of renewable energy, briefly it is a type of energy that continues its natural processes, has continuity, does not end with its transformation into secondary energy, and continues to renew and flow (Gençel and Tarhan, 2019). In addition to diversifying the country's energy resources, renewable energy resources can also reduce the negative pressure on the environment (Koçaslan, 2010).

It is possible to meet the part of electrical energy needs without harming nature and people with renewable energy sources. Electricity generation methods using wind and solar energy sources are the fastest-growing methods in the world. This growth has particularly made wind power an important source of energy worldwide. The wind power is recognized as an essential source of energy worldwide. At the same time, the wind power has been recognized as one of the least environmentally damaging sources of electricity generation (Warren et al.,



2005). It does not cause any harmful pollutant emissions including greenhouse gases such as CO₂. It does not require mining or drilling for fuel, does not produce radioactive or hazardous waste, and does not use steam generation or cooling water (Schiermeier et al., 2008). In this perspective, the wind power generation is of great importance due to its high potential in northwestern parts of Türkiye, ease of use, and being eco-friendly (Taktak and Ili, 2018).

Due to its geographical location, Türkiye has more advantages in terms of wind and solar energy as compared with many countries. In particular, Türkiye should work to expand the wind and solar energy use. In this context, rapidly growing bovine, ovine, and poultry farms that produce plants and animal products can easily benefit from the renewable energy source. Although the initial investment cost of these systems is high, the absence of raw material costs reduces the cost of energy generation. Studies have shown that renewable energy resources can be cost-effectively used in livestock farms way (Yüksel and Yüksel-Türkboyları, 2018; Orhan and Şahin, 2022).

Agricultural production is composed of plant and animal production. Animal husbandry is a major area of production in the world and our country in terms of economic, social, and nutritional aspects. For societies to have a healthy and balanced diet, the nutritional substances that the body needs must be provided. This means that calories, protein, fat, and carbohydrates should be taken in a balanced way (Karacan, 2017). Although it has a great importance in human nutrition, our meat production, which is the source of animal protein, is not sufficient for domestic consumption. Based on 2019 data our country's meat consumption per capita is 36.1 kg (cattle 13.6 kg, poultry 21.0 kg, sheep 1.5 kg), lower than the developed countries (BESD-BİR, 2023).

1.1. Poultry Farming in Türkiye

In terms of poultry broiler production, Marmara and Central Anatolia regions are the leading regions in Türkiye (Dağtekin, 2012). The poultry production sector has an important role in terms of production, national income, and employment. White meat and eggs account for approximately 60% of the annual animal protein production in Türkiye. In recent years, our poultry population and egg production had been increased significantly. This significant increase in production has also been reflected in the number and capacities of poultry houses and has played a major role in the spread of poultry houses having full environmental control (Erensoy et al., 2015).

This development in poultry farming can play an essential role in eliminating our animal protein deficit. Additionally, poultry farming can be carried out in smaller areas and in a faster way as compared with other animal husbandry types. Chicken meat has a strategic value since it is rich in energy, protein, and minerals, easy to digest, and relatively inexpensive. For this reason, the demand for chicken meat has been increasing day by day

recently (Yüksel and Türkboyları, 2019).

1.2. Climate Conditions in Poultry Houses

In the design of modern animal barn systems, efforts should be focused on ensuring animal health and welfare. This will ensure animal welfare in the shelter environment and the efficiency of the business. It is reported that the biggest problem encountered in poultry houses is the regulation of indoor environmental conditions (Karaca et al., 2016; Karacan, 2017). High air temperature, among all environmental conditions, strongly affects the animals. High temperatures decrease feed conversion ratio, increase mortality rates, and decrease live weight gain in chickens (Bilgili and Dağtekin, 2019).

One of the important measures in ensuring environmental control in poultry houses is ventilation. A good ventilation system is needed to ensure adequate ventilation. The ventilation system in the poultry houses should be able to replace the required fresh air with the polluted poultry house air depending on the change in outdoor weather conditions all year round. Therefore, when planning an adequate ventilation system in the poultry houses, first of all, the ventilation capacity should be determined (Atılğan et al., 2010).

In agricultural buildings, electrical energy is needed to meet the desired amount of ventilation (Yüksel and Yüksel-Türkboyları, 2018). In rural areas, in case of a lack of electrical energy or power outage or reducing energy costs, electrical energy might be generated with wind turbines using wind power and it can be used in animal barns.

1.3. Wind Power Potential in Türkiye

Türkiye is located in an advantageous geographical location for wind and solar energy potential as compared to many other countries. The use of these resources will help to reduce dependence on foreign energy resources. In addition, it will contribute to reducing the current account deficit in the state budget due to energy expenses (Karık et al., 2017).

Wind is the result of the solar radiation warming the earth's surface at different levels. This difference in the levels of warming of the earth's surface leads to differences in the air temperature, humidity, and pressure, and to the formation of low- and high-pressure areas. Low- and high-pressure areas allow the air to circulate and therefore create winds. A 2% of the energy of the sun's rays reaching the Earth is converted into wind power. The characteristics of the wind vary depending on local geographical conditions and temperature differences between these geographical locations. Wind is expressed in two different parameters: direction and speed (MENR, 2023).

1.4. Wind Power Potential of Tekirdağ Province

Tekirdağ province, located on the Thracian peninsula, is in a very favorable condition in our country in terms of wind power potential, one of the renewable energy sources. The wind power potential data of Tekirdağ province, where wind speed is high, is given in Table 1.

Table 1. Long-term average monthly predominant wind speed, wind direction, and percentage (%) data (1940-2018) for Tekirdağ (Merkez) (MoEU, 2020)

Months	Wind Speed (ms ⁻¹)	Wind Direction	Months	Wind Speed (ms ⁻¹)	Wind Direction
January	3.1	NW (15.40%)	July	2.7	NE (% 12.60)
February	3.0	NW (12.81%)	August	2.9	NE (% 15.80)
March	2.9	NE (11.56%)	September	2.7	NE (% 12.69)
April	2.3	WNW (10.49%)	October	2.8	NW (% 14.29)
May	2.2	WNW (10.89%)	November	2.7	NW (% 14.77)
June	2.3	WNW (13.09%)	December	3.0	NW (% 15.98)
			Annual Average	2.7	NW (% 13.36)

Wind speeds change as they rise above the ground. As approaches the earth, the wind speed decreases due to the effect of friction force. The wind speed measured at any height can be used to estimate the wind speed measured at another height (Çelikdemir and Özdemir, 2020).

Wind speeds increase as the altitude increases. In a related study conducted in Burdur-Ağlasun area, possible wind speeds at a height of 60 m above the ground were calculated with various methods based on the wind speeds measured in the local meteorology stations. The approximate speed of the wind at a height of 60 m can increase up to 3 times compared to the speed measured at a height of 2 m above the ground (Dikmen and Örgen, 2018). The reason for using the wind speed at 60 m height is that it corresponds to the height of the hub (rotor hub) of the wind turbines. It should be noted that the wind speeds given in Table 1 also increased significantly with height.

This study aims to meet the electrical energy needs required for forced ventilation in poultry houses with the wind turbine energy system. Generally, there is no electricity network in rural areas where poultry houses are located. Ventilation and cooling can be done using the electrical energy obtained from the wind turbine system to be installed in a poultry house, using a fan and wet pad system.

2. Materials and Methods

2.1. Material

Tekirdağ province, the research area, is located on the Thracian peninsula in the southeast of Europe. The Thrace region is located between 26°-29° east longitudes and 40°-42° north latitudes on the continental Europe. Tekirdağ is located to the north of the Marmara Sea and south of the Black Sea and has a surface area of 6313 km². Koru Mountain, located in the province, is the highest point (762 m) and there are no steep slopes, valleys, and high mountains in other places. Tekirdağ generally has rainy winters and dry and hot summers. According to the general humidity indices, it belongs to the semi-humid climate type among the hydrographic regions and is windy in the summer and winter seasons (MCT, 2023).

According to the wind power potential atlas, Tekirdağ and Marmara Sea coasts have high wind speeds in our

country (Karık et al., 2017; Tunus, 2019). Therefore, in Tekirdağ, electrical energy generated by wind turbines can be used for agricultural purposes.

Due to high temperatures causing decreases in animal productivity, the project was designed to ventilate and cool the poultry houses, when the air temperature is high in Tekirdağ. Therefore, the fan-pad system required for evaporative cooling in the poultry house was designed. The floor area of the poultry house is 420 m² and its dimensions are 14x30 m. In the poultry house, 6000 chickens are housed (Şenköylü, 2001).

For the poultry house with these dimensions (14x30 m = 420 m²), ventilation fans and cooling pads (wet pad) sections and a wind turbine system that will generate electrical energy for them were designed.

2.2. Wind Turbine System Design

The wind turbines are machines that convert the kinetic energy of the moving air first into mechanical energy with the turbine blades and then into electrical energy with the generator. The wind turbines can start generating electrical energy only at a certain wind speed (2-4 ms⁻¹). After high wind speeds (25-35 ms⁻¹), wind turbines are automatically switched to the stop position to prevent damage to the system and to protect it (MENR, 2023).

The structure of the wind turbine system may include a wind turbine, batteries, battery charge control unit (charge regulator), inverter, command center, and various electronic circuits (Toprak, 2011; Şenel and Koç, 2015). In this designed system, the wind turbine is used as an energy source. Batteries were added to the system to provide energy in case the wind power cannot generate energy when needed or the system operates off-grid. Batteries store electrical energy as chemical energy and provide electrical energy to the system when needed. To prevent overcharging or discharging of the batteries, a charge regulator is added to the system. This extends the life of the batteries. If the system is on a grid or 220 V 50 Hz alternating current will be used in the system, an inverter should be used in the system (Toprak, 2011; Şenel and Koç, 2015).

2.3. Evaporative Cooling Systems in Poultry House

Providing a certain degree of cooling in the barns during the hot seasons will help minimize the heat stress on the animals. This allows for maintaining a healthy, high-quality, and efficient production. For this reason, the

evaporative cooling method is used in poultry houses located in the southern and hot regions of our country. Fans, which are operated continuously 24 hours a day during the summer season, work as an important element of the cooling system. This increases the energy consumption of the facility. As a result of the increase in the electrical energy consumption, production input costs increase too. This results in expensive products and weakens the competitive edge of producers (Bilgili and Dağtekin, 2019).

With the use of the wind turbine system, a renewable energy source, in the poultry houses in Tekirdağ region, the electricity cost burden on the producer can be reduced significantly. If planning is made properly, the generated excess energy can be given to the system and income can be earned. The system of the study is illustrated in Figure 1.

3. Results and Discussion

3.1. Design of Fan-Pad Systems to Be Used in Poultry Houses

A fan-pad cooling system was designed for the poultry house accommodating 6000 chickens. The width of the

poultry house is 14 meters, the length is 30 meters, and the height is 3 meters (Şenköylü, 2001). The floor plan, ventilation, and cooling system of the projected poultry house are given in Figure 2.

For each 25 m² of floor area (A₁) of the animal barn, 1 m² of wet pad area is needed. The required pad area (A_p) for a barn with a floor area of 420 m² (A_b) can be found as follows (Equation 1) (Yüksel and Yüksel-Türkboyları, 2018).

$$A_p = \frac{A_b}{25} = \frac{420}{25} = 16.8 \text{ m}^2 \quad (1)$$

The daily water requirement of the wet pad is about 1 L on hot days (Bucklin et al., 1993). A small circulation pump is used to wet the pad.

The quantity of ventilation in animal barns is determined by the geographical location of the barn, the season, and the number of animals. The quantity of ventilation in the poultry houses is between 7 and 9 m³h⁻¹ (Q₁) for 1 kg live weight in the insulated poultry houses. Since the average weight of chickens is 1.5 kg, the total quantity of ventilation (Q₂) for 6000 chickens was calculated as follows (Equation 2) (Şenköylü, 2001).



Figure 1. Poultry house, wind turbine system, and elements.

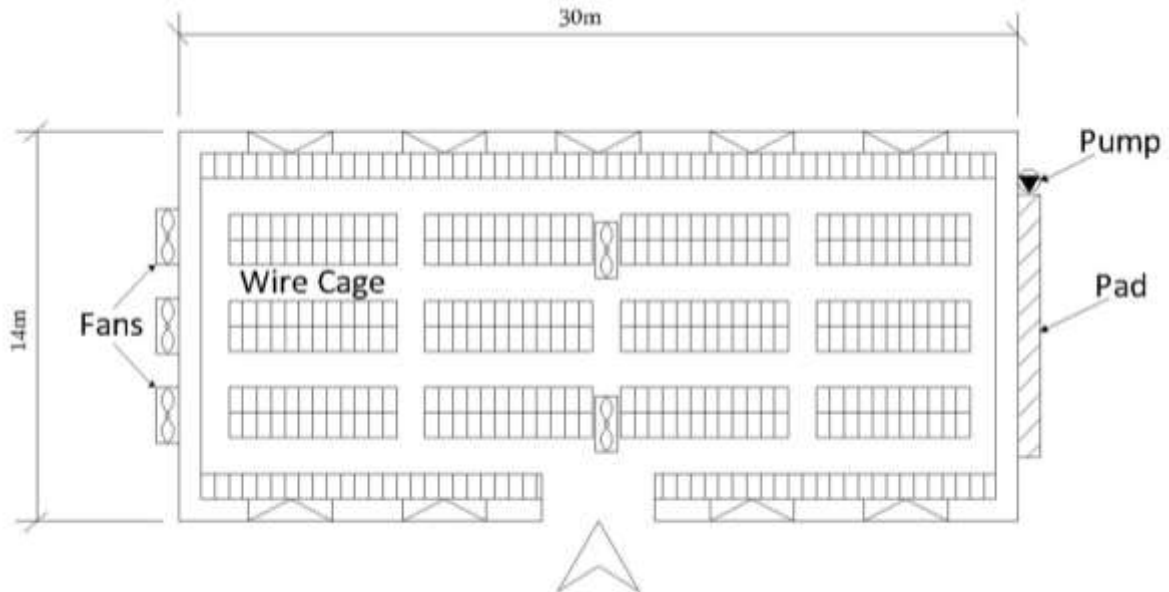


Figure 2. Poultry house floor plan and ventilation-cooling system.

$$Q_t = Q_1 \times 1.5 \times n$$

$$Q_t = 9 \times 1.5 \times 6000 = 81000 \text{ m}^3\text{h}^{-1} \quad (2)$$

If the length of the barn is between 25 and 30 meters, 2 aspirators should be placed in the middle of the barn for the aspirators to have a sufficient effect (Yüksel and Yüksel-Türkboyları, 2018).

The aspirators may be operated individually or in groups according to the needs of the animals in the poultry houses. 1400 rpm (dd^{-1}) and 0.75 kWh aspirators with a diameter of 60 cm and a flow rate of $9500 \text{ m}^3\text{h}^{-1}$ (Q_a) were used to provide this quantity of ventilation in the poultry house (Equation 3) (Anonymous, 2022).

$$n_a = Q_t / Q_a$$

$$n_a = 81000 / 9500 = 8.5 \sim 9 \text{ piece} \quad (3)$$

Since the investigated poultry house is 30 m long 2 aspirators need to be placed in the middle of the house. Accordingly, the number of aspirators in the system is increased up to 11.

The energy requirement of the wind turbine system was calculated as follows (Equation 4):

$$0.75 \times 11 + 0.2 = 8.45 \text{ kWh} \quad (4)$$

This ventilation system needs a wind turbine system of approximately 10 kWh, which is greater than the calculated 8.45 kWh, to operate efficiently. Depending on the wind conditions, the wind turbine system will have periods that it does not generate energy or its output is low. Therefore, a system having a capacity greater than the need should be preferred. When the system is working efficiently, the excess energy from the system can be supplied to the network or stored in off-grid systems in batteries.

3.2. Cost Analysis of Wind Turbine Energy System

Among renewable energy sources, wind turbine and solar panel energy production systems play a leading role. The wind turbine energy system is also suitable for per unit energy cost. The cost of the energy system varies depending on the manufacturer and country. However, the installation cost of the wind turbine system is quite high. It is known that the installation cost is around \$ 2500 per kWh (Erkoç, 2019; Türkdoğan et al., 2020; Türkboyları and Yüksel, 2024).

The wind turbine energy system to be installed is 10 kWh, whose value is 25000 \$. The transportation and installation cost of the system is around \$5000. The total cost of the wind turbine system to be installed in the system will be 30000 \$.

The unit cost of the fans used in ventilation, including transportation and installation, is \$500. The total cost of 11 fans used in the system is \$5500 (Anonymous, 2023a). The unit price of the pad used to cool the air of the chicken coop is \$20. The total price of a 16.8 m² pad is \$336. If transportation and assembly of the pad system are added, it costs \$403 (Anonymous, 2023b). The cost of the water pump used in the system is \$50 (Anonymous, 2023c).

The cost of the ventilation and cooling system to be

installed with the wind turbine is \$35953.

3.3. Environmental Impact of Wind Turbine Energy System

Countries meet their electricity needs from various sources such as coal, natural gas, hydroelectricity, geothermal, biomass, and nuclear. These sources pollute the environment with a wide range of wastes and cause climate change. To reduce this impact, renewable energy sources such as wind and solar energy are preferred as clean energy sources.

Coal-fired thermal power plants have a significant share of 21% of Türkiye's electricity production (Orhan and Şahin, 2022). Thermal power plants that run on coal burn coal to generate electricity and release significant amounts of CO₂ gas into the atmosphere.

According to the Carbon Neutral Charitable Fund, the amount of CO₂ released into the atmosphere by thermal power plants (1 kWh) to generate electricity from coal is 0.94 kg (CNCF, 2023). According to this calculation, the amount of CO₂ that is prevented from being released into the atmosphere is calculated in kg by multiplying the amount of energy produced in kWh per year by 0.94 for a facility that generates electricity with renewable energy sources. This shows how important it is to switch to renewable energy sources in terms of environmental protection.

It is concluded that a 10-kWh wind turbine system was suitable for this project. In other words, the system will generate 10 kWh of electricity. It is expected that the turbine system's operating time is less on some days while more on other days. When it operates for a longer period, excess energy is stored in the network in the on-grid system and the batteries are activated in the off-grid system. On days when the system works for a shorter period, the system is supported either from the grid or from batteries. If the power of the wind turbine system is 10 kWh and assuming operate for 5 hours a day on an average, the amount of energy generated in a year (365 days) can be calculated as follows (Equation 5):

$$10 \text{ kWh} \times 5 \text{ h day}^{-1} \times 365 \text{ day} = 18250 \text{ kWh} \quad (5)$$

This electricity generation will prevent the emission of 17155 kg ($18250 \times 0.94=17155 \text{ kg}$ of CO₂) into the atmosphere. Shifting towards renewable energy sources is a good solution to reduce the high amount of CO₂ to be released into the atmosphere in case of generating electricity with fossil fuels and to protect the environment.

4. Conclusion

In the regions where wind power is sufficient, it is possible to generate and use electrical energy with the wind turbine systems. Thus, on the one hand, energy could be provided to agricultural businesses in rural areas having no electricity network, on the other hand, significant amounts of greenhouse gas emissions into the atmosphere could be avoided.

The main objective in animal production is to ensure

appropriate living comfort in the poultry house environment for a good and high-quality yield. Chickens are very sensitive to high air temperatures. For this reason, the poultry houses should be ventilated and cooled when the air temperature is high. Fans and pads are necessary to ventilate and cool the poultry houses as desired. In the animal barns located in rural areas, the electrical energy required for operating the fans and pads can be supplied by a wind turbine system. At the same time, the cost burden of the business can be reduced with the electrical energy generated from renewable energy sources. If proper planning can be achieved, the excess energy generated can be used in other parts of the facility, or it can be supplied to the network to get income for the facility.

Author Contributions

The percentage of the author(s) contributions is presented below. All authors reviewed and approved the final version of the manuscript.

	E.T.	A.N.Y.
C	50	50
D	50	50
S	50	50
DCP	50	50
DAI	50	50
L	50	50
W	50	50
CR	50	50
SR	100	

C=Concept, D= design, S= supervision, DCP= data collection and/or processing, DAI= data analysis and/or interpretation, L= literature search, W= writing, CR= critical review, SR= submission and revision.

Conflict of Interest

The authors declared that there is no conflict of interest.

Ethical Consideration

Ethics committee approval was not required for this study because of there was no study on animals or humans.

References

- Anonymous. 2023a. URL: <https://www.fansanmarket.com/urun/sanayi-aspiratoru-harici-motorlu-kare-kasa-9500-m3h-cap-60-cm/146/> (accessed date: September 01, 2023).
- Anonymous. 2023b. URL: <https://turkish.alibaba.com/p-detail/Agriculture-60708802282.html?spm=a2700.7724857.0.0.332a4dd40GozfY> (accessed date: September 01, 2023).
- Anonymous, 2023c. URL: <https://www.hepsiburada.com/klpro-klpsp256-100watt-sirkulasyon-pompa-pm-HBC-00000E6SPM> (accessed date: September 01, 2023).
- Anonymous. 2022. URL: www.hvacturk.com/urun/ayas-60-cm-7-kanatli-sanayi-tipi-aspirator (accessed date: October 26, 2022).
- Atılğan A, Coşkan A, Öz H, İşler E. 2010. Etlik piliç kümesinde

- kiş döneminde amonyak gaz düzeyinin vakum sistemi ile azaltılması. Kafkas Univ Vet Fak Derg, 16(2): 257-262.
- BESD-BİR. 2023. Association of Poultry Meat Producers and Breeders. URL: <https://besd-bir.org/assets/uploaded/Tr-kisi-basina-turlere-gore-et-tuketimi.pdf> (accessed date: August 17, 2023).
- Bilgili ME, Dağtekin M. 2019. Adana koşullarında etlik piliç (broiler) kümeslerinde elektrik enerjisinin fotovoltaik güneş panellerinden karşılanması. Çukurova 2. Uluslararası Multidisipliner Çalışmalar Kongresi, 11 Haziran, Adana, Türkiye.
- Bucklin RA, Henley RW, McConnel DB. 1993. Fan and pad greenhouse evaporative cooling systems. University of Florida, Florida Cooperative Extension Service, Circular 1135, Florida, US.
- Çelikdemir S, Özdemir MT. 2020. Adilcevaz bölgesinde rüzgar enerji potansiyelinin incelenmesi. BEÜ Fen Bil Derg, 9(1): 204-214.
- CNCF. 2023. Carbon Neutral Charitable Fund. URL: <https://carbonpositiveaustralia.org.au/calculate/> (accessed date: August 01, 2023).
- Dağtekin M. 2012. Etlik piliç kümeslerinin serinletilmesinde güneş enerjisi kullanımının tekno-ekonomik analizi. ÇÜZF Derg, 27(2): 11-20.
- Dikmen E, Örgen FK. 2018. Ağlasun bölgesi için rüzgar hızı tahmini ve en uygun türbin tespiti. ÖHÜ Müh Bil Derg, 7(2): 871-879.
- Doğan S. 2005. Türkiye'nin küresel iklim değişikliğinde rolü ve önleyici küresel çabaya katılım girişimleri. CÜİB Derg, 6(2): 57-73.
- Erensoy K, Altan A, Bayraktar H. 2015. Tam çevre denetimli yumurta üretim kümeslerinin enerji kullanım karakteristikleri ve enerjiden tasarruf olanakları. 9. Ulusal Zootekni Bilim Kongresi, 3-5 Eylül, Konya, Türkiye.
- Erkoç R. 2019. Güneş enerjisi santrallerinin modellenmesi, ekonomik analizi ve değerlendirme: Almanya ve Türkiye uygulamaları. MSc Thesis, Ordu University, Institute of Science, Ordu, Türkiye, pp: 106.
- Gençel H, Tarhan İ. 2019. Rüzgar enerjisinin önemli geçiş yerlerinden olan Çanakkale bölgesindeki bazı rüzgar enerji santralleri için kapasite faktörü incelemesi. Çanakkale Onsekiz Mart Univ Fen Bil Enst Derg, 5(1): 120-139.
- Karaca C, Yıldız Y, Dağtekin M, Gümüş Z. 2016. Effect of water flow rate on cooling effectiveness and air temperature change in evaporative cooling pad systems. Environ Eng Manag J, 15(4): 827-833.
- Karacan R. 2017. Türkiye'de kırmızı et talebinin, beyaz et tüketimi ve gelir dağılımı açısından değerlendirilmesi. Finans Pol Ekon Yorum, 54(630): 67-73.
- Karık F, Sözen A, İzgeç MM. 2017. Rüzgar gücü tahminlerinin önemi: Türkiye elektrik piyasasında bir uygulama. Politeknik Derg, 20(4): 851-861.
- Koçaslan G. 2010. Sürdürülebilir kalkınma hedefi çerçevesinde Türkiye'nin rüzgar enerjisi potansiyelinin yeri ve önemi. Sos Bil Derg, 4: 53-61.
- Kurucu AA. 2015. Yeşil enerji: Türkiye'nin potansiyelinin ve uygulamalarının Avrupa'dan örneklerle karşılaştırılması. PhD Thesis, Ankara University, Institute of Social Sciences, Ankara, Türkiye, pp: 167.
- MCT. 2023. Republic of Türkiye Ministry of Culture and Tourism. URL: <https://tekirdag.ktb.gov.tr/TR-75726/genel-bilgiler.html> (accessed date: June 15, 2023).
- MENR. 2023. Republic of Türkiye Ministry of Energy and Natural Resources. URL: <https://enerji.gov.tr/eigm-resources-en> (accessed date: July 28, 2023).

- MoEU. 2020. Ministry of Environment and Urbanisation. URL: https://webdosya.csb.gov.tr/db/tekirdag/menu/temiz-hava-eylem-plani-2020-2024-s_20201016045422.pdf (accessed date: July 28, 2023).
- Orhan N, Şahin S. 2022. Bir besi çiftliğinde güneş enerji sisteminin uygulanması ve ekonomik analizi. *Türk Tarım Doğa Bil Derg*, 9(1): 33-40.
- Schiermeier Q, Tollefson J, Scully T, Witze A, Morton O. 2008. Energy alternatives: Electricity without carbon. *Nature*, 454: 816-823.
- Şenel MC, Koç E. 2015. Dünya’da ve Türkiye’de rüzgar enerjisi durumu-genel değerlendirme. *Müh Makina*, 56(663): 46-56.
- Şenköylü N. 2001. Modern Tavuk Üretimi. *Anadolu Matbaacılık, Tekirdağ, Türkiye*, pp: 74.
- Taktak F, İli M. 2018. Güneş enerji santrali (GES) geliştirme: Uşak örneği. *Geomatik Derg*, 3(1): 1-21.
- Toprak A. 2011. Elektrik üretimi için düşük güçlü rüzgar enerji sistemi tasarımı. MSc Thesis, Selçuk University, Institute of Science, Konya, Türkiye, pp: 82.
- Tunus O. 2019. Bursa’da yenilenebilir enerji kaynakları ile elektrik üretim potansiyelinin ekonomik analizi. MSc Thesis, Bursa Uludağ University, Institute of Social Sciences, Bursa, Türkiye, pp: 142.
- Türkboyları E, Yüksel AN. 2024. Rüzgar türbinlerinin tarımsal amaçla hayvan barınaklarında enerji kaynağı olarak kullanılma olanakları. *Osmaniye Korkut Ata Üniv Fen Bil Enst Derg*, 7(2): 610-621.
- Türkdoğan S, Mercan MT, Çatal T. 2020. Şebekeden bağımsız hibrit enerji sistemleri kullanılarak 40 hanelik bir topluluğun elektrik ve termal yük ihtiyacının karşılanması: Teknik ve ekonomik analizleri. *Avrupa Bil Teknol Derg*, 18: 476-485.
- Warren C, Lumsden C, O’Dowd S, Birnie R. 2005. “Green on green”: Public perceptions of wind power in Scotland and Ireland. *J Environ Plan Manag*, 48(6): 853-875.
- Yüksel AN, Türkboyları E. 2019. Ensuring the ventilation and cooling of poultry houses with zero energy. 1st International Congress on Biosystems Engineering (ICOBEN-2019), September 24-27, Hatay, Türkiye.
- Yüksel AN, Yüksel-Türkboyları E. 2018. Using the photovoltaic cells for ventilation and cooling of the animal barns. 1st International 14th National Congress on Agricultural Structures and Irrigation (ICASI-2018), September 26-28, Antalya, Türkiye.



ELEKTRİKLİ ARAÇ DEVRESİNDE KULLANILAN BOOST DÖNÜŞTÜRÜCÜNÜN ANALİZİNE FARKLI YAKLAŞIMLAR

Ayşe Tuğba YAPICI^{1*}, Nurettin ABUT¹, Ali Bekir YILDIZ¹

¹Kocaeli University, Faculty of Engineering, Department of Electrical Engineering, 41100, Kocaeli, Türkiye

Özet: Bu çalışmada, dünya geneli ve ülkemizde oldukça hızlı yayılmaya başlayan elektrikli araç konusu ele alınmıştır. Bu hızlı yayılmanın sebebi yaşanan enerji sorunları ve çevresel faktörlerdir. Olumsuzluklar değerlendirildiğinde, ulaşım araçlarında kullanılan enerjiler açısından elektrik oldukça cazip bir enerji kaynağıdır. Bundan dolayı elektrikli araçlar alanındaki araştırma ve çalışmalar yaşanan hızlı büyüme bakımından ihtiyaç olup katkı sağlamaktadır. Yapılan çalışma ile elektrikli araçlarda tercih edilebilecek dönüştürücü devre seçeneklerinden birisi olan boost (yükselten) dönüştürücü devresinin sayısal yöntemlerle analizine ilişkin iki özgün yaklaşım irdelenmektedir. Dönüştürücü devrede, anahtarlar iki farklı şekilde modellenmiştir. İlk olarak iki değerli direnç yaklaşımı, daha sonra ideal anahtar yaklaşımı kullanılmıştır. Her iki modelleme durumunda da genelleştirilmiş düğüm denklemleri ile analiz yapılmıştır. Bu denklemlerin analitik ve sayısal olarak yapılan çözümleri ile kalıcı hal bölgesinde elde edilen sonuçların aynı olması, uygulanan modellerin ve yöntemlerin doğruluğunu göstermektedir. Analitik ve sayısal olarak çözümlenen devre, MatlabSimulink ortamında simüle edilerek sonuçların doğruluğu teyit edilmiştir. Ayrıca yapılan çalışma ile elde edilen sonuçların gerçek sonuçlara yakın olduğu gösterilmiştir. Böylelikle konu üzerinde çalışma yapacaklar için uygulama çalışması öncesi yapılan inceleme ile sayısal veri örneği de sunulmuş olacaktır.

Anahtar kelimeler: Elektrikli Araç, Boost (yükselten) dönüştürücü, Düğüm gerilimleri yöntemi, Modelleme


Different Approaches to Analysis of Boost Converter Used in Electric Vehicle Circuit


Abstract: In this study, the subject of electric vehicles, which has started to spread very rapidly in the world and in our country, is discussed. The reason for this rapid spread is the energy problems and environmental factors. Considering all these negativities, electric is a very attractive energy source in terms of transportation. For this reason, every study on the electric vehicle will contribute to the rapid growth. In this study, different approaches have been shown regarding the analysis of the boost converter circuit, which is one of the converter circuit options that can be preferred in electric vehicles, by numerical methods. Two different modeling have been implemented in the converter circuit. First, the boost converter circuit was modeled by a dichotomous resistance approach and the model's equations for the analysis of the model were obtained by generalized node equations. Then the boost converter circuit is modeled with the ideal switch approach and the model's equations for the solution of the model were obtained by generalized knot equations. The results obtained from analytical and numerical solutions of these equations and the results obtained in the permanent state region have been shown to be the same. The analytical and numerically analyzed circuit was simulated in MatlabSimulink environment and the same results are confirmed in the simulation environment. In addition, it is aimed that the results obtained with the study are close to the real results. For those who will work on the subject, a numerical data sample will be presented with the work done before the application study.


Keywords: Electric vehicle, Boost converter, Node voltage method, Modelling

*Sorumlu yazar (Corresponding author): Kocaeli University, Faculty of Engineering, Department of Electrical Engineering, 41100, Kocaeli, Türkiye

E mail: a.tgb.yipc@hotmail.com (A. T. YAPICI)

Ayşe Tuğba YAPICI  <https://orcid.org/0000-0003-2471-0835>

Nurettin ABUT  <https://orcid.org/0000-0001-6732-7575>

Ali Bekir YILDIZ  <https://orcid.org/0000-0003-4043-7859>

Gönderi: 04 Mart 2024

Kabul: 10 Mayıs 2024

Yayınlanma: 15 Mayıs 2024

Received: March 04, 2024

Accepted: May 10, 2024

Published: May 15, 2024

Cite as: Yapıcı AT, Abut N, Yıldız AB. 2024. Different approaches to analysis of boost converter used in electric vehicle circuit. BSJ Eng Sci, 7(3): 601-609.

1. Giriş

Günümüzde gelişen endüstri alanı daha fazla kaynak arayışını gündeme getirmiştir (Zimm, 2021). Bu arayış içerisinde öncelik temiz çevre konusunda oluşan hassasiyete uygunluktur. Konu ulaşım açısından değerlendirildiğinde elektrik oldukça uygun bir seçenektir (Hawkins ve ark., 2013; Günaslan ve ark., 2023). Bu sebeple son zamanlarda ulaşımında elektrikli araç çok hızlı bir yayılım göstermektedir (Nilsson ve Nykvist, 2016).

Özellikle mühendislik alanında fiziksel bir yapıyı incelerken, gerçek yapıya benzer şekilde modeller

oluşturulması önemlidir (Yapıcı, 2018). Gerçek sisteme benzeyen bu modeller üzerinde yapılan analitik çözümler, sayısal çözümler ve paket programlar ile elde edilen çözümler, tasarım öncesi büyük kolaylıklar sağlar. Yapılan çalışmada elektrikli araç sisteminde bataryadan çekilen enerjinin yük motorunda kullanıma uygun gerilim seviyesine dönüştürmek için kullanılabilecek dönüştürücü devre seçeneklerinden biri olan boost dönüştürücü tercih edilmiştir (Ortuzar ve ark., 2003; Malik ve ark., 2020; Hançar ve Kaymaz, 2021). Böylelikle bataryadaki gerilim seviyesi yükseltilerek motor için uygun hale getirmek hedeflenmiştir (Moreno ve ark.,



2006; Young ve ark., 2013; Alphonse ve ark., 2012). Boost dönüştürücü devre için modelleme yapılarak hedef sonuçlara ulaşmak amaçlanmıştır. Modelleme konusunun yapılan çalışmalara sağlayacağı katkıdan dolayı, anahtarlama elemanları için iki farklı modelleme seçeneği kullanılmıştır (Yıldız, 2013). Bu modellemelerden biri iki değerli direnç yaklaşımıdır. Bu yaklaşımda iletimde olan temel anahtar ve diyot için çok küçük direnç değeri seçilirken, yalıtımda olan temel anahtar ve diyot için büyük direnç değeri seçilerek modelleme yapılmıştır (Yıldız, 2013). Devre yapısı değişmediğinden, her iterasyon için denklemler aynı kalmakta, sadece başlangıç koşulları güncellenmektedir (Yıldız, 2013). Diğer modelleme yöntemi ise ideal anahtar yaklaşımıdır. Bu yaklaşımda, iletimde olan temel anahtar ve diyot için 0V değerinde gerilim kaynağı, yalıtımda olan temel anahtar ve diyot ise 0A değerinde akım kaynağı olarak modellenmiştir. Devre yapısı değiştiğinden, her iterasyon için denklemler ve başlangıç değerleri güncellenmektedir. Her iki modelleme için de, sistem analizi Genelleştirilmiş düğüm gerilimleri yöntemi ile yapılmıştır. Sayısal analiz için Trapez yöntemi kullanılarak, her iki yaklaşım için sonuçlar elde edilmiştir (Köseni ve Yıldız, 2019).

2. Elektrikli Araç

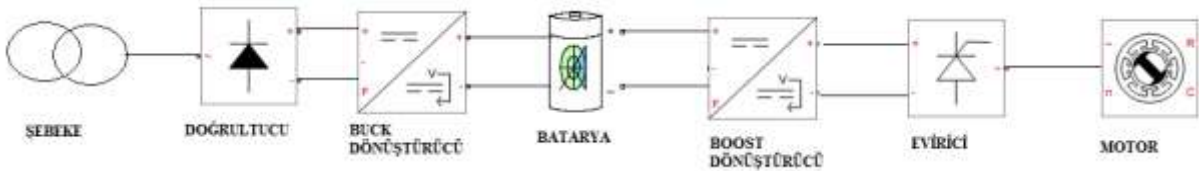
Elektrikli araç temel çalışma prensibi, şebekeden alınarak bataryada depolanan enerjinin daha sonra ihtiyaç duyulduğunda tekrar bataryadan alınarak motor tarafından kullanılması sonucu, tekerleğin hareketinin sağlanmasına dayanmaktadır (Li ve ark., 2016; Sabri ve ark., 2016; Çelik ve Abut, 2022). Şebekeden alınan enerji ilk olarak bataryada depolanmadan önce, bataryada depoalanmaya uygun gerilim seviyesine düşürülmesi gerekmektedir (Khaligh ve Li, 2010; Sousa ve Boris Bouchez, 2010; Clement-Nyns ve ark., 2011; Lunz ve ark., 2012). Depolanan enerji daha sonra motorda kullanılmadan önce motorun çalışması için gerekli uygun

gerilim seviyesine dönüştürülmesi gerekmektedir (Sharma ve ark., 2020). Her iki dönüşüm işlemi için dönüştürücü devreler kullanılmaktadır. Şekil 1 incelendiğinde elektrikli araç için şebekeden başlayarak motora kadar olan kısım genel olarak gösterilmiştir. Şebekeden alınan enerji ilk olarak bataryada depo edilebilecek forma dönüştürülmelidir (Sharma ve ark., 2020). Bu sebeple ilk olarak doğrultucu devre kullanılarak AC sinyal DC sinyale doğrultulmuştur (Kumar ve ark., 2023). Daha sonra ise doğrultulan sinyal buck dönüştürücü devre ile bataryada depo edilebilecek seviyeye getirilir ve depolanır (Kumar ve ark., 2023). Araç hareketi için bataryadan alınan enerji boost dönüştürücü devre ile gerilim seviyesi yükseltildikten sonra evirici ile çıkıştaki AC motor için AC sinyale dönüştürülür (Genç, 2023).

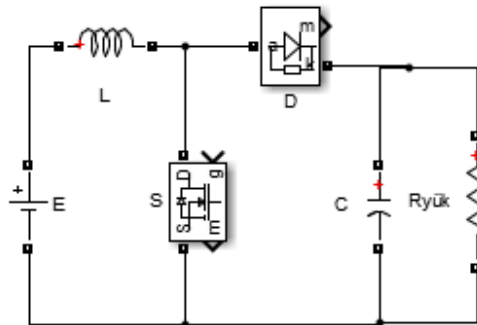
Şarj işlemi AC tip bir şarj istasyonunda gerçekleştiriliyorsa şebekeden alınan enerjinin bataryaya kadar olan kısmındaki dönüşüm işlemi araç içerisinde gerçekleşir (Sun ve ark., 2016; Sivaraman ve Sharmeela, 2021). Eğer DC tip bir şarj istasyonunda şarj işlemi gerçekleştiriliyorsa bu dönüşüm şarj istasyonunda gerçekleşir ve batarya direk hızlıca şarj edilir (Bai ve ark., 2010; Khan ve ark., 2019). Çünkü gerilim bataryada DC olarak depo edilir (Li ve ark., 2016). Yapılan çalışmada ise bataryadan motora kadar olan kısımda tercih edilebilecek dönüştürücü devre seçeneklerinden birisi olan boost devre ele alınmıştır. Şekil 1'deki devrenin boost devre bloğu için modelleme yapılmıştır. Benzer çalışmalar buck dönüştürücü devre, evirici ve motor bloğu için yapılabilir.

3. Boost (Yükselten) DC-DC Dönüştürücü

Boost dönüştürücü devre girişine uygulanan gerilimi çıkışında daha yüksek bir gerilim seviyesine dönüştürür (Baek ve ark., 2005; Chen ve ark., 2006; Prudente ve ark., 2008; Garip ve ark., 2009). Şekil 2'de Boost dönüştürücü devresi görülmektedir.

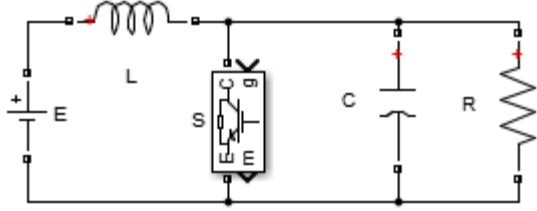


Şekil 1. Elektrikli araç iç yapısı.



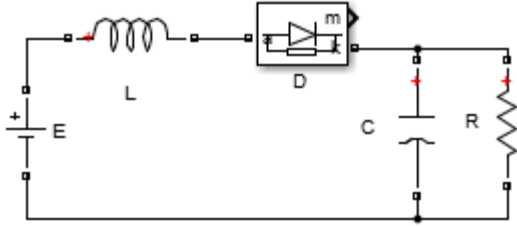
Şekil 2. Boost dönüştürücü devre.

Devre bir temel anahtar (S), bir endüktans (L), bir kapasitör (C), bir diyot (D) ve çıkışa bağlanan dirençten oluşmaktadır (Mert, 2007). Devrede bir temel anahtar vardır, bu nedenle anahtarın iletimde ve kesimde olma durumuna göre iki adet çalışma topolojisi bulunmaktadır (Tofoli ve ark., 2015; Çalışkan ve ark., 2017). Şekil 3’de S anahtarının iletimde iken diyodun kesim durumu gösterilmiştir (Öncü ve Sazak, 2006).



Şekil 3. Boost dönüştürücü devre, anahtar iletimde-diyot kesimde modu.

Bu modda bobin enerjilenmektedir. Şekil 4’de anahtarın kesimde diyodun ise iletimde olduğu mod gösterilmektedir (Öncü ve Sazak, 2006).



Şekil 4. Boost dönüştürücü devre, anahtar kesimde-diyot iletimde modu.

Bu modda endüktansta depolanan enerji yükte aktarılmaktadır.

4. Sistem Denklemlerinin Elde Edilmesi

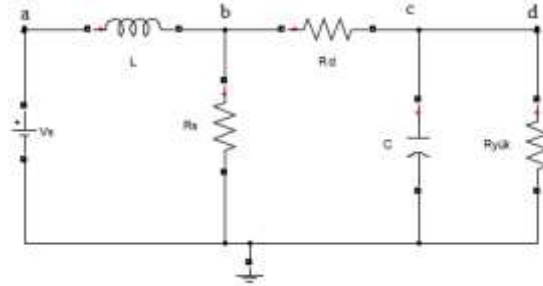
Bölüm 2’de genel çalışma prensibinden bahsedilen boost dönüştürücü devrenin sistem analizini yapabilmek için gerekli olan denklemler bu bölümde elde edilmiştir. Burada diğer devrelerden farklı olarak anahtarlama elemanları bulunmaktadır, Bu sebeple devrenin denklemlerini daha kolay olarak çıkarabilmek için önce anahtarlama elemanlarını modellemek gerekir. Bunun için tercih edilen iki yöntemde çalışmada gösterilmiştir. İki değerli direnç ve ideal anahtar yöntemi ile devre modellendikten sonra sistem denklemleri elde edilecektir. Bu denklemleri elde etmede kullanılan iki yaklaşım vardır: Genelleştirilmiş düğüm denklemleri (GDD), Durum değişkenleri yaklaşımı. Durum değişkenleri yaklaşımında bilinmeyen sayısı az ancak denklemleri elde etmek yoğun işlemler gerekmektedir. Genelleştirilmiş düğüm denklemleri yaklaşımında ise bilinmeyen sayısı fazla ancak denklemleri elde etmek daha kolaydır (Yıldız, 2013; Köseni ve Yıldız, 2019). GDD’nin s ve t domenindeki genel gösterimi Eşitlik (1) ve Eşitlik (2)’ de verilmiştir.

$$(G + sC)X(s) = BU(s) \quad (1)$$

$$Gx(t) + C \frac{dx(t)}{dt} = Bu(t) \quad (2)$$

4.1. Boost (Yükselten) DC-DC Dönüştürücünün İki Değerli Direnç Yaklaşımı İle Modellenmesi ve Sistem Denklemlerinin Elde Edilmesi

Bu bölümde bölüm 3’de bahsedilen anahtarlama elemanlarını modelleme yöntemlerinden biri olan iki değerli direnç yaklaşımı ile eşdeğer devre eldesi ve denklem çıkarımı gösterilmiştir. Şekil 5’de Boost dönüştürücü devresinin iki değerli direnç yaklaşımı ile modellenmiş şekli gösterilmektedir. Burada temel anahtar ve diyot birer küçük değerli ve büyük değerli direnç ile temsil edilmektedir. Anahtarın ve diyodun iletim ve kesim durumuna göre direnç değerleri güncellenerek simülasyona devam edilmektedir. Anahtar iletimde iken çok küçük bir direnç değeri ile temsil edilirken, anahtar kesimde iken çok büyük bir direnç ile temsil edilir. Benzer şekilde iletimde olan diyot çok küçük bir direnç değeri ile temsil edilirken, kesimde olan diyot çok büyük bir direnç değeri ile temsil edilir.



Şekil 5. İki değerli direnç yaklaşımı ile boost dönüştürücü eşdeğer devresi.

Şekil 5’deki devreye ait Genelleştirilmiş düğüm denklemleri eldesi için Eşitlik (1)’deki s domeni ile edilen katsayı matrisleri Eşitlik 3-7’de gösterilmiştir.

$$G = \begin{bmatrix} 0 & 0 & 0 & 1 & 1 \\ 0 & G_s + G_d & -G_d & -1 & 0 \\ 0 & -G_d & G_d + G_{yük} & 0 & 0 \\ 1 & -1 & 0 & 0 & 0 \\ 1 & 0 & 0 & 0 & 0 \end{bmatrix} \quad (3)$$

$$C = \begin{bmatrix} 0 & 0 & 0 & 0 & 0 \\ 0 & 0 & 0 & 0 & 0 \\ 0 & 0 & C & 0 & 0 \\ 0 & 0 & 0 & -L & 0 \\ 0 & 0 & 0 & 0 & 0 \end{bmatrix} \quad (4)$$

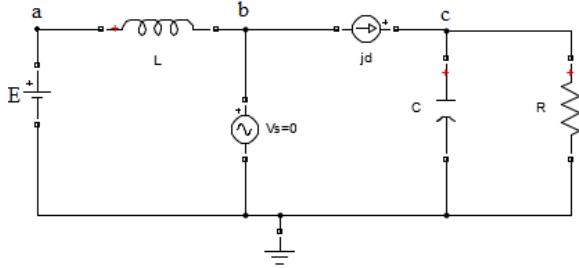
$$B = [0 \ 0 \ 0 \ 0 \ 1] \quad (5)$$

$$X(t) = [V_a \ V_b \ V_c \ I_L \ I_E] \quad (6)$$

$$U(t) = [E] \quad (7)$$

4.2. Boost (Yükselten) DC-DC Dönüştürücünün İdeal Anahtar Yaklaşımı İle Modellenmesi ve Sistem Denklemlerinin Elde Edilmesi

Bu bölümde bölüm 3'de bahsedilen anahtarlama elemanlarını modelleme yöntemlerinden biri olan ideal anahtar yaklaşımı ile eşdeğer devre eldesi ve denklem çıkarımı gösterilmiştir. Burada iki değerli direnç yaklaşımından farklı olarak anahtarlama elemanları bir akım ve bir gerilim kaynağı ile temsil edilmektedir. Bu sebeple devre eşdeğer modellemesi tek şekil üzerinden değil, iki şekil üzerinden incelenecektir. Çünkü iletimde olan anahtarlama elemanı bir gerilim kaynağı ile temsil edilirken kesimde olan anahtarlama elemanı bir akım kaynağı ile temsil edilmektedir. Bu sebeple iletim ve kesim durumları ayrı ayrı modelleme yapmak gerekmektedir. Şekil 6'da Boost dönüştürücü ideal anahtar yaklaşımı ile anahtar iletimde diyot kesim durumunda modellenmiş şekli gösterilmektedir.



Şekil 6. İdeal anahtar yaklaşımı: Temel anahtar iletimde diyot kesimde.

Şekil 6'daki devreye ait Genelleştirilmiş düğüm denklemleri eldesi için Eşitlik (1)'deki s domeni ile edilen katsayı matrisleri Eşitlik 8-12'de gösterilmiştir.

$$G = \begin{bmatrix} 0 & 0 & 0 & 1 & 0 & 1 \\ 0 & 0 & 0 & 0 & 1 & -1 \\ 0 & 0 & G_{yük} & 0 & 0 & 0 \\ 1 & 0 & 0 & 0 & 0 & 0 \\ 0 & 1 & 0 & 0 & 0 & 0 \\ 1 & -1 & 0 & 0 & 0 & 0 \end{bmatrix} \quad (8)$$

$$C = \begin{bmatrix} 0 & 0 & 0 & 0 & 0 & 0 \\ 0 & 0 & 0 & 0 & 0 & 0 \\ 0 & 0 & C & 0 & 0 & 0 \\ 0 & 0 & 0 & 0 & 0 & 0 \\ 0 & 0 & 0 & 0 & 0 & 0 \\ 0 & 0 & 0 & 0 & 0 & -L \end{bmatrix} \quad (9)$$

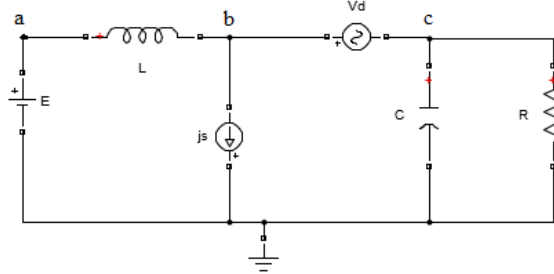
$$B = \begin{bmatrix} 0 & 0 & 0 \\ 0 & 0 & -1 \\ 0 & 0 & 1 \\ 1 & 0 & 0 \\ 0 & 1 & 0 \\ 0 & 0 & 0 \end{bmatrix} \quad (10)$$

$$X(t) = [V_a \ V_b \ V_c \ I_E \ I_s \ I_L] \quad (11)$$

$$U(t) = [E \ V_s \ J_d] \quad (12)$$

Elde edilen matrislerde temel anahtarın iletimde olması durumunda anahtar 0 V değerinde (V_s) bir gerilim kaynağı ile temsil edilirken, bu durumda kesimde olan diyot ise 0 A (J_d) değerinde bir akım kaynağı ile temsil edilmiştir.

Şekil 7'de Boost dönüştürücü ideal anahtar yaklaşımı ile anahtar kesimde, diyot iletimde durumu modellenmiş şekli gösterilmektedir.



Şekil 7. İdeal anahtar yaklaşımı: Temel anahtar kesimde diyot iletimde.

Şekil 7'deki devreye ait Genelleştirilmiş düğüm denklemleri eldesi için Eşitlik (1)'deki s domeni ile edilen katsayı matrisleri Eşitlik 13-17'de gösterilmiştir.

$$G = \begin{bmatrix} 0 & 0 & 0 & 1 & 0 & 1 \\ 0 & 0 & 0 & 0 & 1 & -1 \\ 0 & 0 & G_{yük} & 0 & -1 & 0 \\ 1 & 0 & 0 & 0 & 0 & 0 \\ 0 & 1 & -1 & 0 & 0 & 0 \\ 1 & -1 & 0 & 0 & 0 & 0 \end{bmatrix} \quad (13)$$

$$C = \begin{bmatrix} 0 & 0 & 0 & 0 & 0 & 0 \\ 0 & 0 & 0 & 0 & 0 & 0 \\ 0 & 0 & C & 0 & 0 & 0 \\ 0 & 0 & 0 & 0 & 0 & 0 \\ 0 & 0 & 0 & 0 & 0 & 0 \\ 0 & 0 & 0 & 0 & 0 & -L \end{bmatrix} \quad (14)$$

$$B = \begin{bmatrix} 0 & 0 & 0 \\ 0 & 0 & -1 \\ 0 & 0 & 0 \\ 1 & 0 & 0 \\ 0 & 1 & 0 \\ 0 & 0 & 0 \end{bmatrix} \quad (15)$$

$$X(t) = [V_a \ V_b \ V_c \ I_E \ I_d \ I_L] \quad (16)$$

$$U(t) = [E \ V_d \ J_s] \quad (17)$$

Elde edilen matrislerde temel anahtarın kesimde olması durumunda anahtar 0 A değerinde (J_s) bir akım kaynağı ile temsil edilirken, bu durumda iletimde olan diyot ise 0 V (V_d) değerinde bir gerilim kaynağı ile temsil edilmiştir.

4.3. Sistem Denklemlerine Trapez Yaklaşımının Uygulanması

GDD ile analitik olarak elde edilen denklemlerin bilgisayarda sayısal yöntemlerle belli aralıklarla (adım aralığı) çözümünü elde etmek için, Runge-Kutta, Forward Euler, Backward Euler, Trapezoidal gibi yöntemleri uygulanabilir. Bu çalışmada elde edilen GDD denklemlerinin sayısal yöntemlerle çözümü için Trapezoidal (Yamuk) yöntemi uygulanmıştır. Trapezoidal yöntemi denklemi Eşitlik 18’de gösterilmiştir.

$$X_{n+1} = X_n + \frac{h}{2} [f(X_{n+1}, t_{n+1}) + f(X_n, t_n)] \quad (18)$$

Eşitlik 2’de verilen GDD’nin t domenindeki denklemlerine, bu yöntemin uygulanması ile Eşitlik 19 elde edilir.

$$X_{n+1} = K_A X_n + K_B [U_n + U_{n+1}] \quad (19)$$

Eşitlik 19’daki K_A ve K_B Eşitlik 20’de gösterilmiştir.

$$K_A = K_1^{-1} K_2$$

$$K_B = K_1^{-1} \frac{h}{2} B \quad (20)$$

Eşitlik 20’deki K_1 ve K_2 ise, Eşitlik 21’de gösterilmiştir.

$$K_1 = \left[C + \frac{h}{2} G \right]$$

$$K_2 = \left[C - \frac{h}{2} G \right] \quad (20)$$

5. Bulgular

Elektrikli araç için boost dönüştürücü devrenin analizinde kullanılacak özgün yöntemlerden olan iki değerli direnç ve ideal anahtar yaklaşımını göstermek amacıyla yapılan bu çalışmada kullanılan parametreler Tablo 1 ve Tablo 2’de gösterilmiştir.

Tablo 1’de boost dönüştürücü devre iki değerli direnç yaklaşımı için parametreler verilmiştir.

Tablo 2’de boost dönüştürücü devre ideal anahtar yaklaşımı için parametreler verilmiştir.

Tablo 1 ve Tablo 2’deki parametreler kullanılarak Matlab’te elde edilen kararlı hal sonuçları Tablo 3 ve Tablo 4’de verilmiştir.

Tablo 3 ve Tablo 4’deki sonuçlar iki değerli direnç ve ideal anahtar yaklaşımı için anahtar açık ve kapalı durumdaki sonuçlar alınıp bir sonraki adım da veriler güncellenerek elde edilmiştir. Kararlı hal durumunda elde edilen sonuçlar tablolara eklenmiştir.

Tablo 3’te verilen İki değerli direnç yaklaşımı kararlı hal sonuçları Matlab grafikleri Şekil 8 ve Şekil 9’da görülmektedir.

Tablo 1. İki değerli direnç yaklaşımı parametreleri

E (Giriş Gerilimi)	$R_{smin}-R_{dmin}$	$R_{smax}-R_{dmax}R_{yük}$	C	L
12V	$10^{-3} \Omega$	$10^6 \Omega 5 \Omega 200 \mu F$		1mH

Tablo 2. İdeal anahtar yaklaşımı parametreleri

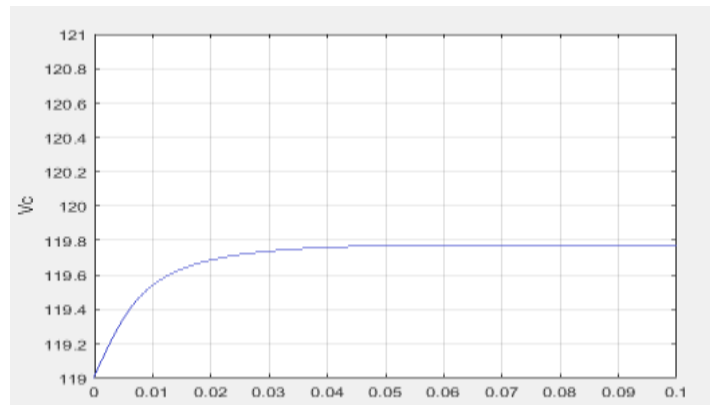
E (Giriş Gerilimi)	$V_s- V_d$	$J_s- J_dR_{yük}$	C	L
12V	0V	0A5 $\Omega 200 \mu F$		1mH

Tablo 3. İki değerli direnç yaklaşımı kararlı hal sonuçları

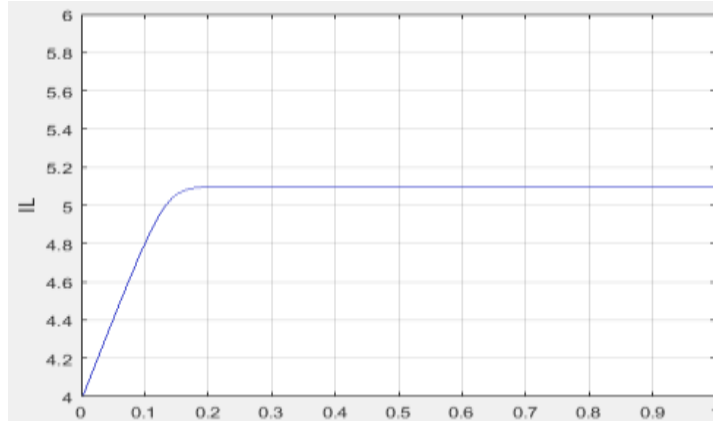
V_a	V_b	V_{cLLE}
12V	110.04V	119.78V 5.3182A
		-1.5129A

Tablo 4. İdeal anahtar yaklaşımı kararlı hal sonuçları

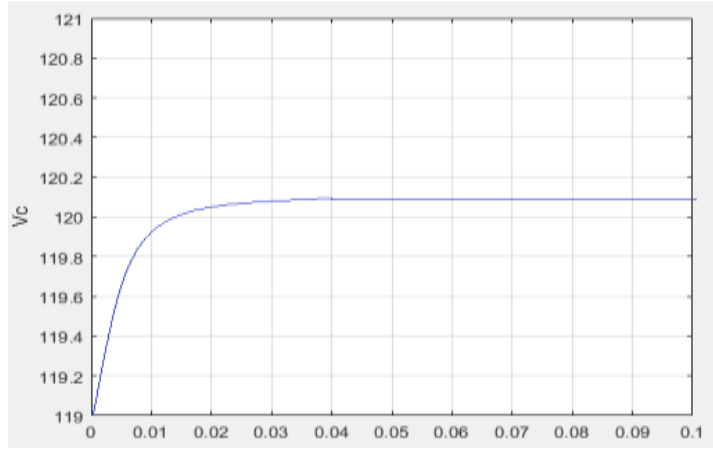
V_a	V_b	V_{cLLE}
12V	109.05V	120.14V 5.4278A
		-1.5132A



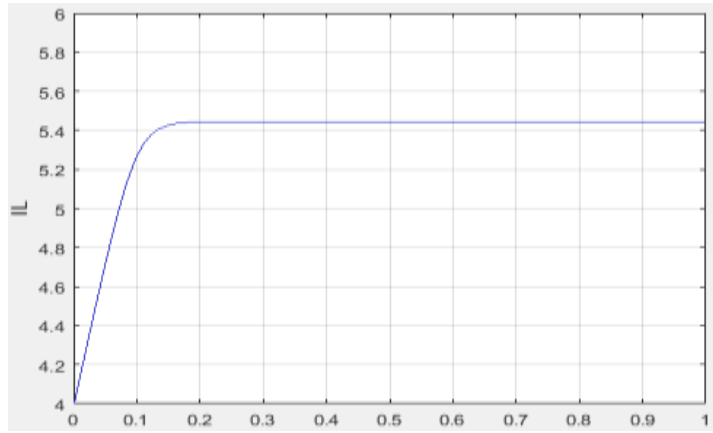
Şekil 8. İki değerli direnç yaklaşımı V_c gerilimi.



Şekil 9. İki değerli direnç yaklaşımı IL akımı.



Şekil 10. İdeal anahtar yaklaşımı VC gerilimi.



Şekil 11. İdeal anahtar yaklaşımı IL akımı.

Şekil 8 incelendiğinde iki değerli direnç yöntemi ile elde edilen denklemler çözümlendiğinde çıkış gerilimi, bu yöntemde VC gerilimi ile gösterilen, yaklaşık olarak 119 V değerini göstermektedir.

Şekil 9 incelendiğinde iki değerli direnç yöntemi ile elde edilen denklemler çözümlendiğinde endüktans üzerindeki akım yaklaşık olarak 5A değerini göstermektedir.

Tablo 4'te verilen ideal anahtar yaklaşımı kararlı hal sonuçları Şekil 10 ve Şekil 11'de verilen grafiklerde görülmektedir.

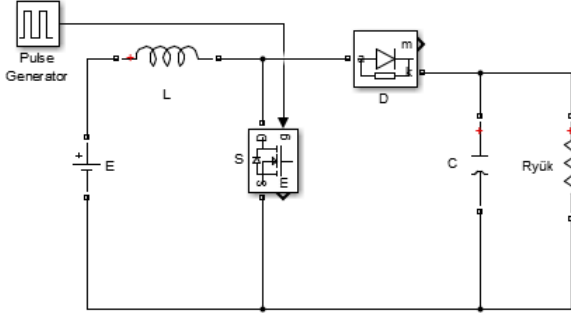
Şekil 10 incelendiğinde ideal anahtar yaklaşımı ile elde

edilen denklemler çözümlendiğinde çıkış gerilimi, bu yöntemde VC gerilimi ile gösterilen, yaklaşık olarak 120 V değerini göstermektedir.

Şekil 11 incelendiğinde ideal anahtar yaklaşımı ile elde edilen denklemler çözümlendiğinde endüktans üzerindeki akım yaklaşık olarak 5A değerini göstermektedir.

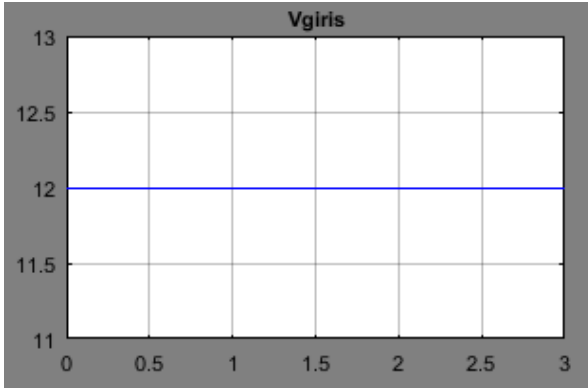
Yapılan çalışmada tercih edilen özgün yaklaşımlar ile elde edilen sonuçlarının birbiri ile yakın sonuçlar olması hedeflenirken bu sonuçların Matlab Simulink'te aynı veriler ile devrenin modellenerek sonuçların desteklenmesi de hedeflenmiştir. Şekil 12'de boost

dönüştürücü devrenin Matlab Simulink modeli gösterilmiştir. Burada iki değerli direnç ve ideal anahtar yaklaşımı ile eşitlikler üzerinden çözülmesi yapılan devrenin Matlab simulinkte modellenmiş şekli görülmektedir. Eşitlikler ile yapılan çözümlerde kullanılan sayısal değerler yapılan modellemede seçilen elemanlara birebir aynı olarak verilmiştir.



Şekil 12. Boost dönüştürücü Matlab simulink modeli.

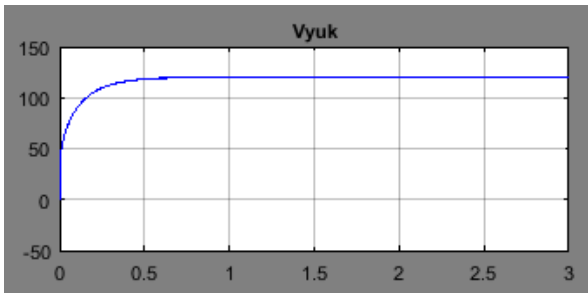
Şekil 13'de boost dönüştürücü devrenin Matlab Simulink modeli giriş gerilimi değeri gösterilmiştir. Buradaki 12 V değeri ortalama olarak bir bataryada depo edilebilecek gerilim değeridir. Yapılan çalışma ile kullanılan boost dönüştürücü devre ile bataryadan çekilen bu 12 V değeri elektrikli araç motoru için uygun gerilim seviyesine yükseltilecektir.



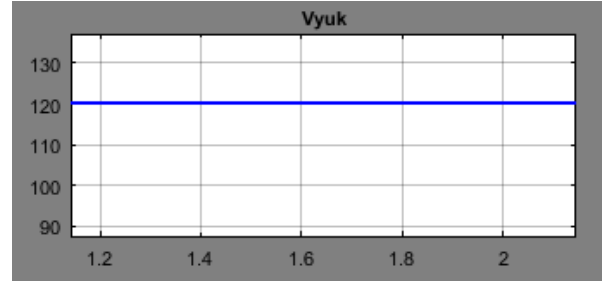
Şekil 13. Boost dönüştürücü Matlab Simulink modeli giriş gerilimi.

Şekil 13 incelendiğinde devrenin giriş geriliminin 12 V olarak belirlendiği görülmektedir.

Şekil 14 ve 15'de boost dönüştürücü devrenin Matlab Simulink modeli çıkış gerilimi gösterilmiştir.



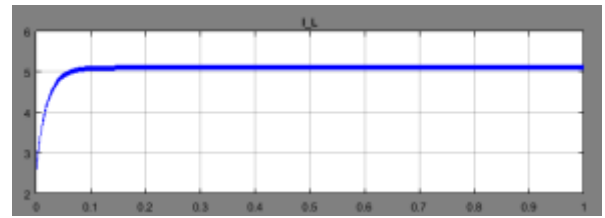
Şekil 14. Boost dönüştürücü Matlab Simulink modeli çıkış gerilimi.



Şekil 15. Boost dönüştürücü Matlab Simulink modeli çıkış gerilimi.

Şekil 14 ve Şekil 15 aynı çıkışın farklı yakınlıktaki görüntüleridir. Şekil 14 ve Şekil 15 incelendiğinde sistemin çıkış geriliminin 120 V olduğu görülmektedir. Elde edilen bu 120 V gerilim değeri elektrikli araç motoru için pratik uygulamada uygun bir değerdir.

Şekil 16 incelendiğinde endüktans akımının 5A olduğu görülmektedir.



Şekil 16. Matlab Simulink modeli IL akımı.

6. Sonuç

Elektrikli araç sistemi üzerinde kullanılabilecek boost dönüştürücü devre analizi için iki farklı özgün yaklaşım incelenmiştir. Konu üzerinde yapılan çalışmada Boost dönüştürücü devresi iki farklı yöntemle modellenmiş ve bu modellerin denklemleri elde edilirken geliştirilmiş düğüm denklemleri yöntemi tercih edilmiştir. Her iki yöntem için ayrı ayrı elde edilen denklemlerin trapez yöntemi ile sayısal analizi yapılmıştır. Kararlı hal analizi için iki yöntemle ait sonuçlar elde edilmiştir. Tablo 3 ve Tablo 4'de iki değerli direnç yaklaşımı ve ideal anahtar yaklaşımı için boost dönüştürücü devrenin kararlı hal sonuçları verilmiştir. Sonuçlar incelendiğinde Tablo 3 ve Tablo 4'de V_c olarak gösterilen sistemin çıkış gerilimi yaklaşık olarak 119 V ve 120 V olarak bulunmuştur. Her iki yaklaşım sonucunun neredeyse birbiri aynı olduğu görülmektedir. Benzer şekilde endüktans akımları da hemen hemen aynı sonucu vermiştir. Aynı devre, aynı veriler ile Matlab simulink ile de gerçekleştirilmiştir. Şekil 8 ve Şekil 10 incelendiğinde matlab modeli için çıkış geriliminin Tablo5 ve Tablo 4' deki V_c değeri 120 V ile aynı sonucu verdiği görülmüştür. Sonuçlar incelendiğinde hem iki değerli direnç yaklaşımının hem ideal anahtar yaklaşımının hem de simülasyon sonuçlarının birbiri ile aynı olduğu görülmektedir. 120 V değeri elektrikli araç motoru için ideal kabul edilebilecek bir değer olmakla beraber çalışmada üç farklı yöntemde aynı sonuç elde edilmiştir. Bunlara ek olarak sistemin girişine uygulanan 12 V

değeri gerçek bir elektrikli aracın batarya giriş değerine uygun olarak seçilmiş ve elde edilen çıkış gerilimi değerinin gerçek bir elektrikli araç için batarya çıkışından motor girişine kadar olan kısımdaki değeri sağladığı görülmüştür. Batarya için 10-15 V arası gerilim ideal kabul edildiği için çalışmada batarya gerilimi 12 V olarak kabul edilmiştir. Motor için ise yaklaşık olarak 120 V gibi bir değer gereklidir. Çalışma için uygulama kısmında elde edilen sonuçların hem birbiri ile aynı olması hedeflenirken hem de gerçek uygulama çalışmalarına da yakın değerler olması hedeflenmiştir. Sonuçlar incelendiğinde girişte 12 V olarak alınan değer motor için gerekli olabilecek 120 V'u sağladığı görülmektedir. Böylelikle çalışma için hedeflenen üç yöntemin sonucunun birbiri ile aynı olması ve aynı zamanda elektrikli araç için gerçek değerlere yaklaşması hedefleri sağlanmıştır.

Katkı Oranı Beyanı

Yazar(lar)ın katkı yüzdesi aşağıda verilmiştir. Tüm yazarlar makaleyi incelemiş ve onaylamıştır.

	A.T.Y.	N.A.	A.B.Y.
K	34	33	33
T	33	34	33
Y	33	33	34
VTI	40	30	30
VAY	40	30	30
KT	34	33	33
YZ	40	30	30
KI	20	40	40
GR	34	33	33
PY	34	33	33
FA	34	33	33

K= kavram, T= tasarım, Y= yönetim, VTI= veri toplama ve/veya işleme, VAY= veri analizi ve/veya yorumlama, KT= kaynak tarama, YZ= Yazım, KI= kritik inceleme, GR= gönderim ve revizyon, PY= proje yönetimi, FA= fon alımı.

Çatışma Beyanı

Yazarlar bu çalışmada hiçbir çıkar ilişkisi olmadığını beyan etmektedirler.

Etik Onay Beyanı

Bu araştırmada hayvanlar ve insanlar üzerinde herhangi bir çalışma yapılmadığı için etik kurul onayı alınmamıştır.

Kaynaklar

Alphonse I, Thilagar H, Singh FB. 2012. Design of solar powered BLDC motor driven electric vehicle. *Int J Renew Energy Res*, 2(3): 456-462.

Baek J, Ryoo M, Kim T, Yoo D, Kim J. 2005. High boost converter using voltage multiplier. 31st Annual Conference of IEEE Industrial Electronics Society, November 6-10, Raleigh, US, pp: 128. <https://doi.org/10.1109/IECON.2005.1568967>.

Bai S, Yu D, Lukic S. 2010. Optimum design of an EV/PHEV charging station with DC bus and storage system. *IEEE Energy Conversion Congress and Exposition*, September 12-16, Atlanta, US, pp: 1178-1184.

Chen J, Maksimovic D, Erickson RW. 2006. Analysis and design of a low-stress buck-boost converter in universal-input PFC applications. *IEEE Transact Power Electron*, 21(2): 320-329.

Clement-Nyns K, Haesen E, Driesen J. 2011. The impact of vehicle-to-grid on the distribution grid. *Elect Power Syst Res*, 81: 185-192.

Çalışkan A, Ünal S, Orhan A. 2017. Buck-boost dönüştürücü tasarımı, modellenmesi ve kontrolü. *Fırat Üniv Müh Bil Derg*, 29(2): 265-268.

Çelik M, Abut N. 2022. Elektrikli araçlar için kablosuz şarj sistemi simülasyonu. *Elektrik-Elektronik ve Biyomedikal Mühendisliği Konferansı*, 24-26 Kasım, Bursa, Türkiye, ss: 53.

Garip İ, Altın N, Sefa İ. 2009. Çift Anahtarlı buck-boost çevirici benzetimi. *TÜBAV Bil Derg*, 2(4): 385-393.

Genç S. 2023. Güç şebekelerinde iletilen yayınımların güç kalitesi analizi ve giderilmesi. *Doktora Tezi*, Ondokuz Mayıs Üniversitesi, Lisansüstü Eğitim Enstitüsü, Elektrik-Elektronik Mühendisliği Ana Bilim Dalı, Samsun, Türkiye, pp: 111.

Günaslan S, Nalbur BE, Cindoruk SS. 2023. Otomotiv endüstrisinde döngüsel ekonomi ve elektrikli araçlar için yaşam döngüsü değerlendirmesinin incelenmesi. *Uluslararası İleri Doğa Bil Müh Araş Derg*, 7(4): 313-318.

Hançar Y, Kaymaz H. 2021. Elektrikli araç batarya yönetim sistemleri için hücre eşitleme yöntemleri. *Akıllı Ulaşım Sist Uyg Derg*, 4(1): 60-73.

Hawkins TR, Singh B, Majeau-Bettez G, Strømman AH. 2013. Comparative environmental life cycle assessment of conventional and electric vehicles. *J Indust Ecol*, 17(1): 53-64.

Khaligh A, Li Z. 2010. Battery, ultracapacitor, fuel cell, and hybrid energy storage systems for electric, hybrid electric, fuel cell, and plug-in hybrid electric vehicles: State of the art. *IEEE Transact Vehic Technol*, 59(6): 2806-2814.

Khan W, Ahmad F, Alam MS. 2019. Fast EV charging station integration with grid ensuring optimal and quality power exchange. *Eng Sci Technol Int J*, 22(1): 143-152.

Köseni H, Yıldız AB. 2019. Geri dönüşlü DC-DC dönüştürücünün geliştirilmiş düğüm denklemleri ile analizi. *Politek Derg*, 22(1): 179-184.

Kumar BA, Jyothi B, Rathore RS, Singh AR, Kumar BH, Bajaj M. 2023. A novel framework for enhancing the power quality of electrical vehicle battery charging based on modified ferdowski converter. *Energy Rep*, 10: 2394-2416.

Li SG, Sharkh SM, Walsh FC, Zhang CN. 2011. Energy and battery management of a plug-in series hybrid electric vehicle using fuzzy logic. *IEEE Transact Vehic Technol*, 60(8): 3571-3585.

Li Z, Hoshina S, Satake N, Nogi M. 2016. Development of DC/DC converter for battery energy storage supporting railway DC feeder systems. *IEEE Transact Industry Appl*, 52(5): 4218-4224.

Lunz B, Yan Z, Gerschler JB, Dauer DU. 2012. Influence of plug-in hybrid electric vehicle charging strategies on charging and battery degradation costs. *Energy Policy*, 46: 511-519.

Malik MZ, Chen H, Nazir MS, Khan IA, Abdalla AN, Ali A, Chen W. 2020. A new efficient step-up boost converter with CLD cell for electric vehicle and new energy systems. *Energies*, 13: 2-14.

Mert T. 2007. Güç faktörü düzeltme yöntemlerinin incelenmesi ve bir uygulama devresinin gerçekleştirilmesi. *Yüksek Lisans Tezi*, Yıldız Teknik Üniversitesi, Fen Bilimleri Enstitüsü, Elektrik Mühendisliği Bölümü, İstanbul, Türkiye, pp: 48.

Moreno J, Ortuzar ME, Dixon JW. 2006. Energy-management system for a hybrid electric vehicle, using ultracapacitors and neural networks. *IEEE Transact Indust Electron*, 53(2): 614-623.

Nilsson M, Nykvist B. 2016. Governing the electric vehicle

- transition – Near term interventions to support a green energy economy. *Appl Energy*, 179: 1360-1371.
- Ortuzar M, Dixon J, Moreno J. 2003. Design, construction and performance of a buck-boost converter for an ultracapacitor-based auxiliary energy system for electric vehicles. *IECON'03. 29th Annual Conference of the IEEE Industrial Electronics Society*, November 02-06, Roanoke, US, pp: 2889-2894.
- Öncü S, Sazak BS. 2006. Tek anahtarlı inverterde bazı kontrol palslerinin silinmesiyle güç kontrolü. *Gazi Üniv Müh Mim Fak Derg*, 21(1): 123-127.
- Prudente M, Pfitscher LL, Emmendoerfer G, Romaneli EF, Gules R. 2008. Voltage multiplier cells applied to non-isolated DC-DC converters. *IEEE Transact Power Electron*, 23(2): 871-887.
- Sabri M, Danapalasingam KA, Rahmat MF. 2016. A review on hybrid electric vehicles architecture and energy management strategies. *Renew Sust Energy Rew*, 53: 1433-1442.
- Sharma S, Panwar AK, Tripathi MM. 2020. Storage technologies for electric vehicles. *J Traf Transp Eng*, 7(3): 340-361.
- Sivaraman P, Sharmeela C. 2021. Chapter 5 - Power quality problems associated with electric vehicle charging infrastructure. *Power Qual Modern Power Syst*, 2021: 151-161.
- Sousa LDB, Boris Bouchez B. 2010. A combined multiphase electric drive and fast battery charger for electric vehicles. *IEEE Vehicle Power and Propulsion Conference*, September 01-03, Lille, France. <https://doi.org/10.1109/VPPC.2010.5729057>.
- Sun B, Dragičević T, Freijedo FD, Vasquez JC, Guerrero JM. 2016. A control algorithm for electric vehicle fast charging stations equipped with flywheel energy storage systems. *IEEE Transact Power Electron*, 31(9): 6674-6685.
- Tofoli FL, Pereira DC, Paula WJ, Júnior DS. 2015. Survey on non-isolated high-voltage step-up dc-dc topologies based on the boost converter. *IET Power Electron*, 8(10): 2044-2057.
- Yapıcı AT. 2018. İndüksiyonla ısıtma sisteminin incelenmesi ve simülasyonu. Yüksek Lisans Tezi, Kocaeli Üniversitesi, Fen Bilimleri enstitüsü, Elektrik Mühendisliği Bölümü, Kocaeli, Türkiye, pp: 62.
- Yıldız AB. 2013. A MNA-based unified ideal switch model for analysis of switching circuits. *J Circuits*, 22(6): 1-12.
- Young K, Wang C, Wang LY, Strunz K. 2013. Electric vehicle battery technologies. In: Garcia-Valle R, Peças Lopes J. (eds) *Electric Vehicle Integration into Modern Power Networks. Power Electronics and Power Systems*, Springer, New York, US, pp: 15-56. https://doi.org/10.1007/978-1-4614-0134-6_2.
- Zimm C. 2021. Improving the understanding of electric vehicle technology and policy diffusion across countries. *Transp Pol*, 105: 54-66.